Studies on Poly (lactic acid) based Microcellular Biocomposite Foams

Thesis submitted in partial fulfillment of the requirements for the degree of

DOCTOR OF PHILOSOPHY

by

SHASANKA SEKHAR BORKOTOKY

(Roll No. 136107011)

Department of Chemical Engineering

Indian Institute of Technology Guwahati

Guwahati-781 039, Assam

May 2019

Dedicated to

My Parents for endless love and support

Department of Chemical Engineering

Indian Institute of Technology Guwahati

Guwahati - 781039, India

STATEMENT

I do hereby declare that the content embodied in this thesis entitled "**Studies on Poly (lactic acid) based Microcellular Biocomposite Foams**" is the result of investigations carried out by me at the Department of Chemical Engineering, Indian Institute of Technology Guwahati, Guwahati, India, under the guidance of **Prof. Vimal Katiyar**. In keeping with the general practice of reporting scientific observations, due acknowledgments have been made wherever the work described is based on the finding of other investigators.

Date: 15 May 2019 **Shasanka Sekhar Borkotoky**

Department of Chemical Engineering

Indian Institute of Technology Guwahati

Guwahati - 781039, India

CERTIFICATE

This is to certify that the thesis entitled "**Studies on Poly (lactic acid) based Microcellular Biocomposite Foams**" submitted by **Mr. Shasanka Sekhar Borkotoky (Roll No.: 136107011)** for the award of the degree of Doctor of Philosophy has been carried out under my guidance and supervision. The work documented in this thesis has not been submitted to any other University or Institute for the award of any degree.

Date:15May 2019

(Prof. Vimal Katiyar)

Professor

Department of Chemical Engineering

Indian Institute of Technology Guwahati

Guwahati - 781039, India

Acknowledgment

"Look at the sky. We are not alone. The whole universe is friendly to us and conspires only to give the best to those who dream and work."

Dr. A. P. J. Abdul Kalam

In the journey of Ph.D., I have learned a lot of new things and it helps me to understand myself. The journey would not have reached a successful end unless the support and guidance of my thesis supervisor, Prof. Vimal Katiyar. The enthusiasm and extremely hard-working nature of Prof. Vimal Katiyar help me a lot towards the completion of the research. I would like to take this opportunity to thank them from the core of my heart. His guidance helped me in all the time of research and writing of this thesis. I could not have imagined having a better advisor and mentor for my Ph.D. study.

I am very much thankful to the doctoral committee members, Prof. Bishnupada Mandal, Dr. Amit Kumar, Dr. Deepak Sharma and Dr. Prakash Kotecha for their useful suggestions and motivations during the research work.

I am really fortunate enough to access the state of art facilities available in the Centre of Excellence-Sustainable Polymer (CoE-SusPol) and Central Instrumentation Facility (CIF), IIT Guwahati for the doctoral research. I am thankful for the head and all authorities of the department of chemical engineering for providing me all research and analytical facilities required for my doctoral work.

I am extremely thankful to the technical staff (teaching and non-teaching) of the chemical engineering department, particularly Ritumoni Kalita, Harsaraj Biswanath, Dipak Kumar Barman, Jayanta Kumar Mout, Dr. Lukumoni Borah, Debajit Borah, Pankaj Sekhar Baruah, Deep Jyoti Sinha, Sailen Das, and Bhagya Boro for providing me all help and assistance for the completion of my work.

I am fortunate to have a large research group of specialists in different areas. I want to thank all my present and past lab members of CoE-SusPol, especially Arvind Gupta, Prodyut Dhar, Surendra Singh Gaur, Gourhari Chakraborty, Medha Mili, Monika, Narendren S, Melaku Tesfaye, Siddhartha Mohan Bhasney, Pankaj Boruah, Khalid Wani, Tabli Ghosh, Neha Mulchandani, Naba Kumar Kalita, Amit Pandey, Deepshikha Das, Bhanupriya Das, Kona Mandal, Dr. Purabi Bhagabati, Dr. Prashanta Baishya, Munmi Das, Chetna M. for their support and encouragement during the research period. I wish to place on record, my

thankfulness to my friends Dibakar Gohain, Kamalesh Verma, Babul Prasad, Atanu Kumar Paul, Dibyajyoti Das, Nemisha Bharadwaj and Sharbani Koushik for boosting my morale at the difficult moments.

I want to acknowledge the Ministry of Human Resources Development (MHRD), Government of India for the scholarship, which helps me financially during the Ph.D. research.

Last but not least, from the core of my heart, I wish to acknowledge the encouragement, support, and love from my parents who took all the burdens of life for the betterment of mine. I wish to thank sincerely one in all who helped me directly or indirectly to complete my research work. I want to acknowledge the internet giants like google scholar, sci-hub, research gate for the contributions in the doctoral research.

Finally and foremost, I thank God for giving me the good times which I enjoyed and the bad times from which I learned many things. I remain thankful for the mental strength given to face adverse situations. Blessings of Almighty are always solicited.

(Shasanka Sekhar Borkotoky)
15 May 2019

Abstract

Development of polymeric foams evolved as major research area due to its unique exclusive properties like lightweight, low density and optimum usage of polymeric materials compared to non-foamed counterparts. However, degradability is a major area of concern for petro-based polymeric foams. The ultimate disposal and environmental aspects of the non-degradable foams leads to the development of bio-based and biodegradable green foams. Major developed biodegradable foam mainly includes starch-based foams, polycaprolactone (PCL) foams, water-soluble polyvinyl alcohol (PVOH) and ethylene vinyl alcohol (EVOH) foam. The applications of these sustainable foams are mainly limited to multilayer packaging applications due to the limitations of oxygen barrier, mechanical properties etc. The improvement in above properties of these foams is a major concern of current research. One of the most promising biodegradable polymers is poly(lactic acid) (PLA) due to its greener routes and comparable properties with some of the conventional petro-based polymers like polystyrene (PS), polypropylene (PP) etc. However, improvement in the properties of PLA-based foams are still lacking in order to substitute the non-degradable foams. The improvement of properties of PLA-based foams can be achieved by incorporation of additives, flame retardants, plasticizers, and so on according to the targeted application. The use of bio-derived nanobiofillers for the improvement of above properties of PLA-based foam provides a greener approach towards the environment point of view. The nanofillers are derived from bio-feedstock that are abundantly available in nature. Therefore, the utilization of these nanobiofillers in PLA foam matrix has both economic and environmental impact. The incorporation of nanobiofillers in the PLA matrix for tailoring various properties is still a growing field of the research.

From the literature, it is observed that a knowledge gap exists towards the fabrication of PLA-based foams using bio-based nanobiofillers for tuning different properties like thermal, mechanical, gas barrier etc. according to the applications. Based on the knowledge gap, the

current doctoral research is mainly focused on the development of a hydrophobic, microcellular interconnected, and highly porous PLA-based foam utilizing lab developed bionanofillers like cellulose nanocrystals (CNC), modified chitosan (MC), modified gum arabic (MG) and silk nanocrystals (SNC). Further, no prior art has been observed regarding the incorporation of these bionanofillers in PLA-based foam matrix for proper tuning of different foam properties. The current research has been performed using the less expensive and innocuous casting and leaching (C/L) technique for foam fabrication utilizing the non-toxic and cost-effective sugar particles as porogen medium. The C/L technique is further modified for better dispersion of porogen particles in the polymer matrix.

The main motivation of the current doctoral research is to investigate the influence of bio-based nanofillers like CNC, MC, MG, and SNC on the foam processing and tailoring of its properties like thermal, wettability, crystallinity, cell size and cell density along with other physicochemical properties. Further, the effect of nanobiofillers in different degradation techniques like thermal, hydrolytic and photodegradation is investigated, first time.

The orientation of the doctoral thesis is as follows:

Chapter 1 mainly focuses on a brief description of non-degradable and biodegradable foams. Different available methods of fabrication of polymeric foams are discussed in this chapter. This chapter also provides a general overview of bio-based foams and its environmental aspects and market shares. This chapter also focuses on available foaming process which are in practice. This chapter consists of a thorough literature review of PLA-based foams. Based on the knowledge gap provided by literature review, different objectives of the research are highlighted in this chapter along with the motivation of current research. Finally, a brief orientation of the thesis is also provided in this chapter.

Chapter 2 provides information regarding various materials and chemicals utilized in the doctoral research. This chapter mainly discusses the technique utilized for the fabrication of the PLA/nanobiofiller-based foams. This chapter also demonstrates the preparation methods of bio-based nanobiofillers used in the thesis. The various analytical methods for characterization of the developed foam and associated sample preparation techniques are discussed in this chapter.

Chapter 3 discusses the fabrication and detailed study of PLA and PLA/CNC-based foams using C/L technique. From this chapter, it is observed that CNC mainly acts as a nucleating agent in the PLA matrix generating smaller pores. CNC improves crystallinity and thermal stability at lower loadings. CNC also influences the thermo-mechanical properties in PLA/CNC-based foams. The wettability phenomena are also affected by the addition of CNC. Both "model-free" and "modelistic" approaches like Kissinger-Akahira-Sinouse, Flynn-Wall-Ozawa, Friedman, Augis Bennet, Criado etc. are utilized to calculate the activation energy of thermal degradation. From the investigation, it is observed that complex degradation mechanism like three-dimensional diffusions is taking place at higher conversions of the fabricated foams. From the non-isothermal crystallization investigations, it can be concluded that CNC acts as a nucleating agent in lower loadings and also supress to the chain folding of PLA at higher CNC loading. The chapter provides a comprehensive characterization of PLA/CNC-based foams.

Chapter 4 demonstrates the fabrication of PLA/modified chitosan (MC) based foams by C/L technique. The results suggest that MC acts as a plasticizing agent in the PLA matrix due to the presence of low molecular weight oligomers. The cell size decreases and cell density improves with the incorporation of MC in the PLA matrix. Increase in surface area with MC loading is also observed. However, decrement in crystallinity and thermal stability is observed

with MC. The hydrophobicity increases with MC addition due to the change in surface morphology.

Chapter 5 provides in-depth analysis of developed PLA/modified gum arabic (MG) based composite microcellular foams by using C/L technique. It is noticed that MG acts as a plasticizing agent for PLA matrix due to pendent oligomer present in it. The thermal stability and crystallinity decrease with MG incorporation. The decrement in cell size and increments in cell density observed with the incorporation of MG bionanofillers. MG also influences the wettability phenomena. The different degradation techniques like hydrolytic and photodegradation of PLA/MG-based foams are examined in this chapter.

Chapter 6 demonstrates the development of PLA/silk nanocrystal (SNC) based microcellular composite foam. It is observed that SNC acts as a nucleating agent in the PLA matrix and helps in the improvement of crystallinity and thermal properties. Increase in cell density and a decrease in cell size is observed with SNC loading in PLA/SNC-based foams. Cell size up to ~0.6 μm is noticed for highest loading (PLA/SNC 3) of SNC. Improvements in hydrophobicity and improvement in thermo-mechanical properties of fabricated PLA/SNC-based foams are observed. The effect of SNC in hydrolytic and photodegradation are carried out in this chapter. It is also observed that SNC gives thermal stability under UV degradation to the PLA/SNC-based foams compared to neat PLA based foams.

Finally, **Chapter 7** mainly focus on a thorough discussion of the research outcomes. The comparative conclusions of the research are drawn in this chapter. The chapter also provides probable future directives of research for PLA/nanobiofiller-based biocomposite foams.

Contents

List of Figures

List of Tables

Nomenclature

Abbreviations Used

2D	Two dimensional
3D	Three dimensional
ASTM	American Society for Testing and Materials
ATR	Attenuated Total Reflectance
Advancing CA	Advancing contact angle
a*	Color parameter indicationg greenness
b*	Color parameter indicating yellowness
cc	Cubic Centimeter
CA	Contact Angle
CBA	Chemical Blowing Agent
CE	Chain Extendar
CFA	Chemical Foaming Agent
CAH	Contact Angle Hysteresis
C/L	Casting and Leaching
CNC	Cellulose Nanocrystals
C.I/I_{Cr}	Crystallinity Index
CO	Carbon monoxide
CO_2	Carbon dioxide
CH	Chitosan
Da	Dalton
DD%	Degree of Deacetylation
DMA	Dynamic Mechanical Analysis
DSC	Differential Scanning Calorimeter
DTG	Derivative of Thermogravimetric Analysis
ER	Expansion Ratio
FDA	Food and Drug Administration
FTIR	Fourier Transmission Infrared
Fig.	Figure
FESEM	Field Emission Scanning Electron Microscope
FWO	Flynn- Wall-Ozawa
GA	Gum Arabic

GRAS	Generally Regarded as Safe
GCF	Green Cell Foam
g	Gram
H_2O	Water
KAS	Kissinger-Akahira-Sinouse
kPa	Kilo Pascal
L*	Colour parameter indicating lightness
LA	Lactic acid
MIP	Mercury Intrusion Porosimetry
MC	Modified Chitosan (Oligomer-*grafted*-chitosan)
MG	Modified Gum Arabic (oligomer-*grafted*-Gum Arabic)
Modified CR	Modified Coats Redfern
M_n	Number average molecular weight
M_w	Weight average molecular weight
N_2	Nitrogen
NaCl	Sodium Chloride
OLLA-g-Chitosan	Oligomer-*grafted*-chitosan
OMMT	Montmorillonite
PLA	Poly(lactic acid)
POM	Polarizing Optical Microscope
PDI	Polydispersity Index
PLGA	Poly(lactic-co-glycolic acid)
PHEE	Poly(hydroxylester ether)
PCL	Polycaprolactone
PGA	Polyglycolic acid
PS	Polystyrene
PP	Polypropylene
PBA	Physical Blowing Agent
PHBV	Poly(3-hydroxybutyrate-co-3-hydroxyvalerate)
PVOH	Poly vinyl alcohol
ROP	Ring Opening Polymerization
RBF	Round bottom flask
rpm	Rotations per minute

sc-CO_2	Supercritical carbon dioxide
s	Seconds
SNC	Silk nanocrystals
TEM	Transition Electron Microscopy
TGA	Thermogravimetric Analysis
TIPS	Thermally Induced Phase Separation
USFDA	United State Food and Drug Administration
VER	Volume Expansion Ratio
XRD	X-ray diffraction

Notations Used

E'	Storage modulus
E''	Loss modulus
T_g	Glass transition temperature
T_c	Crystallization temperature
T_m	Melting temperature
T_{max}	Maximum degradation temperature
T_{onset}	Onset degradation temperature
T_{off}	Offset degradation temperature
M_n	Number average molecular weight
M_w	Weight average molecular weight
N_f	Cell density
ΔH	Enthalpy
ΔG	Gibb's free energy
ΔS	Change in entropy
T	Temperature
ΔE	Energy of crystallization
E_a	Activation energy
T_p	Peak crystallization temperature
X_t	Relative crystallinity
A	Pre-exponent factor

n_T	Tobin exponent
K_T	Tobin rate constant
n	Avrami exponent
k	Avrami rate constant
$t_{0.5}$	Crystallization half time

Greek Letters

θ_Y	Young's contact angle
θ_{adv}	Advancing contact angle
θ_{rec}	Receding contact angle
μ	Micro
β	Expansion ratio/heating rate (in thermal analysis)
α	Conversion

Chapter 1

Introduction and Literature Review

This chapter mainly discusses the biodegradable, non-toxic poly (lactic acid) (PLA) and its advantages over non-degradable petro-based polymers. The main motivation of this research is to fabricate a bio-based, biocompatible PLA-based foam for different probable applications. This chapter also contains different available technique of fabrication of polymeric foams. The advantages of the porous foam materials over their non-foam counterparts is also focused. A brief discussion on degradable and non-degradable polymeric foams is also reported. The different aspects poly (lactic acid) (PLA) is also discussed in this chapter. Different classifications and applications of polymeric foams are discussed thoroughly in this chapter. A detailed literature survey of different aspects of PLA based foams is discussed in this chapter with some important outcomes reported so far. A literature survey is conducted for different bionanofillers used in this investigation followed by knowledge gap in the investigation. The objectives of the research are also highlighted in this chapter. A brief illustration of the thesis chapters is highlighted in the later portion of this chapter.

Parts of this chapter are published/ready to communicate as follows:

1. Narendren Soundarajan, **Shasanka Sekhar Borkotoky,** and Vimal Katiyar *"Up-to date Advances of Biobased Biodegradable Polymers in Food Packaging"* In "*Bio-based Plastics for Food Packaging Applications*". **(Smithers Rapra, ISBN: 9781910242582)**

2. Shasanka Sekhar Borkotoky and Vimal Katiyar "*Biodegradable Nanocomposite Foam: Processing, Structure, and Properties."* (**Book chapter: to be submitted to "Advances in Sustainable Polymers, Springer**)

3. Tabli Ghosh, **Shasanka Sekhar Borkotoky,** Vimal Katiyar "*Porous and Non-Porous Structures of Green Composites: Processing and Application."* **(Book chapter: to be submitted to "Advances in Sustainable Polymers, Springer)**

1.1 General introduction

Polymers are one of the most useful materials developed by humankind. The ease of application, longevity, cost of production, lightweight and applicability in almost every aspect of daily life makes polymer a household name in recent years. Polymers have some added advantages compared to metals and ceramics, as these are not corroded by the atmosphere. Researches are going on to replace metals and ceramics by polymers. Polymers can be broadly classified into two categories: non-degradable polymers and degradable polymers. The petro-based non-degradable polymers like polystyrene (PS), polypropylene (PP) and so on, which mainly dominate the recent market of polymers. The main environmental concern associated with these non-degradable polymers is the end-life disposal [1,2]. Bio-based degradable polymers have some limitations in properties to compete with the major market players [3]. Researches are going on to improve the properties of biodegradable polymers comparable with non-degradable polymers and make it a replacement for different applications. Among available biodegradable polymers, some of the most utilized biodegradable polymers so far includes chemically derived poly (lactic acid) (PLA), microbial-derived poly (hydroxyalkanoates) (PHA) and its various fractions, petrochemical feedstock based polycaprolactone (PCL), and polyglycolic acid (PGA) attaining significant focus due to their potential use in various application in day to day life [4–6]. However, formulation of blends and composites of available biodegradable polymers can provide tailored properties according to the necessity [7–9]. Interestingly, the biocomposites and blends of these polymers with other available biopolymers including cellulose, starch, chitosan, proteins, gelatin are capturing the main focus. Formulations of biocomposites help in improving the polymer properties by transferring the filler load in to the matrix [10].

Another dimension of polymeric research is to reduce the material usage by fabricating foam (porous) structure. Foam is a material, which consists of gaseous voids (75%-95%). Polymeric

foams have some unique properties. It has some added advantages like low weight, low density and less usage of materials compared to non-foam counterparts [11]. The cost of production can also be reduced by these factors. All three types of materials (metals, ceramic and elastomer) can be utilized to fabricate foams. However, elastomeric foams have been widely utilized in different fields of applications. The use of polymer foaming technology is growing day by day and has established as one of the major areas of research. Foaming is gaining importance enormously, where any novel material is targeted for investigating the foaming behaviour immediately for the probable area of applications. The polymeric foam industry was initially developed from the 1930s to 1950s. It took an established shape in the 1980s. Among available polymeric foam materials, polystyrene (PS) foam was firstly developed in 1931. The driving force for the recent investigation of foams are directed towards the tailored property of foamy materials for extensive applications. Polymeric foams can be classified according to different parameters as shown in **Fig. 1.1**. The polymeric foams can also be broadly classified into two major parts: non-degradable foams and biodegradable foams. Non-degradable polymeric foams mainly dominate the current market share of total polymeric foams [12,13]. The recent shares by volume in various applications of polymeric foams are shown in **Fig. 1.2**.

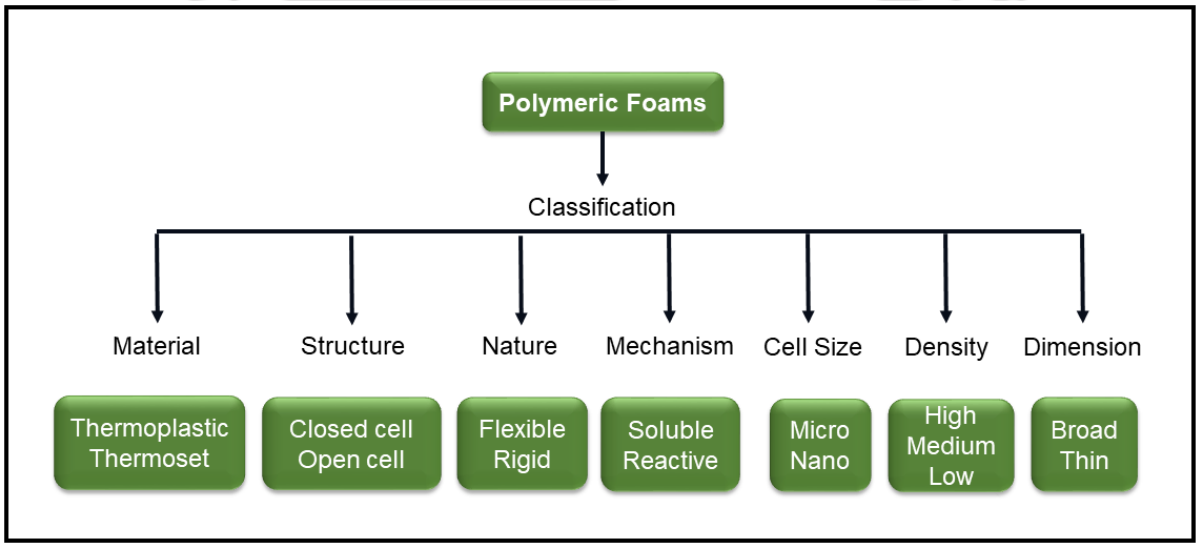

Fig. 1.1 Classifications of polymeric foams based on different parameters.

The demand for polymeric foams in different new areas is rapidly increasing day by day. Researchers are also trying to find new areas of replacement to the conventional non-foamed polymers. A recent market survey suggests the use of high-performance polymeric foams will increase ~4.8% annually due to the growth in emerging technologies. However, the above foam market is mainly dominated by the non-degradable conventional foams. The ultimate disposal of these foams is a major concern in the environmental point of view. The environment-friendly technologies are now a primary requisite followed by international agreements such as the Kyoto protocol, Montreal protocol and so on. Hence, the need for bio-based and degradable foams are gaining attention in recent years. Bio-based and bio-degradable foams show a tremendous and promising impact on different fields like biomedical tissue engineering applications [14,15]. Major differences between biodegradable and non-degradable foams are illustrated in **Fig. 1.3**.

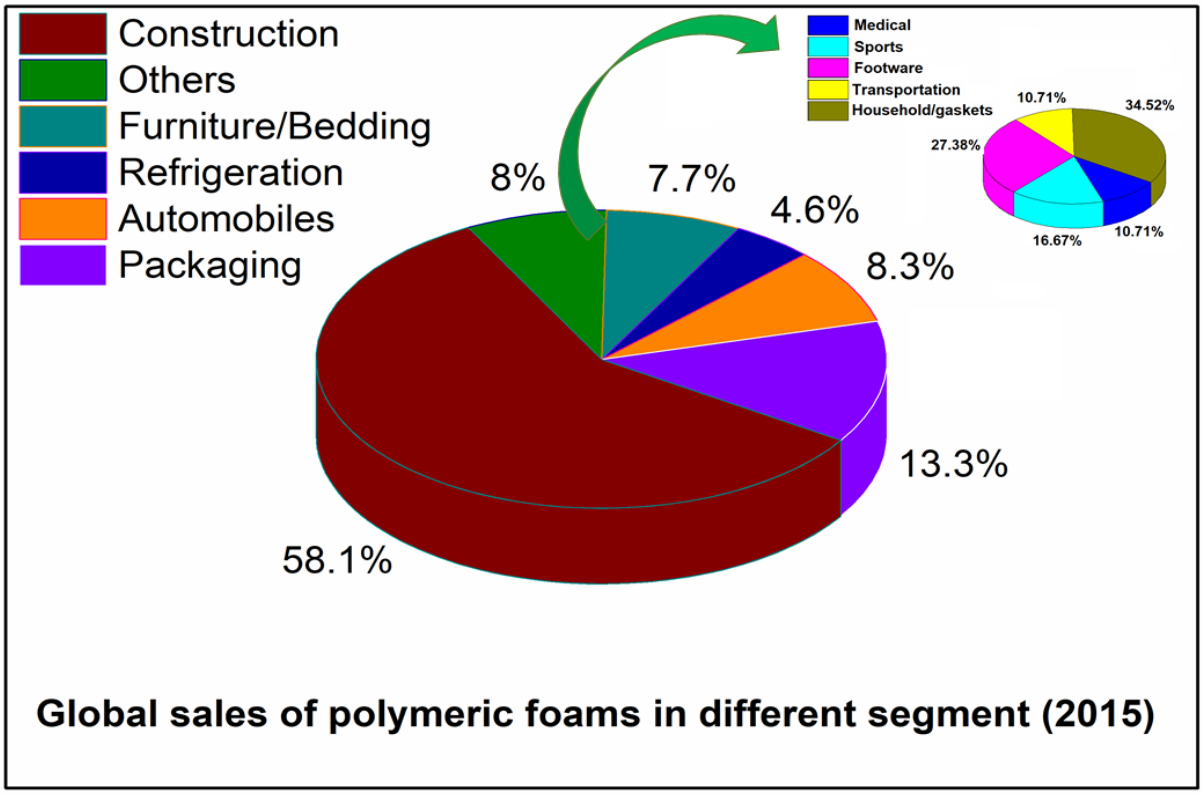

Fig. 1.2 Global market shares of polymeric foams in various segments.

(https://www.smithersrapra.com/resources/2017/february/high-performance-polymer-foams-market-forecast)

From past few years, synthetic biodegradable polymers are acquiring significant attention over fossil-derived conventional polymers due to their non-toxic, biocompatible nature. Further, biodegradable polymers can possibly diminish carbon footprint, plastic-based waste, municipal solid waste, which in turn reduce global warming, and preserves soil fertility through soil composting. Biodegradable foams including starch, polycaprolactone (PCL), polyvinyl alcohol (PVOH) and so on, provides promising properties in some sophisticated biomedical applications [16]. However, it has limitations for replacement of non-degradable foams in various commodity applications. Mainly the use of these biodegradable foams is still limited to packaging, tissue engineering, and thermoformable sheets. The in-depth investigation on biodegradable foams is still required for improved properties to a comparable level with conventional foams [17].

One of the promising biodegradable polymer, which gains attention to the scientific community for the replacement of conventional polymeric foam, is poly (lactic acid) (PLA). Recent researches on bio-based foams are mainly focused in the development of PLA-based foams.

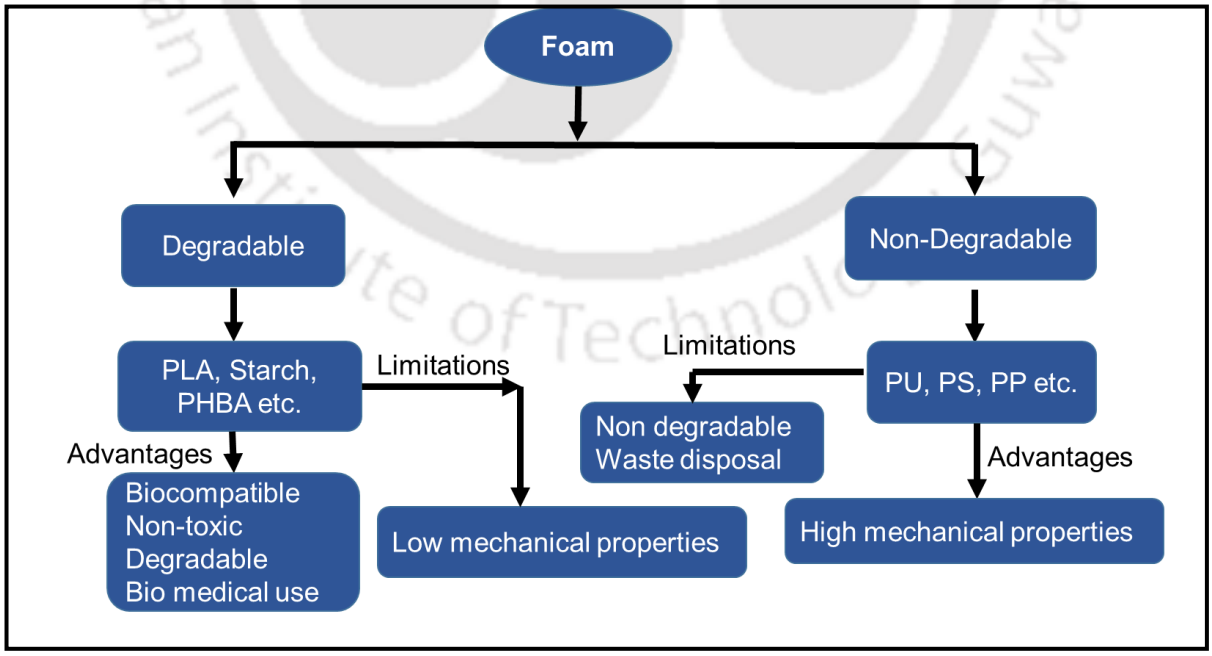

Fig. 1.3 Degradable and non-degradable foam.

1.1.1 Poly (lactic acid) (PLA)

Poly (lactic acid) (PLA) is a bio-based and biodegradable polymer synthesized from natural bio-resources such as corn, sugar feedstock and so on. PLA has the properties comparable to some non-degradable petro-based polymers. The pictorial illustration of the life cycle of biodegradable PLA can be observed in **Fig. 1.4.** PLA has good processability and compostability. Mainly PLA is synthesized by ring opening polymerization (ROP) of lactide monomer [4]. The thermal degradation of PLA leads to the production of environmental friendly products such as CO_2, H_2O and so on due to chain hydrolysis of the ester linkage. PLA is a glossy, transparent and thermoplastic in nature. The production of PLA requires less energy (up to 25-55%) compared to the energy consumed in the production of petroleum-based non-degradable foams. It is semi-crystalline in nature. The content of D-isomer present in PLA influences the ultimate property. The mechanical and other properties of PLA is comparable with most of the petro-based conventional polymers. The properties of PLA can be improved by tuning it with the addition of different nanofillers [18], plasticizers [19,20], chain extenders [21] and so on.

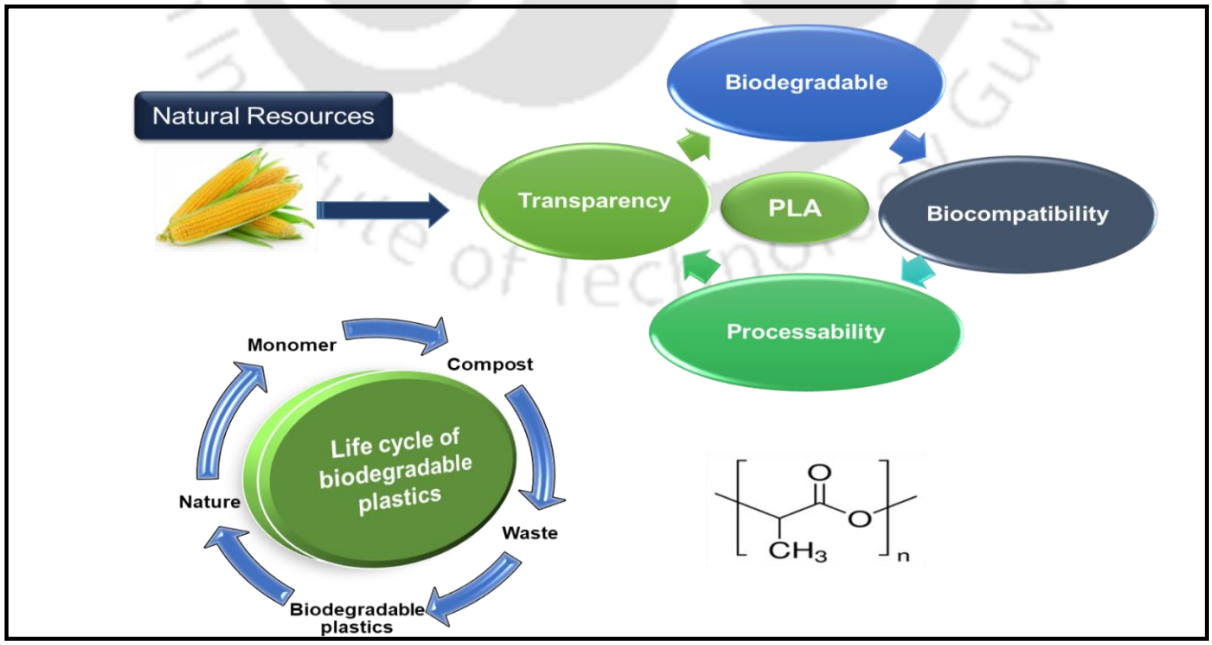

Fig. 1.4 Lifecycle of poly (lactic acid).

One of the limitations of PLA is its low melt strength. The short degradation time of PLA makes it unsuitable for engineering applications. Another limitation of PLA is low thermal properties. The current researches on PLA are mainly in the directions to tune these limitations. PLA-based foams are mainly utilized in sophisticated bio-based medical applications like cell culture, tissue engineering and so on due to its bio-degradability nature. Simultaneously, it can be useful in other applications by properly tuning it. The other applications include mainly packaging, housewares, automobile parts, cushioning applications, insulation, furniture, high-grade decorative items, and electrical appliances. A lot more focused study has to be performed to make it suitable for different areas of application.

1.2 Development of polymeric foam

Polymer foaming can broadly be carried out in different established process classified as batch foaming process and continuous foaming process. Pictorial representation of these two processes can be found in **Fig. 1.5**. The batch process is mainly limited to the research in development fields to investigate the newly developed materials and their foaming behavior. On the other hand, the continuous process is an economically and industrially viable scale-up process in larger magnitude. A continuous process is achieved by an extrusion technique, consisting of steps like mixing with additives and pressurization of inert gases [22].

Batch foaming: Fabrication of polymeric foams can be performed by using batch process. In this process of fabrication, foamed samples are prepared in batch-wise. It is a discontinuous foaming process and the reproducibility of the results of this process is very good by maintaining exact process parameters. This process is mainly utilized to investigate the initial foaming behavior of polymers and composite systems. The process is also industrially viable with some limitations. In this process, carbon dioxide or nitrogen are mainly used as physical blowing agent [9].

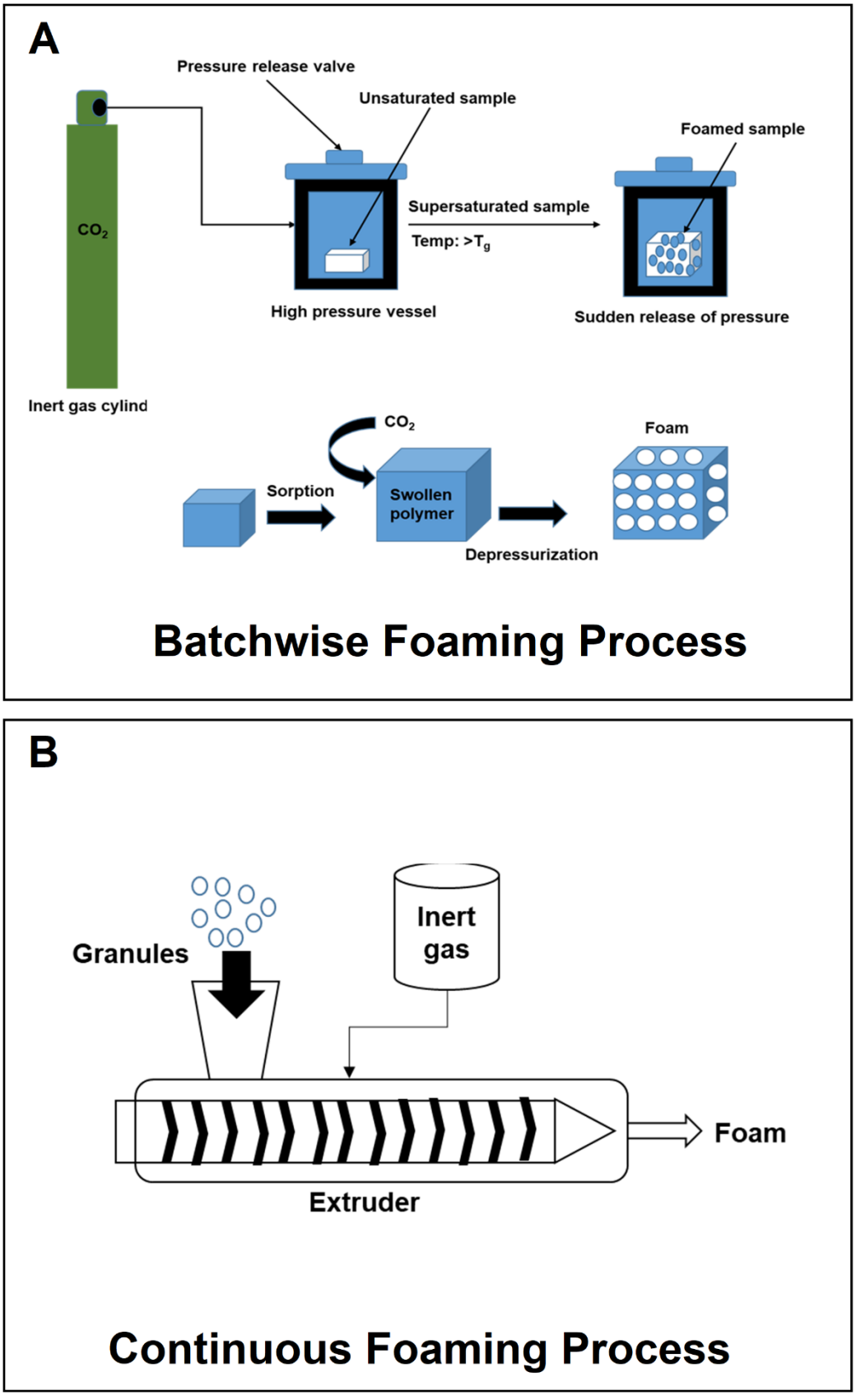

Fig. 1.5 Pictorial representation of A) batch and B) continuous process of foaming.

From very earlier days, two different methods are generally utilized in the batch foaming process. In the first process, pressure drop initiates foaming in the polymer sample resulting thermodynamic disequilibrium. The method is very useful to understand different foaming parameters as well as the influence of additives or blending on cell nucleation. The influence of pressure decrease rate on foaming can be further optimized along with the material and foaming process [23,24].

In the second technique, the thermodynamic disequilibrium is reached due to the temperature increase. The foam processing window of the polymer can be investigated and the temperature of foaming can also be evaluated for foam extrusion process by this method.

Continuous foaming: This process of fabrication of polymeric foam generally consists of extrusion and injection techniques. Different zones of the extruder can be operated at different temperatures, which makes it possible to use temperature sensitive additives to the polymer. This is one of the most beneficial CO_2-based foaming techniques for the addition of different additives to the bio-based polymeric foams. In the die section of the extruder, the pressure is released and ultimately polymer foam is generated. In this continuous process also, the foam parameters like screw speed, saturation pressure, type and amount of additives (clay, plasticizer etc.) etc. process parameters can be optimized. The influence of the die geometry and temperature on the nucleation rate or the expansion ratio of the fabricated foams can be investigated by this process. In this process, the main advantage is the continuous high-speed production and scale up the technology. The different parameters affecting the polymer foam characteristics are shown in **Fig. 1.6**. It can be observed from the figure that different parameters like melt strength, viscosity, solubility, end groups, glass transition temperature and so on effects the polymeric foam [25, 26].

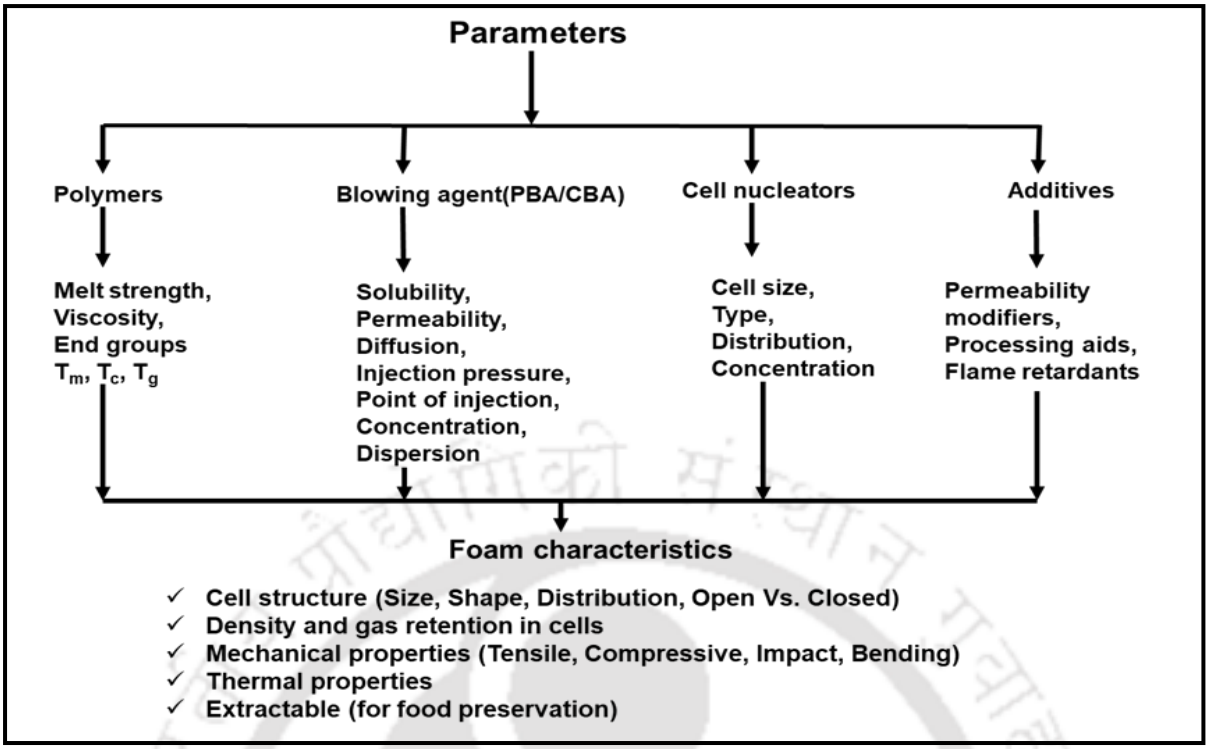

Fig. 1.6 Different parameters affecting the foaming process [27].

1.3 Polymer foam processing techniques

The polymeric foams can be manufactured by the above-discussed processes using different technology. The different techniques used in the above two processes are illustrated in **Fig. 1.7**. Generally, two basic methods are utilized for foaming [28]. In one method, gas is induced directly to the liquid and in the other method, gas bubbles are generated within the liquid phase.

The foaming process involves three general steps [29] as discussed below:

1. Bubble formation

2. Bubble growth

3. Bubble stabilization

Additionally, polymeric foam fabrication can be carried out by using soluble foaming and reactive foaming.

1.3.1 Physical/soluble foaming: It involves the dissolution of physical blowing agents (PBA) in the polymer melt. Extrusion and injection molding with PBA is a common example of this technique. The advantage of this process is that it permits high-speed continuous processing of foams. Soluble foaming can be achieved by using

a) Casting and leaching (C/L) technique

b) Foaming by using gases

c) Thermally Induced Phase Separation (TIPS)

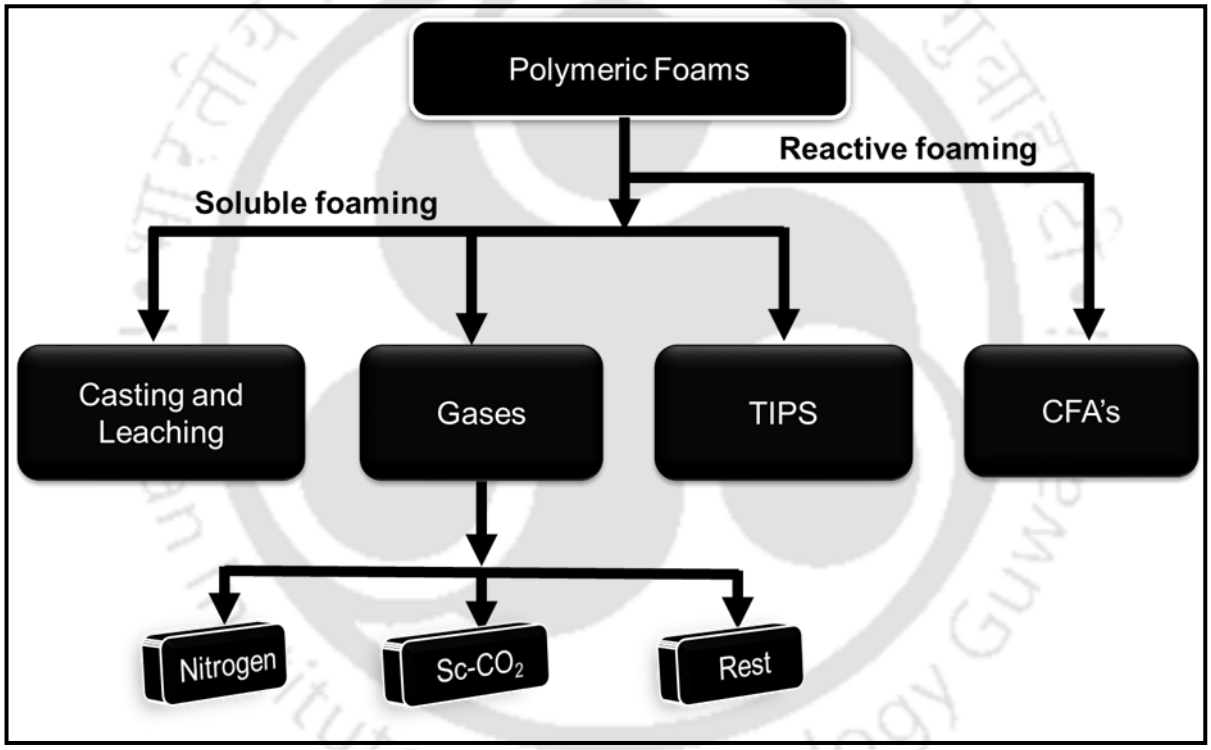

Fig. 1.7 Different techniques used for polymer foaming.

1.3.1.1 Casting and leaching (C/L): This technique involves the dissolution of the polymer into a highly volatile solvent and thereafter casting the prepared solution into a mold (of different shapes of requirements) which contains a solid porogen. The porogen is a particle, which is a water-soluble salt, for example, NaCl, KCl etc. which can be washed out after the solvent has been evaporated. This will ultimately leave a porous and foamed polymeric

structure, which contains gaseous voids in its structure. The pore size and morphology of the fabricated foam can be changed in this method by controlling the size and distribution of the porogen particles and the amount added in the solution [30]. The main advantage of this process involves less machinery usage, low consumption of energy and ease of the operation. The process is illustrated in **Fig. 1.8**.

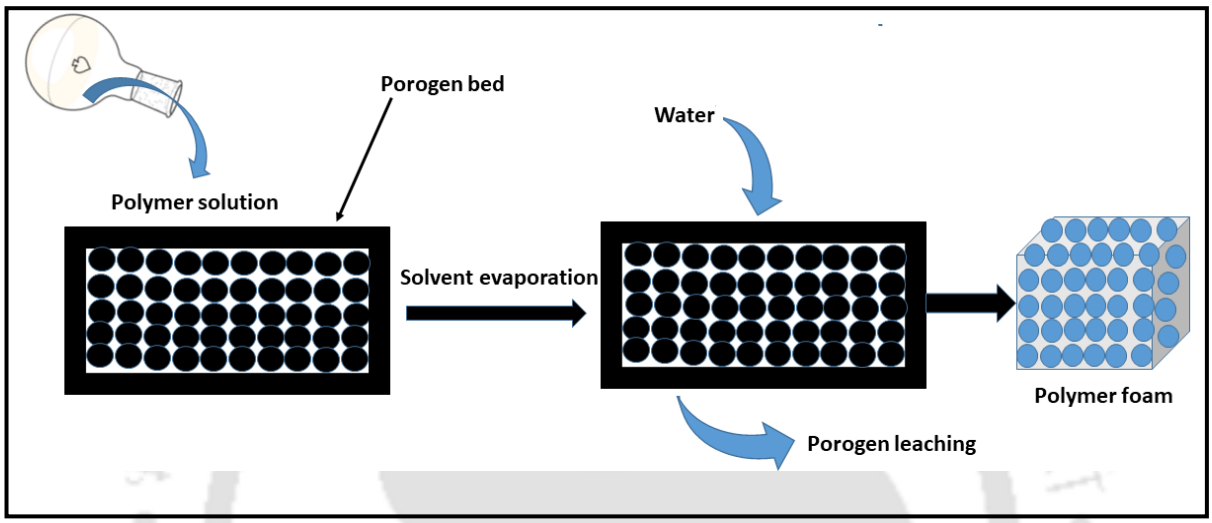

Fig. 1.8 Casting and leaching (C/L) technique for fabrication of polymeric foam.

1.3.1.2 Foaming by using gases: In this technique, Physical blowing agents (PBAs) are used for foaming the polymer. Problems concerning the environment and the need for developing environmentally friendly foaming agents have triggered researchers in this technique. Here mainly inert gases like nitrogen, carbon dioxide are used as a blowing agent, which acts as greener solvent for foaming [14]. The factors affecting the selection of PBAs includes following

a) Physical: Volatility, Critical Temperature, Latent heat etc.

b) Chemical: Reactivity and Stability

c) Transportation: Permeability and Diffusivity

d) Safety: Toxicity and Flammability

e) Environmental issues

f) Availability: Cost and Storage

The main advantages of Foaming by using gasious technique is that it is a non-toxic and environmentally friendly process. Though nitrogen is also used as a blowing agent, extensive use of carbon dioxide as a foaming agent has been observed in literature, as CO_2 helps in enhancing the processability of the polymer. The use of carbon dioxide in the supercritical stage has some added advantages. Because in supercritical fluid there are no distinct liquid and gas phases and it can diffuse through solids like a gas, and dissolve materials like a liquid.

1.3.1.3 Thermally induced phase separation (TIPS): TIPS process mainly involves two steps. Polymer pellets with blowing agents are partly foamed in steam in the first step. These foamed pellets are then transferred into a mold and again comes into contact to steam, in the second step, which results in extra foaming of the pellets. The pellets stick together and take the shape of mold due to the further expansion. Generally, a low boiling liquid such as pentane and hydrochlorofluorocarbons (HCFCs) is used as a foaming agent in this technique [31].

1.3.2 Reactive foaming: In this technique, the final foam production is yielded from a chemical reaction. It initially requires a certain amount of gases, which will finally form a foamed structure. Chemical blowing agents (CBA) are used in this method, where CBAs are capable of liberating gaseous components via reactions and/or thermally induced decomposition [32]. The examples include Azodicarbonamide, Titanium hydride, Isocyanates, where the selection is made based on some properties as described below:

a) Processing capability with the base polymer

b) Type and amount of decomposed gas

c) Appropriate decomposition with other additives

d) Color from leftover or by-products

e) Nucleating effects out of decomposed particles

1.4 Improvement of properties in sustainable polymeric foams using nanobiofillers

The main bioplastic foams used for packaging includes starch, PLA, poly(3-hydroxybutyrate-co-3-hydroxy valerate), poly(hydroxy ester ether) and PHA. However, the combination of the above polymeric materials can also studied for foam packaging applications.

For food packaging applications, Green cell foams® are now available in the market for commercial purposes. Biodegradable Green cell foam® (GCF) made from a proprietary corn-starch blend [33]. Lots of research has been done to improve various mechanical properties (Impact, compression, tension and flexural behavior) so that it can be utilized in the wide area of applications. It was observed that moisture levels and extrusion temperature affect the properties of sustainable foams. Also, the blending of starch with various other bio-plastics was investigated. It was observed that the incorporation of PLA, PHEE, and PHBV promote higher expansion ratio and lower density foams. The foam prepared are found to be more water resistant than normal starch foams [34] Hybrid PLA foams have also been fabricated by compression molding [8]. PLA/starch nanocomposite foams with different organoclays have also improved the foam properties [35].

Poly (lactic acid) foam is now showing a promising impact in the foam industry due to its various properties comparable with non-degradable counterparts. Lots of literature are available for PLA foams in various packaging applications. Applications of PLA foams in cups, thermal insulators, disposable food trays, and cushioning materials have also been explored by researchers [36]. Researchers have also investigated the blending of PLA/Polystyrene (PS) foam and then created an interconnected porous structure by first foaming the PLA/PS blend and then extracting the PS phase. PS phase extraction ensured the interpore connectivity of the cells. The fabricated foam has tissue engineering applications [37]. In recent literature, it can be observed that improvements in biodegradable foams can be done by using nanofillers and other additives. PLA-based foams show a promising improvement in properties compared to

other bio-based foams. Greener approach for improvement in PLA-based foams can be achieved by using some naturally derived bio-based nanofillers like cellulose nanocrystals (CNC), chitosan, silk, gum and so on. These bionanofillers have the potential to tune the properties of PLA-based foams according to the requirements. One of the advantages of these nanobiofillers is their greener route and environment friendliness. Some useful nanobiofillers are discussed below.

1.4.1 Cellulose nanocrystals (CNC): Cellulose nanocrystals are naturally derived nanobiofillers. CNC can improve the mechanical and barrier properties of the neat polymer matrix drastically. CNC has a lot of potentials to improve the property of existing biopolymers. It is observed from recent investigations that CNC has a tensile strength of 500 MPa and stiffness of 140-220 GPa. Incorporation of CNC in the polymer matrix improves the mechanical properties drastically [38–40]. CNC can be fabricated by using acid hydrolysis of nature driven cellulose fibers. CNC has the morphology of rod-like structure with nanometer dimensions. CNC can be referred in several terms such as nanowhiskers, nanocrystals, nanoparticles, microcrystallites or nanofibers. The length of CNC generally observed around ~500-700 nm and width of ~20-30 nm. The rod-like structure of CNC possess various unique morphological aspects like nanoscale dimension, high aspect ratio, high surface area as well as favourable properties such as high specific strength, unique optical transparency and so on [41].

1.4.2 Silk nanocrystals (SNC): Silk nanocrystals (SNC) is relatively new developed nanobiofiller comes from the natural source of silk. Polymer crystals can be generated from a number of living organisms [42]. From silk, crystals can be obtained by removing the amorphous bulky and polar amino acids. Highly organized β-sheet nanocrystal and amorphous region of silk can be interplayed by using molecular modeling [43]. The beta sheet nanocrystals are mainly responsible for the ultimate tensile strength related to the crystal size. The SNC

consists of nanofilaments and the distribution lengths ranged from ~100 nm -~600 nm. The silk nanofilaments are normally ~160 nm long and ~2 nm thick [44].

Silk nanocrystals could be quite promising when compared to organic nanocrystals. They are obtained from nature, thus have the following advantages such as [45] described below:

a) Stable in suspension

b) Renewability

c) Low cost

d) Easy availability

e) Good biocompatibility

f) Easy chemical and mechanical modification

g) Mechanical stability

h) Withstand processing conditions

i) Long-term sustained release of drugs

j) Slow degradability

1.4.3 Chitosan: Chitosan is derived from bio-based chitin, which is abundantly available polysaccharide in nature after cellulose. Conversion of chitosan from chitin depends on the degree of deacetylation (DD%) of chitin. The conversion of chitosan depends on different parameters. Chitosan is a very useful bionanofiller. It has the approval of the Food and Drug Administration (FDA) as a non-toxic material and can be utilized in foods and other biomedical applications. Generally, chitosan is hydrophilic in nature. Some investigations have demonstrated the use of chitosan in the polymer matrix as nanobiofillers. Chitosan has the excellent film-forming ability and high gas barrier applications. It is mainly used in the food

packaging sector. However, due to its hydrophilic nature, some modifications in the surface has to be conducted to make it compatible with hydrophobic biopolymers. Various fields of applications of chitosan include cosmetics, agriculture, biomedical, pharmaceutical, chemical industry, biotechnology and so on. It has the potential to be utilized as nanobiofillers in biopolymer foam matrix for different sophisticated bio-based applications [46,47].

1.4.4 Gum arabic: Gum arabic (GA) is a polysaccharide-based gum obtained from trees like *Acacia Senegal* and *Acacia Seyal*. It has some added advantages like non-toxicity, biodegradability and easy availability as it comes from natural resources. GA has tremendous applications in fields like paints, cosmetics, beverages and pharmaceuticals due to its emulsifying and stabilizing property. GA can be described as a neutral or slightly acidic salt of polysaccharides consisting of Ca, K and Mg cations. The structure of GA can be divided into three main fractions namely arabinogalactan (AG), arabinogalactan-protein (AGP) and glycoprotein (GP). GA has GRAS (Generally Recognized as Safe) certification by USFDA (United States Food and Drug Administration). Hence, it is widely used in food, drug, lithography, ceramics, pharmaceuticals and in different sophisticated biomedical applications [48].

1.5 Literature review and knowledge gaps

This section of the chapter mainly focuses on the literature available on the fabrication of PLA-based foams. Literature available on recent developments in PLA/nanocomposite-based foams and other nanofiller-based PLA foams are discussed thoroughly in this section. This section is divided into five subsections based on biopolymer and PLA-based foams, CNC-based, chitosan-based, gum arabic-based, and SNC related prior arts.

1.5.1 Literatures in nanobiofillers

Many investigations on CNC, chitosan, gum arabic and SNC had been reported regarding the surface modification and its compatibility with biopolymers. In the recent investigations, it is observed that these nanobiofillers can be utilized for the improvement in the ultimate properties of different biopolymers especially PLA. Some existing literatures are discussed below.

Sethi et al. (2017) investigated the impact of CNC with semi-interpenetrating polymer network structure in PLA/PU blends. The investigation was conducted using 1,4-dioxane as a solvent in solution casting technique. They have reported improvements in elastic modulus by ~54% of the composite with 1% CNC concentration. The thermal behavior and thermomechanical properties of the composite improve due to the reinforced PU network in the PLA matrix along with CNC [49].

Braun et al. (2012) developed PLA and CNC based eco-friendly nanocomposites. The hydroxyl-group initiated ring opening polymerization leads to the grafting of PLA chains in the surface of CNC. This surface modification of CNC improves different properties of PLA [50].

The isolation of CNC from microcrystalline cellulose (MCC) and for the improvement of the property has been demonstrated by **Capadona et al. (2009)** [51] Simultaneously, **Zheng et al. (2016)** demonstrated the grafting of CNC with poly(butylene succinate) (PBS) for the improvement of PBS)/ PLA blends. They have demonstrated that the grafting in CNC helps in the dispersion of CNC in the blend phases which enhances the crystallinity and various mechanical properties [52].

Frone et al. (2011) developed two different types of cellulose fiber and fabricated PLA composite. The two types of cellulose fiber were obtained from acid hydrolysis and mechanical disintegration. The surface modification of cellulose fibers was performed by using 3-

aminopropyl triethoxysilane to make it compatible with the PLA matrix. Improvements were observed in storage modulus of PLA [53].

Martinez-Sanz et al. (2011) demonstrated the dispersion of CNC in ethylene-vinyl alcohol copolymer (EVOH). The melt compounding technique was utilized after pre incorporation methods like electrospinning. Improvements in elastic modulus and tensile strength were observed in the EVOH copolymer. The morphology, thermal stability, crystallinity, water barrier, and the mechanical property was also influenced by CNC [54].

Martínez-Sanz et al. (2012) investigated the dispersion of unmodified bacterial cellulose into the PLA matrix. They have used the melt compounding techniques. Electrospinning and solution precipitation was utilized and enhancements in the barrier and mechanical properties were observed [55].

Gupta et al. (2017) recently developed spray-dried lignin coated cellulose nanocrystals (L-CNCs) for the improvement of rheological and thermo-mechanical properties of PLA-based composites. The storage modulus was drastically increased by ~60% due to the improved rheological behavior and blown film processing of PLA-based composite [56].

Haque et al. (2017) studied the effect of reactive functionalization in the presence of glycidyl methacrylate (GMA) in polyvinyl acetate (PVAc) for PLA/CNC composite. The miscibility of the two different phases was improved by this method. PVAc was acting as a dispersing medium for CNC. Chemical modification of CNC was carried out using reactive monomer GMA. They have suggested that this technique can also be effectively used with other biopolymers [57].

Bondeson et al. (2007) also investigated the dispersion of surfactant-modified CNC in the nanocomposite. They have used polyvinyl alcohol (PVA) to improve the dispersion of CNC in the PLA matrix. However, due to the phase separation of PLA and PVA, no significant

improvements in thermal and mechanical property was observed. It was also observed that CNC is more favorable towards the PVA matrix compared to PLA. Hence, it is mainly localized in PVA [58].

Similarly, some prior arts on silk-based nanobiofillers in PLA is observed in the literature. **Cai et al. (2002)** investigated the surface modification of PLA with the help of silk fibroin. They have utilized solvent casting technique for film preparation taking chloroform as a solvent. The investigation gives light to the cell proliferation study in the PLA surface. The modification also helps to incorporate hydrophilicity in the PLA surface [59].

Zhao et al. (2010) fabricated PLA/silk fiber biocomposite utilizing the melt compounding technology. Improvements in storage modulus, stiffness were observed in the matrix, however, the thermal stability noticed to be decreased. They also observed that silk acts as a nucleating agent in the PLA matrix [60]. Similarly, **Cheung et al. (2010)** studied the probable biodegradable implant applications of silk/PLA-based composite materials. They have observed faster biodegradation of ~4 months for the PLA/silk-based composite material. Improvements in stiffness and ductility were observed in the composite material compared to neat PLA [61].

Fabrication of electrospun nanofiber by tussah silk fibroin/PLA composites was demonstrated by **He et al. (2011)** Some improvements were observed in breaking stress and breaking strain, however, increasing in PLA content results phase separation in the matrix [62].

Patwa et al. (2018) investigated the effect of silk nanodisc dispersion on different properties of PLA-based nanocomposites. They have fabricated the silk nano-disc from waste Muga silk by using acid hydrolysis. Improvements observed in crystallinity, thermal and mechanical properties of PLA on the incorporation of silk nano-disc. The uniform dispersion of silk nano-

disc in the PLA matrix leads to the improvement in toughness, storage modulus and percentage elongation [63].

Niamsa et al. (2009) fabricated chitosan-based films using PLA as a solvent with the help of the solution casting method. Different molecular weight chitosan was used for their investigation. They have observed that solvent affected the mechanical properties for PLA. The ratio of L and DL-forms of lactic acid has an impact on the wettability and flexibility of the chitosan films [64].

Svagan et al. (2012) investigated the fabrication of extruded PLA-based films with alternate layers of MMT and chitosan. They have investigated the properties of extruded PLA with 70 bilayers with neat PLA films. The optical clarity remains close to neat counterpart however it affects the transmittance value [65].

Schreiber et al. (2013) demonstrated the fabrication of neat chitosan films with the addition of antioxidants to enhance the functionality [66]. Similarly, **Peng et al. (2013)** also utilized antioxidants such as green tea extracts (GTE) and black tea extracts (BTE) for fabrication of chitosan films in solution casting technique. The reduction in mechanical properties and apparent viscosity was observed on the incorporation of antioxidants in chitosan. However, improvements were observed in solubility and swelling degree of chitosan [67].

Li et al. (2013) utilized chitosan and CNC as coating layers in PET films utilizing the layer-by-layer (LBL) technique for the improvement in oxygen barrier properties. They concluded that the system is very effective for producing films with high gas barrier properties. The reduction up to ~94% in oxygen permeability was observed compared to uncoated films [68].

The applicability of chitosan scaffolds in tissue engineering applications was demonstrated by **Croisier et al. (2013)** They have fabricated 2D and 3D scaffolds of chitosan for different applications. Similar types of investigations are also observed for gum arabic [69]. The

improvement in film forming ability and properties of gum arabic by using plasticizers and cross-linkers was investigated by **Wyasu et al. (2012)** [70]**.**

Sakloetsakon et al. (2016) fabricated chitosan and gum arabic films. They have investigated mechanical and physicochemical properties of the fabricated films. They have utilized a solvent casting method of fabrication. The investigation was useful in the direction of drug delivery and coating applications of gum arabic/chitosan films [71]. The food applications of gum arabic were investigated by **Ali et al. (2010)** They have used gum arabic coating to increase the shelf life of tomato and postharvest quality [72].

From this section of prior arts, it can be concluded that nanobiofillers can be effectively utilized by surface modification or other methods for the improvement of the properties of biopolymers. The utilization of nanobiofillers in biopolymer matrix is a greener approach for the environmental point of view.

1.5.2 Literatures in PLA-based foams

The melt strength and thermomechanical stability are very important properties of polymeric material from processing and application point of view. From the previous literature, it was observed that PLA has low melt strength and some modifications have to be done for tuning of properties for making it as a green replacement for the conventional polymers [73]. Researchers have used various nanofillers to tune the properties of PLA foams. Nanofillers like organically modified montmorillonite (OMMT), organically modified layered silicates (organoclay) have been used in the recent past to tune various properties of PLA foam according to applications [18,74]. Silk composite [75], graphene oxide [76] chain extenders and paraffin spheres [77] are also used by the researchers for various improvement in properties.

Kothapalli et al. (2005) fabricated a biodegradable nano-hydroxyapatite (HA)/PLA scaffold by C/L method and investigated the effect of these nanofiller content on scaffold properties [7]. They observed an increase in compression modulus by increasing the filler content. **Mikos et al. (1994)** fabricated PLA foams by using salt as a porogen particle and investigated the porosity, crystallinity, and morphology of the foam [13]. **Blaker et al. (2005)** investigated the mechanical properties of PDLLA/Bioglass® composite foams with high porosity for possible applications in tissue engineering [78]. **Ma et al. (2014)** used sucrose as a porogen to fabricate biodegradable foam [79]. **Pinto et al. (2016)** investigated the effect of the porous structure of polymeric foam on the remediation of oil spills [80]. They noticed that pore size below 500 microns is able to reach oil absorption capacities. **Preechawong et al. (2005)** prepared and characterized starch/PLA hybrid foams [8]. They have used different type and amount of plasticizers and investigated their effects on water absorption, mechanical properties etc. The flame-retardant properties of PLA foams have been improved up to 28.4% by using starch as a natural charring agent [81]. Some researchers have investigated the non-isothermal melt crystallization behavior of the PLA foams in the recent past.

Dlouhá et al. (2014) investigated cellulose nanofiber/poly (lactic acid) microcellular foams. Their investigation was limited to the mechanical and morphological aspects of the composite foams. One of the interesting observation of their research was the effect of acetylation on cellulose nanofiber in the ultimate tensile properties. Increments in strain at break up to 32 times for foam (containing 3% nanofiller) was reported by them. They also demonstrated the effect of cellulose nanofiber on the specific modulus and specific strength with a comparison to their effect in solid counterparts [82].

Youn Cho et al. (2013) investigated the effect of cellulose nanofibers on poly (lactic acid) foaming. Their research was mainly focused on the physical and morphological aspects of the fabricated foams. They used supercritical carbon dioxide as a physical blowing agent. They

had prepared the nanofibers utilization sonication technique. The decrease in cell size and increase in cell density was also reported by them with the incorporation of cellulose nanofibers. One of the interesting aspects of the research was the relating the observation with viscosity. They have noticed that initially, CNF acted as nucleating agent at low concentrations but at higher concentrations, it physically hinders the chain mobility of PLA. Dynamic rheological studies showed that the PLA/CNF nanocomposites had a higher viscosity than pure PLA. They have demonstrated that the observed foam density of neat PLA was higher than that of the nanocomposites with 1 and 3 wt% of CNFs owing to its weak melt strength to resist the cell expansion [22].

Xiaofei et al. (2015) investigated the method of producing lightweight microcellular injection molded parts with improved ductility and toughness. They used microcellular injection molding. They used nitrogen gas as a physical blowing agent. They used different types of polymeric blends like PP, HDPE, LDPE, PLA, and PHBV at different ratios and studied their mechanical properties like tensile strength, Young's modulus, strain at break etc. for both the foamed and unfoamed counterparts. They have demonstrated that 75/25 PP/HDPE foamed blend showed promising improvement in ductility and toughness as compared to the solid counterpart. It was also observed that PLA typically fails in a brittle manner before plastic deformation occurs [83]

Song et al. (2015) highlighted the designing aspects of biocompatible shape memory polymer (SMP) blend foams. They make biocompatible shape memory polymer (SMP) blend foams composed of thermoplastic polyurethane (TPU) and polylactic acid (PLA). These blends were fabricated by melt blending the TPU and PLA pellets with a twin-screw micro compounder. They used CO_2 as a physical blowing agent in a batch foaming process. They used 50 ºC as the foaming temperature. They investigated the thermal properties of TPU/PLA blends by DSC and found that a significant decrease of the cold crystallization temperatures in the 50/50 and

65/35 TPU/PLA blends compared to neat PLA. They studied mainly the effect of polymer blending (the composition of TPU and PLA) on the porous morphology of TPU/PLA blends. They made three blends of 80/20, 65/35 and 50/50 TPU/PLA. It was found that all the TPU/PLA blends and neat TPU formed close-celled porous structures each containing pores significantly different in size and shape [84].

Di et al. (2005) studied the properties and foam processing of reactively modified PLA. They had utilized the sequential addition of chain extenders (1,4-butanediol and 1,4-butane diisocyanate) to modify poly(lactic acid) for applications, where high melt viscosity and elasticity is prerequisite condition. The thermal and mechanical properties of fabricated foams were compared with the unmodified PLA. In the foaming process, they used the mixture of compressed CO_2 and N_2 (20/80) as a physical blowing agent. Crosslinking increases the T_g of the polymer by introducing restrictions in chain mobility. They concluded that higher viscosity and elasticity for the chain extended/cross-linked resins allowed the production of PLA foams with smaller cell size, higher cell density, and lower foam density compared to neat PLA [85].

Lee et al. (2008) studied the preparation and characterization of tapioca starch-PLA nanocomposite foams. They used the melt intercalation technique. They used four different types of organoclays Cloisite 10A, Cloisite 25A, Cloisite 93A, and Cloisite 15A to produce nanocomposite foams. It was found that Young's modulus (E) of the foams were significantly affected ($p < 0.05$) by type of organoclay. They noticed that the largest increase in E (96%) was obtained from TS/PLA/10A nanocomposite foam as compared to the TS/PLA foam [35].

Lee et al. (2008) studied the preparation and characterization of tapioca starch/poly(lactic acid)/cloisite Na^+ nanocomposite foams. They used the melt intercalation method. They prepared tapioca starch, PLA, and Cloisite Na^+ nanocomposite foams, with different clay contents and their various properties were characterized. It was observed that nanoclay was

intercalated to a lesser extent as clay contents increased. The effect of nanoclays in PLA foam was mainly observed in cell size reduction, increase in cell density and in bulk compressibility [86].

Hwang et al. (2009) investigated the effect of montmorillonite (MMT) content on the mechanical and thermal properties of microcellular injection molded polylactide/clay nanocomposites. They used CO_2 as a physical blowing agent. They prepared the nanocomposite by a twin-screw extruder. It was found that the MMT increases the decomposition temperature and decreases the crystallization temperature. It was also found that the layer spacing of clay was also increased as the increase of clay content. They have observed that PLA/1% organoclay has the highest tensile strength. It is observed that polymer with lesser cell size has low weight residue which increases the tensile strength [87].

Zhai et al. (2009) studied the crystallization, melting, and foaming behaviors of linear polylactic acid in compressed CO_2. It was found that CO_2 exposure significantly increased PLA's crystallization rate. The investigation suggested that crystallinity, foaming window, and cell morphology affects the foaming time due to the crystallization equilibrium of PLA. It is also concluded that strain-induced crystallization has slightly effect on the final crystallinity of the PLA [5].

Ji et al. (2013) investigated the tensile properties of microcellular poly (lactic acid) foams. They had utilized compressed CO_2 for foaming. They also studied the influences of crystallinity, foam density and cell morphology on the tensile properties of PLA foams. The decrease in tensile property was observed for foamed PLA compared to unfoamed counterpart due to volume expansion. The elongation at break of PLA samples was increased to ~15 times. The microcellular foaming of PLA foams increased its specific tensile strength to to ~53%. They have noticed that crystallinity and relative foam density affects the specific tensile

strength and elongation at break. It was also noticed that the presence of open cellular structure tended to decrease the tensile properties of PLA foams due to the breakage of the cell wall [88].

Taki et al. (2011) investigated the effect of growing crystalline phase on bubble nucleation in PLA/CO_2 batch foaming. They found that the number of bubbles increased as a function of the spherulites area (χ_c). The experimental results indicated that increase in χ_c resulted in an increase in the number of bubbles that were present [89].

Zhou et al. (2011) utilized solid-state foaming process for immiscible polymer blends to fabricate tissue engineering scaffolds. They have made polylactic acid (PLA) and polystyrene (PS) blends and then created an interconnected porous structure by first foaming the PLA/PS blend and then extracting the PS phase. The increase in the pore size and porosity was observed after the PS extraction process. They also investigate the cell culture in the fabricated porous structure. It was found that the cells grew well and a fibrous structure was formed. They achieved a very wide range of pore size. PS phase extraction ensured the interpore connectivity of the cells [37].

Liang et al. (2014) fabricated tissue engineering scaffolds with immiscible polymer blends by a solvent-free method. Immiscible polymer blends of PLA and sucrose were obtained using twin-screw extrusion and foamed using the solid-state foaming process. They had achieved PLA scaffolds with above 90% porosity and 25–200 μm pore size. The co-continuous structure of PLA and sucrose was obtained at the 35/65 weight ration. It was reported that pore size and porosity can be controlled with process parameters like extrusion temperature. By adjusting the sucrose particle size and extrusion temperature, large pores can be controlled. They concluded that by controlling the foaming parameters the small pores can be achieved [79].

Tang et al. (2011) prepared expanded polypropylene/ PLA blend bead foams with an autoclave batch foaming process. They used n-pentane as the physical blowing agent. They reported that

parameters like pressure, solubility could control the cellular morphology and expansion of the bead foam. They used nitrogen (N_2) into the autoclave to build up high-pressure drop rate. They observed that n-pentane was highly soluble in polymer due to its plasticizing effects and reduced the foaming temperature. [90].

Ameli et al. (2014) developed high void fraction polylactide composite foams by an injection molding technique. They mainly studied the crystallization and foaming behavior. They used talc at various concentrations. They utilized nitrogen as the physical blowing agent. They had prepared the PLA composite foams by using regular foam injection molding (RFIM) and foam injection molding with mold opening (FIM+MO) techniques. They observed that the combined effects of nanofiller affected the PLA foams morphology to more uniform and finer cell structure (cell size < 50 μm). They found that the PLA's crystallization kinetics were affected by parameters like the foaming action, the presence of talc/nanoclay, the pressurized N_2 and the mold opening stage [91].

Wang et al. (2012) developed a continuous process poly (lactic acid) foams with precise cellular morphology. They utilized CO_2 as the physical blowing agent. They systematically investigated the extrusion foaming behaviors of linear and branched PLAs. They had prepared successfully the foams with a low density, closed-cell microcellular structure, and controllable crystallinity by using branched PLA using a tandem system. They observed that molecular branching increases melt strength and elasticity, and finally it increased the integrity of cells, cell density, and expansion ratio during low- density foaming. One of the major findings of their study suggested that the surface property of PLA foams can be controlled by varying the crystallinity [92].

Frerich et al. (2015) investigated the thermodynamics, foaming behavior and mechanical characteristics of biopolymer foaming with supercritical CO_2 (sc-CO_2). They used direct

foaming of poly(lactide) (PLA), poly (butylene succinate) (PBS) and a blend of poly(lactide) and poly (hydroxybutyrate) (PLA-PHB), under compressed CO_2. They also studied the influence of saturation temperature and applied pressure on the resulting foamed material. They mainly studied the thermal behavior of the foamed sample in the presence of CO_2. They demonstrated that PLA-PHB blend showed a lower value of porosity and the highest values of the compressive modulus. They recommended both PLA and PLA-PHB blend for further examination even under higher pressures [93].

Matuana et al. (2009) utilized endothermic chemical foaming agent for foaming of PLA by melt extrusion process. They investigated the polymer melt flow index, CFA content, the processing speed of cellular structure, void fraction and a cell population density of foamed PLA. They found that void fraction was strongly dependent on polymer melt flow index. The processing speed has also an effect on the morphology of polymeric foams. They concluded that if we properly combined the parameters like polymer melt flow index, CFA content, and processing speed then we can achieve a homogeneous and finer cellular morphology [32].

Makoto et al. (2008) fabricated porous 3D structure from poly (L-lactide) based nanocomposites foams. They also studied the enzymatic degradation. The enzymatic degradation of the resultant nanocomposite foam having different cell density was investigated by them. They used using proteinase-K as a degrading agent. It was observed that the linear degradation rate of nanocellular foam was about two times higher than that of microcellular foam. They have noticed that the enzymatic degradation of foam enhances due to the large surface area available inside the foam structure. The nanocellular foam can take a large amount of water compared with that of microcellular counterparts, which enhances foam swelling and thus assists the enzymatic degradation [94].

Richards et al. (2008) investigated the biodegradable PLA foams using PLA and PHBV by using subcritical CO_2 as a physical blowing agent. They studied mainly the morphology and the thermal properties of the foams. It was found that the PLA and PHBV form an immiscible blend and there is only a physical dispersion of one component to the other. Further, they had prepared cell sizes in the range of 20–1,500 μm and 3–14 μm for PLA and 75/25 PLA/PHBV blend [95].

Preechawong et al. (2005) prepared the starch/poly (L-lactic acid) hybrid foams and investigated their various characteristics. They studied mainly the effects of relative humidity, storage time, PLA content, and type and content of added plasticizer (e.g. glycerol, urea, or ammonium chloride) on moisture and water absorption, mechanical properties, and enzymatic degradability of the prepared foams. They prepared the hybrid foams by baking a mixture of starch, PLA, and other ingredients in a hot mold. They used compression molding technique to prepare the foams and the maximum expansion ratio they acheived was 6 [8].

Hao et al. (2008) studied the different effects on the foaming process of biodegradable PLA/starch composites in compressed/ sc-CO_2. Their main objective was to find the various potential applications of the prepared foam in biomedical applications and as a drug container. They had performed sorption/desorption experiments. They used batch foaming technique for the preparation of foams. They observed that foaming treatment with sc-CO_2 increased the crystallinity of PLA/starch composite. They also reported that the longer is the saturation time, larger is the cell produced and lower is the bulk foam density. They got maximum expansion ratio as 13 and average minimum cell size as 5μm [96].

Mihai et al. (2007) investigated the foaming of PLA and PLA/starch blends by using CO_2 as a blowing agent. They utilized the extrusion foaming process. From this study, we came to know that CO_2 is highly soluble blowing agent for PLA. They got the maximum expansion

ratio as 50 and minimum average cell size as 25μm. They observed a significant increase of crystallization rate associated with CO_2 foaming. For the foaming process, they had observed that crystallinity was mainly affected by chain mobility compared to nucleating sites [19].

Zhang et al. (2007) studied the cellular size distribution, cellular structure and water resistance of biodegradable foams of PLA/starch. They used water as a blowing agent and talc as a nucleating agent. They had utilized extrusion foaming technology. They produced foams with relatively fine cellular size and uniform cellular size distribution under optimized condition of PLA/starch ratio. They found that water was a good blowing agent for PLA/starch systems. They observed maximum expansion ratio as 55 and minimum average cell size as 500 μm. The presence of PLA significantly improved the water resistance of foam in high moisture conditions [97,98].

Yuan et al. (2009) studied the PLA/poly(butylene adipate-co-butylene terephthalate) blend foaming. They used nano silica particles, which helped in the formation of nucleating sites. The maximum expansion ratio was found as 3.2 whereas the minimum average cell size was observed between 10-20μm. They used maleic anhydride (MAH) and 2,5- dimethyl-2,5-di-(tertbutylperoxy)hexane (L101) as an additive to improve the compatibility of PLA with PBAT. They found that the addition of PBAT significantly increased the elasticity and viscosity of blends. They found that cells can grow in a much bigger form if we increase the amount of MAH content. The physical and mechanical properties of the PLA/PBAT composite foams were improved by maleicing reaction [99].

Pilla et al. (2010) investigated the poly(lactide)/ poly (butylene adipate-co-terephthalate) blend foaming utilizing the extrusion process. They had utilized CO_2 as a blowing agent. They used talc to enhance the heterogeneous nucleation. They investigated mainly the effects of different processing parameters on foaming. It was found that the addition of talc has decreased the

average cell size, VER and it improves the cell density along with crystallinity. They had reported the maximum expansion ratio as 1.8 and the minimum average cell size as 10μm [100].

Zhao et al. (2013) investigated the foam processing of PLA/ polyhydroxybutyrate-valerate (PLA/PHBV) blend. They used N_2 in supercritical state as a PBA. They found the minimum average cell size as 25μm. They also noticed the decrease in cell size and increase in cell density with PHBV content in the foamed samples. They observed that at low concentrations of PHBV significantly increases the strain-at-break for both solid PLA/PHBV (85:15) and microcellular PLA/PHBV (70:30) respectively [12].

Pilla et al. (2009) studied the microcellular and solid poly lactide-flex fiber composites. They used silane as a coupling agent. They used an injection molding technique. They found that the degree of crystallinity increased with increase of fiber content. It was found that silane did not have any effect on cell morphology. They have noticed that the degree of crystallinity increased with the fiber content while silane treatment has no effect on it. Interestingly, In microcellular samples, the fiber content and silane treatment have not shown any effect on toughness and strain at break. It was also observed that the glass transition temperature was not affected by fiber content and the silane treatment [101].

Fabrication of PLA/silk composite foam was reported by **Kang et al. (2009)** using sc-CO_2. They had obtained a well-controlled porous structure. They used silk fibroin power with different concentrations to make biodegradable PLA composite by solution processing technique. They had utilized CH_2Cl_2 as a solvent. They used batch foaming technique for preparation of foams. In this investigation, they found that at higher silk content, the composite foam exhibited a reduction in cell size and an increase in cell density compared with PLA foam.

They also noticed that saturation temperature and pressure affected the cellular morphology of the PLA/silk foams. They had achieved the minimum average cell size of 15μm [75].

Fujimoto et al. (2003) prepared a well-controlled biodegradable nanocomposite foam. They prepared PLA/ layered silicate nanocomposite. They utilized sc-CO_2 as a foaming agent. They used batch foaming technology to prepare the foams. They claimed that it was the first report that deals with the possibility of preparing biodegradable nanocellular polymeric foams via nanocomposite technology. They suggested that dispersed silicate particles acted as nucleating sites for cell formation. They achieved a maximum expansion ratio of 2.7 and minimum average cell size of 360 nm [102].

Di et al. (2005) studied the thermal, rheological properties and foam processing of poly(lactic acid)/organoclay nanocomposites. They had used a batch foaming process and a mixture of CO_2 and N_2 was used as a foaming agent. They got the maximum expansion ratio as 13.5 and the minimum average cell size as 25μm. They also observed that as we increase the organoclay content, the cell size was decreased and both cell density and foam density were increased [103].

Ema et al. (2006) studied the foam processing polylactide-based nanocomposites. They had utilized an autoclave for foaming and utilized the batch foaming technique. They used sc-CO_2 as a foaming agent. They reported the processing of PLA and PLA nanocomposites. They got the maximum expansion ratio 5 and minimum average cell size as 200 nm. The nucleating effects of nanoclay and its effects in cell growth and formation was also reported in the investigation. They observed that PLA nanocomposite foams were having high cell density compared to neat counterpart [104].

Pilla et al. (2010) investigated the foam processing of polylactide/hyperbranched polyester/nanoclay composites. They also reported the effects of nanoclay and hyperbranched

polyester on cellular morphology fabricated by both conventional and injection molding process respectively. They used N_2 as a physical blowing agent. They had achieved maximum expansion ratio as 1.2 and minimum average cell size as 10μm. They concluded that the addition of hyperbranched polyester and nanoclay decreases the cell size and increases the cell density. They observed that the reduction in strength was almost similar for microcellular specimens and solid specimens [74].

Matuana et al. (2010) studied the cell nucleation of microcellular poly (lactic acid) foamed. They utilized sc-CO_2 as a physical blowing agent. They utilized the continuous extrusion foaming process. Their main motive of this work was to understand the nucleation mechanism of foaming. They observed that temperature effects the cell nucleation rate for PLA. The addition of nanoclay allowed both heterogeneous and homogeneous nucleation to occur during foaming. They had achieved a minimum average cell size of 6.9 μm. They finally concluded that the processing temperature has an important effect on the rheology and cell nucleation rate of the melt [105].

The effect of surface modified nanoclay on PLA foam processing was investigated by **Tsimpliaraki et al. (2011)** They had used organically modified montmorillonite clay for preparation of nanocomposites. They had utilized supercritical CO_2 as a PBA. The loading of OMMT leading to heterogeneous cell nucleation and also it reduced the cell size and increased the cell density. They had observed that if the clay loading was used more (the longer the alkylammonium surfactant) and higher the modification level of the clay, then the pores of small diameter would form and larger pore densities could be obtained. They observed that supercritical CO_2 also acted as a clay dispersion medium. They achieved a maximum expansion ratio of 6.2 and minimum average cell size of 6μm [73].

Dlouha et al. (2012) investigated the role of CNF in supercritical foaming of PLA and their effect on the foam morphology. It was observed that the CNFs effects the surface morphology of PLA foams. They concluded that parameters like amount of CNFs and surface acetylation affected the cell size and cell density. The result indicated the importance of the shear thinning behavior in the foaming process [106].

Hopmann et al. (2015) studied the foaming technology using gas counter pressure to improve the flexibility of foams. They utilized high amounts of CO_2 as a blowing agent. They observed that if a defined pressure reduction inside the mold, the foaming process can be controlled. They studied on polyurethane foams. A gas counterpressure inside the mold cavity enables the precise control of the physical foaming process. Using this new foaming technology, a density of 116 kg/m^3 was achieved for rigid foams. In the case of flexible foams, density was reduced [107].

The utilization of silk cocoons in synthetic polyurethane foam was demonstrated by **Shah et al. (2015)** They observed that natural silkworm cocoons had the potential to be used as a volume occupying filler in the polymer matrix. They reported that the ultimate properties of cocoon based foams were comparable with volume occupying reinforcements like cork in rigid, low density polymeric foams [108].

Huang et al. (2014) studied the crystallization behavior of porous PLA. They used modified solvent casting and particulate leaching technique for preparation of tissue engineering scaffolds. They obtained pore size of around 250 μm. They used NaCl as porogens. They inserted a step of thermal treatment to recrystallize the polymer matrix before leaching process. They observed that linear cooling is sufficient to achieve certain crystallinity and macro-structure [109]

Jia et al. (2015) investigated the cell morphology and improved heat resistance of microcellular Poly (L-lactide) foam. They introduced stereocomplex crystallites of PLA in the matrix. They utilized stereocomplex crystallites (SC) having improved melting point and heat stability in the PLLA foam matrix. They utilized the melt blending technique for making PLLA and poly (D-lactic acid) (PDLA) composites. They used CO_2 as a physical blowing agent. They reported that heat resistance had improved for PLLA/PDLA foams compared to PLLA foam. The incorporation of SC improved the properties like melting point, heat resistance and cell nucleation ability in the PLLA/PDLA foams [110].

Ludwiczak et al. (2015) studied the foaming of polylactide in the presence of chain extender (CE). The effect of CE on crystallinity and viscosity were investigated. The chain extender utilized was Joncryl 4368. They observed that CE has a significant impact on the foaming process of PLA during the extrusion. They reported that CE affected the crystallization temperature, melt viscosity of the foam. However, reduction in crystallinity and barrier properties was observed by them. They concluded that finest cellular structure (pore size of about 20–50 μm) of PLA can be achieved in the addition of CE (1.0 and 1.5 %). CE also influenced in the density (0.7 g/dm^3) and thermal conductivity (0.1 W/mK) of the foam [111].

Kuang et al. (2015) fabricated poly(lactic acid)/graphene oxide (GO) foams using sc-CO_2. They used solid-state batch foaming process to obtain highly oriented and elongated cell structures. They reported that GO influenced the rheological properties of the PLA/GO nanocomposite foams. The CO_2 absorption of the foams was also improved by the incorporation of GO in the matrix. The increased expansion ratio and d average cell size was observed during the foaming process of PLA/GO nanocomposite [76].

Zhou et al. (2015) studied the crystallization, rheology and foam morphology of branched PLA. They used a novel type of CE. CE utilized was a random copolymer of

polystyrene/poly(glycidyl methacrylate). PLA was branched through melt compounding. They observed that comparing to the neat PLA, the new branched products significantly improved complex viscosity as well as elongational viscosity [112].

Goswami et al. (2013) studied the processing of poly (lactic acid) based composites for medical purposes. They investigated three-components systems such as poly(lactic acid) (PLA), poly(ϵ-caprolactone) (PCL) and wollastonite (W) for possible bio medical applications. They used batch foaming technique using compressed CO_2. They observed that presence of the filler generates heterogeneous nucleation sites in the matrix, which ultimately improves the foamability and producing uniform microcells [113].

Wang et al. (2014) improved the flame-retardant properties of PLA foams using starch as a natural charring agent. They had used microcellular foaming technology with compressed CO_2 as the blowing agent. They had used phosphorus-containing flame retardant (FR) with decomposition temperature higher than 260 °C. They observed a significant improvement in limiting oxygen index (LOI) of PLA foams from 18.2% to 24.8−28.4% at incorporation of 15−25 wt % FR in the matrix. The expansion of PLA foam was also increased from 4.4 to 7.5−16.0. They also reported that LOI could be increased up to 30.6% with addition of starch at 1−5 wt% [81].

Mills et al. (2009) used a finite element micromechanics model to find the impact compression of closed-cell polymer foams [114].

Jun Jin et al. (2001) has fabricated biodegradable polymeric scaffolds by using gas foaming and salt leaching method and studied the hydrolytic behavior. They had used a combination of two effervescent salts, ammonium bicarbonate, and citric acid. They noticed that by adjusting the reaction between the two salts, the porosity and mechanical properties could be controlled. They demonstrated that degradation behaviors of three PLGA scaffolds with different

compositions exhibit significant dimensional changes during degradation depending on their degradation rates [115].

Liao et al. (2002) has fabricated biodegradable polymeric scaffolds by utilizing C/L technique. They fabricated a solvent merging/particulate leaching method for preparing 3D porous scaffolds. They observed that ratio and particle size of porogens effects the porosity and the pore size of the scaffold [116].

Lizundia et al. (2017) investigated the tunable hydrolytic degradation of poly(L-lactide) scaffolds triggered by ZnO nanoparticles. They have successfully fabricated the porous PLLA and PLA/ZnO scaffolds with porosity ranging from 10-90% and average pore diameter of 125-250 µm. They had utilized the solvent casting/particulate leaching technique to produce the foam. They have observed that the addition of ZnO nanoparticles into PLLA matrix accelerates the hydrolytic degradation kinetics of scaffolds [117].

Ikada et al. (1997) investigated the photodegradation behavior of aliphatic polyesters. From the investigation, they have concluded that the photodegradation of PLA follows the Norish II type of photocleavage [118].

Schliecker et al. (2003) investigated the effect of oligomers on degradation rate and crystallinity of hydrolytic degradation of poly(lactide-co-glycolide) films. They have observed that With increasing oligomer concentration the glass transition temperature (T_g) and the molecular weight of films decreased prior to erosion. They thoroughly investigated the role of oligomers on the degradation process. They also studied the influence of the average molecular weight and the concentration of d,l-lactic acid oligomers added on the degradation rate and crystallinity of PLGA 50:50 film [119].

Elsawy et al. (2017) investigated the hydrolytic degradation of PLA and its composites. They had observed that the degradation of the PLA polymer matrix is restricted to its surface if the temperature remains below the T_g value [120].

From the above literature, it is observed that researchers are developing new technologies to tune the properties of the existing PLA foams. Different types of additives are used to get the desired properties. Nanotechnology is becoming one of the vibrating sectors in biodegradable foaming.

1.6 Knowledge gaps in the existing literature

From the literature study, we observed that the fabrication of biodegradable PLA foam is a vibrant area of current research studies in the world. It is because of

a) Biocompatible, non-toxic and degradable in nature,

b) Competitive material and processing costs, that of non-degradable foams,

c) Comparable mechanical properties to that of petroleum-based foams,

d) Various properties can be tuned by using additives.

PLA has the potential to replace the non-degradable PS and PU foams in near future. From the literature, it is observed that various researchers utilized nanofillers to tune different properties of PLA foams. The nanofillers acts as a nucleating site in the polymer matrix.

However, a lot needs to be done in this area. Based on the prior art as discussed in earlier sections, it is observed that no investigation (as per best of our knowledge of concern) has been demonstrated on the use of different nanobiofillers like CNC, SNC, modified gum arabic, and modified chitosan in PLA-foam matrix. The study of their effects on the ultimate properties

of foam has not been extensively done yet. The crystallization behavior of the nanobiofillers in PLA matrix needs to be performed extensively with different established methods. The effect of these nanobiofillers in different degradation techniques like thermal, hydrolytic and photodegradation (UV) needs to be investigated for different fields of applicability of the PLA-based foams. The degradation mechanism of the PLA-based foams needs to be thoroughly investigated with the help of established models. Further, the effect of nanobiofillers on important foam properties like cell size and cell density needs to be analyzed thoroughly. On the other hand, focus and modifications need to be done in some less expensive and easy techniques like casting and leaching (C/L). The selection of porogens in C/L technique needs to be carried out in a perfect and in an economical way.

1.7 Hypothesis and motivation

The fabrication of completely bio-based and biodegradable polymer foam is growing interest in worldwide due to its environmental friendliness. The improvements in PLA foams by utilizing natural resources and bio-derived nanobiofillers (as cellulose, chitosan, gum, and silk are abundantly available in nature) has the potential to meet the required environmental and bio safety protocols with required properties for different sophisticated biomedical and other applications.

The main aim of this doctoral research is to fabricate PLA and PLA/bionanofillers based open cellular, hydrophobic, interconnected and highly porous foam structure. The required improvements in properties can be achieved by the addition of bionanofillers. The fabrication of PLA-based foams will be performed by utilizing less expensive and easy techniques like casting and leaching (C/L) with easily available and cost effective porogen like sugar which can easily be leached out by water. The batch process of foaming will help to maintain the foaming parameters constant in different systems of PLA/CNC, PLA/chitosan, PLA/gum

arabic, and PLA/SNC. The formulations by C/L technique will also help in the cost-effectiveness of the fabrication process.

1.8 Objective of the current research

To achieve the above-discussed knowledge gaps in PLA-based foams, the preliminary doctoral research has to be conducted towards the following directions.

a) Fabrication and characterization of biodegradable PLA/CNC, PLA/chitosan, PLA/gum arabic and PLA/silk-based foams.

b) Different degradation investigations (hydrolytic, UV and thermal) in the mechanistic approach of the fabricated foams.

c) Comparative studies of properties.

d) Porosimetric investigations of the fabricated foams.

1.9 Orientation of the doctoral thesis

The current doctoral thesis provides in-depth analysis and fundamental research of PLA/CNC, PLA/ chitosan, PLA/ gum arabic and PLA/SNC-based foams. The method of fabrication of foams and detailed investigations will be described systematically in the following chapters and schematic representation is presented.

Chapter 1: Introduction and Literature Review.

In this chapter, a brief introduction of the development of polymer foams and different techniques of foam fabrication has been discussed along with a comprehensive study of prior arts in the related fields to find out the knowledge gap in the current research. The objectives of the doctoral research are formulated from the gaps of the prior arts.

Chapter 2: Materials and Methods.

In this chapter, different materials used in this research and fabrication process along with different analytical methods are thoroughly discussed.

Chapter 3: Fabrication and Characterization of poly (lactic acid) and cellulose nanocrystals (CNC) based microcellular composite foams.

This chapter mainly focuses on the fabrication of development of PLA/CNC-based foams by using casting and leaching (C/L) technique. Different foam related investigations like mechanical, wettability, physicochemical, porosimetric properties and thermal properties have been discussed thoroughly in this chapter. Crystallization kinetics and thermal degradation behavior of the fabricated PLA/CNC-based foams are discussed in this chapter. This chapter gives a deep insight into the developed PLA/CNC-based foams for their probable applications.

Chapter 4: Poly (lactic acid)/Modified Chitosan (MC) based Nanocomposite Foams: Non-isothermal Crystallization and Thermal Degradation Kinetics with Wettability and Porosimetric Investigations.

This chapter mainly deals with the development of PLA/modified chitosan (MC) based microcellular foams. The structure-property relationship of the developed foams has been addressed in this chapter. The crystallization kinetics behavior and thermal degradation kinetics of the fabricated PLA/MC-based foams have been discussed in this chapter along with porosimetric investigations.

Chapter 5: Prospects of Poly (lactic acid)/Modified Gum Arabic (MG) based Microcellular Composite Foams.

This chapter is mainly focuses on the development of PLA/modified gum arabic (MG) based foams. The different physicochemical characterizations along with wettability and

crystallization studies of the developed foam have been discussed in this chapter. The non-isothermal crystallization kinetics of the developed foams along with different degradation studies like hydrolytic, photodegradation and thermal degradation have also been thoroughly discussed in this chapter.

Chapter 6: Development of Silk-based Poly (lactic acid) Microcellular Composite Foams.

This chapter mainly deals with the fabrication and characterization of PLA/silk nanocrystal (SNC) based foams. The structure-property relationship of the developed foams has discussed in this chapter. Thermal stability along with crystallization behavior and different degradation (photodegradation and hydrolytic) behavior of the fabricated PLA/SNC-based foams are discussed thoroughly in this chapter. This chapter provides useful and through insight into the PLA/SNC-based foamed structure.

Chapter 7: Conclusions and Future Prospects.

This chapter delivers concluding remarks based on doctoral research work. A brief comparison of fabricated PLA/nanobiofillers-based foams in the current research has been discussed along with useful information regarding the future scope and directions of the current research work.

Chapter 2

Materials and Methods

This chapter deals with materials used in the current doctoral research and different methods of fabrication for the PLA and PLA/nanobiofiller based foams. The selection procedure of the porogen particles along with the pre-treatment of porogen are discussed in this chapter. The modified casting and leaching technique (C/L) is discussed in details with schematic representations. It also contains brief information about the preparation of cellulose nanocrystals (CNC), modified chitosan (MC), modified gum arabic (MG) and silk nanocrystals (SNC) used in this research. The detailed fabrication process of PLA and PLA/CNC, PLA/MC, PLA/MG and PLA/SNC-based foams are also reported in this chapter. This chapter also includes the brief description of different analytical instruments and their experimental procedures utilized for analysis of the fabricated foams.

2.1 Materials

Poly (L-lactic acid) (PLA) 2003D grade (granules form, L-lactic acid: 98.6%, D-lactic acid: 1.4%, density: 1.24 gcm^{-3}; number average molecular weight (M_n): ~150000 Da; weight average molecular weight (M_w): ~200000 Da; melt flow index (MFI): 0.73 g min^{-1} at 210ºC) used in the research was procured from NatureWorks® LLC, USA. The sugar cubes were purchased from Dourala Pvt. Ltd. (India). The 1, 4 dioxane used as a solvent in the research, was supplied by Loba Chemie Pvt. Ltd. For preparation of CNC, we have used chemicals like sodium hydroxide (NaOH), sodium hypochlorite (NaOCl), sulphuric acid (H_2SO_4), hydrogen peroxide (30% (wt/v) H_2O_2), acetone and chloroform (analytical grade) which were purchased from Sisco Research Laboratories (SRL Chemicals, India). Chitosan (commercial grade with medium molecular weight and degree of deacetylation (DD)>70%), L-lactic acid with 20% assay and acetic acid were purchased from Sigma-Aldrich, India. HPLC grade chloroform was supplied by Merck (India). Millipore water (Metrohm, ELIX 3) was used for the wettability investigations. Biopolymer gum arabic (GA), was supplied by Sigma-Aldrich, India. Muga silk (Antheraea assama) was supplied by Regional Muga Research Station (RMRS), Boko, Assam, India, which was utilized for fabrication of silk nanocrystals (SNC). Sodium carbonate (>97%) (analytical grade) supplied by Merck, India was used for degumming of silk. Sulphuric acid (>99%) was utilized as a hydrolyzing agent for SNC preparation was supplied by Sisco Research Laboratories (SRL Chemicals, India). Nitrogen cylinders used for creating inert atmosphere, were supplied by Jainex Pvt. Ltd., Assam, India. All chemicals were used as purchased without any purification or treatment.

2.2 Methods

This section of this chapter mainly discuss about the different methods utilized for the fabrication of nanobiofillers and PLA/nanobiofiller-based foams along with the pre-treatment procedure of the porogen.

2.2.1 Synthesis of nanobiofillers for PLA matrix

In the current research, four different nanobiofillers (cellulose nanocrystals, chitosan, gum arabic, and silk nanocrystals) were prepared to investigate the effect on various properties of PLA foam. Since, chitosan and gum arabic is hydrophillic in nature, so surface modifications needs to be carried out to make it compatible in hydrophobic PLA-based systems. Silk nanocrystals (SNC) were extracted from Muga silk, which is abundantly available in the northeastern state of India, Assam. All these nanobiofillers were lab developed and their detailed investigations have been demonstrated elsewhere [63,121–123].

2.2.1.1 Preparation of cellulose nanocrystals (CNC)

CNCs were fabricated through acid hydrolysis from the purified cellulose extracted from the bamboo pulp through a pre-treatment method using sulphuric acid as a hydrolyzing agent. In brief, pretreatment of cellulose pulp was carried out with soda pulping method with 2 wt % NaOH at 85 °C for 2 h, followed by bleaching with H_2O_2 (2 wt %) and hypochlorite treatment with NaOCl (2 wt %) at 90 °C for 2 h respectively. The pulp was filtered out, washed with of Milli-Q at each step three times and further dried in an oven (at~80 °C), to remove the trace amount of chemicals. CNCs were fabricated by hydrolyzing the pretreated cellulose pulp (2 g) with sulphuric acid (64 wt%, 100 ml) under vigorous magnetic stirring for 2 h, at room temperature (~25 °C). After 2 h, the reaction was stopped instantly by adding equal volumes of the chilled deionized water. The CNC suspension was centrifuged (Remi, India) at 10000 rpm for 20 min and the precipitate was collected. It was thereafter transferred to cellulose

acetate dialysis membrane with cut-off molecular weight 12-14 kDa (Sigma Aldrich, India). Dialysis was carried out in a water bath until the pH of the CNC suspension reached at pH~7 [121]. Pictorial representation of the fabrication process can be observed in **Fig. 2.1**.

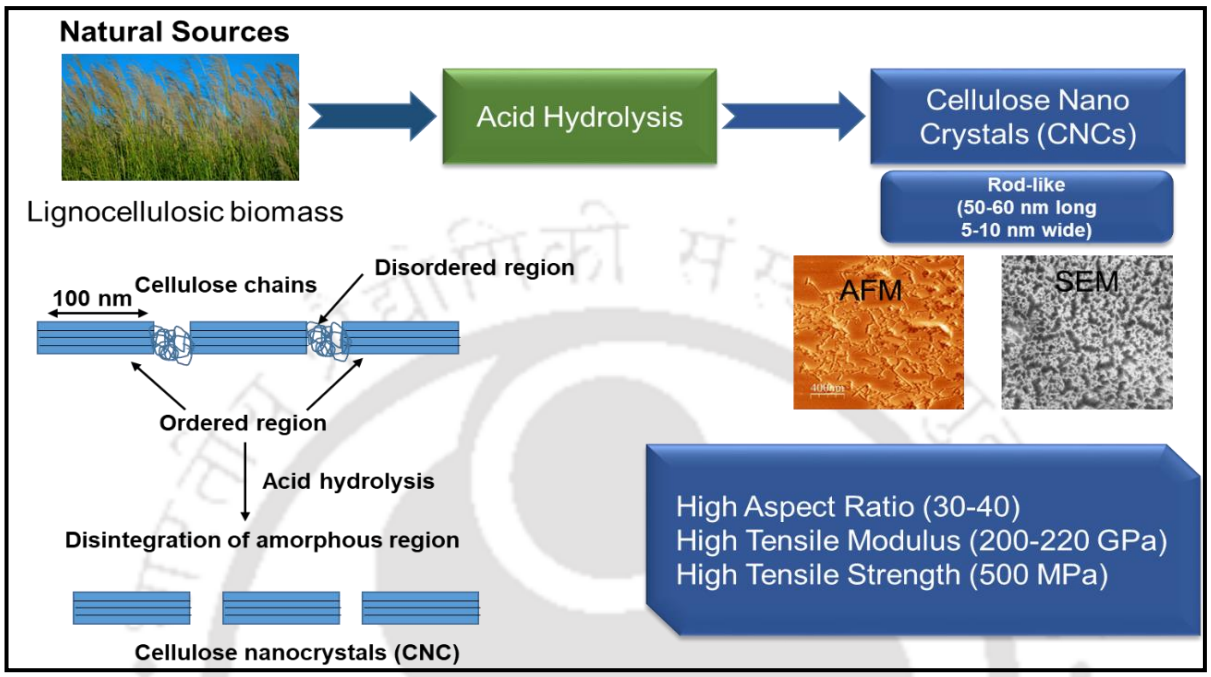

Fig. 2.1 Pictorial representation of fabrication of CNC.

2.2.1.2 Preparation of modified chitosan (chitosan -*g*- oligo L-lactic acid) (MC)

Initially, chitosan and lactic acid (LA) were mixed in 1:3.33 (wt/wt %) in a round bottom flask and properly mixed. The inert atmosphere was maintained for the mixture. The addition of chitosan to the LA was performed under constant magnetic stirring (~400 rpm). The whole mixture was kept for 12 h in the round bottom flask at room temperature for complete soaking of LA. The setup was placed in a microwave under an inert nitrogen atmosphere for microwave assisted condensation polymerization. The temperature of the microwave was maintained at 110 °C for 30 min at 240 W. The microwave was set at "convection cum microwave" mode. A heating belt (maintained at ~100 °C) was utilized as a connector between the round bottom flask and the condenser to avoid condensation of unbound water and other by-products. A dark brown color product was obtained with high viscosity. LA was grafted on the chitosan

backbone. The M_w and M_n of the obtained product were calculated and was found as 1400 Da and 3000 Da respectively. Generally, PLA foam is brittle in nature, MC has been used to improve elongation and flexibility of PLA foams. Pristine chitosan is hydrophilic in nature and cannot be used with PLA (hydrophobic) due to the phase separation problems. So, chitosan has been modified to transform its hydrophilic nature into hydrophobic and subsequently, used as a filler in the PLA matrix [123].

2.2.1.3 Preparation of modified gum arabic (GA-graft-oligo L-lactic acid) (MG)

The modification of biopolymer GA was done in order to make it compatible with PLA for improved properties of formulated foams. The synthesis was done by taking LA: GA in the ratio of 5:1 (wt/wt%), which was mixed prior to synthesis in a round bottom flask. Microwave-assisted synthesis of MG was carried out at temperature 130 °C for 45 min at 240 W under convection cum microwave mode. To avoid any clogging of by-products formed, a temperature of 100 °C was maintained between the outlet of the round bottom flask and the condenser. The formulated MG were used as filler to the PLA for developing foams [122].

2.2.1.4 Preparation of silk nanocrystals (SNC)

Synthesis of silk nanocrystals (SNC) was carried out in two steps: degumming process (removal of sericin) and isolation of SNCs. The extraction process of fibroin from Muga silk cocoons was performed using the degumming process. In the degumming process, firstly sulphuric acid was utilized as a hydrolyzing agent. For the extraction process, 0.02 M Na_2CO_3 maintained at 98 °C for 30 min was utilized. The extracted degummed silk was filtered out and washed with Mili-Q water three times.

In the next step, ~5 g of this extracted degummed silk has been acid hydrolyzed with ~50 ml of sulphuric acid (64 wt%) under a combined atmosphere of mechanical stirring (Speed: ~500 rpm) and sonication (Temp: 45 °C, ~40 kHz). The process of SNC fabrication was then

followed by centrifuging at 10,000 rpm and the precipitate was dialyzed (Cellulose acetate membrane with cut-off molecular weight 12-14 kDa supplied by Sigma Aldrich) to obtain neutral medium. The process was followed by freeze-drying using a lyophilization setup (Scanlaf, Denmark) at ~-110 °C [124]. The schematic presentation of the SNC preparation is shown in **Fig. 2.2** below.

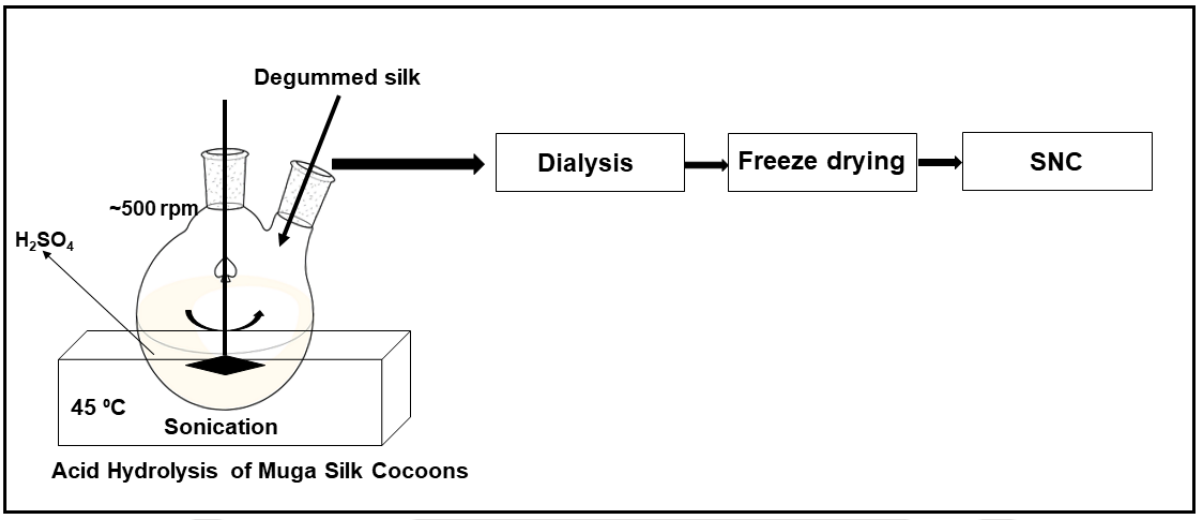

Fig. 2.2 Schematic representation of the preparation process of SNC.

2.2.2 Fabrication of PLA and PLA/nanobiofillers-based foams

In the current investigation, fabrication of PLA and PLA/bionanofiller-based foams were carried out by using less expensive and easy casting and leaching method (C/L method). The aim of this research is mainly to fabricate biodegradable PLA based foams for probable biomedical and other applications. C/L method is generally used for fabrication of foams for biomedical applications. In this study, the C/L technique of fabrication of foam is slightly modified then the conventional C/L technique for better dispersion of porogen in the polymer matrix.

Generally, in the C/L technique, the polymer solution was cast in a porogen bed followed by drying and leaching to remove the porogen particle. However, it has some disadvantages like the non-uniform dispersion of porogen in the polymer matrix and comparatively large size of

the porogen particles, which affected the ultimate foam properties. In view of this, to maintain proper dispersion of porogen in the PLA matrix and to decrease the size of the porogen particles in the current investigation modifications has been introduced in the conventional C/L technique.

The fabrication of PLA and PLA/nanobiofiller-based foams were carried out batch wise. Four different batches of fabrications of foams are as follows: PLA and PLA/CNC-based foam, PLA and PLA/MC-based foam, PLA and PLA/MG-based foam and PLA and PLA/SNC-based foam. Different parameters like temperature, amount of porogen, time of rotation has been changed according to the nanobiofiller batch and its prior arts available for incorporation in the PLA matrix. The protocols for the fabrication of PLA/CNC, PLA/MC, PLA/MG, and PLA/SNC are optimized by several trials and errors. The same protocol was used for fabricating foams consisting of PLA as well as nanobiofillers of the same batch. The protocols followed for the fabrication of different batches are discussed below.

2.2.2.1 Selection and pre-treatment of porogen particle

From the literature, it was observed that generally salts like NaCl are generally used as porogens for C/L technique of foam fabrication. However, it was observed that salts are not so easily leached by water and maintaining the size of porogen is difficult. In addition, it was observed that salt, as porogen, is not so suitable for flexible foam preparation by C/L technique. One of the easily available particles, which have the potential to be used as a porogen in C/L technique, is sugar. In the first phase of this research, to check the applicability of sugar as a porogen, we have utilized table sugar cubes directly in PLA solution followed by leaching. Sugar is easily available and less expensive material. The initial experiments indicated that sugar could be utilized as a porogen medium. However, to get better foam structure, size of the

porogen particles must be decreased. The schematic representation of the initial experiments is shown in **Fig. 2.3**.

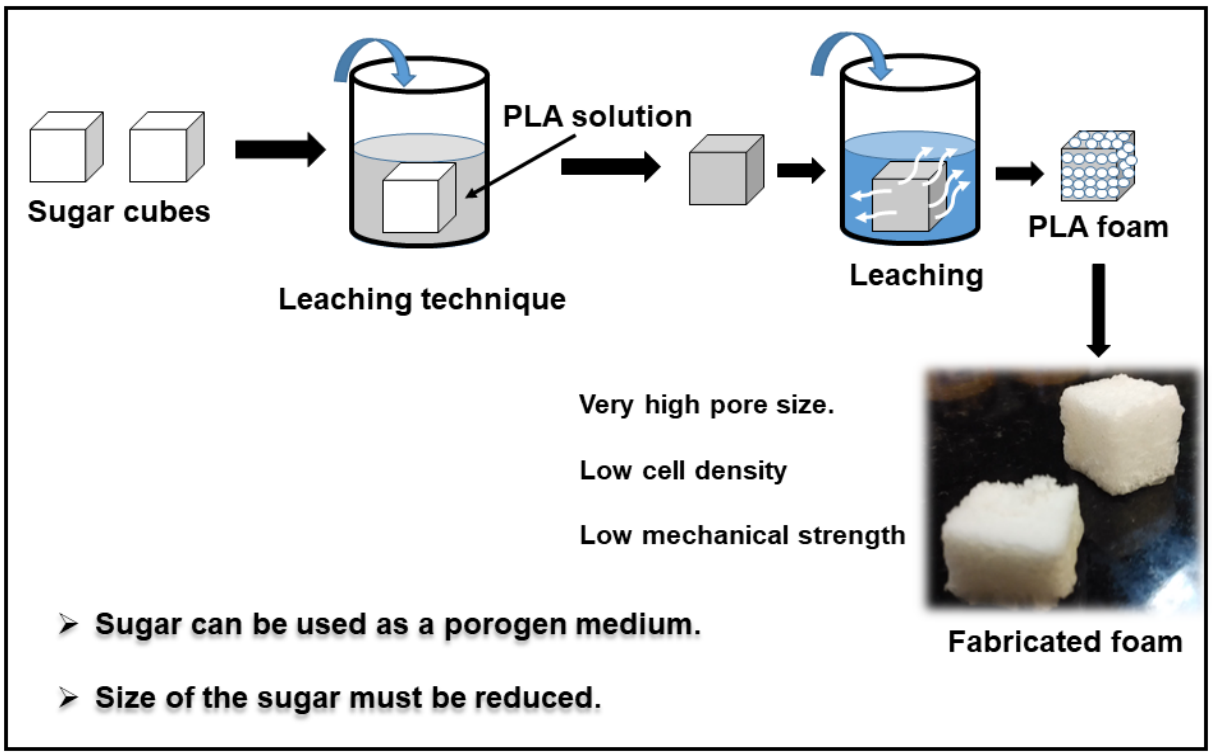

Fig. 2.3 Initial experiments for selection of porogen for PLA matrix.

In our investigation, we have used sugar as porogen for foam fabrication. Very less literature was observed for sugar as a porogen medium. For reducing the size of the pores of foam, finely ground table sugar cubes has been utilized in this investigation. Porogen size was responsible for the ultimate cell size and cell density of the fabricated foam [30]. One of the other reason for taking sugar as porogen was that it can easily be dispersed in 1,4 dioxane solvent, which also happens to be a good solvent for PLA. Hence, some modifications in the C/L technique is feasible in this process.

The process of pre-treatment of the porogen is shown in **Fig. 2.4**. The table sugar cubes were finely grinded using a marble grinder and the fine sugar power was obtained. The fine sugar (~30 g) was dispersed in 20 ml of solvent (1, 4 dioxane). The mixture was placed under constant

magnetic rotation (~800 rpm) for ~12 h. This pre-treated porogen has been used for PLA foam preparation in the next step.

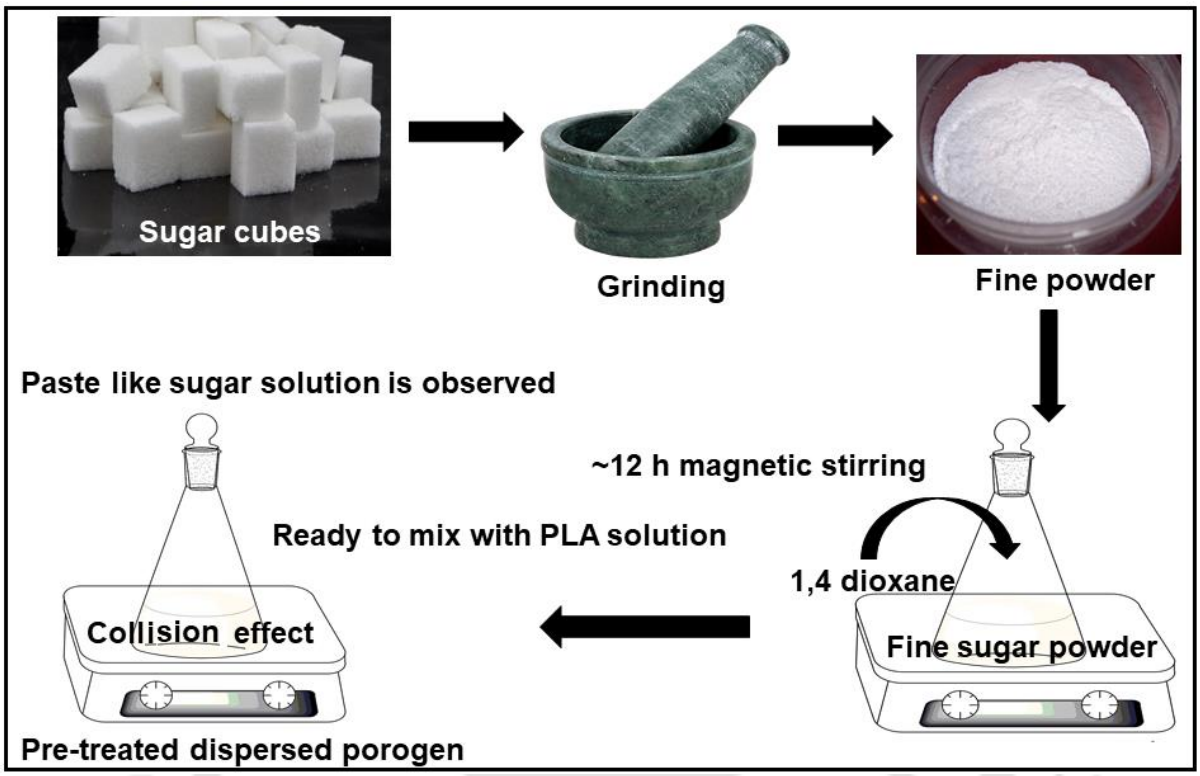

Fig. 2.4 Pre-treatment of porogen dispersed in PLA matrix.

The conventional C/L technique and the modified C/L technique can be seen in **Fig. 2.5**. In the modified C/L technique, the collision between particles in solvent influences the ultimate size of the porogen. In the modified C/L technique, the pre-treated porogen particles were mixed to the polymer solution in 1, 4-dioxane solvent and allowed to stir magnetically for ~12 h. The mixed solution was then cast in Teflon petri dish followed by drying and leaching.

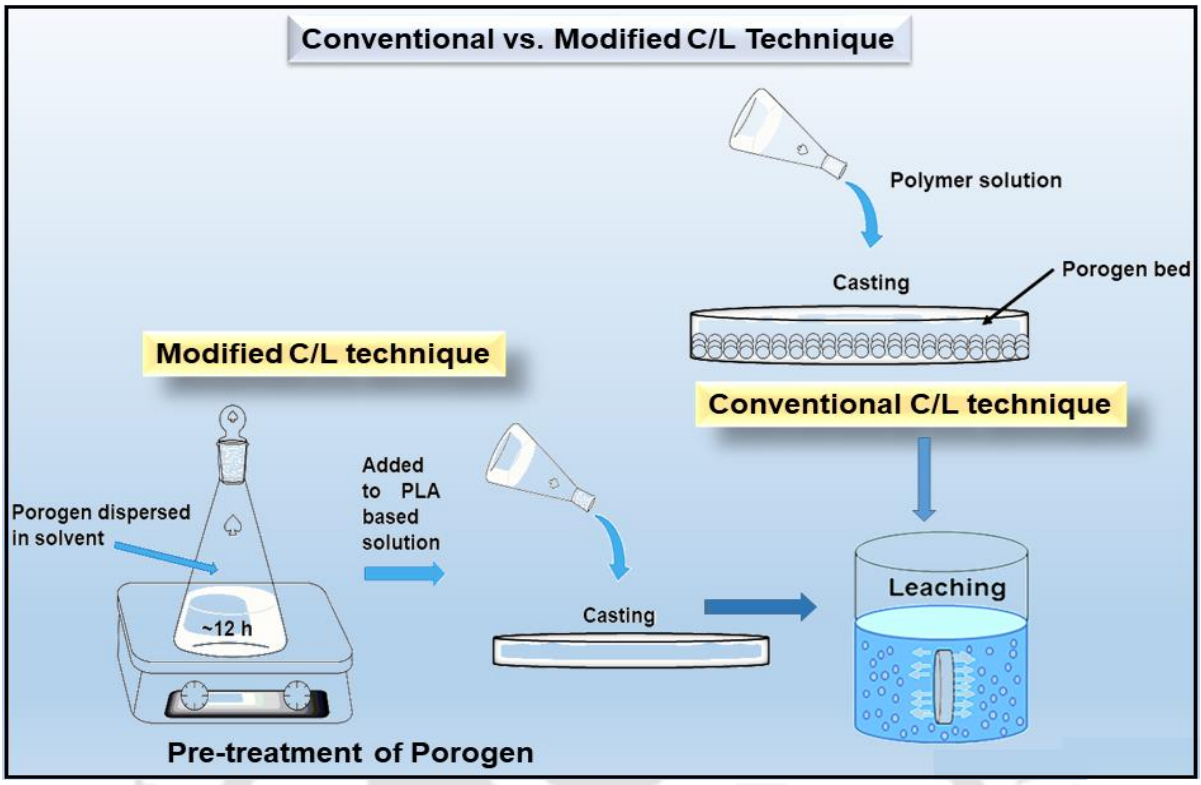

Fig. 2.5 Conventional and modified C/L technique.

The general representative scheme of the fabrication process of the PLA-based foam is shown in **Fig. 2.6** below.

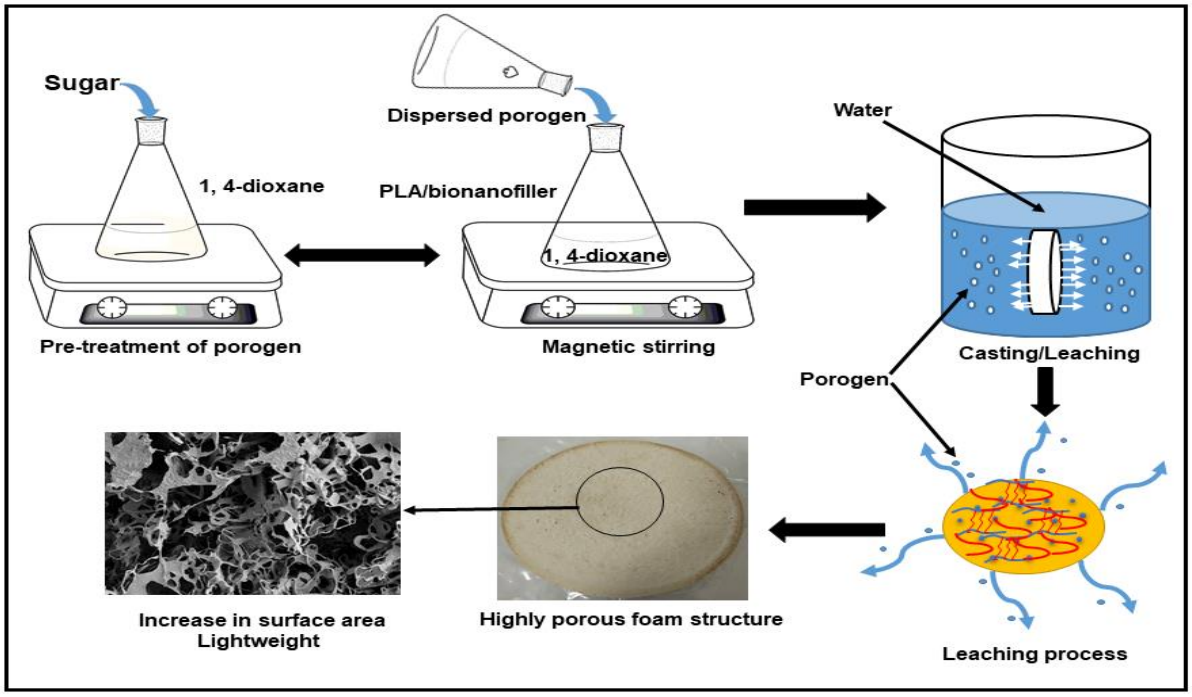

Fig. 2.6 General representation of the fabrication process of PLA-based foams.

2.2.2.2 Fabrication of PLA and PLA/CNC-based foam

For the fabrication of PLA and PLA/CNC based foams, C/L technique has been utilized. Sugar cubes were taken and grinded in a grinder to prepare fine sugar particles. An amount of ~30 g of sugar powder was taken and dispersed in 25 ml of 1, 4-dioxane and kept it under continuous magnetic stirring for ~12 h. Simultaneously, PLA solution was prepared by dissolving ~4 g of PLA granules in 20 ml of 1, 4-dioxane and kept under magnetic stirring for 6 h in a 250 ml conical flask followed by transfer of pre-treated sugar solutions to this. The mixed solution was kept under magnetic stirring for another 12 h. After 12 h, the mixed solution was cast in a glass petri dish of diameter 14 cm and height of 2 cm. The dish was kept under fumehood for 6 h followed by hot air oven for 2 h. After complete removal of the solvent, the samples were peeled-off from the glass petri dish surface and the dry weight was measured. Then the sample was placed in a water bath for leaching out of the sucrose particles. The water was continuously replaced in every half an hour. The process was continued until the removal of all the porogen particles. The sample was dried in a hot air oven at 35°C. An amount of ~4 g of PLA was dissolved in 20 ml of 1, 4 dioxane and allowed to stir under constant magnetic stirring for 6 h. After that CNCs were mixed in the solution and the temperature was raised to 70 ºC and the solution was allowed to stir for an hour. After complete dispersion of CNCs in the mixture, the solution was mixed with the sucrose solution and allowed to stir for 12 h at 70 °C. Rest of the protocol for PLA/CNC foam is similar to the PLA foam, as described in the above. PLA/CNC nanocomposite foams were fabricated by using three different loading of CNCs, 1%, 2%, and 3% and will be abbreviated in the subsequent sections as PLA/CNC 1, PLA/CNC 2 and PLA/CNC 3 respectively whereas neat PLA foam will be abbreviated as nPLA. All samples were dried at 35 °C overnight to remove any residual solvent or moisture present in it before analysis.

2.2.2.3 Fabrication of PLA and PLA/MC-based foam

For the fabrication of PLA and PLA/MC based foam, marble grinder was utilized to grind the sugar cubes (1cm×1cm) into a fine powder as discussed in an earlier section. Approximately, ~30 g of sugar particles were added to the solvent (1, 4 dioxane) and kept under magnetic stirring (rpm: ~800) for 8 h. Simultaneously, ~4 g of PLA was added to the 1, 4 dioxane solvent under magnetic stirring (rpm: ~800) for 4 h. The sucrose solution was then mixed with PLA solution under continuous stirring (rpm: ~800) for 6 h. After 6 h of mixing, a Teflon petri dish was used for casting the solution. The sample was placed under water for leaching the sugar particles present in the sample. The water was replaced in every 30 min for 4 h. Subsequently, sugar was removed (by using weight analysis to get an idea of sugar leached in water) from the sample, the sample was dried and the dry weight was observed. If the weight was observed more than 4 g (as we have taken ~4 g of PLA initially for casting), then we again executed the leaching and measured the weight until a steady weight (below ~4 g on a dry weight basis) of foam was observed. The sample was dried and ready for further analysis.

For the fabrication of modified chitosan-based PLA/MC foams, MC was first kept in a conical flask (250 ml) and placed under constant magnetic rotation (~600 rpm) with 10 ml of 1,4 dioxane. After 1 h, the MC solution was filtered by using Whatman® filter paper. The filtrate was collected and mixed with PLA solution (as discussed above) and magnetically stirred for 1 h. The PLA/MC solution was then mixed with the sugar solution. The final mixture was placed under continuous magnetic stirring for 6 h. The rest of the process of fabrication of the PLA/MC based foams was same as that of the PLA foam. PLA/MC based foams were fabricated by using three different concentrations of MC (i.e. 1%, 2%, and 3%) and abbreviated as PLA/MC 1, PLA/MC 2 and PLA/MC 3. The percentage calculation of MC (1%, 2%, and 3%) has been performed on wt/wt% basis of PLA as the solvents used in fabrication are not the part of the final product. Before analysis, all the fabricated foams were kept in a vacuum

oven at 35 °C overnight for removal of any moisture present. The process for the fabrication of PLA/MC-based foam can be represented by the schematic shown in **Fig. 2.7.**

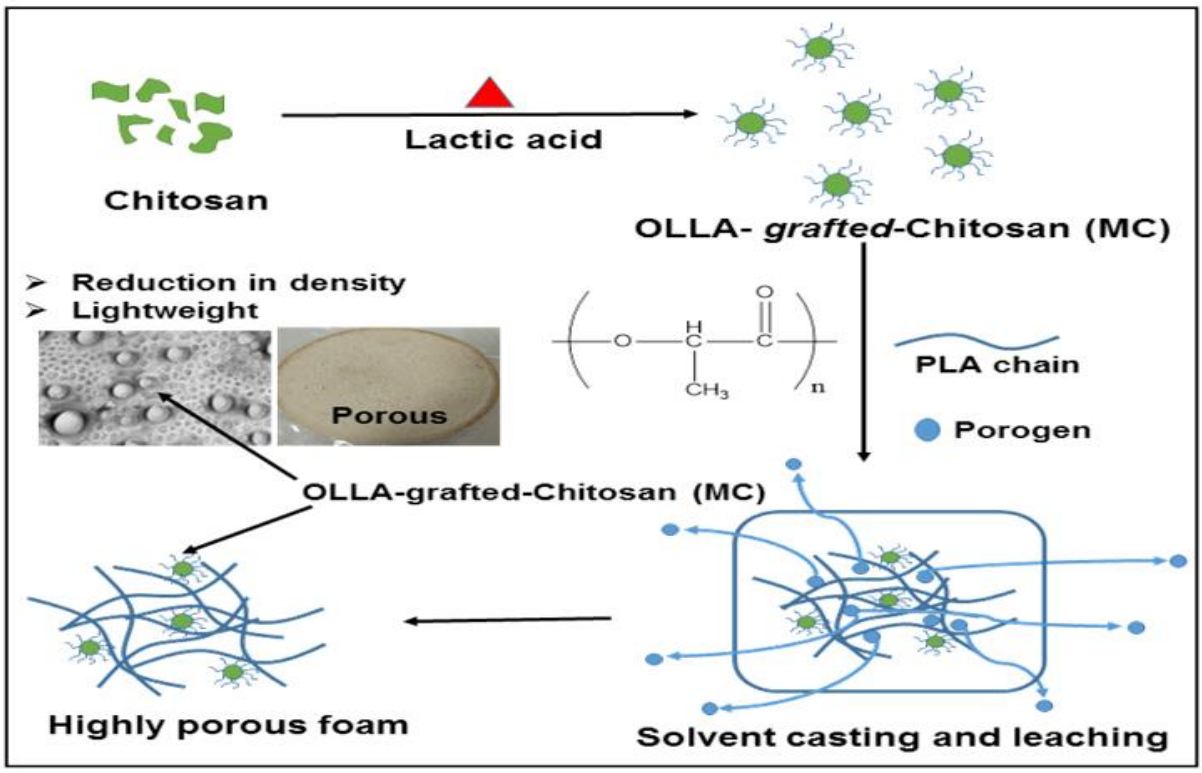

Fig. 2.7 Process of fabrication of PLA/MC based foams.

2.2.2.4 Fabrication of PLA and PLA/MG-based foam

The supplied sugar cubes were grounded using a marble grinder for obtaining the fine sugar particles for developing foams. The influencing factors for developing foams are quantity and size of porogen, which in turn affect the foam properties such as its pore volume, porosity, pore size, density, wettability, surface area etc. The porosity of polymeric foams plays a significant role in determining various properties. The fabrication of foams was performed by dissolving sucrose in 1, 4-dioxane followed by vigorous stirring for 12 h in the ratio of 1:1.2 (w/v) (solution A). Consecutively, PLA granules were dissolved in 1, 4-dioxane (1:3 w/v %) and kept under magnetic stirring for 2 h. After this, the prepared PLA solution was transferred to the solution A and was magnetically stirred for 6 h. The final solution was cast on a Teflon petri

dish and further kept in a hot air oven for 2 h to ensure the removal of the solvent. Thereafter, the dry weight was taken and the casted films containing sugar were placed in deionized water (replaced with new water after equal intervals), where porogen particles got leached out. The complete leaching was confirmed by taking the dry weight at an equal time interval (weight must be constant at final stages) as discussed earlier. Finally, the obtained foams were dried and the final weight was taken. A highly porous and lightweight foam structure was obtained, which was further utilized for different analysis. For developing PLA/MG based fabricated foams, the process is similar as above mentioned. Additionally, the required amount of MG was added in 10 ml of solvent and kept under stirring for an hour and filtered by using Whatman® filter and the filtrate was collected and mixed with PLA solution. The PLA/MG solution was further kept stirring for 2 h. The solution was transferred to the sugar solution and magnetically stirred for 6 h at 60 °C. Then the final casting and leaching method was followed as discussed earlier. The MG based foam were made incorporating nanobiofiller in the ratio (w/w%) of 1%, 2% and 3%, which were named as PLA/MG 1, PLA/MG 2, PLA/MG 3. All the developed samples were dried (~45°C) overnight for removing any residual in the foam and ready for various analysis.

2.2.2.5 Fabrication of PLA/SNC-based foams

For the fabrication process, approximately ~4 g of PLA granules were dissolved in ~20 ml of solvent and the mixture was kept under magnetic stirring for ~2 h. After that, the required amount of SNC powder (w/w%) was added to the above PLA solution and the system was kept under magnetic stirring (~800 rpm) for ~6 h for proper dispersion of the nanobiofillers. After the time period, the pre-treated porogen particles (as discussed in the earlier section) were mixed with the PLA/SNC solution. The mixed solution was again kept under magnetic stirring (~800 rpm) for ~4 h. The mixed solution was then cast on a Teflon petri dish and allowed to dry under the fume hood for ~2 h and placed under vacuum oven at temperature 40 °C for ~6

h. The leaching process of the samples was performed by using Mili-Q millipore water and the protocol of the leaching process was similar as utilized for the previously described fabricated foams.

After the leaching process, the samples were dried to obtain a highly porous foam structure. The fabricated PLA/SNC based foams were dried overnight at 35 °C in a vacuum oven to remove any entrapped water present before characterizing the foams. The fabricated foams were abbreviated as PLA/SNC 1, PLA/SNC 2 and PLA/SNC 3 for 1%, 2%, and 3% loading of SNC nanobiofillers. Neat PLA foam was abbreviated as nPLA.

2.3 Analytical methods and instrumentation

This section of the chapter provides discussion about different analytical methods and instrumentation used in the current doctoral research.

2.3.1 Fourier transform infrared spectroscopy (FTIR)

For the investigation of various functional groups present in the PLA/bionanofillers based foams, FTIR analysis was performed. FTIR analysis was carried out by using Frontier FTIR (Perkin-Elmer, USA). All the samples were dried at 50 ^{o}C for 2 h before analysis to remove the moisture present in the samples. The samples were prepared by cutting the homogeneous parts of the foam into small pieces (3cm×3cm). The samples were analyzed under ATR (Attenuated Total Reflectance) mode scanned in the range of 4000−700 cm^{-1} with a resolution of 4 cm^{-1} for 128 scans at room temperature. The FTIR spectrum was taken in transmittance mode for all the samples.

2.3.2 X-ray diffraction (XRD) analysis

The crystallographic investigations of the developed foam were executed by diffractometer (Model: D8 Advanced™; Make: Bruker, Germany) equipped with Cu-Kα radiation (λ=0.1541

nm) and voltage (40 kV). The investigations were performed under scan speed (1 s/scan) with an increment (0.05°/s). All the fabricated foam samples were placed in a hot air oven at a temperature of 80 °C for 2 h before the analysis. The % crystallinity index (C.I.) values were measured by the equation below

$$C.I. = \frac{A_{Crystalline}}{A_{Crystalline} + A_{Amorphous}} \quad (2.1)$$

Where, $A_{Crystalline}$ and $A_{Amorphous}$ are the area under the crystalline peaks and area under the amorphous peaks, respectively.

2.3.3 Density (ρ), porosity (P) and volume expansion ratio (VER) of fabricated foams

The density and porosity of the foam are considered as one of the important characteristics of foam as they influence various properties. The density of the fabricated foams was measured by using an International Equipment® densitometer, India. For the density calculations, small squares of (2 cm×2 cm) were cut from different locations of the foam. Further, the volume expansion ratio (VER) is a very important parameter of foam as it is required for calculation of cell density (N_f) and also its value is significant of the type of foam. Five samples were prepared for each fabricated foam and the average density value was calculated [125]. The average density was calculated from the data. Volume expansion ratio was calculated from the equation below.

$$VER = \frac{\rho_{Solid}}{\rho_{Foam}} \quad (2.2)$$

Where ρ_{Solid} and ρ_{Foam} are the respective densities of material and foam, respectively.

The classification of foam can also be done by VER values as

VER ≤4 (high-density foam), 4≤ VER ≤10 (medium density foam) and VER>10 (low-density foam).

Porosity (P) of the foam samples can be calculated by using density values using the equation below [78].

$$P = 1 - \frac{\rho}{\rho_o} \tag{2.3}$$

Where P is the porosity, ρ is the density of the foam and ρ_0 is the density of the material before foaming.

2.3.4 Gel permeation chromatography (GPC)

With the aid of GPC, the M_w, M_n, polydispersity index (PDI) of developed foams were determined using refractive index detector (RID-10A), taking polystyrene for calibration purpose. For the experiment, the eluent flow rate and sample injection volumes were 1 ml/min and 40 ml, respectively. The developed foams (20 mg) were dissolved in 1 ml of HPLC grade chloroform. The solution was then collected by using Dispo Van® syringe and filtered by using Axiva® syringe filter of 0.2µm. The M_w, M_n and polydispersity index (PDI) values were measured with the help of standard polystyrene prepared in chloroform ($CHCl_3$).

2.3.5 Color investigations

The color factors (L*, a* and b*) of the developed foams were measured using color measurement spectrophotometer supplied by Datacolor Technology, Suzhou Co. Ltd., China (Model: Datacolor 550). The foam samples were prepared by cutting in the square (2cm×2cm) from the different locations of the surface. Colorimetric investigations was carried out in three different locations and the value was calculated by taking average triplicates. The meaning of different values of color parameters is given below.

L* scale: Light vs. dark where a low number (0-50) indicates dark and a high number (51-100) indicates light.

a* scale: Red vs. green where a positive number indicates red and a negative number indicates green.

b* scale: Yellow vs. blue where a positive number indicates yellow and a negative number indicates blue.

2.3.6 Porosimetric investigation (mercury intrusion porosimetry)

Porosimetric investigations of the prepared foams were performed by mercury intrusion porosimeter (MIP) (Model: AMP-60K-A-1) procured from Porous Materials Inc., India. Sample weight of ~0.2 gm was taken for the analysis. The contact angle of mercury (~140°), surface tension (480 dyn/cm) with pressure (Range: 0 to 10000 psia) was utilized for the investigations. Porosimetric studies are very important in the context of foams as it gives an idea of porosity (%), surface area and average pore diameter of the fabricated foams. Porosimetric investigations of the fabricated PLA and PLA/nanobiofiller-based were carried out for deep understanding of average pore size, surface area and porosity. The average cell size were also measured from the FESEM micrographs. The results obtained from porosimetric investigations were further corroborate with the results obtained from visual observation methods (FESEM).

2.3.7 Thermogravimetric analysis (TGA)

The thermal stability analysis of the developed foams was executed using TG analyzer (Model: TGA-4000, Make: PerkinElmer, USA) under the inert environment (Rate: 50 mL/min) inside the chamber. For the analysis, the selected amount of sample (~8 mg) was placed in the alumina crucible and analysis was performed (Scanning range: 30 °C -700 °C; Rate: 10 °C/min). From

the TGA, onset degradation temperature (T_{onset}), maximum degradation temperature (T_{max}) and 90% degradation temperature (T_{90}) were measured.

The isothermal TGA investigations were performed by heating the sample from 30 °C to 150 °C at the rate of 10 °C/min and then kept it isothermally for 25 min at that temperature followed by heating at the rate of 10 °C/min to 200 °C and kept isothermally for 25 min at that temperature. The sample was again heated to 250 °C at the rate of 10 °C/min and kept isothermally for 25 min in that temperature. In the last cycle, the samples were heated from 250 °C up to 700 °C at the rate of 10 °C/min.

2.3.8 Differential scanning calorimetry (DSC)

The thermal and crystallization behavior of developed foams were determined by using DSC (Model: Netzsch DSC Phonix, Germany) in the flow of inert gas flow condition (50 ml/min). For this investigation, an approximate of ~8 mg samples were taken for each analysis. For the investigation, two thermal cycles were used, in the first heating cycle, samples were heated from 30 °C to 200 °C (Rate: and isothermally kept for 2 min, which was again cooled to 30°C and again kept for 2 min in the second cycle. Finally, the samples were again heated to 200 °C (Rate: 10 °C/min). The second heating cycle was utilized for our investigation after erasing the processing history of the first heating cycle. The degree of crystallinity, X_c (%) of the samples are calculated by using the equation below [126]

$$X_C = \frac{\Delta H_m^a}{\Delta H_m^o} \times 100 \qquad (2.4)$$

Where ΔH_m^a is the melting enthalpy of the second heating cycle, ΔH_m^o is the melting enthalpy for 100% crystalline PLA (taken as 93 J/g).

For non-isothermal crystallization investigations, samples are investigated at different heating/cooling rates of 2.5 °C/min, 5 °C/min, 7.5 °C/min and 10 °C/min.

2.3.9 Dynamic mechanical analysis (DMA)

The developed foams were analyzed for their thermomechanical properties using dynamic mechanical analyzer (DMA242, Netzsch, Germany) under tensile and compressive mode. Both the tensile and compressive modes were used for the analysis. For tensile mode, samples were prepared (measuring 15mm×5mm) from the homogeneous regions of the fabricated foams. All the analysis was carried under an inert nitrogen atmosphere (flow rate=100ml/min). For the compressive mode of analysis, circular cubic samples were cut from homogeneous sections of the fabricated foam (circle diameter 15 mm). For all the samples thickness were measured using Schut® electronic micrometer. All samples were investigated at frequency of 1Hz with dynamic force of 2 N (for compressive mode), 1 N (for tensile mode) and heating at the rate of 3 °C/min from 30 °C to 100 °C (tensile mode) and from 30 °C to 120 °C (compressive mode). The measurement of compressive strength was done at frequency 1 Hz applying 2 N dynamic force for a temperature range of 30 to 120 °C. This investigation provides information about the storage and loss modulus at dynamic temperature range.

2.3.10 Polarized optical microscope (POM)

Polarized Optical Microscope (Eclipse LV100N POL, Nikon Co., Japan) was used to analyze the particle size of the sucrose. The finely grinded sucrose particles were manually placed in a glass slide and placed under POM to analyze the particle size. The size of the sucrose particles was then analyzed by using Image J® software.

2.3.11 Hyphenated TGA-FTIR investigations

Hyphenated TGA (TGA4000, Perkin-Elmer, USA) coupled with FTIR (Frontier, Perkin-Elmer, USA) analysis was carried out for fabricated foams at temperature ranges from 30 °C to 700 °C (heating rate= 10 °C/min) under inert nitrogen atmosphere (flow rate= 50 mL/min) to investigate the evolved gases from TGA instrument at various temperatures. TGA instrument

was coupled with FTIR by using an interface line containing a gas transfer tube and gas cell. The interface line was heated to 250 °C to avoid any condensation of evolved gas. The evolved gases were analyzed by FTIR.

For the better understanding of the gaseous products evolved at different conversions and the better understanding of the reaction mechanism, isothermal hyphenated TGA-FTIR investigations were carried out at conversion (α=0.3 and 0.7). The investigations were done for nPLA and the PLA/CNC fabricated foam, which has the highest activation energy suggested from different models. For the investigations, ~8-9 mg sample was taken for all the cases. Samples were first heated to the desired temperatures at 10 °C/min heating rate and kept at the corresponding temperature of the conversion for 1 h under inert nitrogen atmosphere and then reached to 400 °C at a heating rate of 10 °C/min. The gaseous products evolved was investigated with the help of the IR spectrometer.

2.3.12 Transmission electron microscopy (TEM)

Transmission electron microscopy (TEM) (Model: JEM-2100, Make: JEOL, USA) was used for the morphological investigations of modified chitosan (MC). HPLC grade chloroform was used to disperse the prepared nanobiofillers (MC and MG) and placed for 2 h under constant magnetic stirring (~600 rpm) for proper uniform dispersion of nanobiofillers (MC and MG) followed by drop casting on carbon-coated grids (Tedpell, USA). The prepared sample was kept at 60 °C overnight before analysis. ImageJ® software was used to measure the dimension of nanobiofillers. On the other hand, SNC samples were first sonicated for ~30 min in water (0.01 wt%) before drop casting. Rest of the protocol was same as above.

2.3.13 Field emission scanning electron microscopy (FESEM)

Field Emission Scanning Electron Microscopy (FESEM) analysis was carried by using Zeiss™, Germany, Model Sigma, installed at CIF, IIT Guwahati, India to investigate the

morphology of the foam surfaces of the fabricated foams. The foam samples were placed on a stub with carbon tape and further coated in gold sputtering unit for 270 secs and then characterized at an accelerating voltage of 2-4 kV. Both the fractured cross-section and surface of the foam were investigated. For cross-sectional view, the samples were prepared by dipping into liquid nitrogen and fractured. The fractured surface was then cut by using a sharp Wilkinson Blade® in downward direction carefully so that there is no effect of compression on cell structure of foams. The cell morphology of the foam samples was investigated. The micrographs were analyzed by using Image J® software for cell density (N_f) and average cell size. The cell density (N_f) and average cell size were calculated for all the samples. The following equation [127] was used for calculation of cell density (N_f)

$$N_f = VER\left[\frac{n}{A}\right]^{1.5} \tag{2.5}$$

where VER is the volume expansion ratio, n is the number of bubbles detected in the area A of the FESEM micrograph. The diameter of pores was measured at different locations of the micrograph and average value of pore diameter with standard deviation was reported.

In the investigation, the meaning of cell size and pore size was same. However, pore was used for the porosimetric investigations to avoid any confusion with the cell size measured from FESEM.

2.3.14 Particle size analysis (Delsa Nano)

The particle size of the porogen after dispersing into the solvent after different hours of magnetic stirring was measured by a particle size analyzer (Make: Beckman Coulter (Switzerland), model: Delsa Nano C). A very dilute solution of the sucrose after 2 different hours (7 h and 12 h) of magnetic stirring of the sample was first diluted in a solvent and kept under sonication for 15 mins. The diluted solution was transferred to a cuvette and was examined. For the irradiation of the sample, HeNe laser of 632.8 nm wavelength was used.

This produced intensity fluctuation occurred rapidly for smaller and faster-moving particles, and slowly for the larger and slower moving particles. The size distribution was directly observed from the software associated with the instrument.

2.3.15 Wettability investigation

Contact Angle Measurements were carried out by using Kruss® DSA 25 Contact Angle instrument. The samples were first dried at 40 °C in a hot air oven for 2 h and then the samples of dimension 2cm × 2cm dimensions were pasted on a glass slide for analysis. The static contact angles values were measured at three different locations on the foam surface and the drops were allowed to settle for ~200 s and then the value was taken. The static contact angle was taken as the average value of the contact angles. On the other hand, the static contact angle was calculated for compressed foam in order to eliminate the effect of surface texture. The compressed sample was prepared by applying a load of 150 kg/cm^2 for 10 mins on the samples using a hydraulic press supplied by Kimaya Engineers, India. The advancing and receding contact angles for the foam surface were measured as the liquid initial droplet of volume 1 µL was continuously increased to a volume of 11 µL at a rate of 10 µL/min and again it was decreased back to 1 µL at the same rate. The whole process was observed and the contact angle hysteresis was measured along with the Young's contact angle. The above process was carried out at three times at different locations of the fabricated foam.

2.3.15.1 Dynamic contact angle and linear modeling

Wetting is an interesting phenomenon. It is the interaction of the liquid with the solid surfaces, which forms a contact angle with the solid surfaces. This is a very important property of any material. Wetting and non-wetting phenomena are one of the most important criteria of selection of material for a specific usage. If the contact angle is greater than 90°, than it can be considered as a non-wetting surface in some of the cases. Hydrophobicity can be defined by

the contact angle analyses. So to define the wetting on the textured surface contact angle measurements were investigated. Advancing contact angle, θ_{adv} is the maximum contact angle at the three-phase contact line and receding contact angle, θ_{rec} is the minimum contact angle at the three-phase line. The difference between the advancing and receding contact angle is known as contact angle hysteresis (CAH). Surface roughness is the major cause of CAH. Generally, a large no of surfaces shows contact angle hysteresis. There are generally two methods to measure contact angle hysteresis. One method is the tilted plane method and the second method is the sessile drop method or the captive bubble method. In this investigation, the second method was used to calculate the contact angle hysteresis [128–131].

For general ideal surfaces, the equilibrium contact angle is the Young's contact angle. Young's contact angle is very much essential along with CAH to understand the wettability of surfaces. Young's CA and CAH govern the various phenomenon occurring in the surface (solid/liquid interface) like spreading and sliding the liquid drops.

Young's contact angle can be defined as,

$$\cos\theta_Y = \frac{(\cos\theta_{adv} + \cos\theta_{rec})}{2} \tag{2.6}$$

where θ_Y is the Young's contact angle. For ideal smooth surfaces, young's contact angle is the equilibrium contact angle. But in some of the literatures, it was found that Young's contact angle can be determined by simple averaging of advancing and receding contact angles [132–134].

For partially wetting surfaces, three factors are affecting, they are the interfacial tensions of solid-vapor, solid-liquid, and liquid-vapor. So equilibrium contact angle (θ_e) is the function of all three parameters[135].

$$\cos\theta_e = \frac{(\gamma_{SV} - \gamma_{SL})}{\gamma_{LV}} \tag{2.7}$$

where γ_{SV} , γ_{SL} and γ_{LV} are the interfacial tensions of solid-vapor, solid-liquid, and liquid-vapor respectively.

Schulze et al. in their investigation suggested a plot of advancing/receding contact angles in the function with hysteresis [134]

$$H = \theta_{adv} - \theta_{rec} \tag{2.8}$$

They suggested that,

$$\theta_{adv} = \theta_Y + kH \tag{2.9}$$

$$\theta_{rec} = \theta_Y - (1-k)H \tag{2.10}$$

where $0 \leq k \leq 1$ and k is the positive slope of the curve $\theta_{adv} - H$. In some of the solid-liquid systems, the curves $\theta_{adv} - H$ deviate from the linearity at high H values.

In the current investigation, a linear model was used to predict the young's contact angle and analyze the predicted values with the experimental ones.

2.3.16 Water immersion test

The water immersion test of the fabricated foam samples was performed as per ASTM D570-98. The fabricated samples were prepared (5 cm×5 cm) and kept under vacuum oven at 80 °C for 24 h. The weight of the sample was measured and immersed in water for 24 h at a temperature of 25±2 °C. During the period, the sample was collected and the surface was cleaned to remove the other water droplets by a blotting paper periodically at every 3 h and weight of the sample was measured. Three replicates of each sample were used and the average value was reported.

2.4 Thermal degradation investigation of the fabricated foams

The thermal investigations of PLA and PLA/bionanofiller based foams were carried by using TGA 4000 (Perkin Elmer, USA) analyzer. The fabricated foam samples (~8 mg) were placed

in a platinum crucible and started heating ranging from 30 °C-700 °C under an inert nitrogen atmosphere. The samples were heated at four different heating rates for dynamic TGA analysis (5 °C/min, 10 °C/min, 15 °C/min and 20 °C/min) to investigate the non-isothermal degradation kinetics behaviour of the fabricated PLA and PLA/nanobiofiller-based foams by using some well-known "model-free" and "modelistic" approaches. These methods help to determine the apparent activation energy (E_a) of the fabricated foams without prior knowledge of the degradation mechanism.

2.4.1 Non-isothermal degradation kinetics studies

The fundamental rate equation for all type of kinetic investigations is given below [136]

$$d\alpha/dt = kf(\alpha) \tag{2.11}$$

Where k denotes rate constant and $f(\alpha)$ denotes reaction model. α denotes the rate of conversion and can further be expressed as

$$\alpha = (W_o - W_t)/(W_o - W_f) \tag{2.12}$$

Where W_0 is the initial weight of the sample, W_t is the weight of the sample at time t and W_f is the final weight of the sample.

In equation 2.11, the k represents rate constant, which can further be expressed as

$$k = A\exp\left[-E_a/RT\right] \tag{2.13}$$

Where E_a is the apparent activation energy in kJ/mol, R is the gas constant (8.314 J/K mol), T is the temperature in Kelvin, A is the pre-exponential factor [137]

By putting the value of k

$$d\alpha/dt = A\exp\left[-E_a/RT\right] f(\alpha) \tag{2.14}$$

For the dynamic thermogravimetric analysis (TGA) the heating rate is very important. So by introducing the term " β " in the above equation where $\beta = dT/dt$

$$d\alpha/dT = \left(A/\beta\right)\exp\left[-E_a/RT\right] f(\alpha) \tag{2.15}$$

The above equation is the basic equation for dynamic TGA kinetic analysis for the calculation of kinetic parameters. There are normally two approaches model free and model fitting approach for thermal degradation kinetics. The model fitting approach is generally more popular due to the direct finding of kinetic triplets. However, it has a disadvantage of inability to predict reaction model [138].

2.4.1.1 Iso-conventional methods ("model-free" approach)

The iso-conventional method is used to calculate the activation energy (E_a) at different conversion rates (α) without any prior modelistic assumptions [139]. The main advantage of these methods is that it does not require any previous knowledge of reaction mechanisms. We have used the most common established "model-free" methods like Flynn-Wall-Ozawa (FWO), Kissinger-Akahira-Sunose (KAS), Friedman method, Augis and Bennett model to calculate kinetic parameters at different heating rates.

Friedman method: This method is a useful iso-conventional method for calculation of activation energy. The method can be written as

$$\ln\left[\frac{d\alpha}{dt}\right] = \ln\left[\beta\frac{d\alpha}{dT}\right] = \ln\left[Af(\alpha)\right] - \frac{E_a}{RT} \tag{2.16}$$

Graphs are plotted between $\ln\left[\frac{d\alpha}{dt}\right]$ vs 1/T for constant conversions and from the slope of the linear lines, we can calculate the activation energy [140].

Kissinger-Akahira-Sunouse method: KAS method is based on Murray and White approximation for temperature integral [141].

$$\frac{d\alpha}{f(\alpha)} = \frac{A}{\beta}\exp\left[-\frac{E_a}{RT}\right]dT \tag{2.17}$$

This method utilizes the initial condition of α=0 and T=T_o for obtaining the expression below

$$g(\alpha) = \int_0^{\alpha}\frac{d\alpha}{f(\alpha)} = \frac{A}{\beta}\int_{T_o}^{T}\exp\left[-\frac{E_a}{RT}\right]dT = \frac{AE}{\beta R}p\left[\frac{E_a}{RT}\right] \tag{2.18}$$

The KAS method can be written as given below

$$\ln\frac{\beta}{T^2} = \ln\frac{AR}{E_a g(\alpha)} - \frac{E_a}{RT} \tag{2.19}$$

This method is based on Coats-Redfern approximation [142]. The assumption of this method is that A, f(α) and E_a are independent of temperature T. A and E_a are also assumed of independent of conversion. In this method, plots have been made in between $\ln(\beta/T^2)$ vs 1/T. Straight lines are obtained at each conversion and the slope from these lines we can calculate activation energy (E_a).

Flynn-Wall-Ozawa method: This method is an integral isoconversional method, based on Doyal's linear approximation [143]. The equation comes from the Arrhenius rate equation. The FWO equation can be expressed as given below

$$\ln \beta = \ln\left[{AE_a}/{Rg(\alpha)} \right] - 5.331 - 1.052\, {E_a}/{RT} \tag{2.20}$$

In this method, we have plotted a graph between ln β vs 1/T for PLA and PLA/CNC based fabricated foams. Straight lines should be obtained at various conversions in different heating rates. The slopes of these lines can be utilized to calculate the activation energy (E_a) [144,145].

Augis and Bennett model: This is an iso-conversional method in which temperature dependency on heating rates is established [146]. The equation can be written as

$$\ln\left[\frac{\beta}{T_m - T_o} \right] = -\frac{E_a}{RT_m} + \ln A \tag{2.21}$$

In this method, single activation energy is obtained for the samples at maximum degradation temperature (T_m). Graphs are plotted between $\ln\left[{\beta}/{T_m - T_o} \right]$ vs $1/T_m$. Straight lines are obtained. From the slope and intercept of the lines, we can calculate activation energy and pre-exponential factor (A) [146].

Modified Coats Redfern (Modified CR) model: This method is a combination of Coat-Redfern and Friedman method. The method can be expressed as below.

$$\ln\left(\frac{\beta}{T_\alpha^{\,2}} \right) = \ln\left[\frac{-AR(1 - 2RT_\alpha / E_a)}{E_a \ln(\alpha)} \right] - \frac{E_a}{RT_\alpha} \tag{2.22}$$

Graph is plotted against left side of the above equation vs $-\frac{1000}{T}$ and a series of linear curves are generated for each conversion and activation energy (E_a) values is calculated for each conversion.

All the equations are summarized in **Table 2.1.**

Table 2.1 Equations used for thermal degradation investigation

Method	Equation	Plots
FWO	$\log\beta = \log\left(AE_a/Rg(\alpha)\right) - 2.315 - 0.4567E_a/RT$	$\log\beta$ vs 1/T
Kissinger	$\ln\left(\beta/T_P^2\right) = \ln\left(AR/E_a\right) + \left(1/T_P\right)\left(-E_a/R\right)$	$\ln\left(\beta/T_P^2\right)$ vs $1/T_p$
KAS	$\ln\left(\frac{\beta}{T^2}\right) = \ln\left(\frac{AR}{E_a g(x)}\right) - \frac{E_a}{RT}$	$\ln(\beta/T^2)$ vs 1/T
Friedman	$\ln\left[d\alpha/dt\right] = \ln\left[Af(\alpha)\right] - E_a/RT$	$\ln\left[d\alpha/dt\right]$ vs 1/T
Augis and Bennett	$\ln\left[\beta/T_m - T_o\right] = \ln A - E_a/RT_m$	$\ln\left[\beta/T_m - T_o\right]$ vs $1/T_m$
Modified CR	$\ln\left(\frac{\beta}{T_\alpha^{\,2}}\right) = \ln\left[\frac{-AR(1-2RT_\alpha/E_a)}{E_a \ln(\alpha)}\right] - \frac{E_a}{RT_\alpha}$	$\ln(\beta/T^2)$ vs 1/T

2.4.1.2 Model-fitting approach

By using the model-fitting approach, also we can calculate activation energy, pre-exponential factor by different model fitting at a particular temperature. One of the most popular models fitting approach is the Kissinger method. We have used the Kissinger method for the calculation of activation energy and pre-exponential factor (A).

Kissinger method: The assumption of the Kissinger method is that the reaction rate is maximum at T_{max} (maximum degradation temperature) which can be found from the DTG curve. It is used for calculating E_a values for solid-state reactions. This method calculates the activation energy at T_{max}. Only one activation energy can be obtained for each sample. The assumption

also includes the constant degree of conversion (ά) at maximum degradation temperature. At T_{max} , the first and second derivative of conversion "α" is zero. The Kissinger equation can be written as

$$\ln\left[\beta/T_m^2\right] = -E_a/RT_m = \ln\left[AR/E_a\right] \tag{2.23}$$

Activation energy (E_a) can be obtained from the slope of the straight lines plotted between $\ln\left[\beta/T_m^2\right]$ vs $1/T_m$ [147,148]

Criado method: This method is mainly used for a better understanding of the reaction mechanism if the activation energy of the system is known. Criado method is used to determine the mechanism of mainly solid state reaction process [149,150]. Master plots are used for different types of the mechanism by plotting between Z(α) vs α, where Z(α) can be expressed as

$$Z(\alpha) = \frac{\left[d\alpha/dt\right]}{\beta}\pi(x)T \tag{2.24}$$

Where $x = E_a/RT$ and $\pi(x)$ is an approximation of temperature integral, $\pi(x) = xe^x P(x)$

Different mechanisms are shown for Z(α) in **Table 2.2**. For master plots, the expression used as given below

$$Z(\alpha) = f(\alpha)g(\alpha) \tag{2.25}$$

In Criado method, the experimental curve is plotted by using the expression given below

$$Z(\alpha) = \frac{d\alpha}{dT}\frac{E_a}{R}e^{E_a/RT}P(x) \tag{2.26}$$

Where $P(x) = \frac{e^{-x}}{x}\frac{x^3 + 18x^2 + 86x + 96}{x^4 + 20x^3 + 120x^2 + 240x + 120}$

The degradation mechanism can be determined by comparing the experimental curves with master plots.

2.4.2 Measurements of thermodynamic variables

Entropy of activation (ΔS) can be defined as the difference between change in entropy of the activated complex and the summation of the entropies of the reactants [151]. This can be represent mathematically as

$$\Delta S = R\left[\ln\left(\frac{Ah}{kT_m}\right)\right] \tag{2.27}$$

Where k is the Boltzmann constant (1.38×10^{-23} m^2 kg/s^2k^1), h is the Plank's constant (6.626×10^{-34} m^2kg/s), R is the gas constant (8.3144598 J $mol^{-1}K^{-1}$), A is the pre-exponential factor and T_m is the maximum degradation temperature given by DTG curves. The other thermodynamic parameters ΔG (Gibb's free energy) and ΔH (Enthalpy of activation) were calculated by using the equations 2.28 and 2.29 below.

$$\Delta G = \Delta H - T_m\Delta S \tag{2.28}$$

$$\Delta H = E_a - RT_m \tag{2.29}$$

Table 2.2 g(α) and f(α) values for the master plot of Criado method.

Mechanism: Solid state process	$g(\alpha)$	$f(\alpha)$
A_2: Nucleation and growth (Avrami Eq. 1)	$[-\ln(1-\alpha)]^{1/2}$	$2(1-\alpha)[-\ln(1-\alpha)]^{1/2}$
A_3: Nucleation and growth (Avrami Eq. 2)	$[-\ln(1-\alpha)]^{1/3}$	$3(1-\alpha)[-\ln(1-\alpha)]^{2/3}$
A_4: Nucleation and growth (Avrami Eq. 3)	$[-\ln(1-\alpha)]^{1/4}$	$4(1-\alpha)[-\ln(1-\alpha)]^{3/4}$
R_1: Phase boundary controlled reaction (One-dimensional movement)	α	1
R_2: Phase boundary controlled reaction (contracting area)	$[1-(1-\alpha)]^{1/2}$	$2(1-\alpha)^{1/2}$
R_3: Phase boundary controlled reaction (contracting volume)	$[1-(1-\alpha)]^{1/3}$	$3(1-\alpha)^{2/3}$
D_1: One-dimensional diffusion	α^2	$(1/2)\alpha$
D_2: Two-dimensional diffusion (Valensi equation)	$(1-\alpha)\ln(1-\alpha)+\alpha$	$[-\ln(1-\alpha)]^{-1}$
D_3: Three-dimensional diffusion (Jander equation)	$[1-(1-\alpha)^{1/3}]^2$	$(3/2)[1-(1-\alpha)^{1/3}]^{-1}$ $(1-\alpha)^{2/3}$
D_4: Three-dimensional diffusion (Ginstling-Brounshtein equation)	$[1-(2/3)\alpha]-(1-\alpha)^{2/3}$	$(3/2)[1-(1-\alpha)^{1/3}]^{-1}$
F_1: Random nucleation with one nucleus on the individual particle	$-\ln(1-\alpha)$	$1-\alpha$
F_2: Random nucleation with two nuclei on the individual particle	$1/(1-\alpha)$	$(1-\alpha)^2$
F_3: Random nucleation with three nuclei on the individual particle	$1/(1-\alpha)^2$	$(1/2)(1-\alpha)^3$

2.5 Non-isothermal melt crystallization studies

Generally, two types of crystallization occur in polymers i.e. cold crystallization and melt crystallization. When the crystallization occurs from a melting state of polymers it is known as melt crystallization and when crystallization occurs from the glassy state than it is known as cold crystallization. Various physical and mechanical properties of polymers are directly and indirectly dependent on the crystallization [152,153].

In this present research, crystallization of microcellular foam is investigated. The DSC kinetics investigations were carried out by using Netzsch® DSC (201 F1 Phoenix™) under an inert nitrogen atmosphere. For nonisothermal melt crystallization study, the analysis was carried out at three different temperatures of 2.5 °C/min, 5 °C/min and 7.5 °C/min. Samples were first heated from room temperature (30 °C) to 200 °C at 10 °C/min and kept isothermally for 5 min at that temperature for removal of any thermal history and moisture present in it. Samples were then cooled at 3 different cooling rates of 2.5 °C/min, 5 °C/min and 7.5 °C/min respectively for the second cycle from 200 °C to 30 °C and kept isothermally at that temperature for 5 min. In the third cycle, samples were again heated to 200 °C at respective heating rates of 2.5 °C/min, 5 °C/min and 7.5 °C/min. The cooling cycle was taken for kinetic analysis. Approximately ~8 mg of sample mass was taken for each analysis.

For non-isothermal cold crystallization investigations, different heating rates of 2.5 °C/min, 5 °C/min, 7.5 °C/min and 10 °C/min were taken for analysis. The first heating cycle was from 30°C to 200 °C at the above mentioned heating rates and then isothermally kept at that temperature for 2 min. Sample were than cooled down to 30 °C at 10 °C/min and isothermally kept for 2 min. Finally, in the second heating cycle samples were again scanned at the above mentioned different temperatures to 200 °C. The second heating cycle was taken into consideration for the cold crystallization kinetics investigations.

Relative Crystallinity: The relative crystallinity (X_t) can be expressed in terms of time of crystallization (t) by integrating the exotherms of melt crystallization for PLA and PLA/CNC based fabricated foams. The relative crystallinity as a function of temperature can be expressed as given below

$$X_t = \frac{\int_{T_o}^{T} \frac{\Delta H_c}{dT} dT}{\int_{T_o}^{T_\infty} \frac{\Delta H_c}{dT} dT} \tag{2.30}$$

Where T_o denotes the onset and T_∞ denoting final melt crystallization temperature. T is the temperature at crystallization time (t) can relate as

$$t = \frac{T - T_o}{\beta} \tag{2.31}$$

Where β is the heating rate.

Crystallization half-time ($t_{0.5}$): This is the time required by the sample for 50% crystallization. This is a very important parameter for prediction of the rate of crystallization.

Avrami model: For non-isothermal crystallization of polymers, the Avrami model is generally utilized to investigate kinetic parameters [154].

$$X_t = 1 - \exp(-kt^n) \tag{2.32}$$

$$\log\left[-\ln(1 - X_t)\right] = \log k + n \log t \tag{2.33}$$

where 'X_t' indicates relative crystallinity at a time 't', 'k' indicates the crystallization rate constant and 'n' denotes the Avrami exponent. The 'n' and 'k' values are a very important parameter for crystallization and can be calculated from the slope and intercepts of the straight

line between $\log\left[-\ln(1-X_t)\right]$ vs $\log t$. The 'n' value signifies the mechanism of nucleation and growth of crystals.

Ozawa model: This method can be considered as the modified version of the Avrami model. Time variable of the Avrami model is replaced by cooling rate in this model. The assumption of this model is that the sample was cooled from a molten state in a constant cooling rate. The general equation can be expressed as;

$$1-X(T)=\exp\left[-K(T)/\beta^{m}\right] \tag{2.34}$$

Where $X(T)$ is the relative crystallinity degree, $K(T)$ is the kinetic parameter at temperature 'T', 'β' is the cooling rate and 'm' is the Ozawa exponent. The equation can be rearranged as

$$\log\left[-\ln(1-X(T)\right]=\log K(T)-m\log\beta \tag{2.35}$$

The graph can be plotted between $\log\left[-\ln(1-X(T)\right]$ vs $\log\beta$ to get the value of $K(T)$ and 'm' from the intersection with the Y-axis and slope of the line [153].

Mo model: Mo model is a developed model which is in relation with Avrami and Ozawa model. Avrami model is based on the relation between X_t with t and Ozawa model relates to X(T) with β. In this model relationship between 't' and 'β' can be established. This two terms can relate as

$$t=\frac{T_o-T}{\beta} \tag{2.36}$$

Where T_o is the temperature at initial crystallization (at t=0), 'T' is the temperature at time't'. The following equation was developed from the Avrami and Ozawa model assumptions

$$\log K_t + n\log t = \log K(T) - m\log\beta \tag{2.37 a}$$

$$\log\beta = (1/m)\log[K(T)/K_t] - (n/m)\log t \tag{2.37 b}$$

$$\log\beta = \log F(T) - a\log t \tag{2.37 c}$$

where $F(T) = \left[\frac{K(T)}{K_t}\right]^{1/m}$ and $a = n/m$

Slopes and intercepts can be calculated from the reasonable linear graph plotted between ln β vs ln t to calculate the ' a ' and "$\log F(T)$".The physical significance of $\log F(T)$ and a is very important for crystallization point of view [155].

Tobin model: Avrami model only gives an idea of initial crystallization, it cannot describe the whole crystallization process alone. Secondary crystallization is also taking place in most of the cases. Tobin model is very much useful for the understanding of primary and secondary crystallization process. This model gives a better insight into the phase transformation kinetics and growth impingement. The Tobin model can be expressed as

$$X_t = \frac{K_T t^{n_T}}{1 + K_T t^{n_T}} \tag{2.38}$$

Where 'K_T' is Tobin parameter for crystallization rate constant, 'n_T' is the Tobin exponent and 'X_t' is the relative crystallinity at a time 't', 'n_T' is responsible for different nucleation and growth mechanisms.

$$\log\left[\frac{X_t}{1 - X_t}\right] = \log K_T + n_T \log t \tag{2.39}$$

The graph is plotted between $\log\left[\frac{X_t}{1-X_t}\right]$ vs log t and the values of 'K_T' and 'n_T' can be calculated from the intercept and slope of the linearly fitted lines [156].

Kissinger method for effective activation energy of crystallization: Energy of activation of crystallization generally depends on two factors

1. Minimum requirement of the diffusion energy to reach the crystallization sites.

2. The requirement of energy to form crystallites of a critical size from where growth starts. ΔE is a temperature dependant term and it depends on the morphology and dimensions of the nanofillers

The effective change in the activation energy of crystallization (ΔE) by using the Kissinger equation below [157]

$$\frac{\partial\left[\ln\left(\frac{\beta}{T_P^2}\right)\right]}{\partial\left(\frac{1}{T_P}\right)} = -\frac{\Delta E}{R} \qquad (2.40)$$

where 'β' is the heating rate (°C/min), 'T_P' is the peak crystallization temperature and 'R' is the universal gas constant [156].

2.6 Hydrolytic degradation investigations of the fabricated foams

With the aid of hydrolytic degradation of developed nanocomposite foams, the change in a property of foams with respect to different condition (pH and temperature) can be analyzed. The hydrolytic degradation was carried out at temperatures 35 °C ± 2 °C and 55 °C ± 2 °C with acidic (pH=2), neutral (pH=7) and basic (pH=12) solution. The degradation temperature was selected as per various previous literature [158,159]. The pictorial representation of the process can be found in **Fig. 2.8**. The targeted samples for hydrolytic degradation were cut into uniform

pieces of dimension 2 cm×2 cm and dipped into the above-mentioned solutions. A similar amount of solutions (~50 ml) was taken for all the samples. For the experiment, the samples were taken off from the solution after a regular interval, washed twice with MiliQ (millipore water), then dried at 60 °C for 2 h and further taken for analysis. The residual weight fraction of the foams was determined by gravimetric analysis, where the weight of the samples before and after degradation measures. The residual weight fraction was measured following the below equation as a function of degradation time (t).

$$\phi = \frac{W_t}{W_o} \times 100\% \qquad (2.41)$$

Where ϕ is the residual weight fraction, W_t is the weight after time t and W_o is the initial weight of the sample. The hydrolytic investigations were carried out for 120 h and degraded samples were dried at ~40 °C for 6 h for further analysis. Different investigations like XRD, FESEM, TGA, DSC, GPC, colour, wettability phenomena etc. were performed for the degraded samples to study the effect of hydrolytic degradation on foam properties.

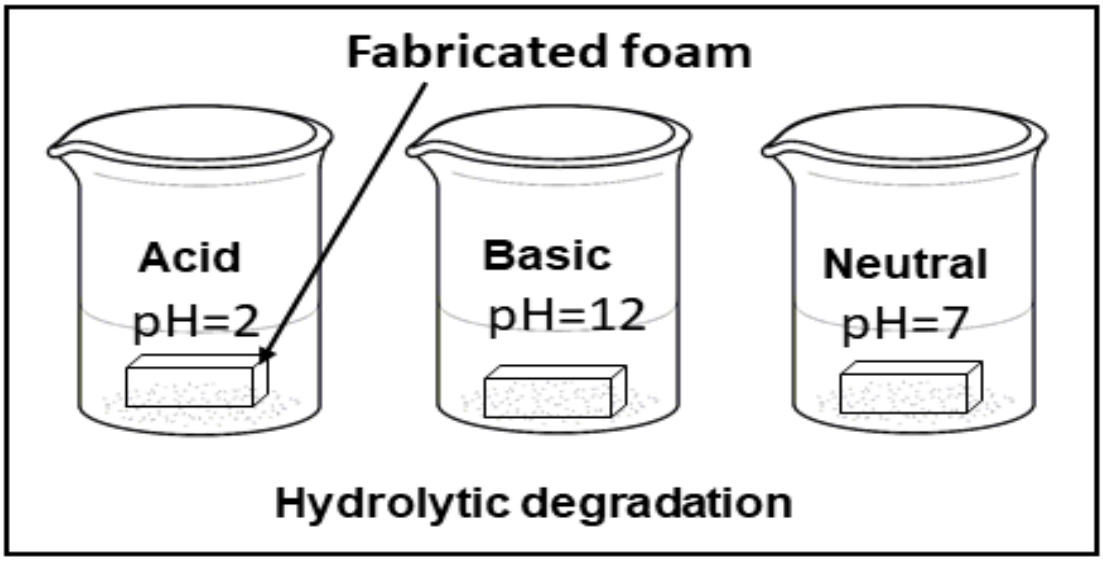

Fig. 2.8 Hydrolytic degradation investigation of fabricated foams.

The different hydrolytic samples used in this research (MG and SNC-based fabricated foams) were abbreviated as nPLA_acid_35, PLA/MG 1_acid_35, PLA/MG 2_acid_35, PLA/MG 3_acid_35, PLA/SNC 1_acid_35, PLA/SNC 2_acid_35 and PLA/SNC 3_acid_35 for acidic medium at 35 ºC. Similarly, samples for basic medium at 35 °C were abbreviated as nPLA_basic_35, PLA/MG 1_basic_35, PLA/MG 2_basic_35, PLA/MG 3_basic_35, PLA/SNC 1_basic_35, PLA/SNC 2_basic_35 and PLA/SNC 3_basic_35. The samples for neutral medium at 35 °C were abbreviated as nPLA_neutral_35, PLA/MG 1_neutral_35, PLA/MG 2_neutral_35, PLA/MG 3_neutral_35, PLA/SNC 1_neutral_35, PLA/SNC 2_neutral_35 and PLA/SNC 3_neutral_35.

Similarly, for 55 °C, the MG and SNC-based fabricated foams were abbreviated as nPLA_acid_55, PLA/MG 1_acid_55, PLA/MG 2_acid_55, PLA/MG 3_acid_55, PLA/SNC 1_acid_55, PLA/SNC 2_acid_55 and PLA/SNC 3_acid_55 for acidic medium at 55 °C. Similarly, samples for basic medium at 55 °C were abbreviated as nPLA_basic_55, PLA/MG 1_basic_55, PLA/MG 2_basic_55, PLA/MG 3_basic_55, PLA/SNC 1_basic_55, PLA/SNC 2_basic_55 and PLA/SNC 3_basic_55. Samples for neutral medium at 55 °C were abbreviated as nPLA_neutral_55, PLA/MG 1_neutral_55, PLA/MG 2_neutral_55, PLA/MG 3_neutral_55, PLA/SNC 1_neutral_55, PLA/SNC 2_neutral_55 and PLA/SNC 3_neutral_55.

2.7 UV irradiated degradation of fabricated foams

For the photodegradation (UV) investigations, the fabricated PLA and PLA/bionanofiller based foam samples (5 cm×5 cm) were exposed to UV lamp. The UV lamp (8 W, dominant wavelength: ~360 nm, Narva, Germany) was installed 25 cm above the exposed top foam surface. The temperature of the UV chamber was maintained at ~40 °C. Samples were collected after an interval of 1 week, 2 weeks and 3 weeks for further analysis. Different analytical methods like FTIR, FESEM, TGA, DSC, GPC, contact angle, color etc. were investigated to

study the effect of UV irradiation on the fabricated PLA based foams. The photodegraded MG and SNC-based fabricated foam samples in the current investigation were abbreviated as according to the week of degradation as 1 week, 2 weeks and 3 weeks.

भारतीय प्रौद्योगिकी संस्थान गुवाहाटी
Indian Institute of Technology Guwahati

Chapter 3

Studies on Poly (lactic acid) and Cellulose nanocrystals (CNC) based Microcellular Composite Foams

This chapter addresses the fabrication and detailed investigations of PLA and PLA/CNC based foams. The pore size of less than 10 microns is achieved for the fabricated foams. From the porosimetric investigations of the fabricated foams, an increase in surface area with nanofiller concentration is observed. CNC mainly acts as a nucleating agent in the PLA foam matrix. Effect of CNC is mainly observed in thermal, wettability and thermo-mechanical properties of the fabricated foams. Static and dynamic wettability investigations are performed for the fabricated foams. Thermal degradation investigations along with a mechanistic approach to degradation behavior of PLA/CNC based foam has discussed thoroughly in this chapter. Isothermal TGA hyphenated FTIR investigations are carried out to understand the degradation mechanism. Both "model free" and "modelistic" approaches like Kissinger-Akahira-Sinouse, Flynn-Wall-Ozawa, Friedman, Augis Bennet, Criado etc. are utilized to calculate the activation energy. From the investigation, it is observed that complex degradation mechanism like three-dimensional diffusions might be taking place at higher conversions of the fabricated foams. From the non-isothermal crystallization investigations, it can be concluded that CNC acts as a nucleating agent at lower loadings and gives hindrance to the chain folding of PLA at higher loading. Combined effects of porosity and CNC are mainly observed in thermal degradation studies whereas the effect of CNC is mainly observed in the crystallization studies. A detailed comparison between porous and non-porous PLA/CNC system is also included in this chapter.

Parts of this research work has received scientific recognition as follows:

1. Shasanka Sekhar Borkotoky, Prodyut Dhar and Vimal Katiyar. *"Biodegradable poly (lactic acid)/Cellulose nanocrystals (CNCs) composite microcellular foam: Effect of nanofillers on foam cellular morphology, thermal and wettability behavior."* International Journal of Biological Macromolecules 106 (2018): 433-446.

2. Shasanka Sekhar Borkotoky, Gourhari Chakraborty and Vimal Katiyar. *"Thermal degradation behavior and crystallization kinetics of poly (lactic acid) and cellulose nanocrystals (CNC) based microcellular composite foams."* International Journal of Biological Macromolecules 108 (2018): 1518-1531.

3.1 Introduction

The importance of bio-based and biodegradable porous polymers is growing day by day due to the generation of plastic waste, which in turn raises the ultimate disposal materials, carbon footprint, global warming etc. In this regard, porous materials have some very important properties such as high surface area, low thermal conductivity, lightweight, high permeability, low density etc. Foams can be prepared from all three types of materials e.g. metal, ceramic and elastomers. However, the use of elastomeric foam is tremendous in our daily life. The polymeric foams got attention in the market due to the demand for materials such as shock and sound absorbers, lightweight materials etc. Due to its huge demand in the above fields, the annual production of polymeric foams has a large share of the total polymer production in the world [27,160–162]. At present, the major market players for polymeric foams are the conventional non-degradable foams like polyurethane, polystyrene, polypropylene etc. However, due to the ultimate disposal problems of these non-degradable polymers, biodegradable polymeric foams can play a major role in the future. Recently, a handful of investigations have been reported in biodegradable poly (lactic acid) (PLA) foams. PLA foams can be a better replacement in green packaging to the non-degraded foams [163]. PLA foams have the potential to compete with conventional non-degradable petroleum-based foams like polyurethane, polystyrene etc. in some of the applications where degradability is a major area of concern [164]. Foam materials have to fulfill some requirements for the specific type of applications (biomedical applications, drug delivery etc.) including cell size, cell density and porosity. In recent investigations, it was observed that the melt strength of polymers is the most important parameter to fabricate desired foams [165,166]. PLA has poor melt strength, where some modifications need to be carried out for improved melt strength of PLA. The properties of the biodegradable PLA foams can be tuned by using various nanofillers, additives etc. Various properties of the degradable PLA foams may be improved by incorporation of clay

nano particles [167]. However, the addition of bionanofillers in the PLA foams has not been extensively investigated yet. The cellulose nanocrystals (CNC) are smart nanobiomaterials, which can be derived from natural resources [38,39,168]. It has the potential to be used in various applications like sensor, biomedical and pharmaceutical and in packaging industries [169,170]. CNCs has lots of advantages over other nanoparticles such as high surface area, high aspect ratio, non-toxicity, biodegradability and other optical properties [40]. In general studies, CNCs are used to improve various mechanical and barrier properties of various biopolymers [121].

The thermal degradation behavior of the polymeric foams is very important to investigate for their ultimate mode of application. It is observed in various literature that at high temperatures polymeric chains starts to separate and react with one another [171]. Researches are going on for the thermal degradation kinetics of polymeric foams. The thermal degradation kinetics of PLA foams have investigated by **GePu et al.** [172]. Thermal degradation investigations are very important to understand the thermal behavior and degradation mechanism of PLA foam and the product formed during degradation. Various factors affects the degradation of PLA such as molecular weight distribution, nanofillers, oligomers, monomers and catalyst [173]. From literature, it is observed that the main degradation products of PLA based foams are mainly cyclic oligomers, carbon monoxide, carbon dioxide, acetaldehyde, hydrocarbons and so on. The intensity of this product can vary with concentrations of nanofillers, catalyst and so on [7,174,175].

Crystallization of polymer is the process of formation of a particular array of polymer chains from a random state. Nucleation and crystal growth are the two major phenomena, which govern the crystallization process. The nano reinforcement materials acting as nucleating substance can alter the crystallization behavior of virgin polymer. Therefore, the rate of crystallization, the morphology of crystals of polymer composites sometimes gets affected

because of the presence of reinforcements, thus the property of the composites also changes. The efficiency of properties for biodegradable polymers like PLA is very much relied on the degree of crystallinity of the matrix. Therefore, investigation of crystallization kinetics is highly needed to understand the effect of the reinforcement on chain folding behavior. Non-isothermal and Isothermal crystallization kinetics study are the two general methods to study the polymer crystallization.

In our investigation, CNC nanobiofillers are used at different loadings in the foam matrix to investigate the effects on surface morphology and other properties of the foam. The effects of CNCs in PLA foam at different loadings in thermal properties have been investigated in this chapter. Dynamic mechanical analysis has been performed for the foamed samples to investigate the thermo-mechanical behavior of the fabricated foam both in tensile and compressed mode. The detailed wetting investigations have been performed in all the samples in foamed and compressed conditions to see the effects of CNCs in the surface morphologies on wetting. Wettability study is very important for various types of applications like coating, printing, waterproofing etc. We have performed both the static and dynamic contact angle studies of the fabricated foams. Contact angle hysteresis (CAH) has been investigated to see the effects of nano bio-fillers in wetting. The morphological changes, changes in density and porosity with CNCs loadings has also investigated in the current study. A linear model has been used to find the Young's contact angle and is compared with experimental values. The study has been conducted to develop an approach to fabricated biodegradable PLA foams in a cheap and comparatively easy way than the conventional techniques like solid-state foaming. The cell density and average cell size has been calculated by using FESEM micrographs. The thermal degradation kinetics behavior of the fabricated foams is thoroughly investigated by dynamic TGA studies at different heating rates. The activation energy (E_a) values of the fabricated foams are calculated using different approaches (Flynn-Wall-Ozawa (FWO),

Kissinger-Akahira-Sinuose (KAS), Friedman Augis-Bennet and Kissinger). Finally, the degradation mechanism of the fabricated PLA and PLA/CNC based foams are proposed by using Criado method and isothermal hyphenated TGA-FTIR investigations at two different conversions as suggested by the Criado plots. The crystallization kinetics of the fabricated foams are investigated thoroughly in this chapter. Different models for crystallization kinetics like Avrami, Tobin, Ozawa, Mo etc. have been utilized in this investigation. This chapter provides enough information on the thermal degradation kinetics, degradation mechanism along with product formed during degradation process and crystallization kinetics of the fabricated PLA and PLA/CNC based foams for their probable applications in fields like biomedical, packaging etc. The main objective of this chapter is to develop a biodegradable foam with improved properties for various useful applications so that the fabricated foam can be a possible green replacement to the conventional foams.

3.2 Results and discussions

In this section of the chapter, the results and observations obtained from various analytical methods is discussed along with probable scientific explanations.

3.2.1 Chemo-physical properties of foams

The average density of PLA granules is found to be 1.223 g/cm^3. However, in the case of nPLA foam, the density is found as 0.20±0.01 g/cm^3. The significant reduction in the density is mainly due to the leaching of porogen molecules with subsequently filling of spaces with air in the pores, which decreases the mass of the sample and ultimately affects the density. However, the density (**Table 3.1**) shows an increasing pattern with the addition of CNCs into the polymer matrix. The addition of CNCs in the matrix increases the number of cells in the matrix and hence influenced the ultimate density of the foam samples. The densities are found to be 0.22±0.01 g/cm^3, 0.23±0.01 g/cm^3 and 0.24±0.01 g/cm^3 for PLA/CNC 1, PLA/CNC 2 and PLA/CNC 3 respectively. It is essential to mention here that low density of foam is always

desirable for several applications like biomedical scaffold applications, drug delivery applications etc. This is a phenomenon that could be explained by FESEM images of the foams. The increase of the density of PLA based foams with CNC loading might be due to the effect of CNC in the PLA matrix which influences the mass of the foam [11]. The results of the weight analysis are shown in the table below. The volume expansion ratio (VER) of the fabricated foams (**Table 3.1**) are calculated by using the formula discussed in the previous chapter. The porosity (P) values are calculated as shown in **Table 3.2.**

Table 3.1 Weight analysis, density and expansion ratio of PLA/CNC-based foams.

Samples	**Dry weight (before leaching) (g)**	**Dry weight (after leaching) (g)**	**Avg. density (g/cc)**	**VER**	**Foam Type**
nPLA	34.6	2.8	0.20±0.02	6.05±0.38	Medium density
PLA/CNC 1	31	3.6	0.22±0.02	5.49±0.31	Medium density
PLA/CNC 2	34	3.8	0.23±0.02	5.21±0.30	Medium density
PLA/CNC 3	32	3.5	0.24±0.02	5.05±0.30	Medium density

Avg. density of the PLA granules is found to be 1.22±0.01 g/cc.

X-ray diffraction patterns of nPLA foams and PLA/CNC foams with different loadings are shown in **Fig. 3.1**. The sharp peak is observed at 16.6° and 19.1° that corresponds to the (1 0 1) and (1 1 0/2 0 0) planes of α-crystals in nPLA foam. In the case of CNC, two peaks corresponding to (1 1 0) and (2 0 0) plane are observed at 19.8° and 21.9°. In the case of PLA/CNC based foams, these peaks are found at 19.1° and 22.4° with 1% loading of CNCs. Peaks at 22.4° represent the presence of CNCs in the composite foams and indicate the existence of hydrogen bond type of interaction between PLA and CNC in nanocomposites foam

[121,176]. An increase in peak intensity is observed in PLA/CNC based foams while other parameters of experiments and XRD analysis are kept identical. The increase in peak intensity is due to the higher crystallinity, which may be due to the nucleating effect of CNCs within the PLA matrix. This is only possible when a good degree of polymer-filler interaction exists between the two. The crystallinity index (I_{Cr}) values are calculated from the XRD graph, where the crystallinity of the nPLA foam is measured as 42.9%. Further, with the increase in CNCs content, the crystallinity (%) are also increasing. Crystallinity (%) values of PLA/CNC 1, PLA/CNC 2 and PLA/CNC 3 are found to be 43.6%, 44.0% and 55.6% respectively. The crystallinity of the highly expanded foams is mainly occurred during processing of the material. The α-crystals are mainly dominant in the PLA foams. This affirms that the presence of CNCs in the matrix promotes nucleating sites, which causes the increase in crystallinity without changing the crystal structure.

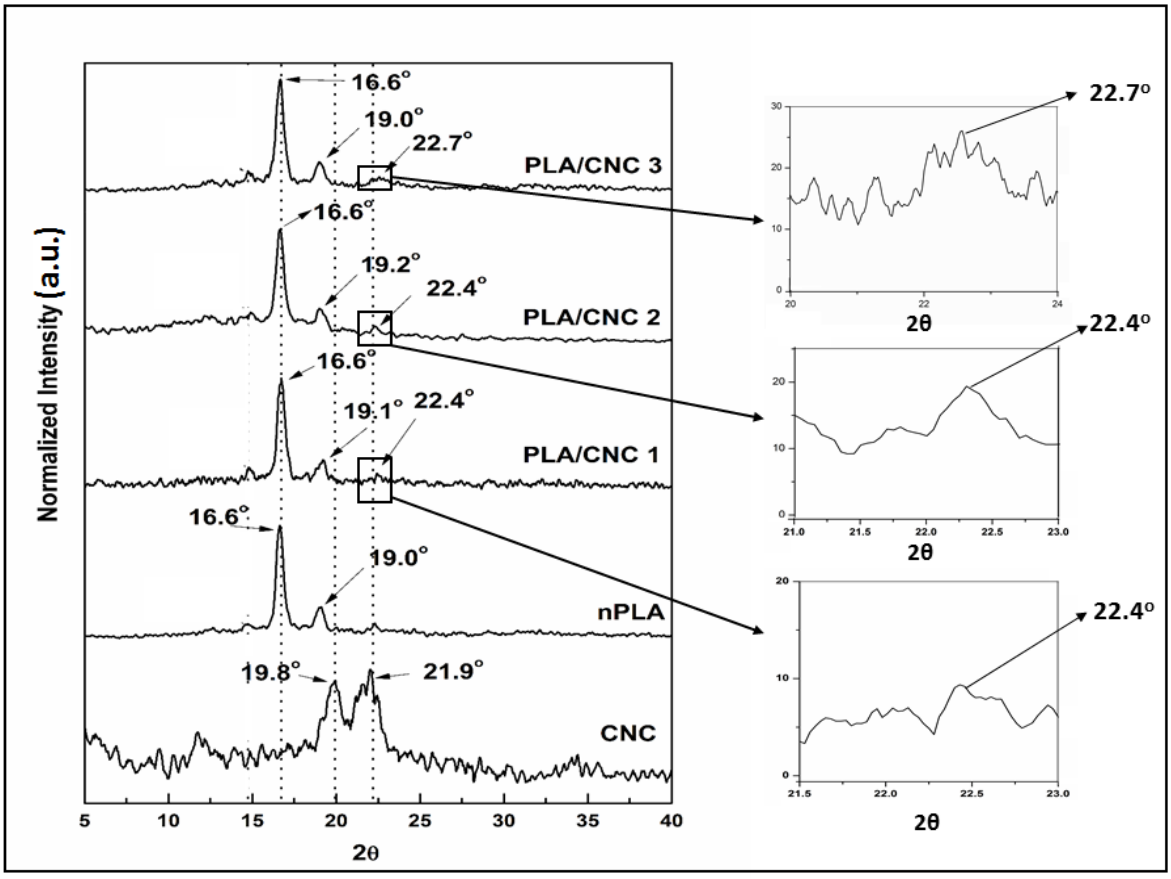

Fig. 3.1 XRD patterns of various samples of PLA and PLA/CNC-based foams.

Additionally, number average molecular weight (M_n), weight average molecular weight (M_w) and polydispersity index (PDI) values (**Table 3.2**) are calculated by using GPC system. It is observed that nPLA foam has a M_n and M_w value of ~124580 Da and ~219750 Da. The introduction of CNCs in the foam matrix has not affected the molecular weight values of the foam samples. No significant changes in molecular weight are observed in PLA/CNC 1, PLA/CNC 2 and PLA/CNC 3 foam samples. The PDI values are observed in the range of ~1.74 to ~1.76 for the foam samples.

Table 3.2 TGA, Porosity and molecular weight investigations of PLA/CNC-based foam.

Sample	**TGA Analysis**			**Porosity (%)**	**GPC Analysis**		
	T_{onset} (°C)	T_{max} (°C)	T_{90} (°C)	**(P)**	M_n (Da)	M_w (Da)	PDI
nPLA	359.7°	376.4°	385.9°	83.4±1.2	124580	219750	1.76
PLA/CNC 1	353.0°	372.3°	381.9°	81.7±1.0	125760	215560	1.71
PLA/CNC 2	360.1°	378.0°	385.5°	80.7±1.3	126990	223140	1.76
PLA/CNC 3	352.3°	373.7°	383.4°	80.1±1.0	125200	217330	1.74

From the FTIR spectrum (**Fig. 3.2**), distinct characteristic FTIR peaks are observed around ~866 cm^{-1}, ~1073 cm^{-1}, ~1454 cm^{-1}, ~1742 cm^{-1} and 2926 cm^{-1} corresponding to –C–O–C– bond stretching, $–CH_3$ asymmetric vibrations, –CH bending vibrations, –C=O vibrations and $–CH_3$ symmetric vibrations respectively for nPLA foam. The characteristic peaks of sucrose are present in lower wavenumbers. The peak at 908 cm^{-1} attributed to –C–O stretching vibrations of sucrose. Peaks around ~1300 cm^{-1} and ~1400 cm^{-1} attributed to the bending vibrations of –OH group and bending vibrations of C–H group of sucrose respectively. The peaks observed

at 3380 cm^{-1} and 3556 cm^{-1} attributes to the stretching vibrations of –OH group of sucrose [177]. For the case of CNCs, peak at 2908 cm^{-1} represents the –CH stretching band, peaks around ~1163 cm^{-1} represents the C-O-C stretching in β-1,4- D glycosidic linkage present in CNCs and peaks at ~1427 cm^{-1} represents the symmetric $–CH_2$ bending peak. The prominent peaks of ~908 cm^{-1} for –C-O stretching vibrations and ~3556 cm^{-1} for stretching vibrations of –OH of sucrose are not present in other samples. A broad peak at around ~3500 cm^{-1} in all the PLA/CNC foamed samples represents the –OH functional groups. This peak indicates the formation of strong intra or intermolecular hydrogen bond of CNCs with the PLA matrix. The presence of peaks near ~1750 cm^{-1} in all the nanocomposite foams indicates the presence of free –C=O groups. Similarly, the peaks around ~1450 cm^{-1} and ~2940 cm^{-1} in all the nanocomposites represents the symmetric $–CH_2$ bending and stretching vibrations, respectively [40,121,176].

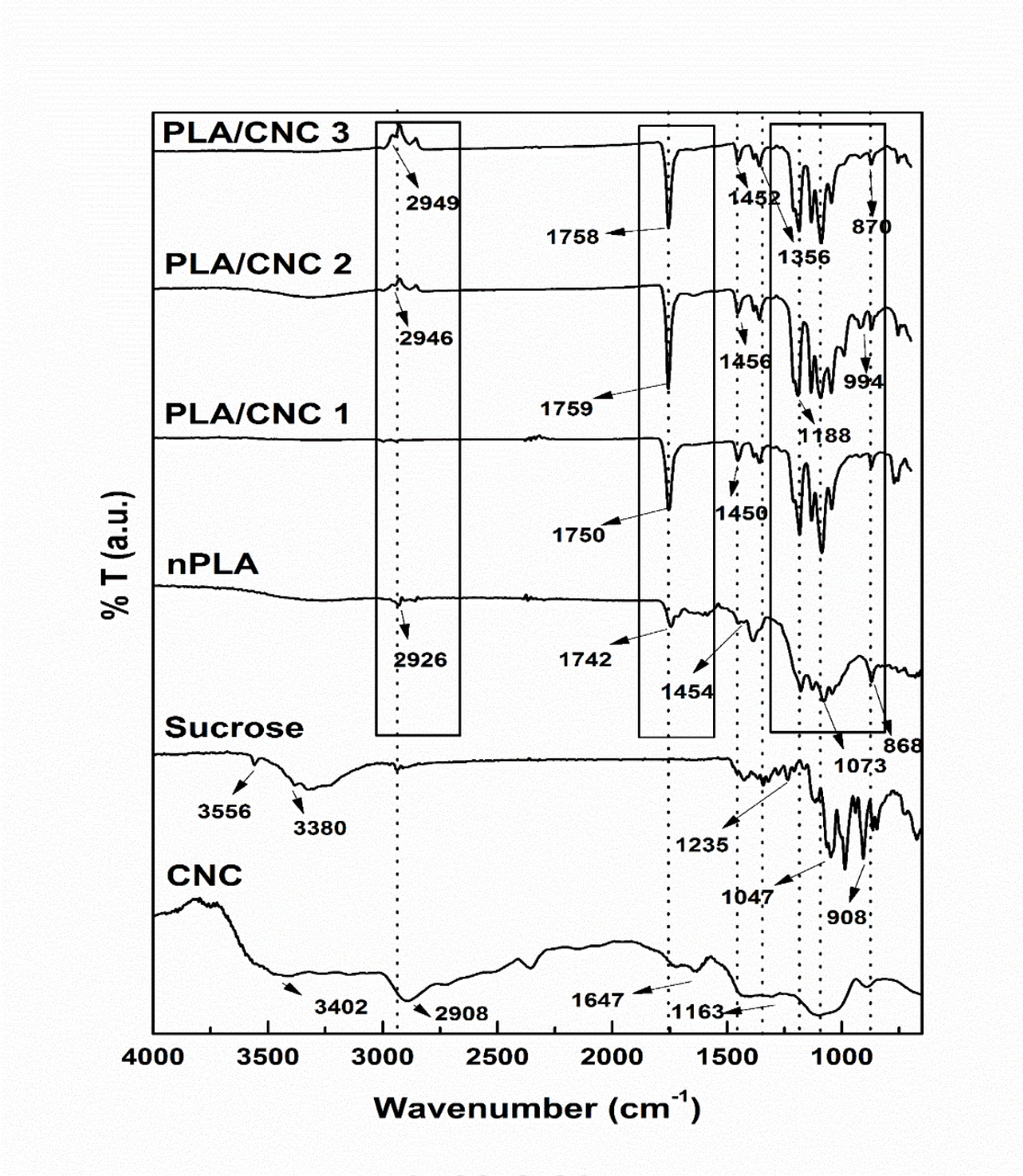

Fig. 3.2 FTIR spectrum of the CNC, sucrose, PLA and PLA/CNC-based foams.

3.2.2 Thermal properties of PLA/CNC-based foams

Thermogravimetric analysis (TGA) (**Fig. 3.3**) is used to determine the onset degradation (T_{onset}), maximum degradation (T_{max}) and temperatures at which 90% reduction of weight occurs (T_{90}) of nPLA and PLA/CNC based foams (**Table 3.2)**. In case of nPLA foam, the onset

degradation is found to be ~ 359.8 °C and T_{max} of ~376.48 °C, which is due to hydrolysis, and oxidative chain scissions of PLA chains present in the matrix [178]. All the graphs show a single step degradation of foams. The introduction of CNC did not show any significant improvement in the thermal properties of the foam. In the case of PLA/CNC 1 the T_{onset} value slightly decreases (~5 °C) to a value of 353.1 °C compared to PLA. The DTG plot (**Fig. 3.3**) suggests the maximum degradation temperature (T_{max}). The T_{max} value also decreases (~4 °C) compared to the neat counterpart. However, in case of PLA/CNC 2, a comparable value of T_{onset}, T_{max} is found in regards to PLA, which may be due to the uniform dispersion of CNCs in the matrix compared to PLA/CNC 1. At higher loading of CNC (PLA/CNC 3) the T_{onset} and T_{max} values decrease (~7 °C for T_{onset} and ~3 °C for T_{max}) than neat PLA counterpart. It is observed that CNC enhances the degradation of PLA and hence effects the thermostability [121] of the fabricated foam.

Non-isothermal melt crystallization behavior of nPLA and PLA/CNC foams are investigated at a heating rate of 10 °C/min by using Differential scanning calorimetry (DSC) analysis under inert atmosphere (**Fig. 3.4**). For the analysis, DSC second heating thermographs of nPLA and PLA/CNC foams are considered. The single peak in the melting region indicates a homogeneous distribution of crystals in an ordered arrangement. However, the addition of CNC into the matrix is not affecting much in the melting point of the foams as seen from the endothermic peak for PLA/CNC 1, PLA/CNC 2 and PLA/CNC 3. At higher temperatures, the peak indicates the melting of the perfect crystals [179]. From the thermographs, it was observed that in the case of nPLA foam, the T_g was at 61.4 °C. Temperature of crystallization (T_c) value for all the samples are found near ~110 °C, indicating that CNCs has no significant effect in T_c. The T_g value of the PLA foam was not changing much on the incorporation of the CNC which indicates that there is no formation of short-chain PLA molecules. Single T_g values are found in all the samples which indicate the good compatibility of CNC in the PLA matrix.

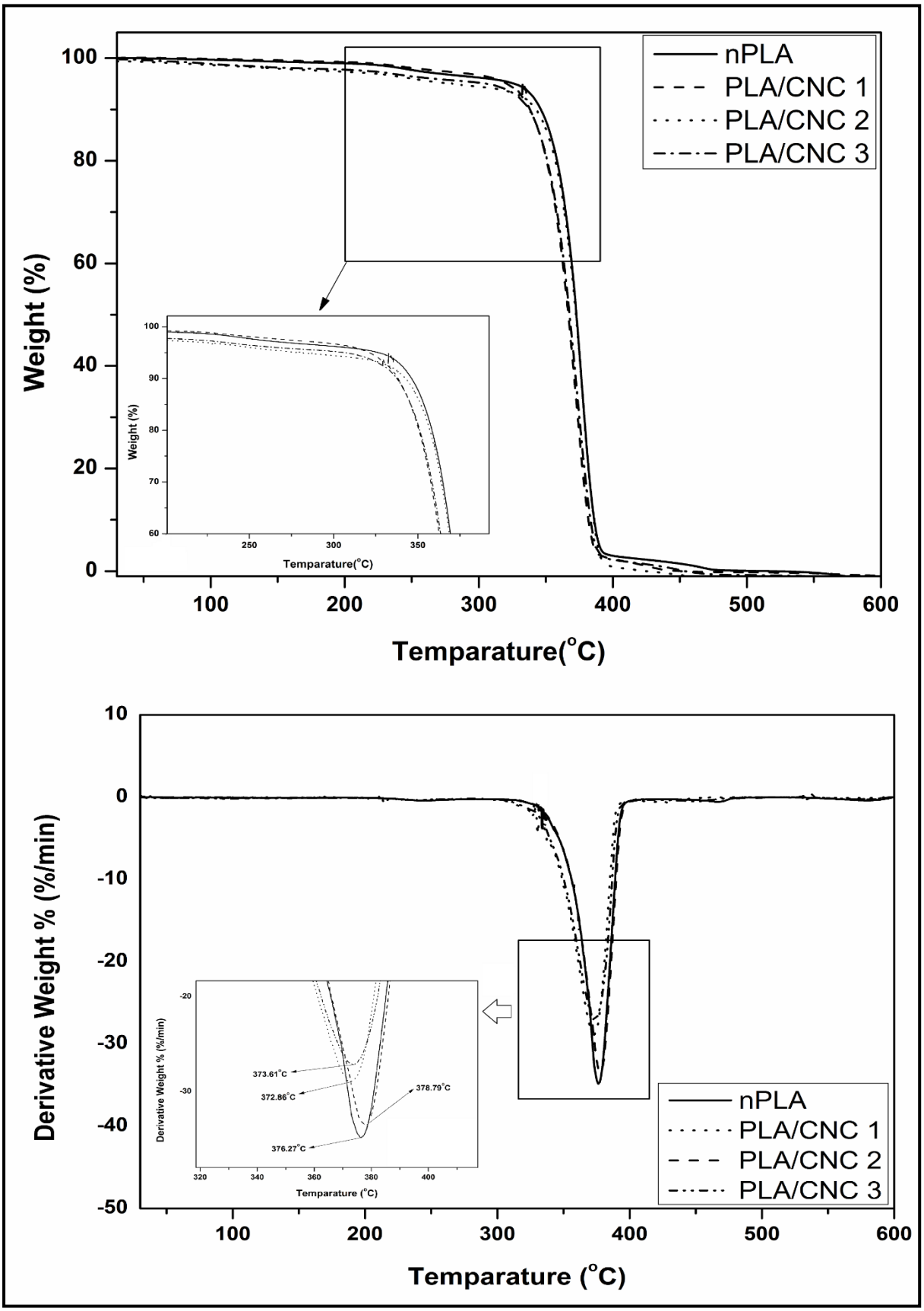

Fig. 3.3 TGA and DTG curves for PLA and PLA/CNC-based foams.

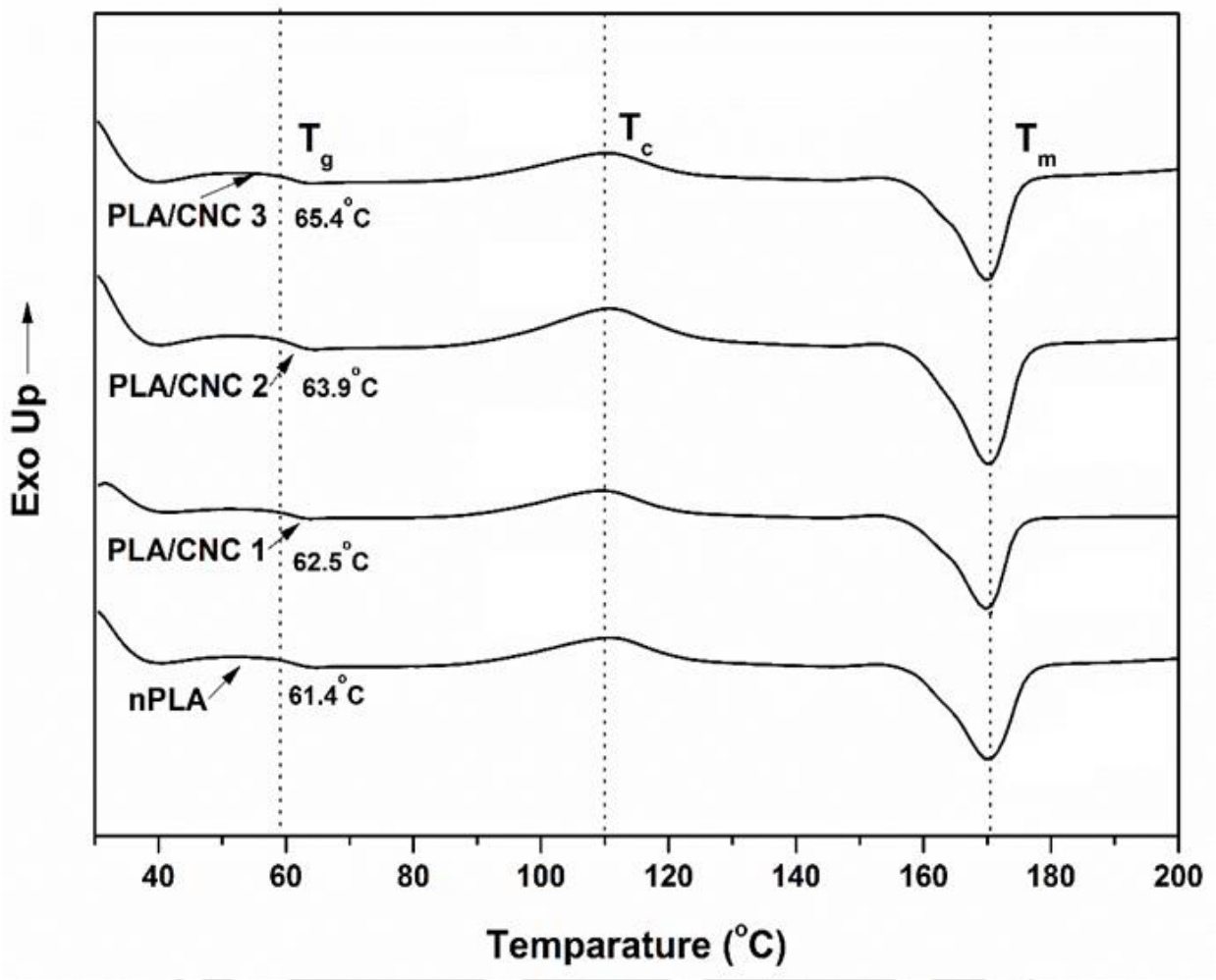

Fig. 3.4 DSC thermographs PLA and PLA/CNC-based foams.

3.2.3 Characterization of the gaseous products evolved using TGA-FTIR hyphenated system

To understand the thermal decomposition behavior of the fabricated foams, the generated gaseous products from TGA are analyzed by hyphenated TGA-FTIR system for nPLA and PLA/CNC 3 foams. The 3-D graphs of the samples in a dynamic temperature range of 30 ºC-700 ºC are shown in **Fig. 3.5**. The weight loss observed from the graph is similar for all the samples and a single step degradation pattern is observed for all the samples as discussed earlier. The evolution of various gaseous products is observed beyond ~300 ºC. The main degradation of PLA/CNC foam is observed in a temperature range of ~320 ºC-~450 ºC with

two prominent peaks, representing cyclic oligomers (~1790 cm^{-1}) and carbon dioxide (CO_2) (~2350 cm^{-1}). The FTIR peaks corresponding to various degradation temperatures (with ~20 °C increments) are shown (from ~300 ^oC to ~400 ^oC) in **Fig. 3.6**. The intensities of the peaks of degraded products are found to be highest at T_{max} for the samples, which indicates that decomposition of PLA is maximum at that temperature. The main degraded products obtained from the nPLA and PLA/CNC 3 foam are identified as water (H_2O) (~3577 cm^{-1}), hydrocarbons (HC) (~2952 cm^{-1} and ~3010 cm^{-1}), carbon dioxide (CO_2) (~2350 cm^{-1}), carbon monoxide (CO) (~2180 cm^{-1} and ~2106 cm^{-1}) and cyclic oligomers or lactides (~1790 cm^{-1}) [124,180,181]. Other noticeable FTIR peaks include -CH- stretching (~1377 cm^{-1}), -C=O- stretching (~1240 cm^{-1}), -C-O- stretching (~1100 cm^{-1}) and -C-C- stretching (~930 cm^{-1}).

The prominent peak of oligomers is generated around ~340 °C and vanishes after ~400 °C, which indicates that maximum decomposition of foam is happening at this temperature range for the samples. Carbon dioxide (CO_2) is generated beyond 360 °C corresponds to the chain hemolysis of PLA [180]. Formation of carbon monoxide might be due to some extent of decomposition of hydroxyl end initiated ester and the reduction of peak intensity after ~380 °C might be due to the insignificant effect of hydroxyl end initiated ester decomposition [124,182]. The main degraded products of nPLA and PLA/CNC foam are same and they follow the same pattern of degradation, hence it can be concluded that the incorporation of the CNC fillers in small loadings does not alter the main degradation products of the foam.

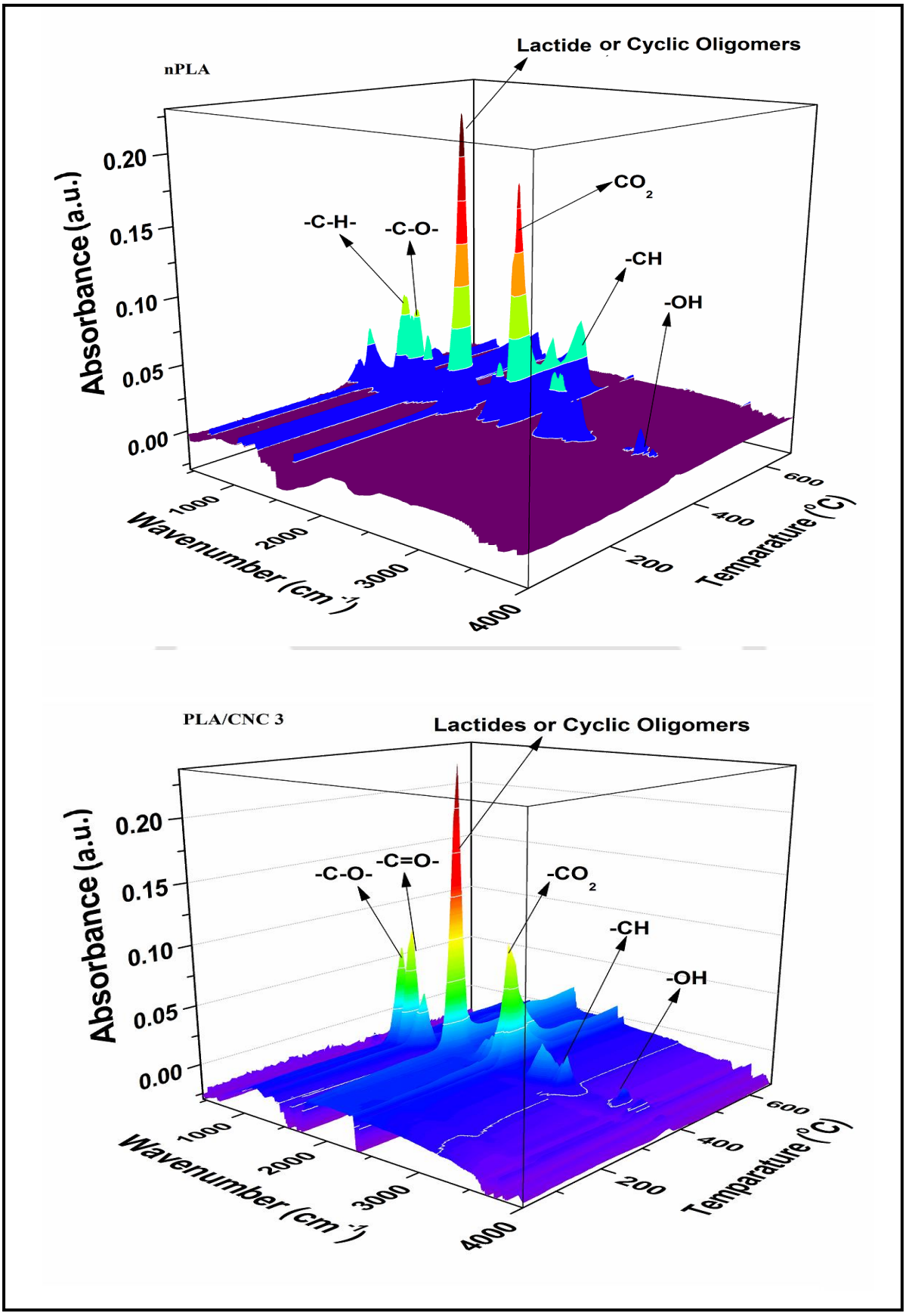

Fig. 3.5 3D curves of TGA-FTIR hyphenated system of nPLA and PLA/CNC 3 foam.

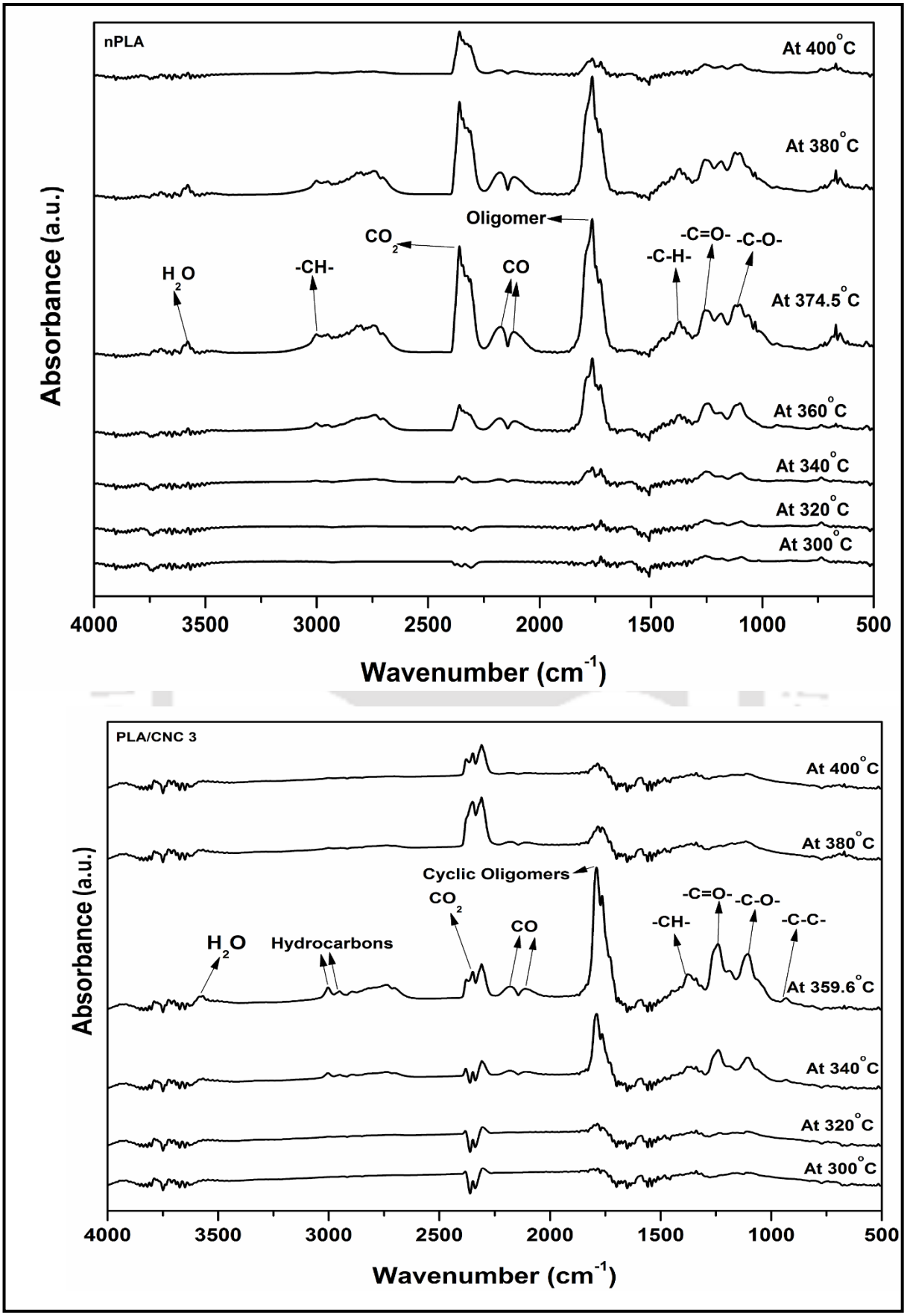

Fig. 3.6 FTIR spectra of various gaseous products evolved in nPLA and PLA/CNC 3 foam.

3.2.4 Thermo-mechanical analysis

The dynamic mechanical response of the various foams as a function of temperature in terms of storage modulus (E') and loss modulus (E") in compression and tensile mode of analysis are shown in **Fig. 3.7**. The influence of the CNC on the thermos-mechanical behavior in terms of E' and E" are investigated. In the compressive mode, it is observed that on the introduction of CNCs in the foam matrix, the E' values increases by ~1.5 times for PLA/CNC 3 compared to nPLA foam. The increase in E' with CNCs concentration might be due to the formation of cross-linked structure, crystallinity (more ordered regions developed) and better dispersion of CNC in the PLA matrix which leads to better adhesion of CNC. It is observed that no effect of parameters until the onset of the softening of the foam. After 55 ^{o}C, there is a sudden increase in the value of storage modulus in all the samples is noticed, which is due to the sudden densification of the foams in the onset of glass transition temperature (T_g) of the foam [78]. In case of E" curve also similar phenomenon is observed.

It is observed from the curve that in the tensile mode, the storage modulus values of the foams increase with the increase in filler concentration (~2.5-fold increase in PLA/CNC 3 compared to nPLA foam), which can be supported by crystallinity values as discussed above in subsequent section. The CNC are uniformly dispersed in the PLA matrix which leads to the formation of more ordered crystalline regions in the matrix and leads to the effective transfer of CNC modulus to the PLA matrix which might be the reason of increasing values of E' which is accompanied by the values of E".

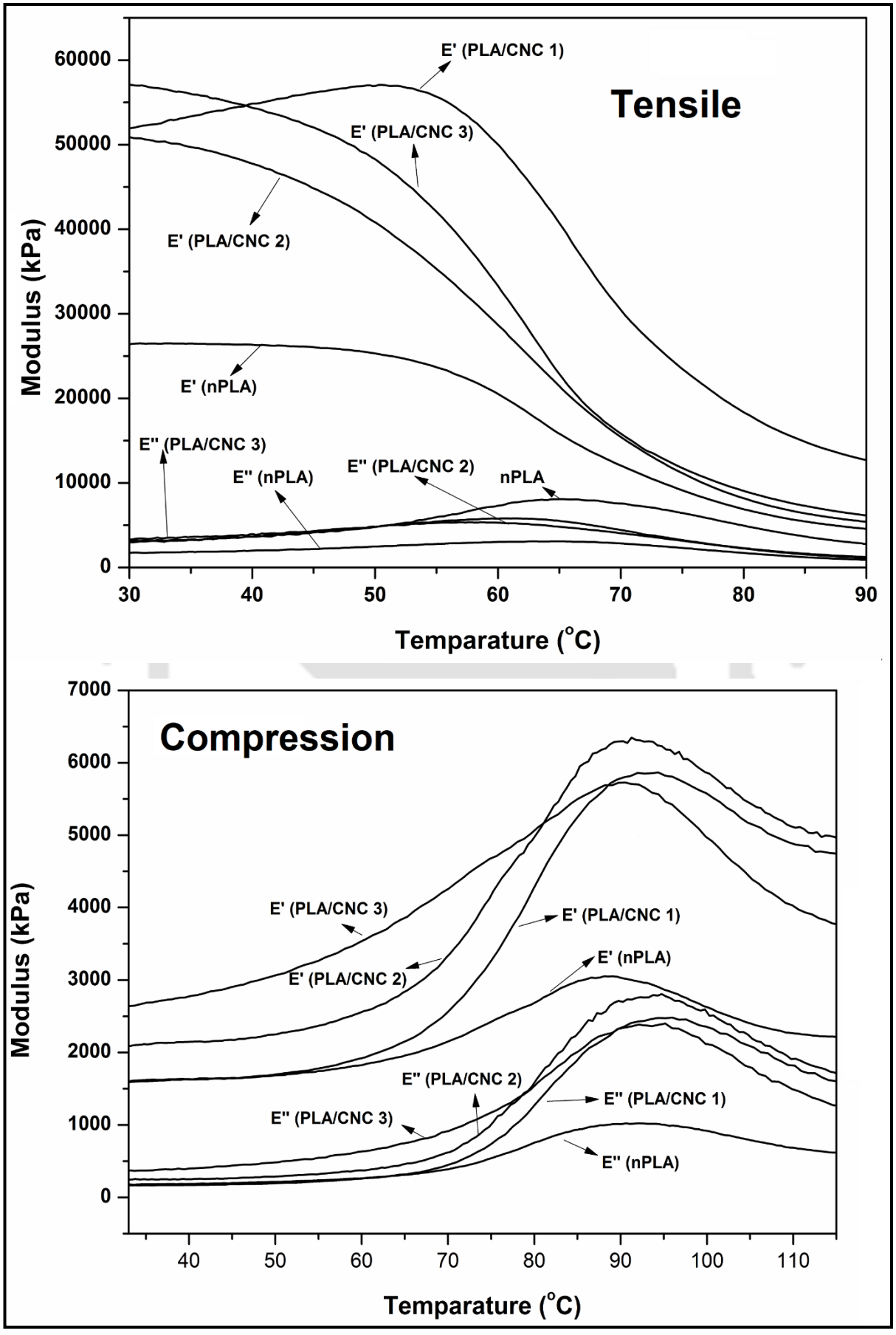

Fig. 3.7 E' and E'' values of the foam by DMA (tensile and compressive mode).

3.2.5 Wettability studies of PLA based foams

Wettability investigations are carried out by using contact angle analysis (**Fig 3.8**). The static contact angle for nPLA is found to be 127.0°±3.2°, which indicates the hydrophobic nature of the foam surface. The hydrophobic nature of the foam surface might be due to the surface texture. To understand the wetting phenomenon, we have analyzed the wettability of the compressed foam, foamed surfaces are compressed to investigate the effect of surface morphology in the contact angle. Due to which the foamed structure is collapsed and a smooth surface is obtained. From the results (**Table 3.3**) it can be concluded that the contact angles are decreased to a large extent (~53˚) in case of nPLA, which is due to the absence of the effects of foamed morphology. The static contact angle decreased to (~60°) in case of PLA/CNC based foams due to the possible rearrangement of CNC fillers in the PLA matrix, which is possibly due to the combined effects of PLA and CNCs present on the surface.

Table 3.3. Static contact angle values of PLA and PLA/CNC-based foams.

Samples	Static Contact Angle (Surface with texture)	Static Contact Angle (Compressed surface without texture)
nPLA	127.0°±3.2°	74.1°±2.1°
PLA/CNC 1	131.0°±2.4°	75.0°±2.1°
PLA/CNC 2	138.0°±1.8°	77.0°±1.1°
PLA/CNC 3	140.0°±1.5°	80.0°±2.2°

It is also found from the studies that on increasing the concentration of CNC, the contact angle increases to 140.0°±1.5° in case of PLA/CNC 3. The dispersion of nanobiofillers alters the surface morphology affecting the wettability of the foams. The better dispersion of the nanobiofillers in the matrix generates more pores in the sample, which ultimately gives a comparative uniform, and smaller pores (~1.79±0.31 µm). The introduction of CNC increases

a total number of pores, which affects the contact angle as the contact angle is depending on the surface morphology and roughness. However, higher contact angles are observed in rougher surfaces [183]. All the values of contact angles are measured and it is observed that all the surfaces act similarly in wetting phenomena. From the study, we can conclude that the higher angles present in the foamed structure are due to the effects of surface morphology and texture along with the combined effects of PLA and CNC present in it. Due to the collapse of the foamed structure, we observe a similar trend in wettability. Therefore, the previously made assumption on the effect of surface texture and morphology of foam on its wettability property can be justified here. To understand more into the reason behind such behavior, we have made a rigorous study on the dynamic contact angles of the PLA foam and its nanocomposites in the next section of the linear model.

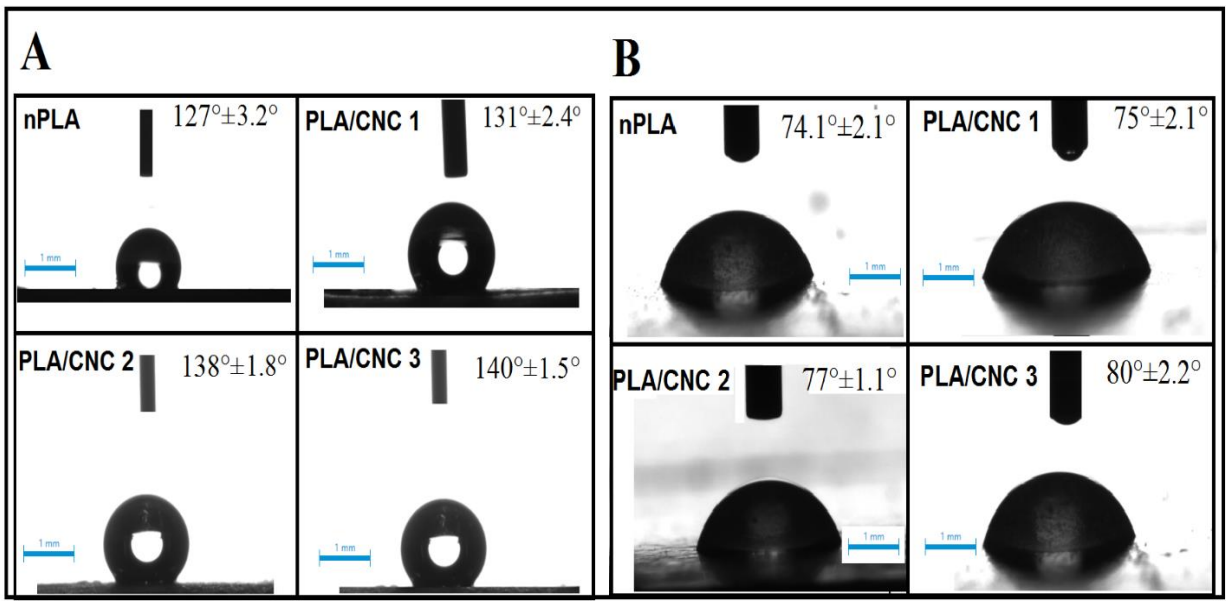

Fig. 3.8 Static contact angle values of PLA and PLA/CNC based foams in A) surface with texture, B) surface without texture (compressed surface).

3.2.5.1 Comparison between experimental and predicted values of Young's contact angle

The linear modeling of the dynamic contact angle in all the foam samples are carried out to evaluate the concept behind the effect of CNC onto the PLA foams **(Fig. 3.9)**. The advancing contact angle and receding contact angle values are calculated from both experimental and as

predicted by the linear model **(Table 3.4)** at 27 °C. The advancing and receding contact angles strongly suggest the applicability of this model in the studied system of PLA/CNC 2, which may be due to more numbers of pores generated and the dispersion of CNC on the foam surface. The slope (k) values for the curves ($\theta_{adv} - H$) and hysteresis (H) values are shown in **Table 3.5**. The CNCs has no such significant effect on advancing and receding contact angle of the fabricated foams.

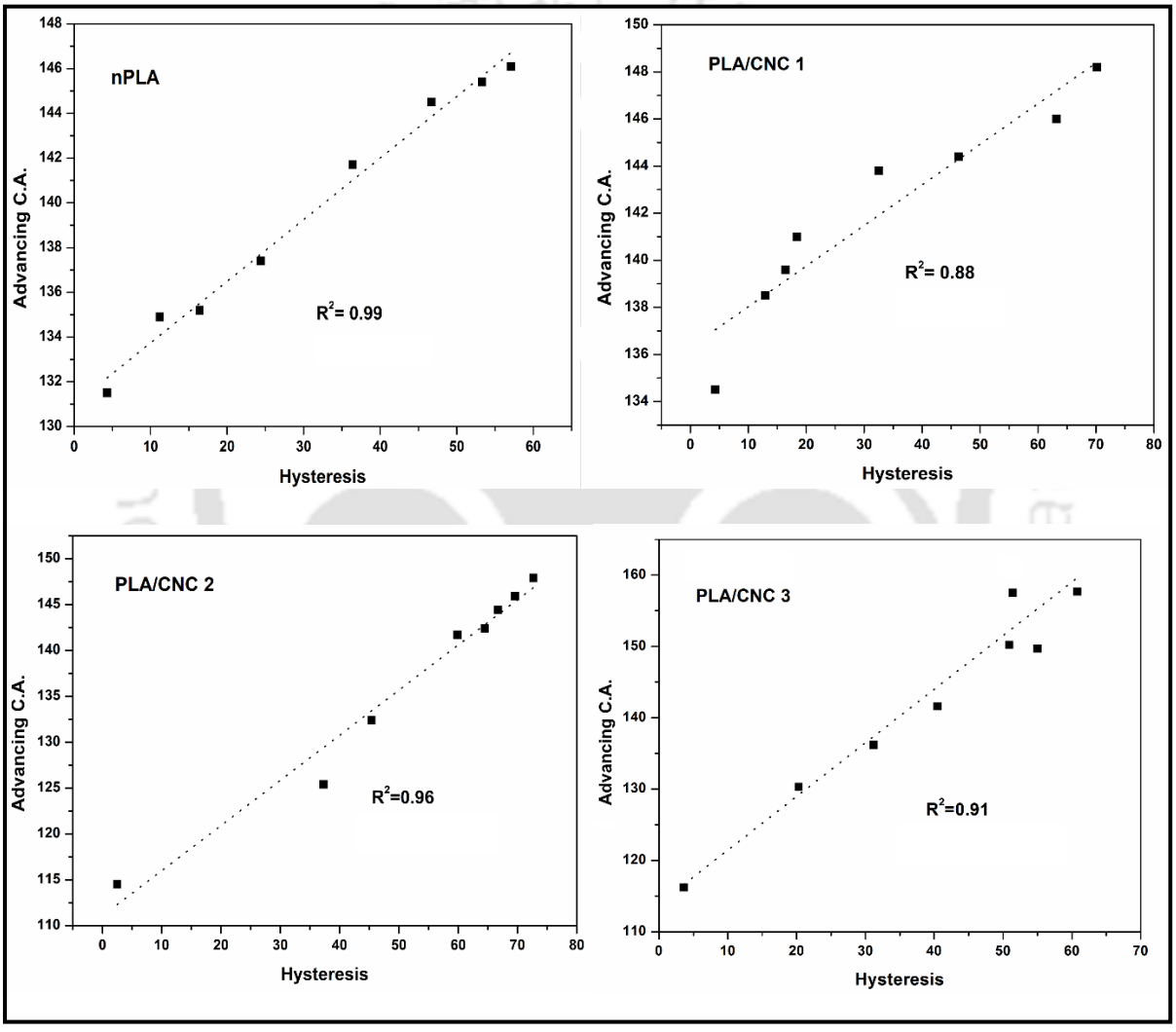

Fig. 3.9. Advancing C.A. vs. Hysteresis for PLA and PLA/CNC-based foams.

Young's contact angles are calculated for all the samples of PLA/CNC foams along with nPLA foam. In the case of PLA/CNC 1, the regression value is 0.88, which means the model slightly

deviates from linearity. In the case of PLA/CNC 2, the model has strong applicability than the other samples (regression value 0.96). Higher loading of CNCs may lead to some agglomeration effecting the overall state of nanofiller dispersion within its polymer matrix. Nevertheless, it is understandable from the analysis that the hydrophobic nature of a polymeric foam is greatly determined by the surface topography, which again is dictated by the incorporated nature of bionanofillers. Young's contact angle from both experimental and predicted by the linear model is tabulated in **Table 3.6.**

Table 3.4 The experimental and predicted values of advancing and receding contact angles.

Samples (foamed)	**Advancing Contact Angle**		**Receding Contact Angle**	
	Experimental	**Predicted**	**Experimental**	**Predicted**
nPLA	139.5°±5.1°	131.12°±4.2°	108.3°±13.6°	100.0°±9.8°
PLA/CNC 1	142.0°±4.1°	129.5°±3.9°	108.9°±18.9°	96.4°±11.6°
PLA/CNC 2	136.8°±10.9°	134.2°±6.2°	84.5°±11.3°	81.8°±7.5°
PLA/CNC 3	144.3°±13.8°	152.1°±8.9°	103.8°±5.8°	111.6°±8.8°

Table 3.5 The value of slope (k) from the graph ($\theta_{adv} - H$) and hysteresis (H= $\theta_{adv} - \theta_{rec}$)

Samples	**Slope (k)**	**Hysteresis (H)**
nPLA	0.27	31.2°±3.3°
PLA/CNC 1	0.17	33.0°±2.9°
PLA/CNC 2	0.49	52.3°±4.9°
PLA/CNC 3	0.75	40.5°±3.7°

Table 3.6 Young's contact angle values (experimental vs predicted)

Samples	Young's C.A. (experimental)	Young's C.A. (predicted)
nPLA	122.5°±7.8°	114.5°±6.6°
PLA/CNC 1	123.8°±9.9°	112.0°±8.5°
PLA/CNC 2	108.4°±8.0°	106.1°±6.8
PLA/CNC 3	121.7°±6.5°	128.7°±6.0

It can be observed from the table that in the case of PLA/CNC 2, the linear model is more accurate compared to other cases.

3.2.6 Morphological studies

The morphology of the PLA based foams can be observed from FESEM micrographs (**Fig. 3.10**). From the FESEM it is confirmed the presence of open cells in all types of foams. The CNCs having dimensions ranging from ~500 nm to ~600 nm in length and ~70 nm to ~98 nm in diameter are shown from FESEM images (**Fig. 3.11**). In case of CNC based foams, the dispersion of needle-like CNC in the foam matrix is clearly visible in the cross-sectional views of PLA/CNC-based foam micrographs at different magnifications (**Fig. 3.12**) with porous foam structure observed in all samples. The foam samples are highly dominated by open cell interconnected structures.

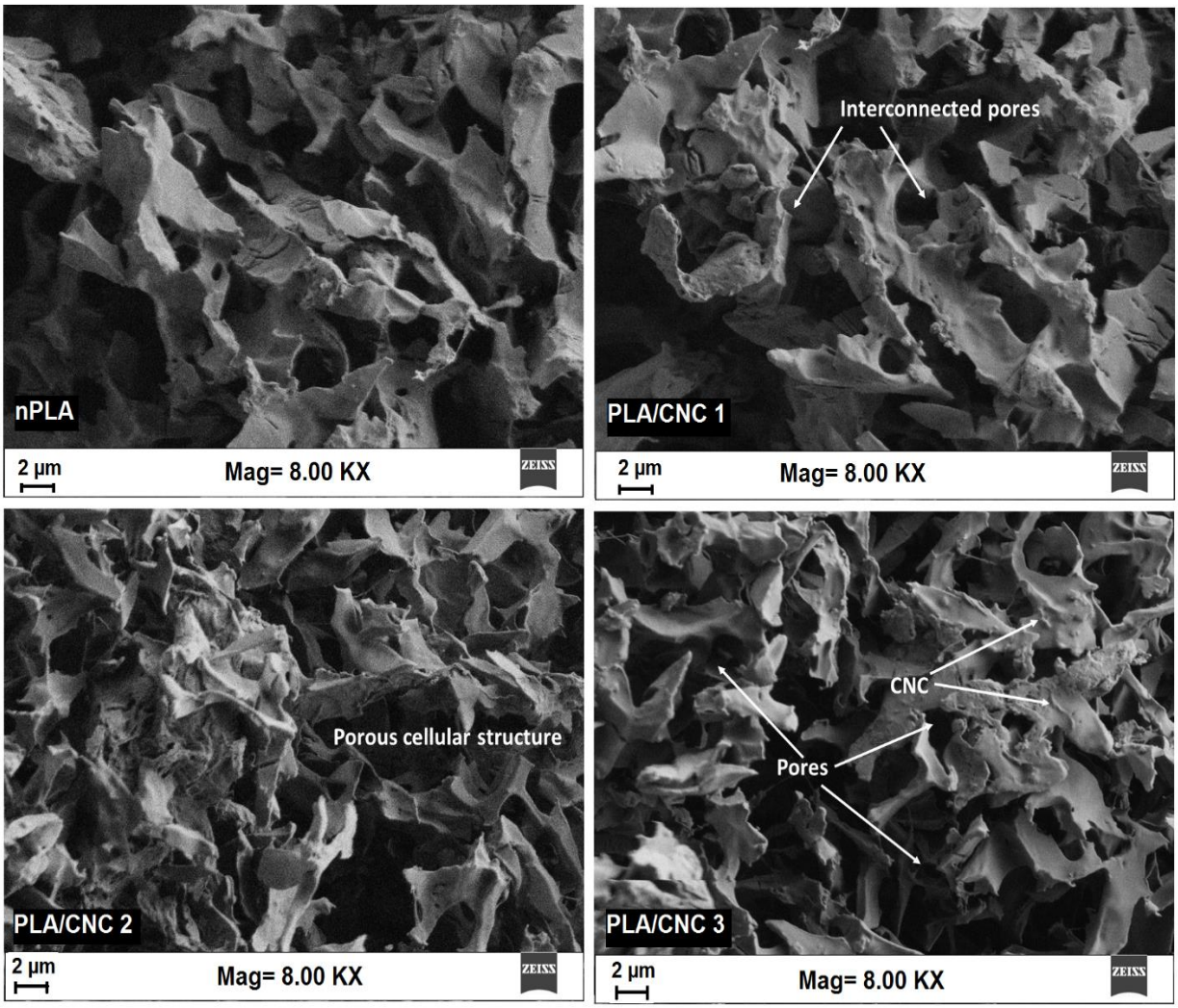

Fig. 3.10 FESEM image of nPLA and PLA/CNC-based microcellular foam.

The cell density and average cell size are calculated in all the foam samples **(Fig. 3.13)**. In case of nPLA foam, the cell density (N_f) is found to be 2.1×10^8 cells/cm^3 with an average pore diameter of 2.8±1.3 µm. In the case of PLA/CNC 1, the cell density is found to be 3.0×10^8 cells/cm^3 and the average cell diameter is found to be 1.04±0.43 µm. The cell density of PLA/CNC 2 is calculated as 2.7×10^8 cells/cm^3 with an average diameter of cells as 1.5±0.54 µm. The cell density increases to a value of 2.9×10^8 cells/cm^3 with an average cell diameter of 1.81±0.61 µm in the case of PLA/CNC 3. The value of cell density is increased than the value of nPLA foam, which might be due to the formation of more number of nucleating sites by the

nanobiofiller results in the formation of more number of cells in the foam matrix. The reason for the observed increasing pore numbers is associated with reduced average pore size on the incorporation of CNC into the PLA matrix could be attributed to the nucleating effect of the nanobiofiller [24,27,29]

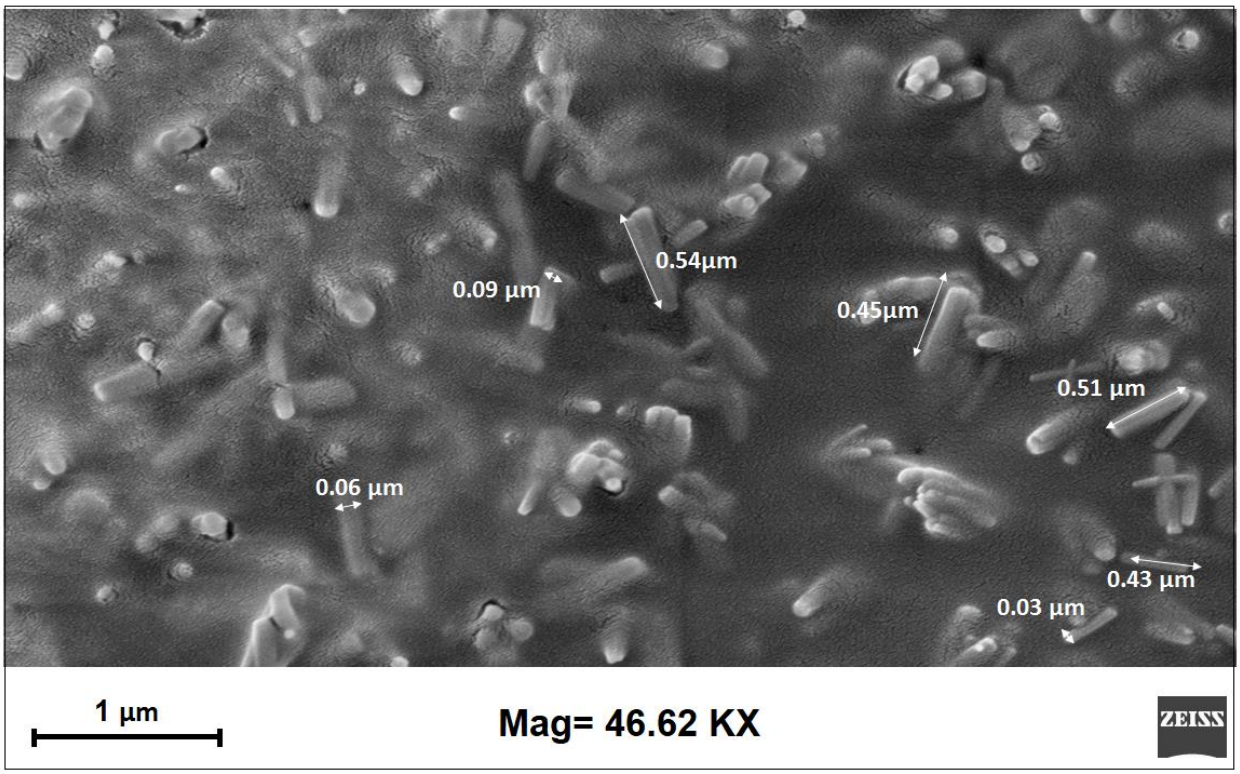

Fig. 3.11 FESEM image of fabricated CNC.

The average particle size of the sugar (finely grinded) before dispersed in the solvent is analyzed by a polarized optical microscope (POM) (**Fig. 3.14**). The average particle size (diameter) is calculated by measuring particle size at different locations of the micrograph and averaging the values. The average particle size (diameter) is found to be 1.23±0.45 µm. The sucrose particles are then dispersed in the solvent for fabrication of foams.

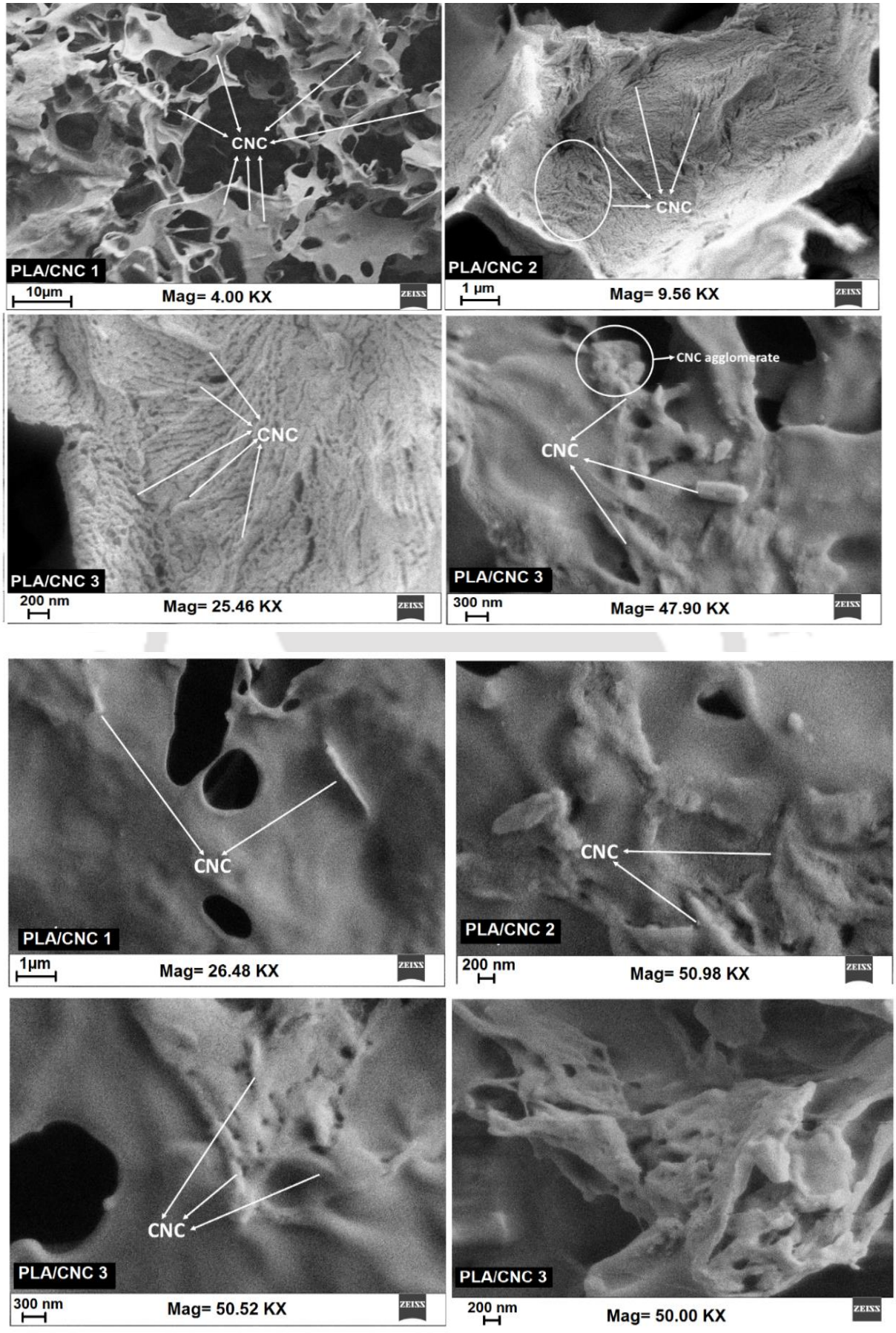

Fig. 3.12 CNC nanofiller in PLA/CNC based microcellular foams at different magnification.

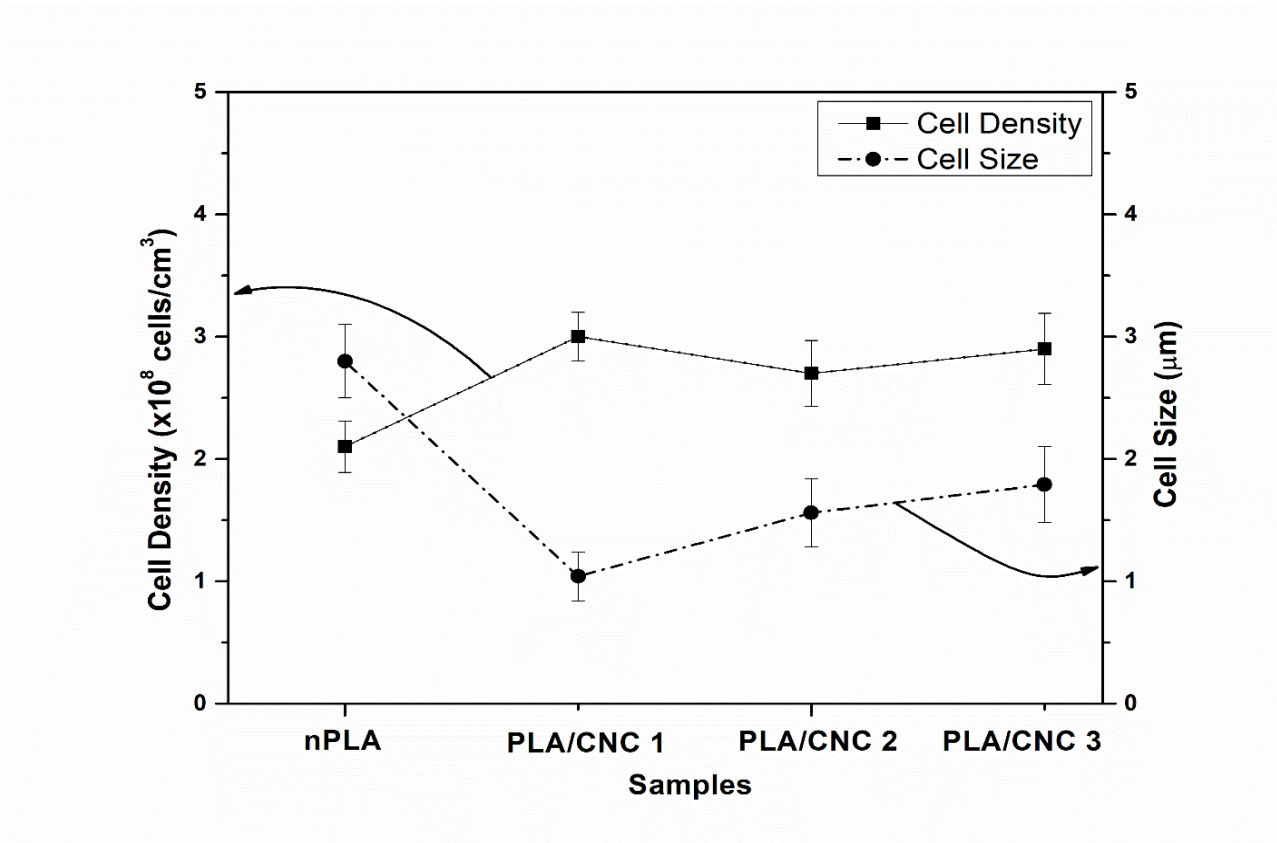

Fig. 3.13 Cell density, average cell size and volume expansion ratio of foams at different concentrations of CNC.

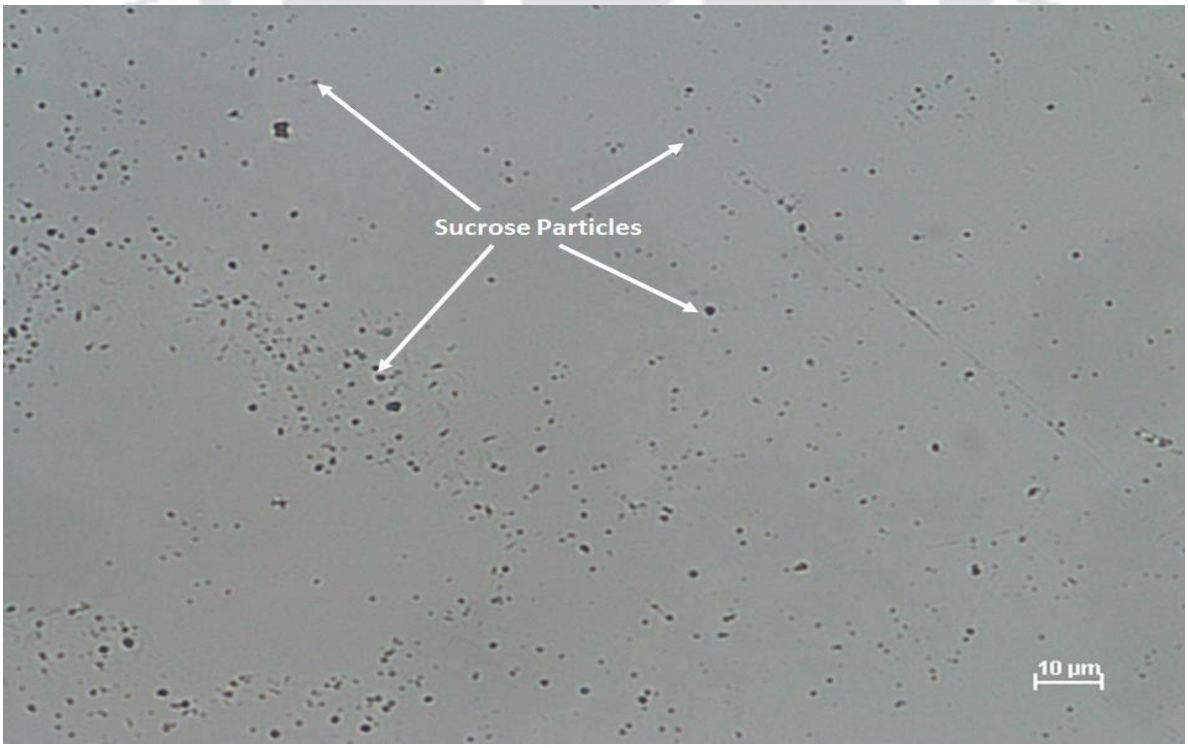

Fig. 3.14 POM images of sucrose particles before dispersed in the solvent.

3.3 Dynamic thermal degradation studies of PLA and PLA/CNC based foams

Thermogravimetric analysis (TGA) and DTG plots of the PLA and PLA/CNC based fabricated foams are shown in **Fig. 3.15**. The dynamic TGA analysis is performed at four different heating rates (5 °C/min, 10 °C/min, 15 °C/min and 20 °C/min). The thermal degradation investigations of the PLA and PLA/CNC based foams are carried out by using different "model-free" and "modelistic" approaches.

Friedman plots are shown in **Fig. 3.16.** The model is more suitable at higher conversion values as observed from the result. At lower conversion values, the method is deviating from linearity. We have calculated the apparent activation energy values from this model and the values are found to be ~201.0 kJ/mol, ~205.1 kJ/mol, ~198.2 kJ/mol and ~195.3 kJ.mol for nPLA, PLA/CNC 1, PLA/CNC 2 and PLA/CNC 3 respectively.

FWO plots for the PLA and PLA/CNC based fabricated foams are shown in **Fig. 3.17** parallel straight lines are observed at different conversions for all the foams. The parallel lines observed in each conversion ranging from α=0.1 to 0.9 for every sample indicates the suitability of the FWO model to our system. The slopes of the straight lines increase with an increase in the conversion after α=0.4. The calculated activation energy (E_a) values are tabulated in **Table 3.7.** In the case of nPLA foam, the apparent activation energy is observed as ~174.8 kJ/mol and a similar value is observed earlier [184]. The activation energy is almost similar till α=0.4 which indicates the less energy requirement for bond breaking at the initial level of conversions and also indicates the breakage of a similar type of bonds [185]. After $\alpha \geq 0.5$ an increase in activation energy is observed in nPLA foam. This indicated that the thermal decomposition of the nPLA foam follows a complex mechanism that may include random scission, depolymerization, diffusion, inter and intramolecular esterification and so on [186].

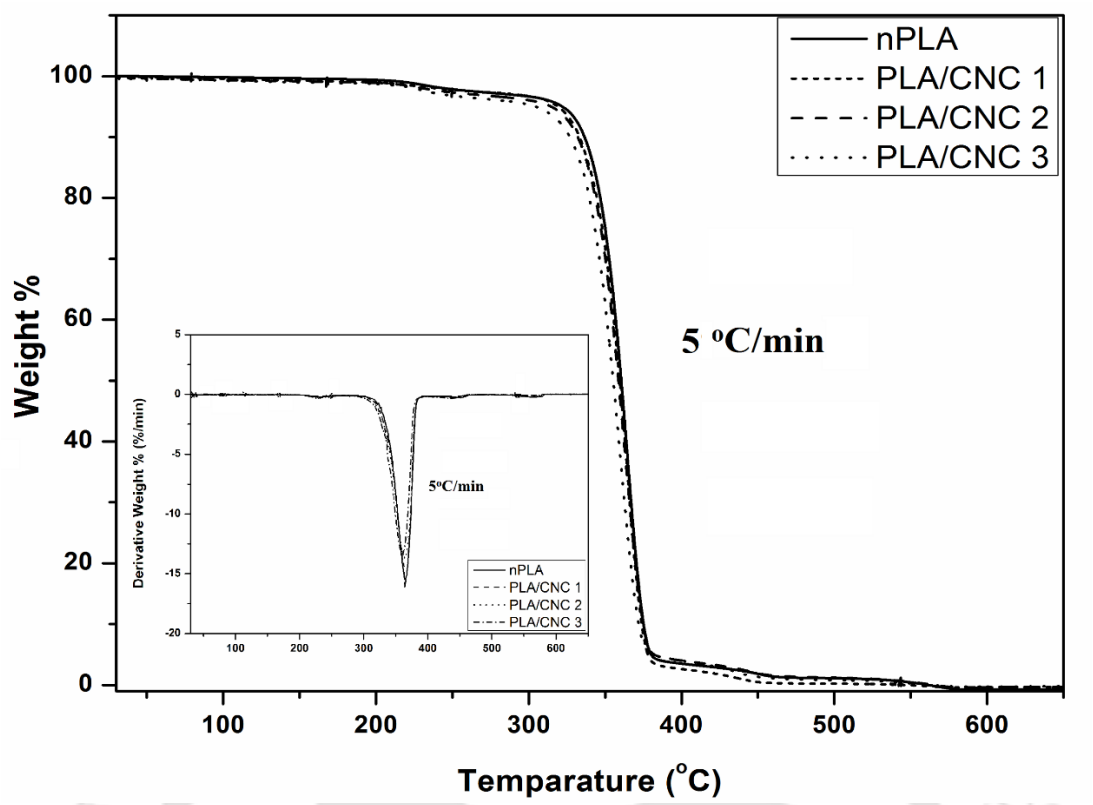

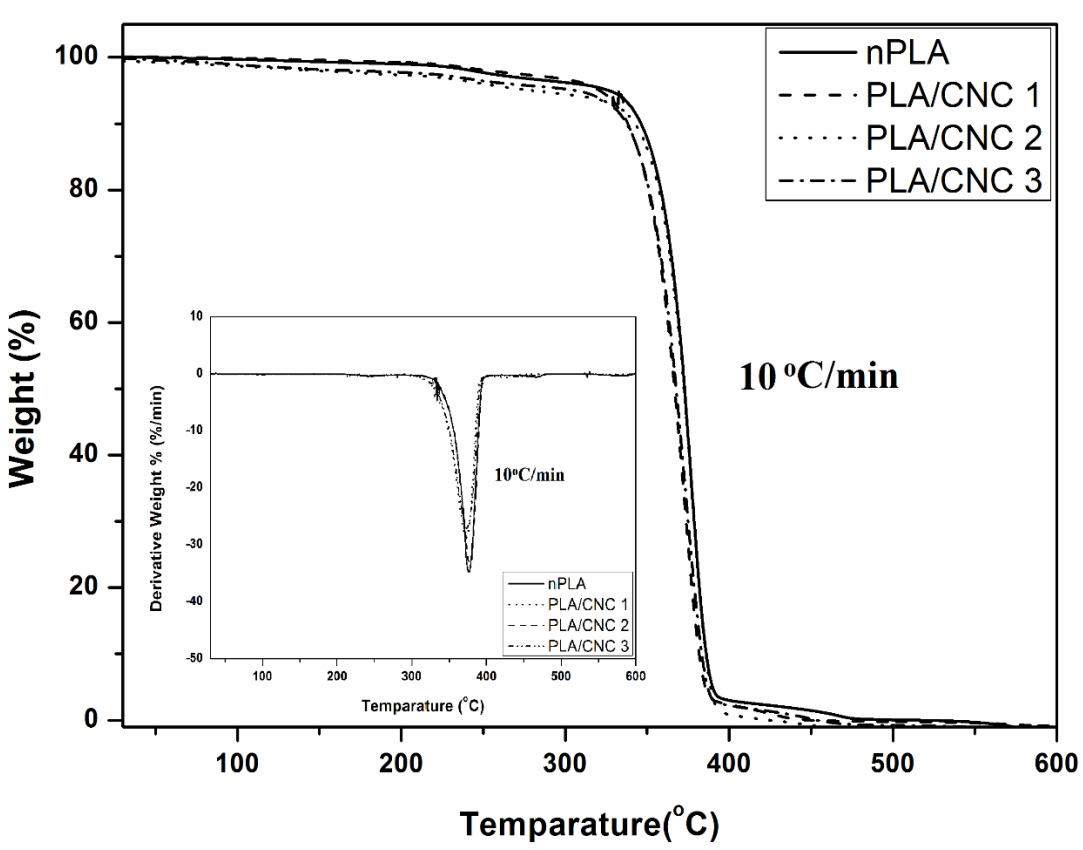

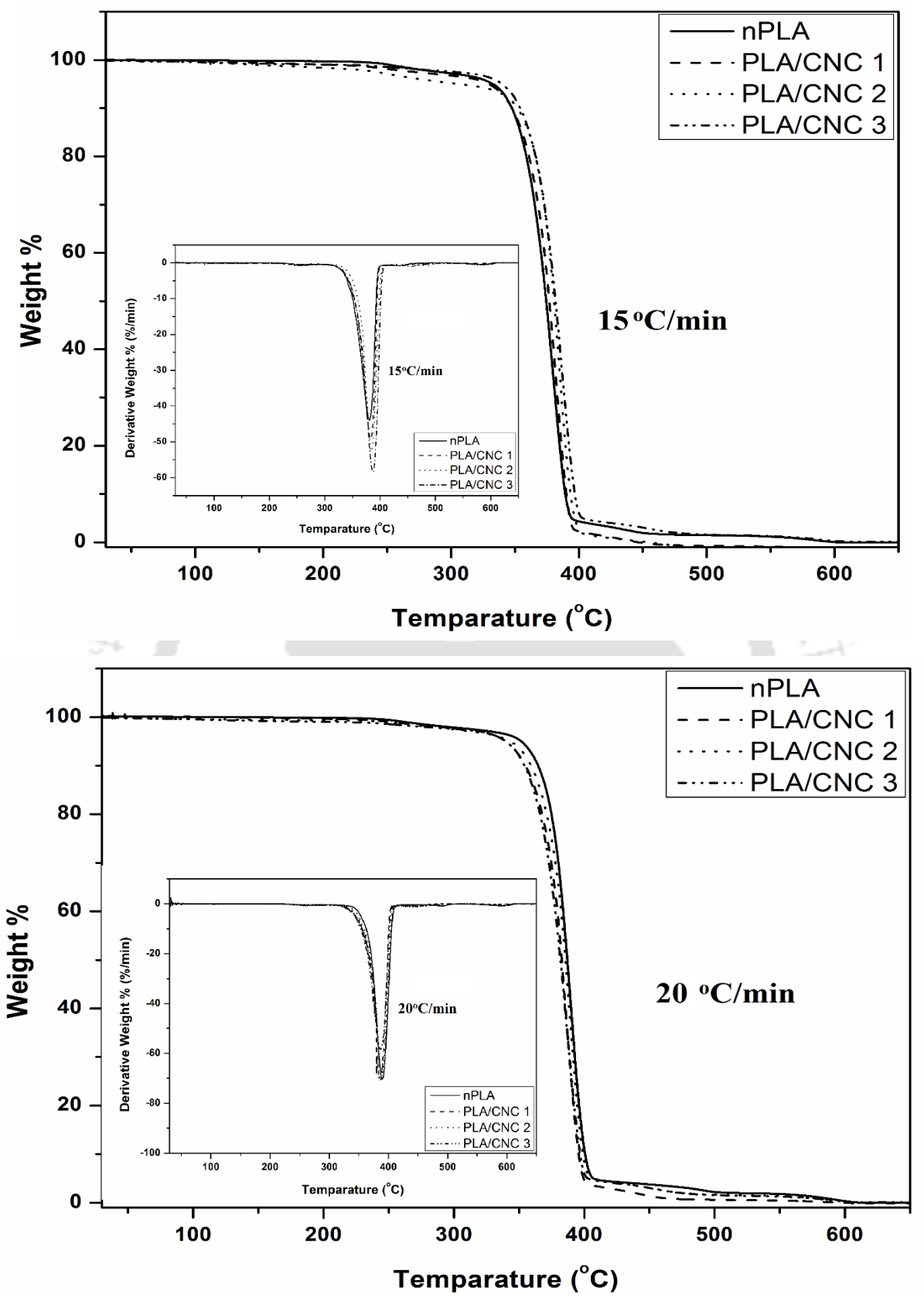

Fig. 3.15 TGA and DTG profiles of PLA and PLA/CNC based foams at different heating rates.

It can be observed from all the PLA/CNC foam systems that there is a variation of activation energy with respect to conversion, which indicates that the decomposition of nanobiofillers also proceeds through a complex mechanism. The apparent activation energy of PLA/CNC 1 foam is observed as ~194.6 kJ/mol. In PLA/CNC 1 foam, the dependence of E_a with α is observed mainly in two regions. The first region is α=0.1 to 0.3, where a similar E_a value is observed. In the second region, α=0.4 to 0.9, a gradual increase in E_a value is observed (as shown in **Fig. 3.18**) which suggests a complex process of decomposition of nanocomposite foam with at least two different mechanisms. The increase in activation energy might be due to the effect of CNC nanobiofillers. More energy is required to break the bonds due to the uniform dispersion of nanobiofillers as suggested by FESEM images. At higher loadings of CNC, in case of PLA/CNC 2, it is observed that the apparent activation energy is ~175.5 kJ/mol and in case of PLA/CNC 3, apparent activation energy value is ~171.8 kJ/mol. The decrease in apparent activation energy compared to PLA/CNC 1 might be due to the presence of an increasing number of sulfate groups at higher loadings, which may degrade the PLA, and hence the reduction in activation energy is observed [121]. However, in both the cases of PLA/CNC 2 and PLA/CNC 3, two similar regions are observed as in PLA/CNC 1 for the dependency of E_a with α. This also suggests the complex mechanism of degradation of the fabricated foams.

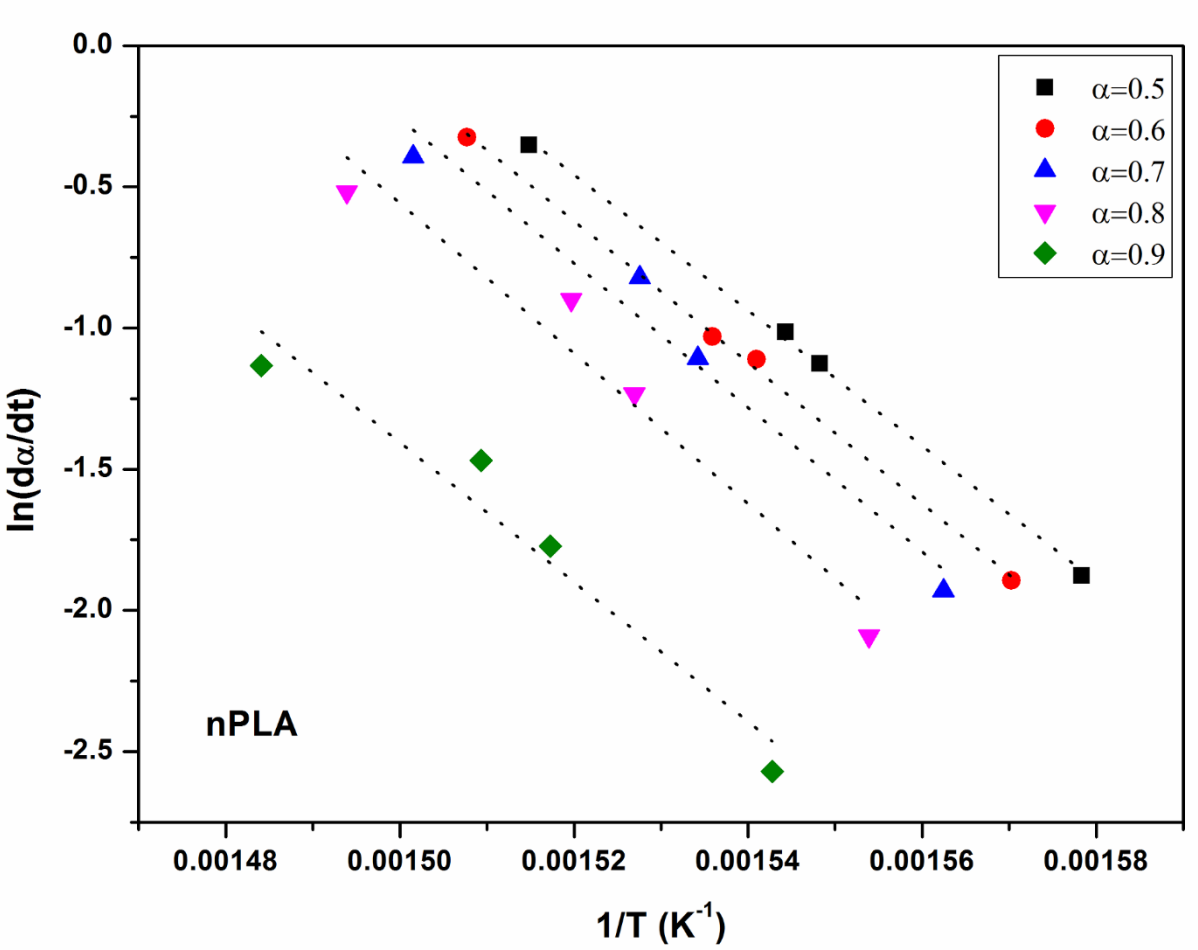
0.0
-0.5
-1.0
-1.5
-2.0
-2.5
ln(dα/dt)
0.00148
0.00150
0.00152
0.00154
0.00156
0.00158
1/T (K-1)
α=0.5
α=0.6
α=0.7
α=0.8
α=0.9
nPLA

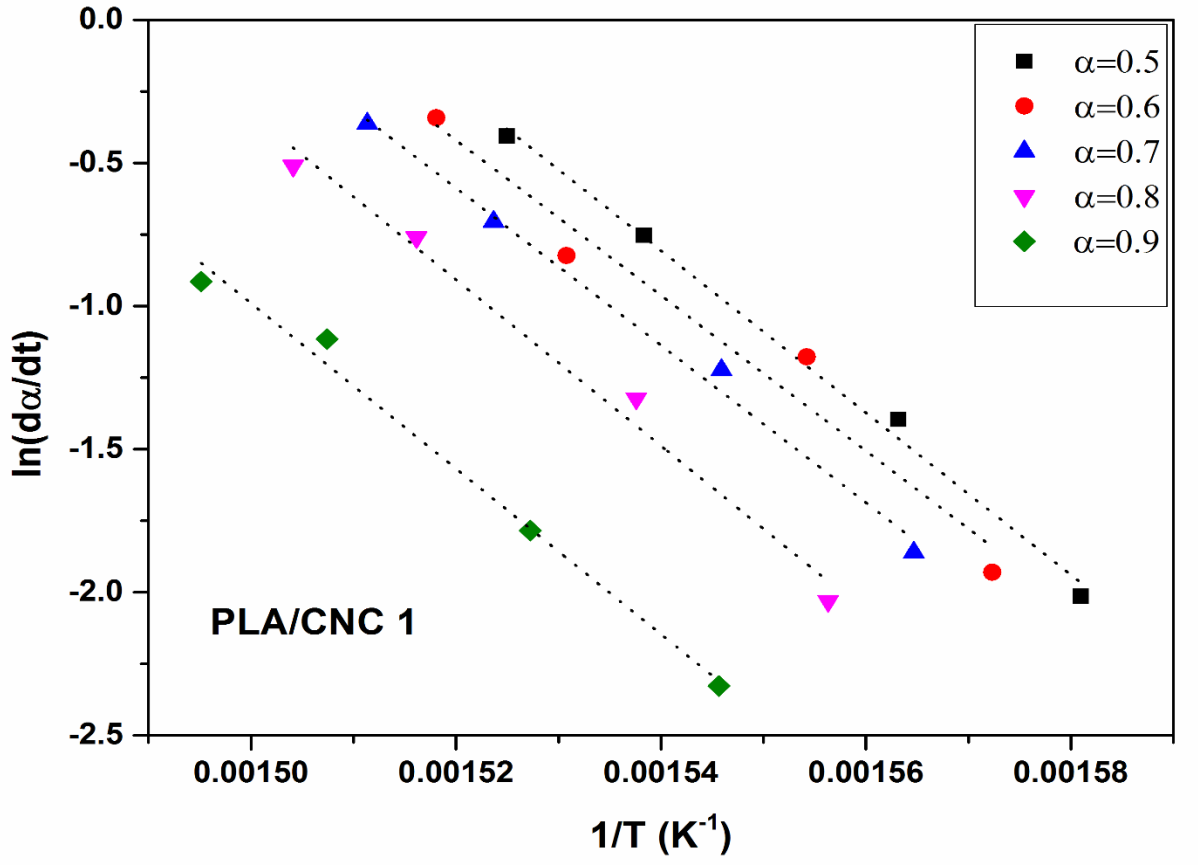
0.0
-0.5
-1.0
-1.5
-2.0
-2.5
ln(dα/dt)
0.00150
0.00152
0.00154
0.00156
0.00158
1/T (K-1)
α=0.5
α=0.6
α=0.7
α=0.8
α=0.9
PLA/CNC 1

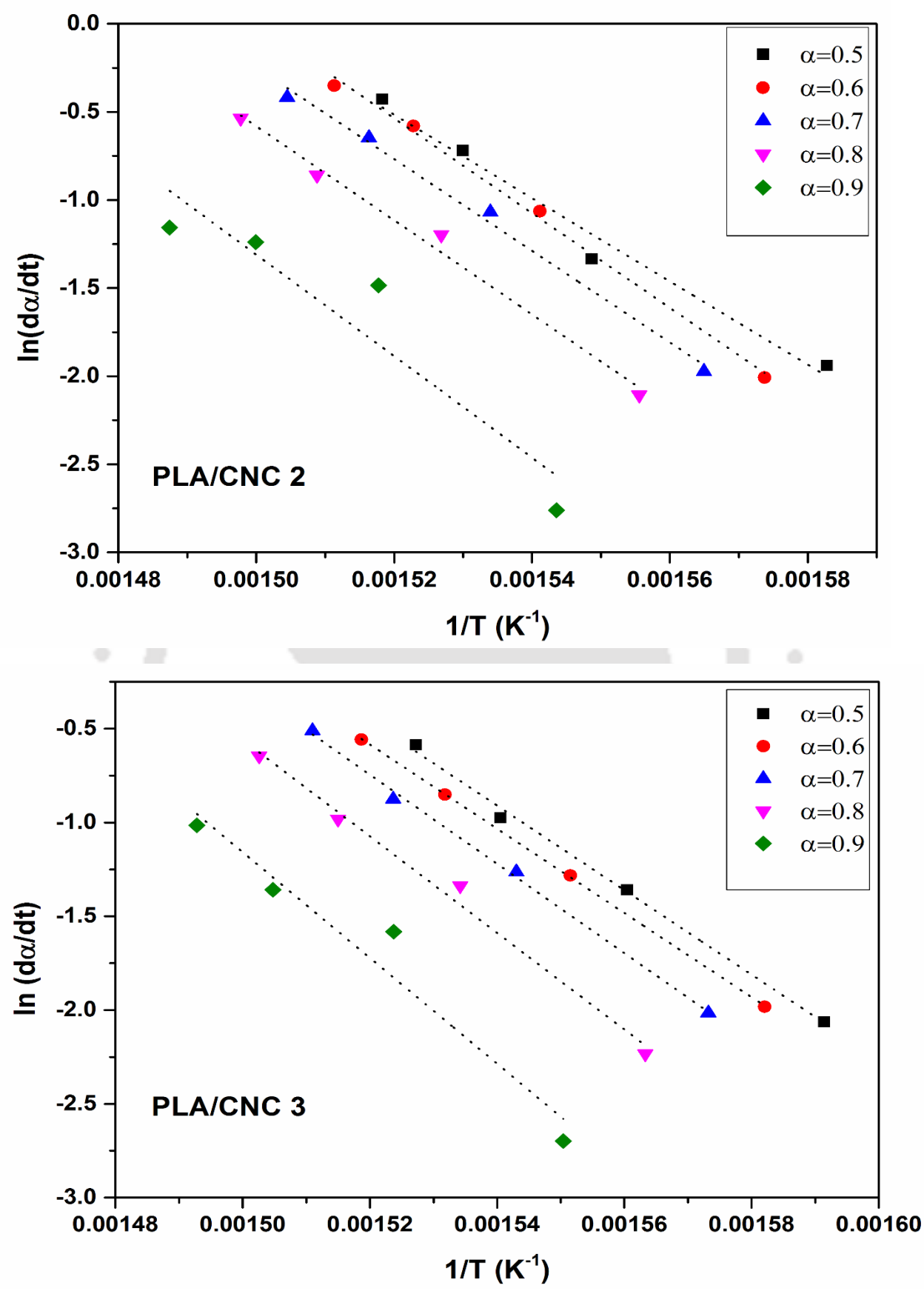

Fig. 3.16 Friedman plots for PLA and PLA/CNC based foams.

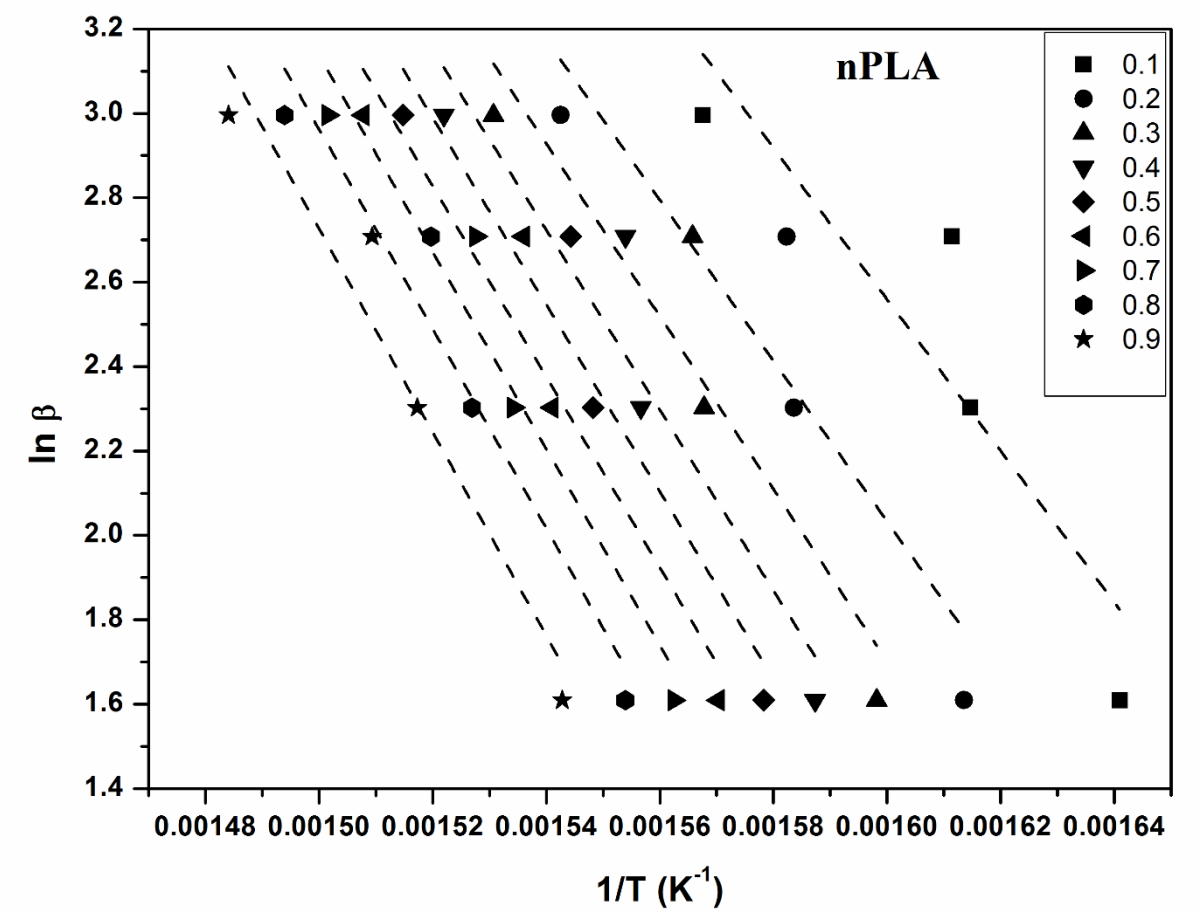

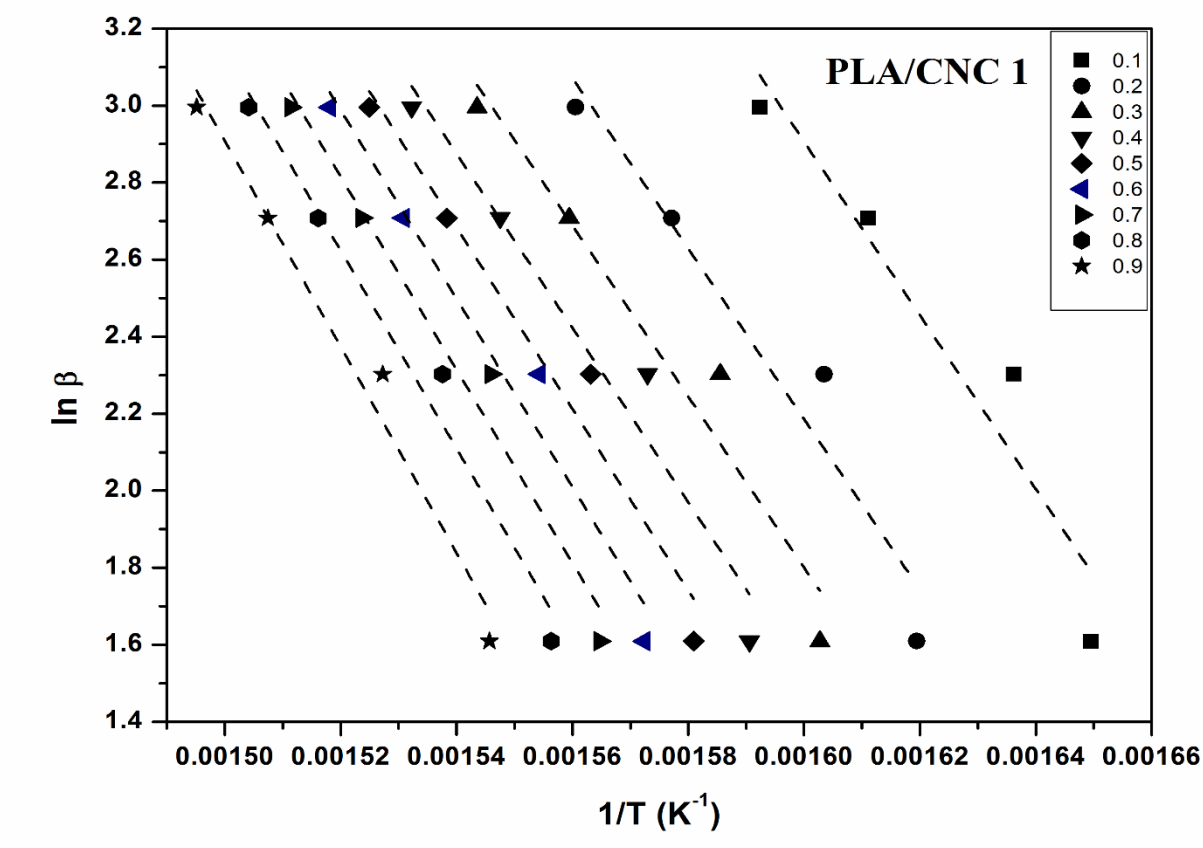

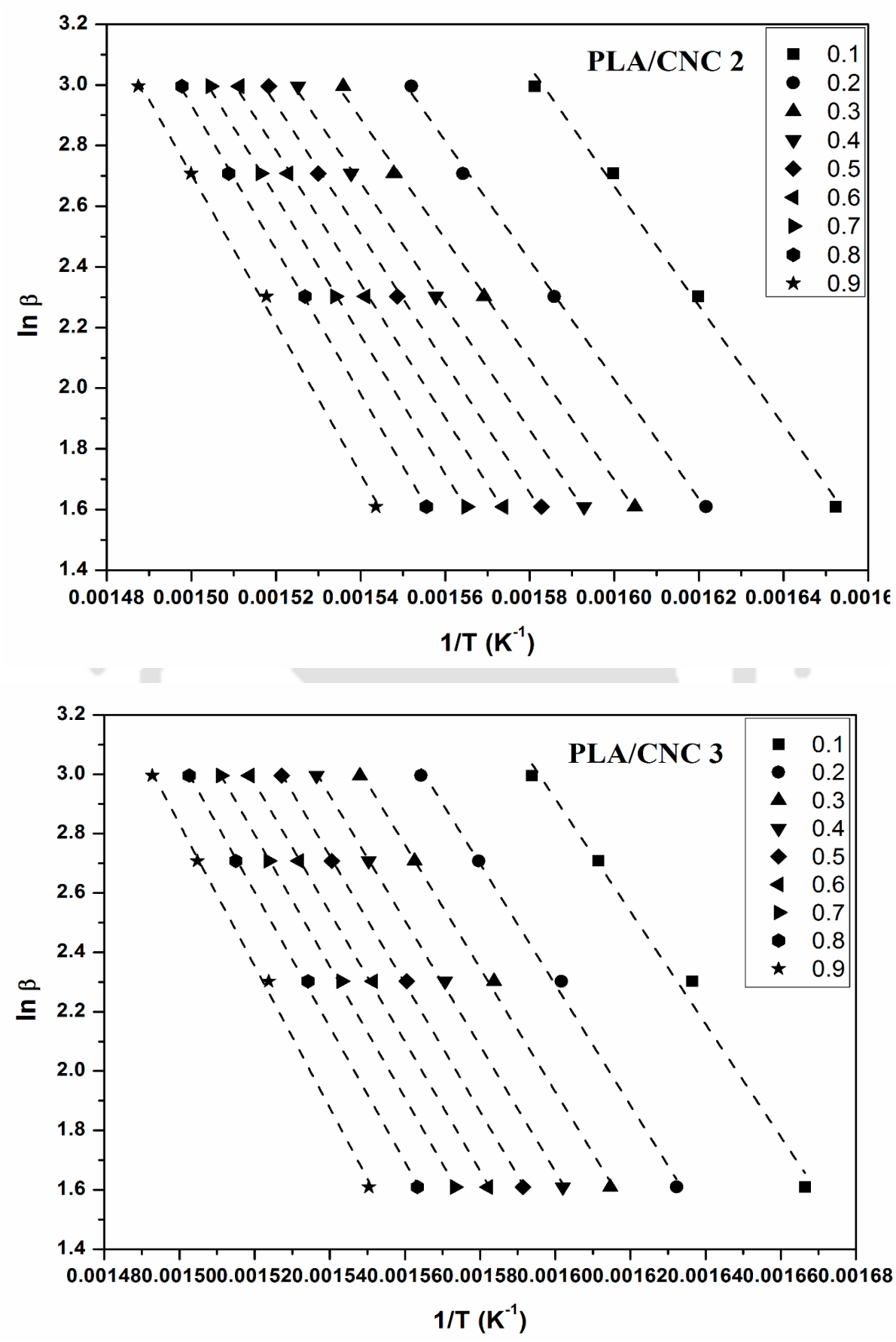

Fig. 3.17 FWO plots for PLA and PLA/CNC-based foams.

Table 3.7. Apparent activation energy (E_a) at different conversions for PLA and PLA/CNC-based foams.

Samples	FWO	KAS	Friedman
	E_a (kJ/mol)	**E_a (kJ/mol)**	**E_a (kJ/mol)**
nPLA	174.8	165.3	201.0
PLA/CNC 1	194.6	183.8	205.1
PLA/CNC 2	175.5	165.1	198.2
PLA/CNC 3	171.8	164.3	195.3

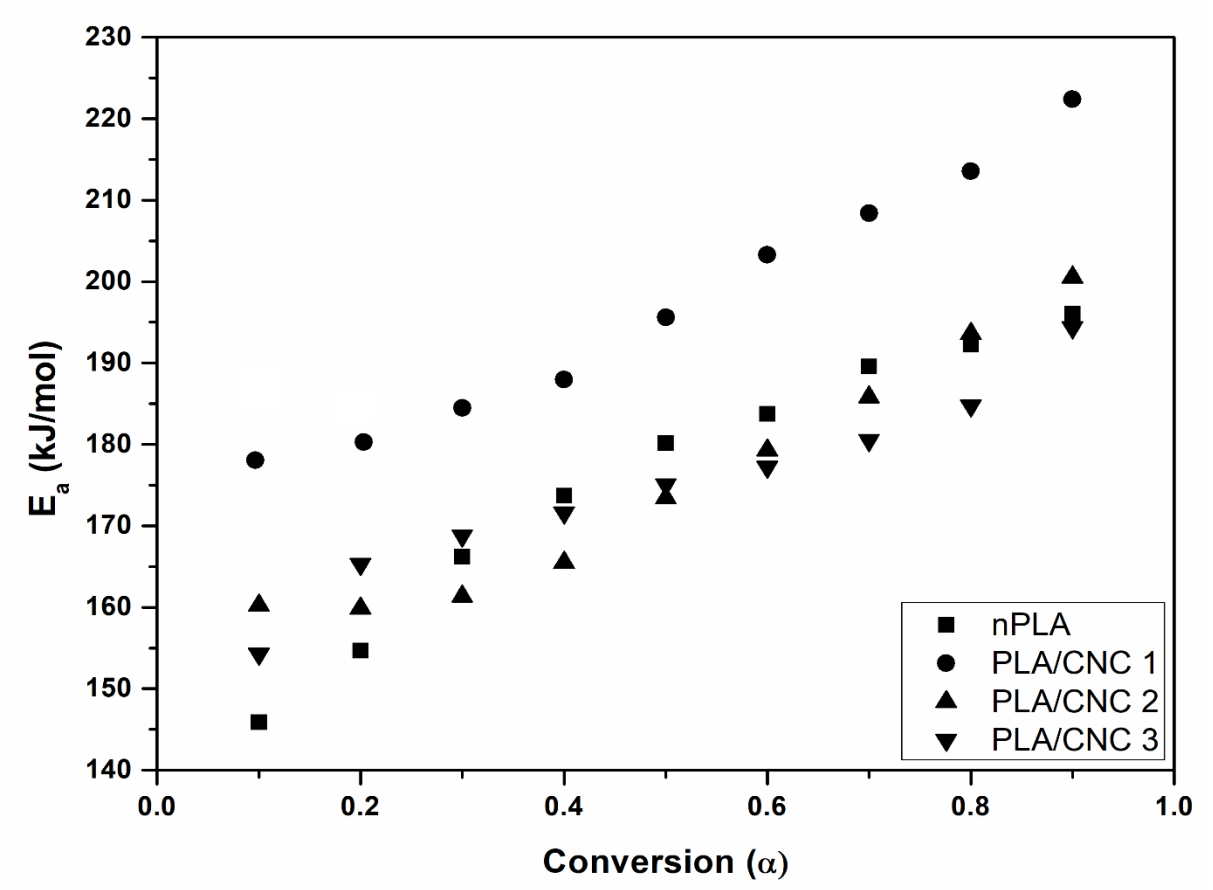

Fig. 3.18 Activation energy (E_a) values from FWO for PLA and PLA/CNC based foams.

KAS plots for PLA and PLA/CNC based fabricated foams are shown in **Fig. 3.19**. Straight parallel lines are observed for different conversions which indicate the suitability of the model

to this system. Linearity is observed in this method. It is observed that the activation energy values are increasing on increasing the conversion. The slope of the lines is also increases on increase in conversion values. The apparent activation energy for nPLA is found to be ~165.3 kJ/mol. In case of PLA/CNC 1, PLA/CNC 2 and PLA/CNC 3, the apparent activation energy is observed as ~183.8 kJ/mol, ~165.1 kJ/mol, and ~164.3 kJ/mol. The E_a values observed is this method (**Fig. 3.20**) is in a similar trend as the FWO method, which indicates both iso-conversion method is suitable for our foam system. However, Friedman method is not suitable for lower conversion rates. The graphs obtained from Augis and Bennett model is shown in **Fig. 3.21** Almost parallel straight lines are obtained for each sample.

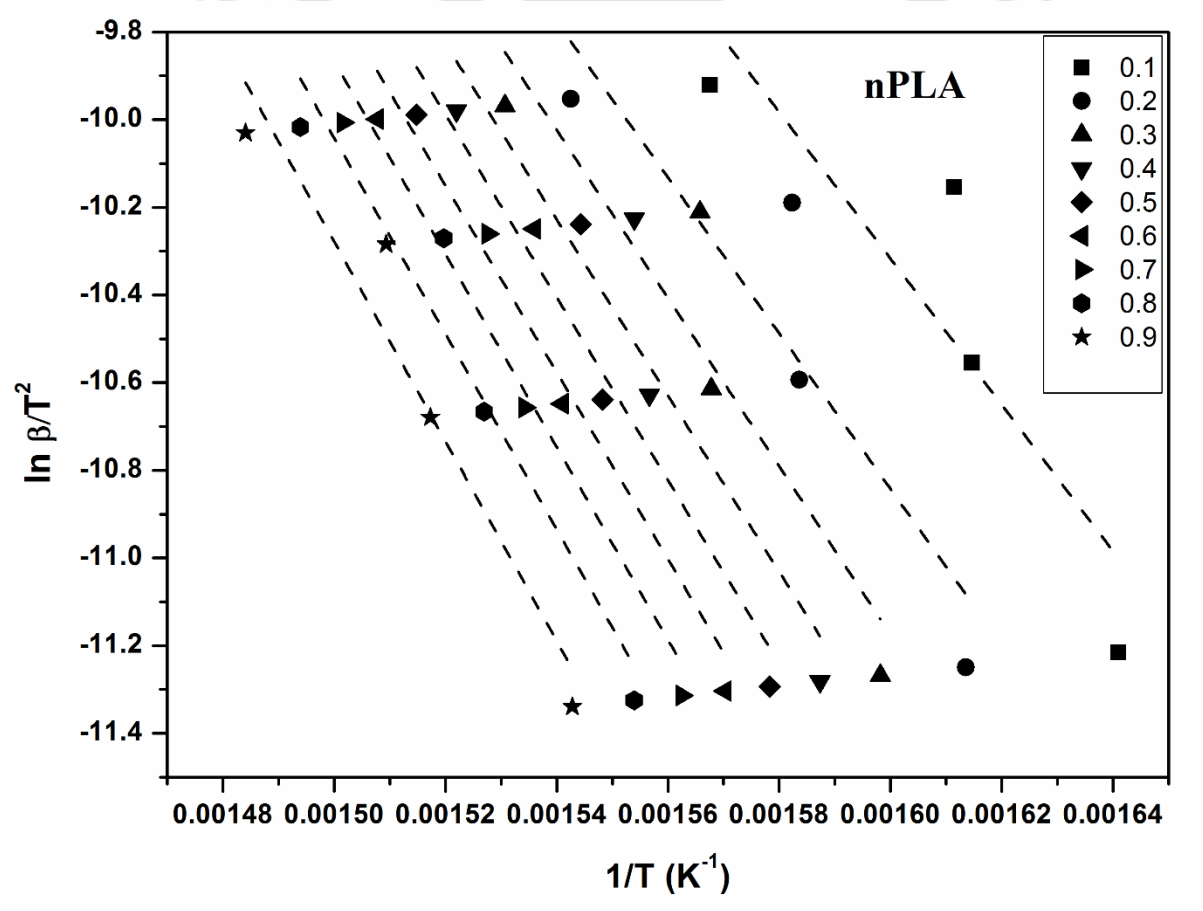

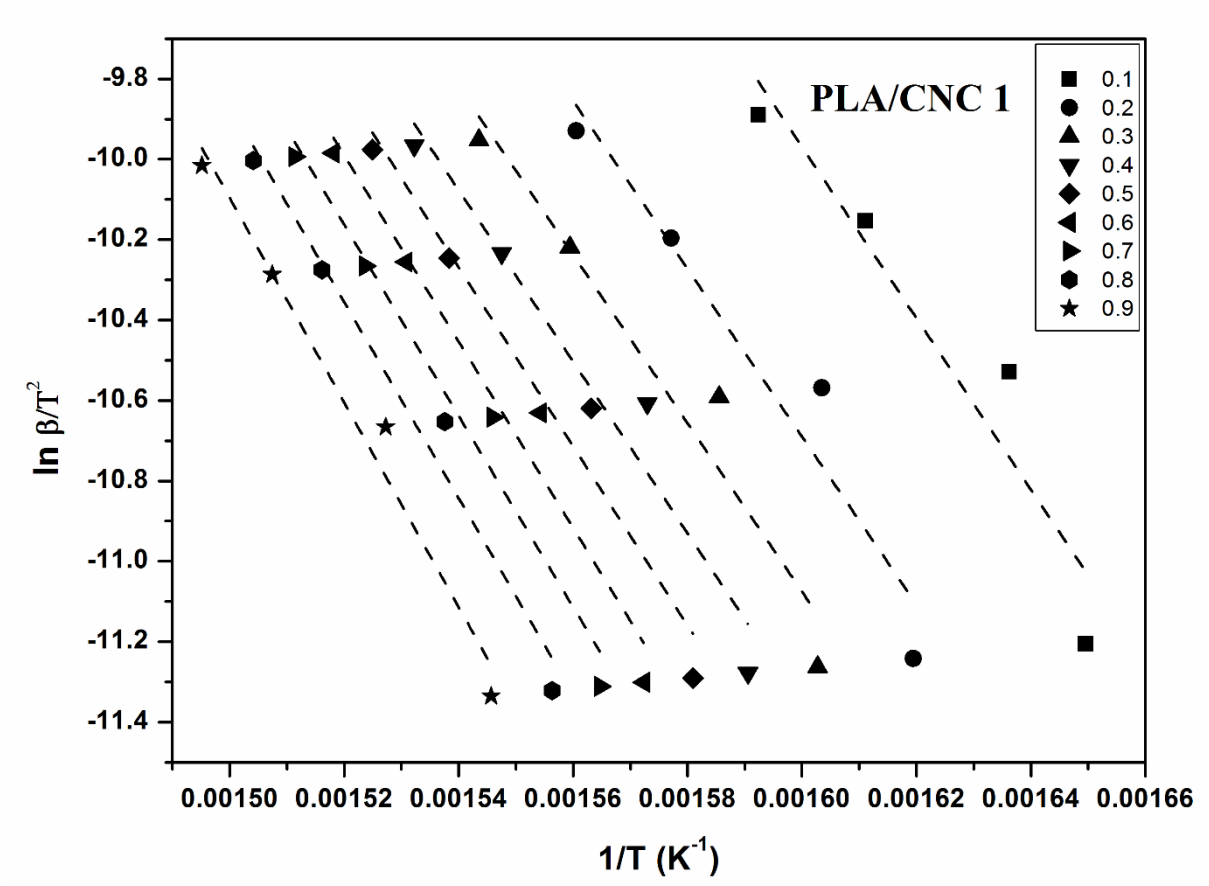

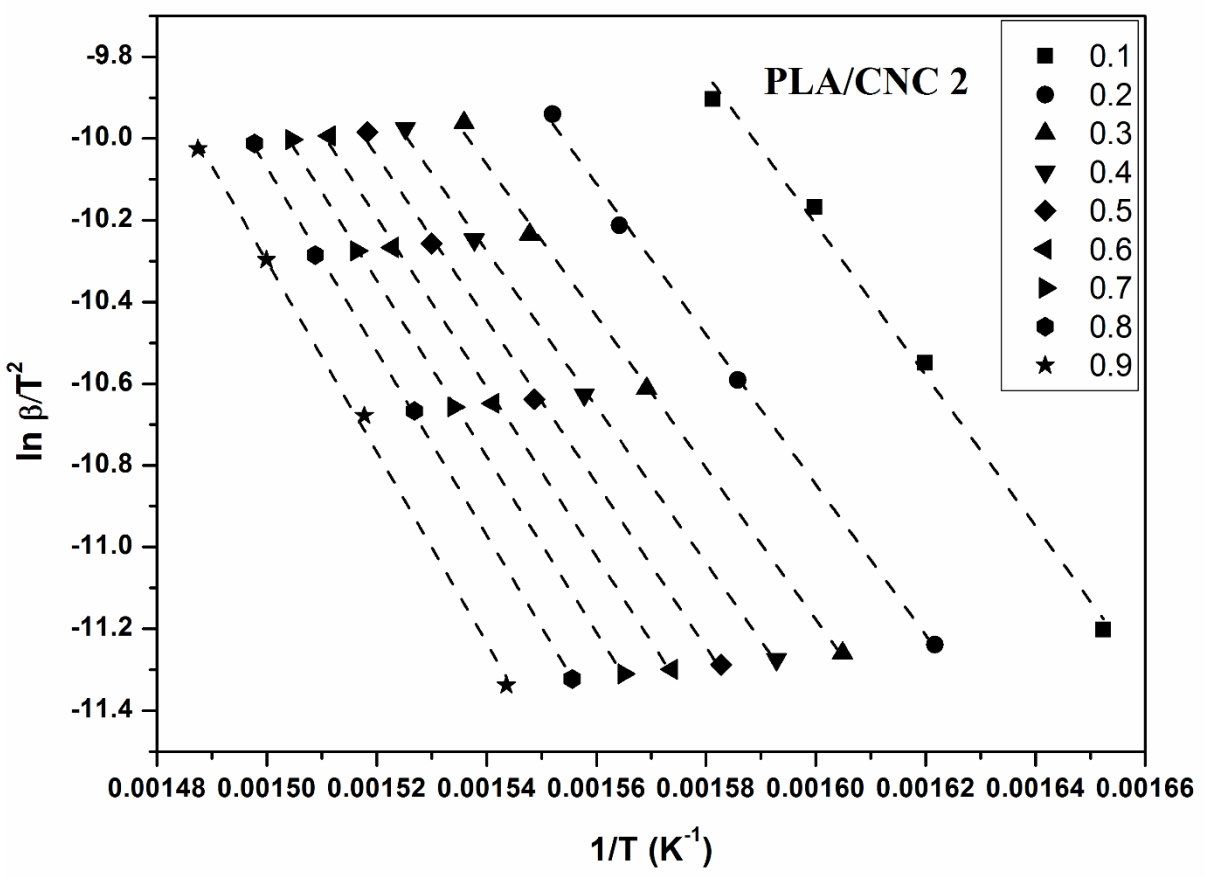

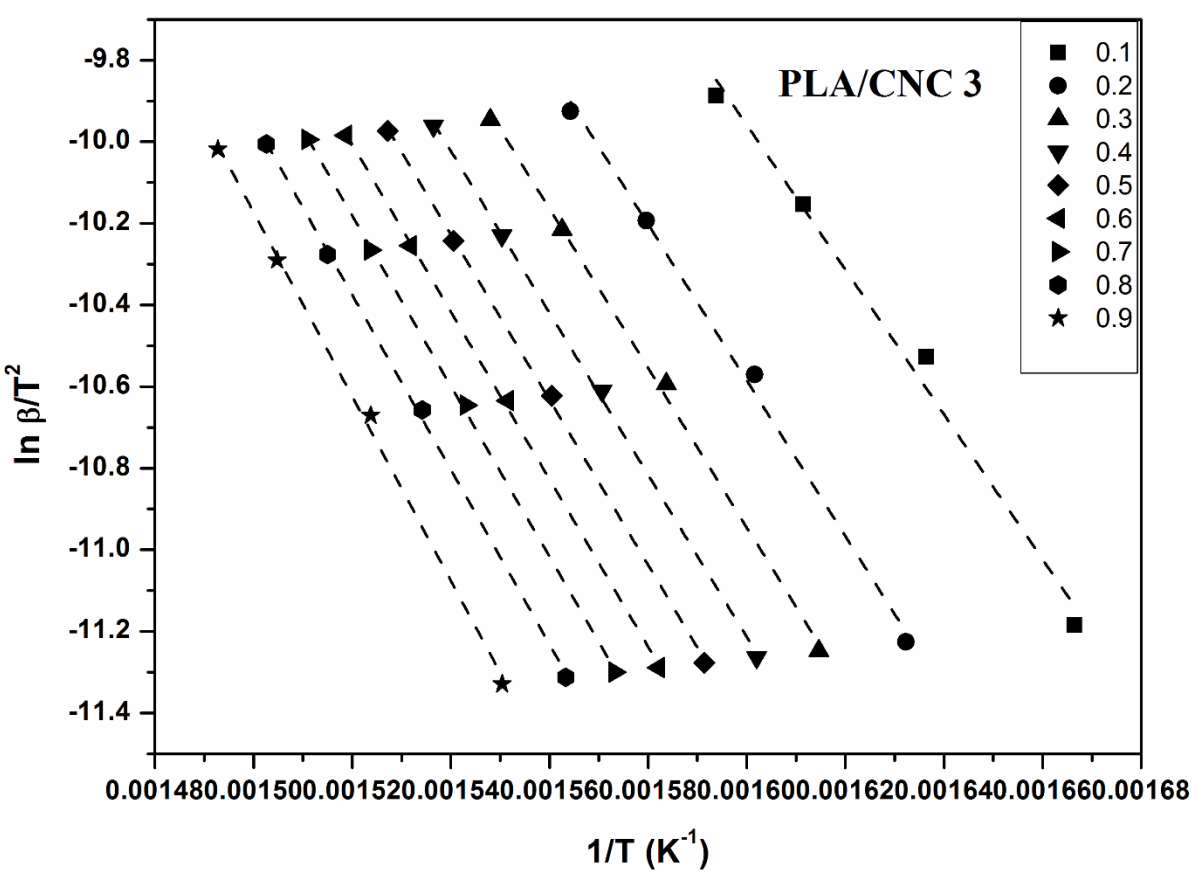

Fig. 3.19 KAS plots for PLA and PLA/CNC-based foams at different conversions.

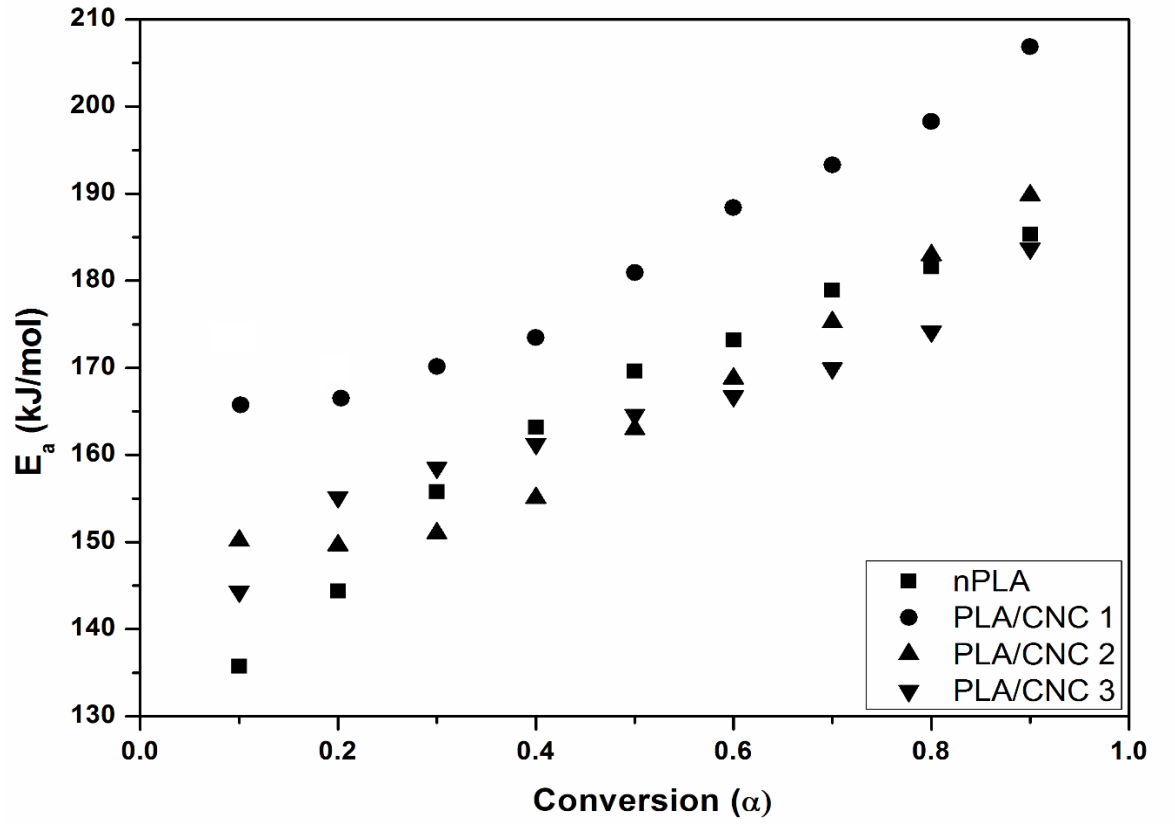

Fig. 3.20 Activation energy (E_a) values from KAS for PLA and PLA/CNC-based foams.

Single E_a is observed from samples. The activation energy obtained for nPLA is ~186.9 kJ/mol. The activation energies of PLA/CNC based foams are found to be ~217.3 kJ/mol, ~198.2 kJ/mol and ~182.5 kJ/mol for 1%, 2% and 3% loading of CNC. The suitability of the model is judged by the R^2 values obtained. The R^2 values of FWO and KAS are found to be ~0.99. The above results are found to be in accordance with the above models. We have calculated the values of "A" (**Table 3.8**) from this model. These values are also in accordance with the values obtained from other methods. Pre-exponential factor depends on the collision of the molecules while degradation taking place.

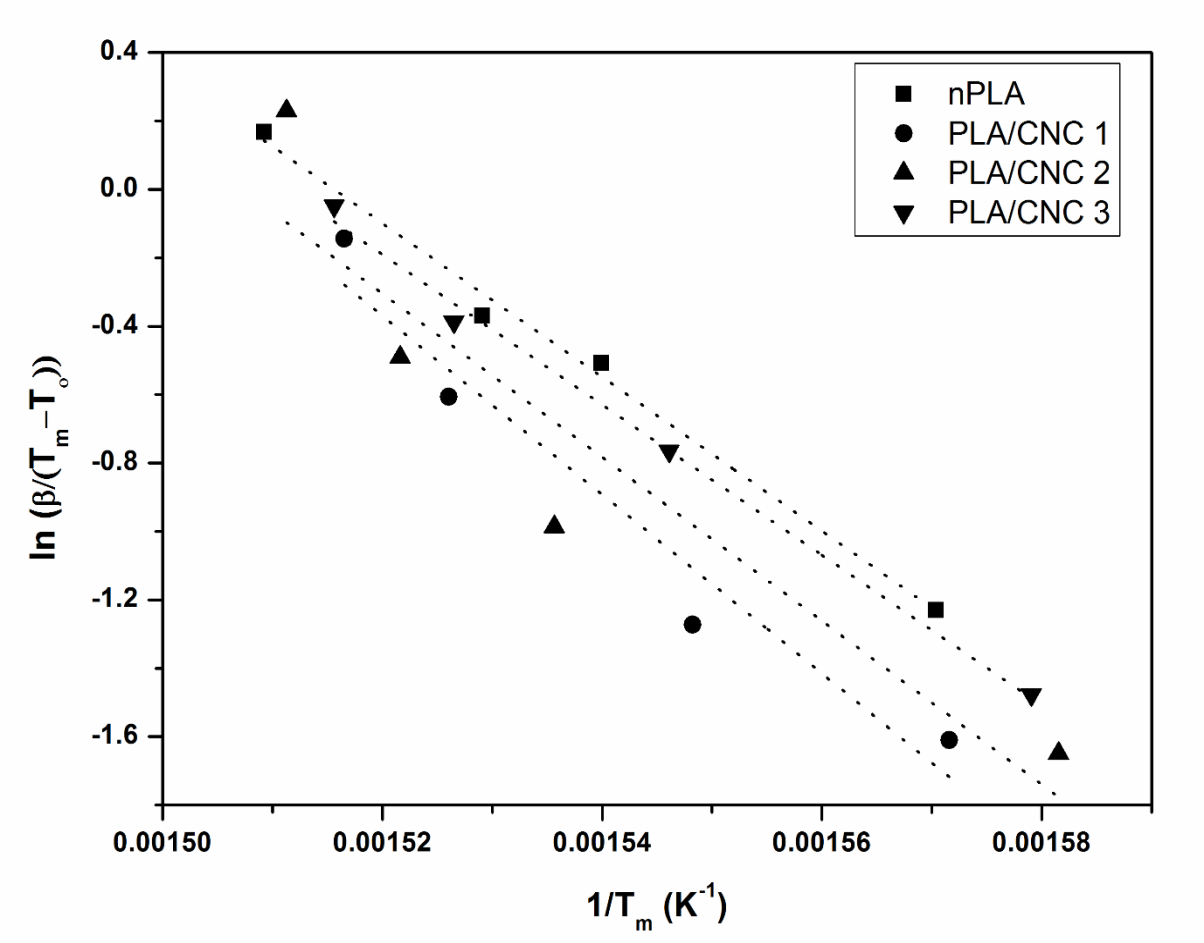

Fig. 3.21 Augis and Bennett plots for PLA and PLA/CNC based foams.

Table 3.8 Activation energy (E_a), regression and pre-exponential factor (A) for PLA and PLA/CNC-based foams at a heating rate of 10 °C/min.

Sample	**Augis & Bennett model at 10 °C/min**			**Kissinger model at 10 °C/min**		
	E_a (kJ/mol)	R^2	A (s^{-1})	E_a (kJ/mol)	R^2	A (s^{-1})
nPLA	186.9	0.99	6.3×10^{14}	183.6	0.97	3.3×10^{11}
PLA/CNC 1	217.3	0.92	1.2×10^{17}	198.9	0.96	6.3×10^{12}
PLA/CNC 2	198.8	0.81	4.5×10^{15}	185.4	0.99	4.3×10^{12}
PLA/CNC 3	182.6	0.99	2.5×10^{14}	167.0	0.99	1.6×10^{10}

For the case of "modelistic" approaches, we have calculated the activation energy and the mechanism of degradation of the PLA and PLA/CNC based foams.

From the Kissinger plots (**Fig. 3.22**), single activation energy is calculated for each sample. For nPLA the activation energy is found to be ~183.7 kJ/mol. For PLA/CNC based fabricated foams, activation energy values are found to be ~198.9 kJ/mol, ~185.4 kJ/mol and ~167.0 kJ/mol for PLA/CNC 1, PLA/CNC 2 and PLA/CNC 3 respectively. From Kissinger method, we have calculated the value of pre-exponential factors (A), which is required to calculate the values for thermodynamic parameters. The trend observed from Kissinger is also in good accordance with the "model-free" approaches.

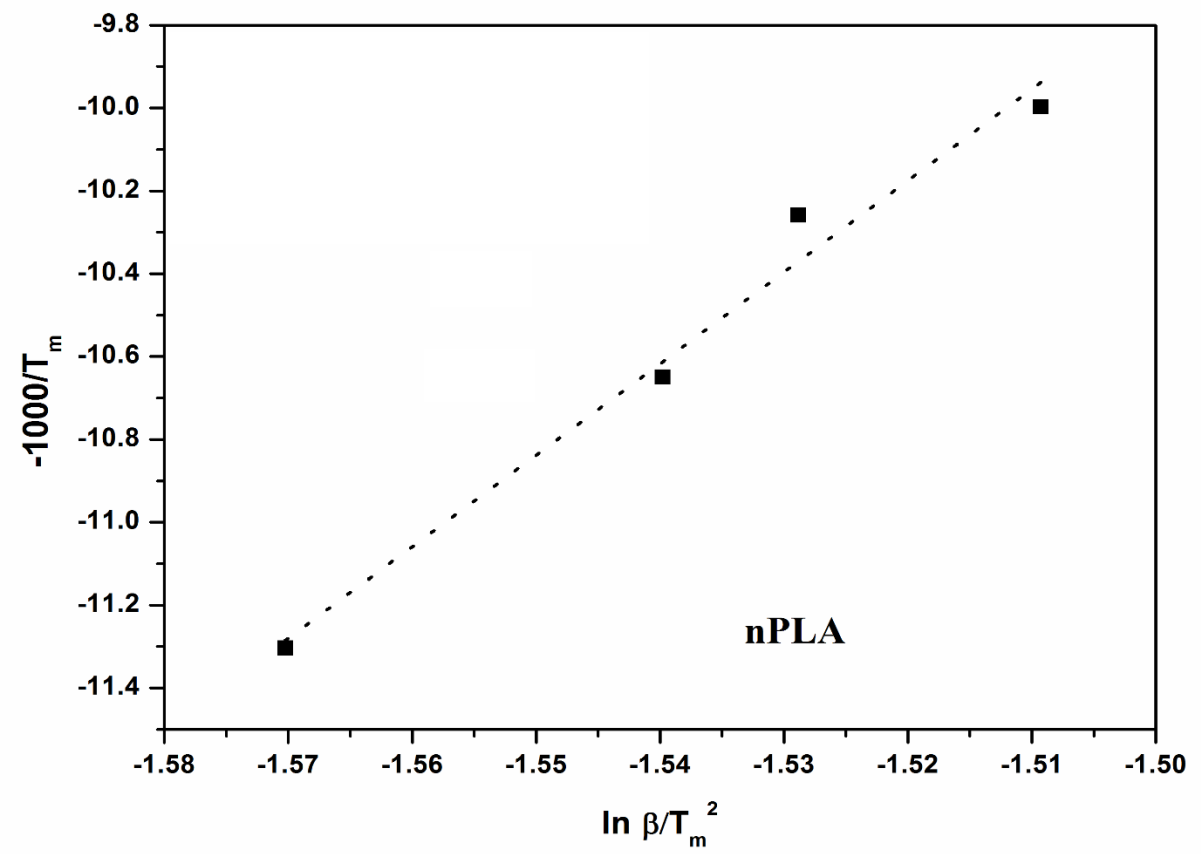
-9.8
-10.0
-10.2
-10.4
-10.6
-10.8
-11.0
-11.2
-11.4
-1000/T_m
nPLA
-1.58
-1.57
-1.56
-1.55
-1.54
-1.53
-1.52
-1.51
-1.50
ln β/T_m^2

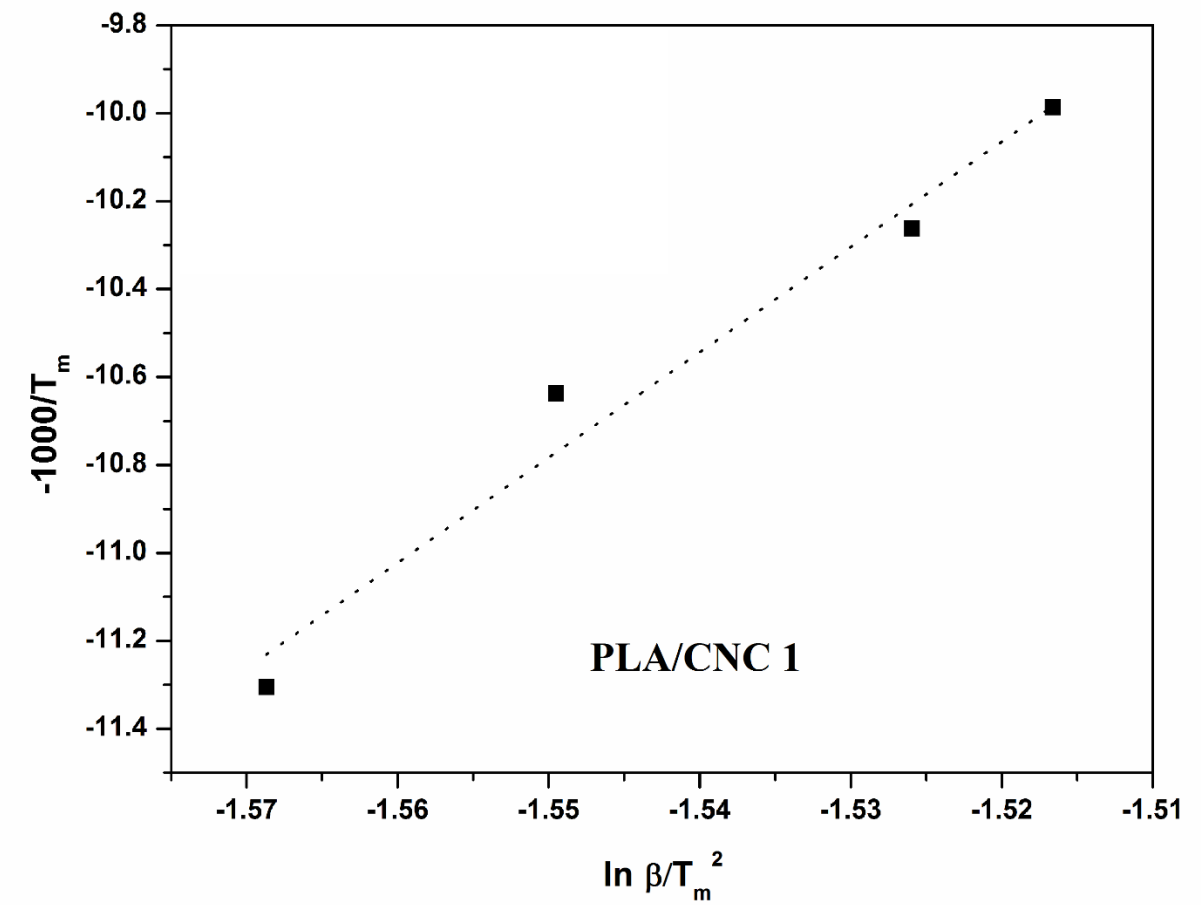
-9.8
-10.0
-10.2
-10.4
-10.6
-10.8
-11.0
-11.2
-11.4
-1000/T_m
PLA/CNC 1
-1.57
-1.56
-1.55
-1.54
-1.53
-1.52
-1.51
ln β/T_m^2

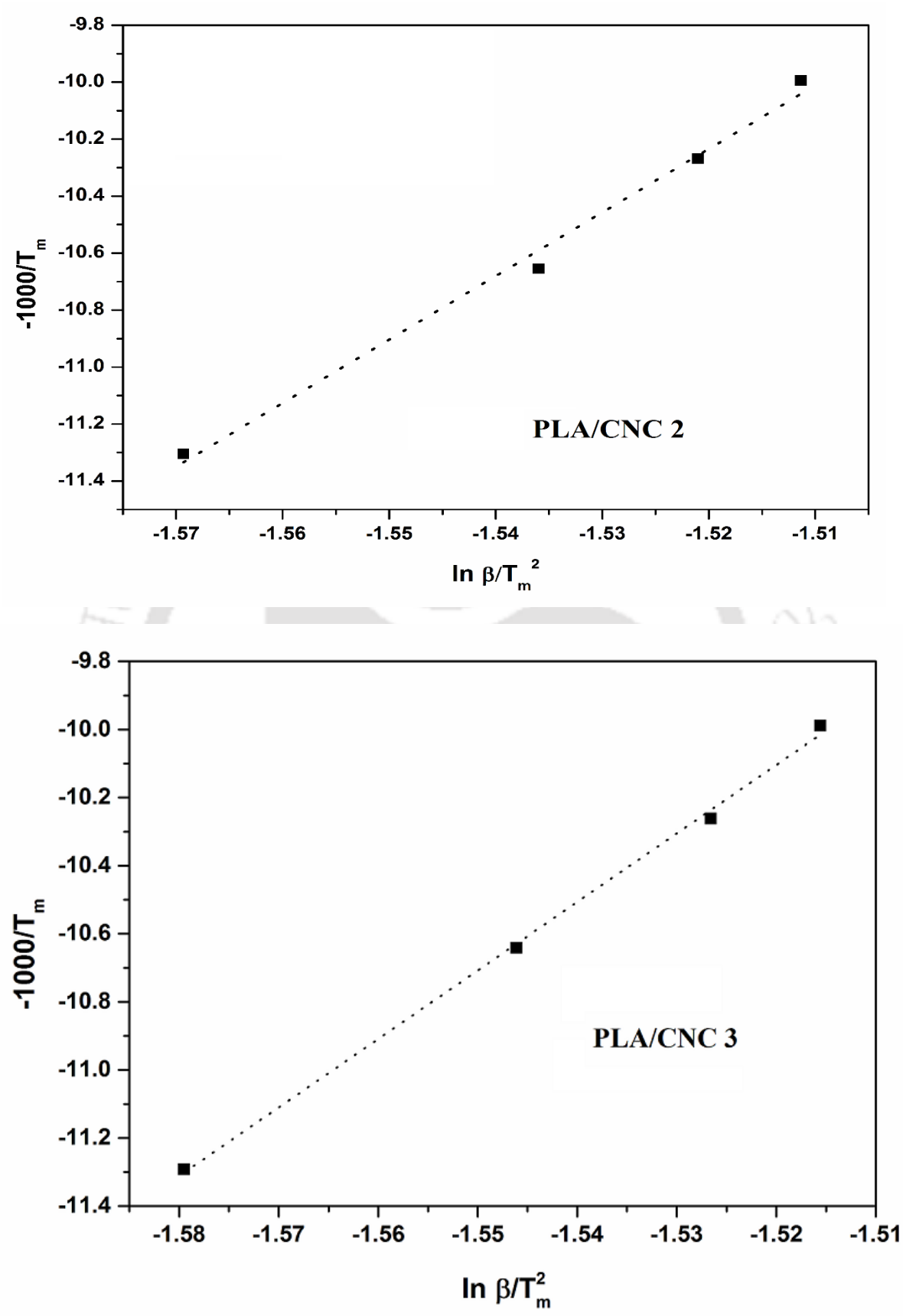

Fig. 3.22 Kissinger plots for PLA and PLA/CNC-based foams.

The degradation mechanism of PLA and PLA/CNC based microcellular composite foams are proposed by using Criado method. The Criado plots at 10 °C/min are shown in **Fig. 3.23.** The master and experimental curves are shown for PLA and PLA/CNC based fabricated foams. Master curves are plotted for different degradation mechanisms as discussed in the earlier chapter. The activation energy (E_a) calculated by using the Kissinger method was used for the calculations of Criado method.

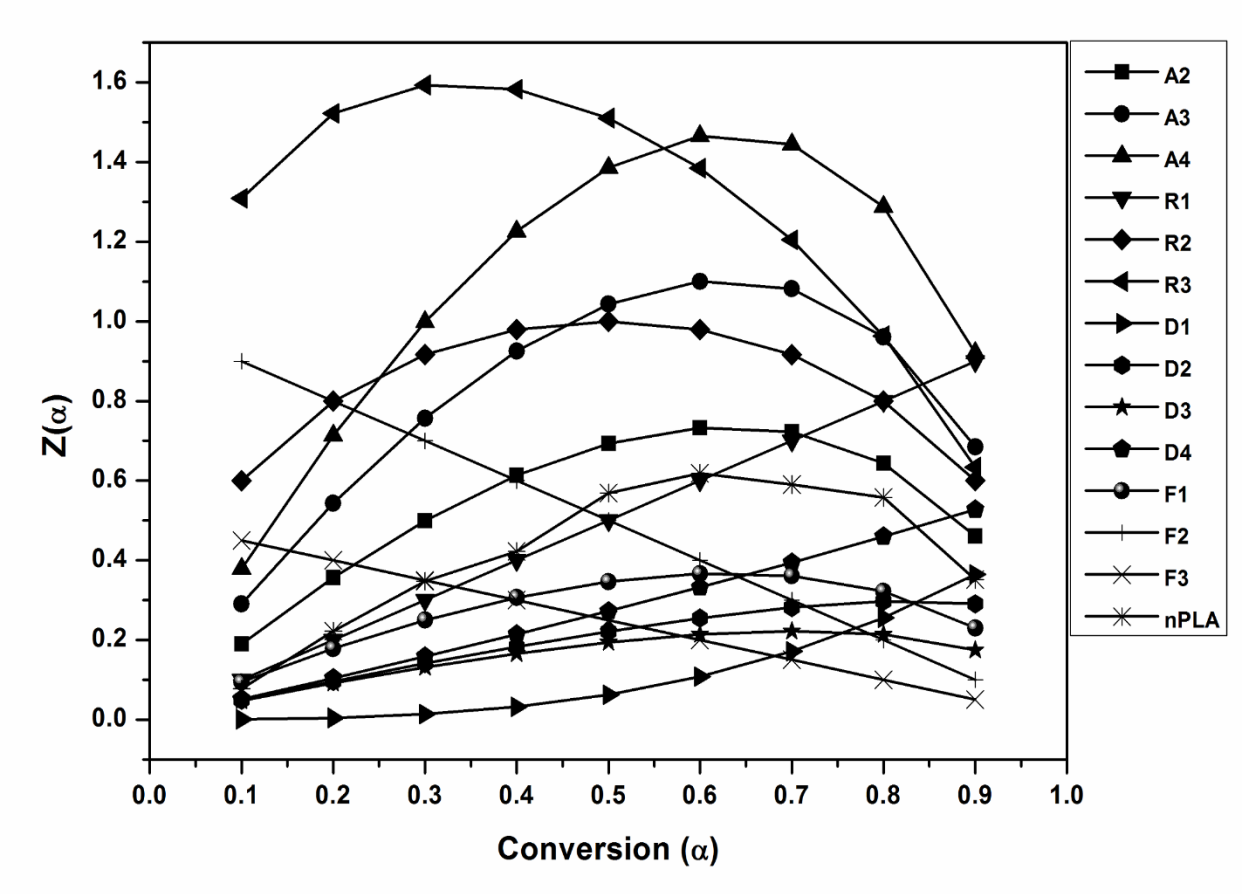

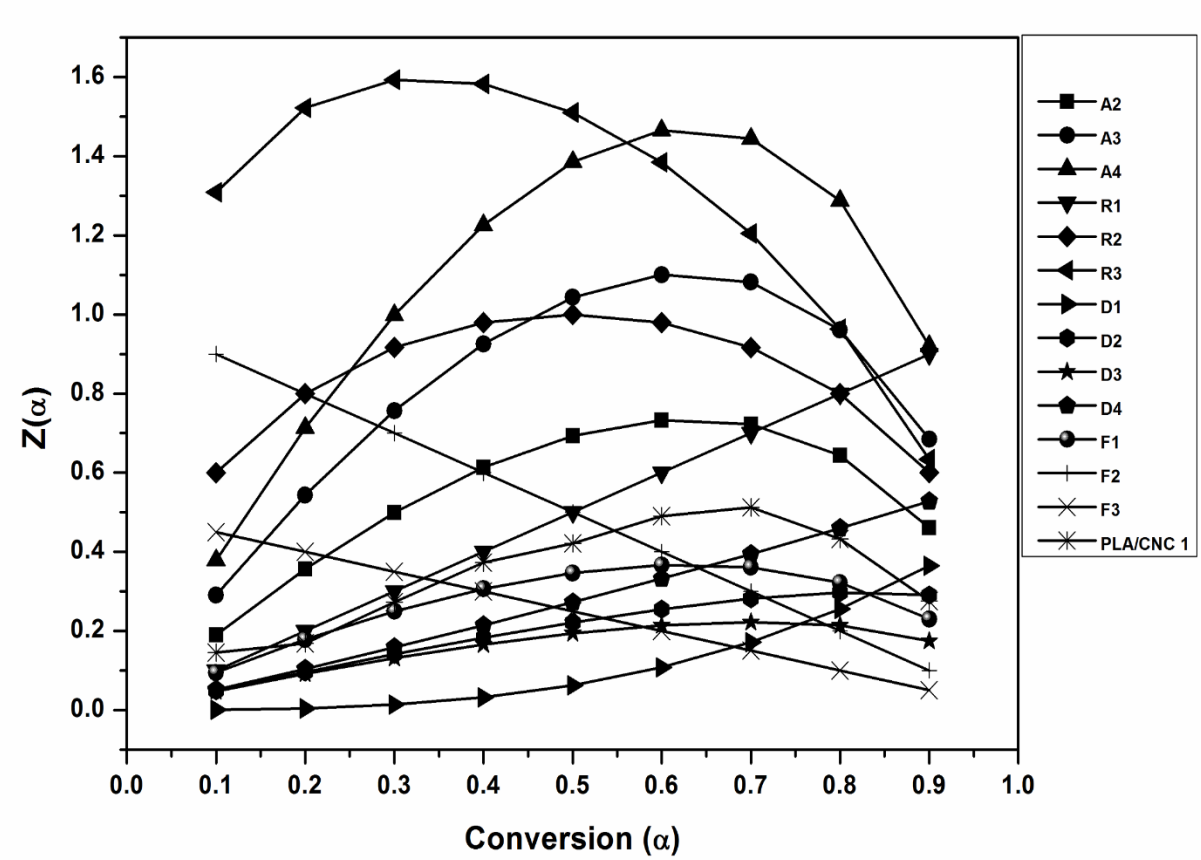
Z(α)
Conversion (α)
A2
A3
A4
R1
R2
R3
D1
D2
D3
D4
F1
F2
F3
PLA/CNC 1

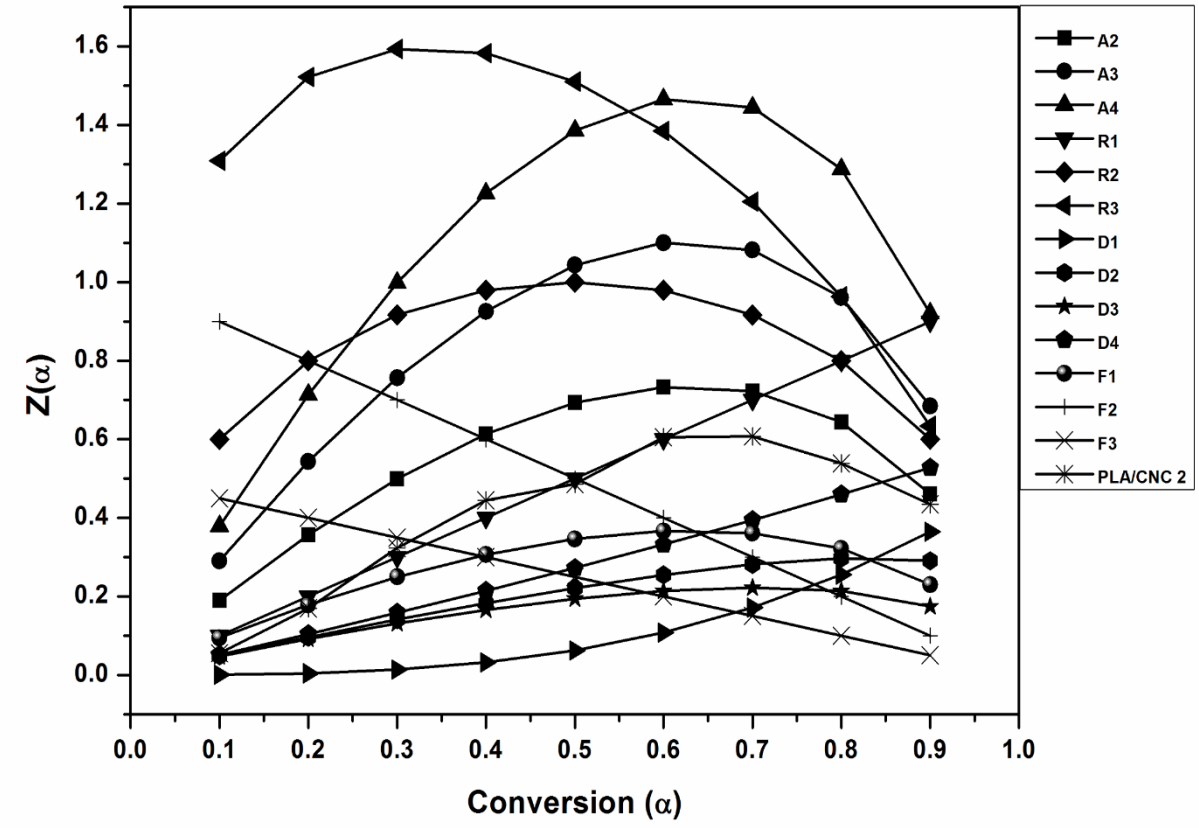
Z(α)
Conversion (α)
A2
A3
A4
R1
R2
R3
D1
D2
D3
D4
F1
F2
F3
PLA/CNC 2

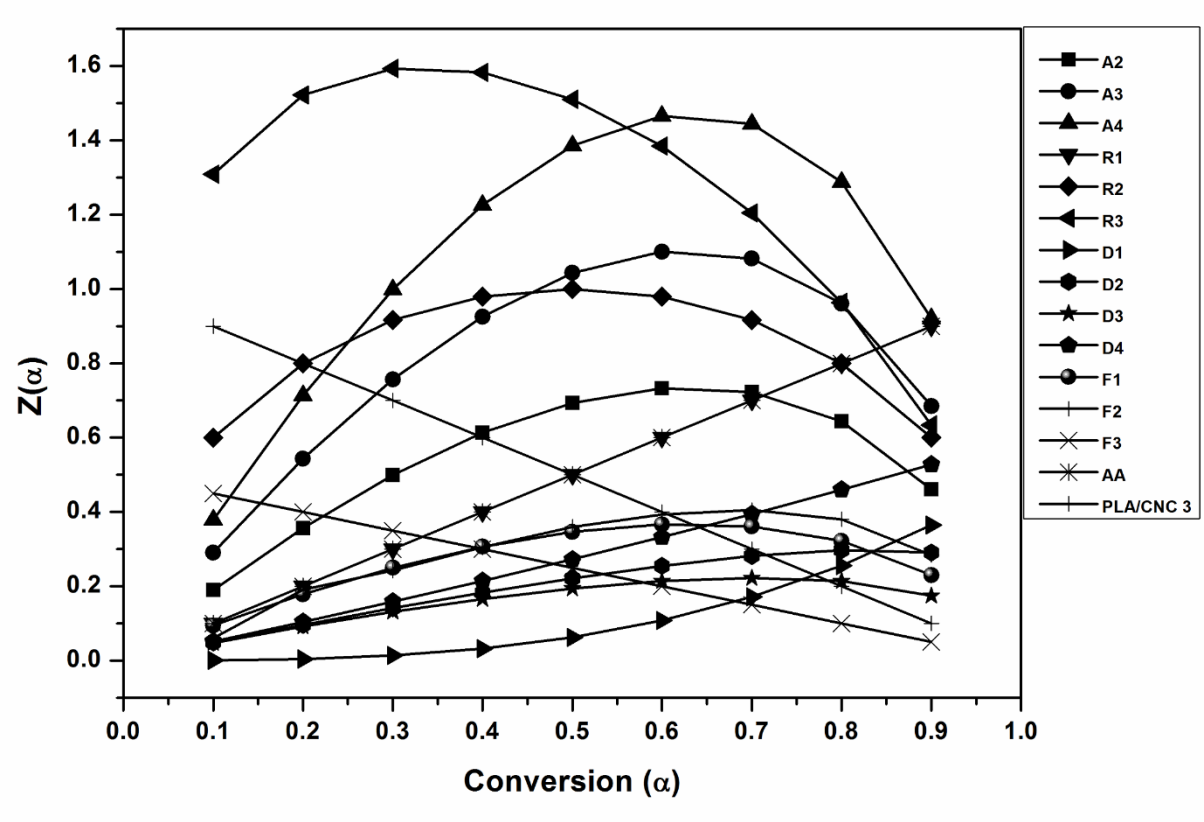

Fig. 3.23 Criado plots for PLA and PLA/CNC-based foams.

From the shape of the experimental curves, we can propose the degradation mechanism of the fabricated PLA and PLA/CNC based foams. It is observed from nPLA, Criado experimental curves that at lower conversions (α=0.1) overlap F1 and R1 mechanism. On higher conversion, the mechanism shifted to D3 at α=0.3. Degradation mechanism follows R1 in the range α=0.4-0.6. The degradation of nPLA follows F2 mechanism at α=0.4-0.6. At higher conversion α≥0.8, mechanism follows D4 type mechanism followed by D1 mechanism. In the case of PLA/CNC-based foams, it is observed that all the composite foams behave almost similar type of degradation mechanism. In the case of PLA/CNC 1, the degradation mechanism follows F1/R1 mechanism till α≤0.2. Mechanism shifted towards F3 in conversion ranging from α=0.3-0.4. It follows the F2 mechanism at α=0.6. At higher rates of conversion (α>0.7), the reaction mechanism follows D4 followed by D1 mechanism. Similar types of degradation mechanism can be observed at higher loadings of CNC. In PLA/CNC 2, initially, the degradation follows

F1/R1 mechanism till α≤0.3. The experimental line overlaps on R1 and F2 at α=0.5 followed by R1 mechanism till α=0.6. At higher conversions, degradation mechanism follows D4 mechanism of degradation (α≥0.7). For the case of PLA/CNC 3, it follows F1 mechanism till α≤0.4. At α=0.4, the experimental line overlaps F3 and F1 mechanisms. The degradation mechanism follows, F1 till α=0.6. On conversion of α=0.6, it follows, F2 mechanism. At the higher conversion of α≥0.7, the degradation mechanism follows, D4 followed by D1 and D2 mechanisms. From the above Criado plots, we can conclude that the mechanism of degradation of all the composite microcellular foams is similar.

3.4 Investigations from isothermal TGA hyphenated FTIR

The isothermal studies of TGA-FTIR system for PLA and PLA/CNC based fabricated foams are shown as the 3D plot in **Fig. 3.24**. The various gaseous products obtained on degradation is investigated. The investigations are done in two conversions (α=0.3 and α=0.7). The two conversions are selected on the basis of Criado plots as it suggests a change in the mechanism of degradation at these conversions for PLA and PLA/CNC based fabricated foams. The analysis is done for nPLA and PLA/CNC 1 foam at their respective conversion temperatures for 1 h. nPLA foam is kept isothermally at ~365 °C and ~379 °C. It is observed from the figure that the intensity of peaks increased at higher conversion. However, some new peaks are also observed at higher conversion. Peaks around ~2022 cm^{-1} at α=0.3 corresponds to -C-O- can be seen for both the component after 2000 s. Peaks around ~1756 cm^{-1} indicate the formation of cyclic oligomers. Other small peaks are also observed around ~1110 cm^{-1}, ~1246 cm^{-1} and ~1382 cm^{-1} indicating –C-O stretching, -C=O stretching and –CH stretching. At higher conversion (α=0.7), A new peak is observed around ~2344 cm^{-1} indicating the formation of carbon dioxide at higher conversion. This peak is not present at lower conversion. Other prominent peaks at higher conversion include ~1228 cm^{-1} and ~1804 cm^{-1} indicating -C=O stretching and cyclic oligomers respectively. So a change in the mechanism of degradation is

observed at higher conversions. Polymers degrade via random depolymerization to produce the above products. However, at higher conversion, complex mechanisms like three-dimensional diffusion (D1, D2, and D3) might be occurring which produces products like carbon dioxide due to chain homolysis of PLA [182].

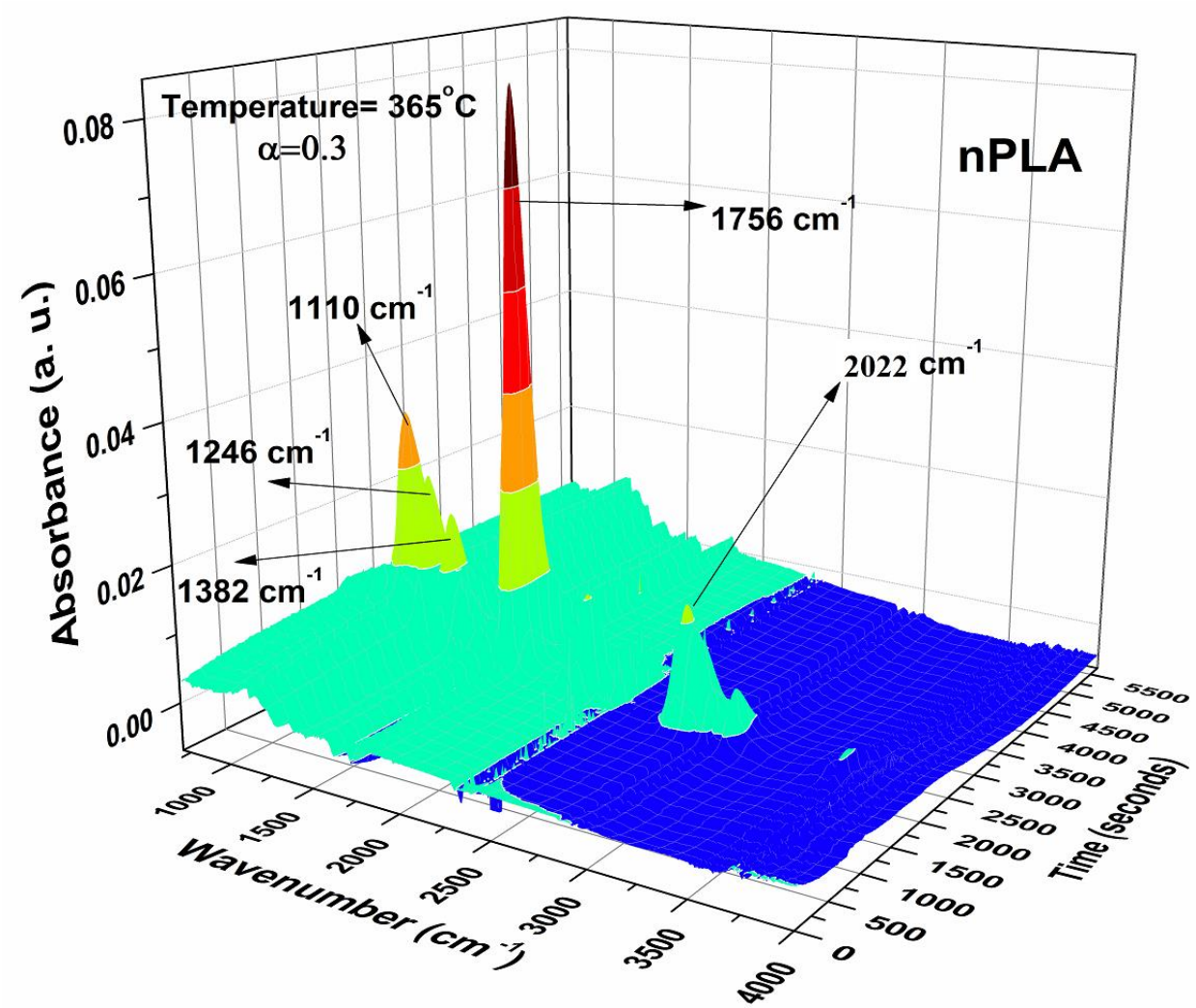

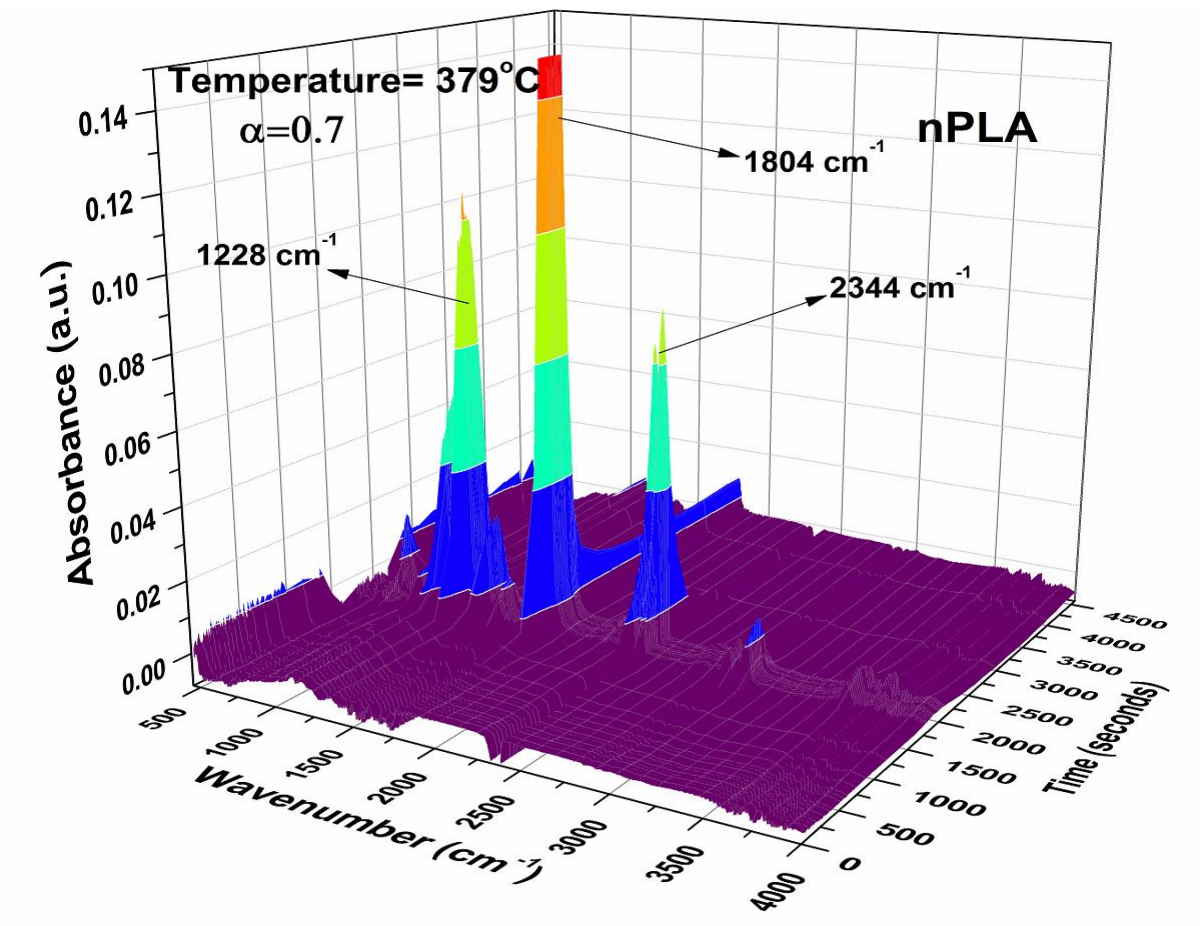

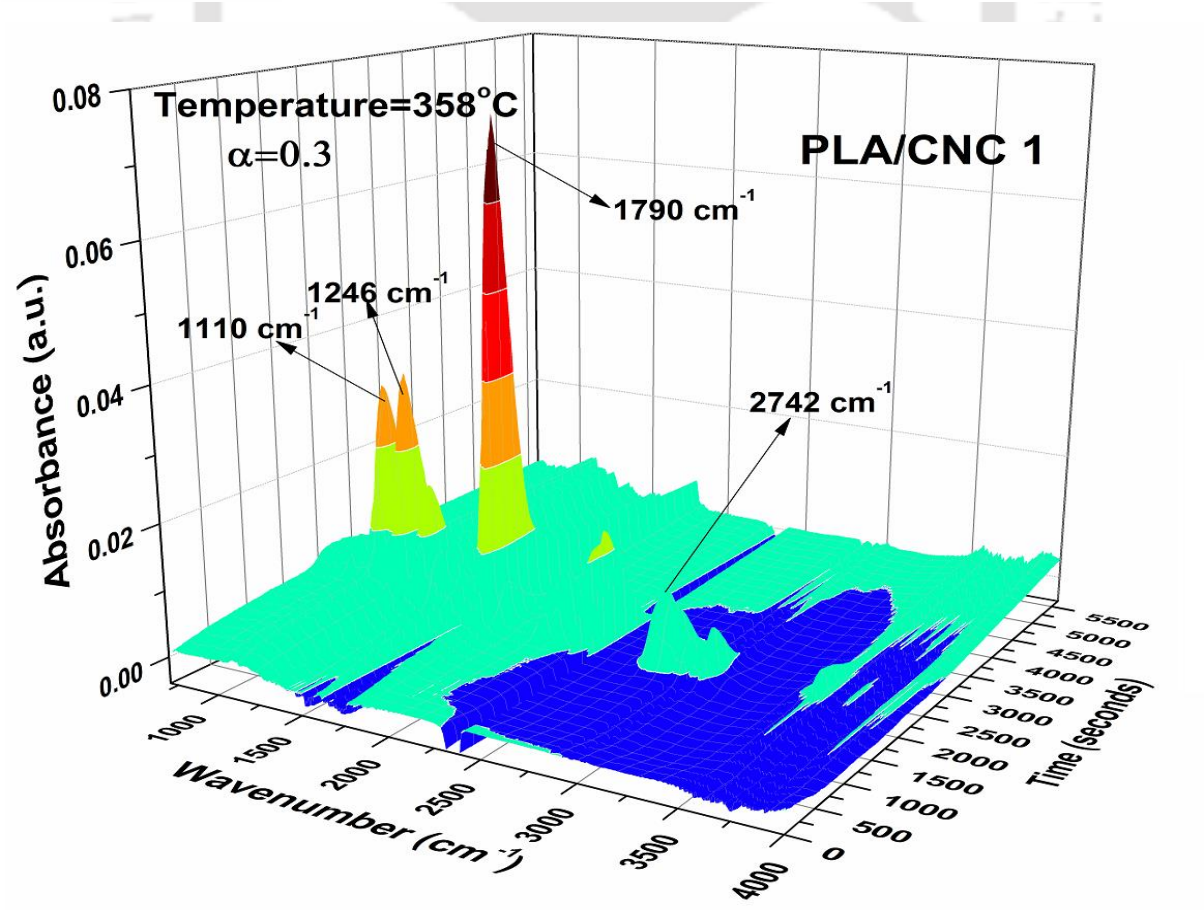

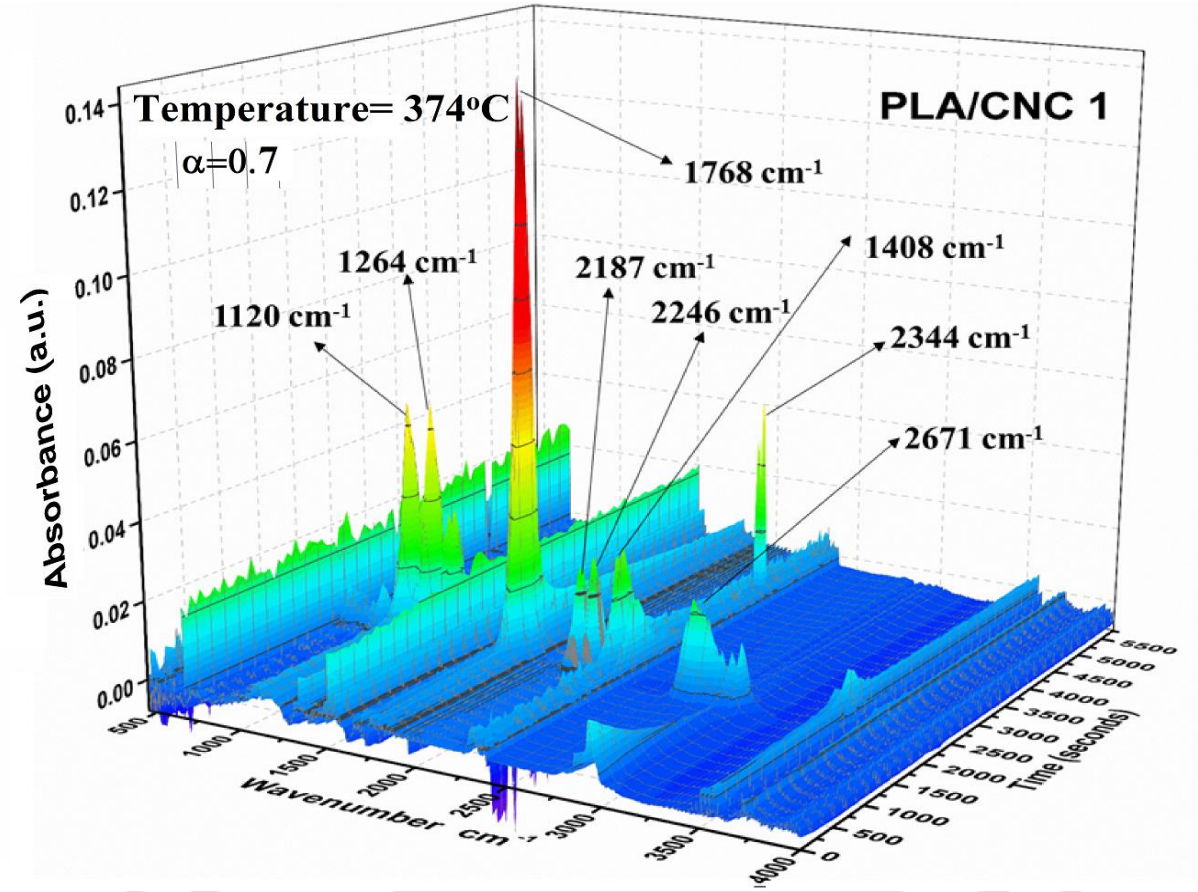

Fig. 3.24 Isothermal TGA-FTIR of nPLA and PLA/CNC 1 at conversion (α=0.3 and α=0.7).

The results are in accordance with the mechanisms suggested by the Criado method as discussed earlier. For the case of PLA/CNC 1 foam, it is observed that at lower conversion (α=0.3) at ~358°C, prominent peaks are observed at ~1790 cm^{-1} indicating the formation of cyclic oligomers after ~1800 s in isothermal conditions. Other peaks are observed around ~1110 cm^{-1} and ~1246 cm^{-1} indicating the formation of –C-O- stretching and –C=O stretching.

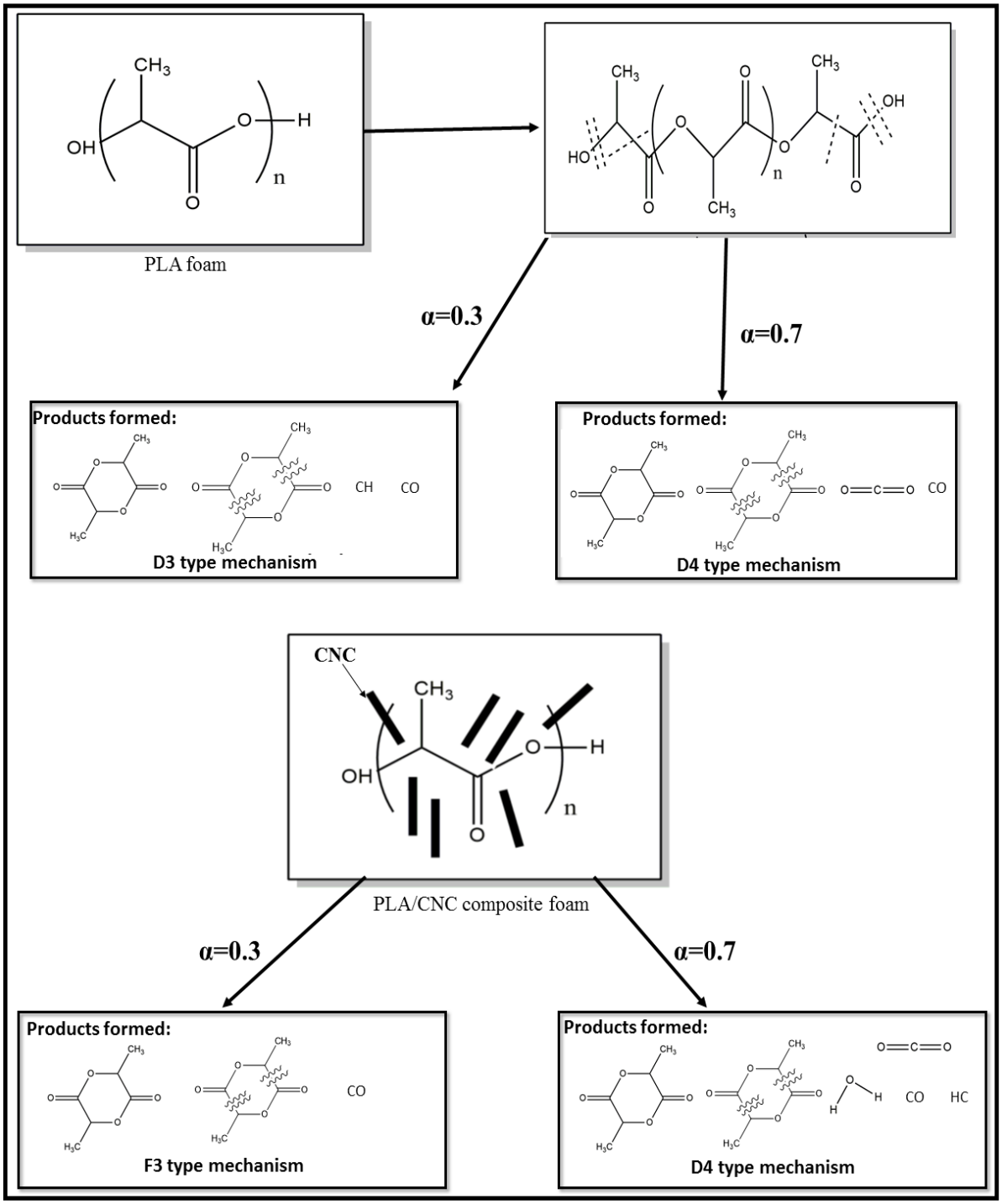

Fig. 3.25 Schematic representation of the degradation mechanism of PLA and PLA/CNC-based foams.

These peaks are also observed in nPLA at lower conversion. At higher conversion (α=0.7) and at 374 °C, for PLA/CNC 1, a prominent sharp peak is noticed around ~1768 cm^{-1} indicating the formation of cyclic oligomers after 2000 s of the isothermal condition. Other prominent

peaks at higher conversion include ~1120 cm^{-1} and ~1264 cm^{-1} indicating the formation of –C-O- stretching and –C=O stretching after ~1800 s. Peaks are also observed around ~2344 cm^{-1} and ~2187 cm^{-1} indicating the formation of carbon dioxide and carbon monoxide at higher conversions. Peak around ~1400 cm^{-1} indicates hydrocarbon formation at this conversion. Peaks are also observed around ~2671 cm^{-1}, ~3000 cm^{-1} and ~3500 cm^{-1} indicating the formation of C-H=O, hydrocarbons, and water at higher conversions [186]. Therefore, it can be concluded that the degradation of PLA/CNC follows a complex mechanism and the mechanism changes at higher conversion. At higher conversions the production of various products like carbon dioxide, carbon monoxide, water etc. might be due to a complex mechanism like 3-dimensional diffusion (D1, D2, and D4) causes chain homolysis of PLA and some extent of hydroxyl end initiated ester decomposition [187]. A schematic representation of the degradation mechanism of the PLA and PLA/CNC-based foams are shown in **Fig. 3.25**. It can be concluded that PLA and PLA/CNC-based foams degraded in similar mechanisms. CNCs does not alter the degradation mechanism of the PLA based foams. The results from TGA-FTIR is in accordance with the results obtained from the Criado method [136].

3.5 Melt crystallization kinetics of the PLA and PLA/CNC-based foams

Crystallinity is a very important phenomenon for foams as it influences the cell integrity and degree of expansion of cells [188–191]. Effects of nanobiofillers in crystallinity, nucleation rate, spherulite size and temperature of crystallization are well established [124]. It can be seen from the relative crystallinity curve (**Fig. 3.26**) that at 2.5 °C/min cooling rate over all time of crystallization is less for the CNC loaded composite as compared to nPLA. In the case of nPLA the value is 5.7 min. Whereas the values are observed as ~5.5 min, ~5.8 min and ~5.7 min for PLA/CNC 1, PLA/CNC 2 and PLA/CNC 3 respectively. However, in the case of higher cooling rates (5 °C/min and 7.5 °C/min), it is similar. At 5 °C/min cooling rate, the value is observed as ~3.7 min for nPLA whereas, the value is observed as ~4.2 min, ~4.0 min and ~3.5

min for PLA/CNC 1, PLA/CNC 2 and PLA/CNC 3 respectively. In the case of 7.5 °C/min cooling rate, the values are found as ~2.4 min, ~2.7 min, ~2.3 min and ~2.3 min for nPLA, PLA/CNC 1, PLA/CNC 2 and PLA/CNC 3 respectively. It can be concluded that half time of crystallization i.e. $t_{0.5}$ is not affected by CNC loading where as for the CNC loaded composites $t_{0.5}$ decreased with the loading of CNC. It may be due to the nucleation effect of the CNC nanobiofillers in the PLA matrix.

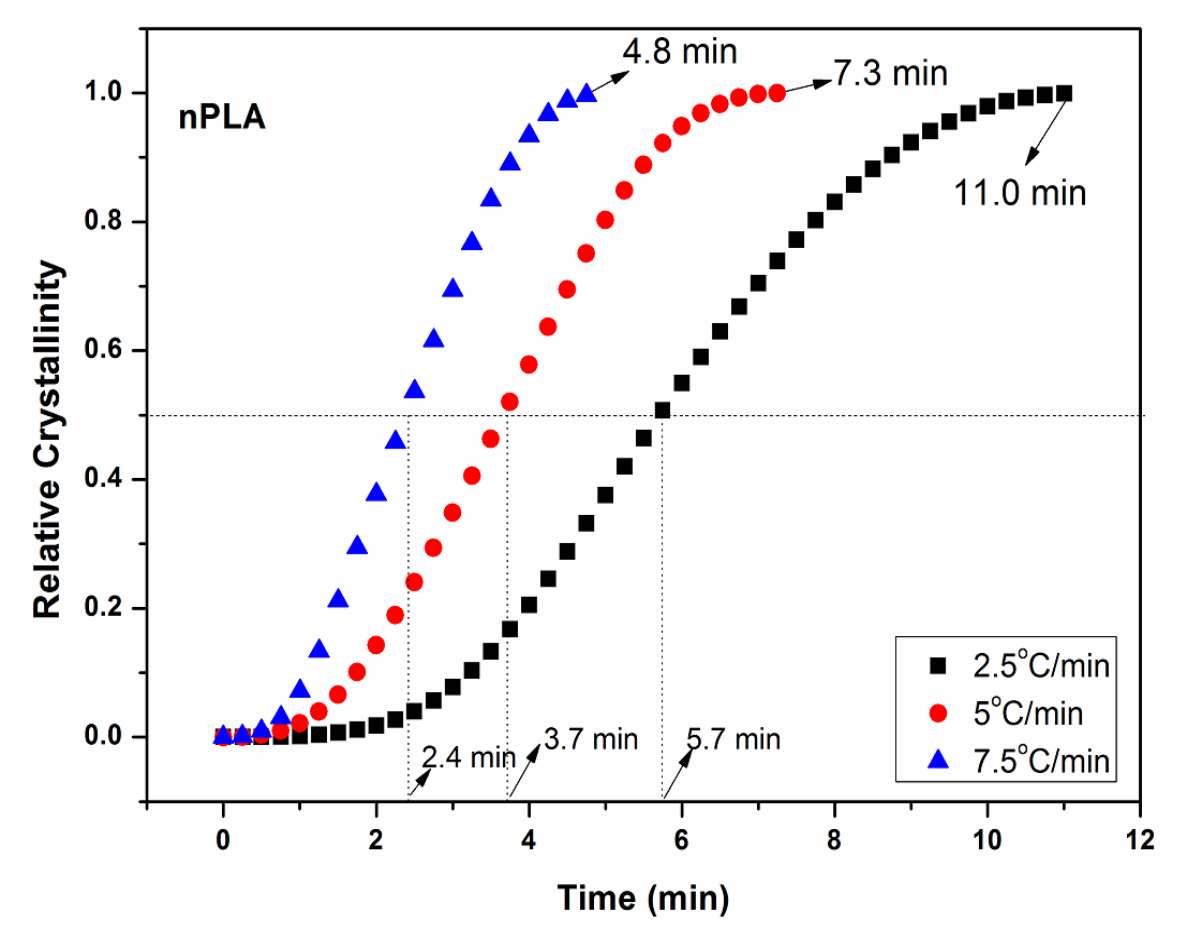

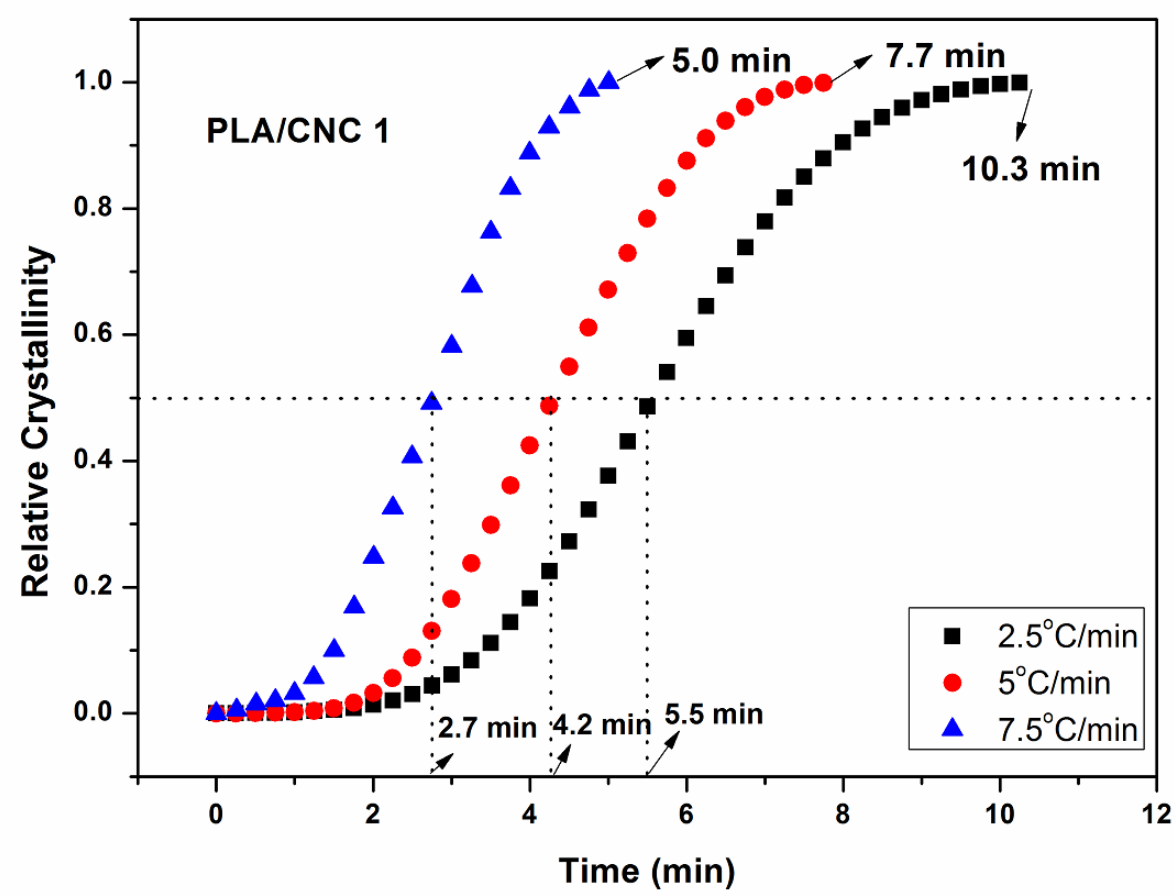
PLA/CNC 1
5.0 min
7.7 min
10.3 min
2.7 min
4.2 min
5.5 min
2.5°C/min
5°C/min
7.5°C/min
Relative Crystallinity
Time (min)

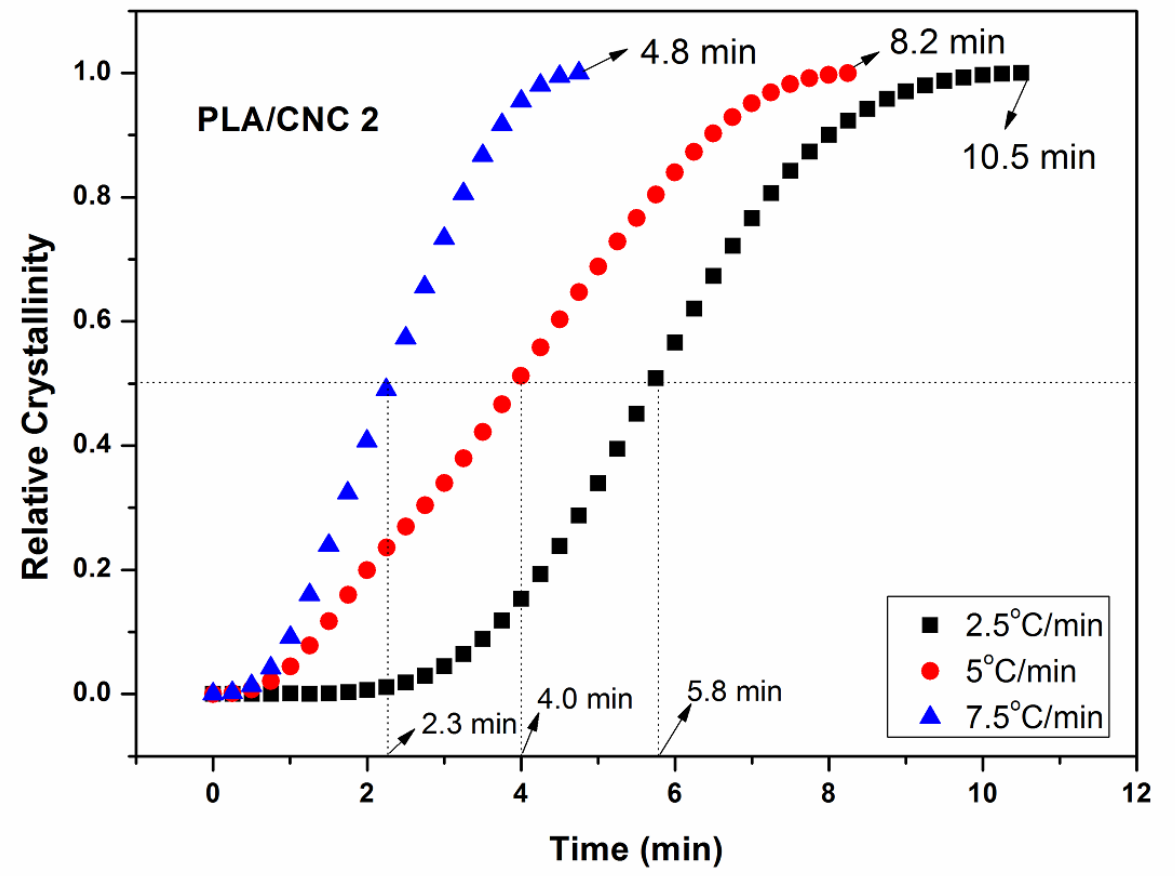
PLA/CNC 2
4.8 min
8.2 min
10.5 min
2.3 min
4.0 min
5.8 min
2.5°C/min
5°C/min
7.5°C/min
Relative Crystallinity
Time (min)

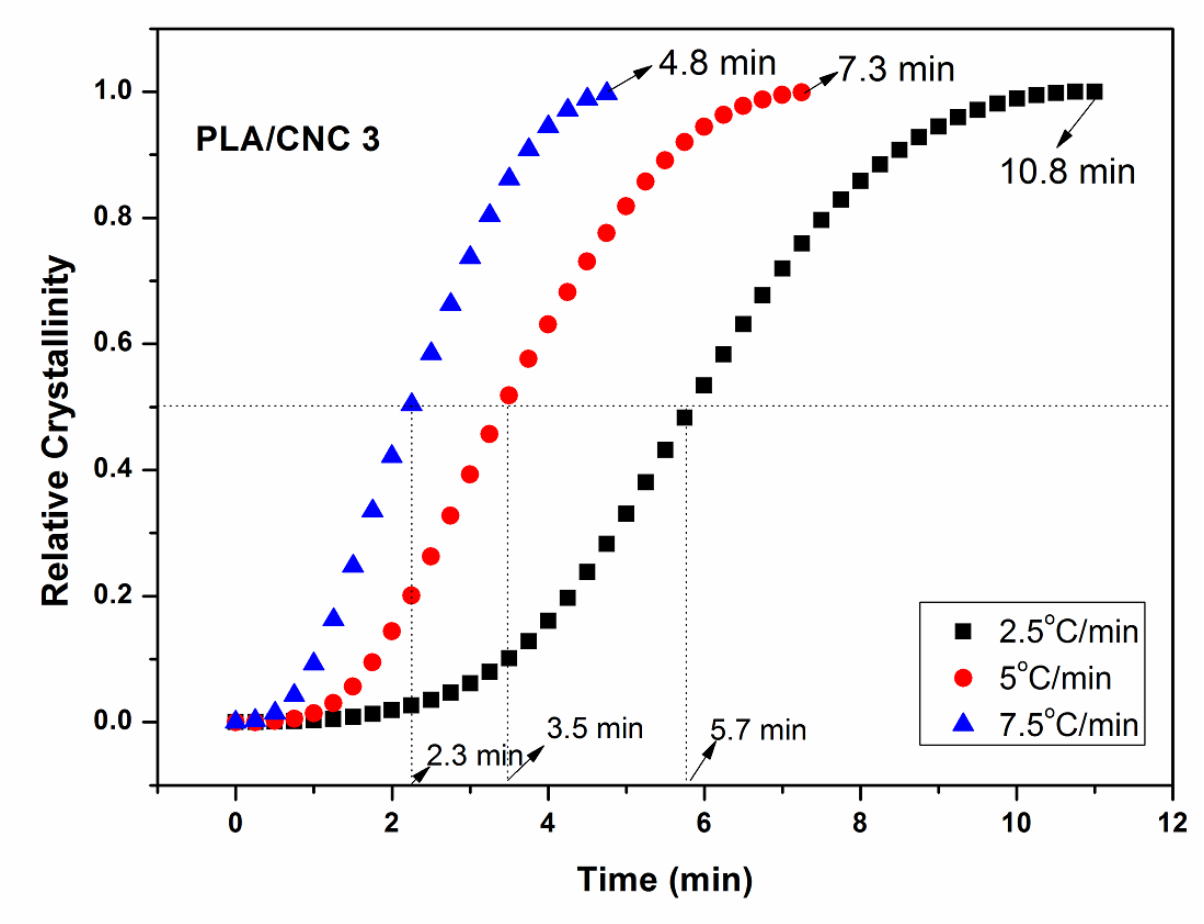

Fig. 3.26 Relative crystallinity plots for PLA and PLA/CNC-based foams.

Avrami plots for PLA and PLA/CNC based fabricated foams are shown in **Fig. 3.27**. From the plots we have calculated the values of Avrami exponent "n" and crystallization rate constant "K" and values are summarized in **Table 3.9**. The values are calculated from the slope and intercept of the linear region of the plots. These to parameters are useful for understanding the crystallization process. Avrami exponent gives an idea of the nucleation mechanism of CNC in the PLA matrix in terms of growth of crystals. It can be seen from the plot that all the fabricated foams behave similarly. A slight deviation from linearity is observed in all the cases indicating the presence of both primary and secondary crystallization [11]. Avrami plot suggests the presence of two different types of crystal growth rate in low crystallinity region and high crystalline region. From the linear region of Avrami plot exponent and rate, constants

were determined. It is found that the "n" value is ranging from ~2.5-~4.0. In most of the cases, it is observed that "n" value is found near to ~3 which indicated the plate-like growth of nuclei over the time.

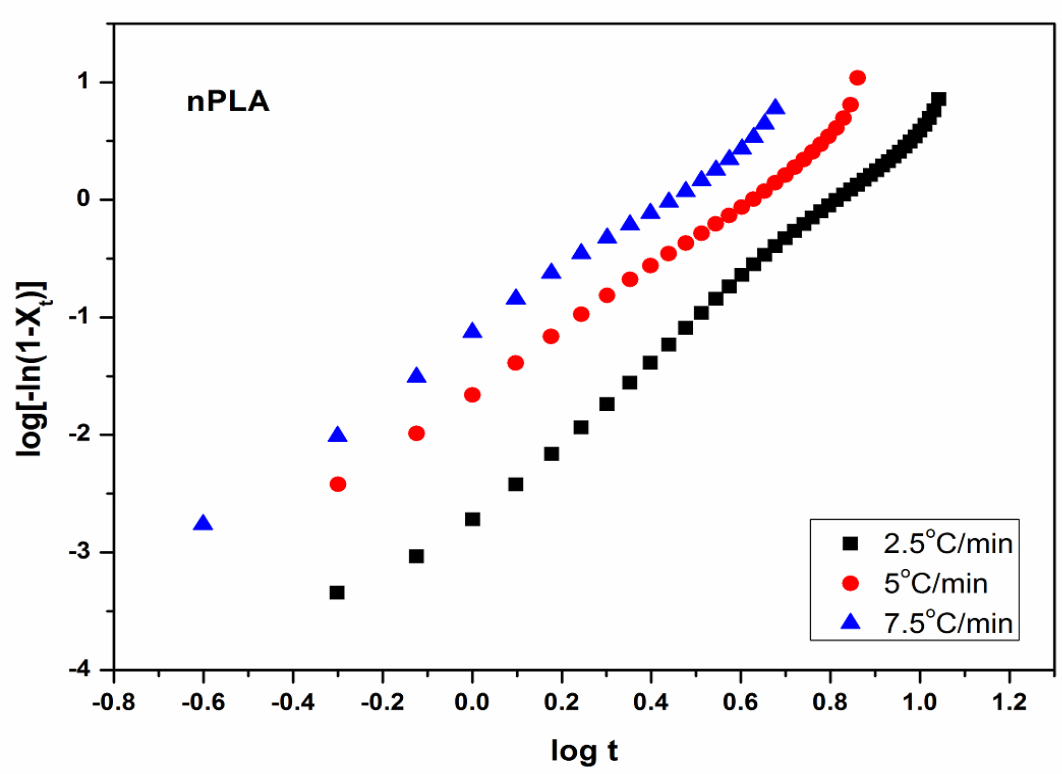

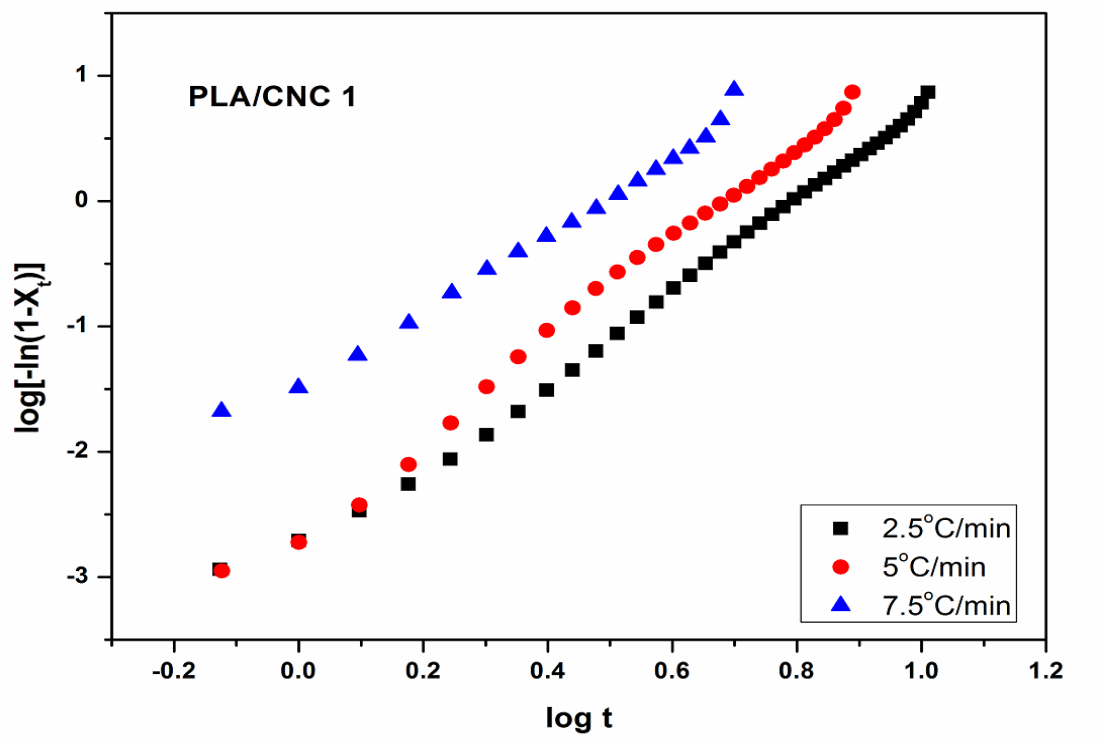

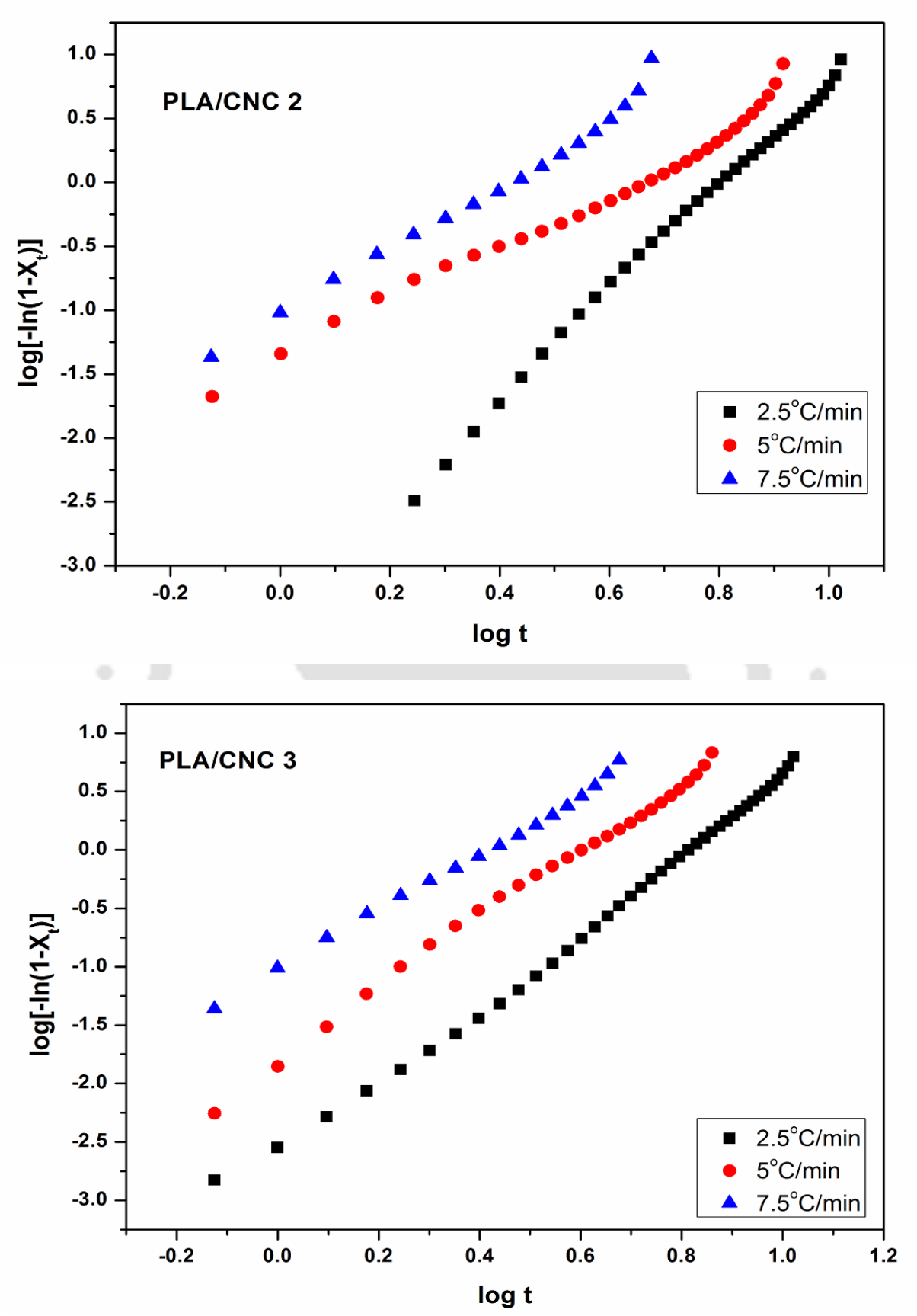

Fig. 3.27 Avrami plots for PLA and PLA/CNC-based foams.

As the value comes nearer to ~2 it indicates the two-dimensional growth of crystals [124]. It is also observed from the rate constant value that it increases with an increase in cooling rate. A similar type of observation is noticed for all the PLA and PLA/CNC based foams. From the rate, constant values it can be confirmed that CNCs act as a nucleating agent and helps in generation of more numbers of nucleating sites in the PLA matrix and thus affecting the crystallization rate of the PLA and PLA/CNC-based fabricated foams. The non-integral values of "*n*" suggesting both thermal and athermal nucleation in the crystallization process.

Table 3.9 Crystallization parameters from the Avrami and Kissinger.

Sample	**Cooling Rate (°C/min)**	**$t_{0.5}$ min**	***k*** **(min^{-n})**	n	**ΔE (kJ/mol)**
nPLA	2.5	5.7	0.002	3.2	72.4
	5	3.7	0.02	2.7	
	7.5	2.4	0.07	2.7	
PLA/CNC 1	2.5	5.5	0.001	3.5	81.3
	5	4.2	0.002	3.8	
	7.5	2.7	0.03	3.0	
PLA/CNC 2	2.5	5.8	0.0004	4.0	153.5
	5	4.0	0.04	2.2	
	7.5	2.3	0.09	2.6	
PLA/CNC 3	2.5	5.7	0.002	3.2	316.2
	5	3.5	0.02	2.9	
	7.5	2.3	0.09	2.5	

Ozawa plots for fabricated foams are shown in **Fig. 3.28**. Nonlinearity of the curves are increasing in the incorporation of CNC nanofillers, which may be due to the nucleation effect of the

nanobiofiller. The composites are not following homogeneous crystallization behavior like PLA. Mo plots of the fabricated foams are shown in **Fig. 3.29**. The value of "*a*" and $F(t)$ are calculated from the slope and intercepts of the curves obtained. The range of "*a*" value of the components are similar it is in the range of 0.9 to 1.9. In case of nPLA, the values are found as ~1.1, ~1.3, ~1.3 and ~1.4 respectively for 20%, 40%, 60% and 80% relative crystallinity. Almost similar trends are observed for PLA/CNC based foams. The change in value at a different degree of crystallinity suggests the change in the mechanism of crystallization. The nonlinearity in the curves also suggests the primary and secondary crystallization in accordance with the previous methods. The different values of "*a*" and *"F(t)"* at different degrees of crystallinity are summarized in **Table 3.10**. Increase in *"F(t)"*value with a degree of crystallization indicating higher cooling rate is required for higher crystallinity. Tobin plots for PLA and PLA/CNC based fabricated foams are shown in **Fig. 3.30.** This method is useful for prediction of the crystallization process as alone Avrami method cannot predict the whole crystallization process. Tobin method describes the crystallization with growth site impingement. The value of "n_T " and "K_T" are calculated from the plots and summarized in **Table 3.10**.

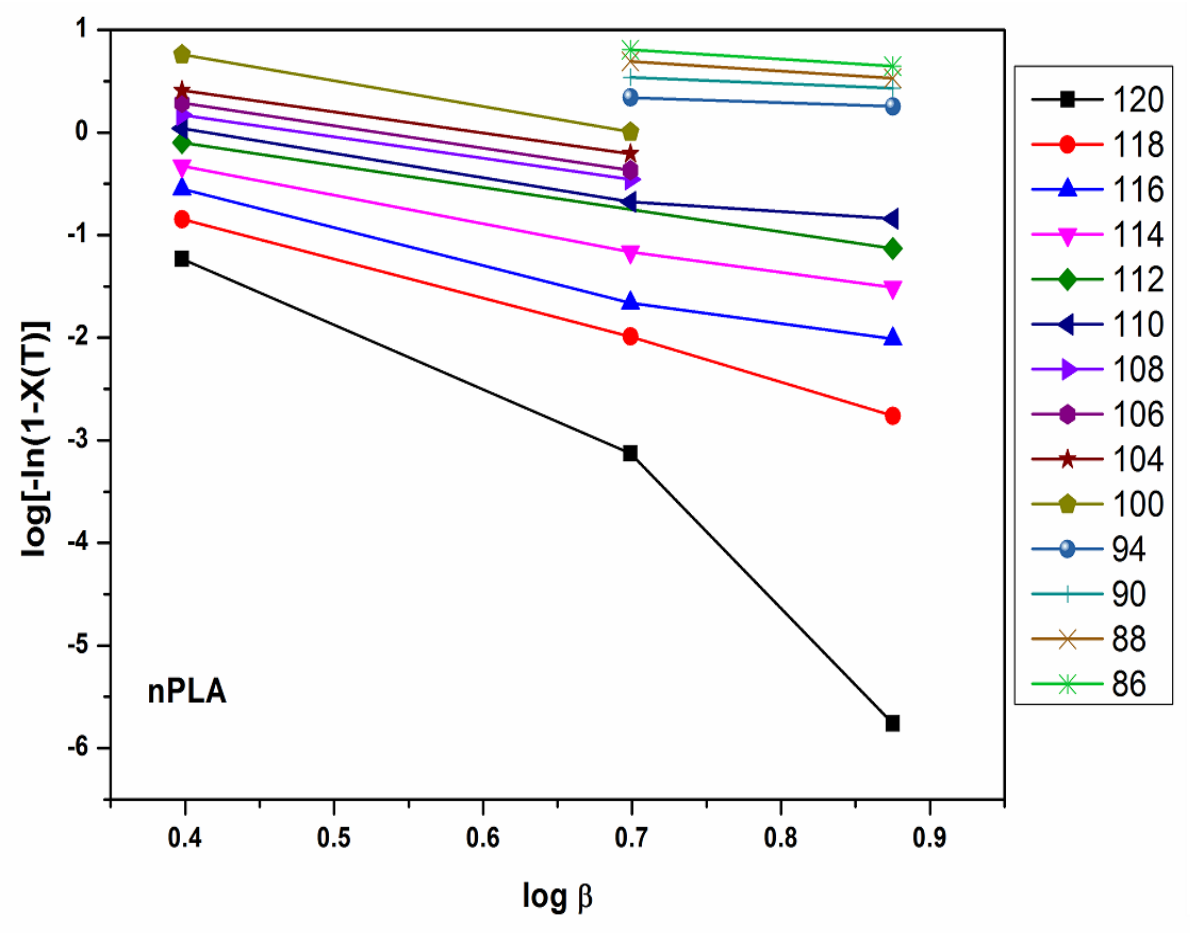

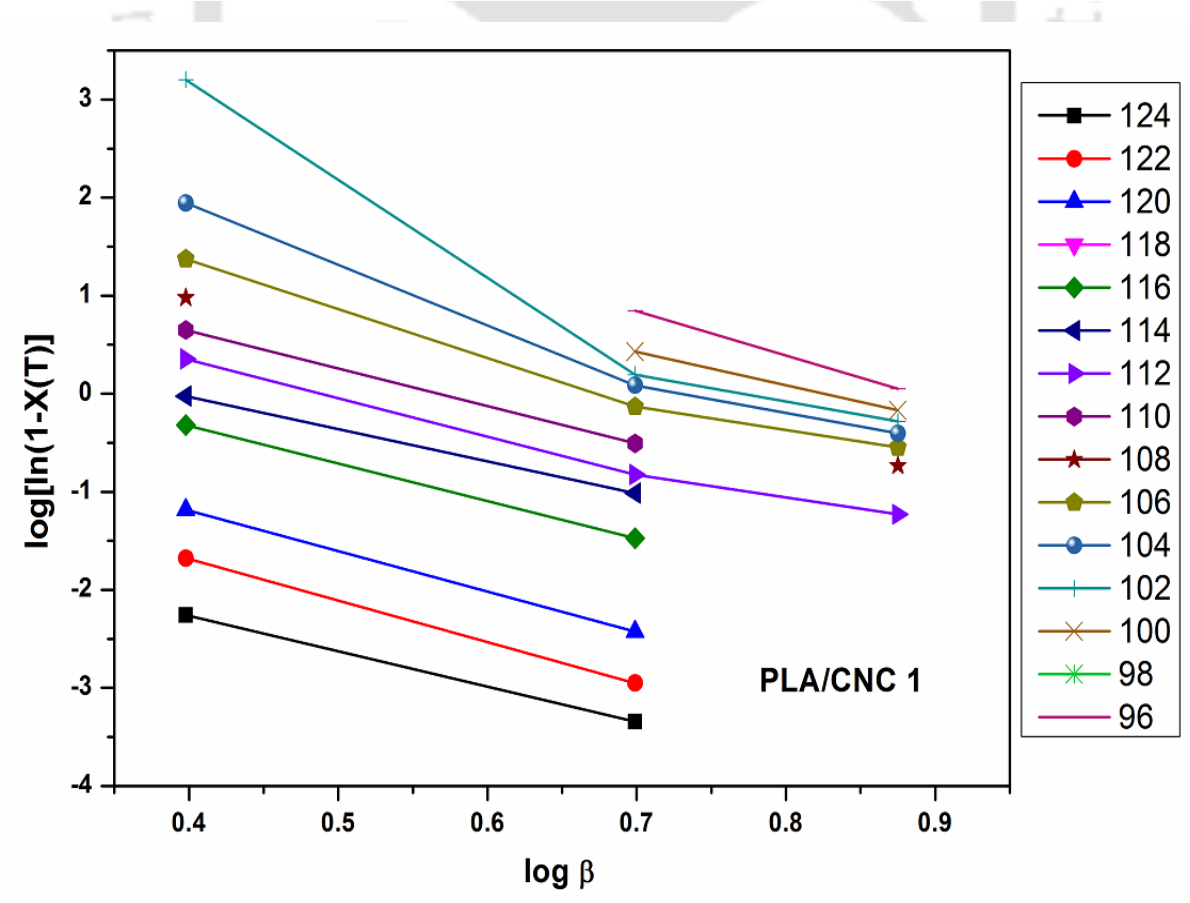

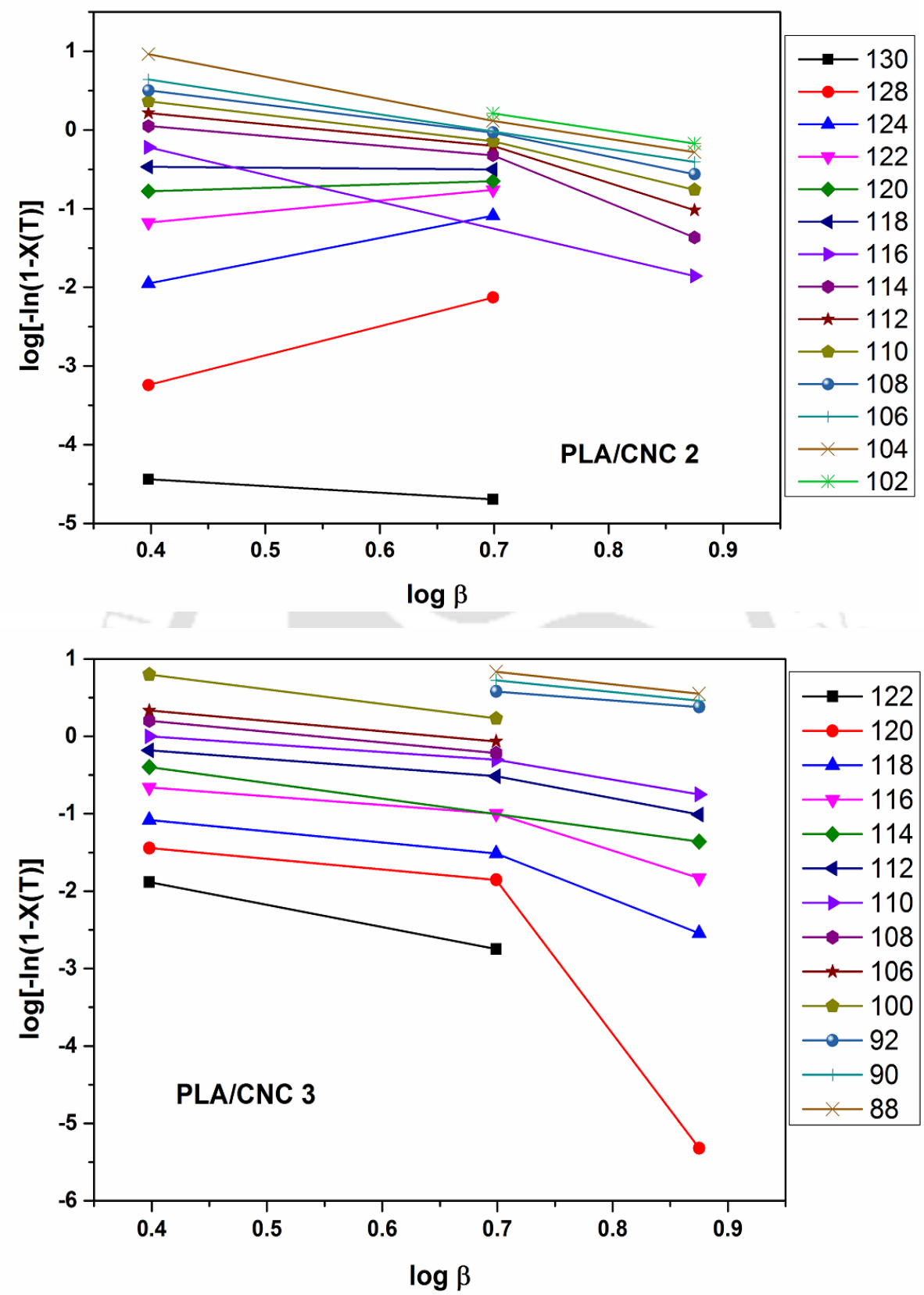

Fig 3.28 Ozawa plots for PLA and PLA/CNC-based foams.

The n_T values are found in a range of ~2.0-~5.2. The value is observed in the range of ~3.0-~3.9 for nPLA, ~3.4-~4.2 for PLA/CNC 1, ~2.0-~5.2 for PLA/CNC 2 and ~2.8-~3.5 for PLA/CNC 3 respectively. A similar range of Tobin rate constant (K_T) and Avrami crystallization rate constant (k) is observed. Tobin exponent (n_T) is also in accordance with Avrami exponent "n". Hence, good accordance of Tobin kinetic parameters with Avrami is observed. It is also observed that n_T value is generally higher than n value of Avrami at same sample and the same cooling rates. Tobin plots also deviate slightly from linearity indicating secondary crystallization in the PLA and PLA/CNC-based fabricated foams [192].

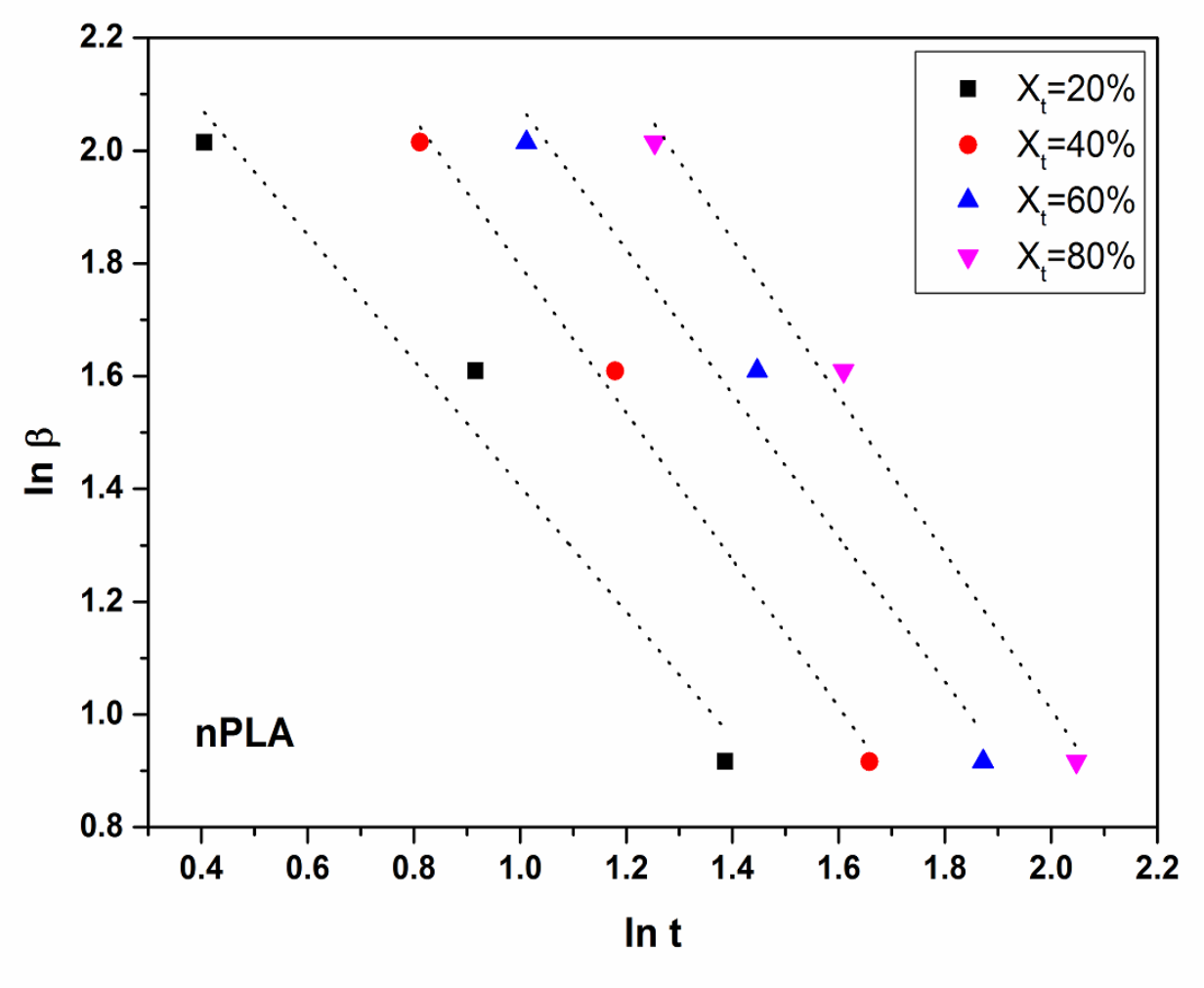

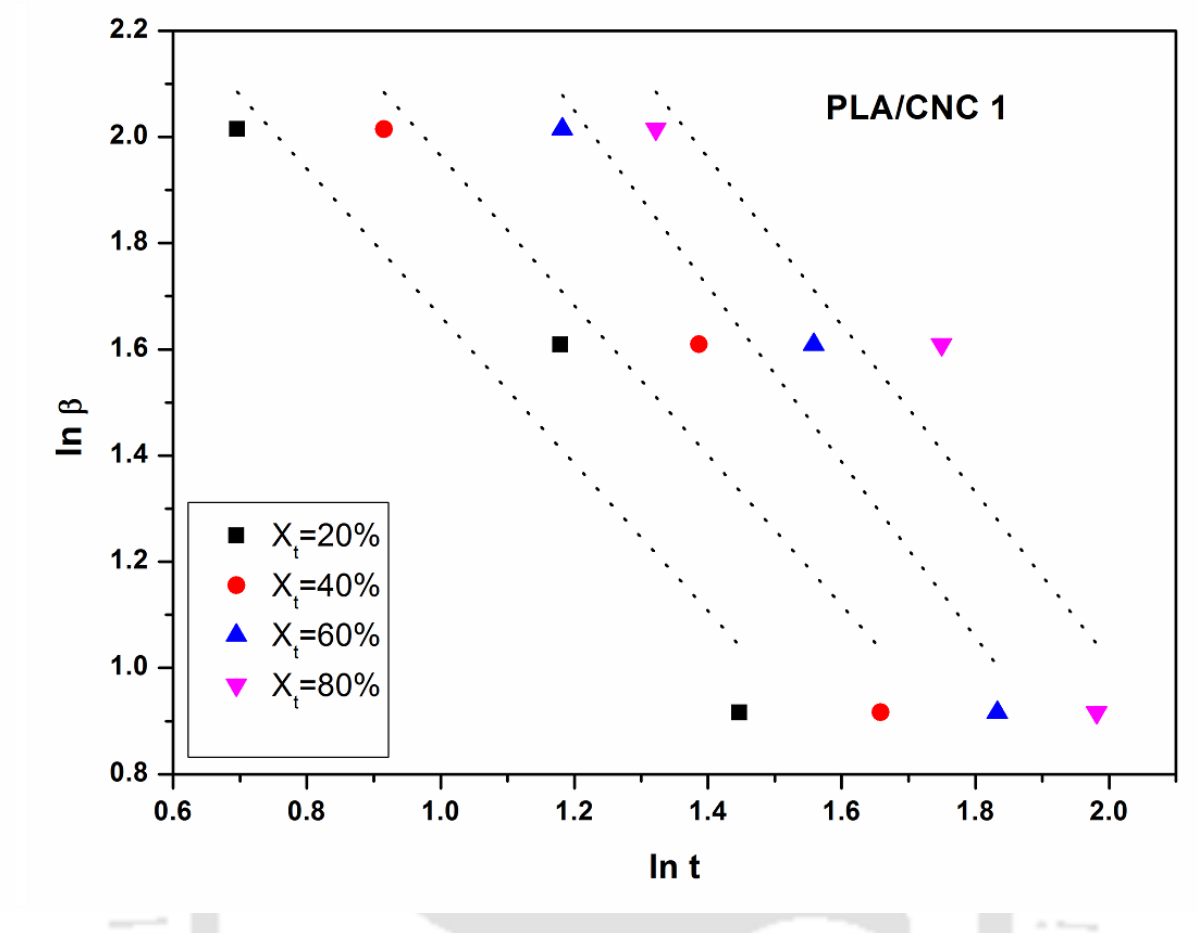
PLA/CNC 1
ln β
ln t
X_t=20%
X_t=40%
X_t=60%
X_t=80%
2.2
2.0
1.8
1.6
1.4
1.2
1.0
0.8
0.6
0.8
1.0
1.2
1.4
1.6
1.8
2.0

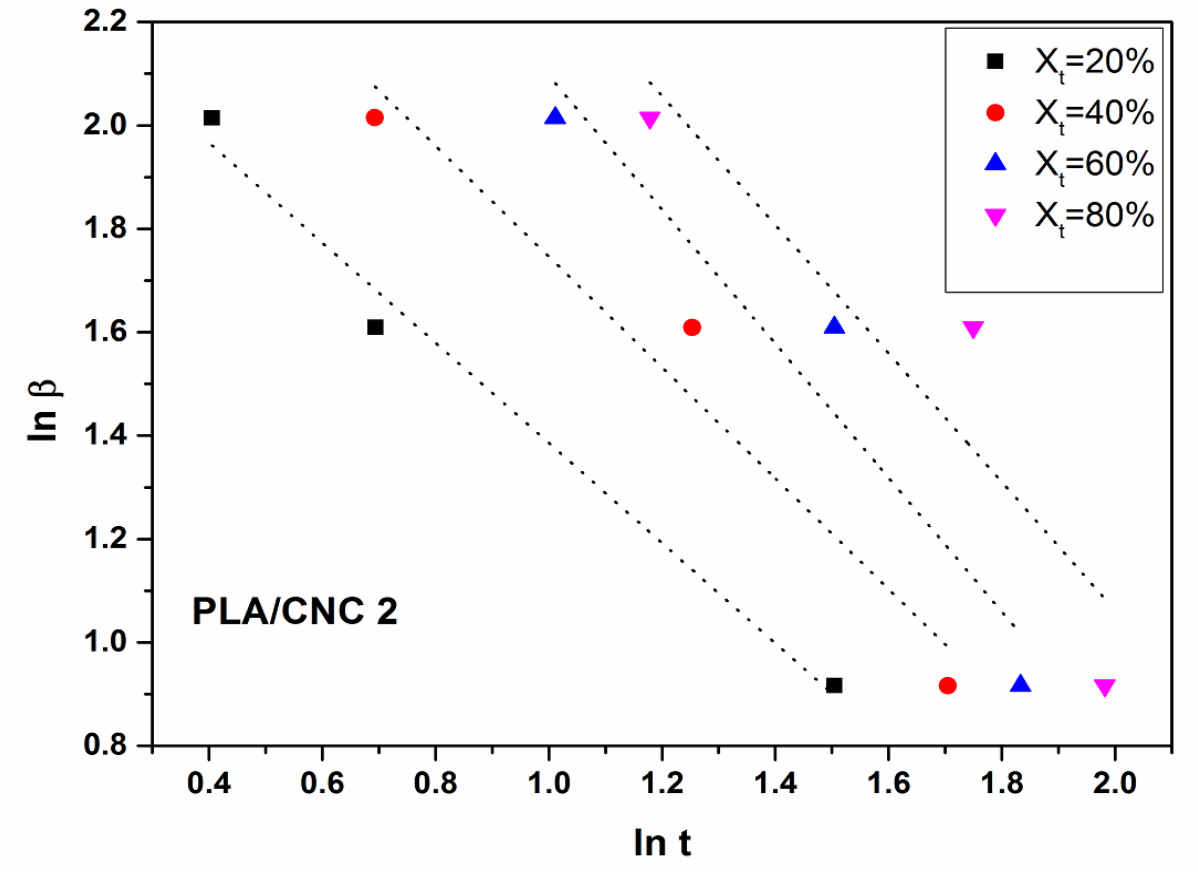
PLA/CNC 2
ln β
ln t
X_t=20%
X_t=40%
X_t=60%
X_t=80%
2.2
2.0
1.8
1.6
1.4
1.2
1.0
0.8
0.4
0.6
0.8
1.0
1.2
1.4
1.6
1.8
2.0

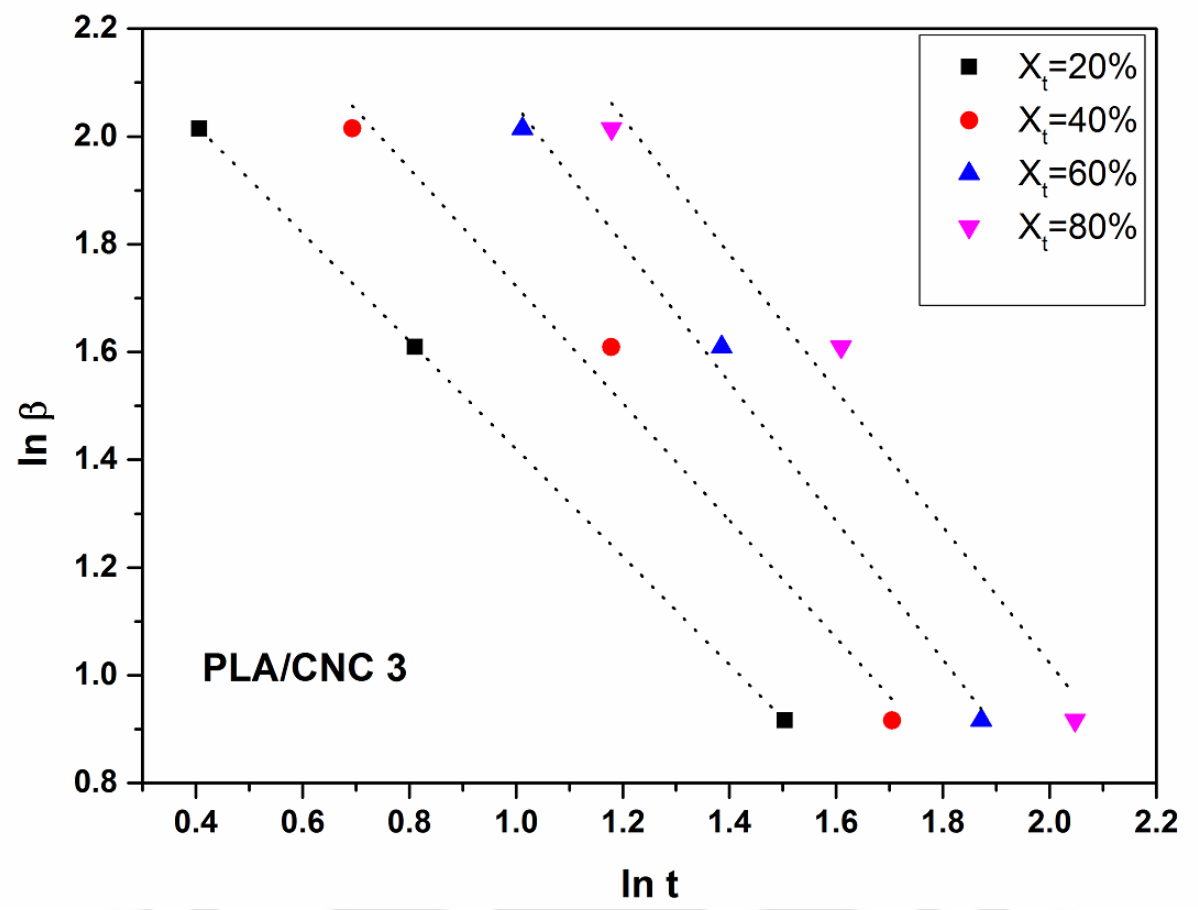

Fig 3.29 Mo plots for PLA and PLA/CNC-based foams.

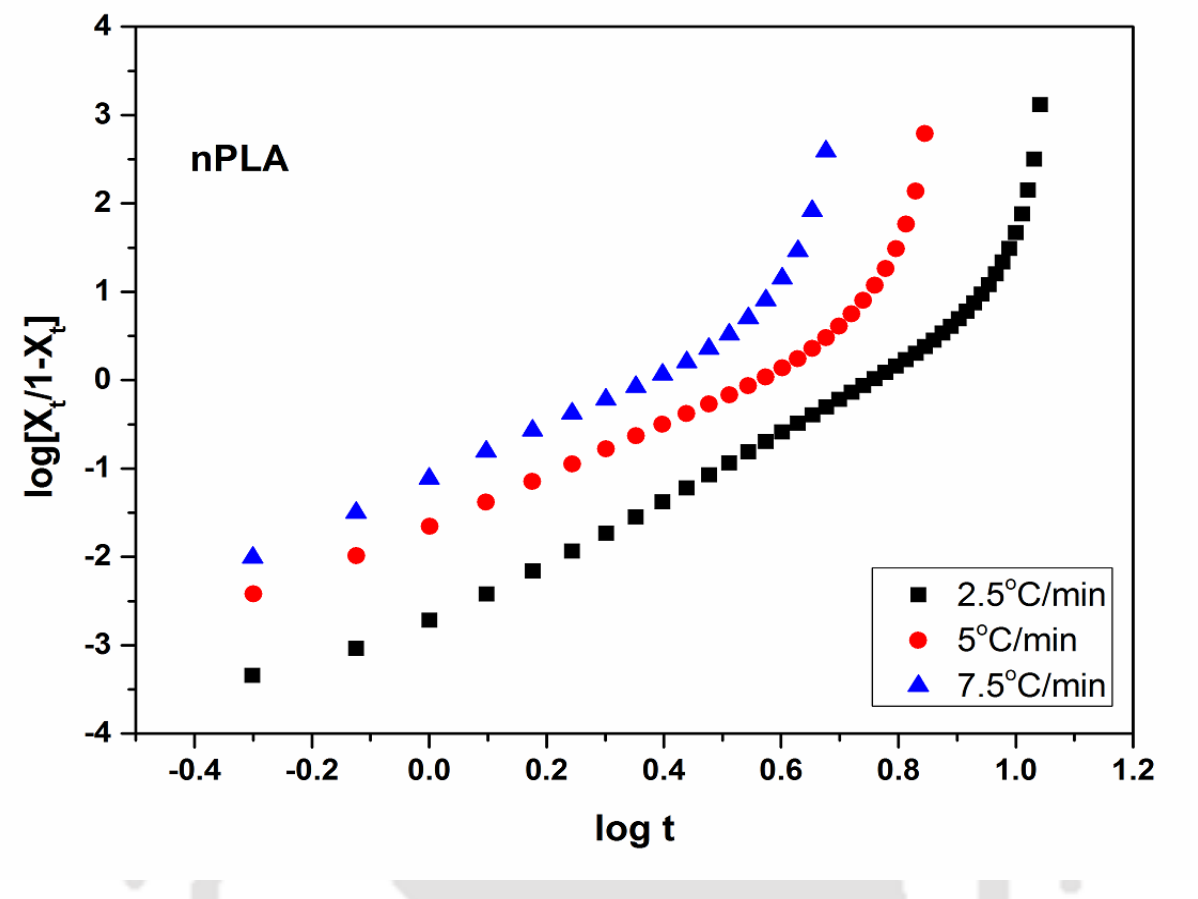
nPLA
log[X_t/1-X_t]
log t
2.5°C/min
5°C/min
7.5°C/min

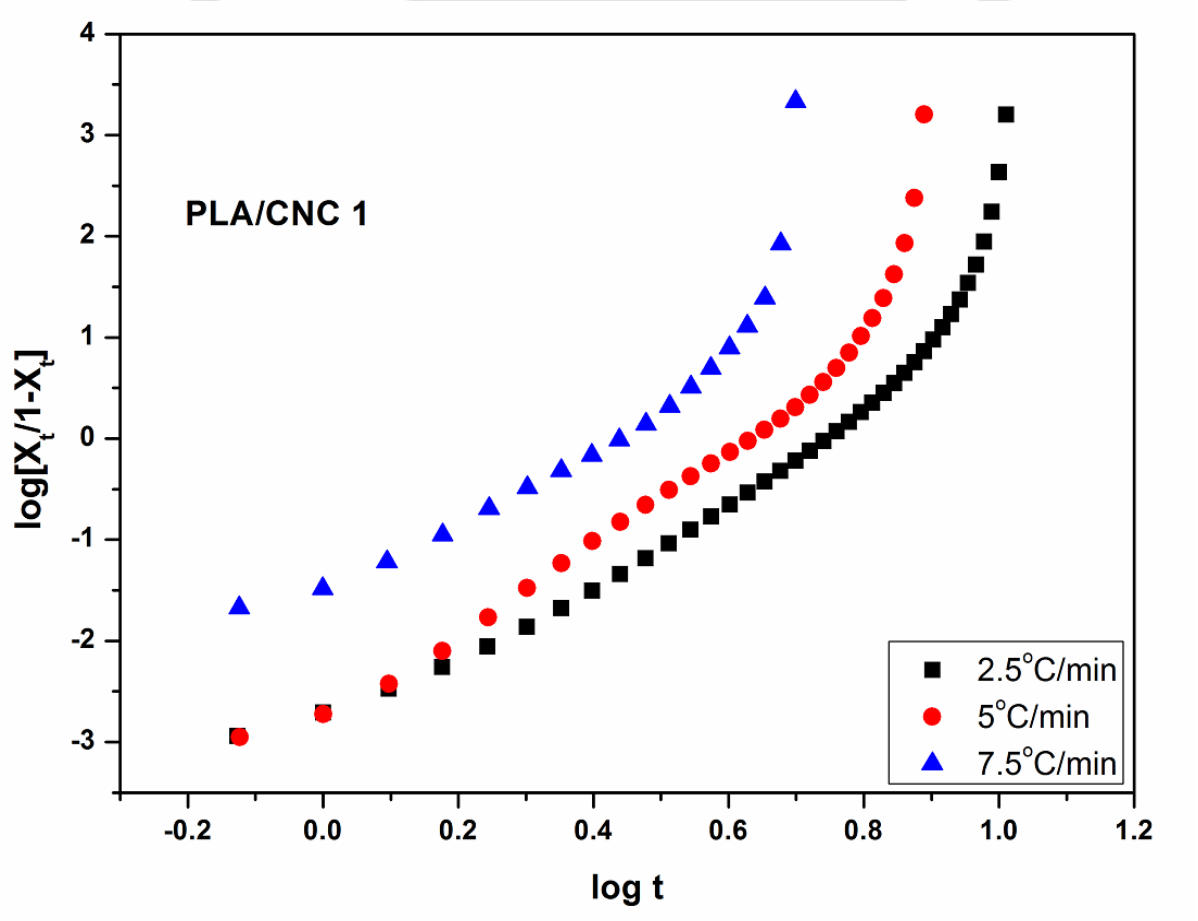
PLA/CNC 1
log[X_t/1-X_t]
log t
2.5°C/min
5°C/min
7.5°C/min

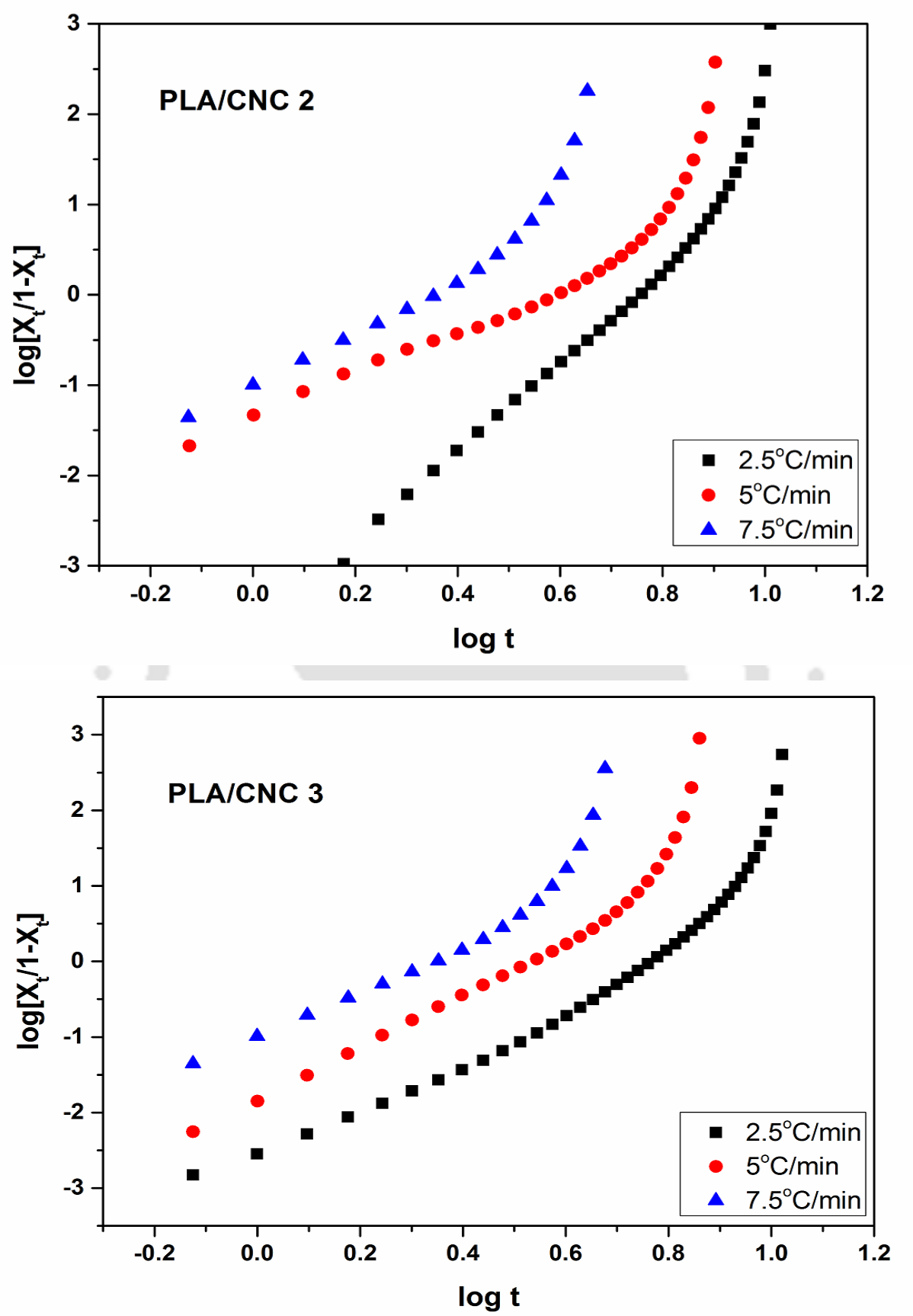

Fig 3.30 Tobin plots for PLA and PLA/CNC-based foams.

The change in energy for crystallization is calculated by using the Kissinger method and the ΔE values are summarized in **Table 3.9**. It is observed from the literature that energy of activation of crystallization is very much related to the transportation of the macromolecular chains of the polymer in the growing surface. Some earlier investigations of isothermal crystallization of PLA/CNC film indicates the presence of nucleating effects of CNC nanobiofillers and also the restriction of chain mobility by the nanobiofillers affecting the crystallization [193–195]. A more prominent effect of CNC as a nucleating agent and restriction in chain mobility in non-isothermal crystallization of poly(β-hydroxybutyrate) composite films is also reported [196]. Increase in crystallization energy on the incorporation of CNC compared to neat PLA films and CNC acted as a chain diffusion barrier in non-isothermal crystallization kinetics of PLA/CNC films is also reported by **Dhar et.al.** [157]. Similarly, in our investigation of non-isothermal crystallization of PLA/CNC based foams, it is observed that an increase in CNC loading, the ΔE value also increases. For the case of nPLA the value is observed as ~72.4 kJ/mol. An increase of ~4 fold is observed for PLA/CNC 3. For PLA/CNC 1, the value is found to be ~81.3 kJ/mol. The value further increased to ~153.5 kJ/mol for PLA/CNC 2. The increase in the value of ΔE might be due to the introduction of CNCs hinders the chain folding of PLA, and thus change in activation energy becomes higher. The higher value indicates that the crystallization is slower in the case of PLA/CNC based foams than nPLA [197]. At highest loading of CNC (PLA/CNC 3), an abrupt increase in ΔE value is observed which might due to the agglomeration of CNC nanobiofillers in the PLA matrix which may cause phase separation and more energy is required for crystallization [157].

It is observed from the literature that CNCs act as a nucleating agent and it also restricts the movement of polymer chains in PLA/CNC based composite films [193,196]. In our PLA/CNC foam system, it can be concluded that at lower concentrations, CNC mainly acts as a nucleating

agent, however at higher concentration, due to the agglomeration, CNC gives hindrance to the movement of polymer chains.

Table 3.10 Crystallization parameters from the Mo and Tobin Analysis.

Sample	**Mo**			**Cooling Rates (°C/min)**	**Tobin**	
	X_t (%)	$F(t)$	a		K_T	n_T
nPLA	20	12.4	1.1	2.5	0.002	3.3
	40	22.2	1.3	5	0.02	3.0
	60	28.6	1.3	7.5	0.06	3.9
	80	44.2	1.4			
PLA/CNC 1	20	28.8	1.9	2.5	0.002	3.4
	40	33.9	1.6	5	0.002	4.2
	60	81.4	1.9	7.5	0.03	3.9
	80	90.9	1.8			
PLA/CNC 2	20	10.5	0.9	2.5	0.0002	5.2
	40	16.7	1.1	5	0.06	2.0
	60	29.7	1.3	7.5	0.07	3.5
	80	34.8	1.2			
PLA/CNC 3	20	11.3	1.0	2.5	0.003	2.8
	40	16.6	1.1	5	0.01	3.5
	60	28.3	1.3	7.5	0.09	3.1
	80	34.9	1.3			

From the above discussion, it can be concluded that PLA and PLA/CNC-based foams undergo both primary and secondary crystallization and CNCs acts as a nucleating agent in the matrix.

3.6 Porosimetric investigations of PLA and PLA/CNC-based foams

The various properties of fabricated foams investigated by MIP are summarized in **Table 3.11**. The average pore diameter is decreasing on increasing the CNC loading which might be due to the nucleating effect of the nanobiofillers, which creates nucleating sites in the PLA matrix leads to the generation of more number of smaller pores. The increase of ~66% and ~96% in surface area is observed for PLA/CNC 1 and PLA/CNC 2 respectively compared to their neat counterpart can also be justified by the above logic. However, for the highest loading (PLA/CNC 3), a comparable average pore diameter (~1.28µm) and surface area (14.48 m^2/g) is observed with nPLA. This decrease in surface area and increase in average pore diameter might be due to the agglomeration of the CNC nanobiofillers, which creates a phase separation in the PLA matrix. The porosity of the fabricated PLA/CNC based foam decreases on increasing the filler concentration due to the generation of smaller pores and larger surface area. However, in the case of PLA/CNC 3, the porosity observed near to nPLA foam due to the presence of larger pores compared to other PLA/CNC based foams. CNC is agglomerating and phase separation is taking place at higher CNC loading.

Table 3.11 Summary of Mercury Intrusion Porosimetry (MIP) Investigation.

Sample	Average pore diameter (µm)	Porosity (%)	Surface area (m^2/g)
nPLA	1.45	82	13.62
PLA/CNC 1	0.59	76	22.66
PLA/CNC 2	0.45	74	26.80
PLA/CNC 3	1.28	81	14.48

3.6.1 Corroboration of foam properties with respect to porosity

In literature, up to ~2-fold increase in crystallization activation energy (ΔE) of PLA/CNC non-porous system is reported for the loading of 1% CNC to its neat counterpart [157]. An increment of ~1-fold in ΔE than the neat counterpart is also reported for poly(β-hydroxybutyrate)/CNC based non-porous system at 2% loading indicating the nucleating effect of CNC in the non-porous system [196]. Similarly, in our porous PLA/CNC system, ~1-fold and ~2-fold increment in ΔE is observed for PLA/CNC 1 and PLA/CNC 2 respectively indicating the nucleation of CNC. However, at highest loading the CNC agglomerates and acts as a physical barrier for chain movements. The change in ΔE increments in both the porous and non-porous system is quite similar. In this investigation, non-isothermal melt crystallization is performed, where samples are first melted to the desired temperature and then allowed to cool. So the effect of porosity is not so prominent and the effect of nanofiller is mainly governing the crystallization process. However, the thermal degradation activation energy of the PLA/CNC based non-porous system from various models are comparatively less than the results we found in our PLA/CNC based foam system as discussed earlier. An increment of ~40-~50 kJ/mol in activation energy is observed in the case of PLA/CNC based porous system [182,186]. The probable reason might be due to the presence of gaseous voids in the foam system that effects the transfer of heat in the foamed structure and ultimately requires slightly higher energy for degradation. In addition, it retards the gas diffusion because of the increase of the tortuous path length due to the porous nature of the fabricated foams. Due to the presence of voids, the effective heat transfer coefficient reduces. From the previous findings (in section 3.3), mainly diffusion is the governing mechanism of thermal degradation of PLA/CNC system and the above-mentioned features of porous system effects both heat diffusion and gas diffusion within the system during thermal degradation. A schematic representation of the

process is shown in **Fig. 3.31**. It is observed that in the case of thermal degradation kinetics, the effect of both the porous morphology and nanofiller is prominent in degradation.

The porosity of the fabricated foams can be correlated with the activation energy of thermal degradation. It can be concluded from the MIP investigation that on decreasing the porosity, the activation energy improves along with thermal stability. However, at the highest concentration of CNC, the porosity increases and the thermal stability along with activation energy decreases due to the presence of comparatively larger pores and agglomeration of CNC nanobiofillers. Porosity increases mean the presence of more gaseous voids in the foams, which reduces the heat transfer rate [187]. The surface area of PLA/CNC 3 is observed near to that of nPLA foam. Due to the reduction in a surface area, less number of degradation cites will generate which ultimately decreases the energy of activation required for thermal degradation to take place. Results are in accordance with our previous discussions of thermal degradation kinetics.

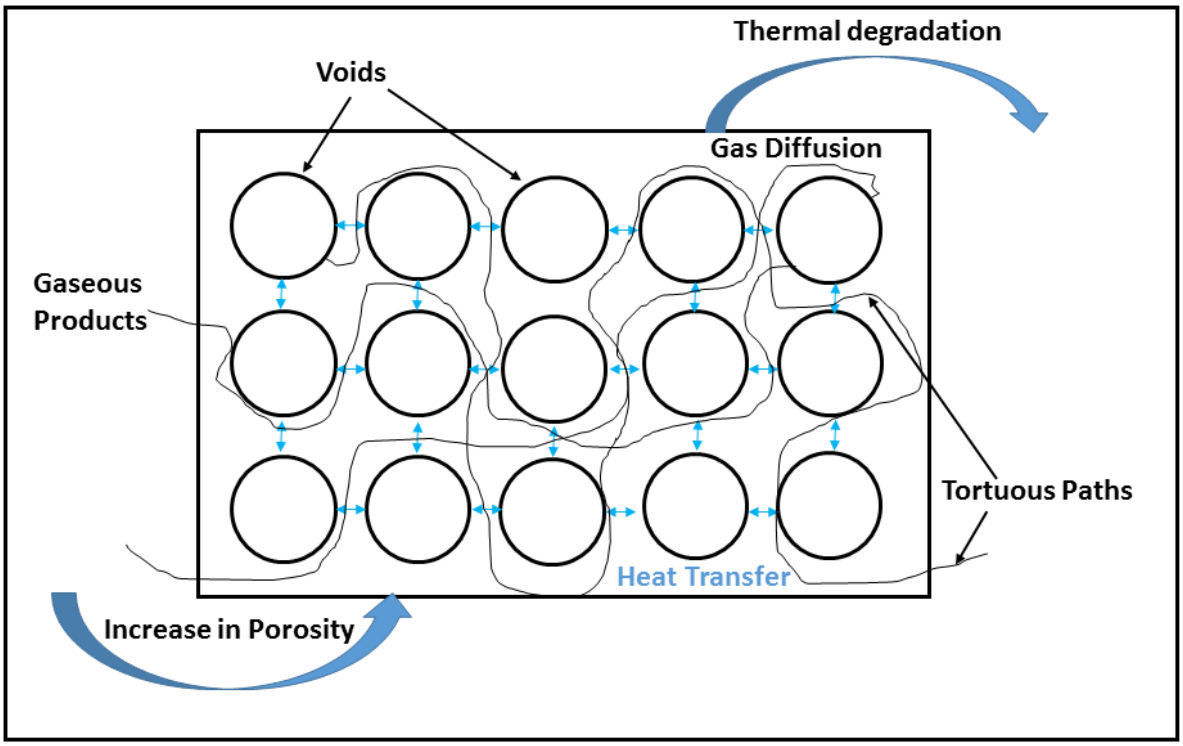

Fig. 3.31 Schematic representation of thermal degradation in porous PLA/CNC based system.

3.7 Summary

This chapter demonstrates the fabrication of biodegradable PLA and PLA/CNC based foams with porous, cellular and open cell structure and interconnected pores, which have been developed using sucrose as porogen medium. This investigation is successfully demonstrated an elegant method for the production of biodegradable foams. The density of composites foams is successfully reduced to ~6.1folds compared to PLA granules. The introduction of CNCs affects the surface morphology and wettability of the fabricated foam due to the generation of more nucleating sites with the loading of CNCs. From the FESEM images, it is observed that the PLA/CNC foams have a porous structure with uniformly dispersed CNC nanobiofillers. However, while compression of the foamed surface, the contact angle is decreased, which indicates the effect of surface morphology on wetting. It is further observed that the storage modulus (E') and loss modulus (E'') values of the foams increases with CNC loading. It is noteworthy to mention that due to a reduction in cell size with CNCs loading, which eventually generates more nucleating sites, which enhances the cell density (N_f). Crystallinity increases on increasing the CNCs content, highest crystallinity is observed for PLA/CNC 3 foam that is around ~55%. However, the effect of CNCs onto the thermal degradation stability of the nPLA and PLA/CNC foam samples are observed, which later aggravated its thermal degradation at higher CNC loading. The rigorous study on wettability property, morphology, mechanical and thermal property of CNC based PLA nanocomposite foams may open up a new prospect towards its applicability in the field of biomedical and drug delivery application.

Thermal degradation kinetics and non-isothermal crystallization kinetics of PLA and PLA/CNC based fabricated foams are also thoroughly investigated in the present chapter. From the MIP investigations, it can be concluded that CNC nanobiofillers are acting as nucleating agent in the PLA matrix thus a decrease in pore diameter and porosity is observed on increase in CNC loading. However, at higher loading, CNC agglomerates results in increasing average

pore diameter and a decrease in surface area. From the "model-free" and "modelistic" approaches, it is observed that on increasing the conversion value the E_a values increase for the fabricated foams. The results obtained by the different methods are in good agreements. The decreasing value of E_a on higher loading is due to the presence of more number of sulfate groups on higher loading, which affects thermal stability, and agglomeration might be taking place in the matrix. This investigation confirms that PLA/CNC 1 (E_a is in range of ~183.8 kJ/mol-~205.1 kJ.mol) has the most thermostable compared to higher loading. The degradation mechanism of the PLA and PLA/CNC based foams are proposed by using Criado method. Complex degradation mechanism like three-dimensional diffusions might be taking place at higher conversions as suggested by the formed products from hyphenated TGA-FTIR studies which are in accordance with Criado method. From the non-isothermal crystallization investigations, it can be concluded that CNC acts as a nucleating agent in lower loadings and hinders the PLA chain folding at higher loading. It is observed that both primary and secondary crystallization is taking place in all the PLA and PLA/CNC based fabricated foams. It can be concluded that the effect of porosity is more prominent in thermal degradation than in crystallization. The investigation is useful to understand the probable applications of the fabricated PLA and PLA/CNC-based microcellular composite foams. The fabricated bionanocomposite PLA/CNC-based foam has the ability as a green replacement for the petroleum-derived non-degradable foams and can be useful in applications such as biomedical, packaging due to the fact that CNC improved various properties of the fabricated foam.

Chapter 4

Poly (lactic acid)/Modified Chitosan (MC) based Nanocomposite Foams: Non-isothermal Crystallization and Thermal Degradation Kinetics with Wettability and Porosimetric Investigations

This chapter mainly deals with the development of PLA/modified chitosan (MC) based microcellular foams. The detailed investigations of crystallization kinetics and thermal degradation behavior is thoroughly discussed in this chapter. The structure-property relationship along with porosimetric investigations of the developed foams is also reported. The decrease in the pore diameter up to ~33.3% and increase in the surface area up to ~30.2% for the highest concentration (3%) is also observed from the porosimetric study with an increase in MC. MC also influences the hydrophobicity (up to ~10° increment in contact angle) of the foams. Thermal degradation kinetics and degradation mechanism of the fabricated foams are investigated by using different approaches like modified Coats Redfern (modified CR), Flynn-Wall-Ozawa (FWO), Kissinger and Criado. Crystallization behavior of the fabricated foams is also discussed thoroughly in this chapter. The crystallization studies of the PLA and PLA/MC based foams suggest the nucleating behavior of MC in the PLA matrix. Porosimetric investigation of the fabricated foam also corroborates the nucleating effect of MC. From the porosimetric investigation, it can be concluded that the effect of porous morphology is prominent in the thermal degradation compared to crystallization.

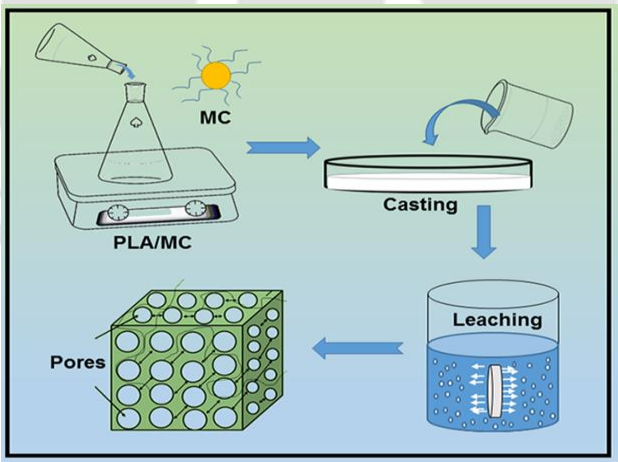

Parts of this research work has received scientific recognition as follows:

Shasanka Sekhar Borkotoky, Akhilesh Kumar Pal and Vimal Katiyar *"Poly (lactic acid)/Modified Chitosan (MC) based Nanocomposite Foams: Non-isothermal Crystallization and Thermal Degradation Kinetics with Wettability and Porosimetric Investigations*". Journal of Applied Polymer Science, 136 (2019) 47236. doi: http://doi.org/ 10.1002/app.20181697.

4.1 Introduction

Recently polymeric foams gain many attentions in research due to its unique characteristics over non-foamed counterparts like lightweight and low density. These unique properties make it suitable to penetrate in almost all aspects of our daily life. The cost of production of these materials is also comes down due to the less usage of material [198]. The ultimate disposal and recycling of petro-based foams have some detrimental effects in nature. Due to this reason, now researchers are mainly focused on the development of green biodegradable foams, which can be easily fed to the ecological system [2,3]. Foamed materials already made their strong presence in some sophisticated areas of application like drug delivery, tissue engineering, and other biomedical applications. The need for new greener sustainable polymeric foam for the environmental point of view is opening new opportunities for biobased, non-toxic and biodegradable polymers like poly (lactic acid) (PLA), polycaprolactam etc. In some sophisticated applications, biodegradability is a major area of concern. In the recent past, PLA based foams get more attention in the research community due to its comparable properties with petroleum-based conventional polymeric foams. It can be used as green packaging for various applications. The requirements of foam properties (like cell size, cell density etc.) varies with the applications [5,6]. Hydrophobicity of PLA foam is required for some applications in the biomedical field.

Chitosan is derived from chitin and it is the most recommended biopolymer for food packaging and biomedical applications. One of the most important properties that make chitosan more favorable for various applications is its film-forming ability. Chitosan is a green biopolymer with properties like biodegradability and non-toxicity. Chitosan is hydrophilic and can be used for edible purposes [123,199]. In recent researches, it is observed that chitosan microspheres have been utilized in the PLA matrix as a carrier for peptide [200]. Additionally, chitosan is used for the fabrication of porous PLGA/PLA micro particles as a scaffold for investigations

of breast cancer cells [201]. Chitosan in the PLLA matrix shows an excellent cell study by Jiao et al.[202] Biocompatibility studies of poly (chitosan-g-lactic acid) scaffolds were investigated by **Zhang and his co-workers** [203]. Some investigations on hybrid PLA/chitosan scaffold were carried out by **Haaparanta et al.** [204]. They have used the freeze-drying technique for the fabrication of the scaffold. However, in all the above investigations the incompatibility of chitosan in PLA is a major concerned area. For sophisticated applications like cell culture, tissue engineering etc. increase in surface area with interconnected and highly porous foam structure is favorable and much-needed prerequisite condition [205]. From the literature, it is observed that the mixing of chitosan and PLA is a challenging task due to the hydrophilic nature of chitosan in hydrophobic nature of PLA matrix. Researchers used different techniques to address this issue. To overcome this obstacle some modifications in the chitosan have been carried out by making it hydrophobic and thus make it compatible in the PLA matrix by **Pal et al.** Their investigations were mainly focused on PLA/chitosan-based films for different applications [123,174]. Thermal degradation of the polymer is very much essential to establish technology for processing applications and it also gives an insight to the thermal decomposition mechanism, which is really very helpful in the recycling of polymeric materials [136]. From the above discussion, it is observed that a knowledge gap is existing in a systematic investigation of the effect of chitosan in PLA based foam's degradation mechanism, crystallization, wettability and porosimetric behavior for different applications along with a comparison between porous and non-porous system.

In this chapter, the fabrication of PLA/modified chitosan (MC)-based foams applying casting and leaching technique using sucrose as porogen medium has been thoroughly discussed. This chapter mainly focuses on the thermal and wettability phenomena of the fabricated foam. The influence of MC at different concentrations in the properties of PLA foam (physicochemical, thermal etc.) has been investigated in this study. The thermal degradation investigations have

been thoroughly investigated and activation energies have calculated by using different models. The degradation mechanism has been investigated by using Criado method [206] for the fabricated foams. The crystallization behavior of the fabricated foam at dynamic heating rates have been thoroughly investigated. Wettability phenomenon is very important for the foams for application point of view like coating, waterproofing, and printing etc. Wettability phenomenon has been thoroughly investigated for both static and dynamic conditions. Dynamic study of wettability is important because Young's contact angle along with CAH governs some phenomenon in the surface like spreading and splitting of the liquid drop in the surface. The influence of MC in the morphology, cell size and cell density of the foam samples have been thoroughly investigated in this chapter. The main motivation towards the investigation is to fabricate a biodegradable PLA/chitosan-based foam using a less expensive and innocuous method for potential applications in biomedical fields. The major requirements of foam for applications like cell culture are wettability, increased surface area, interconnected pore structure with high porosity. In this investigation, we are mainly focused in these areas to make it compatible for different applications as chitosan is already an established material for biomedical applications [207]. The structure-property relationship is also well investigated in the study to establish the probable thermal window with degradation mechanism useful for different applications to replace the established conventional petrol based foams. As per authors' knowledge of concern, no such investigations have been reported on bio-based modified chitosan (MC) as a nanofiller for the fabrication of hydrophobic, microcellular interconnected PLA/MC-based foam with significantly improved flexibility and porosimetric results. Schematic representation of the fabrication process of PLA/MC-based foams is shown in **Fig. 4.1**.

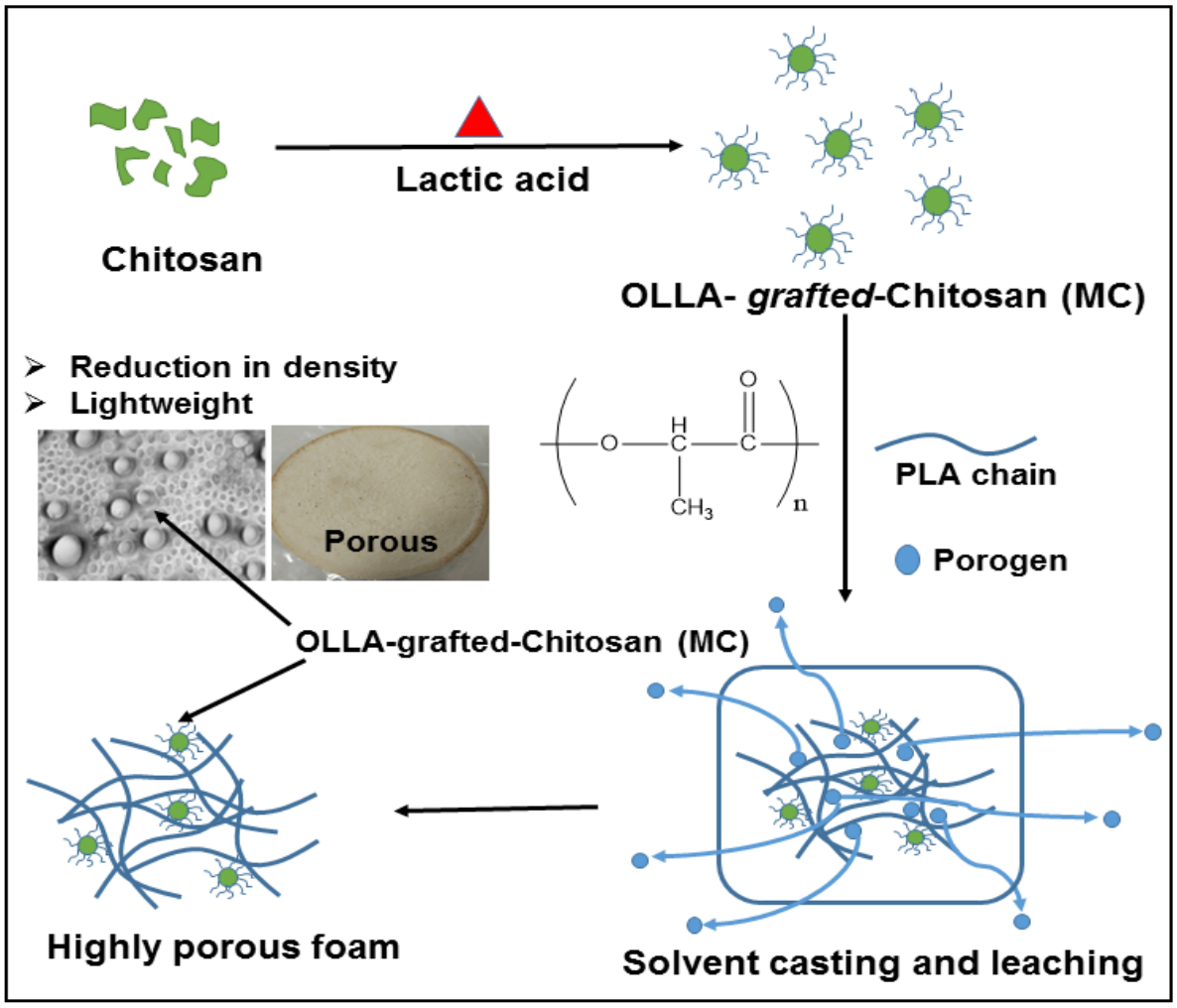

Fig. 4.1 Schematic representation of the fabrication process of PLA and PLA/MC-based foams.

4.2 Results and discussions

In this section of chapter, the results and observations are discussed with probable scientific conclusions.

4.2.1 Chemo-physical properties

The chemo-physical properties of the fabricated foams are investigated. The density of PLA based foam is significantly reduced to 0.16±0.02 g/cc (~7.7-fold reduction) compared to PLA granules (1.24±0.02 g/cc) (**Table 4.1**). The reduction in the bulk density of the foam sample might be due to leaching of porogen particles and subsequently, the void spaces filled with air

are generated which is responsible to the reduction of the mass per unit volume of the sample. Whereas, a slight increase in density of the PLA/MC-based foams is observed while the increase in the MC loading. It is observed that the addition of MCs in the PLA matrix has no significant influence in the bulk densities of the fabricated composite foams. The addition of the nanobiofillers increases the number of pore generation might be due to the nucleating effect and influences the amount of air that can be accommodated in the pores. The low density and lightweight characteristics of these biodegradable foams are prerequisite for applications like drug delivery, tissue engineering, and biomedical scaffold. It is observed from the average density values that all the fabricated foams are lies in the range of ~0.2 g/cc which falls under 80% reduction in the bulk density of the pristine polymer matrix. Further, from the observed β values (**Table 4.1**), all the fabricated foams can be categorized as medium density foams. This value is further utilized to calculate the cell density (N_f) of the fabricated foams.

Table 4.1 Weight, density and volume expansion ratio (VER) of PLA and PLA/MC-based foams.

Sample	Dry weight before leaching (g)	Dry weight after leaching (g)	Avg. density (g/cc)	VER	Foam Type
nPLA	33.8	3.8	0.16±0.02	7.8	Medium density
PLA/MC 1	34.2	3.5	0.19±0.01	6.5	Medium density
PLA/MC 2	34.8	3.1	0.21±0.02	5.9	Medium density
PLA/MC 3	32.8	3.9	0.22±0.01	5.6	Medium density

Avg. density of PLA granules is found to be 1.24±0.02 g/cc; g/cc: gram/cm^3

The XRD patterns of the fabricated foams are shown in **Fig. 4.2**. From the figure, it is observed a sharp peak around 2θ=16.65° for all the fabricated foams from [2 0 0/1 1 0] planes indicating the α-form of the crystalline structure of PLA. The pattern of [2 0 0] reflections indicating the

orthorhombic crystal structure of the PLA [123]. Three more peaks are observed at 2θ=14.8°, 19.15° and 22.35° indicating reflection patterns of [0 1 0], [2 0 3] and [0 1 5] respectively. These peaks confirm the presence of α-form (19.15° and 22.35°) and β-form (14.8°) of crystals in the matrix. However, no significant shifting in peaks is observed in the XRD indicating that no phase separation ordered crystal structures are noticed due to the introduction of the nanobiofillers. The semi-crystalline nature of the fabricated foams can be confirmed from the discussion above.

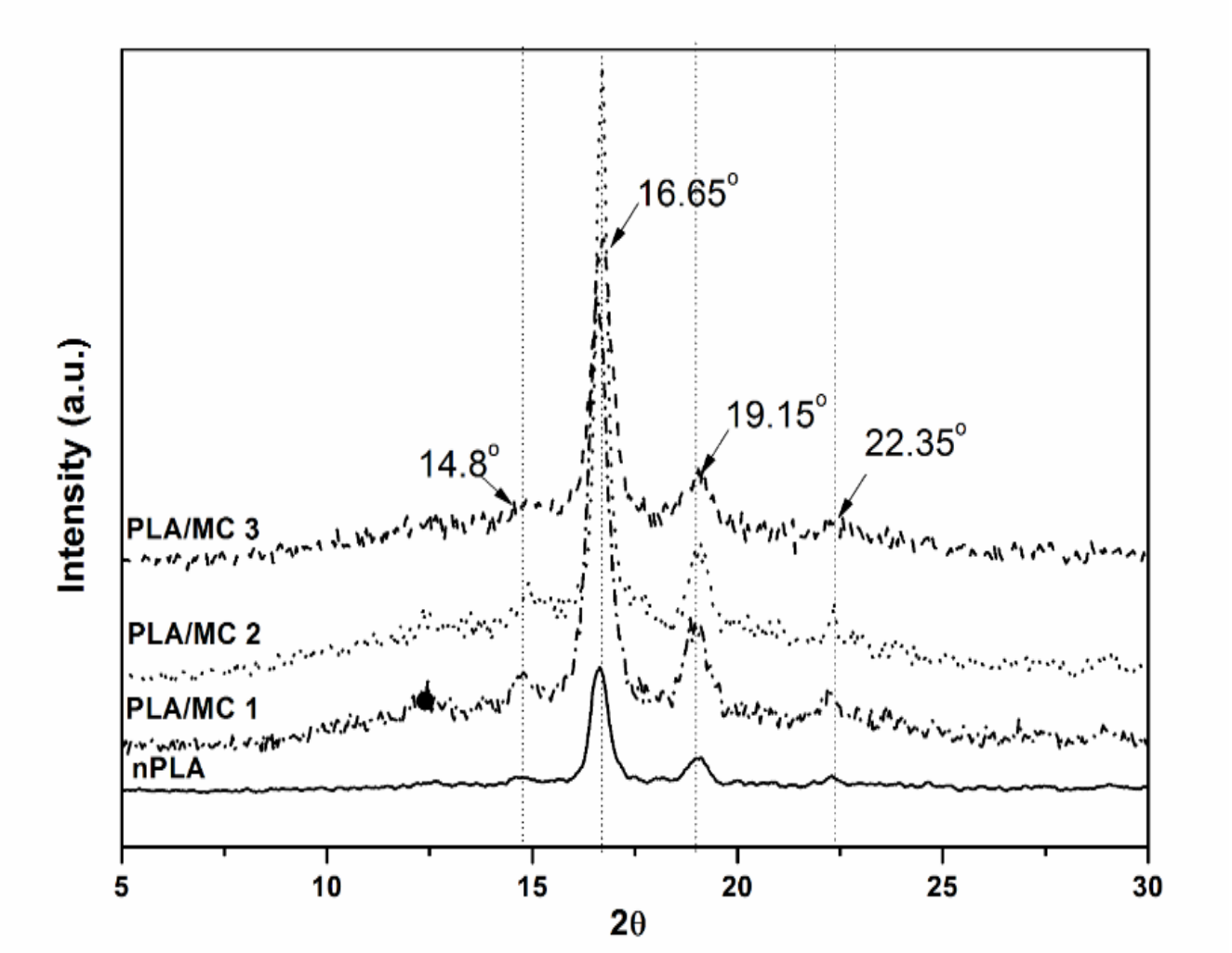

Fig. 4.2 XRD patterns of PLA and PLA/MC-based foams.

From the FTIR spectrum (**Fig. 4.3**), It is observed that distinct characteristic peaks around ~753 cm^{-1}, ~869 cm^{-1}, ~1450 cm^{-1} corresponding to -CH bending of the molecular structure of PLA,

-C-C- bond stretching (amorphous phase of PLA) and -CH_3 bending vibrations or methyl asymmetric deformation of PLA respectively present in PLA and PLA/MC-based foams. An intense peak around ~1750 cm^{-1} attributes to –C=O (carbonyl stretching) valance vibrations of fabricated foams. Peaks around ~1082 cm^{-1} and ~1182 cm^{-1} represent the –CO stretching of PLA. Peak around ~1383 cm^{-1} attributes to –CH bending in PLA. In the case of sucrose, characteristics peaks are present at lower wavenumbers. Characteristics peaks of sucrose are observed around ~908 cm^{-1}, ~1295 cm^{-1} and ~1418 cm^{-1} corresponds to –CO stretching vibrations, –OH bending vibrations and −CH bending vibrations respectively. Peaks around ~3556 cm^{-1} and ~3380 cm^{-1} represents the–OH group of sucrose (stretching vibrations). It is observed that prominent peaks of sucrose (~908 cm^{-1} and ~3556 cm^{-1}) are absent in fabricated foams. In the case of MC, prominent peaks are observed around ~1450 cm^{-1} and ~1750 cm^{-1} attributing to –CH_3 bending and –C=O stretching. The grafting of oligomer on chitosan can be confirmed by the presence of peaks around ~1543 cm^{-1} and ~1638 cm^{-1} of MC representing amide I band (-C=O stretching) and amide II band (-N-H bending) [123].

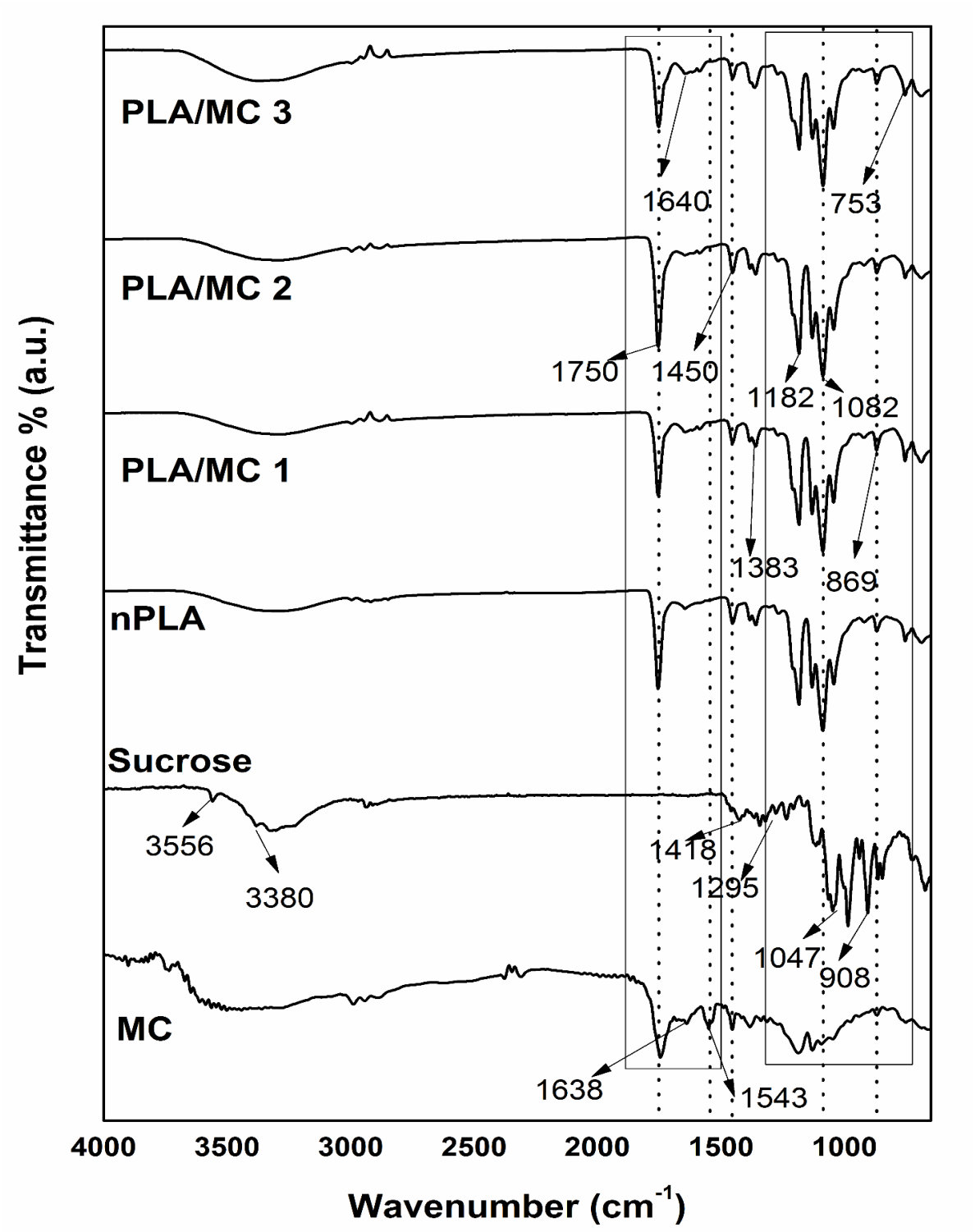

Fig. 4.3 FTIR spectra of MC, Sucrose, PLA, and PLA/MC-based foams.

Gel Permeation Chromatography (GPC) results of the fabricated PLA/MC-based foams are shown in **Table 4.2**. The M_n and M_w values of nPLA are observed as of ~114300 Da and

~202400 Da respectively. The presence of low molecular weight oligomer (OLLA) in the MCs might be responsible for the reduction of molecular weight of fabricated PLA/MC-based foams. On increasing the MC (increase in OLLA) loading to the PLA matrix the M_n decreases because M_n is sensitive to molecules of low molecular weight. However, M_w values increased slightly due to more contribution of the large chain while calculation of M_w. In the leaching process, some of the low molecular weight oligomers may come out from the surface of the foam matrix. The PDI values are observed between ~1.6 to ~1.8 for the foam samples.

Table 4.2. Values obtained from DSC (2.5 °C/min), TGA (10 °C/min) and GPC analysis of PLA and PLA/MC based foams.

Sample	DSC Analysis		TGA Analysis			GPC Analysis		
	ΔH_m^a (J/g)	X_C (%)	T_{onset} (°C)	T_{max} (°C)	T_{90} (°C)	M_n (Da)	M_w (Da)	PDI
nPLA	-28.6	30.7	359.6	376.4	385.9	114270	202380	1.77
PLA/MC 1	-27.8	29.8	351.7	375.3	385.3	110000	181050	1.64
PLA/MC 2	-27.3	29.4	349.6	374.7	384.6	107430	185920	1.73
PLA/MC 3	-26.3	28.4	337.1	367.9	375.2	104350	188420	1.80

4.2.2 Thermal properties

From DSC thermographs (**Fig. 4.4**) the crystallization and melt behavior of the fabricated foams were investigated with two heating cycles at a heating/cooling rate of 10 °C/min. During the first heating cycle, the thermal history and physically bound water or moisture present in the sample were removed. It is observed from the graph that the glass transition (T_g) temperature was reduced up to ~7 °C with the increase of the MC loading. The decrease value of T_g might be due to the plasticizing effect of MC (presence of low molecular weight OLLA) as the diffusion of short polymeric chains (low molecular weight) are easy. The glass transition

is effected by the change in molecular weight. This justifies the reduction of molecular weight of the fabricated foams as discussed earlier in this article. A small reduction of ~4 °C is observed in cold crystallization temperature (T_{cc}) at the highest loading of MC, which might be due to the presence of some deformed crystals in the PLA. A slight decrease (~2 °C) in melting point (T_m) is observed for PLA/MC based foams at the highest loading of MC (PLA/MC 3). The decrease in melting point can be justified with the reduction in thermal stability of the PLA molecules with an increase in bionanofiller. Single T_g is observed in all the cases which indicates that no phase separation is taking place in the foams. The DSC graphs at different heating rates (at 2.5 °C/min, 5 °C/min and 7.5 °C/min) for crystallization kinetics investigation can be found in **Fig. 4.5**. The percentage crystallinity of the fabricated samples is calculated from the enthalpy values and tabulated (**Table 4.2**). A slight decrease in crystallinity is observed with increase in MC might be due to the presence of short PLA chains, which may affect in the chain folding [208].

Thermogravimetric analysis (TGA) plots are shown in **Fig. 4.6**. It can be observed that single step degradation behavior is followed by all the fabricated samples. The maximum stability is observed in case of pristine PLA foam and the values of T_{onset}, T_{max} and T_{90} are found to be 359.6 °C, 376.4 °C, and 385.9 °C respectively (**Table 4.2**). It is observed that on increasing the MC concentration, the values of T_{onset}, T_{max} and T_{90} decreases. A reduction of ~20 °C in T_{onset}, ~10 °C in T_{max} and ~10 °C in T_{90} are observed in the case of highest loading of nanobiofiller foam (PLA/MC3). This observation can be justified by the fact that on increasing the loading of bionanofiller, the generation of acidic sites during the degradation is also increased in the PLA matrix of the foam, which attributes to the degradation of the foam at a lower temperature. The weight loss (%) at T_{max} is found to be 37% (nPLA), 31% (PLA/MC 1), 32% (PLA/MC 2) and 27% (PLA/MC 3) for the fabricated foams.

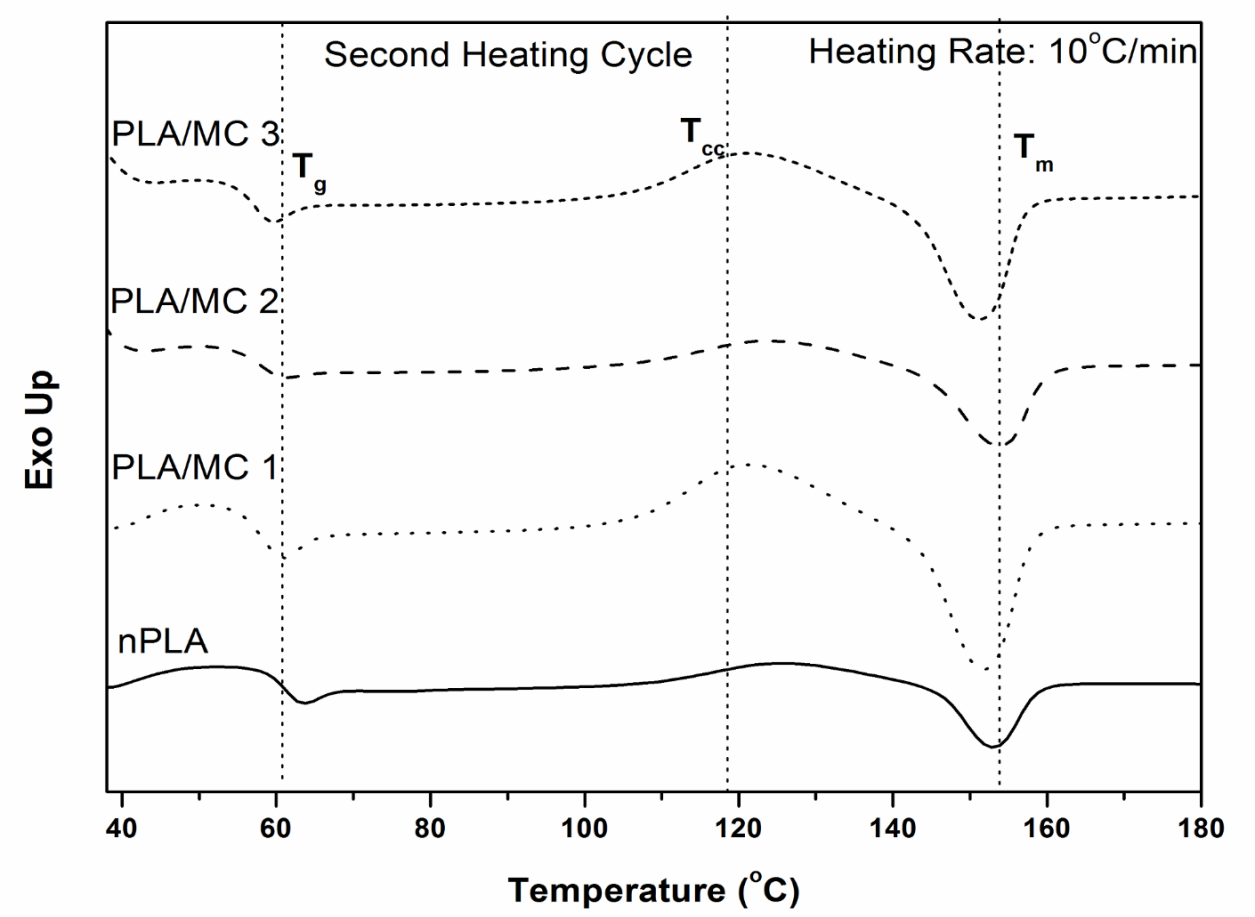

Fig. 4.4 DSC thermographs of PLA and PLA/MC-based foams.

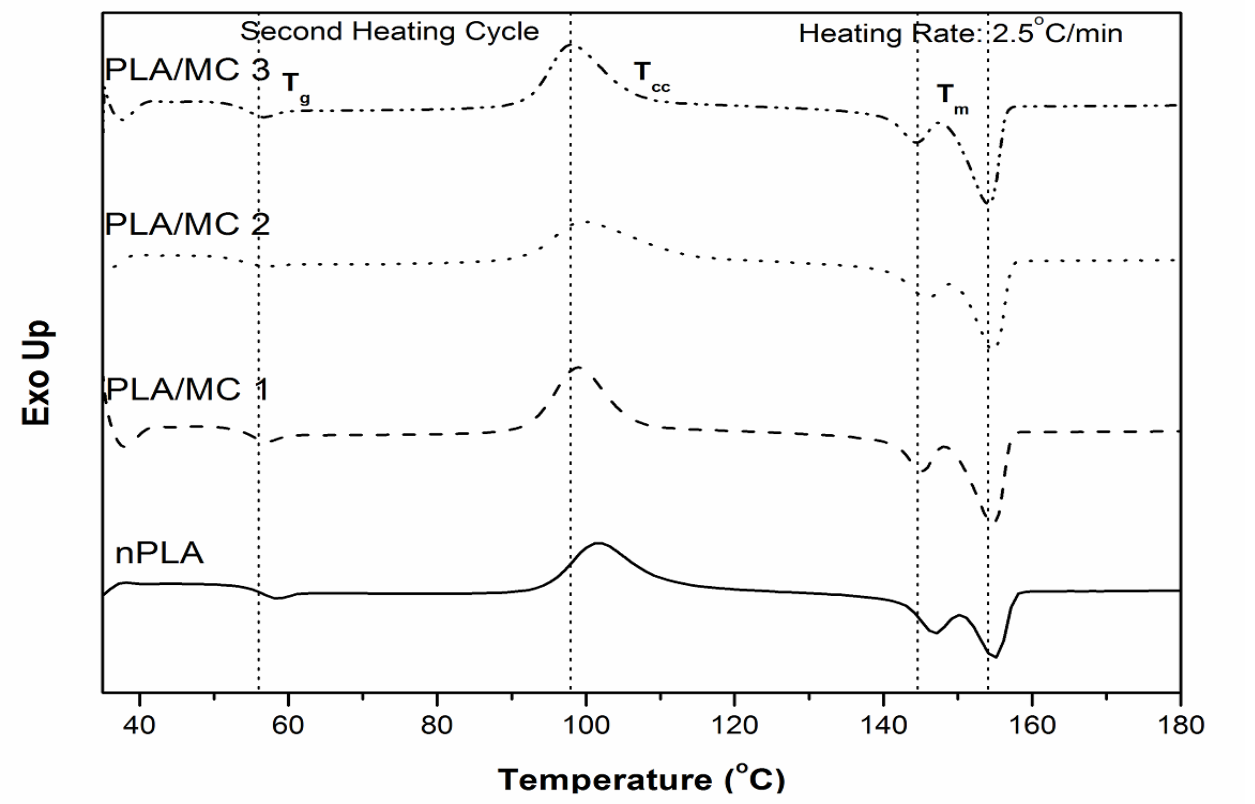

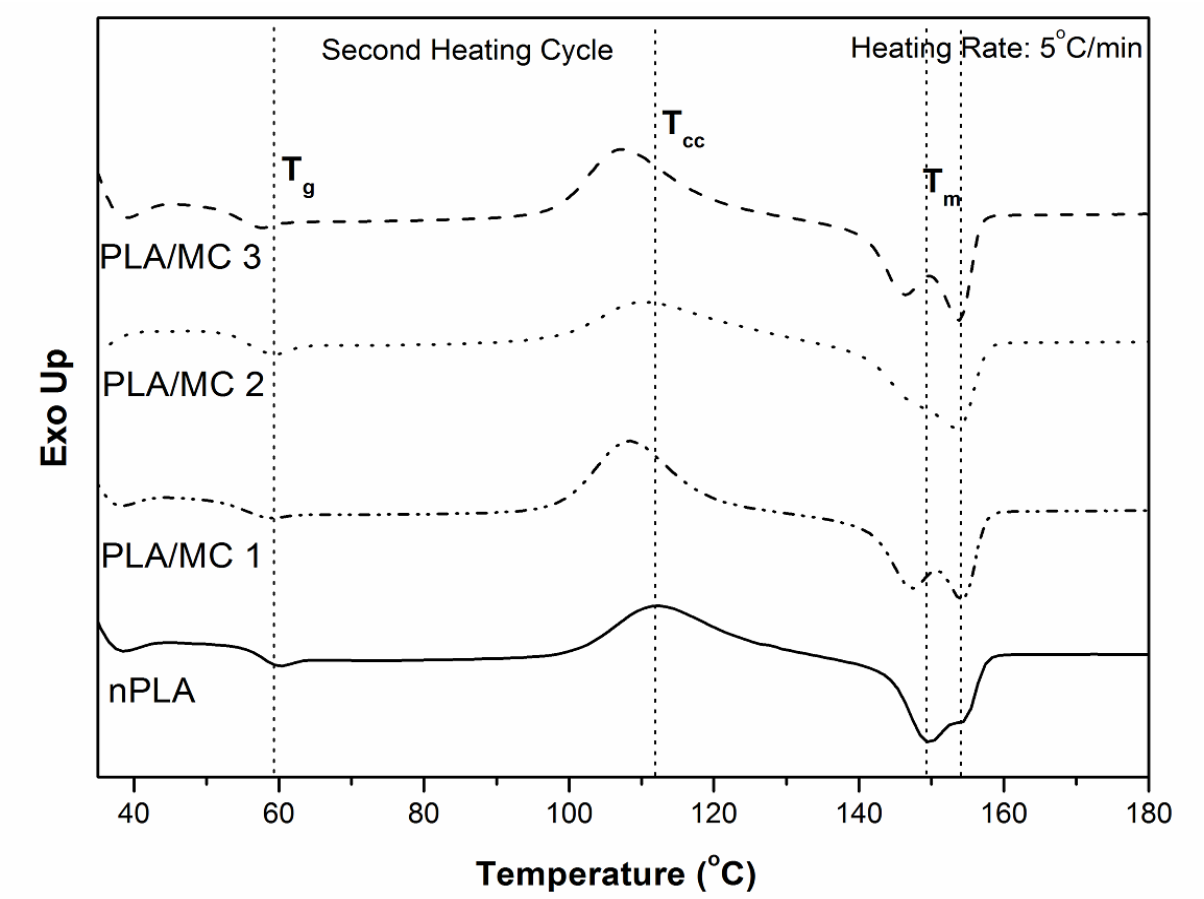

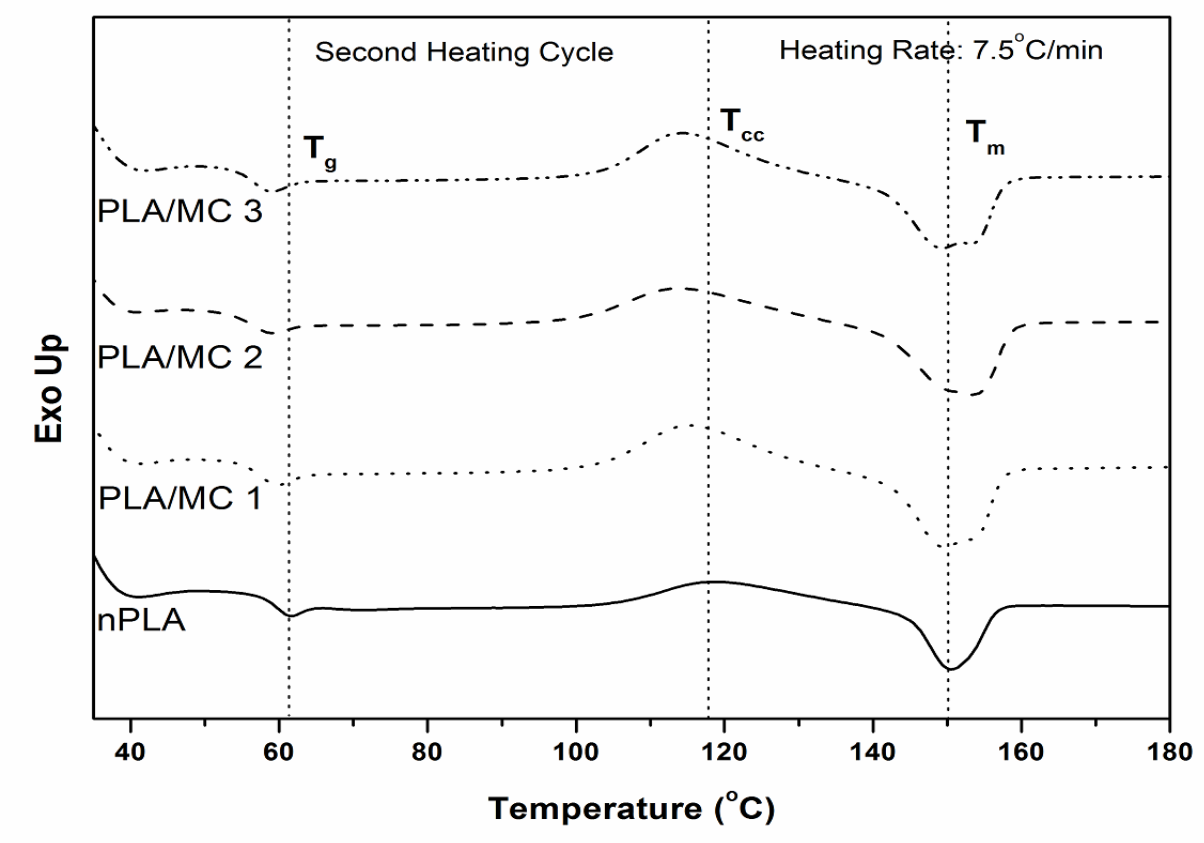

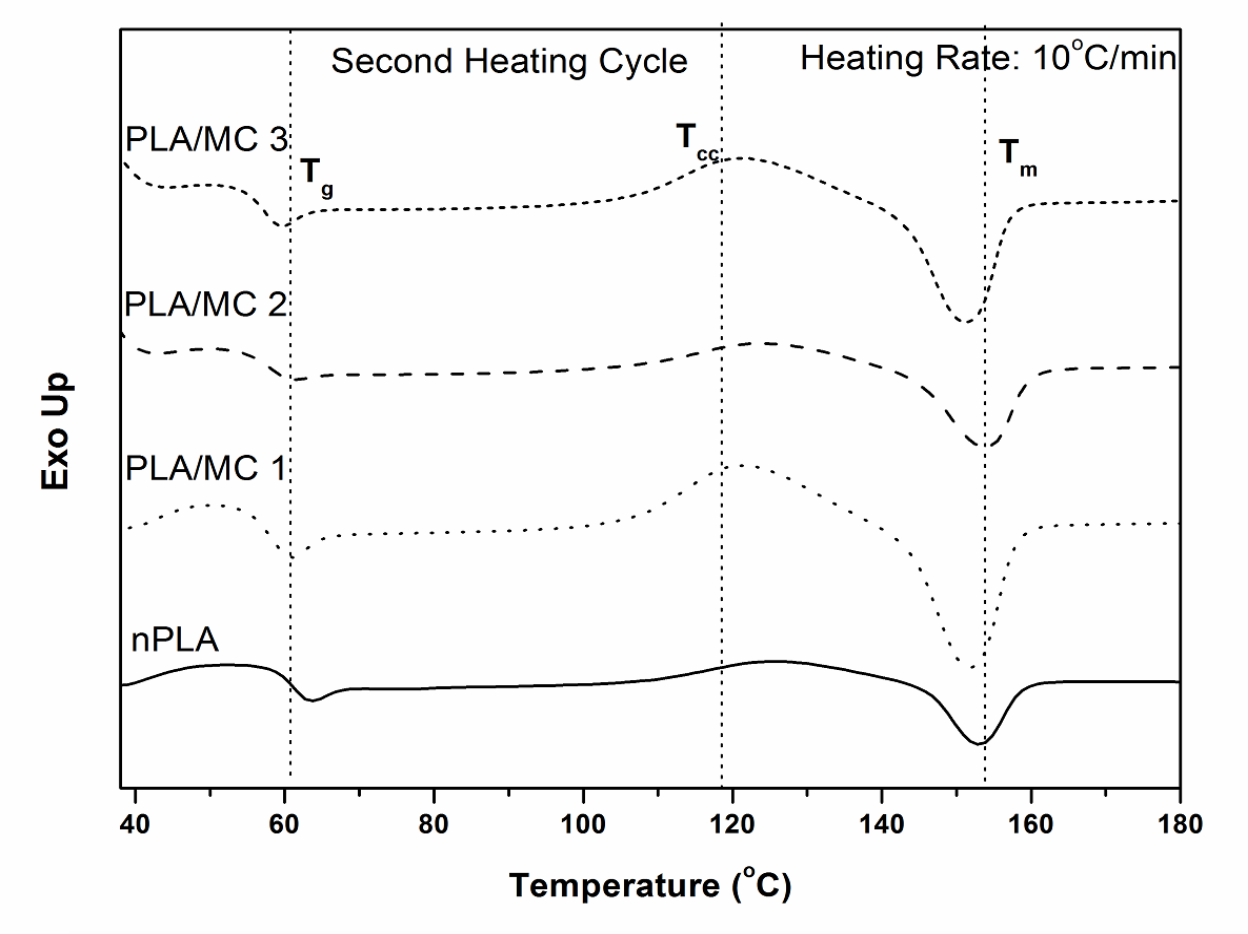

Fig. 4.5 DSC thermographs of PLA and PLA/MC-based foams at different heating rates.

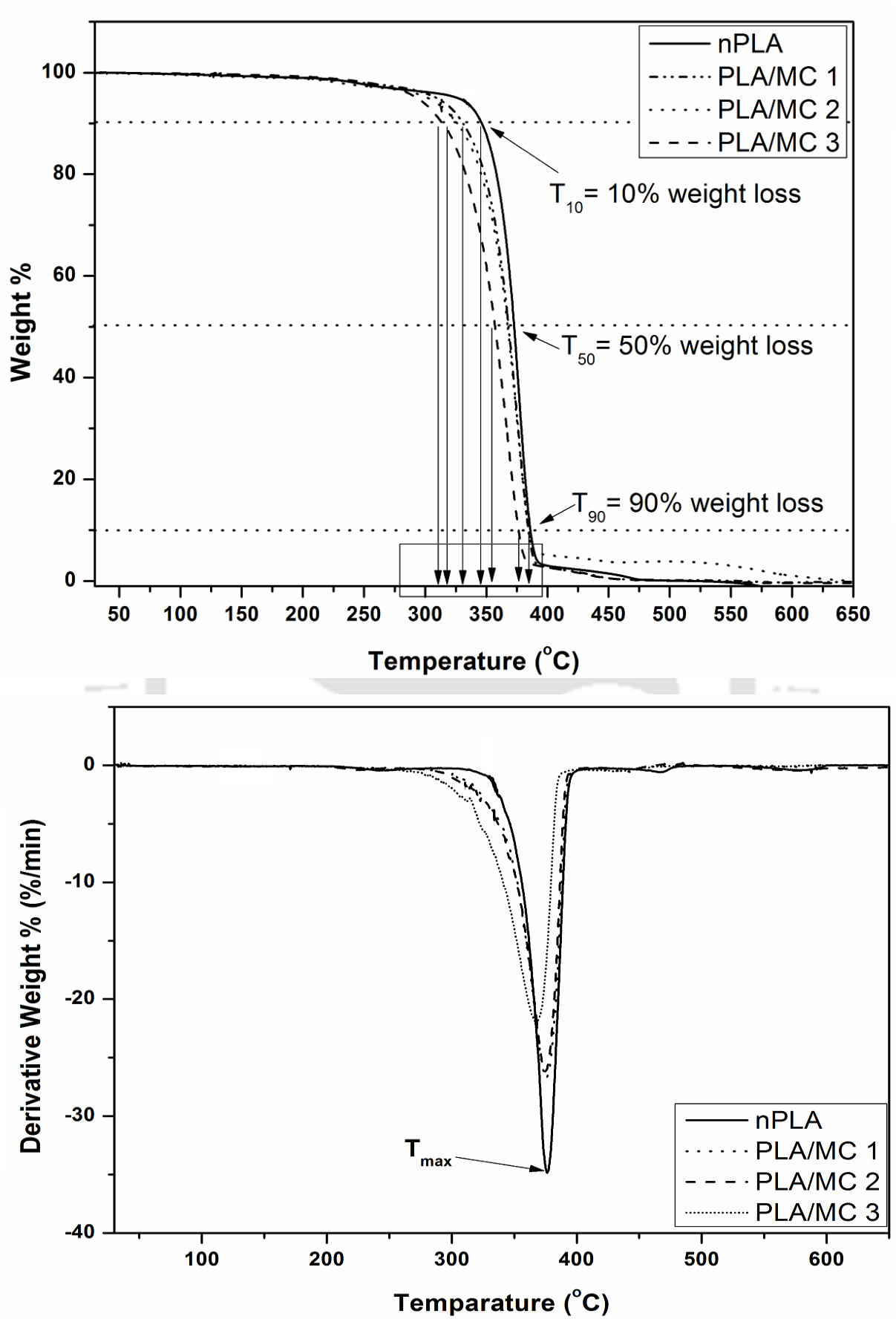

Fig 4.6 TGA and DTG graphs of PLA and PLA/MC-based foams.

4.2.3 Wettability of PLA and PLA/MC-based foams

From wettability investigations (**Fig. 4.7**), it can be observed that nPLA foam has a contact angle value 123.5°±4.5° indicating hydrophobic nature. This hydrophobicity can be attributed to the influence of surface texture as observed from FESEM. An increase in contact angle is observed on the increasing of nanobiofillers content to the PLA matrix. An increment of ~8° is observed for the highest loading (PLA/MC 3). The increment in contact angle of the fabricated foam can be explained from the **Fig. 4.8**. PLA is hydrophobic in nature whereas the fabricated modified chitosan has a hydrophobic shell with the hydrophilic core. As the loading of MC increases the effect of the hydrophobic shell also increases and hence the increase in contact angle. It is also evident from the FESEM images that MC is uniformly dispersed in the surface of the fabricated foam. Introduction of MC influences the pore generation and the size of the cell. The higher contact angle is observed in rough surfaces [183]. The contact angle for the foam samples without any surface texture is also measured (**Table 4.3**). The decrease of contact angle up to ~49° is observed for PLA/MC 3. Hence, it can be concluded from the analysis that both the surface texture and the nanobiofillers influence the wettability behavior of the fabricated foams [121]. From the dynamic contact angle investigations, it is observed that Young's contact angle value also increases with increase in filler concentration. Young's contact angle utilizes both the splitting and spreading phenomenon of liquid in the contact surface. Young's contact angle values are also in good agreements with the static contact angle analysis. The increment in hydrophobicity along with an increase in MC is quite useful for various biomedical applications [207]. Similar behavior of wetting phenomena is observed for all the fabricated foams.

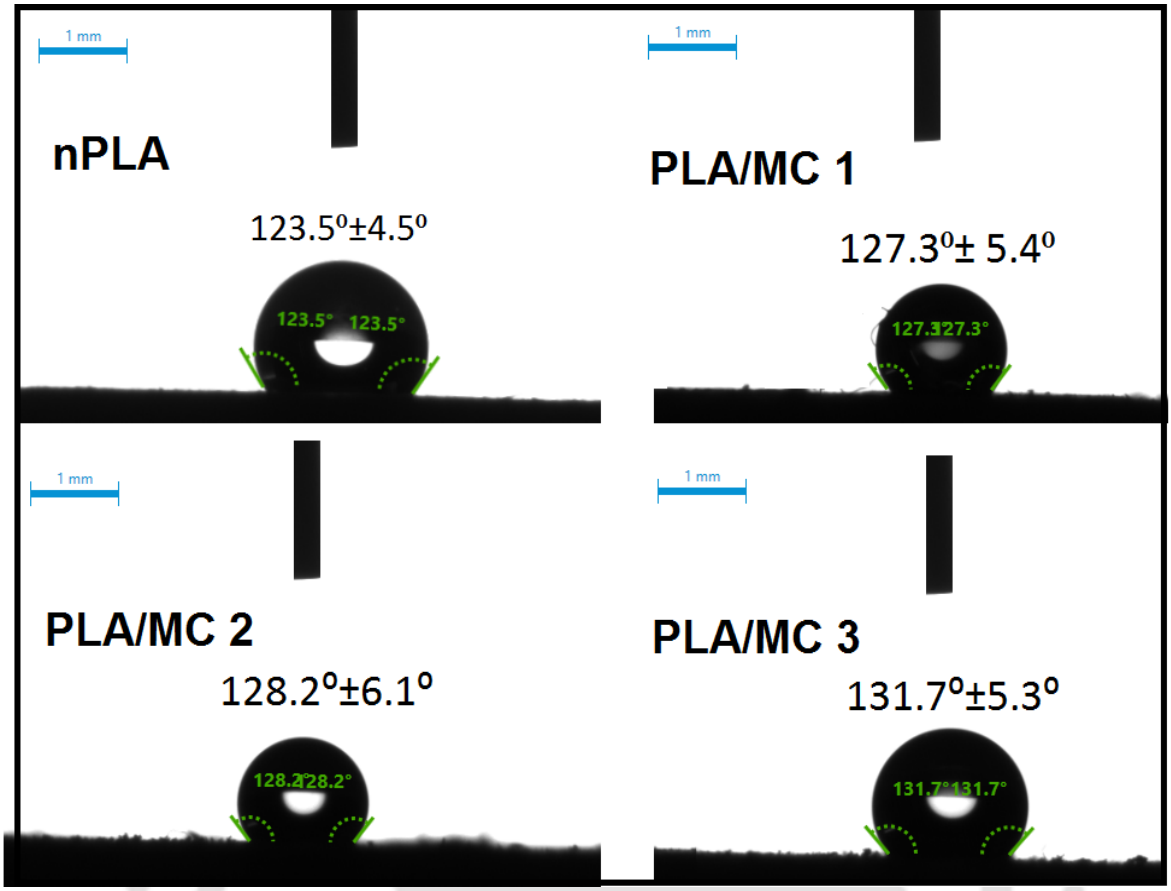

Fig. 4.7 Static contact angles of PLA and PLA/MC-based foams.

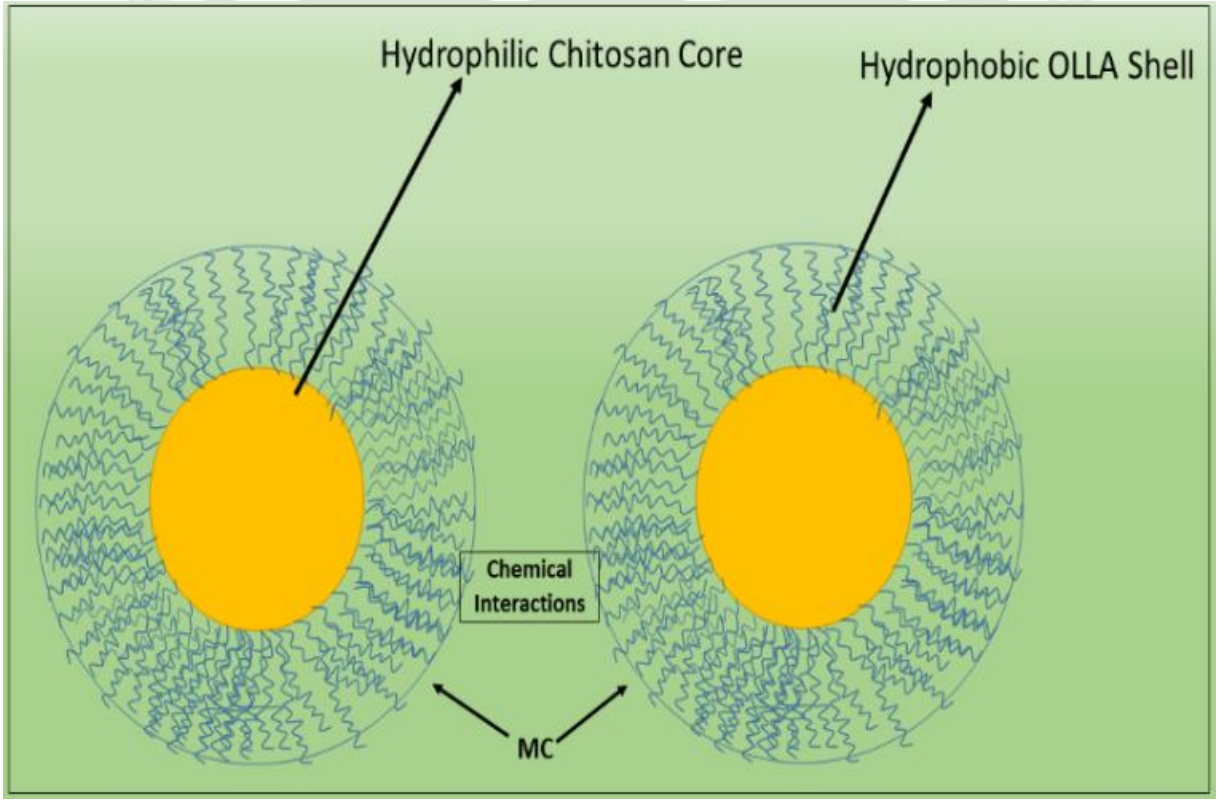

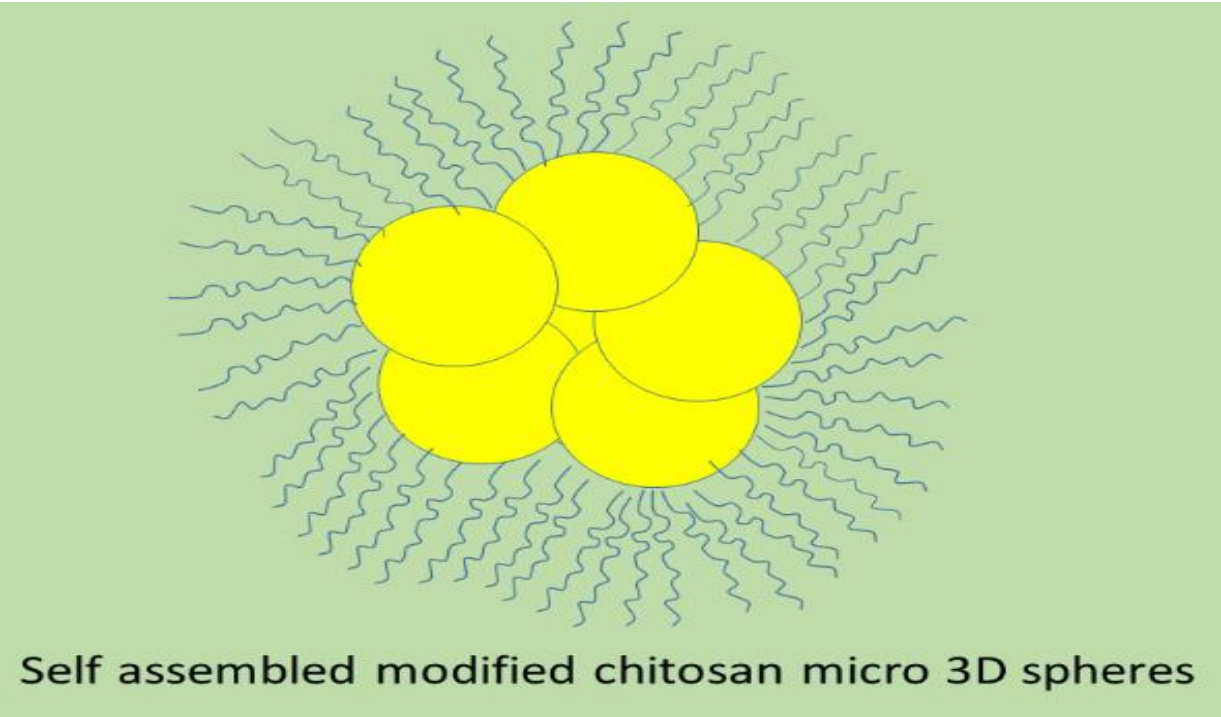

Fig. 4.8 Schematic of OLLA-g-chitosan (MC).

Table 4.3 Static and dynamic contact angle values of PLA and PLA/MC based foams.

Sample	Static Contact Angle		Dynamic Contact Angle		
	Surface with texture	Surface without texture	Advancing θ_{adv}	Receding θ_{rec}	Young's θ_Y
nPLA	123.5°±4.5°	76.1°±3.7°	134.2°±10.3°	94.5°±8.6°	112.8°
PLA/MC 1	127.3°±5.4°	78.8°±2.8°	135.6°±13.6°	98.2°±9.8°	115.4°
PLA/MC 2	128.2°±6.1°	81.6°±3.1°	140.8°±14.5°	104.5°±11.2°	120.8°
PLA/MC 3	131.7°±5.3°	82.8°±2.9°	139.5°±5.1°	108.3°±13.6°	122.5°

It can be concluded from the porosimetric investigation that effect of porous morphology and MC nanobiofiller is mainly prominent in thermal degradation than in the crystallization process of the fabricated foams.

4.2.4 Morphological investigations of PLA/MC-based foams

Polarized optical microscopy (POM) micrograph is shown in **Fig. 4.9 A**. The average particle size of the sucrose is observed as ~1.13±0.34 µm. These porogen particles are further utilized for the fabrication of foams.

The surface topography has been observed using TEM analysis, which is the most evident observation to check the distribution of nanofiller in the matrix **(Fig. 4.9 B).** It is clearly visible that the various size of spherical form of chitosan nanoparticles are uniformly dispersed in the matrix. The diameter of spherical chitosan particles varies in the range of ~20-80 nm. It is also noticed that the spherical particles are attached with the OLLA chain.

Hence, such kind of arrangement of spherical particles with low molecular weight OLLA chain may be termed as a nano-amphiphilic molecule in which the tail shows hydrophobic nature and the head represents hydrophilic nature. It can be observed from the FESEM micrographs that all the fabricated foams have an open cell porous structure.

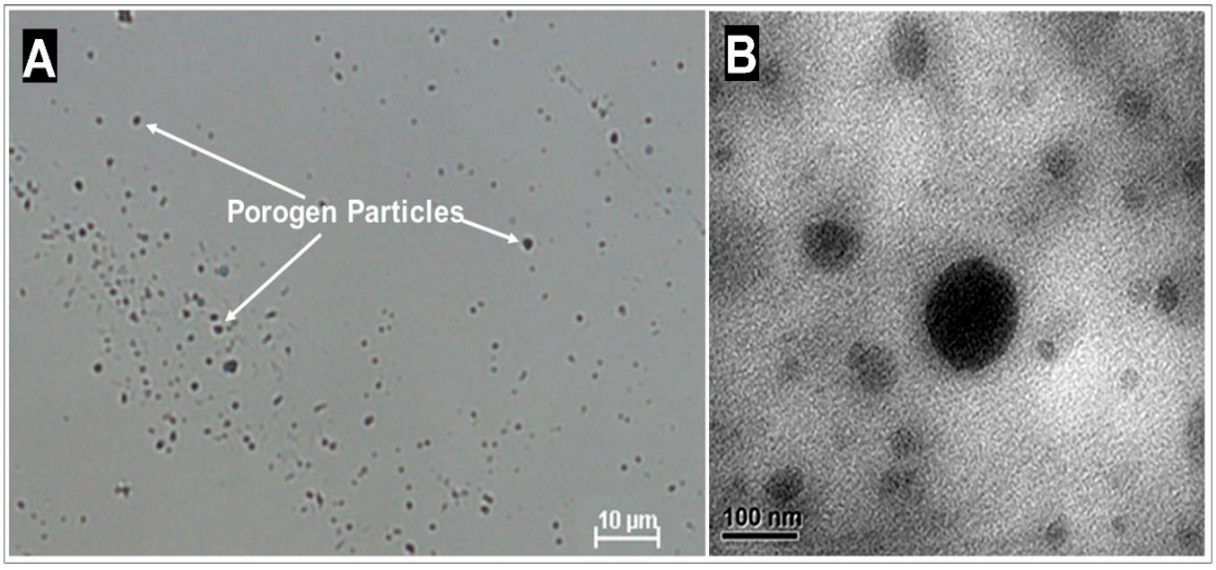

Fig. 4.9 A) Optical microscopy image of porogen particles and, **B)** TEM image of OLLA-*g*-chitosan (MC).

It is observed from the cross-sectional view of the fractured surface of the PLA and PLA/MC based foam (**Fig. 4.10**) that all the foam morphology has highly dominated by the interconnected porous structure. The dispersion of MC nanobiofillers in the cell walls of the fabricated foams can be observed from **Fig. 4.11**. The MC nanobiofillers are self-assembled and form agglomerates and uniformly dispersed in the cell walls of the fabricated foams as shown from the fractured and horizontal surfaces of foam (**Fig. 4.12**). The average size of the self-assembled MC in the cell walls is found to be ~0.24 µm (PLA/MC 1), ~0.39 µm (PLA/MC 2) and ~0.40 µm (PLA/MC 3). The increase in the size of the self-assembled MC is due to the fact that more the loading of nanobiofillers more number of nanobiofillers gets assembled in the matrix and hence the increase in diameter. The uniformly dispersed MC nanobiofillers observed in the PLA matrix are in the range in micrometers due to the micellar behavior of MC in the PLA matrix, which also has self-assembling property in the matrix. The spheres that are observed in the PLA matrix foam are an aggregate of MC (chitosan behaves as head and attached oligomer chain denotes the tail of polymeric micelles) due to its self-assemble properties [123].

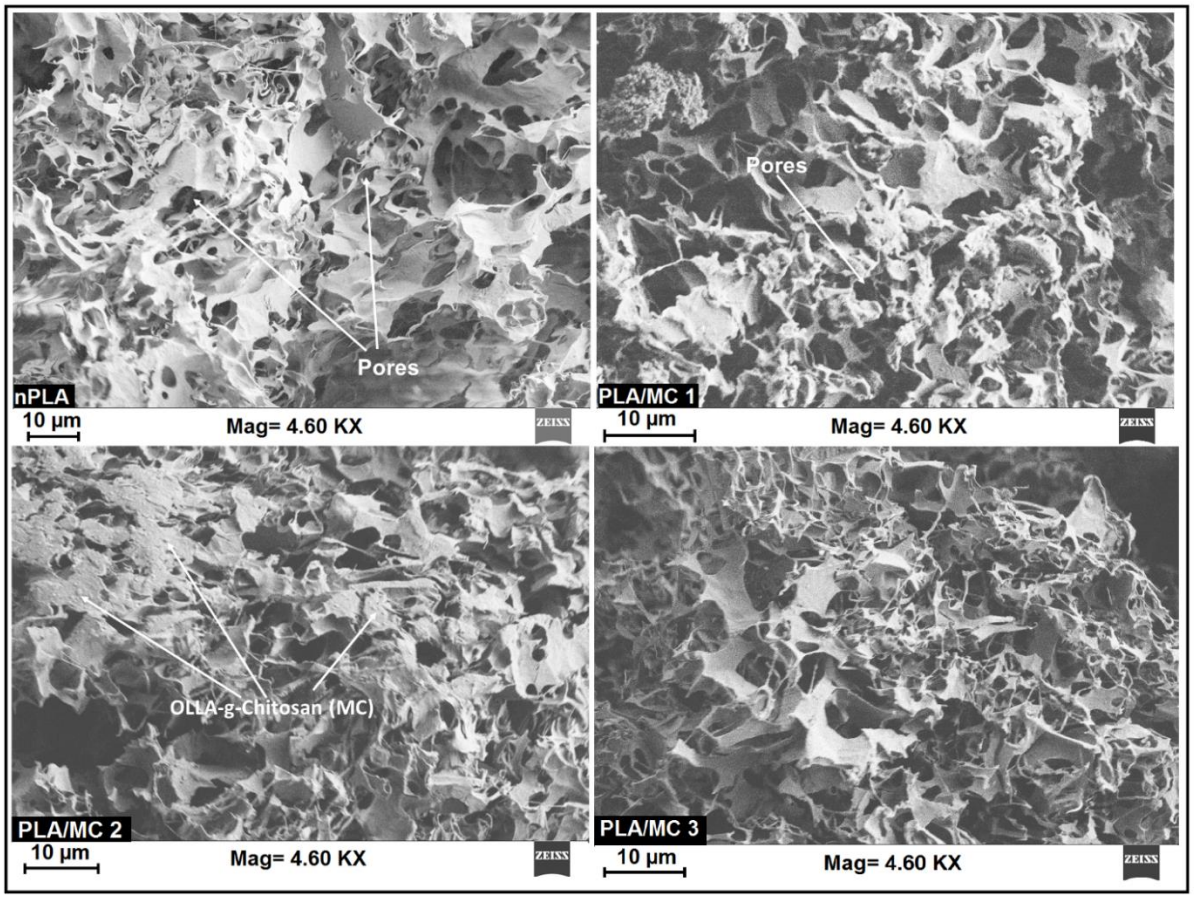

Fig. 4.10 FESEM micrographs of cross sections of the fractured surface of PLA and PLA/MC-based foams.

A representative image of MC micelle is shown in **Fig. 4.8**. The cell density (N_f) and cell sizes (**Fig. 4.13**) are also calculated from the FESEM micrographs. It is found the nPLA has cell density value of ~1.02×10^{11} cells/cm^3. The cell density value increases on increasing of MC. The generation of more number of uniform cells per unit volume on the introduction of MC might be due to the possible availability of more nucleating sites, which helps in generation of more number of cells per unit volume.

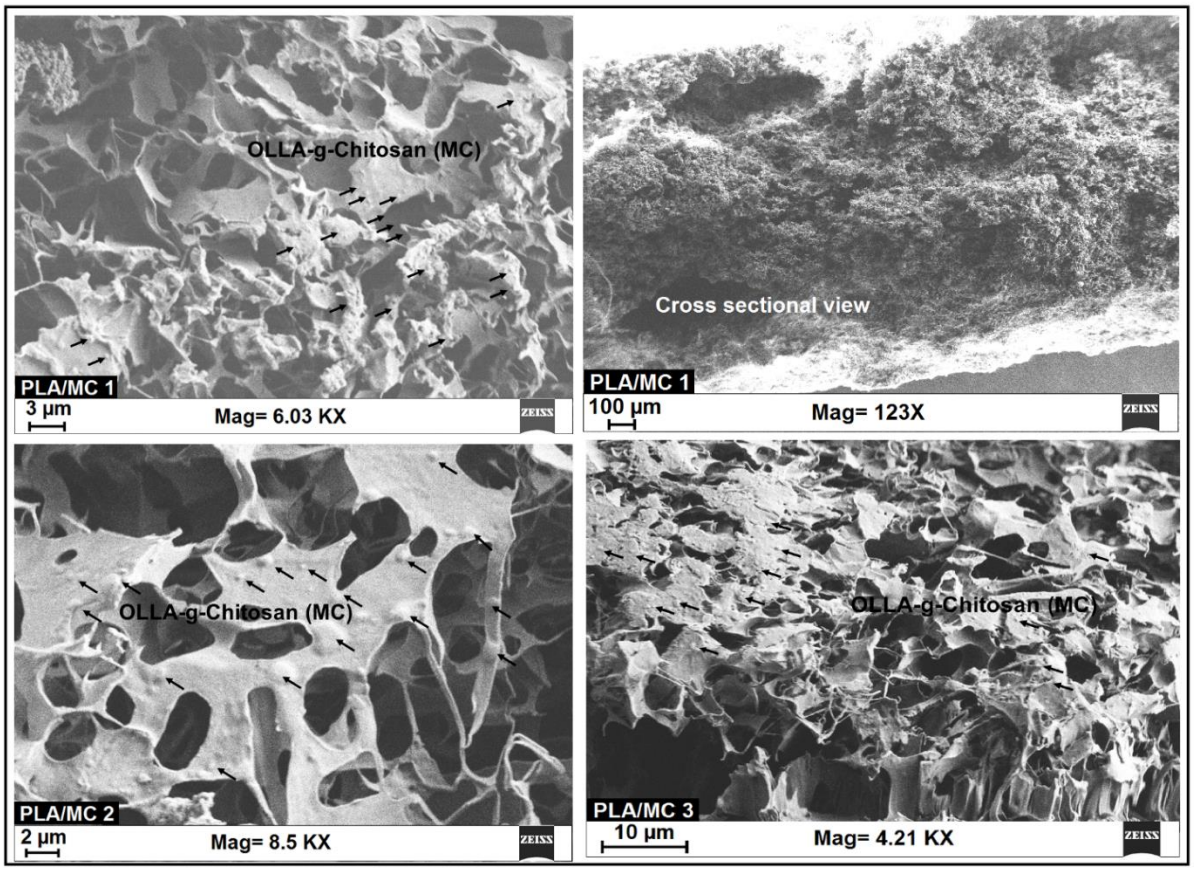

Fig. 4.11 Dispersion of MC in the cell walls of the PLA/MC-based foams.

The cell densities of PLA/MC 1, PLA/MC 2 and PLA/MC 3 are observed as ~1.92×10^{11} cells/cm^3, ~2.13×10^{11} cells/cm^3 and ~2.3×10^{11} cells/cm^3 respectively. From FESEM micrograph, the average cell size of the nPLA foam is found to be ~2.23±0.08 µm. The value of cell size decreases on increase in nanobiofillers loadings. The average cell size of PLA/MC based foams are found to be ~2.03±0.09 µm, ~1.88±0.07 µm and ~1.79±0.04 µm for 1%, 2% and 3% loadings of MC as suggested by FESEM. The reason of reduced average cell size of the PLA/MC-based foams can be associated with the increase in cell density of the fabricated foams due to the nucleating effect of the nanobiofiller.

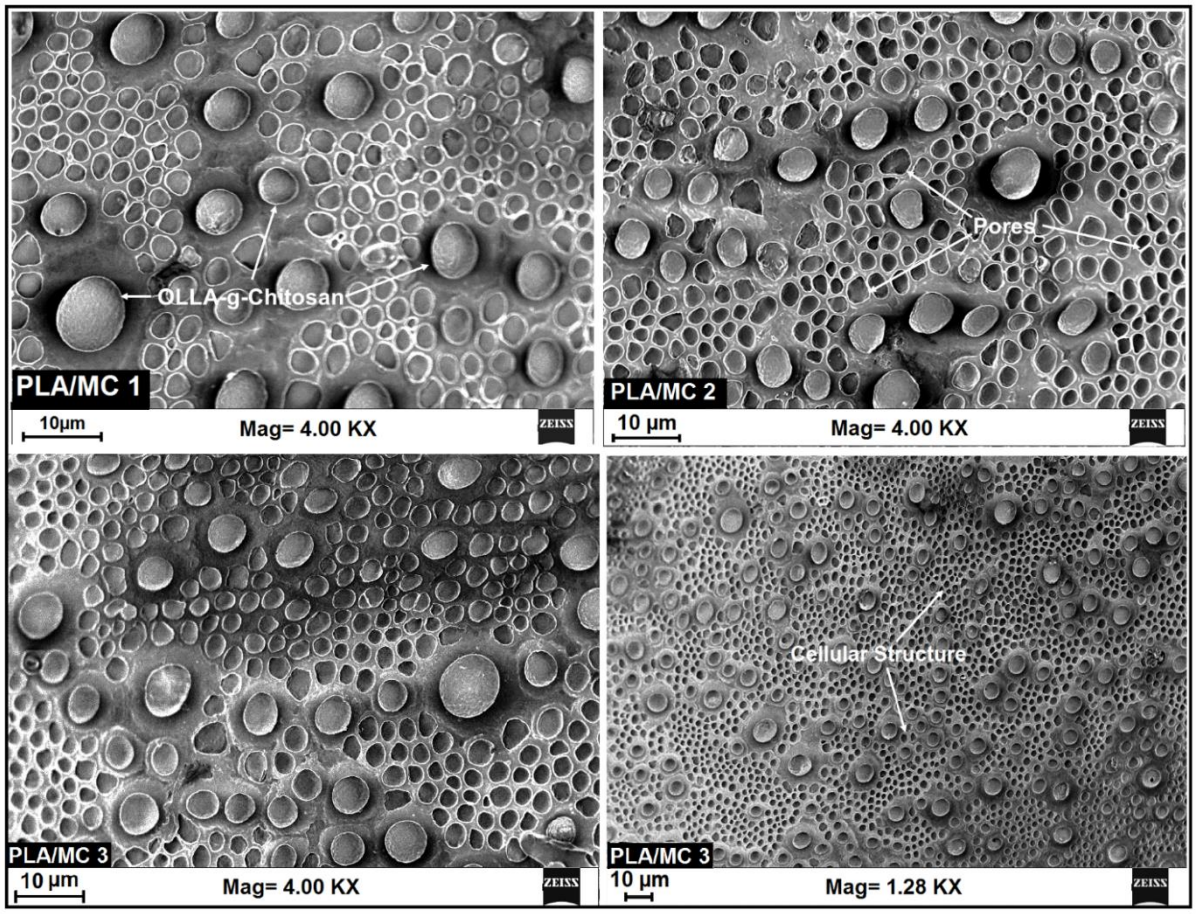

Fig. 4.12 FESEM micrographs of horizontal surfaces of PLA/MC-based foams.

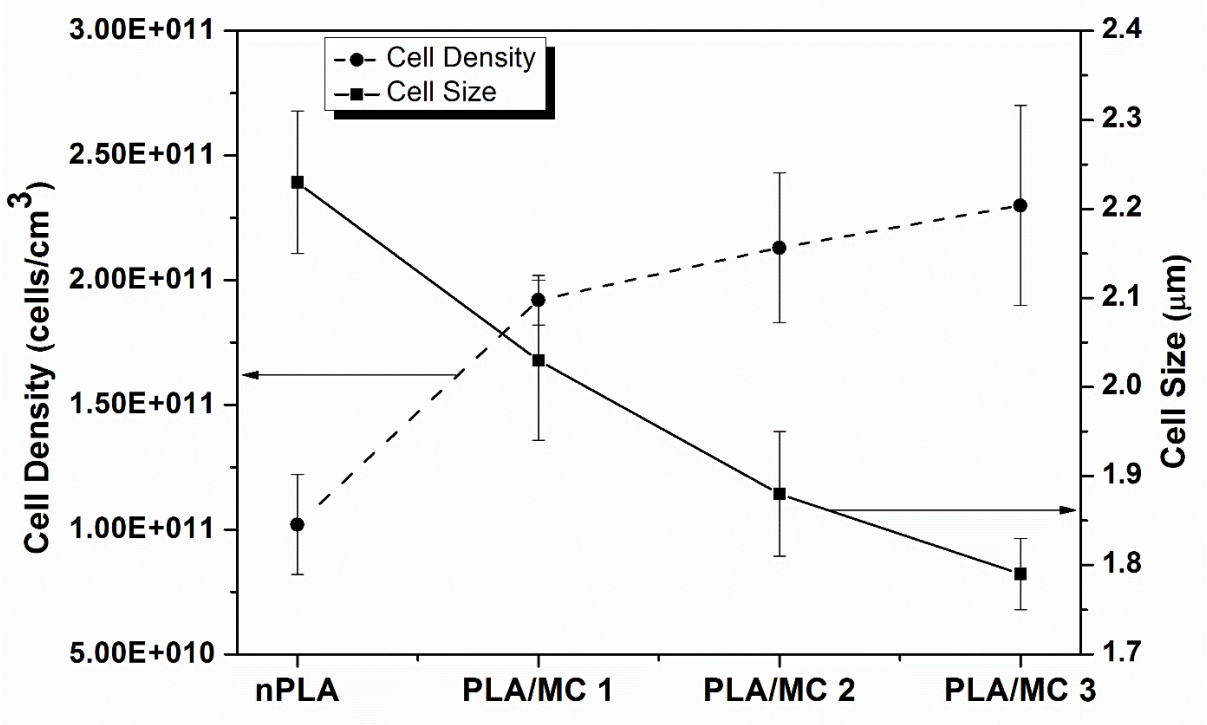

Fig. 4.13 Cell density and cell size of the PLA and PLA/MC-based foams.

4.3 Thermal degradation kinetics investigation of the fabricated PLA/MC-based foams

The non-isothermal thermal degradation behaviour of the fabricated PLA and PLA/MC-based foams are investigated utilizing different "model-free" and "modelistic" approaches as discussed below.

4.3.1 Analysis of non-isothermal degradation kinetics

Non-isothermal degradation kinetics has been performed at dynamic heating rates (**Fig. 4.14**) under an inert nitrogen atmosphere. From DTG curves (**Fig. 4.15**), it can be observed that on increment heating rates, the peak degradation temperatures shifted to a higher temperature due to the faster release of gaseous products. The main information obtained from different theoretical approach is the measurement of activation energy (E_a) with respect to conversion (**Table 4.4**).

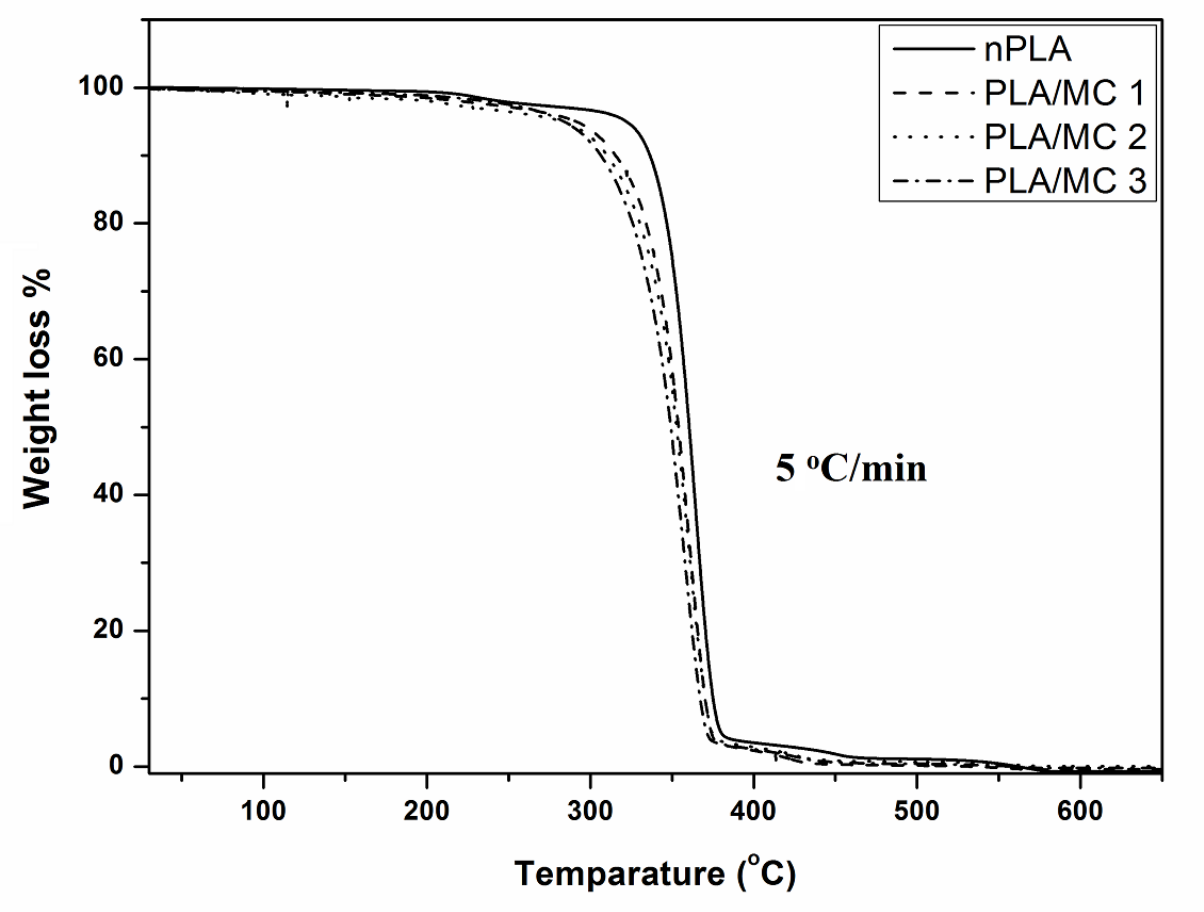

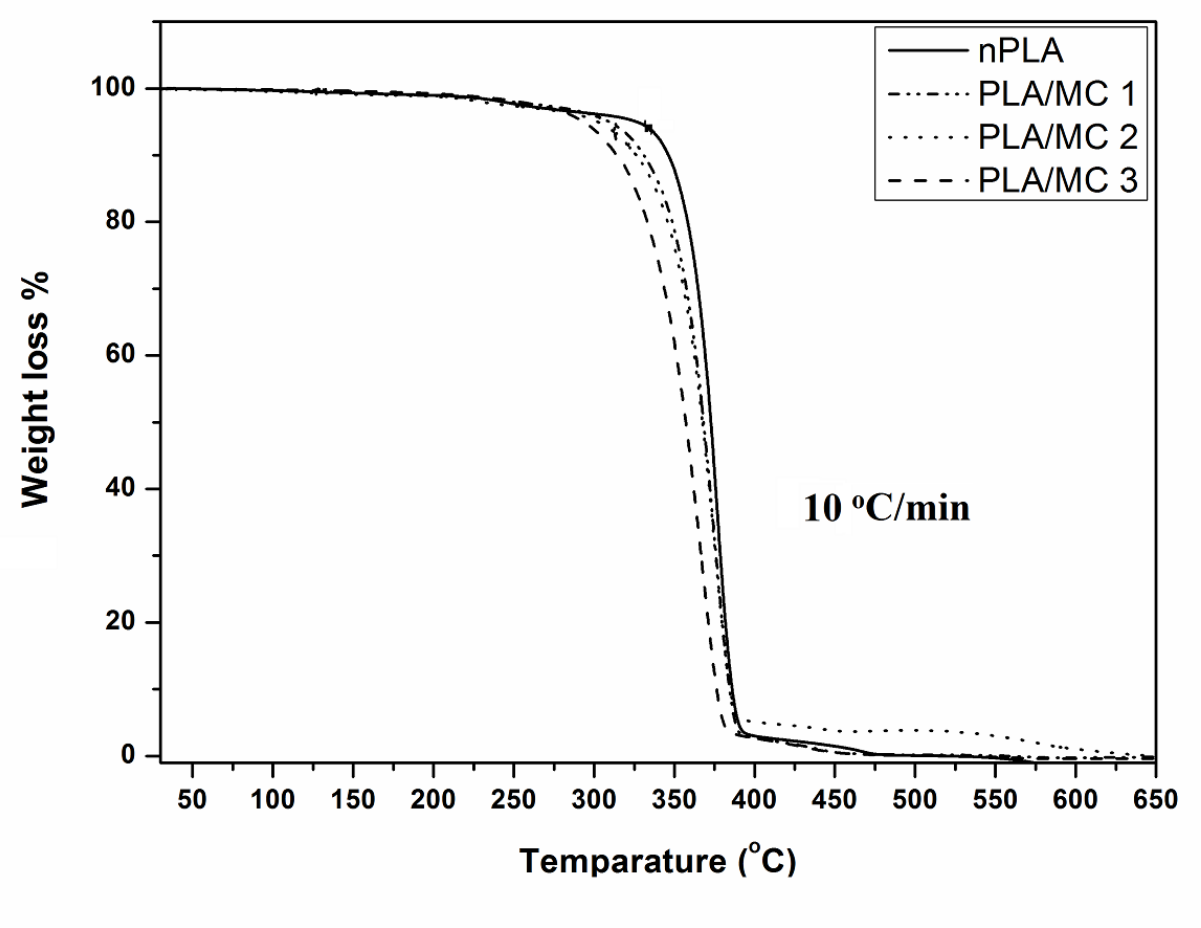

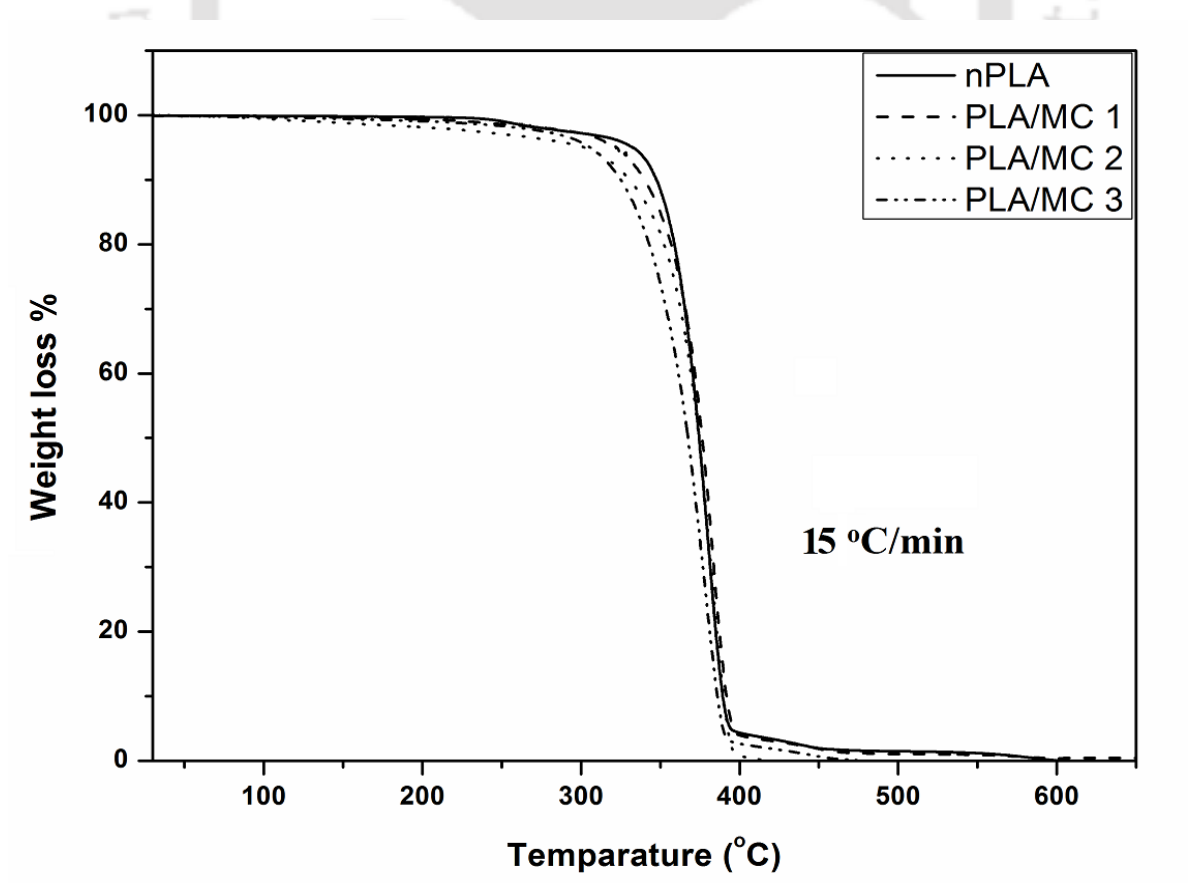

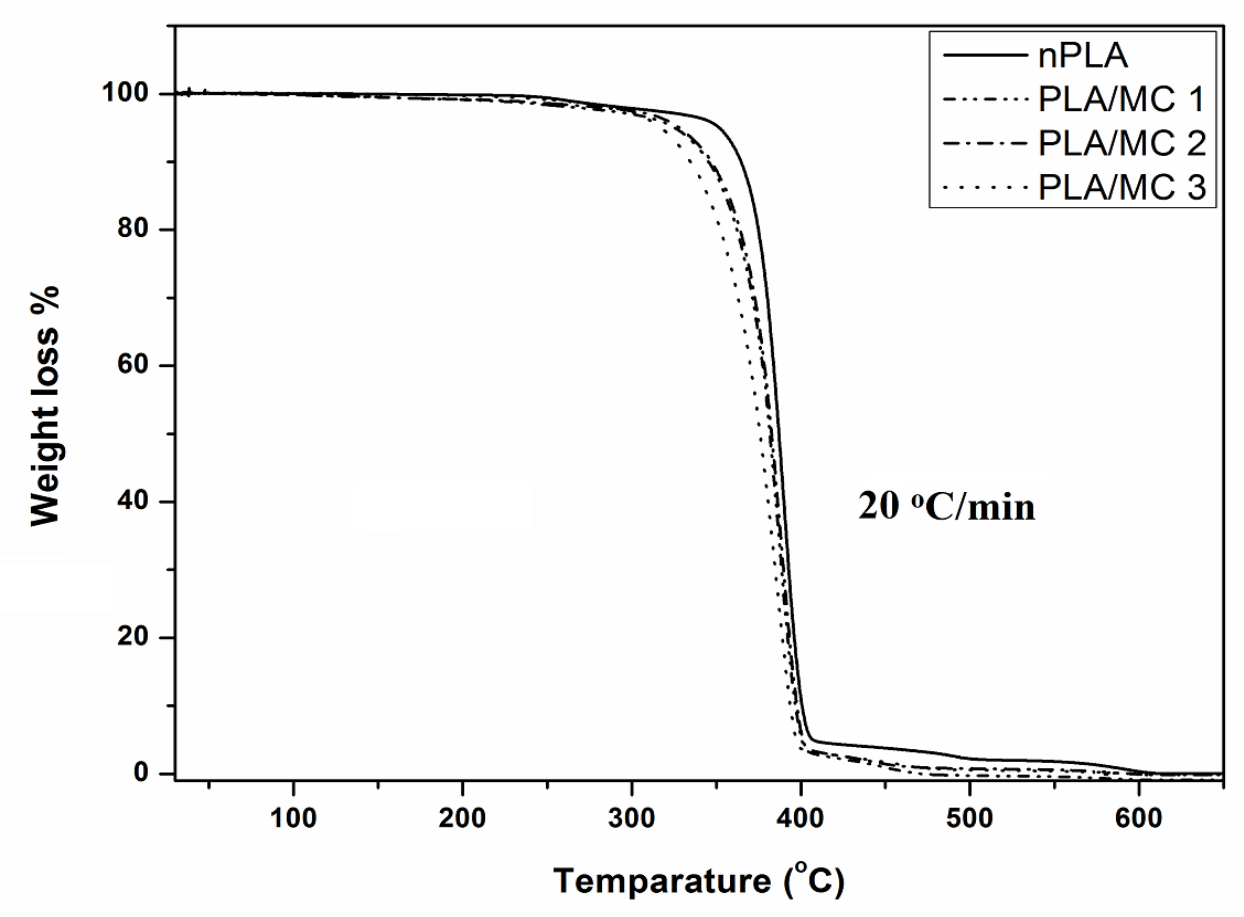

Fig. 4.14 TGA thermographs of PLA and PLA/MC-based foams at different heating rates.

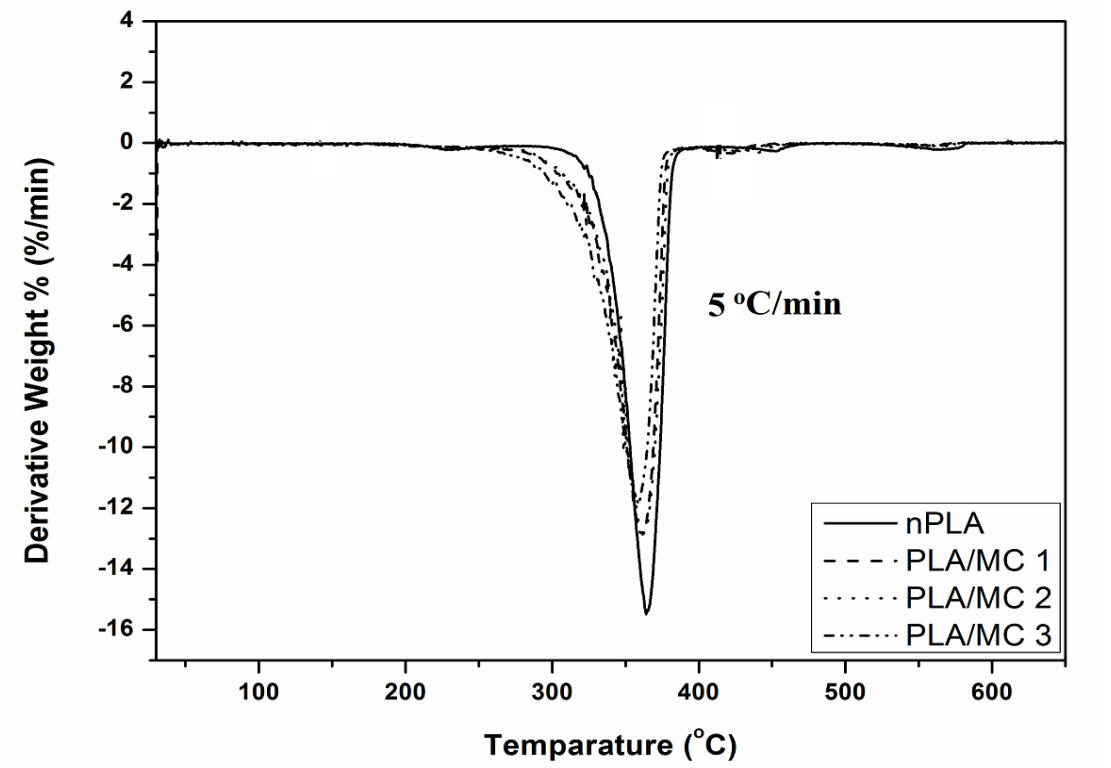

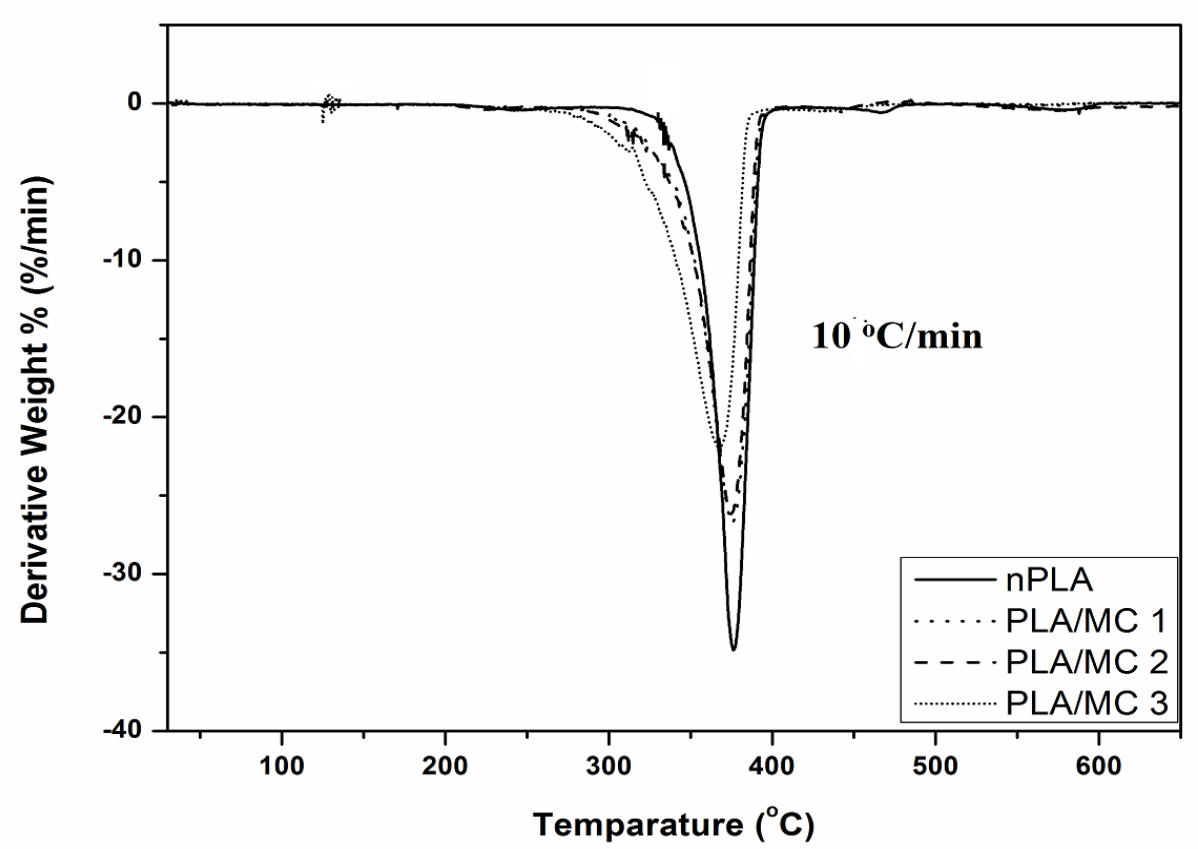

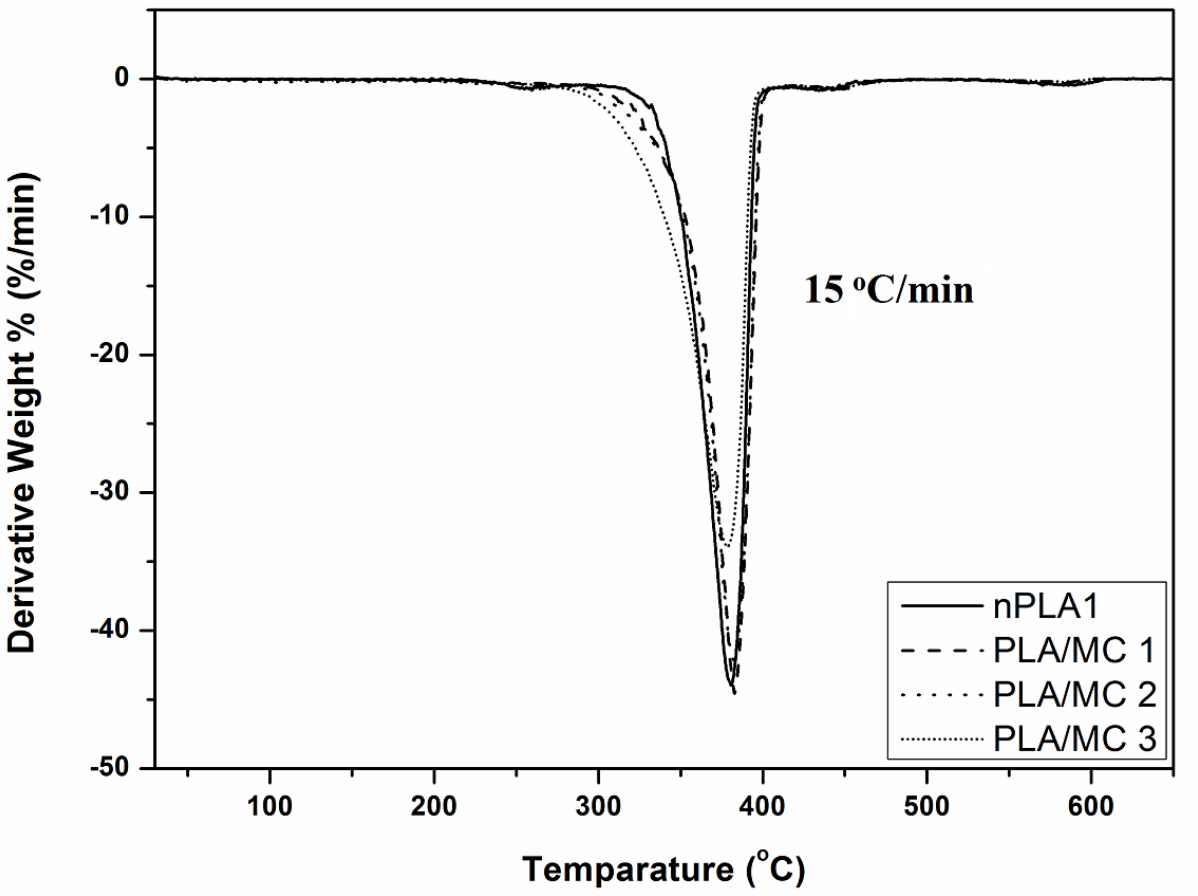

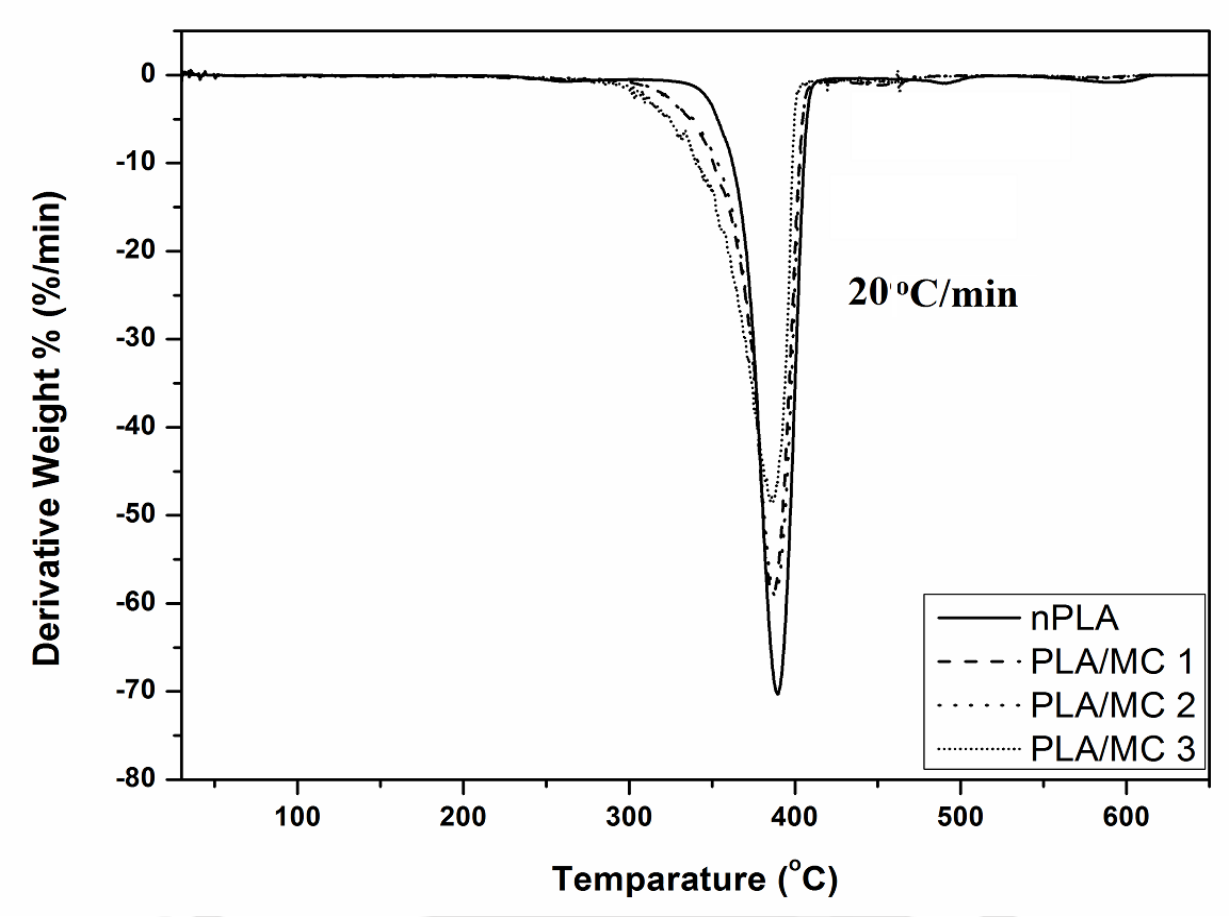

Fig. 4.15 DTG graphs of PLA and PLA/MC-based foams at different heating rates.

Table 4.4 Apparent activation energy distribution with conversion (α) for PLA and PLA/MC-based foams.

Sample	**α**	**FWO**		**Coats-Redfern (Modified)**	
		E_a (kJ/mol)	**R^2**	**E_a (kJ/mol)**	**R^2**
nPLA	0.1-0.9	145-196	0.94	135-185	0.92
PLA/MC 1	0.1-0.9	139-186	0.99	129-175	0.99
PLA/MC 2	0.1-0.9	114-185	0.99	104-174	0.99
PLA/MC 3	0.1-0.9	138-182	0.99	129-171	0.98

4.3.1.1 Flynn-Wall-Ozawa model

The activation energies are calculated by using the FWO method (**Table 4.4**). Graphs are plotted by taking ln β vs -1/T. It can be observed from **Fig. 4.16** that parallel lines are achieved at conversion rates (α= 0.1-0.9), which also confirms the applicability of this model to our system. The activation energy (E_a) of nPLA is calculated as 175.8 kJ/mol, which is in accordance with previously obtained results [184]. The E_a values gradually decrease on increase in nanofiller loading which means that lesser energy requirement for bond breaking higher loading of MC. Therefore, we can conclude that nanobiofiller reduces the thermal stability of the fabricated foams. Distribution of activation energy with conversion is shown in **Fig. 4.17.**

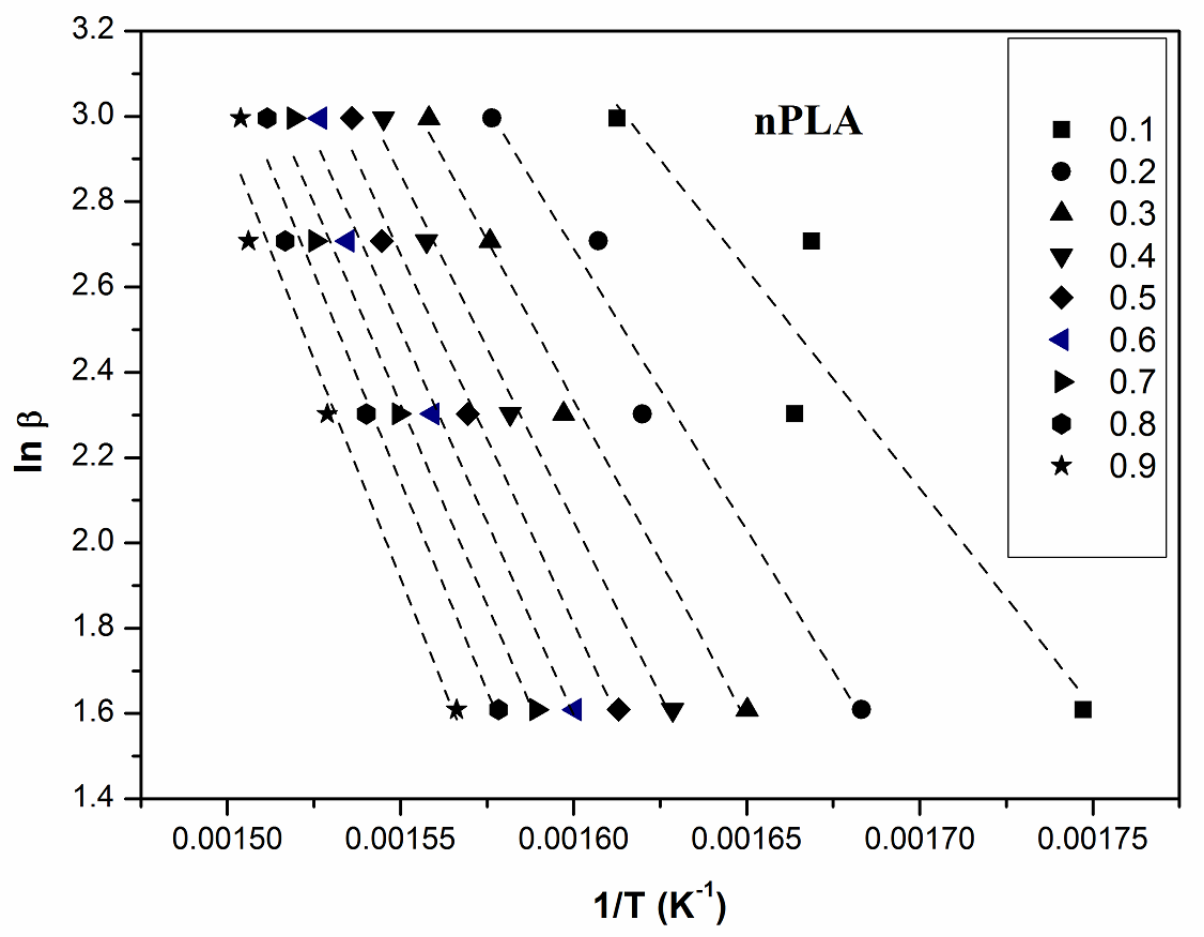

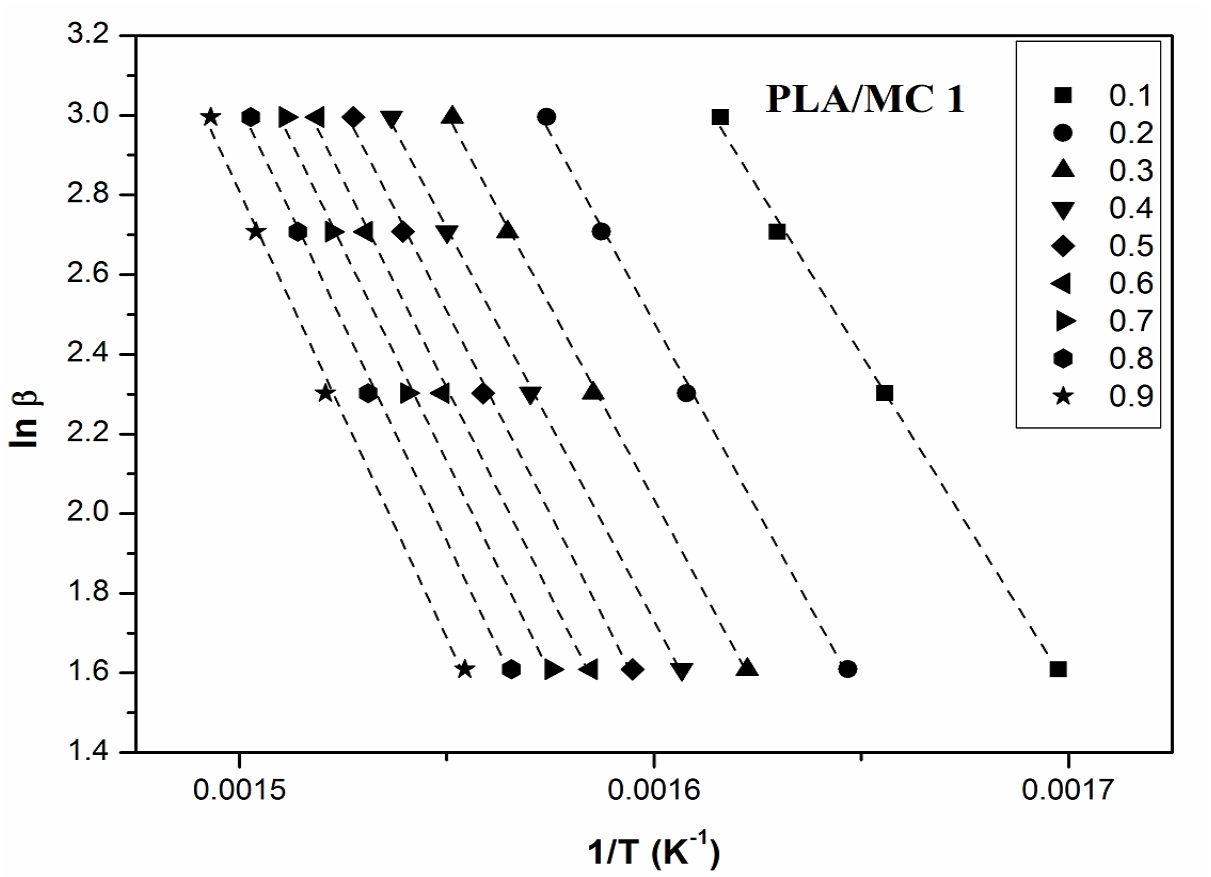

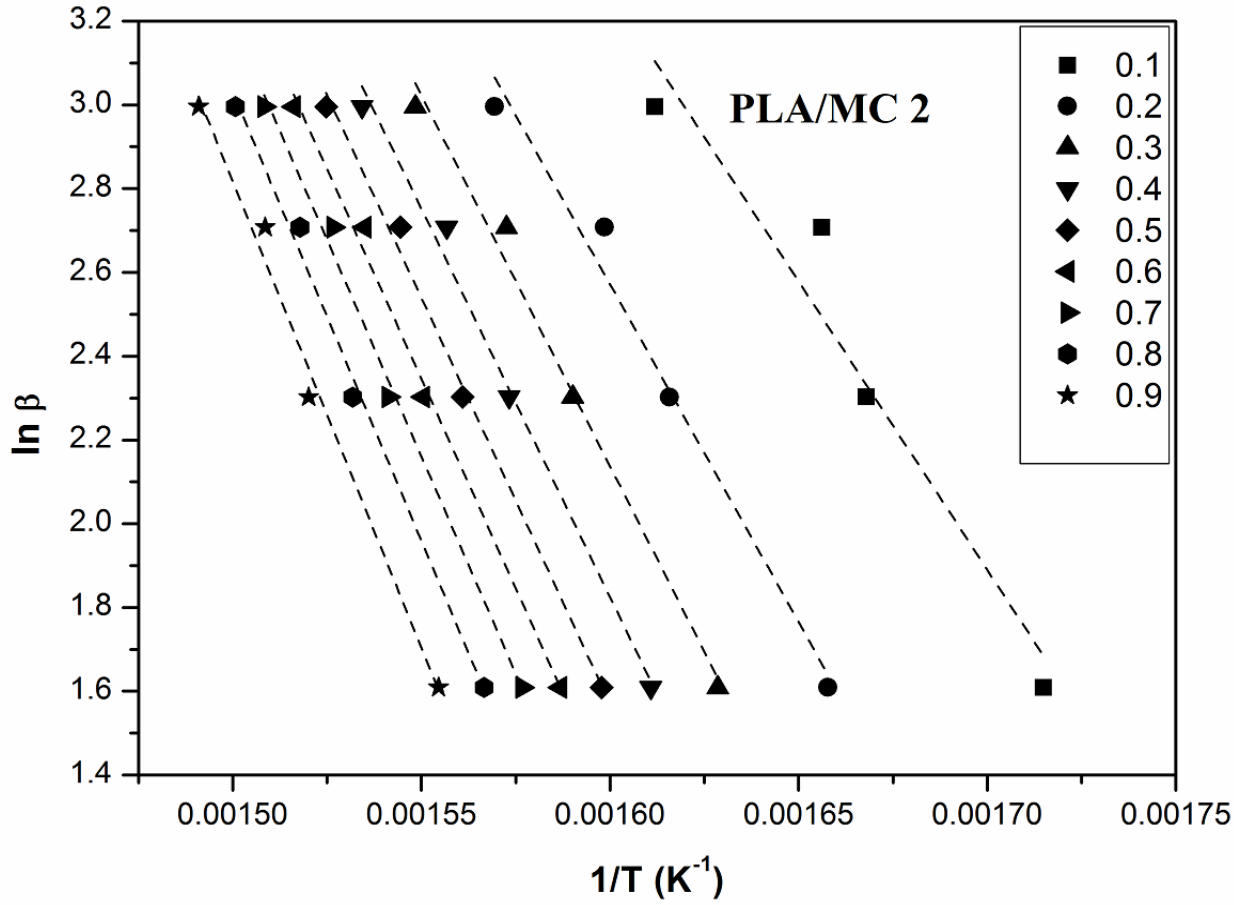

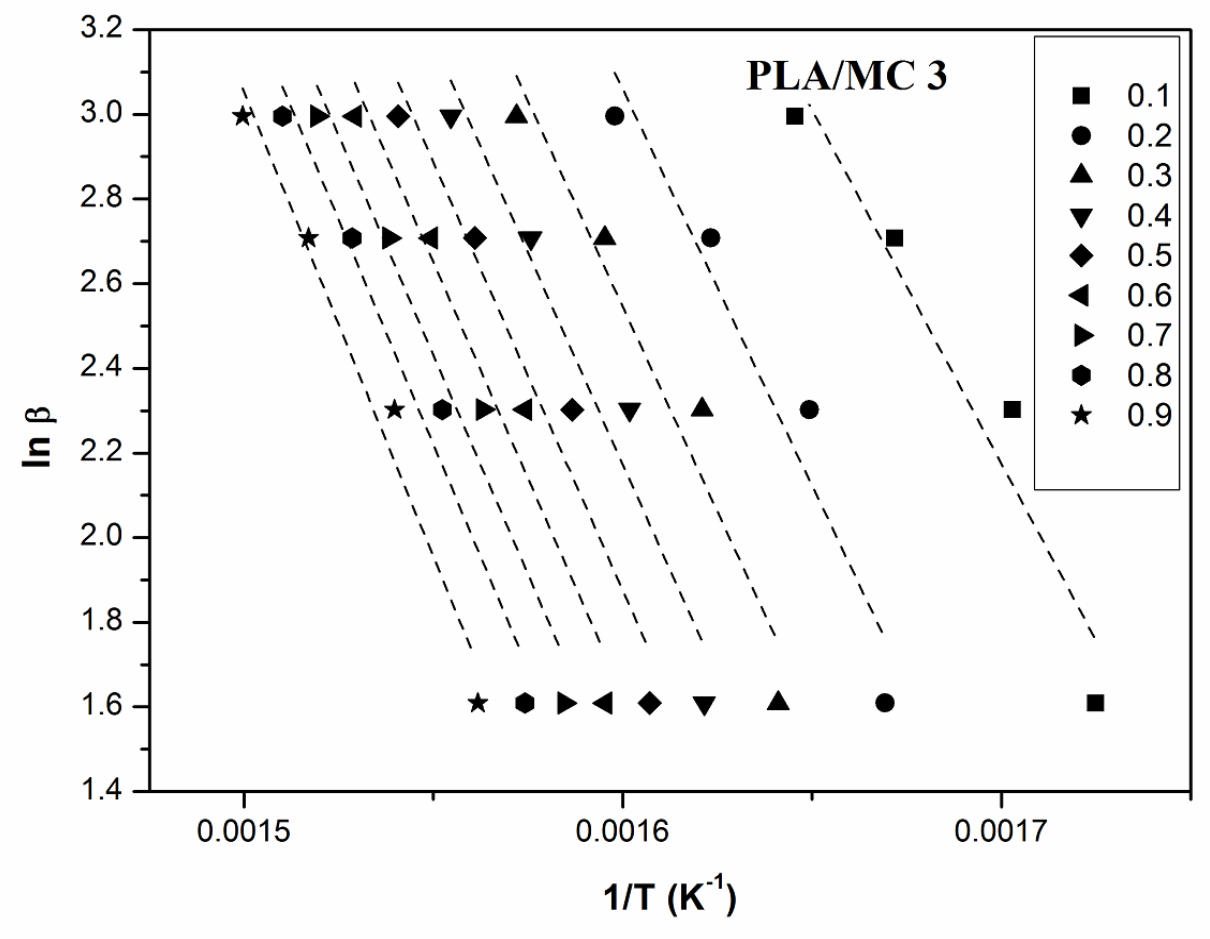

Fig. 4.16 FWO plots for PLA and PLA/MC-based foams.

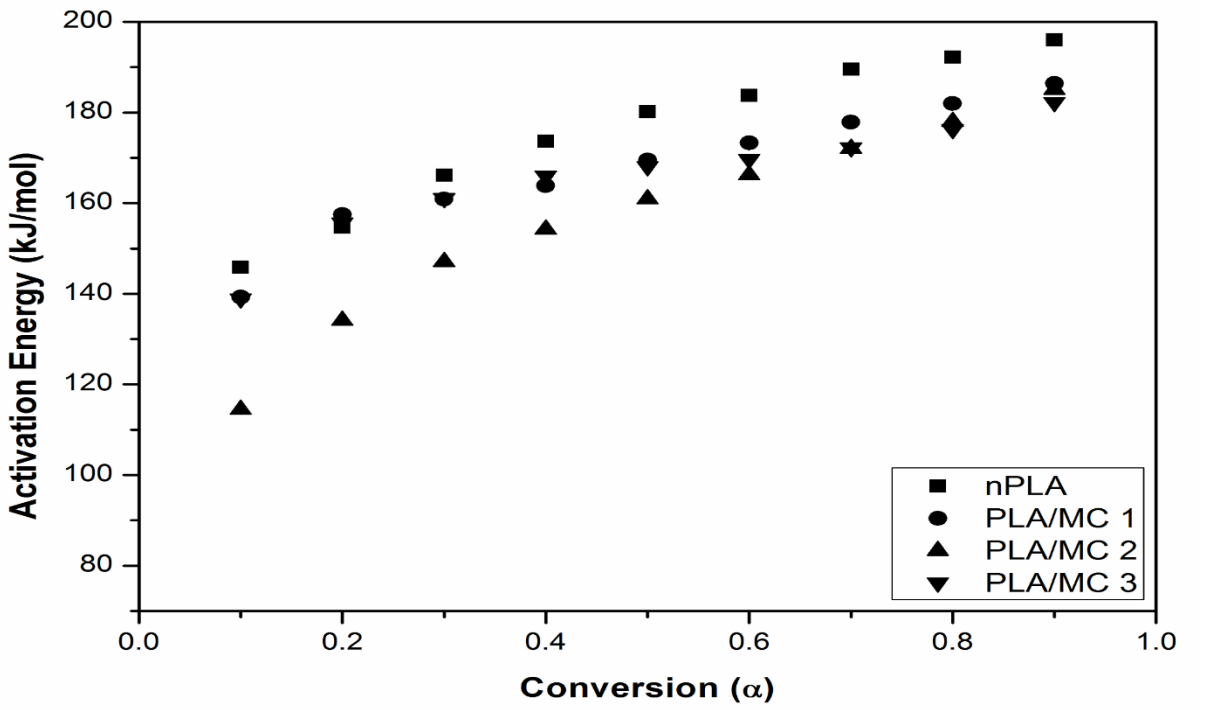

Fig. 4.17 Distribution of activation energy for PLA and PLA/MC-based foams at different conversions from FWO model.

4.3.1.2 Modified CR model

The distribution of activation energy with different conversions are shown in **Table 4.4**. The graph was plotted between ln β/T^2 vs 1/T for fabricated foams. It is observed that parallel lines are obtained (**Fig. 4.18**) at different conversions in case of all the fabricated foams, which justifies the applicability of this model to the used polymeric system. It is noticed that with the conversion, the slope of the lines increases. It is observed from the table, that activation energy value decreases with increase in nanobiofillers. The activation energy distribution with conversion can be observed in **Fig. 4.19**. The values of activation energies calculated by modified CR and FWO models are close enough to each other, which indicates the applicability of these isoconversional model to PLA/MC foam.

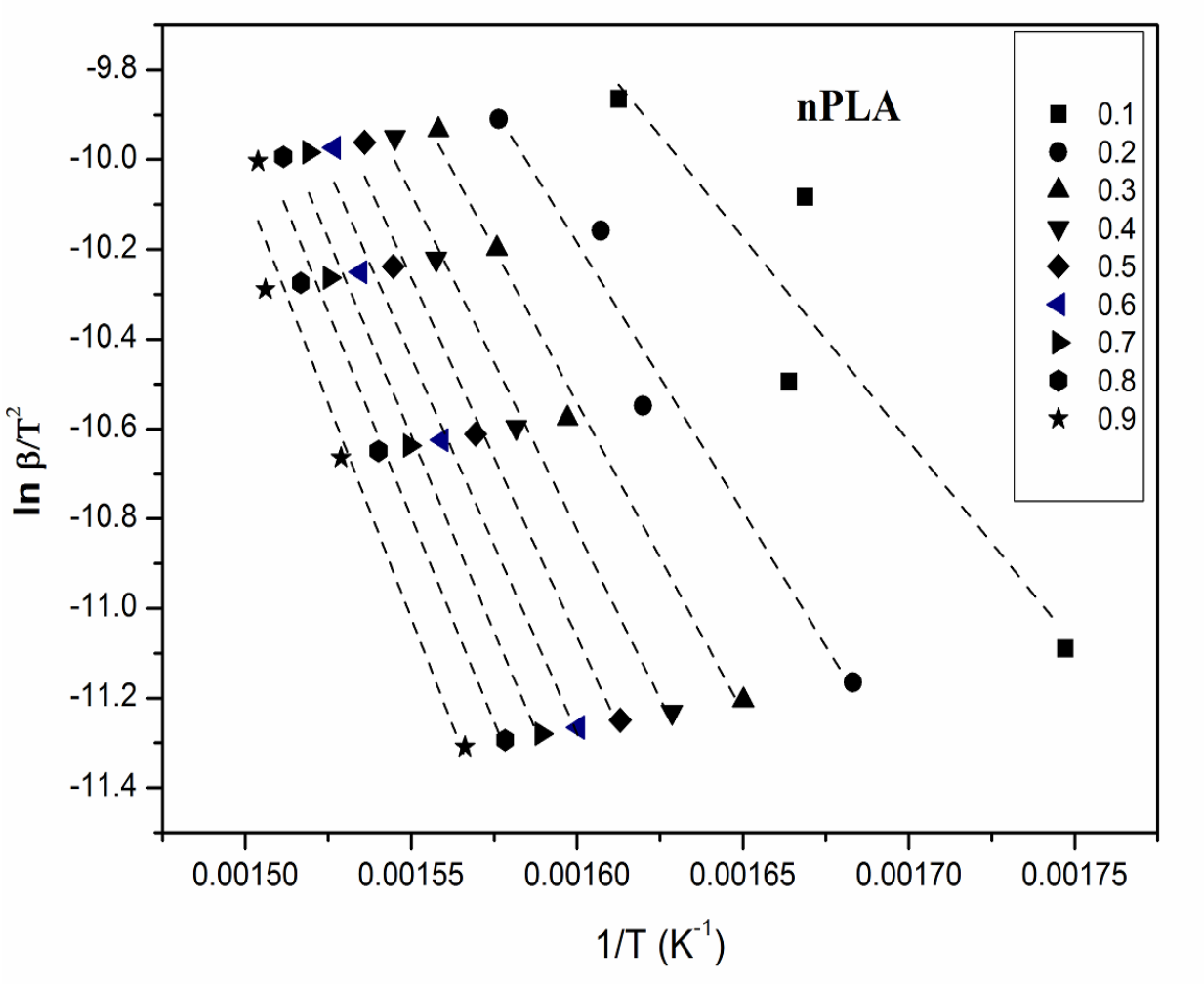

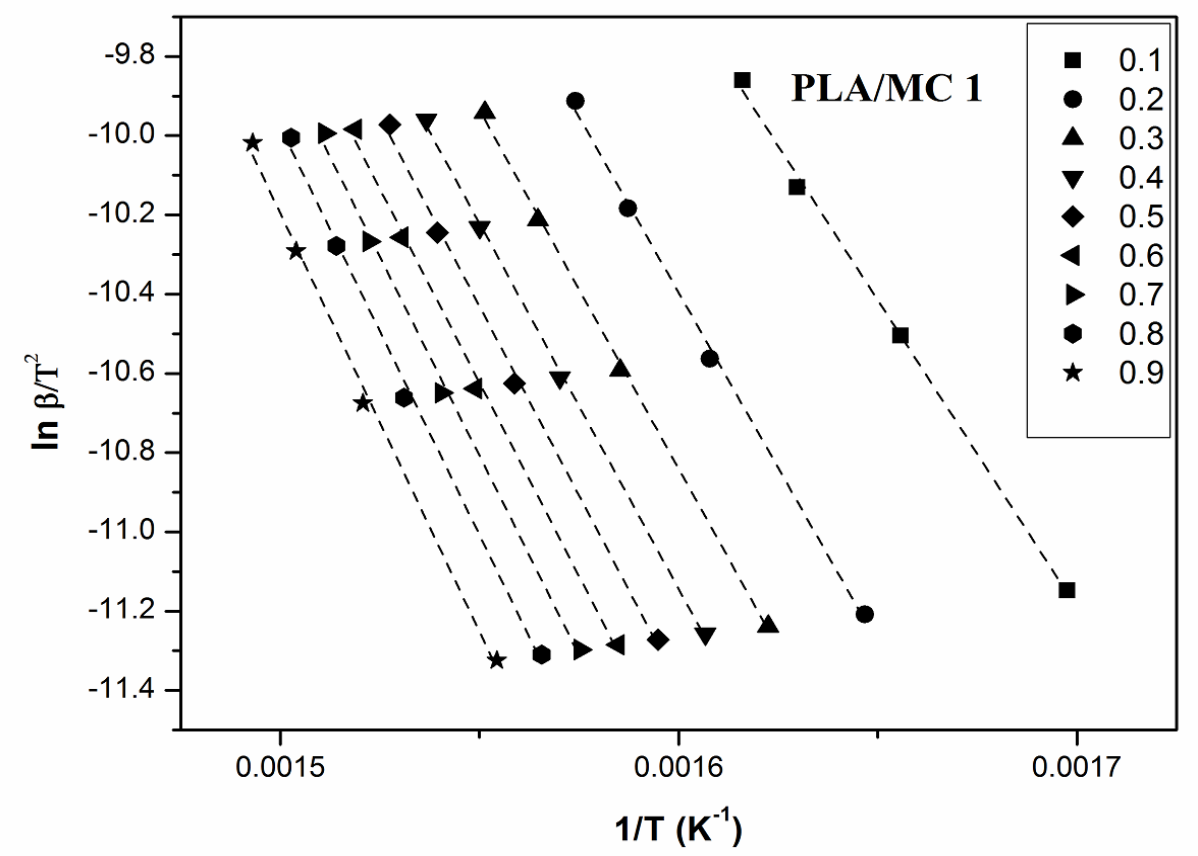

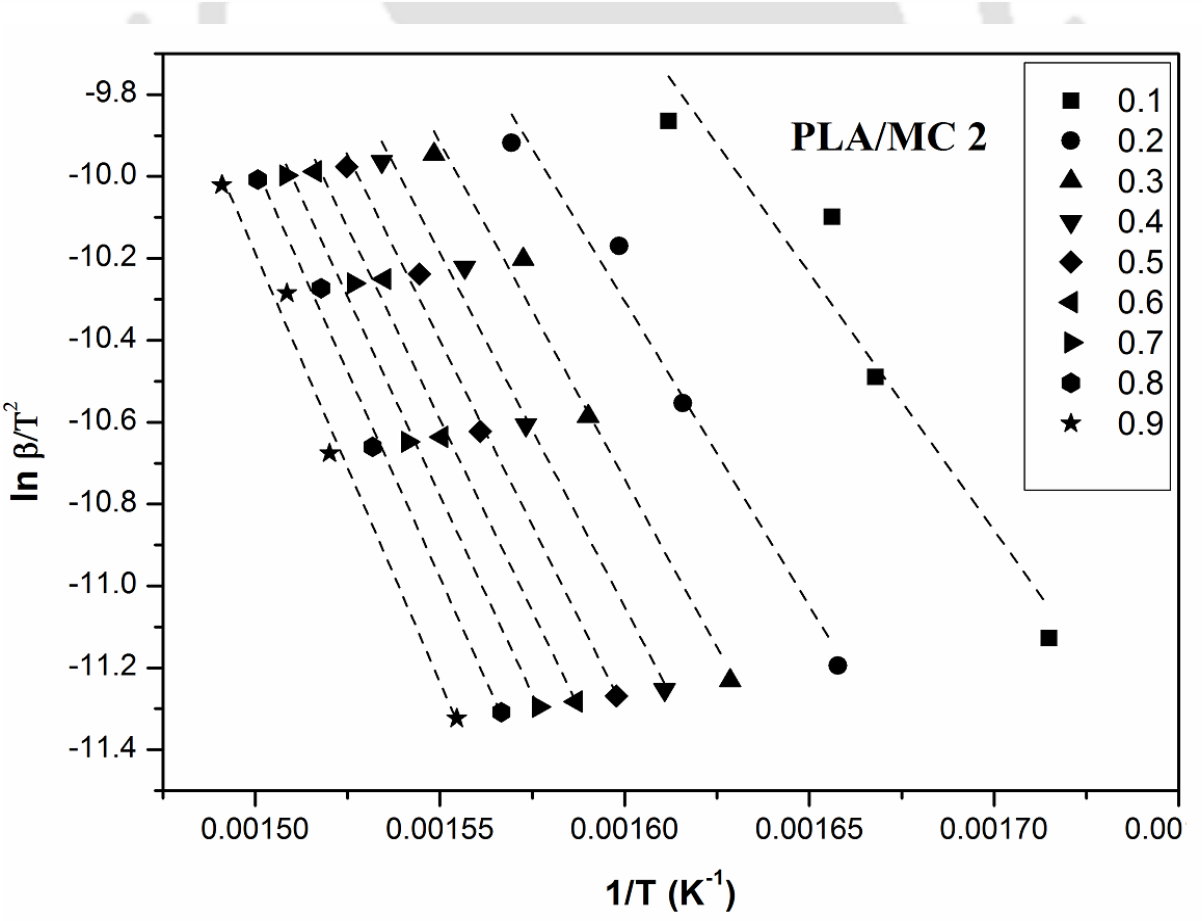

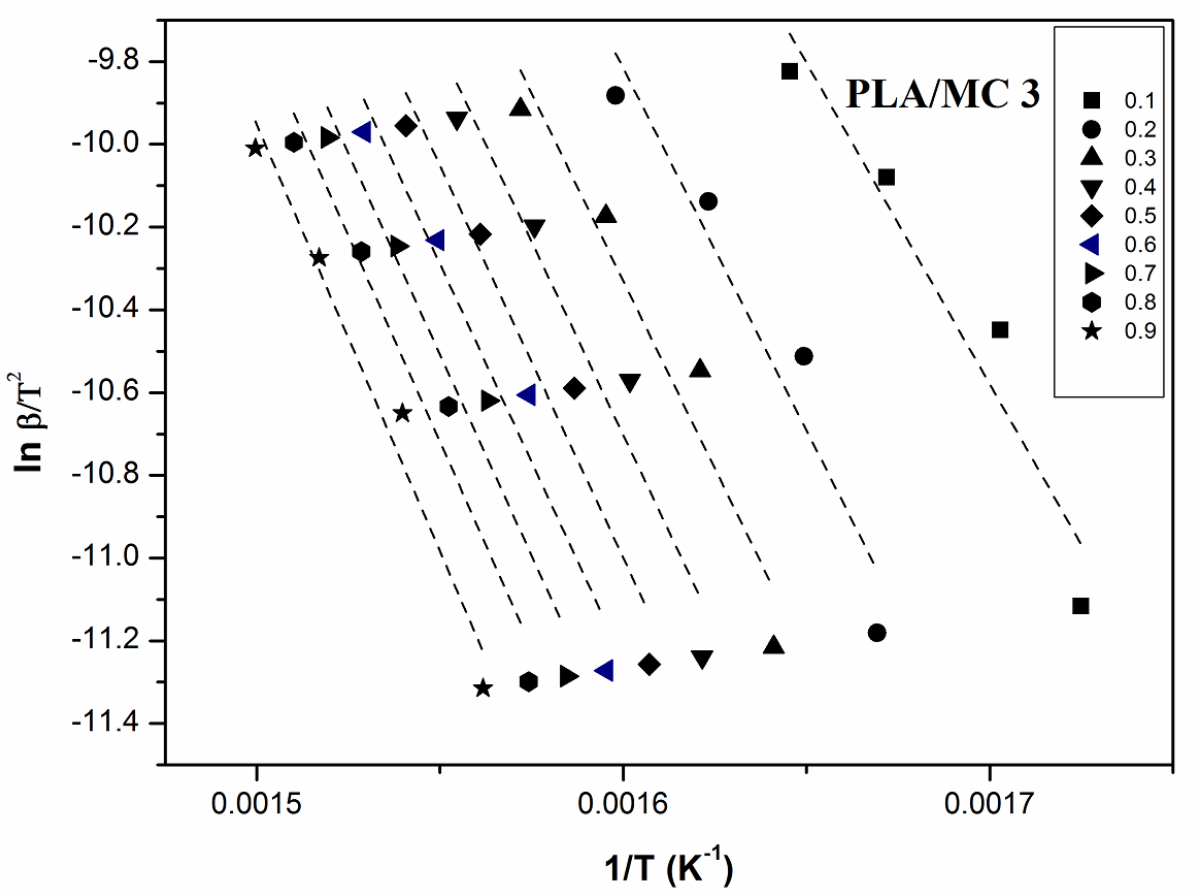

Fig. 4.18 Modified CR plots for PLA and PLA/MC-based foams.

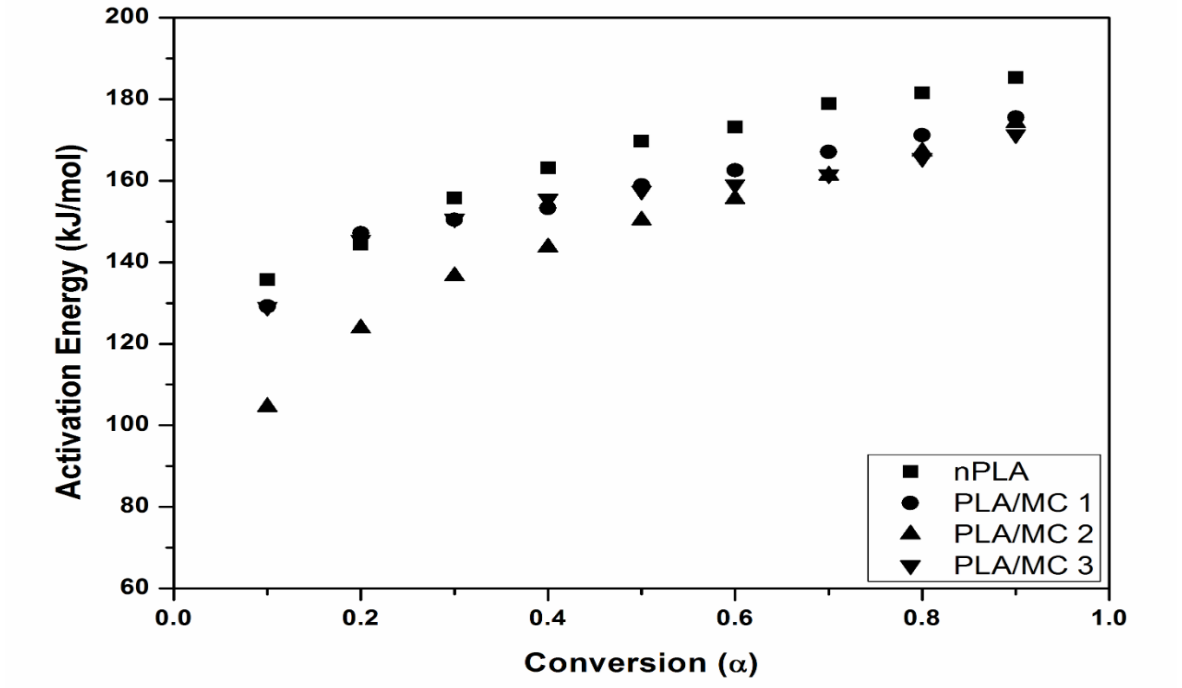

Fig. 4.19 Distribution of activation energy for PLA and PLA/MC-based foams at different conversions from modified CR model.

4.3.1.3 Kissinger model

This method is used to calculate the activation energy at T_{max}. The graph was plotted (**Fig. 4.20**) between ln β/T^2_{max} vs $(-1000/T_{max})$ for the calculation of slope values. The lines are fitted properly indicating the applicability of this model to the current polymeric system. From the Kissinger method, the same trend of activation energy is noticed as shown by FWO and modified CR methods (**Table 4.5**). This model gives only one E_a at T_{max}, However, in case of FWO and modified CR provide E_a values at each conversion. The calculated values of activation energies by Kissinger method have been used to measure various thermodynamic parameters. The reduction in activation energy with nanobiofiller loading is due to the increase in acidic sites. The acidic site increases the degradation and decreases the activation energy. During thermal degradation, hydrolysis of ester group taking place, which again converts to acids. Higher acidic sites enhance the random chain scission of ester groups in PLA backbone [204].

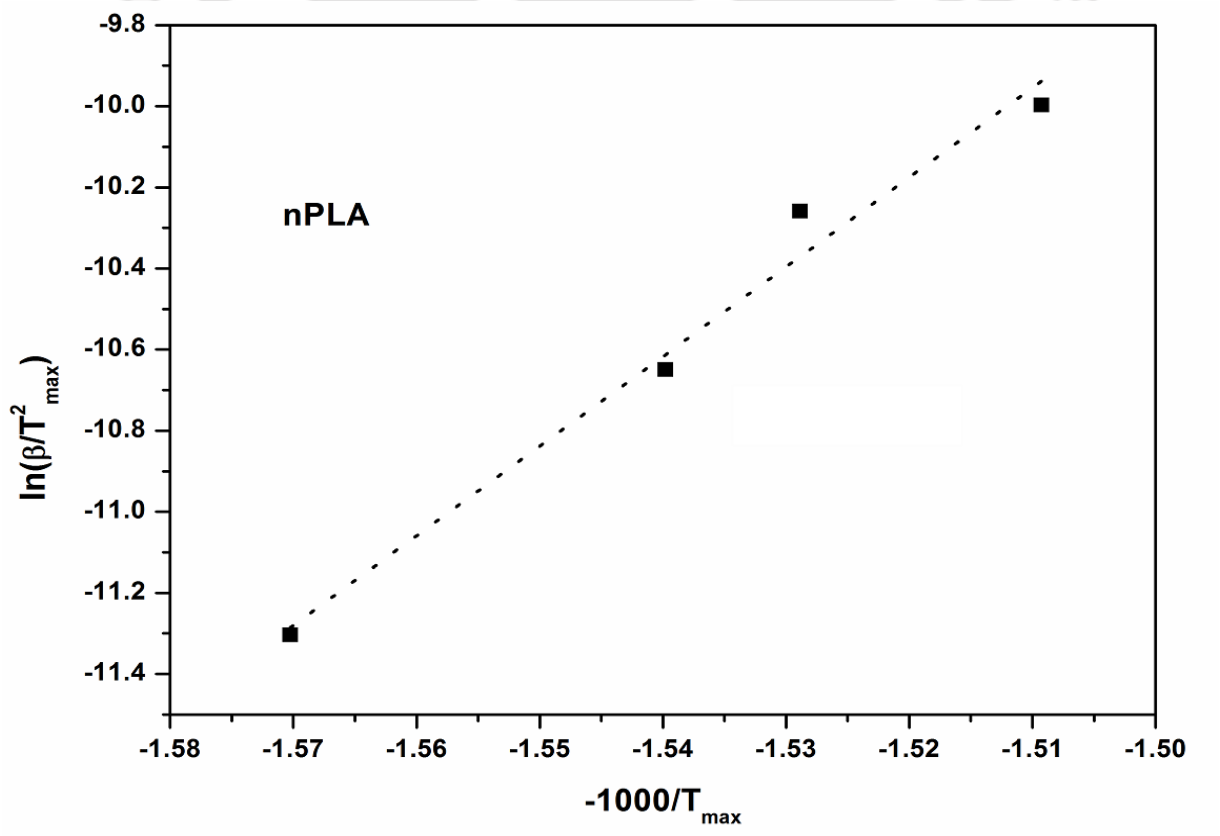

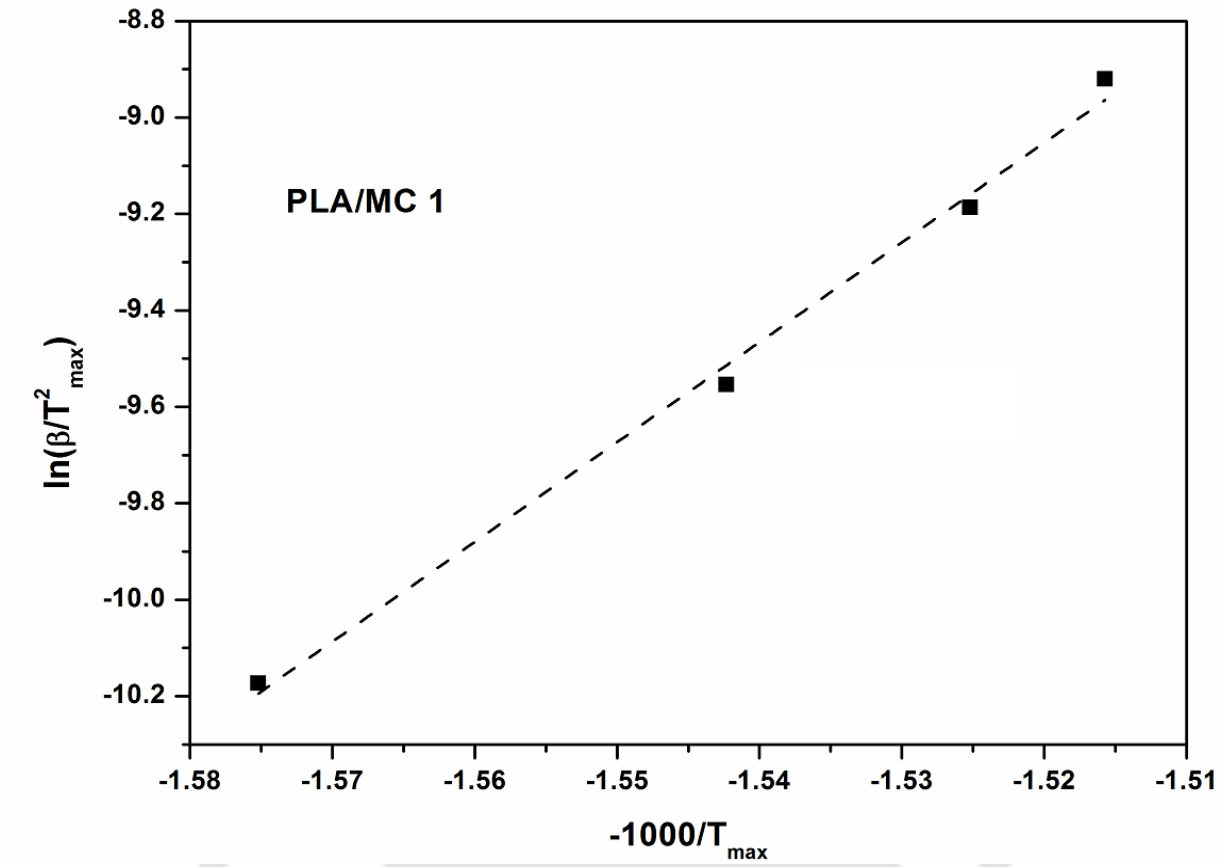
PLA/MC 1
-8.8
-9.0
-9.2
-9.4
-9.6
-9.8
-10.0
-10.2
-1.58
-1.57
-1.56
-1.55
-1.54
-1.53
-1.52
-1.51
ln(β/T2max)
-1000/Tmax

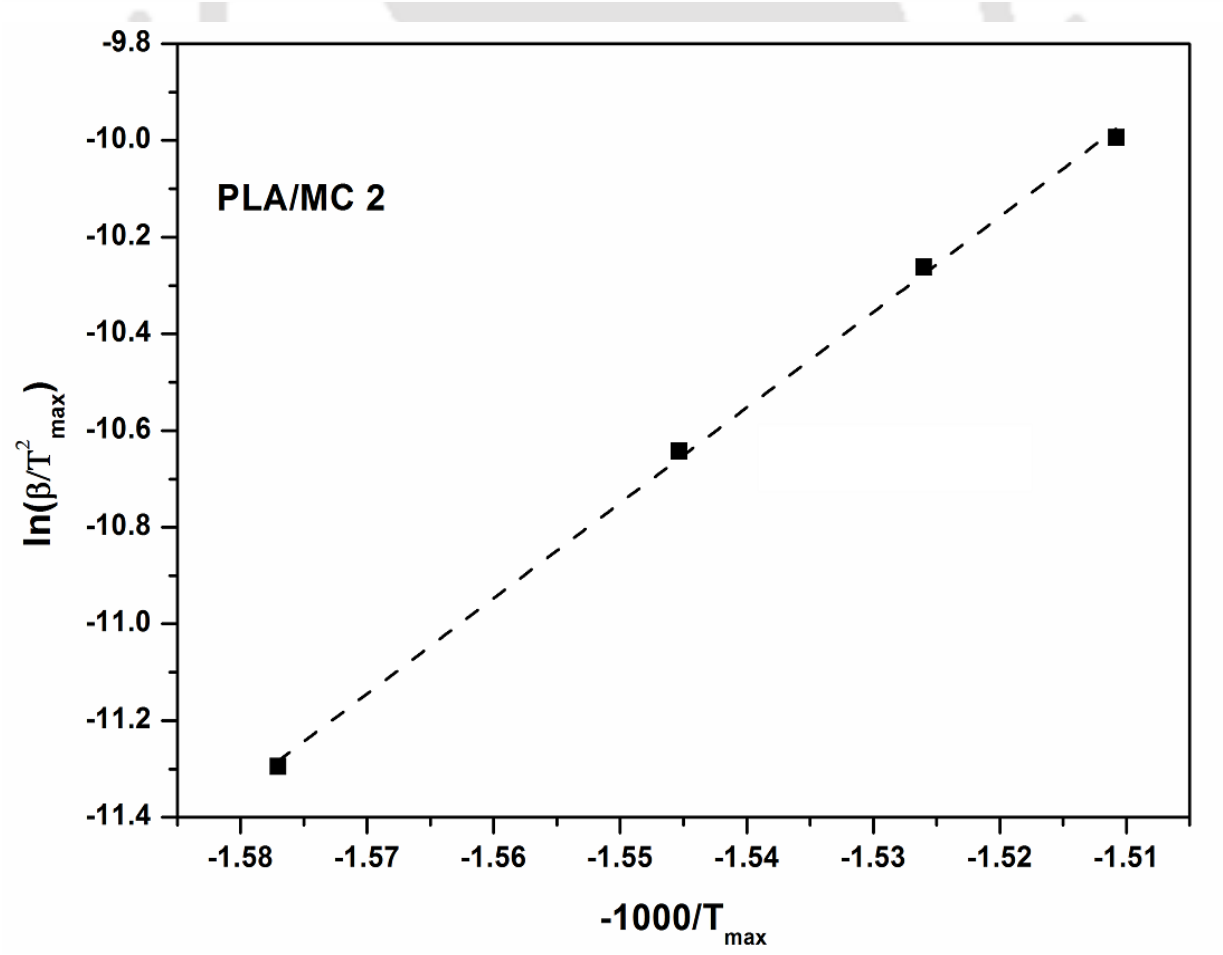
PLA/MC 2
-9.8
-10.0
-10.2
-10.4
-10.6
-10.8
-11.0
-11.2
-11.4
-1.58
-1.57
-1.56
-1.55
-1.54
-1.53
-1.52
-1.51
ln(β/T2max)
-1000/Tmax

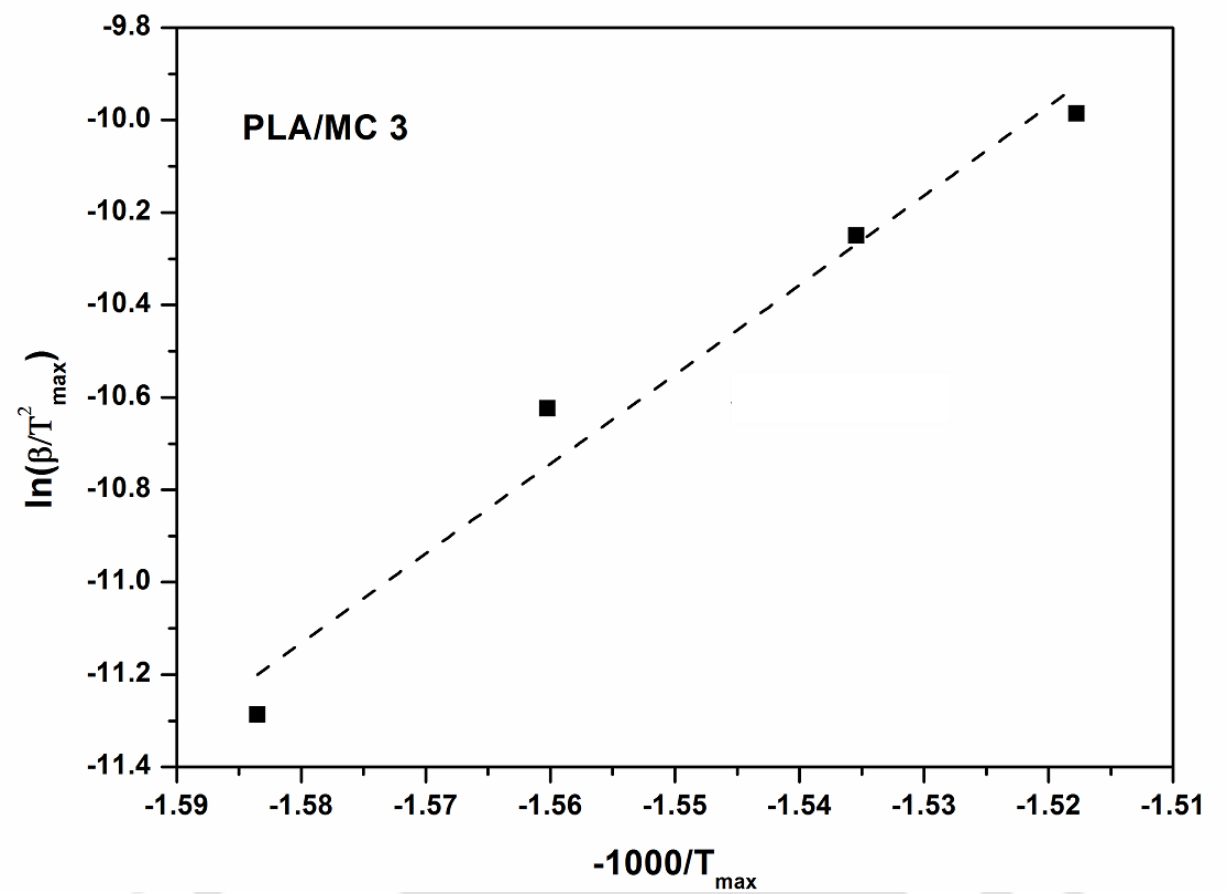

Fig. 4.20 Kissinger plots of PLA and PLA/MC-based foams.

Table 4.5 Kinetic parameters and thermodynamic variables for PLA and PLA/MC-based foams from Kissinger method at a heating rate of 10 °C /min.

Sample	**Kinetic Parameter**			**Thermodynamic Variables**		
	E_a (kJ/mol)	**R^2**	**A (s^{-1})**	**ΔG (kJ/molK^{-1})**	**ΔH (kJ/mol)**	**ΔS (kJ/mol)**
nPLA	183.6	0.97	3.25×10^{11}	1.5×10^{4}	-5215.8	-31.1
PLA/MC 1	171.9	0.99	1.11×10^{11}	2×10^{4}	-5218.6	-39.9
PLA/MC 2	164.0	0.99	8.2×10^{9}	3.4×10^{4}	-5215.9	-61.6
PLA/MC 3	160.9	0.96	5.5×10^{9}	3.6×10^{4}	-5167.7	-64.8

4.3.2 Estimation of thermodynamic parameters

Thermodynamic variables are calculated for fabricated foams (summarized in **Table 4.5**). It is observed that ΔS value for all the fabricated foam is negative. This negative value indicates that the activated complex was formed at higher temperatures and some extent of chain alignment is taking place in polymeric chains. It also indicates that the degree of disorder of product is lower than an initial disorder of the reactants. The negative value of ΔH for all the fabricated foam indicates the process bond dissociation is exothermic in nature. The value of ΔG is observed as positive for all the cases indicating the non-spontaneous nature of the dissociation process [151,209,210].

4.3.3 Reaction mechanism for degradation

Criado method is utilized for a better understanding of the degradation mechanism. Activation energy values obtained from Kissinger model are utilized to evaluate the mechanism (Heating rate:10°C/min). The master and experimental curves of the fabricated foams are shown in **Fig. 4.21**. It is observed that all the foam follows F3 and F2 mechanism initially at low conversions. At higher conversions ($\alpha \geq 0.6$), it undergoes R1 mechanism followed by D4 mechanism. In $F_{n,}$ mechanism decomposition begins with random nucleation which propagates thermal degradation of the sample. R1 mechanism involves phase boundary controlled one-dimensional movement reactions. The D4 mechanism promoting an acceleration in decomposition by three-dimensional diffusion process at higher temperatures. It can be concluded from the study that all the fabricated foams follow similar degradation mechanism for thermal decomposition [211].

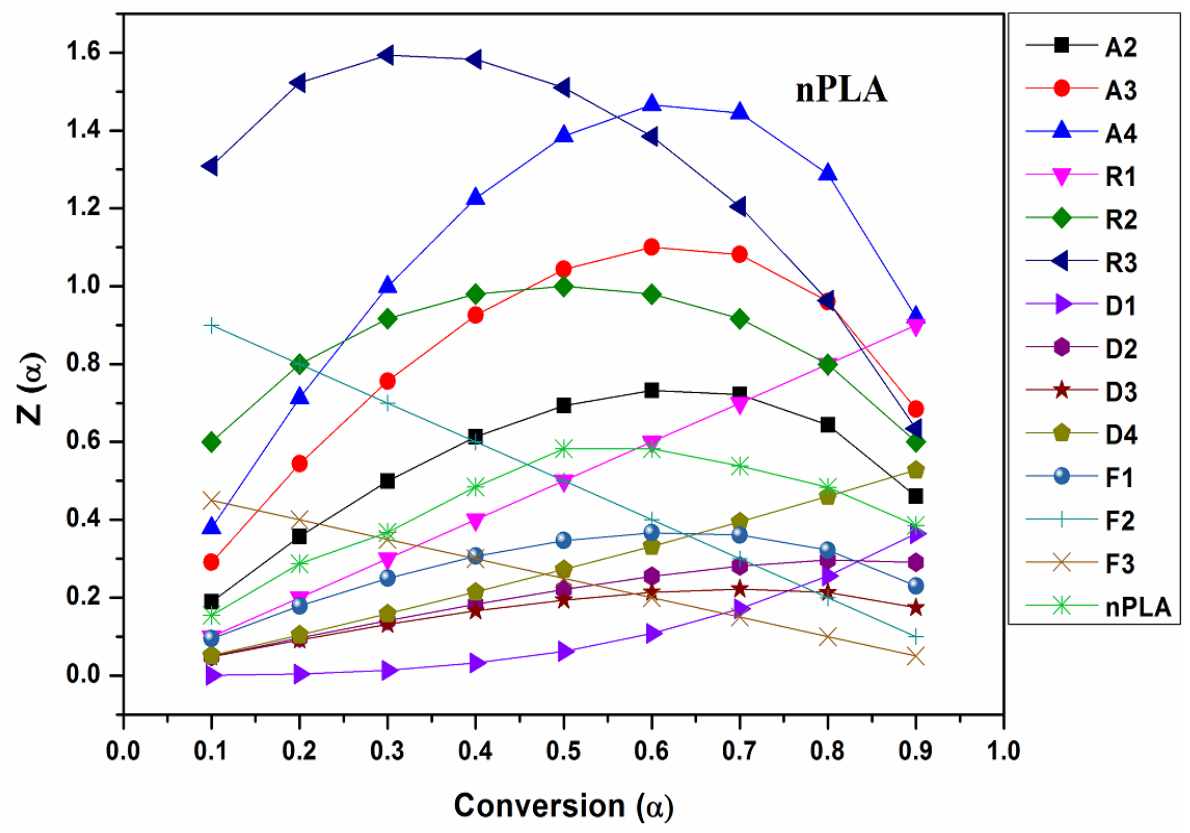
nPLA
Z (α)
Conversion (α)
A2
A3
A4
R1
R2
R3
D1
D2
D3
D4
F1
F2
F3
nPLA

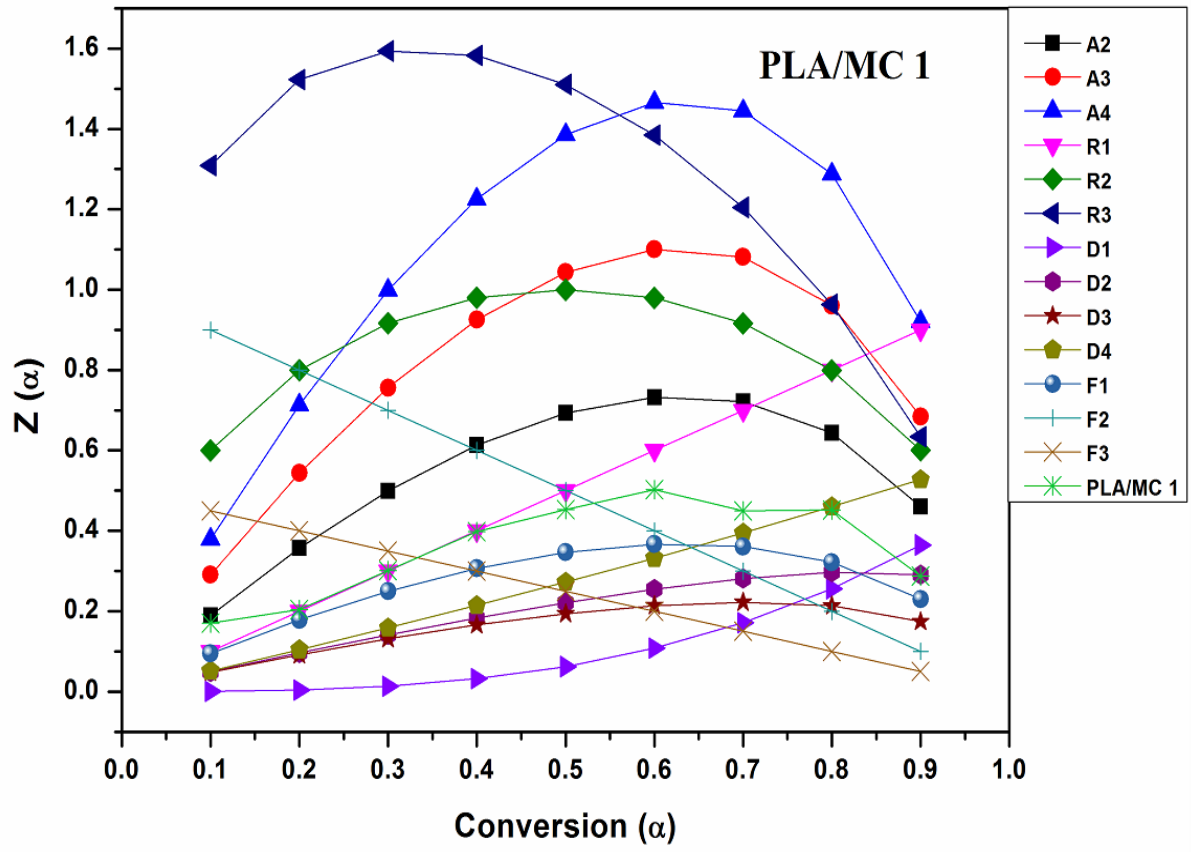
PLA/MC 1
Z (α)
Conversion (α)
A2
A3
A4
R1
R2
R3
D1
D2
D3
D4
F1
F2
F3
PLA/MC 1

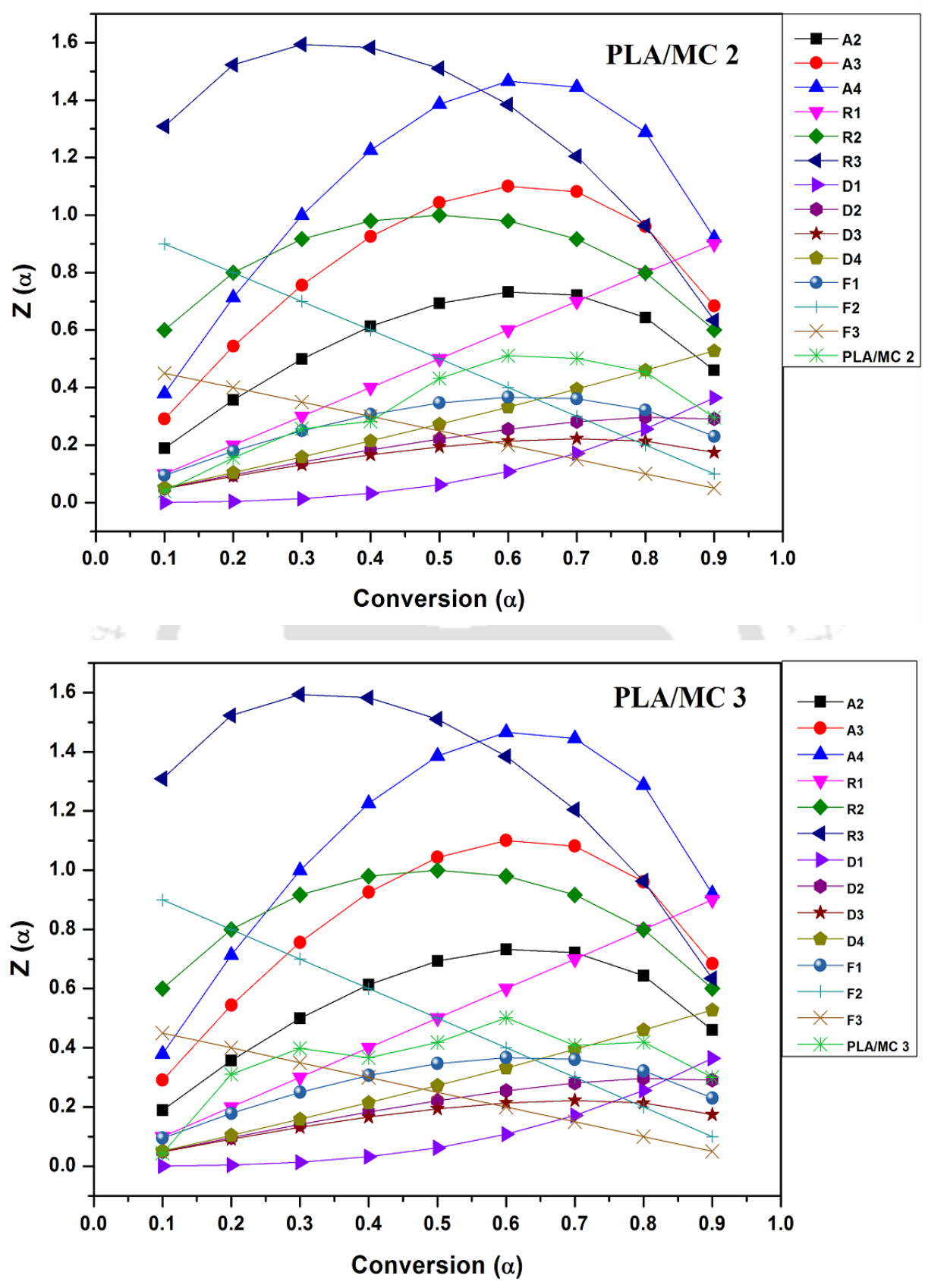

Fig. 4.21 Criado master and experimental plots for PLA and PLA/MC-based foams.

4.4 TGA-FTIR investigations of the PLA and PLA/MC-based foams

TGA coupled with FTIR investigations have been carried out for detailed observation of the volatile gaseous products obtained during thermal degradation of the fabricated foams. This information can be utilized for justification of the reaction mechanism followed by the PLA and PLA/MC-based foams. The height of the IR peaks indicates the concentration variations of the products obtained.

4.4.1 Release of volatile products from PLA based foams

The 3D and 2D FTIR spectra at a dynamic temperature ranging 30 °C to 700 °C are shown in **Fig. 4.22**. Plots at different degradation temperature indicate that the gaseous volatile products are mainly observed above the temperature of ~360 °C, which is in accordance with the TGA investigations discussed earlier. The main volatile products obtained from TGA-FTIR for nPLA with two prominent peaks at ~1790 cm^{-1} representing lactide or cyclic oligomers and at ~2350 cm^{-1} representing the carbon dioxide (CO_2) generated. The intensities of these products are found to be maximum at T_{max}. Other products obtained are identified as water (~3577 cm^{-1}), hydrocarbons (~2952 cm^{-1} and ~3010 cm^{-1}) and carbon monoxides (~2180 cm^{-1} and ~2106 cm^{-1}). Generation of CO is mainly due to decomposition of the ester with hydroxyl end initiation.[6] Some peaks are also noticed around ~1377 cm^{-1} (-CH stretching), ~1240 cm^{-1} (-C=O stretching), ~1100 cm^{-1} (-CO stretching) and 930 cm^{-1} (-C-C- stretching). The prominent peaks vanish after ~400 °C, indicating maximum decomposition of the fabricated foam happens at a temperature range of 360 °C-400 °C. Generation of CO_2 at a temperature above ~360 °C might be due to chain homolysis of PLA. The above results suggest that the degradation follows a random chain scission mechanism [3,6].

4.4.2 Release of volatile products from PLA/MC-based foams

The TGA-FTIR 3D spectra of PLA/MC 3 is shown in **Fig. 4.22**. It is observed from the FTIR spectra at different temperatures that the volatile products generated in thermal decomposition are almost similar to that of PLA based foam (nPLA). However, it is observed that the intensities of the peaks are less compared to that of nPLA. Maximum peak intensity is observed in the range of 367.9 °C-380 °C. The peaks are positioned at similar wavenumbers as in the case of nPLA. Three new small intensity peaks are observed in the case of PLA/MC 3. Peaks at 1650 cm^{-1}, 1542 $cm^{-1,}$ and 1529 cm^{-1} indicating amide I, amide II and –NH stretching of MC. This also indicates the grafting between OLLA and chitosan. The amount of polymers present is in a trace amount in MC, so the intensities of these bonds are very small. Intensities of the peak of CO are very less compared to the nPLA, which is an advantage for the environmental point of view. The decrease in peak intensities of the PLA/MC based foam compared to nPLA might be due to the generation of radicles in the thermal decomposition of MC. Radical reactions can take place at higher temperatures due to the formation of these gaseous products [174].

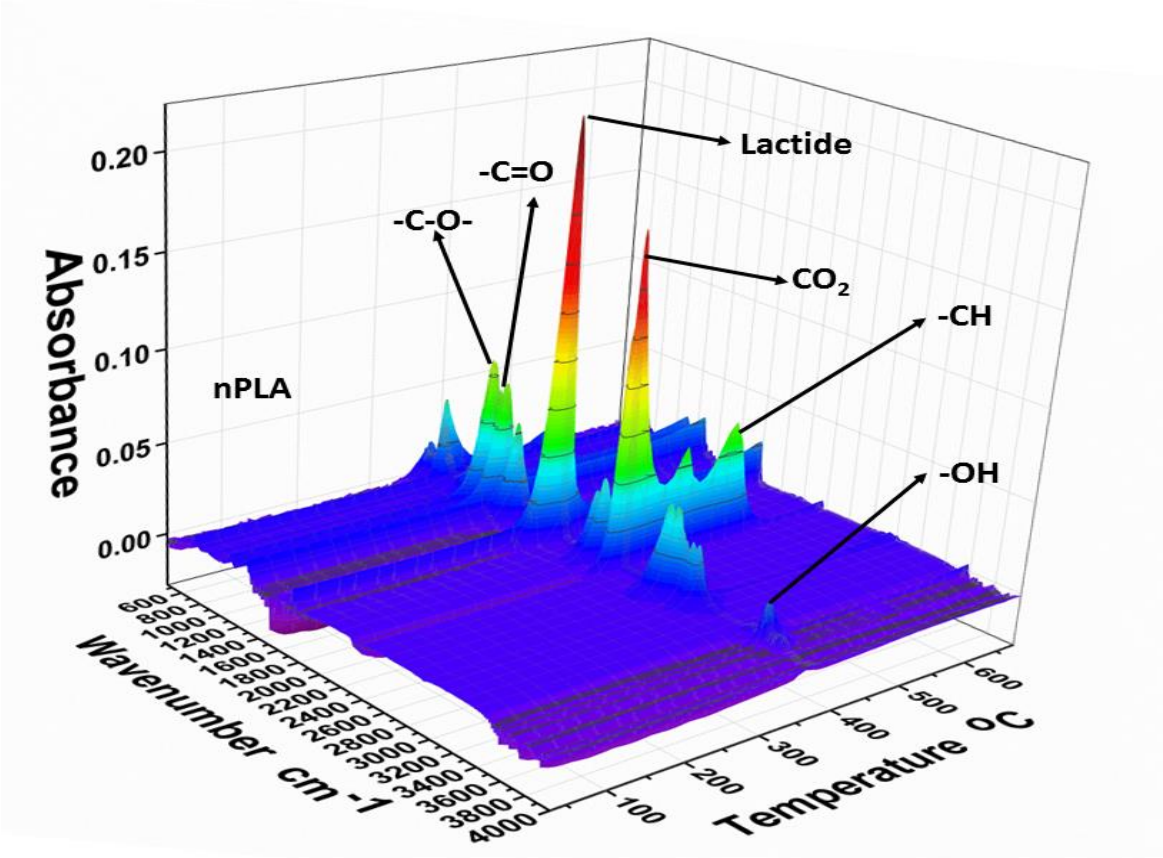
Absorbance
0.20
0.15
0.10
0.05
0.00
nPLA
-C-O-
-C=O
Lactide
CO_2
-CH
-OH
Wavenumber cm -1
600
800
1000
1200
1400
1600
1800
2000
2200
2400
2600
2800
3000
3200
3400
3600
3800
4000
Temperature oC
100
200
300
400
500
600

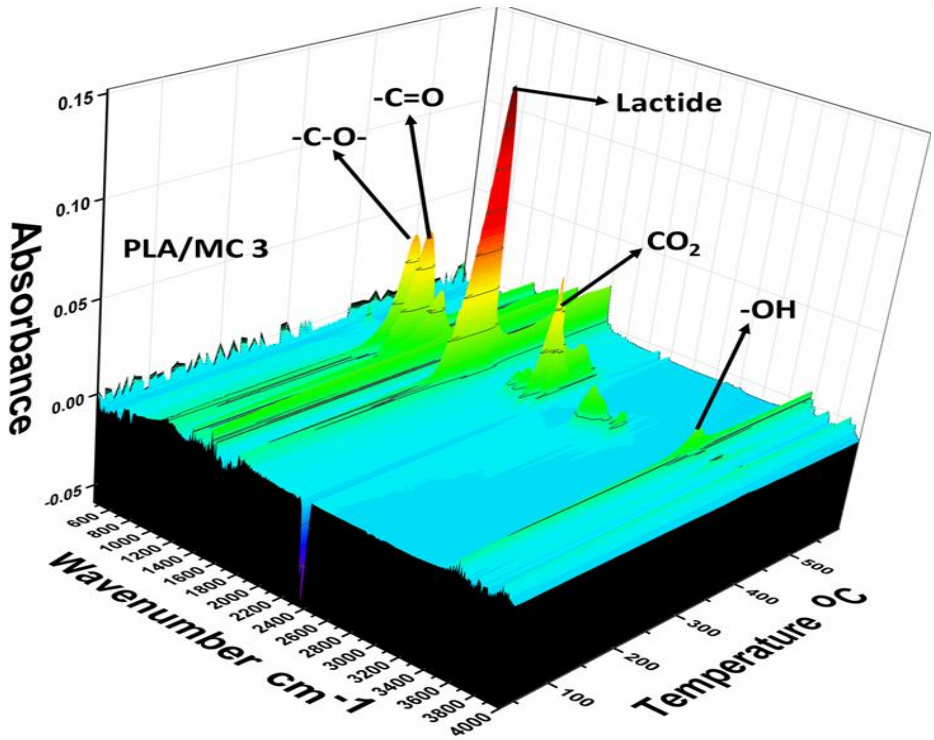
Absorbance
0.15
0.10
0.05
0.00
-0.05
PLA/MC 3
-C-O-
-C=O
Lactide
CO_2
-OH
Wavenumber cm -1
600
800
1000
1200
1400
1600
1800
2000
2200
2400
2600
2800
3000
3200
3400
3600
3800
4000
Temperature oC
100
200
300
400
500

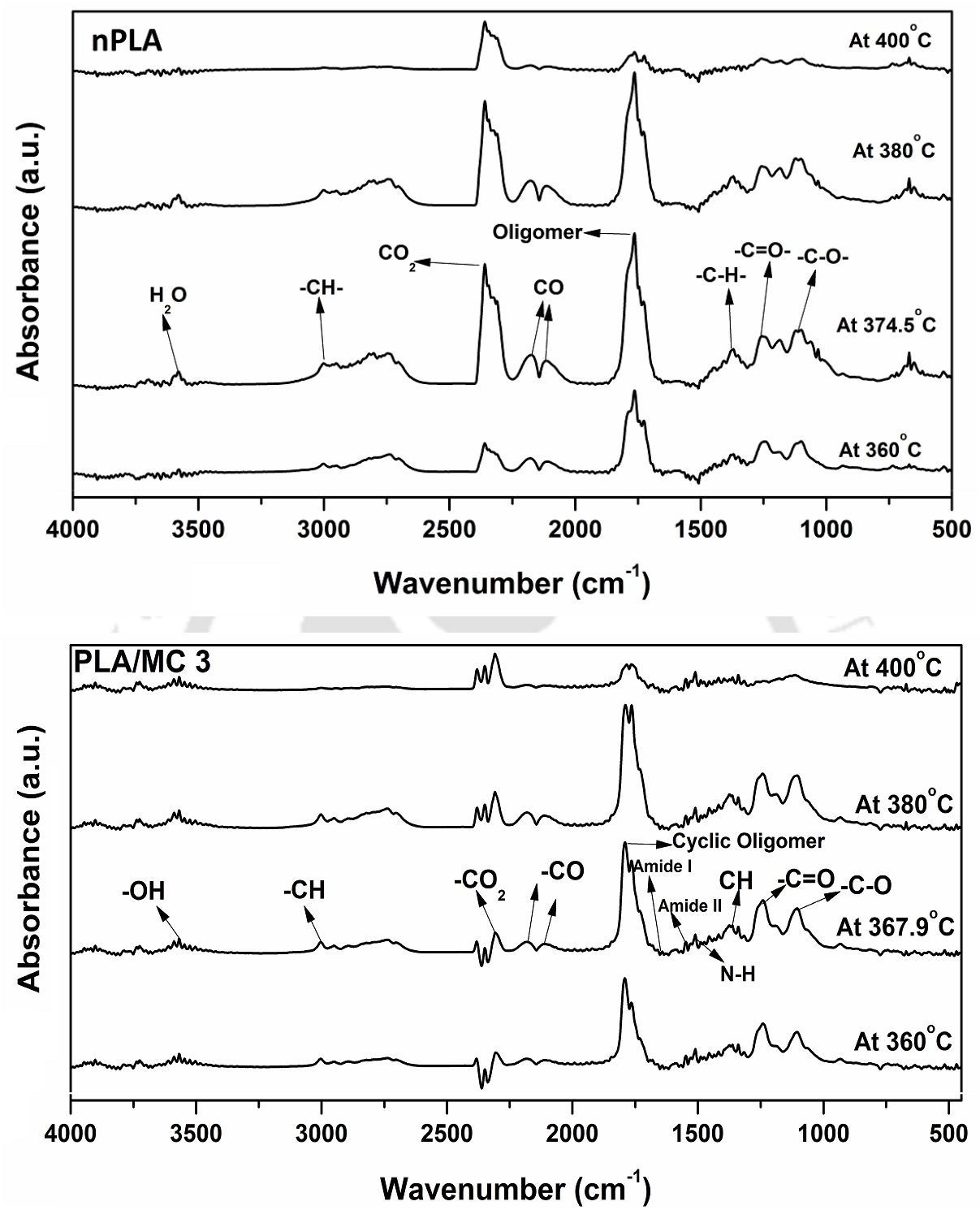

Fig. 4.22 3D and 2D spectra of hyphenated TGA-FTIR for nPLA and PLA/MC 3.

4.5 Crystallization behavior at dynamic heating rates

Crystallization can be explained on the basis of arrangement of polymer chains. Crystallization of polymeric foam plays a crucial role in the degree of expansion and integrity of cellular

structure [11]. DSC plots at different heating rates are shown in **Fig. 4.5**. The non-isothermal crystallization studies have been investigated to study the effect of MC in the PLA crystallization. The results obtained from various methods are summarized in **Table 4.6**.

Table 4.6 Crystallization parameters from the Avrami and Kissinger Analysis.

Sample	**Heating Rate (°C/min)**	**$t_{0.5}$ min**	***k*** **(min^{-n})**	***n***	**ΔE (kJ/mol)**
nPLA	2.5	7.7	0.0009	1.9	66.8
	5	5.9	0.003	1.9	
	7.5	3.3	0.02	2.4	
	10	2.8	0.04	2.3	
PLA/MC 1	2.5	11.1	0.0003	2.0	69.2
	5	7.0	0.003	1.5	
	7.5	4.5	0.006	2.3	
	10	3.9	0.01	2.2	
PLA/MC 2	2.5	9.6	0.001	1.5	65.3
	5	5.7	0.004	2.1	
	7.5	4.6	0.005	2.0	
	10	3.3	0.04	1.9	
PLA/MC 3	2.5	9.1	0.0004	2.3	65.4
	5	6.2	0.002	2.3	
	7.5	3.2	0.02	2.3	
	10	2.7	0.05	2.2	

`

Avrami equation is utilized to plot a graph between $\ln[-\ln(1-X_t)]$ vs $\ln t$ (**Fig. 4.23**). The values of Avrami exponent (*n*) and crystallization rate constant (*k*) was measured from the slopes and intercepts from the linear region. The straight linear pattern indicates the primary crystallization. In the Avrami plots, deviation from linearity is observed for foams suggesting the presence of secondary crystallization. The primary crystallization indicates the growth of lamellar structure whereas the secondary crystallization indicates the perfection of crystallization with spherulite impingement. The value of "*n*" is useful to understand the mechanism of nucleation and form of crystal growth [212].

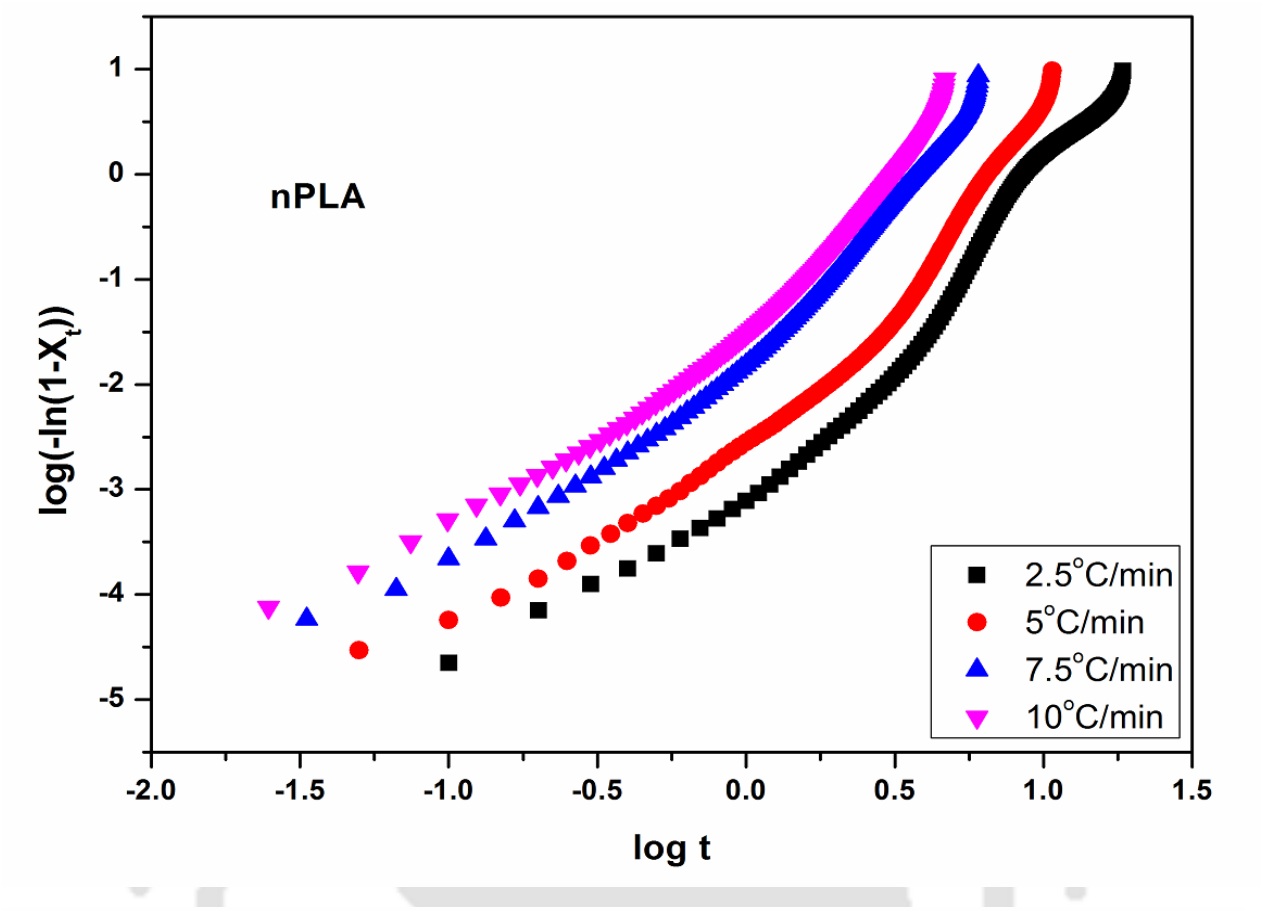
nPLA
log(-ln(1-X_t))
log t
2.5°C/min
5°C/min
7.5°C/min
10°C/min

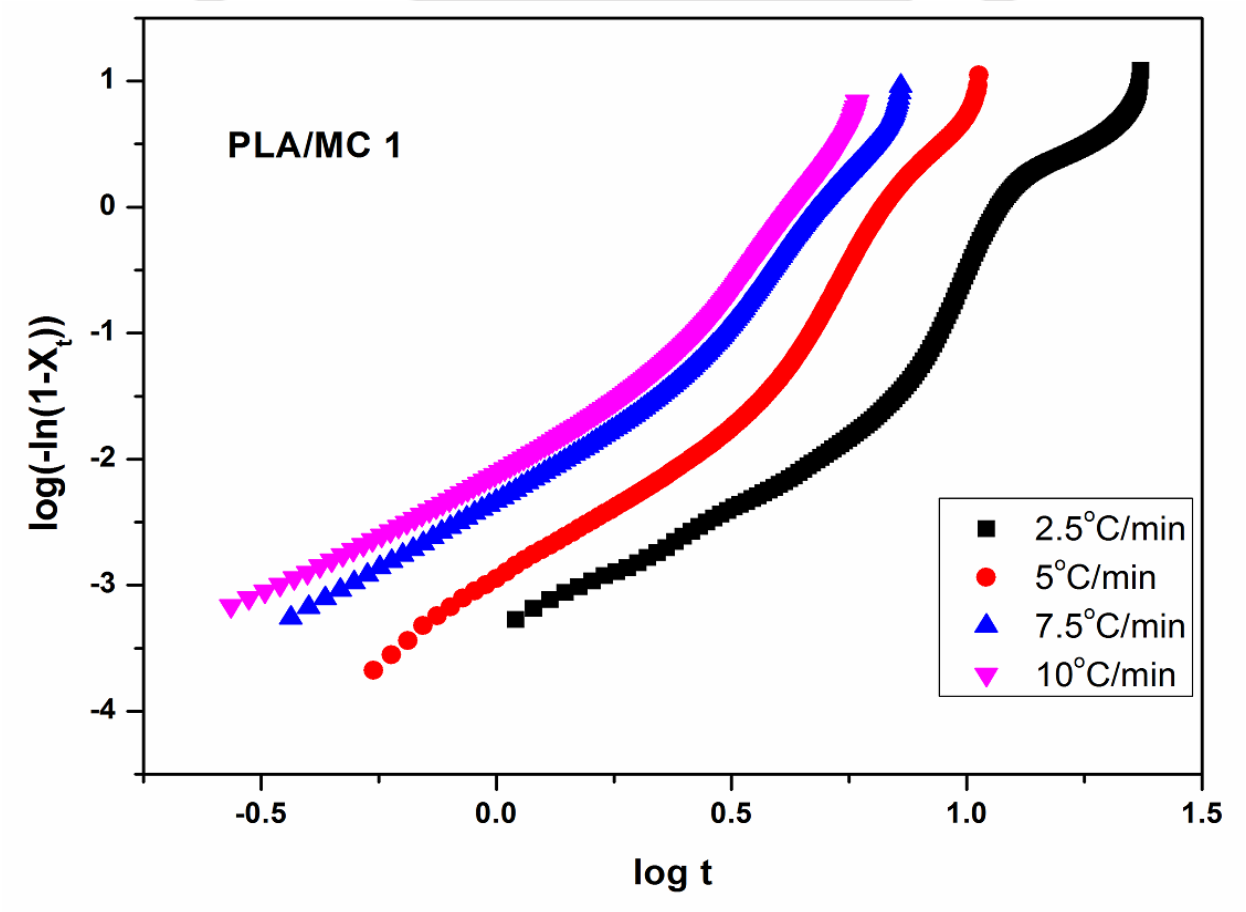
PLA/MC 1
log(-ln(1-X_t))
log t
2.5°C/min
5°C/min
7.5°C/min
10°C/min

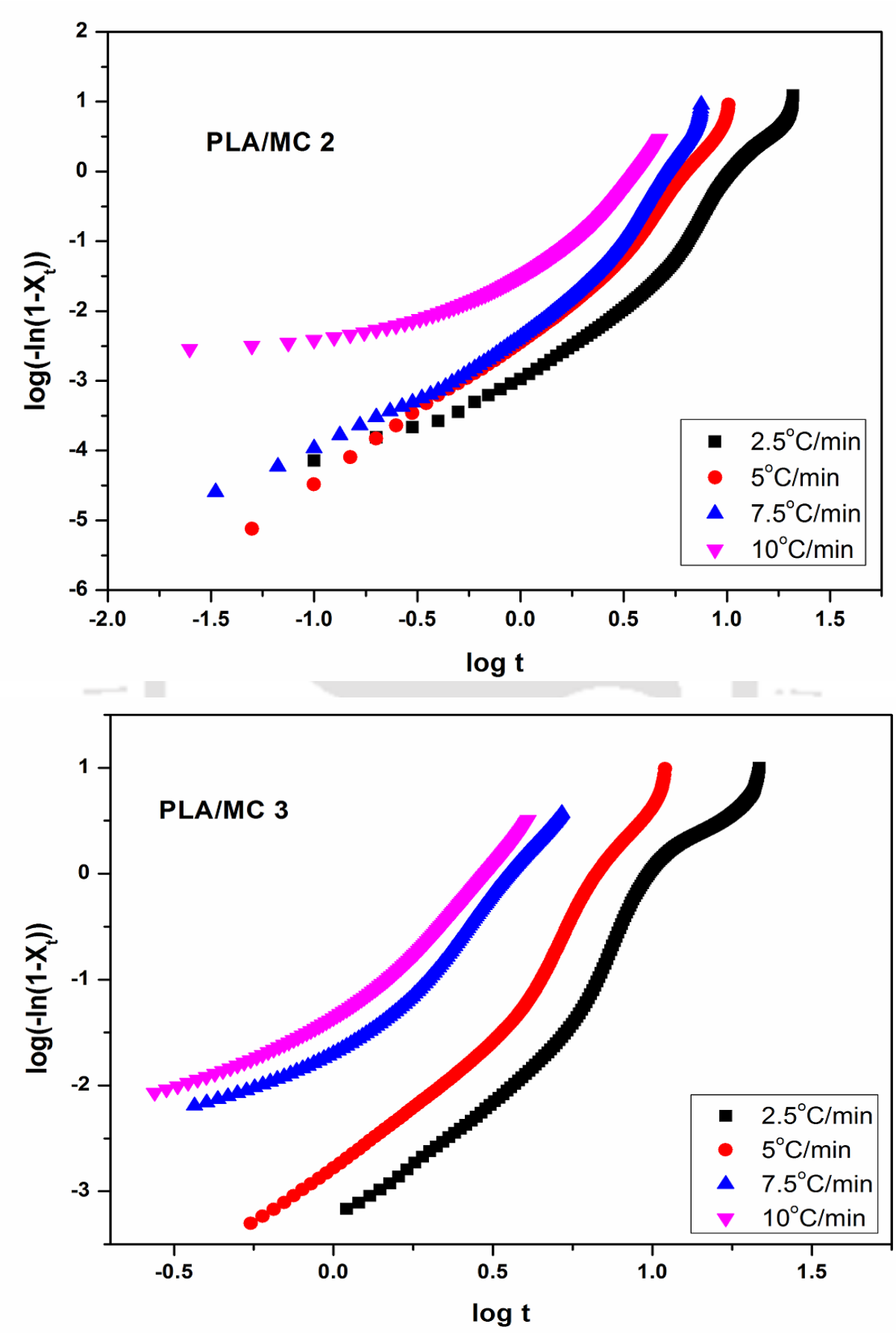

Fig. 4.23 Avrami plots for PLA and PLA/MC-based foams.

In this study, we observed that "*n*" value of the fabricated foam is ~2 which indicates truncated spherical structures. The "*n*" value also suggests the two-dimensional nucleation and growth of crystals. The non-integral values of "*n*" suggests the presence of thermal and athermal nucleations in the mechanism of nucleation [123]. The "*k*" values are in accordance with $t_{0.5}$ values, suggested that nanofiller helps in producing more nucleating sites and hence effects the crystallization rate of PLA. The presence of both primary and secondary crystallization in the fabricated foams can also be observed from Tobin plots (**Fig. 4.24**) in accordance with Avrami plots. The $t_{0.5}$ value decreases on increasing the heating rate (**Fig. 4.25**) suggesting that the rate of heating effects the crystallization of the PLA and PLA/MC-based foams.

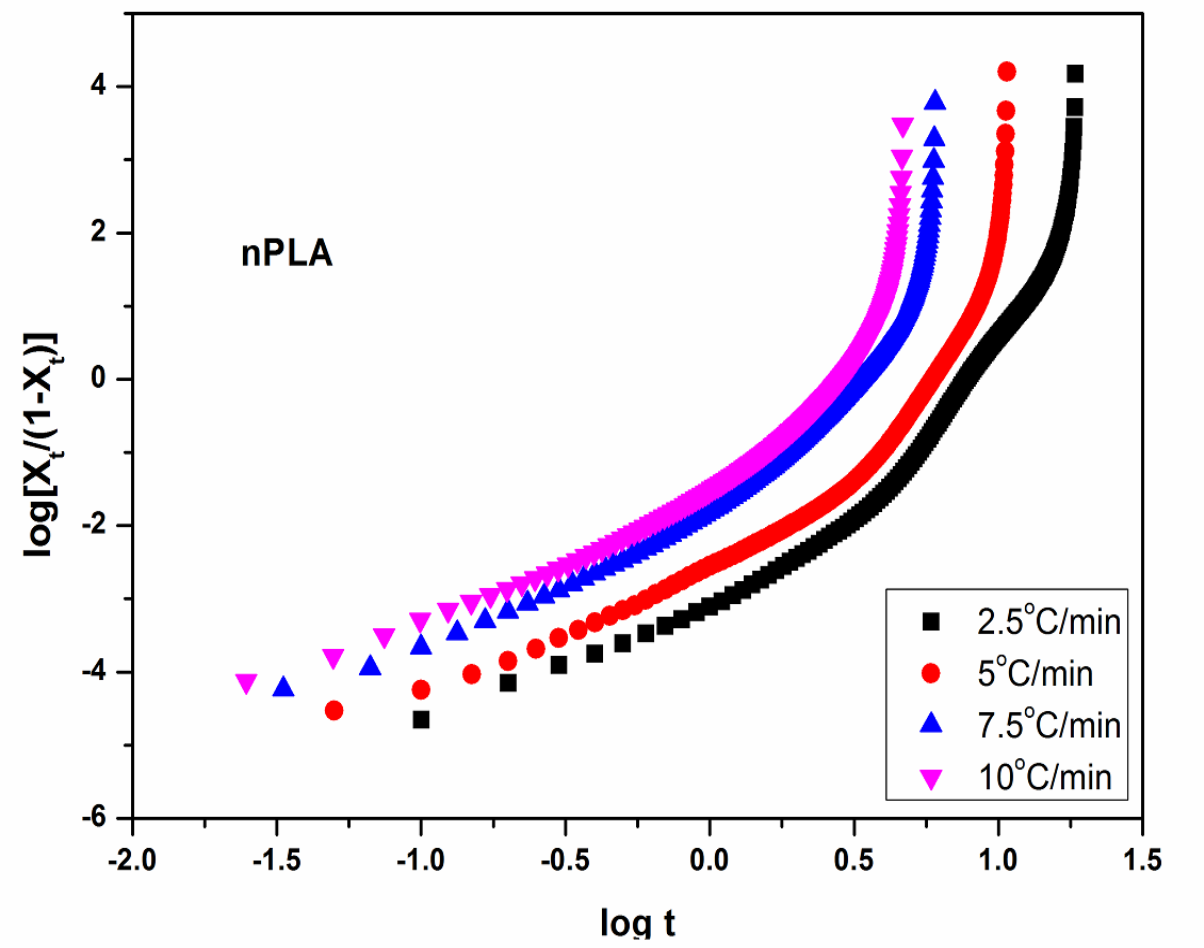

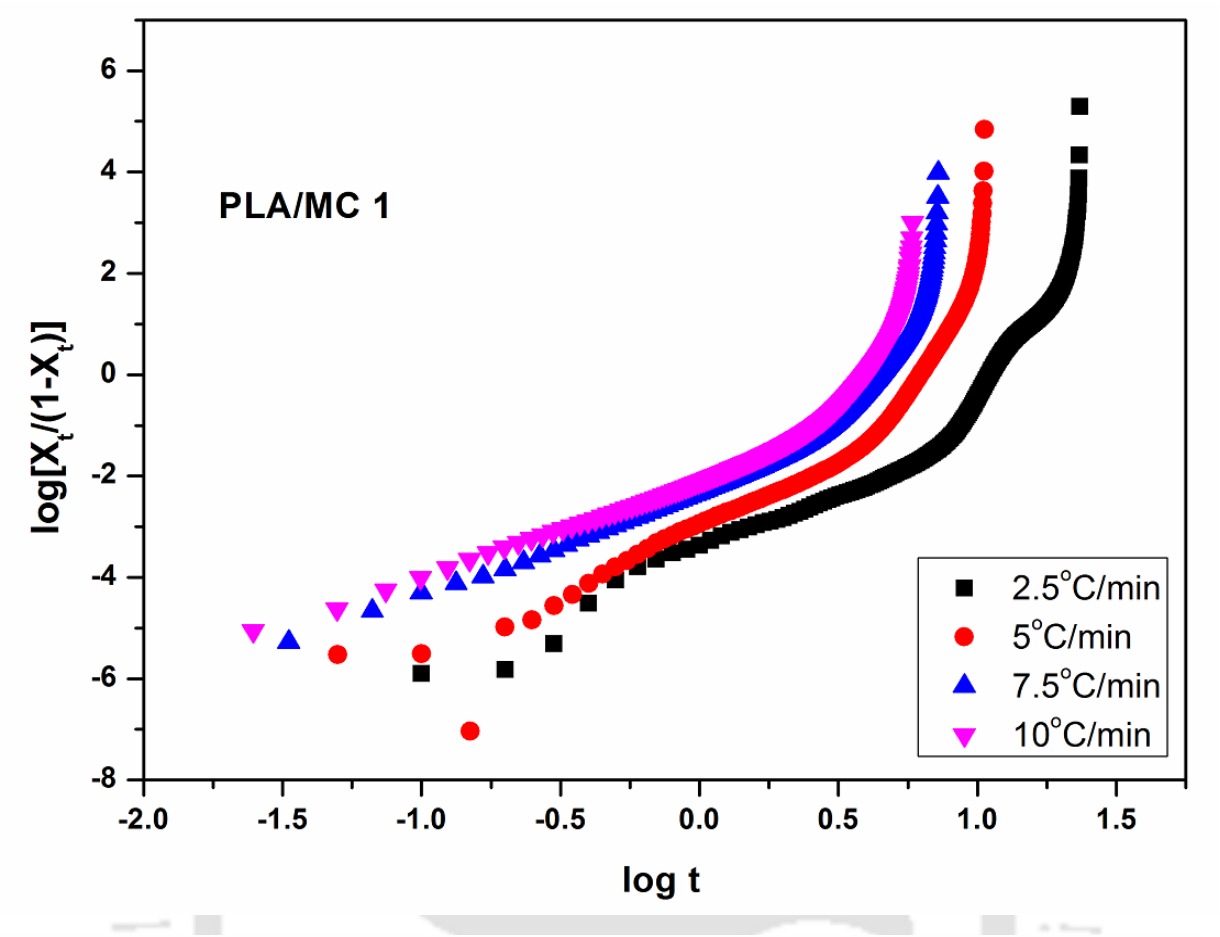
PLA/MC 1
log[X_t/(1-X_t)]
log t
2.5°C/min
5°C/min
7.5°C/min
10°C/min

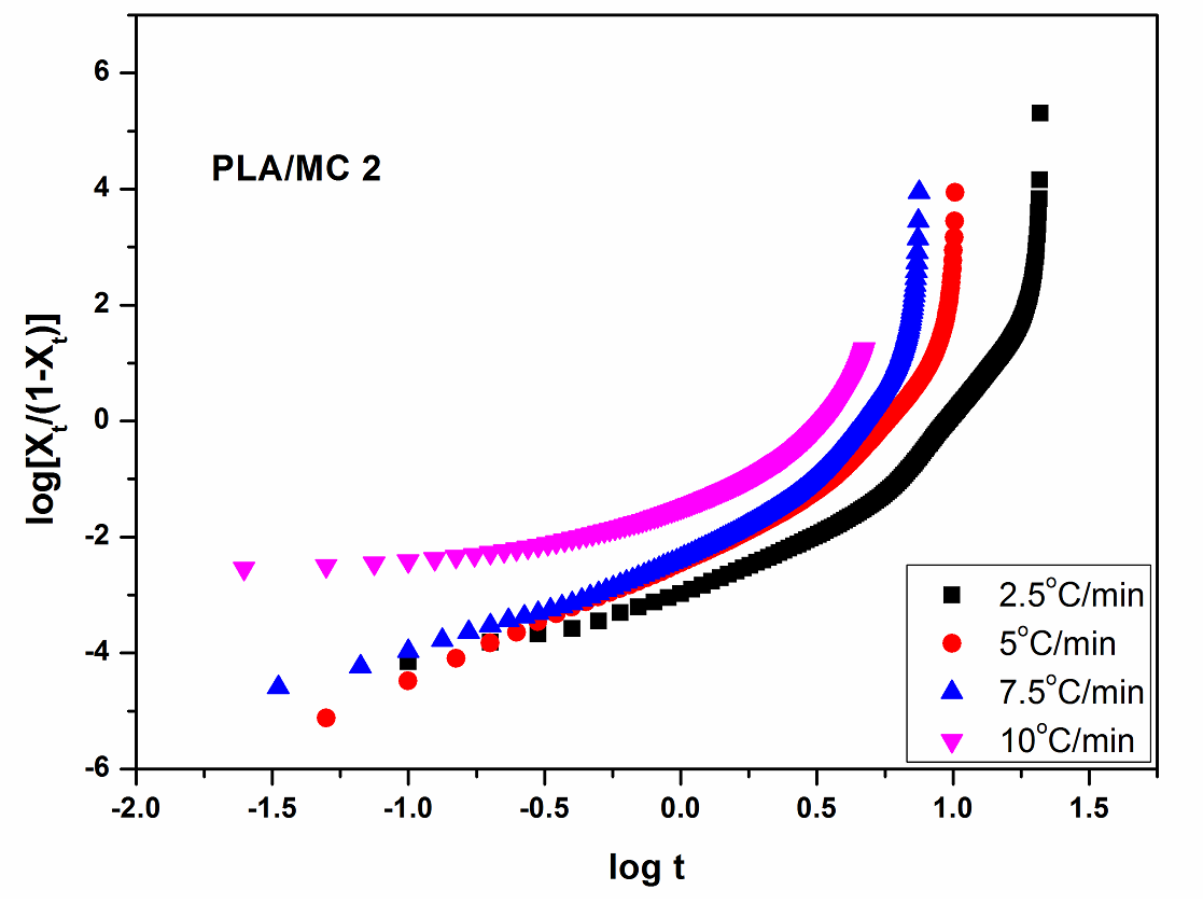
PLA/MC 2
log[X_t/(1-X_t)]
log t
2.5°C/min
5°C/min
7.5°C/min
10°C/min

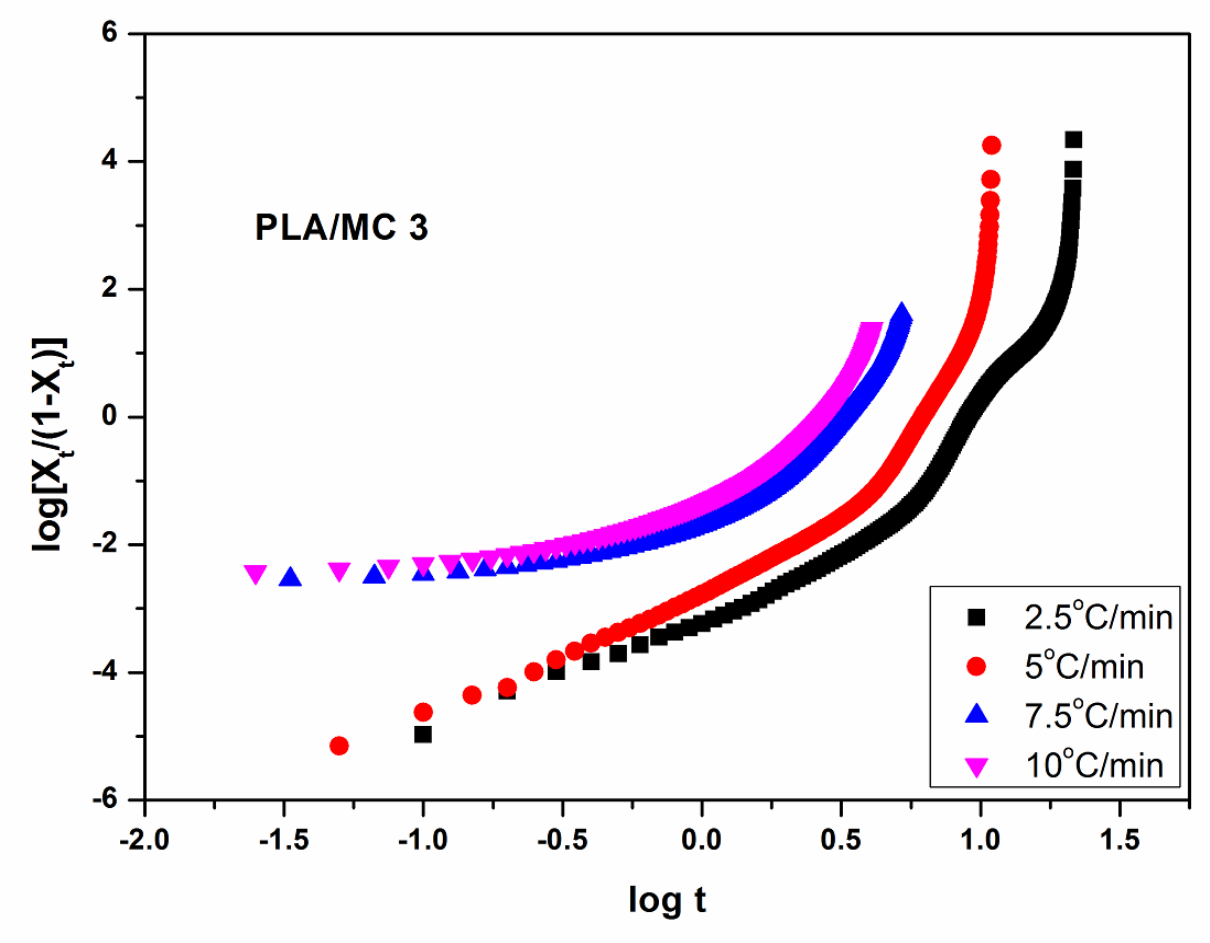

Fig. 4.24 Tobin plots for PLA and PLA/MC-based foams.

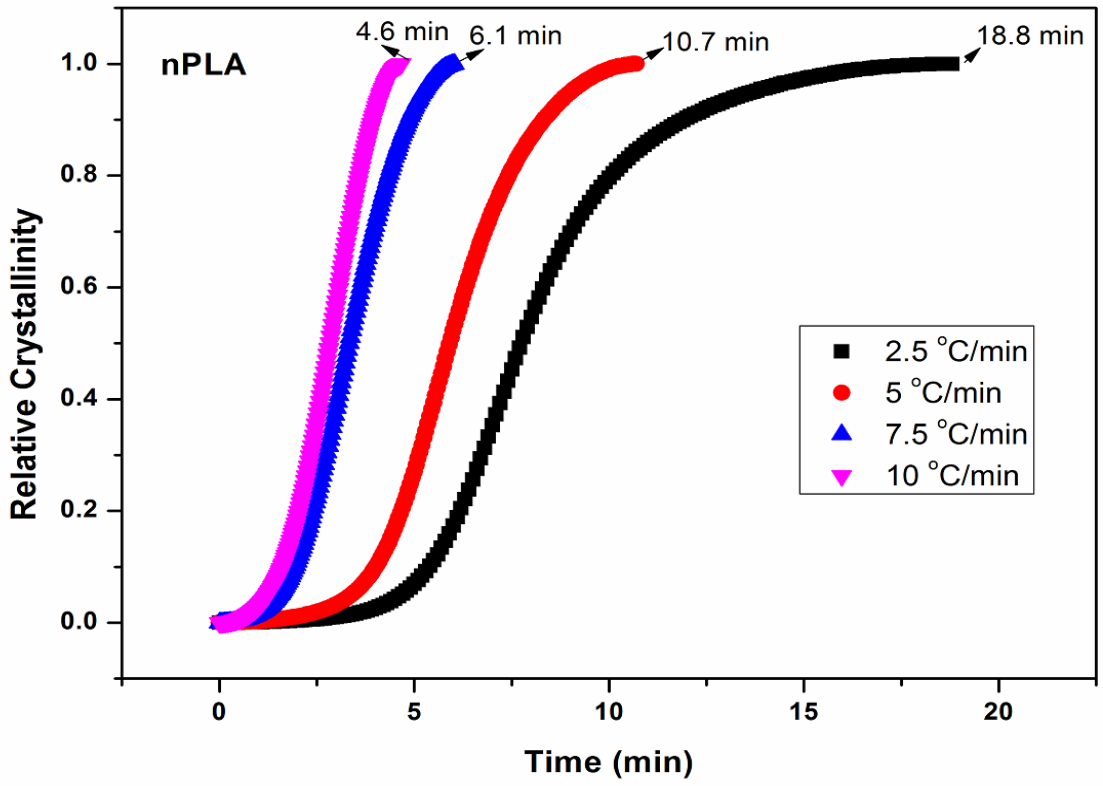

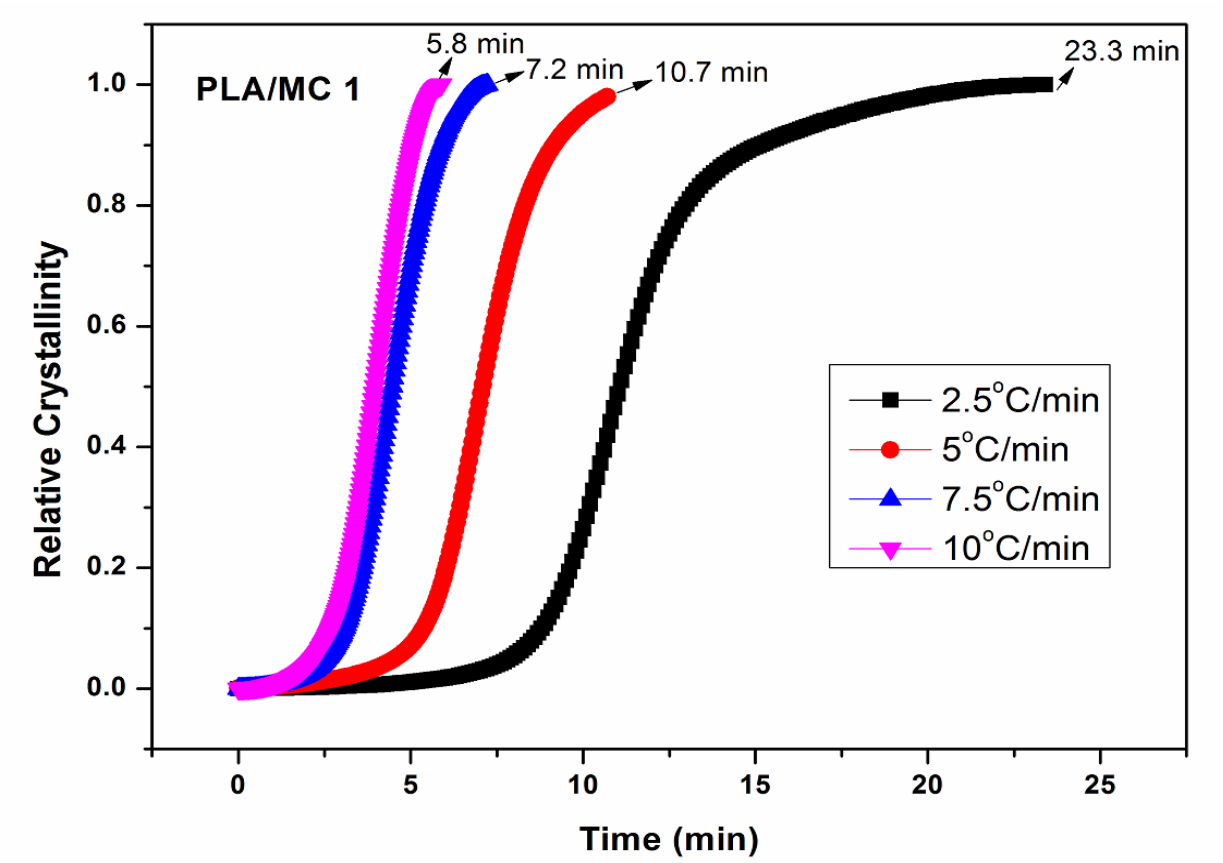

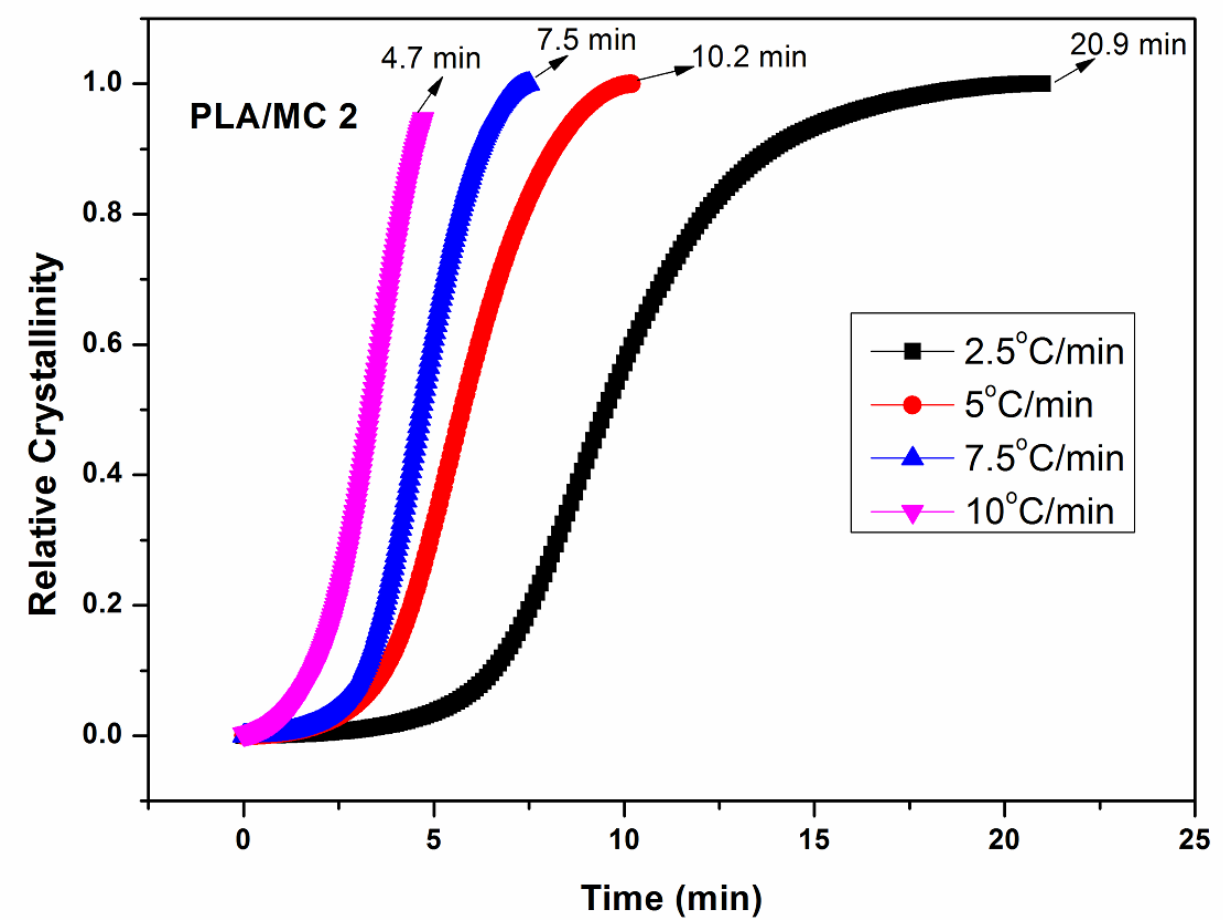

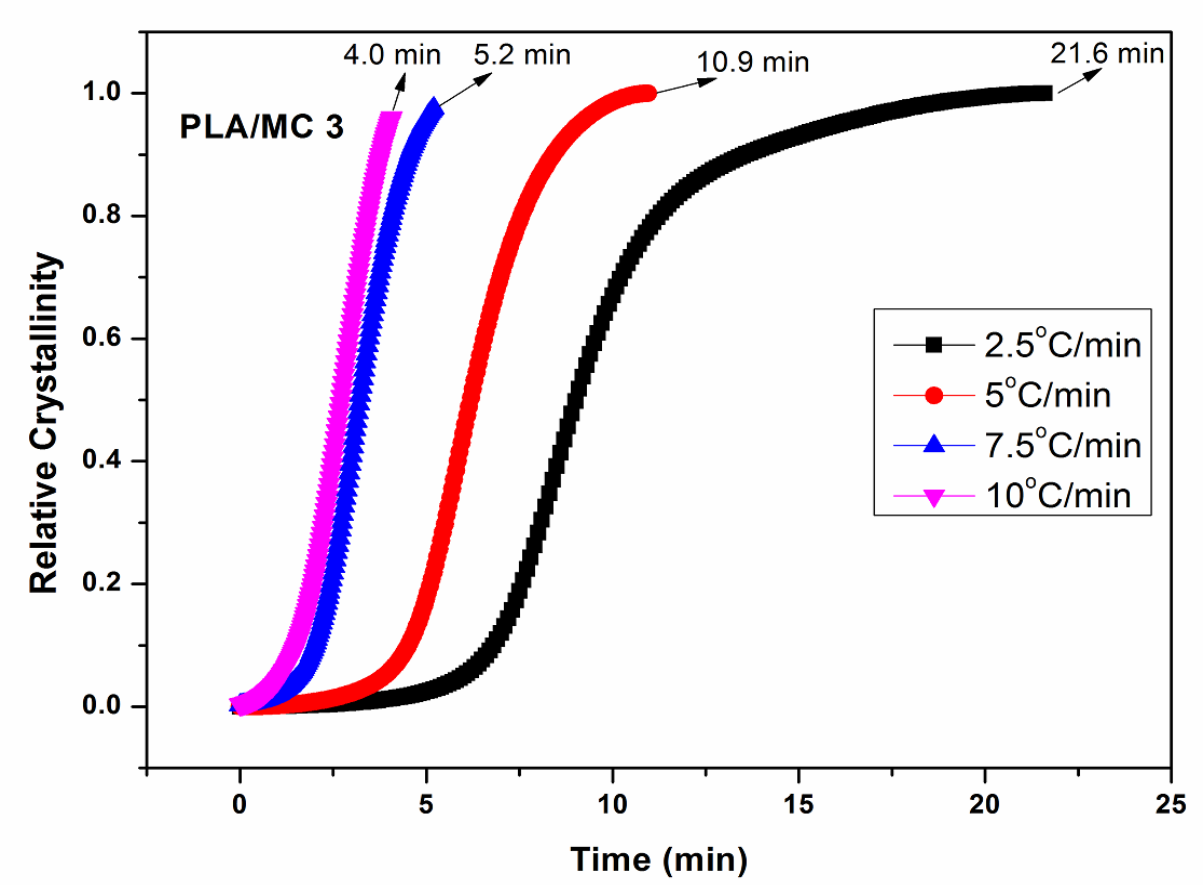

Fig. 4.25 Relative crystallinity vs time plots for PLA and PLA/MC-based foams.

Crystallization also depends on the dilution effects of gas molecules present in the fabricated foams [212]. The change in the activation energy of crystallization (ΔE) of the fabricated foams are measured by utilizing Kissinger plot (ln (β/T_p^2) vs $1/T_p$) (**Fig. 4.26**). It is observed from **Table 4.6** that by increasing nanobiofillers the ΔE values slightly decreases compared to nPLA. The ΔE value slightly increases for PLA/MC 1 compared with nPLA. Nanofiller at higher loading increases the mobility of the polymer chains due to which the energy required for retraction and folding of molecular chain decreases [213]. It can be concluded that MC enhance the folding of PLA chains and hence the change in energy becomes less. The slight reduction observed in cold crystallization temperature (T_c) is mainly due to the presence of some deformed shape and size crystals in the PLA matrix. Crystal growth depends on short chain

diffusion, which hampers crystallization. Subsequently, the nucleating effect of MC is also justified by the crystallization kinetics studies.

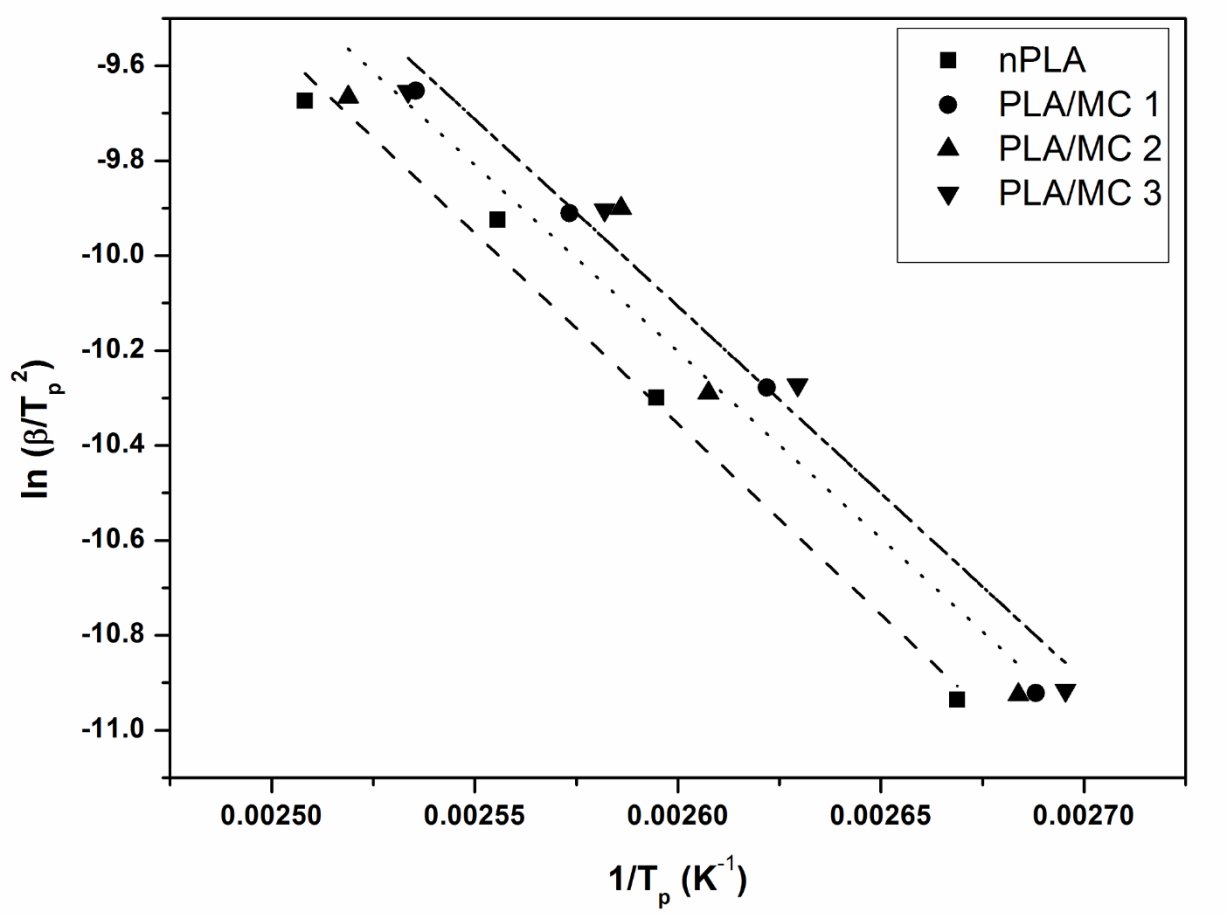

Fig. 4.26 Kissinger plots for PLA and PLA/MC-based foams.

4.6 Porosimetric investigations of PLA/MC-based foams

The results obtained from porosimetric investigations are summarized in **Table 4.7**. The porosity of the nPLA foam is observed as ~82% and no significant change is observed in porosity with a change in MC loading. The porosity of PLA/MC 1, PLA/MC 2 and PLA/MC 3 are found to be ~81%, ~81%, and ~82% respectively. However, a reduction in the surface area and average pore diameter is observed, indicating the possible nucleation of the nanobiofillers in the PLA matrix. On increasing the loading, the MC generates more nucleating sites in the PLA matrix, which generates more number of smaller pores, thus there is a decrease

in pore diameter. The highest surface area is observed in the case of PLA/MC 3 (~17.7 m^2/g). The increase in surface area is helpful in the generation of cell culture studies as observed in the literature [214]. It can be concluded from the MIP study that MC nanobiofillers are acting as nucleating sites in the PLA foam matrix and generating more number of pores in the PLA/MC- based fabricated foams [121]. The results obtained from porosimetry investigations are in line with the earlier investigation of cell density and cell size obtained from FESEM.

Table 4.7 Porosimetric investigations of the PLA and PLA/MC-based foams.

Sample	Porosity (%)	Avg. Pore Dia. (µm)	Surface Area (m^2/g)
nPLA	82	1.5	13.6
PLA/MC 1	81	1.2	14.5
PLA/MC 2	81	1.1	15.7
PLA/MC 3	82	1.0	17.7

Porosimetry can also be related to the thermal degradation of PLA/MC-based foams. The increase in surface area with MC loading indicating generation of more degradation sites available for thermal degradation of foams so ultimately less activation energy is required as per our earlier discussion. From the results obtained from thermal degradation kinetics, it is observed that PLA/MC 3 requires less activation energy for degradation compared to nPLA. The degradation process is schematically represented in **Fig. 4.27**. Comparisons can be made with available literature on PLA/OLLA-g-chitosan non-porous system and it can be seen that the activation energy required for thermal degradation is slightly higher in the non-porous system (up to ~31% for 3% loading of MC) than the porous system [174]. The presence of porous structure, effective heat transfers between pores, dispersion of MC in the cell walls and more available degradation sites (more easily available surface area for degradation) might be

responsible for the less energy requirement for degradation [187]. The pore size achieved in our investigation is very much less than the available literature on some chitosan-based foam system indicating generation of smaller pores with increasing surface area which are favorable in tissue culture application study in the fabricated system [203,204]. However, in the crystallization process, the effect of pores present is not so prominent in the porous system of PLA/MC based foams as the second heating cycle is considered for crystallization studies to remove any thermal history present [215]. Effect of nanobiofiller is mainly dominating the crystallization process.

It can be concluded from the porosimetric investigation that effect of porous morphology and MC nanobiofiller is mainly prominent in thermal degradation than in the crystallization process of the fabricated foams.

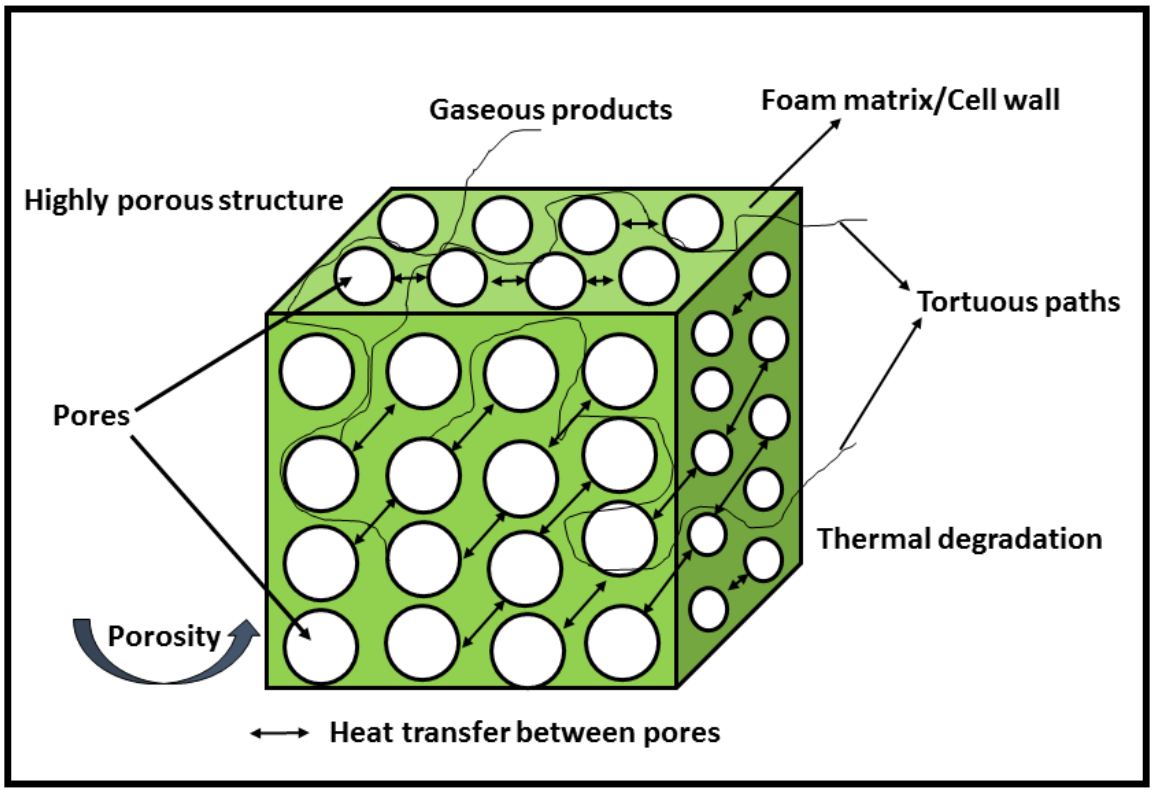

Fig. 4.27 Schematic representation of the degradation process of PLA and PLA/MC-based foams.

4.7 Summary

This investigation successfully demonstrated an elegant and less expensive technique for fabrication of porous cellular and interconnected open-cell structured hydrophobic biodegradable PLA and modified chitosan-based foams using casting and leaching method. The highly porous structure is observed from FESEM analysis where MC is uniformly dispersed in the cell walls of fabricated foams. The density of the fabricated foams is reduced successfully up to ~7.8-folds compared to PLA granules. An increase in cell density (up to ~2.3-fold) on the introduction of MC and reduction of cell size is observed in the fabricated foams. The hydrophobic shell of the MC along with surface texture influences the wettability phenomenon of the fabricated foams. Static contact angle values along with dynamic contact angle (Young's contact angle) increased to ~9° (for static contact angle) and ~10° (for Young's contact angle) for highest loading of MC compared to nPLA foam. It is also observed from TGA studies that the MC reduces the thermal stability (T_{onset} ~20°C for PLA/MC 3) along with a number average molecular weight of the fabricated foam. Thermal degradation investigation suggests the plasticizing effect of MC nanobiofiller in the PLA matrix. Degradation mechanism of the fabricated foams are investigated by Criado method and it is observed that PLA and PLA/MC based foams follow the same degradation mechanism. The crystallization studies of the PLA and PLA/MC based foams have suggested the nucleating behavior of MC in the PLA matrix. Porosimetric investigation of the fabricated foam also corroborates the nucleating effect of MC. From the porosimetric investigation, it can be concluded that the effect of porous morphology is prominent in the thermal degradation compared to crystallization. The decrease in pore diameter up to ~33.3% and increase in the surface area up to ~30.2% for PLA/MC 3 is also observed from the porosimetric study with an increase in MC. From the investigation it can be concluded that fabricated hydrophobic interconnected porous PLA and PLA/MC-based foams with increased surface area might be effectively utilized in biomedical applications such

as tissue engineering, drug delivery, cell proliferation studies due to the bio-friendly nature of both PLA and nanofillers and the lightweight characteristics gives added advantages compared to other PLA/MC-based biocomposite films.

Chapter 5

Development of Poly (lactic acid)/Modified Gum Arabic (MG) based Microcellular Composite Foams

This chapter mainly investigates the development of PLA/modified gum arabic (MG) based composite foams. The different physicochemical characterizations along with wettability and crystallization studies of the developed foam has thoroughly discussed in this chapter. It has been observed that there is a decrease in ~7% crystallinity of fabricated composite foams, which might be due to the plasticizing effect of MG. The thermomechanical and thermal investigations also confirm the plasticizing effect of MG. Further, an increment of ~16% contact angle is observed for highest loading than the neat counterpart. The hydrophobic nature of MG along with the surface texture might be responsible for the change in wettability behavior with MG. The porosimetric investigations reveal the increment in surface area and decrement in pore diameter with MG indicating the nucleating effect of nanobiofiller at lower concentrations. Interestingly, the increase in surface area, decrease in pore size, and hydrophobic nature is favorable for biomedical applications. The different degradation studies like hydrolytic and photodegradation of the fabricated foams have been discussed in this chapter. Hydrolytic degradation is performed under three conditions of acidic, basic and neutral medium for 120 h. Various characterization techniques including TGA, DSC, GPC, XRD, colorimetric studies, FESEM, and wettability is investigated and the effect of MG in degradation are discussed in this chapter.

Parts of this research work are published/ready to communicate as follows:

1. Shasanka Sekhar Borkotoky, Tabli Ghosh, Purabi Bhagabati and Vimal Katiyar *"Poly (lactic acid)/Modified Gum Arabic (MG) based microcellular composite foam: Effect of MG on foam properties, thermal and crystallization behavior."* International Journal of Biological Macromolecules, 125 (2019), 159-170.

2. Shasanka Sekhar Borkotoky, Tabli Ghosh and Vimal Katiyar *"Hydrolytic and UV irradiate degradation of Modified Gum Arabic (MG) reinforced Poly (lactic acid)-based microcellular nanocomposite foams: A mechanistic approach"* **(To be submitted to "Polymer Degradation and Stability", Elsevier).**

5.1 Introduction

Recently, polymeric foams have gained a lot of attention over non-foamed materials due to its unique advantages such as lightweight, less usage of materials etc. that positively affects the production cost. The detrimental effects of non-degradable polymeric foams can be overcome by replacing with biodegradable polymeric foams [216–219]. Biodegradable polymeric foams are now showing their presence in different acoustic, thermal insulation, commodity, biomedical and commodity applications. Nowadays, the use of PLA based polymeric foam is increasing due to their potentiality in the field of food packaging, tissue engineering for developing scaffolds for tissue [220,221]. In a greener approach, bio-based and biodegradable PLA foams are now commercialized for packaging applications and are projected as an alternative to nondegradable conventional polystyrene (PS) foams [222]. Interestingly, increase in surface area and a decrease in the cell size of the foam are two important parameters for biomedical applications including cell proliferation study, tissue engineering etc. [205]. In literature, some investigations are observed on the effect of polysaccharide-based gums like gum tragacanth, gum karaya and so on in PLA matrix. Recently, investigations on Gum tragacanth/poly(L-lactic acid) scaffolds have been demonstrated by **Ranjbar-Mohammadi et al.** They mainly focused the investigations for regeneration of peripheral nerve [223]. Gum arabic (GA) is a biocompatible and biodegradable polysaccharide, which can be derived from Acacia trees mainly include *Acacia Senegal* and *Acacia Seyal*. GA has distinct advantages over other available polysaccharide gums due to its vast applications in the paint industry, food industry, beverage industry, cosmetics, and biomedical fields. It has the status of GRAS (Generally Recognized as Safe) by USFDA (United States Food and Drug Administration). Moreover, GA acts as adhesives having properties of antimicrobial, antibacterial, adhesiveness, stabilizers etc., which imparts its wide application including food and pharmaceuticals for stabilizing the emulsion, for acting as encapsulating agents to engulf bioactive materials etc. [48,122]. GA is a kind of biopolymer having highly

branched chains of galactose units with β-1,3-glycosidic linkage. Adversely, the hydrophilicity of GA makes it unsuitable for filler materials, so in this regard, modification of GA can make it compatible for PLA, where grafting of GA with oligomers of lactic acid or use of cross-linking agent and compatibilizer can put a good impact on formulating PLA based biocomposites. Several reports are also available for the food and biomedical applications of GA [224–227]. The availability of GA is abundant in Indian subcontinent compared to other polysaccharide gums and also it is an established gum for different food and biomedical applications. However, there are certain other polysaccharide gums of similar characteristics like gum karaya, gum olibanum, gum tragacanth etc., but their use in food or different biomedical applications is limited unlike gum arabic.

The present study aims towards developing biodegradable PLA/ modified gum arabic (MG) based foams using a simple and cost effective technique, where sugar is used as porogen particles. Interestingly, sugar is extensively available, cost-effective, non-toxic, biocompatible material and mainly consists of glucose and fructose molecules. A schematic representation of the fabrication process of PLA/MG-based foam is shown in **Fig. 5.1**.

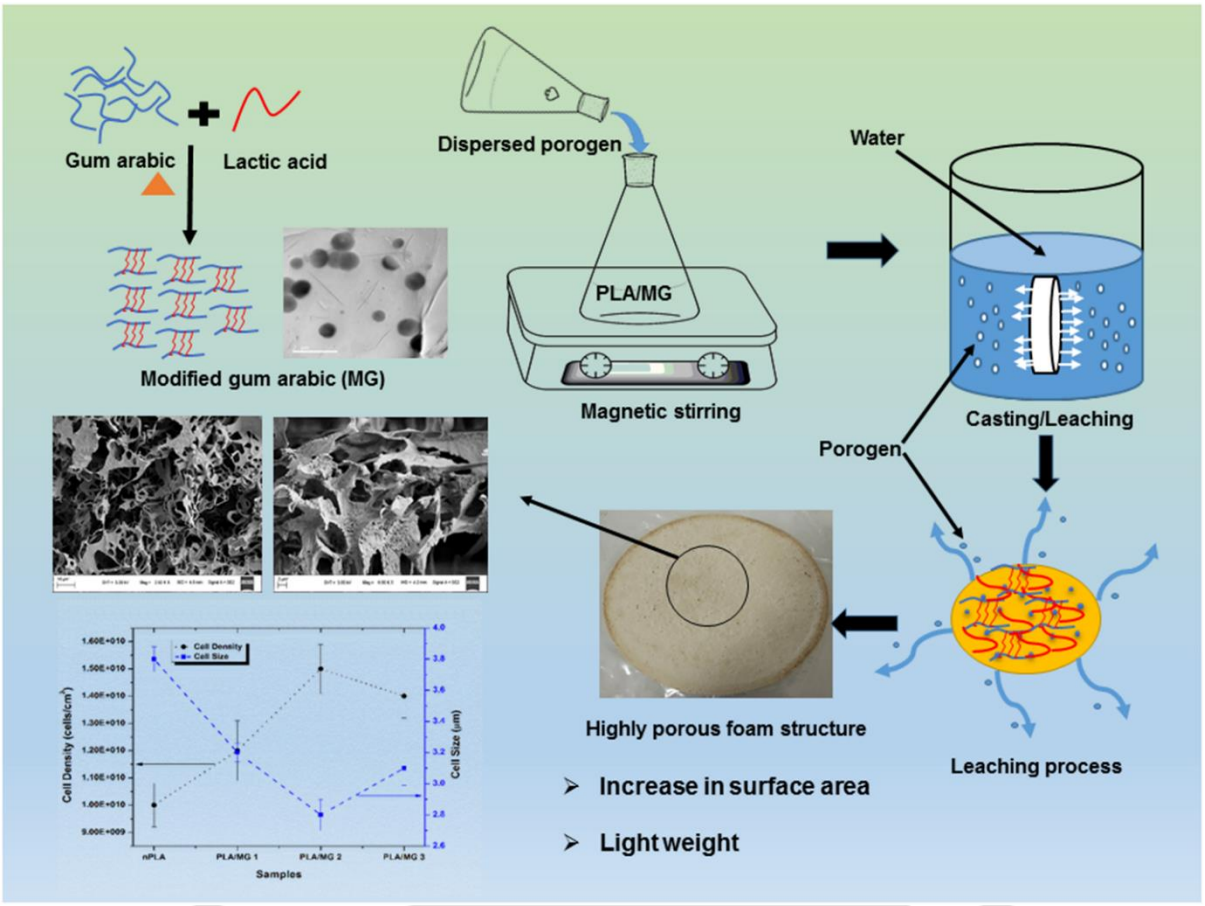

Fig. 5.1 Schematic representation of the fabrication process of PLA/MG-based foam.

5.2 Results and discussions

In this section, the results and observations obtained from various analytical techniques are scientifically discussed with probable conclusions and explanations.

5.2.1 Morphological investigations of the PLA/MG-based foams

The FESEM images of both the horizontal and cross-sectional surfaces of the prepared foams can be observed in **Fig. 5.2** and **Fig. 5.3**. Presence of open cellular interconnected porous structure of the foams can be visualized from the figures. The dispersion of MG in the cell walls can be visible from FESEM images. The MG nanobiofiller having particle dimensions of 80 nm to 900 nm in length are shown in **Fig. 5.4**. From the FESEM image, the measured average cell size (diameter) of PLA based foams was ~3.8±0.08 µm. However, the incorporation of MG

nanobiofiller effects the average cell size. In the case of PLA/MG 1, the cell size was observed as ~3.2±0.06 µm, which was further decreased to ~2.8±0.1 µm for PLA/MG 2. For the biocomposite foam with the highest loading of 3% MG (PLA/MG 3), the value of cell size was observed as ~3.1±0.1 µm.

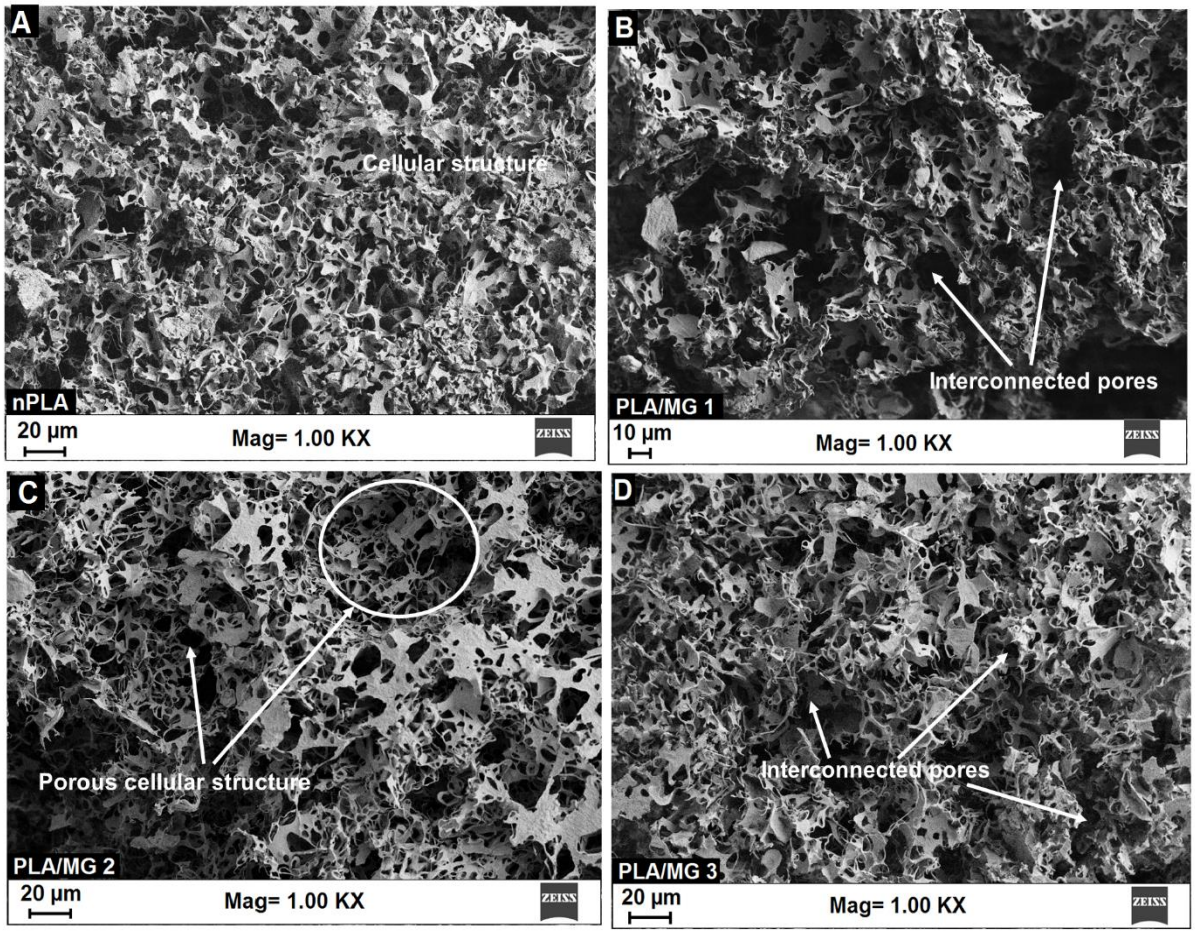

Fig. 5.2 FESEM micrographs of PLA and PLA/MG-based foams.

Similarly, the cell density (N_f) of the fabricated foams were also calculated by FESEM micrographs as shown in **Fig. 5.5**. The cell density of the neat PLA foam is observed as ~1.0×10^{10} cells/cm^3 whereas the value was increased to ~1.3×10^{10} cells/cm^3 for PLA/MG 1. Moreover, the cell density is increased to ~1.5×10^{10} cells/cm^3 for PLA/MG 2, which is further increased to ~1.4×10^{10} cells/cm^3 for the loading of 3% MG. The increase in cell density and a decrease in cell size is observed with increasing filler concentration. However, at highest

loading, the value is little bit decreased due to probable agglomeration of MG. This phenomenon may have attributed to the nucleation effect of MG, which results in increasing the generation of cell numbers. Further, reports suggest that β-lactoglobulin/ acacia gum generates number of nucleating sites for nucleation and growth mechanism [228].

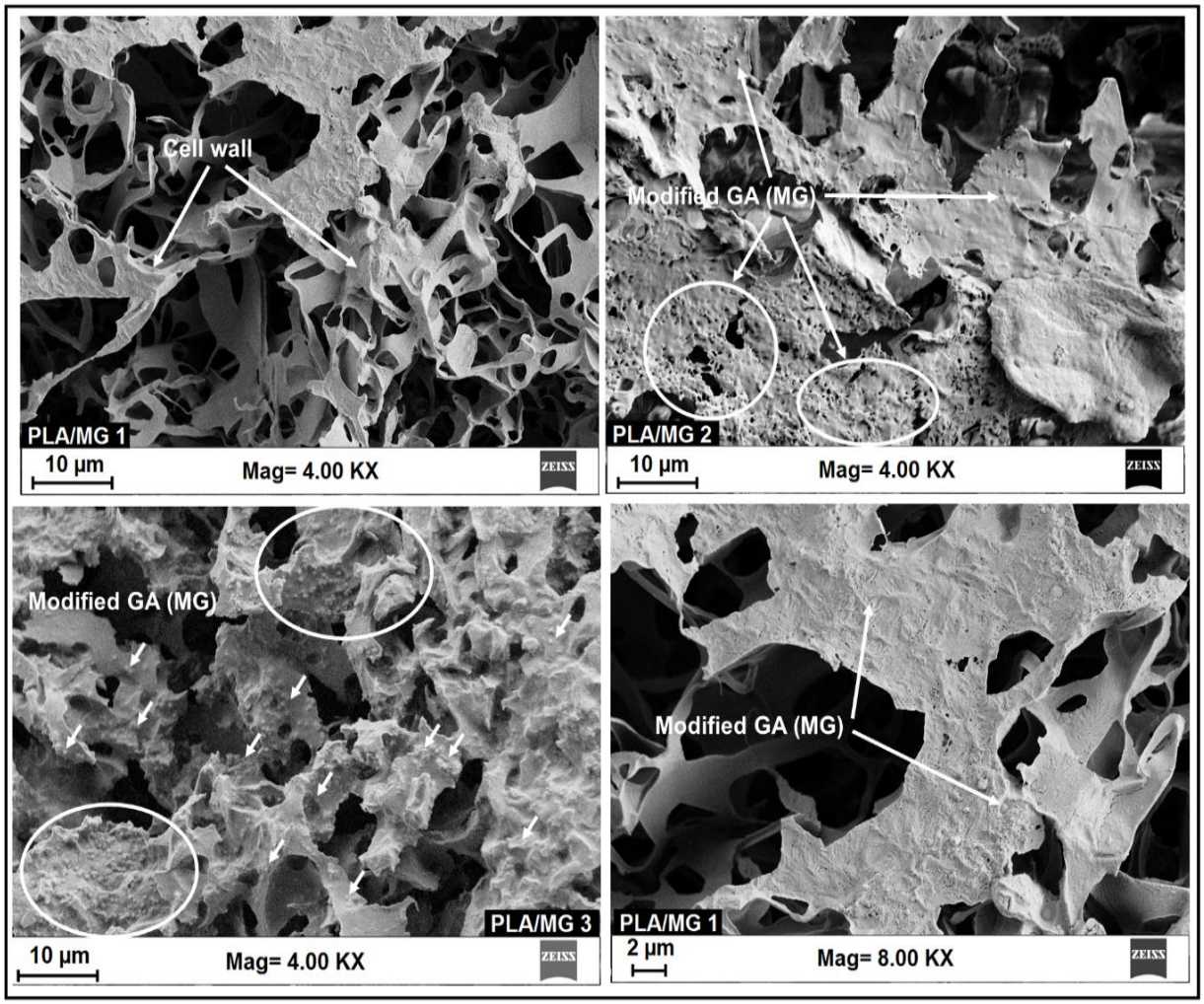

Fig. 5.3 Cross-sectional FESEM view of PLA/MG-based foams.

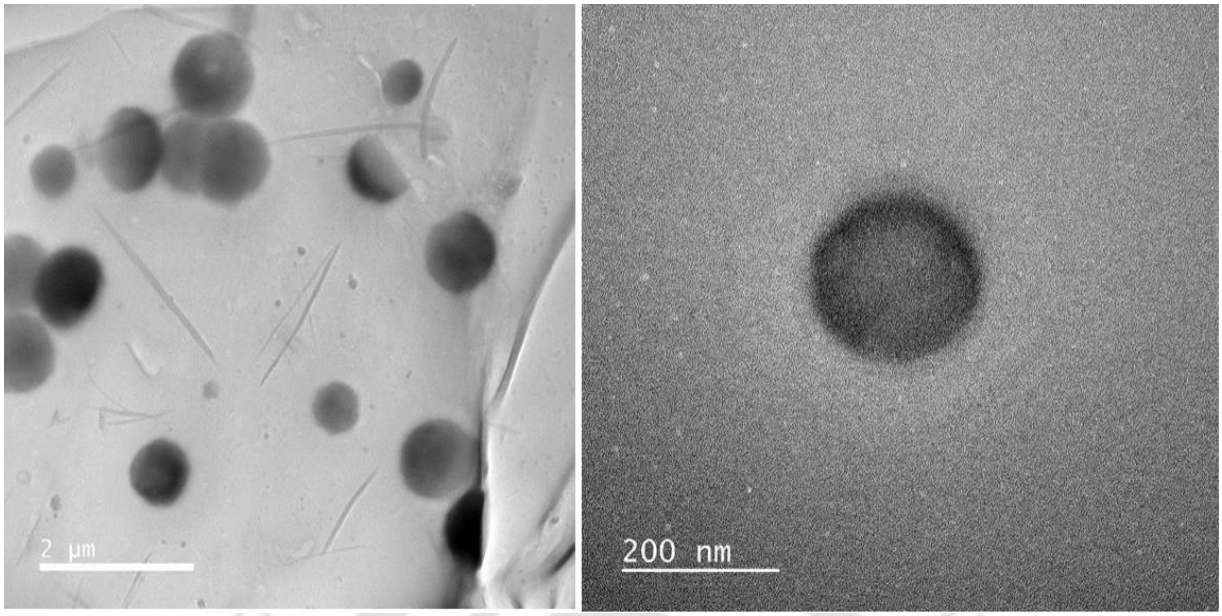

Fig. 5.4 FETEM images of Modified GA.

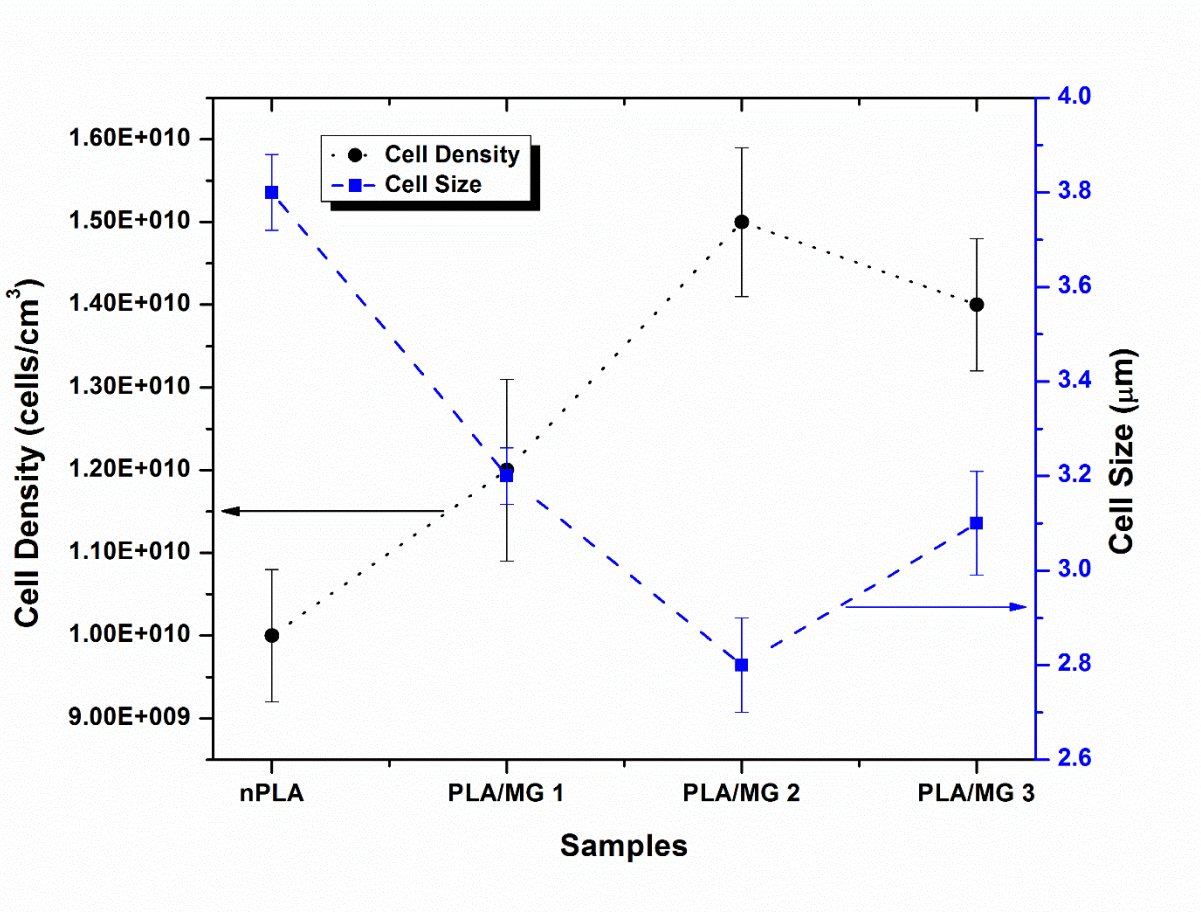

Fig. 5.5 Cell density and cell size of the PLA and PLA/MG-based foams.

5.2.2 Chemo-physical investigations

The average density of the fabricated foams was calculated and tabulated in **Table 5.1**. The average density of the nPLA foam was found to be ~0.17±0.01 g/cc, whereas the density of the PLA granule was observed as ~1.24±0.1 g/cc. The significant reduction of density in case of foams is mainly due to the presence of voids in the matrix, which caused by the leaching of porogen particles. The presence of air voids in the PLA matrix reduces its weight, which directly affects the density. The lightweight foam materials are preferable in various applications with the aid of cost reduction for using a lesser amount of materials. The measured density of PLA/MG 1 was found to be ~0.17±0.01 g/cc, which is similar for nPLA. Subsequently, in the case of PLA/MG 2 and PLA/MG 3 the average density values are observed as ~0.15±0.01 and ~0.16±0.01 g/cc, respectively. The small reduction in density at higher loadings can be attributed to the phenomena of nucleation of MG nanobiofiller, which contributes to more number of pores by reducing the mass and finally effects the average density [228].

Table 5.1 Dry weight, density and volume expansion ratio (VER) of foams.

Sample	Dry weight before leaching (g)	Dry weight after leaching (g)	Avg. density (g/cc)	VER	Foam Type
nPLA	34.6	3.8	0.17±0.01	7.5±0.4	Medium density
PLA/MG 1	33.8	3.5	0.17±0.01	7.1±0.3	Medium density
PLA/MG 2	34.8	3.2	0.15±0.01	8.4±0.5	Medium density
PLA/MG 3	32.8	3.6	0.16±0.01	7.7±0.3	Medium density

Avg. density of PLA granules is found to be 1.24±0.02 g/cc.

The VER of the foams are calculated and are summarized in **Table 5.1**. The VER of nPLA foam is observed as 7.5±0.4 indicating medium density foam. It can be observed from Table 1 that all the fabricated foams can be categorized as medium density foam. The FTIR spectra of porogen, MG, and fabricated foams are shown in **Fig. 5.6**. The characteristic FTIR peaks of sucrose can be observed around ~908 cm^{-1} (–C-O- stretching), ~1300 cm^{-1} attributes to the –OH group (bending vibrations) and peak around ~1400 cm^{-1} indicates to –CH group (bending vibrations) of sucrose. Two peaks (~3380 cm^{-1} and ~3556 cm^{-1}) indicates the –OH groups (stretching vibrations) of sucrose [177]. Further, for MG peaks around ~1750 cm^{-1} (-C=O- stretching) and 1128 cm^{-1} (–C-O- stretching) are observed. The peaks observed at MG are also observed in PLA/MG based fabricated foams. Characteristic peaks are observed for nPLA around ~868 cm^{-1} (–C-O-C- stretching), ~1073 cm^{-1} (-CH_3 asymmetric vibrations), ~1450 cm^{-1} (-CH bending vibrations) and ~1742 cm^{-1} (–C=O vibrations). Moreover, the peak around ~2930 cm^{-1} represents the –CH_3 symmetric vibrations. For the case of all PLA/MG based foams, a broad peak around ~3500 cm^{-1} representing –OH is observed. In case of all the fabricated foams, sharp peaks around ~1750 cm^{-1} (–C=O- stretching) and 1454 cm^{-1} (–CH_3 stretching) are observed [122,123]. Peaks around ~1198 cm^{-1}, ~1133 cm^{-1} and ~1083 cm^{-1} representing –C-O- stretching in the structure of MG [188]. Other characteristic peaks are observed around ~1045 cm^{-1} and ~1595 cm^{-1} indicating –OH stretching and –C=O stretching as well as –N-H- bending, respectively [229]. The XRD patterns of fabricated foams are represented in **Fig. 5.7**. For nPLA foam, a sharp peak was observed at 2θ=16.6° which indicates [1 1 0]/ [2 0 0] planes. This sharp intense peak confirmed the α-form of crystals, which presents in the structure. Other peaks were observed at 2θ=14.9°, 19.5° and 22.5° corresponding to [0 1 0], [2 0 3] and [0 1 5] planes, respectively [122]. Sharp peaks around 2θ=~16.6° are present in all concentrations of PLA/MG-based foams, which confirms the presence of ordered crystals in the fabricated foams. It was also observed from the figure that no significant shifting of

peaks occurs which confirmed that no phase separation of ordered crystals held in PLA/MG based foams. MG nanofiller acting as plasticizing agent may also affect the crystallinity of the fabricated PLA/MG based foams compared to their neat counterpart. The peak intensity of 2θ=~16.6° for PLA/MG 1 is observed as I_{max}=4479, for PLA/MG 2 the value is I_{max}=4153 and for PLA/MG 3 the value is observed as I_{max}=3159 whereas I_{max}= 3833 for nPLA keeping other parameters constant for XRD analysis. The increase in intensity value may also be due to a good degree of interaction of polymer-filler and the nucleation effect of MG filler in the polymer matrix. It is observed from the investigation that α-form of crystals are mainly dominating the fabricated foams.

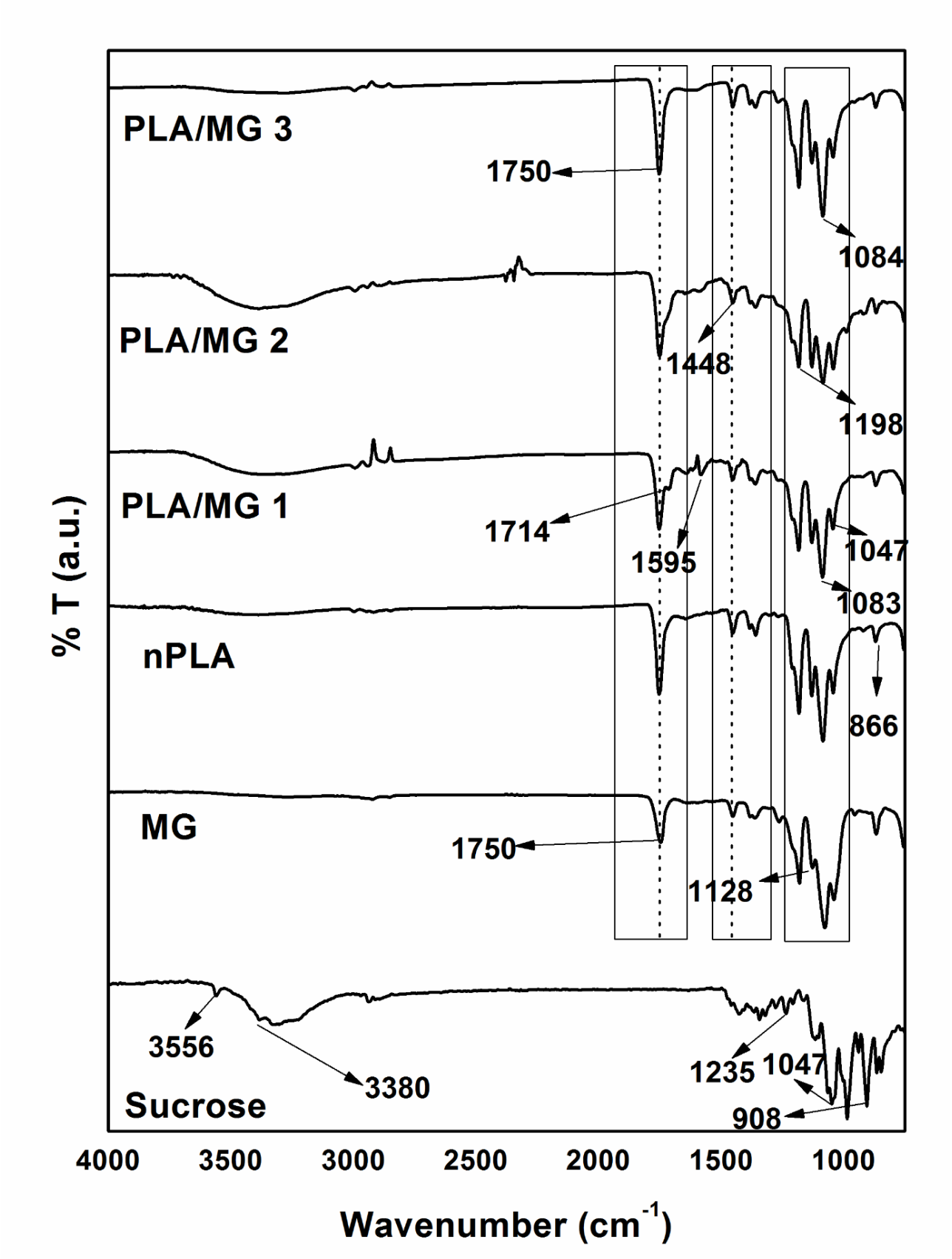

Fig. 5.6 FTIR spectra of Sucrose and PLA/MG-based foams.

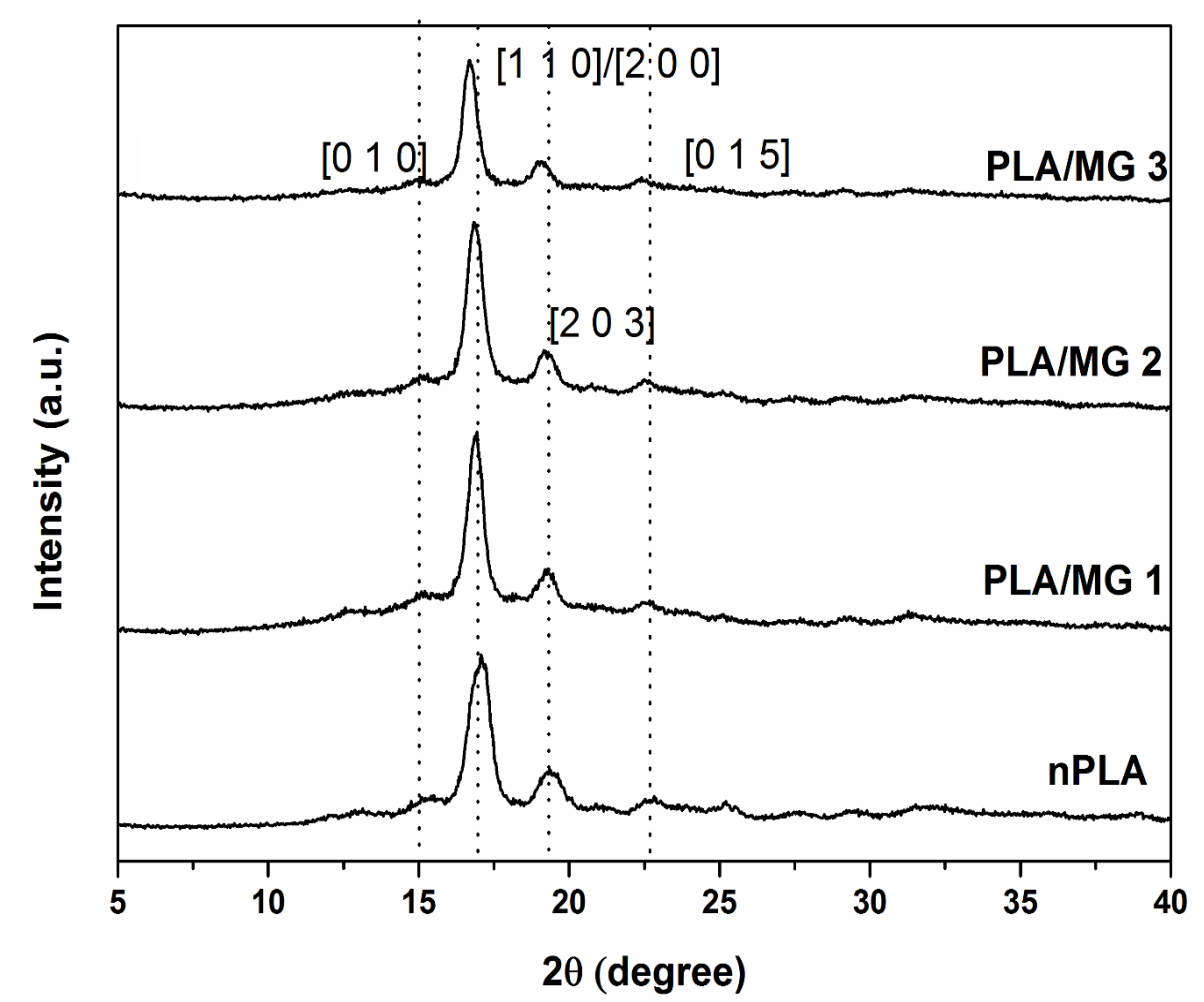

Fig. 5.7 XRD spectra of PLA and PLA/MG-based foams.

The calculated values of M_n, M_w, and PDI from GPC analysis are summarized in **Table 5.2**. The M_n and M_w values of nPLA foam were observed as ~114270 Da and ~202380 Da, respectively. The PDI value of nPLA foam was observed as ~1.8. However, on the addition of MG nanobiofillers, a reduction in molecular weight was observed. This phenomenon is occurring due to the presence of low molecular weight oligomer (OLLA) present in MG, which was used as a filler material to fabricate the composite foams. It can be seen from the table that M_n value decreases with MG due to the presence of low molecular weight oligomer. Moreover, the M_w value is also decreasing on increasing the filler concentration. Further, the PDI of the fabricated foams lies in the range of ~1.7-~1.8.

Table 5.2 Thermal analysis data and molecular weight investigations.

Sample	TGA Analysis			GPC Analysis		
	T_{onset} (°C)	T_{max} (°C)	T_{90} (°C)	M_n (Da)	M_w (Da)	PDI
nPLA	358	392	403	114270	202380	1.8
PLA/MG 1	349	389	398	107450	184010	1.7
PLA/MG 2	345	388	397	95240	17480	1.8
PLA/MG 3	342	387	397	90070	153070	1.7

5.2.3 Colorimetric investigations of the fabricated PLA and PLA/MG based foams

The color parameters of formulated polymeric foam materials using PLA and its biocomposites are significantly influenced by the use of various loading of MG as shown in **Table 5.3**. The observed L value of the prepared nPLA foam was found to be 96.48±0.51, which is having a close agreement to 92.1±0.2 obtained by **Samsudin et al.** [230]. Further, incorporation of MG to the PLA materials reduce the L value by ~18.2, ~28.90 and ~44.66 % with the loading of 1, 2, and 3% biofiller materials, respectively, where the fabricated dark brown color of MG is responsible for such change. Further, color factor shows a drastic change to redness from greenness due to the incorporation of filler material and observed values significantly switch from -0.04±0.02 to 6.50±0.13 with an increase in loading of bionanofiller. Interestingly, there was also found an increment in b* values where there is shown a significant improvement of yellow color which may be due to the effect of temperature and % loading during processing of filler materials. The chroma values are also observed to be influenced by filler materials and are found to be enhanced which shows the increase in saturation values of color with increasing MG nanobiofiller. It can be concluded that MG significantly effects the color parameters of the fabricated foams.

Table 5.3 Colour properties of biodegradable composite foam.

Parameters	nPLA	PLA/MG 1	PLA/MG 2	PLA/MG 3
L	96.48±0.51	78.96±0.19	68.59±0.39	53.39±1.05
a*	-0.04±0.02	3.63±0.07	4.79±0.09	6.50±0.13
b*	0.89±0.09	13.85±0.14	18.38±0.13	19.39±0.22
Chroma	0.89±0.09	14.31±0.14	19.00±0.10	20.45±0.24

5.2.4 Thermal investigations

The thermogravimetric plots of fabricated foams are represented in **Fig. 5.8**. The calculated T_{onset}, T_{max} and T_{90} from the TGA profile are summarized in **Table 5.2**. The hydrolysis along with the oxidative scissions of PLA chains might be responsible for the T_{max} value obtained for nPLA (~392 °C) [178]. It can be observed from the TGA profile that degradation is undergoing in a single step for all the cases. However, on the introduction of MG filler, no such significant changes were observed. At the highest concentration of MG (PLA/MG 3), there was a reduction of ~5 °C in T_{max} value. In the case of T_{onset}, it was observed that PLA/MG 3 has a reduction of ~16 °C compared to nPLA foam. A reduction of ~6 °C was also observed in T_{90} for PLA/MG 3 than its neat counterpart. The degradation process of PLA is enhanced by MG and thus affecting the thermostability. On increasing the concentration of MG, the generation of acidic sites are also increased which enhances the degradation at a slightly lower temperature.

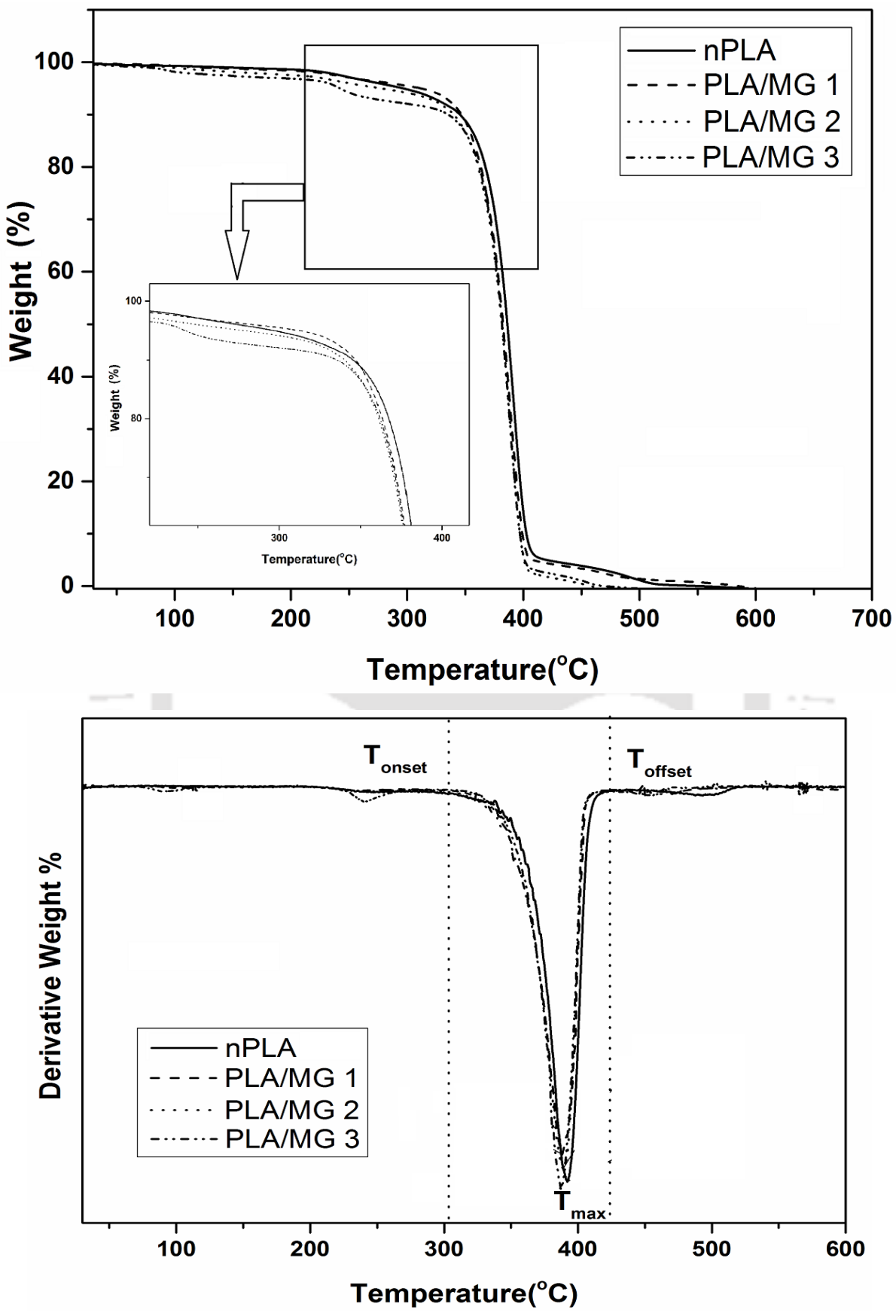

Fig. 5.8 TGA and DTG profile of PLA and PLA/MG-based foams.

The crystallization behaviors of the fabricated foams are represented in **Fig. 5.9** and the second heating cycle of the analysis were considered for the present experiment. The glass transition temperature (T_g), crystallization temperature (T_c) and melting temperature (T_m) of PLA and PLA/MG based foams can be measured from the DSC plot. T_g value of nPLA was found around ~63.7 °C. However, a reduction in T_g value was observed on increasing MG filler concentration which might be due to the plasticizing effect of MG and formation of short chains. Single T_g indicates good compatibility of nanofiller in the polymer matrix. No such significant reduction in melting point was observed in PLA/MG based foams compared to nPLA. The single endothermic melting peak indicates the homogeneous distribution of MG filler in the PLA matrix. The melting peaks indicate the melting of perfect crystals at higher temperature [179]. So it can be concluded that introduction of MG has no significant effects in melting temperatures of PLA/MG based foams. However, there was a reduction in T_c value was also observed in PLA/MG-based foams compared to the neat counterpart.

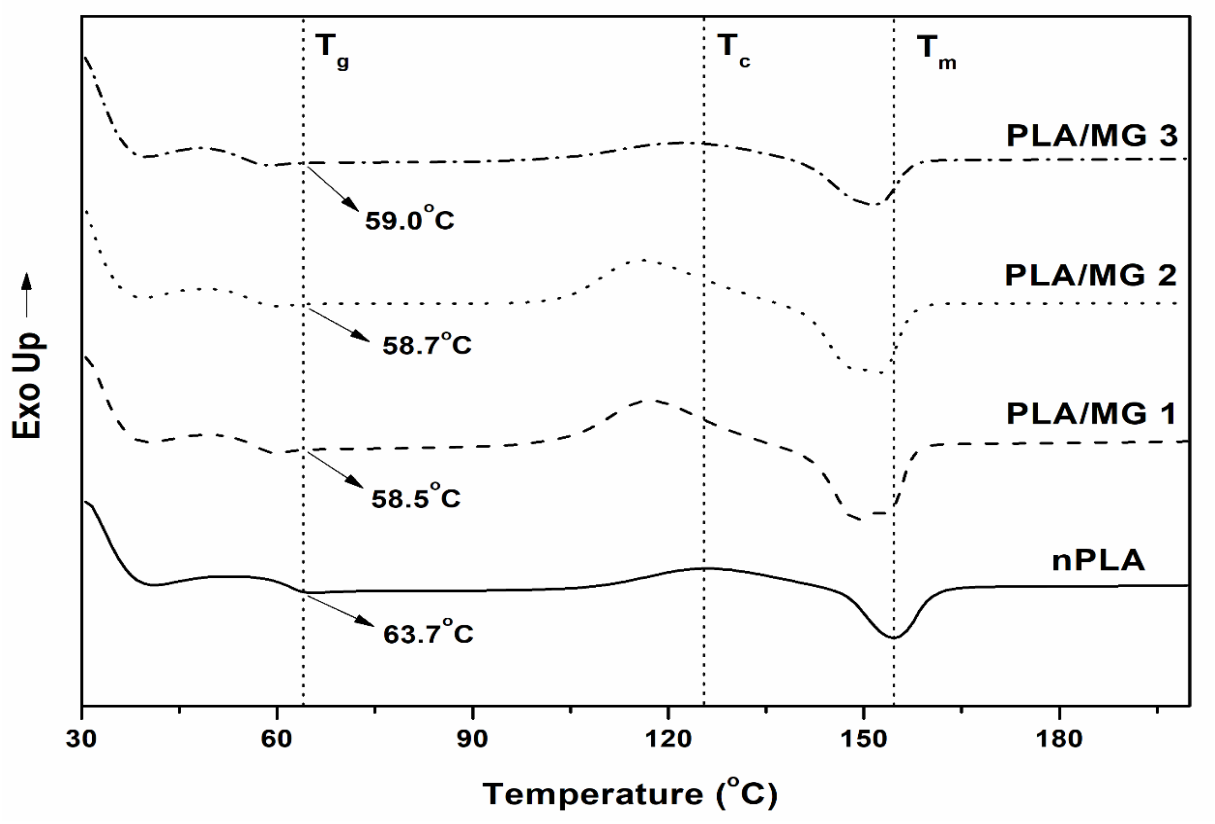

Fig. 5.9 DSC thermograms of PLA and PLA/MG-based foams.

5.2.5 Wettability Phenomena

Wettability investigations of developed foams (**Fig.5.10A**), are performing observing both static and dynamic contact angle values (**Table 5.4**). The static contact angle value of nPLA was observed as ~118.4°±2.2°. On introduction of MG nanobiofiller, the increase in hydrophobicity in PLA matrix was observed. Further, the static contact angle also increases with MG nanofiller concentration. Almost ~20° increment in contact angle was observed for PLA/MG 3. The increase in contact angle for both PLA/MG 1 and PLA/MG 2 was found to be around ~17°. The contact angle studies of the compressed foam (surface without texture) has been performed to understand the influence of surface morphology in wettability. It can be seen from the table that a reduction of ~45° contact angle is observed in nPLA foam, whereas the contact angle reduction for PLA/MG 1 and PLA/MG 2 are ~60°. Similarly, in the case of PLA/MG 3, a reduction of ~55° in contact angle was observed. The reduction in contact angle of compressed foams might be due to the collapse of the foamed structure in the matrix. However, an increase in contact angle with MG loading was also observed in compressed foam surfaces. Hence, we can conclude that MG fillers along with the surface morphology has combined effects in wettability of foams. Due to the hydrophobic nature of MG, the contact angle might be affected. The probable reorganization of MG in the PLA might be responsible for the decrement of the contact angle of compressed surface effecting wettability. From the dynamic contact angle analysis, a slight increase (~2°) in Young's contact angle was observed for the fabricated foams. Dynamic wettability analysis considers both the spreading and splitting phenomena of the liquid drops in the surface. As discussed in the previous section, the MG nanofiller increases the generation of the number of pores which directly increases the cell density and decreases pore size as supported by FESEM (~2.8±0.1 µm for PLA/MG 2). Parallel conclusions can also be made from the contact angle hysteresis (CAH) values (**Table 5.4**) obtained. It is observed that on increasing MG concentration in the PLA matrix, the hysteresis value also increases. The CAH value depends on

the surface morphology and in our investigation, the highest value of CAH is observed for PLA/MG 3. The change in surface morphology of the PLA based fabricated foams with the increase in MG might be the reason behind this change in CAH value. The observations are in agreement with some previous investigation of wettability in PLA based foams [128]. Hence, comparatively smaller pores are present in PLA/MG-based foams, which affects the wettability, as it depends on surface roughness and morphology [183]. It can be concluded that the combined effect of MG nanobiofiller along with surface morphology of the fabricated foams is responsible for wettability phenomena.

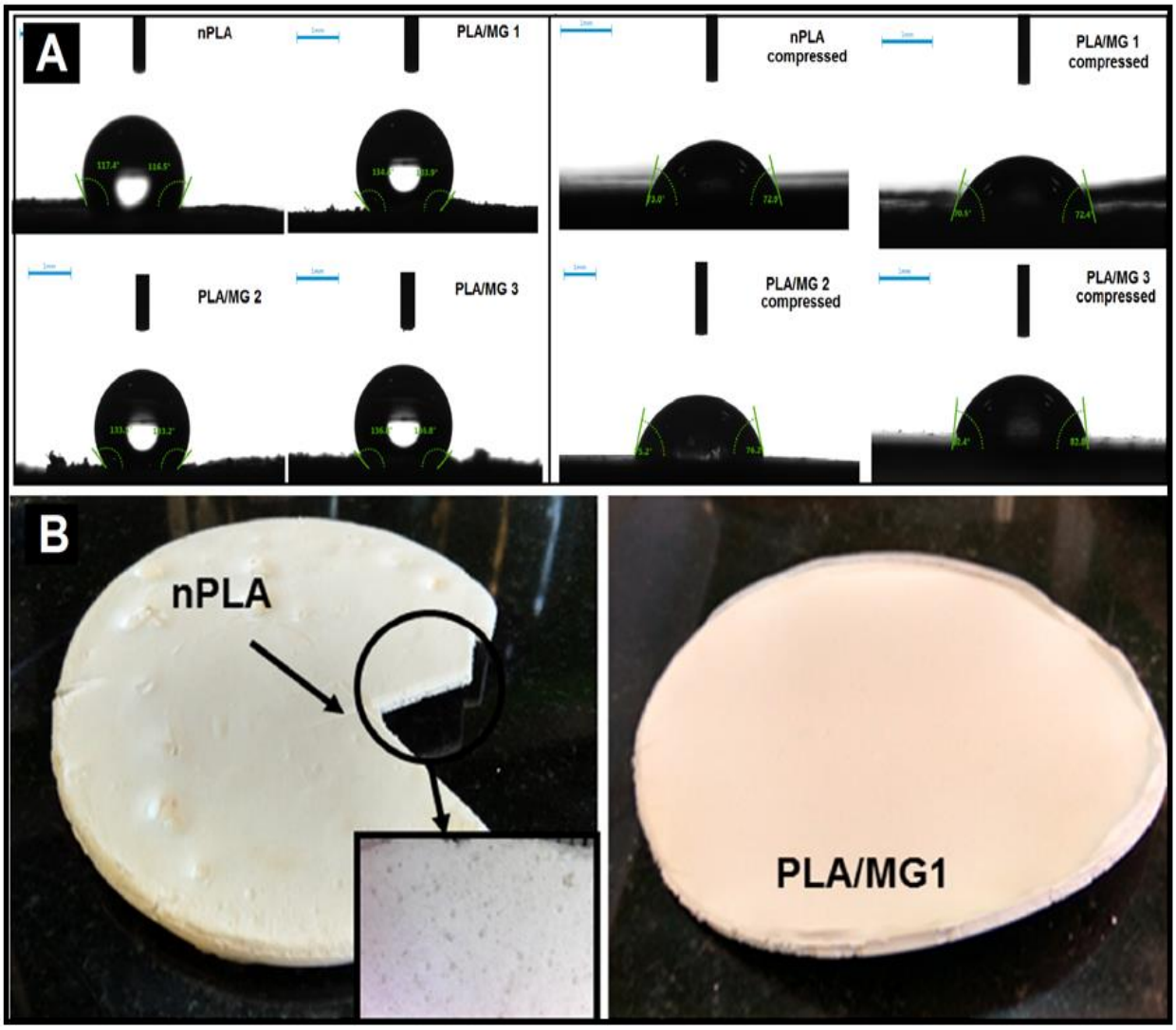

Fig. 5.10 A) Static contact angle of PLA and PLA/MG-based foams, **B)** Digital photograph of

the fabricated foams.

Table 5.4 Wettability analysis of the fabricated PLA and PLA/MG-based foams.

Sample	Static Contact Angle		Dynamic Contact Angle			
	Surface with texture	Compressed surface without texture	Advancing θ_{adv}	Receding θ_{rec}	Young's θ_Y	Hysteresis CAH
nPLA	118.4°±2.2°	73.0°±3.6 °	136.5°±5.1°	95.8°±8.8°	114.4°±4.8°	40.7°
PLA/MG 1	135.2°±3.2°	73.5°±2.8°	141.5°±9.8°	98.8°±6.8°	117.9°±7.5°	42.7°
PLA/MG 2	134.2°±2.6°	76.2°±2.6°	140.8°±8.8°	96.4°±8.4°	116.3°±6.8°	44.4°
PLA/MG 3	137.5°±3.1°	82.8°±3.4°	145.6°±7.7°	93.8°±6.8°	116.4°±5.8°	51.8°

5.2.6 Porosimetric investigations

The digital photograph of fabricated foams can be observed in **Fig. 5.10 B**. The results obtained from porosimetric investigations are summarized in **Table 5.5**. A reduction of ~ 20 % and ~ 53.3 % average pore diameter is observed for PLA/MG 1 and PLA/MG 2 compared to nPLA respectively. However, the average pore diameter value slightly increases for foam with highest MG loading. Interestingly, the reduction in average pore diameter can be related to the nucleation of MG. The increase in MG generates more nucleating cites which might enhance the number of pores. The agglomeration of MG at highest loading might be the probable reason of the slight increment in average pore diameter. The average cell diameter observed from this investigation are in good agreements with the cell size obtained from FESEM micrographs as discussed in the previous section. The surface area is also related with the pore size and it is observed that an increment of ~15.4 % and ~59.6 % in surface area was caused with an increase in MG for PLA/MG 1 and PLA/MG 2 compared with PLA foam, respectively. Similarly, a slight decrease of surface area is observed for PLA/MG 3, where an increase in surface area

can be related to the decrease in pore size. As discussed earlier, the increase in surface area and a decrease in pore size is very much useful for different applications including cell proliferation and tissue culture [205]. The porosity value also slightly decreases with an increase in surface area due to the presence of smaller pores. The porosity of the PLA foam is observed as ~82% and the value slightly decreases to ~80% and ~78% for 1% and 2% loading of MG respectively.

Table 5.5 Porosimetric investigation of PLA and PLA/MG based foams**.**

Sample	Porosity (%)	Avg. Pore Dia. (µm)	Surface Area (m^2/g)
nPLA	82	1.5	13.6
PLA/MG 1	80	1.2	15.7
PLA/MG 2	78	0.7	21.7
PLA/MG 3	80	1.0	17.5

5.3 Crystallization kinetics investigations of PLA/MG-based foams

The DSC thermogram of different heating rates for non-isothermal crystallization kinetics of developed foams is shown in **Fig. 5.11**. Crystallinity is a phenomenon, which can be explained on the basis of arrangements of polymer chains in the matrix. The nanofillers effects the crystallinity, nucleation rate, crystallization temperature and spherulite size [231] The crystallinity is also important for the degree of expansion and integrity of the cellular structure of foams [232]. The investigation is mainly focused on the effect of MG nanobiofiller on the crystallization properties of PLA foams. The non-isothermal cold crystallization kinetics of PLA and PLA/MG based foams are carried out at 4 different heating rates 2.5 °C/min, 5 °C/min, 7.5 °C/min and 10 °C/min and relative crystallinity plots and summarized values are shown in **Fig. 5.12** and **Table 5.6**. It is observed from the table that $t_{0.5}$ value got decreased on

increasing the heating rate of PLA and PLA/MG based foams, suggesting the rise in the rate of crystallization on increase in heating rate.

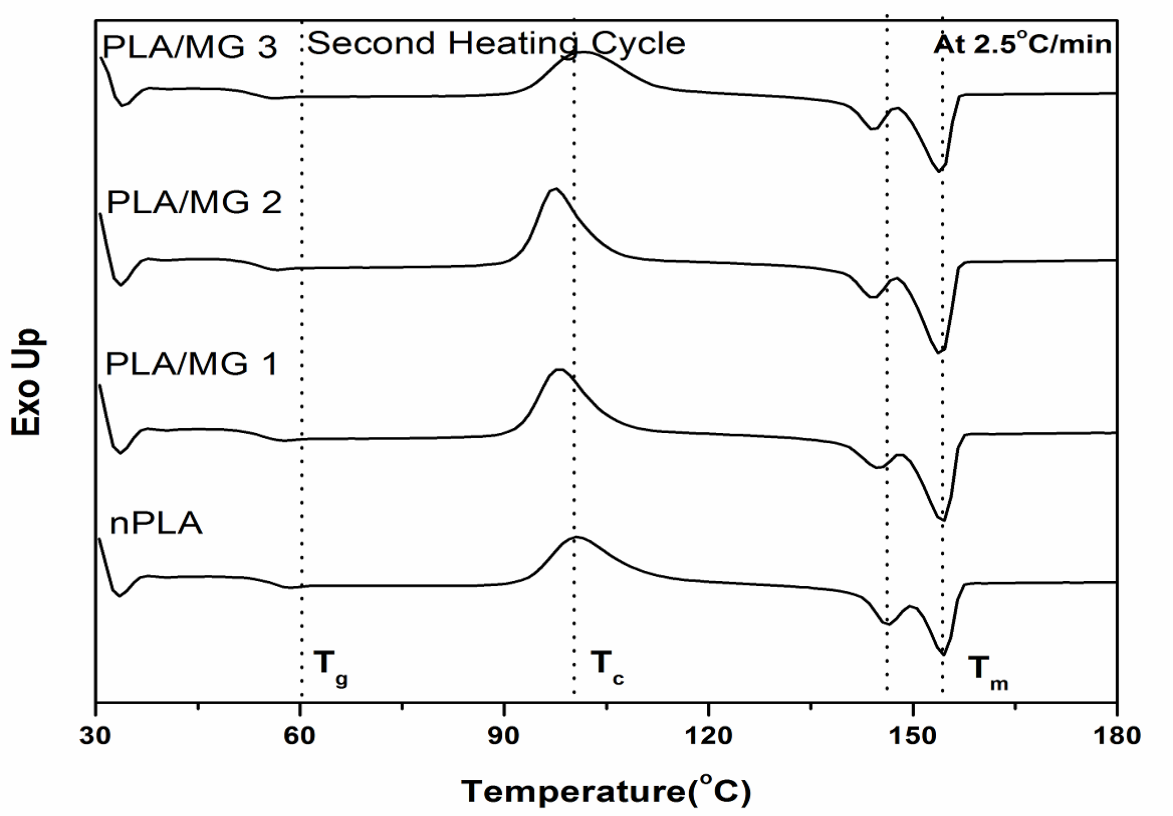

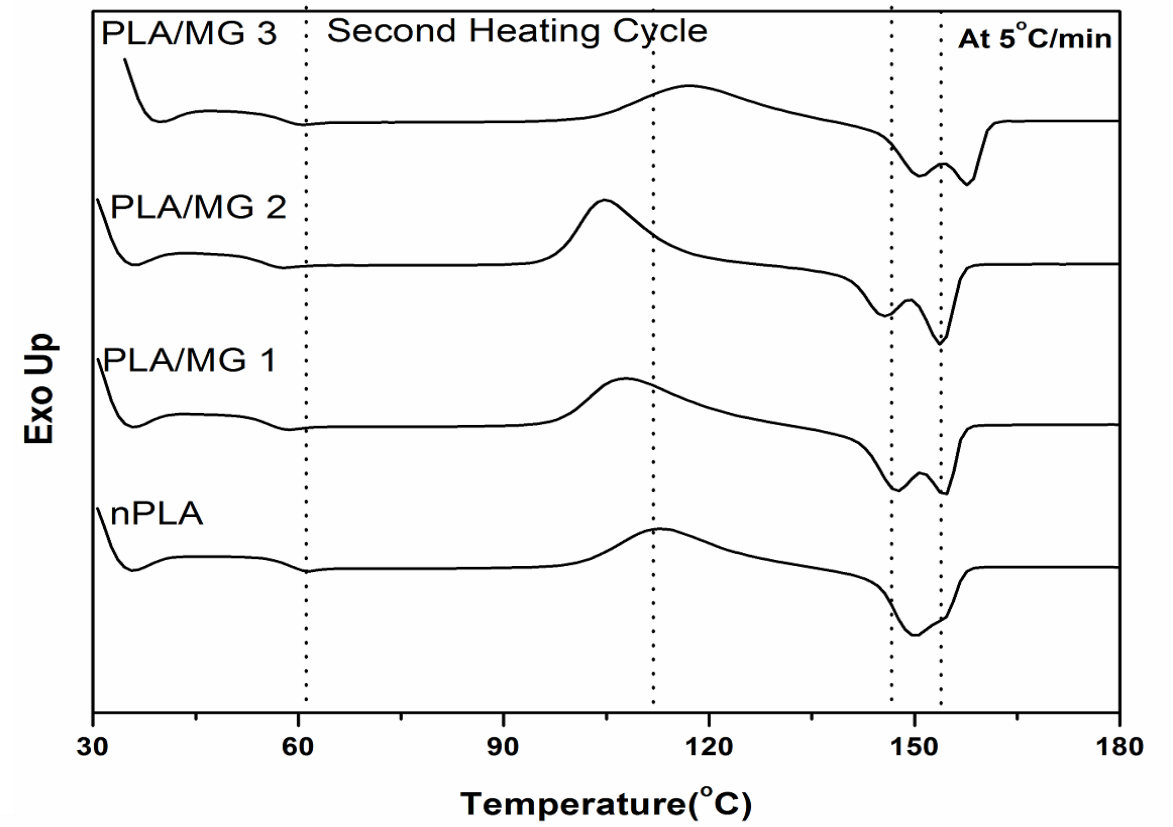

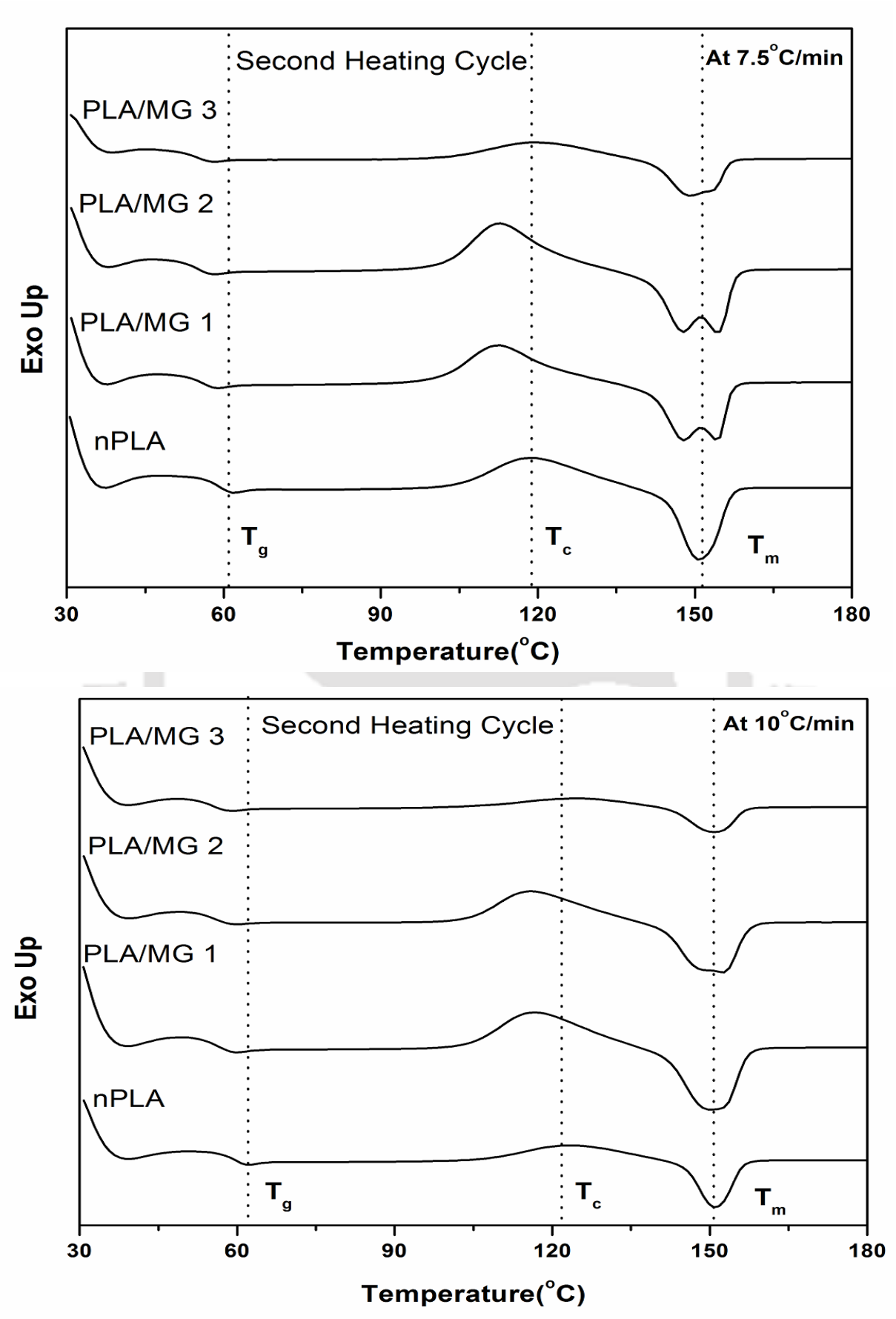

Fig. 5.11 DSC thermograms of PLA and PLA/MG-based foams.

The Avrami plots of the PLA and PLA/MG based foams are shown in **Fig. 5.13**. The values of Avrami exponent (n) and crystallization rate constant (k) are calculated and tabulated in **Table 5.6**. The values are calculated from the slope and intercept of the linear region of the Avrami plots and the linear pattern of the plot suggests primary crystallization.

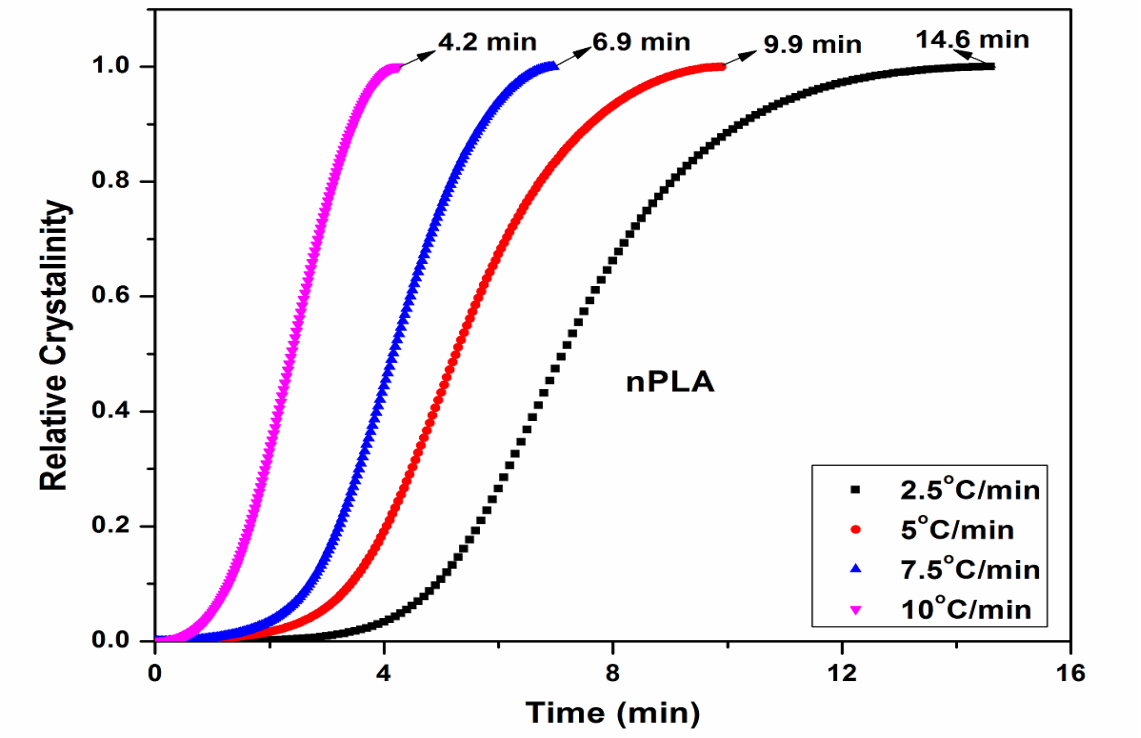

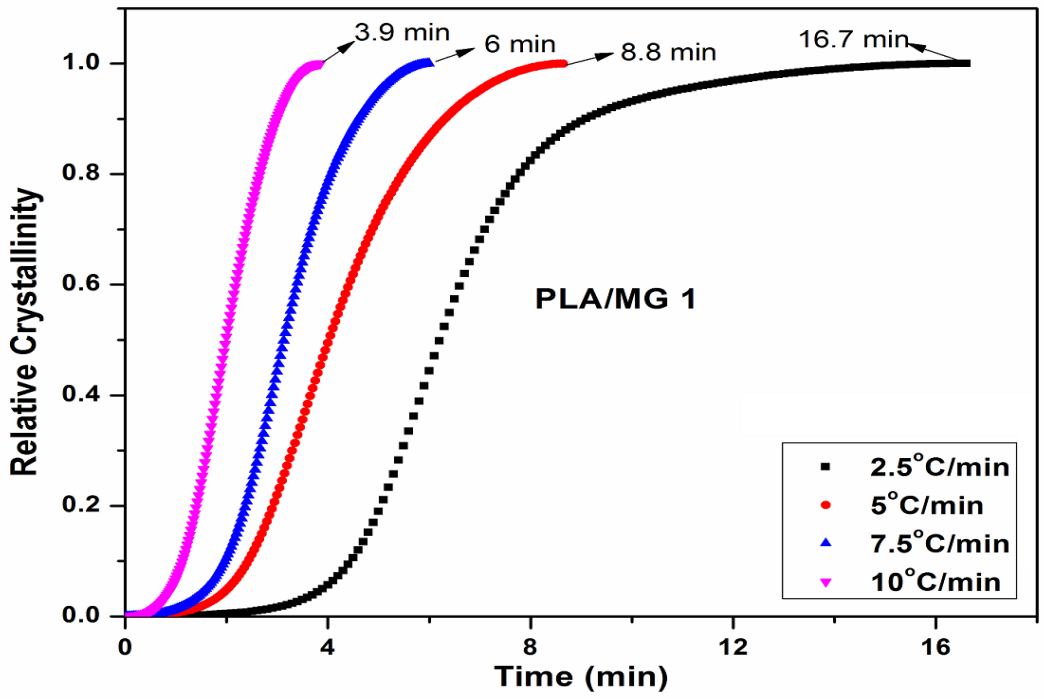

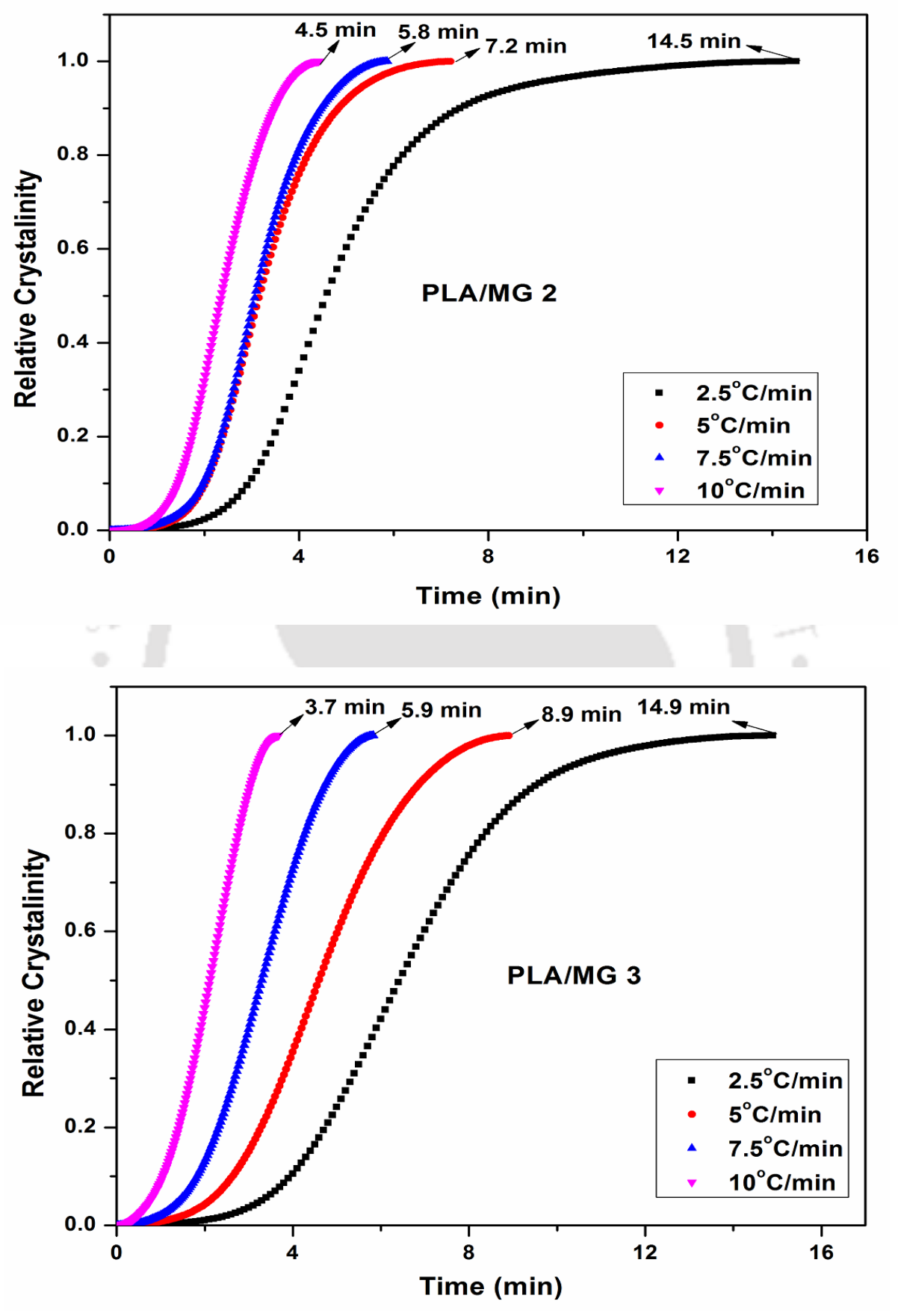

Fig. 5.12 Relative crystallinity vs time plots of PLA and PLA/MG-based foams.

However, it was observed that all the fabricated foams behave similarly and slightly deviates from linearity, suggesting the occurrence of secondary crystallization [123]. The primary crystallization suggests the outward growth of lamellar stacks depicting the perfection of internal spherulite crystallization and impingement of spherulite. Avrami exponent value is used to have an idea of nucleation mechanism of MG and form of crystal growth. In this investigation, it is observed that "*n*" value ranging from ~1.9-~3.0. The value of "n" nearer to ~2 suggesting two-dimensional nucleation and growth of the crystals [231], whereas the value of "*n*" close to ~3 suggesting plate-like growth from nuclei initiated over time [233]. The non-integral values of "*n*" suggesting that the nucleation mechanism consists of both thermal and athermal nucleation [123].

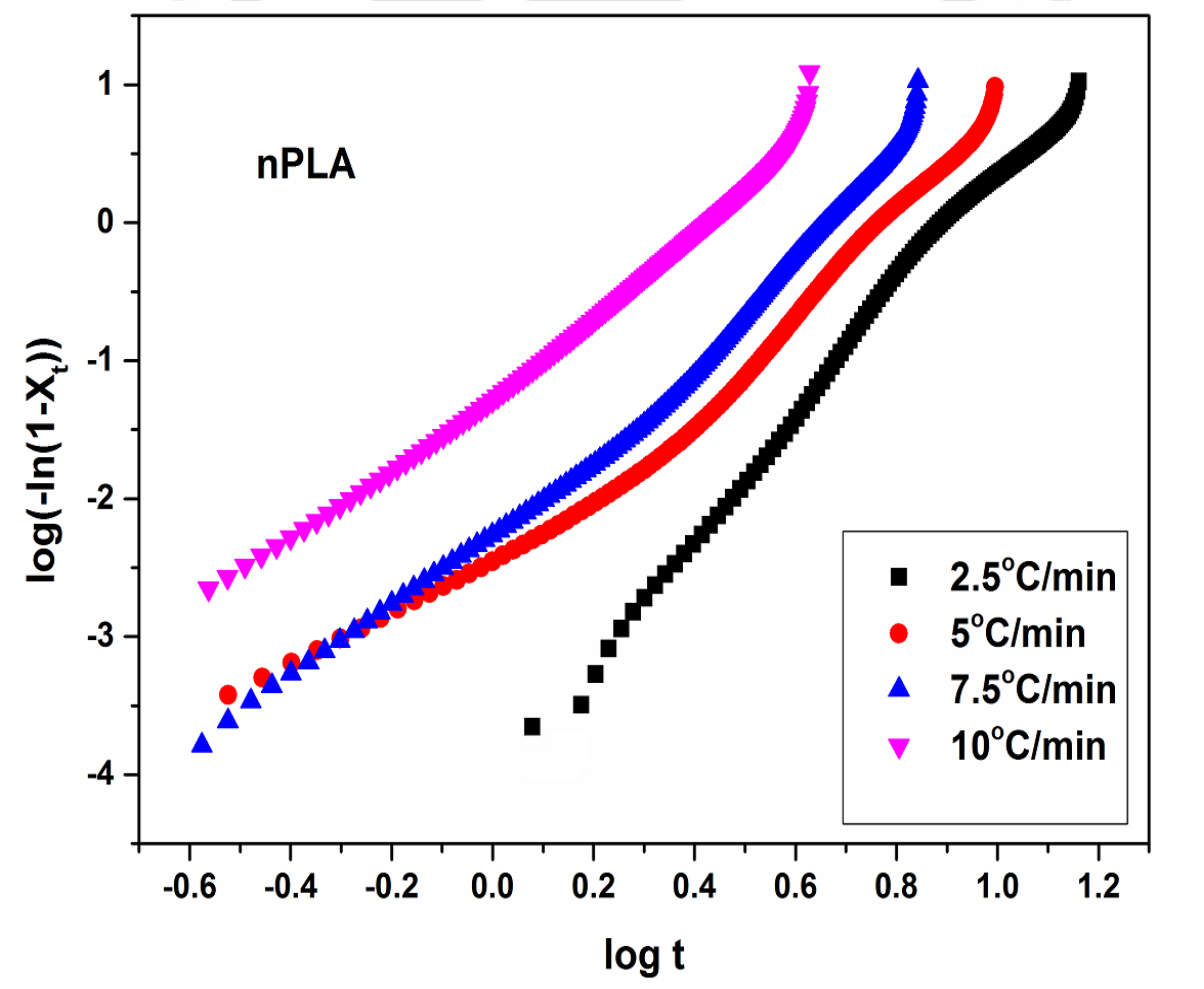

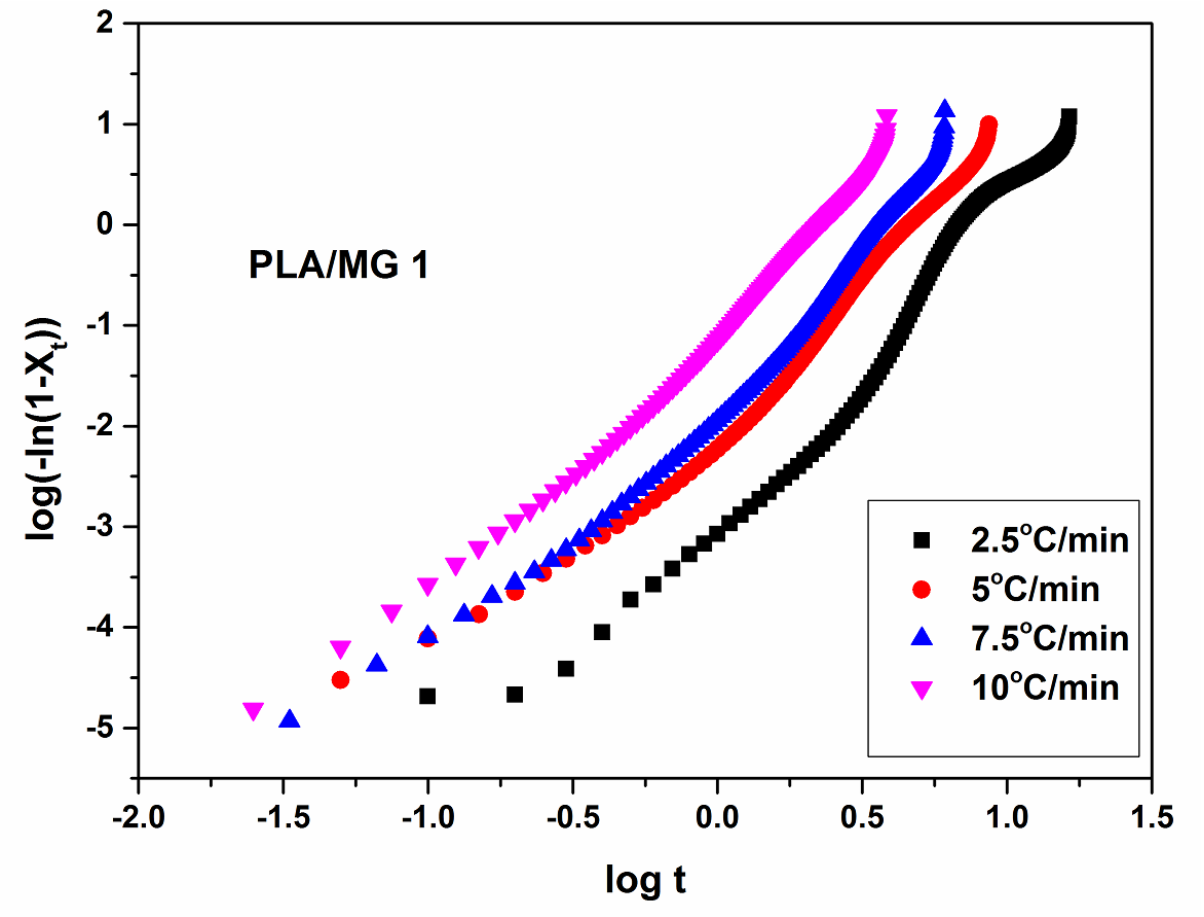

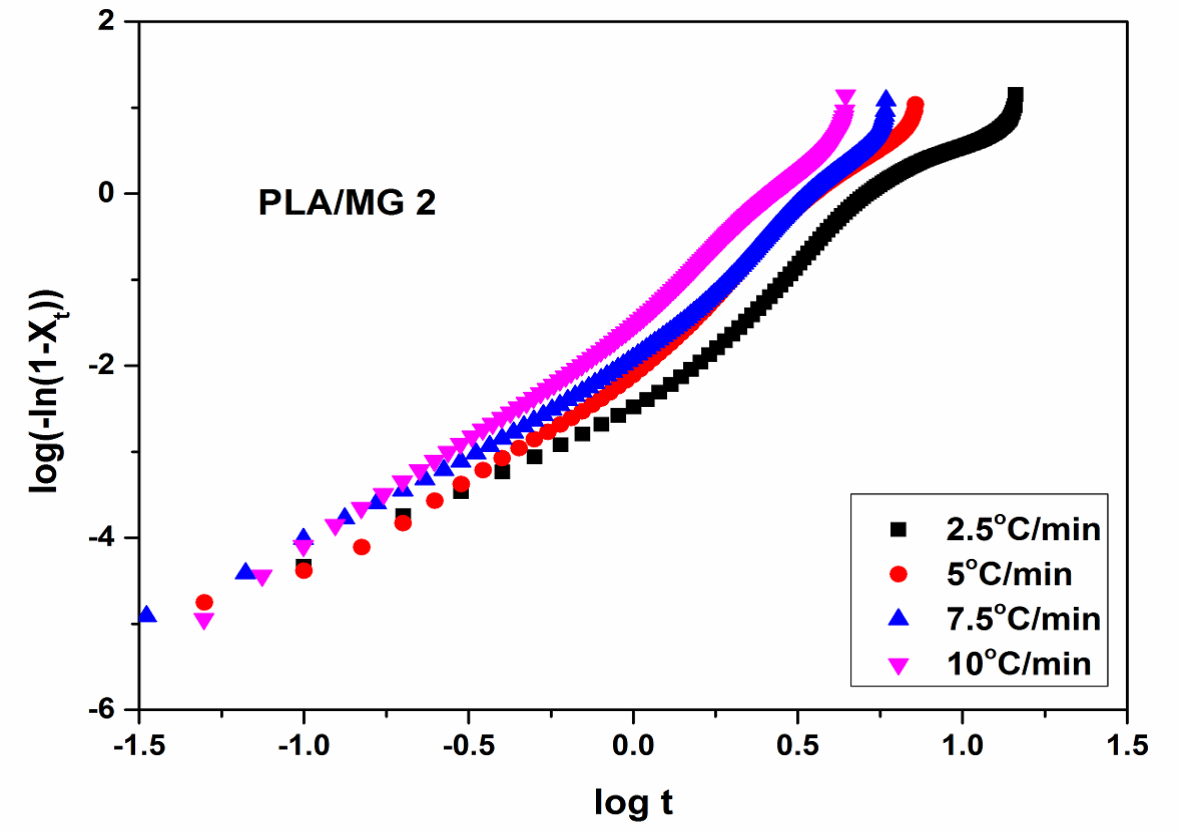

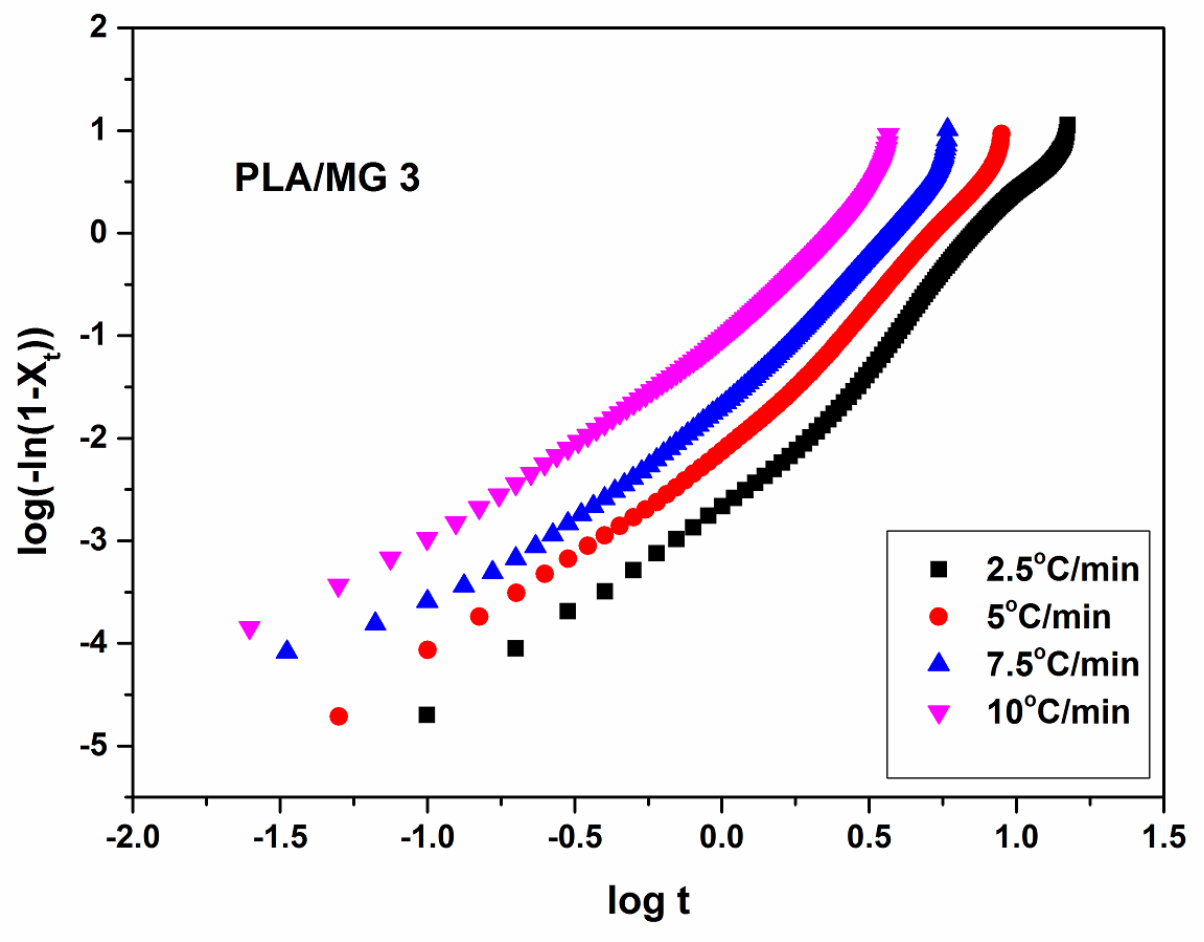

Fig. 5.13 Avrami plots of PLA and PLA/MG-based foams.

From the value of "k" we can confirm that MG fillers helps in generation of more nucleating sites and thus affecting the crystallization rate of PLA and PLA/MG based foams. Ozawa plots for PLA and PLA/MG based fabricated foams are shown in **Fig. 5.14**. The plots are mostly linear in nature, however, the non-linearity of the plots suggests the secondary crystallization process taking place in the fabricated foams. From the Mo plots (**Fig. 5.15**) the values of "a" and $F(t)$ are calculated and tabulated in **Table 5.6**. The values are found to be in the range of ~1.08-~1.25, ~1.10-~1.27, ~2.02-~2.04 and ~1.12-~1.22 for nPLA, PLA/MG 1, PLA/MG 2 and PLA/MG 3 respectively at a different degree of crystallization suggesting a change in crystallization mechanism. The $F(t)$ values are increasing with the degree of crystallization

indicating higher heating rate is required for higher crystallinity. The non-linearity is also observed in Mo plots suggesting primary and secondary crystallization. Tobin plots (**Fig. 5.16**) also indicates non-linearity and thus in accordance with the previous investigations.

Table 5.6 Crystallization parameters from the Avrami and Mo plots**.**

Sample	**Heating Rate (°C/min)**	**$t_{0.5}$ min**	k **(min^{-n})**	n	**X_t%**	a	$F(t)$
nPLA	2.5	7.2	0.0009	1.9	20	1.08	20.26
	5	5.3	0.004	2.3	40	1.18	28.98
	7.5	4.1	0.006	2.8	60	1.24	38.25
	10	2.3	0.06	2.8	80	1.25	47.98
PLA/MG 1	2.5	6.3	0.0009	2.5	20	1.10	16.58
	5	4.1	0.009	2.5	40	1.18	22.60
	7.5	3.2	0.02	2.6	60	1.25	29.95
	10	1.2	0.1	2.8	80	1.27	39.08
PLA/MG 2	2.5	4.6	0.005	2.4	20	2.02	33.19
	5	3.2	0.01	2.9	40	2.13	55.36
	7.5	2.9	0.02	2.6	60	2.13	78.81
	10	2.3	0.04	3.0	80	2.04	105.37
PLA/MG 3	2.5	6.4	0.002	2.2	20	1.12	16.80
	5	4.6	0.01	2.3	40	1.19	24.32
	7.5	3.3	0.03	2.5	60	1.23	31.87
	10	2.0	0.1	2.3	80	1.22	38.81

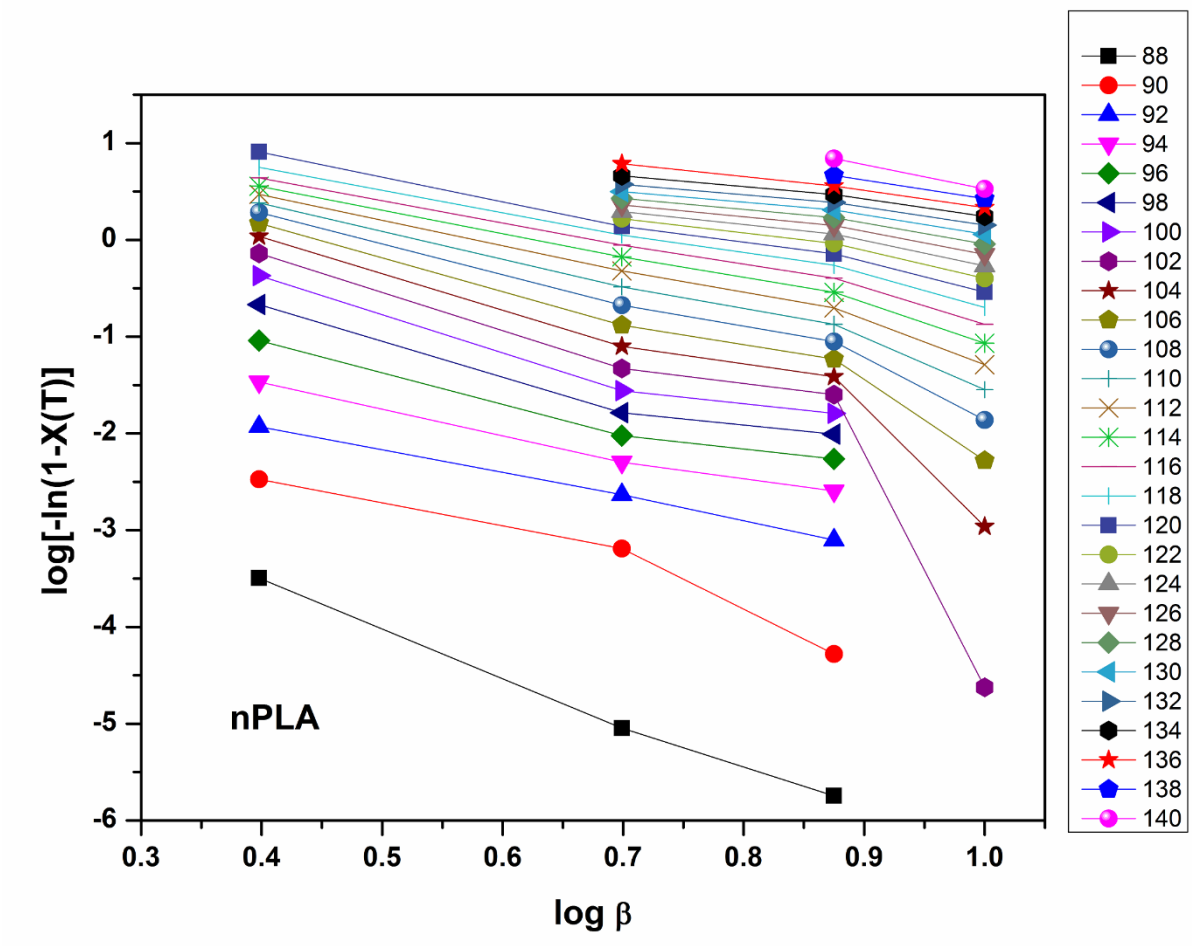
log[-ln(1-X(T))]
log β
nPLA
88
90
92
94
96
98
100
102
104
106
108
110
112
114
116
118
120
122
124
126
128
130
132
134
136
138
140

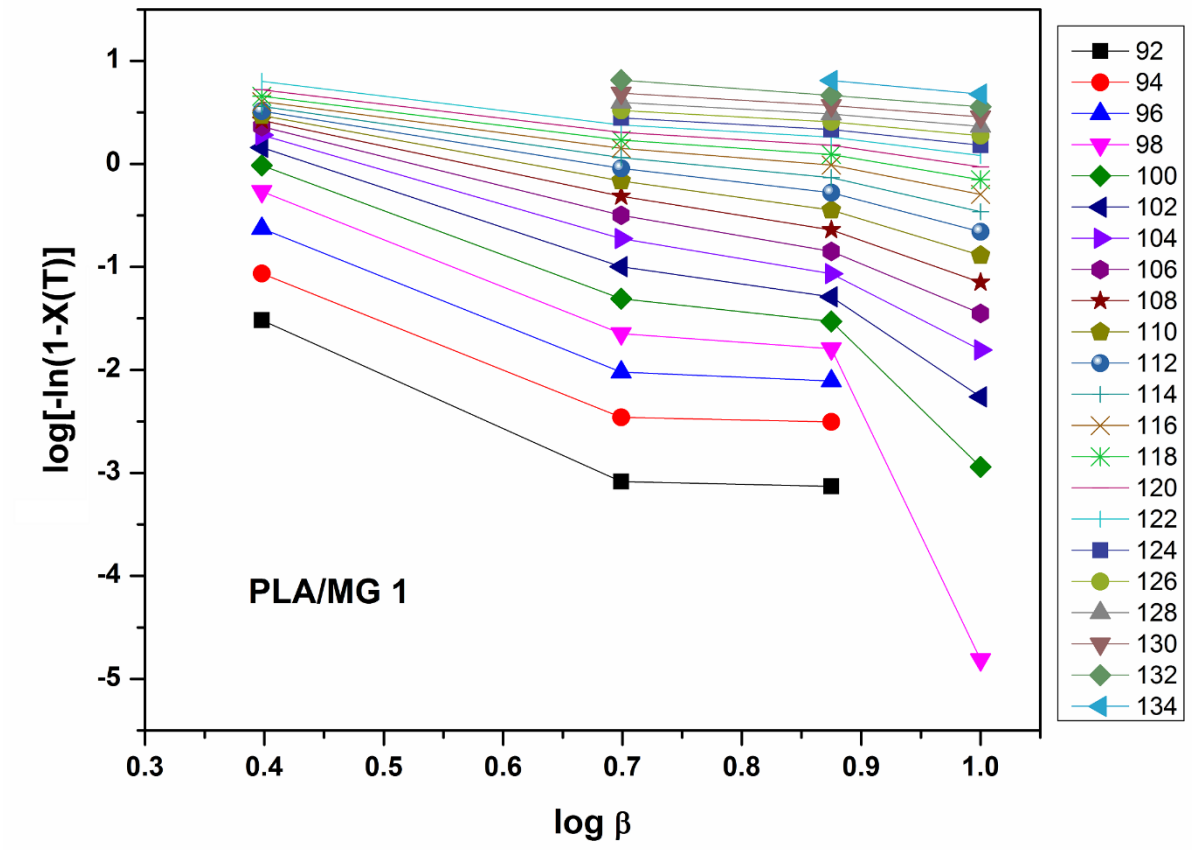
log[-ln(1-X(T))]
log β
PLA/MG 1
92
94
96
98
100
102
104
106
108
110
112
114
116
118
120
122
124
126
128
130
132
134

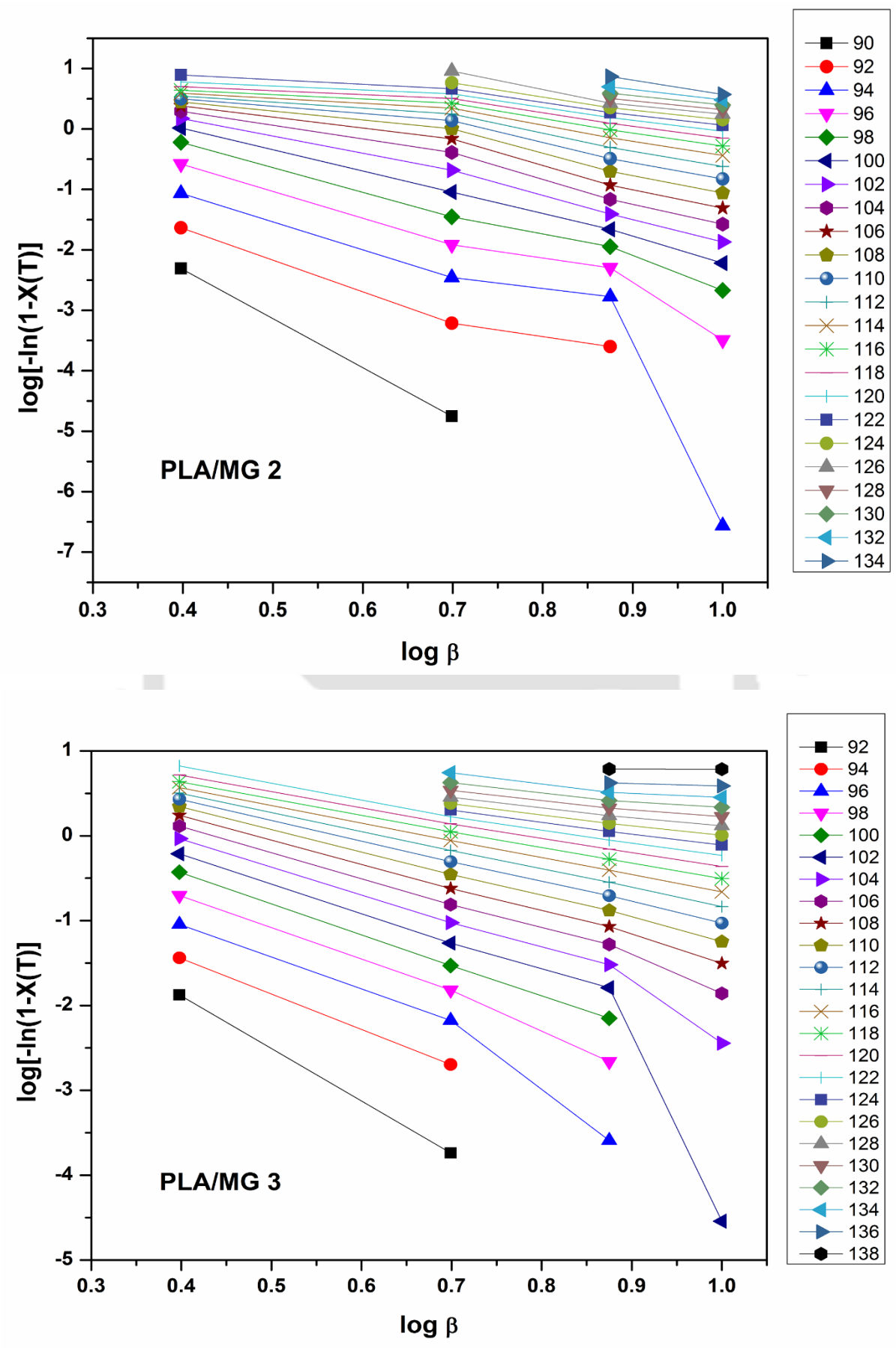

Fig. 5.14 Ozawa Plots for PLA and PLA/MG-based foams.

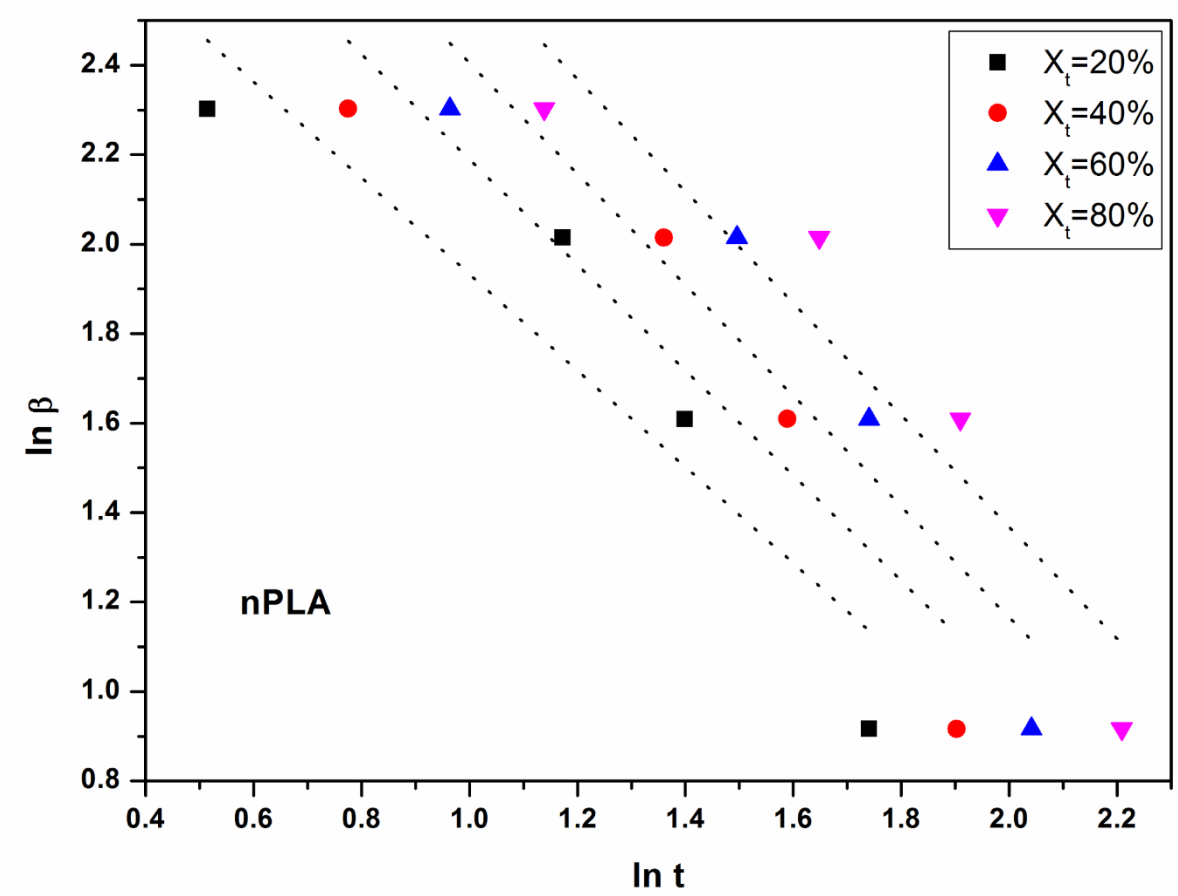

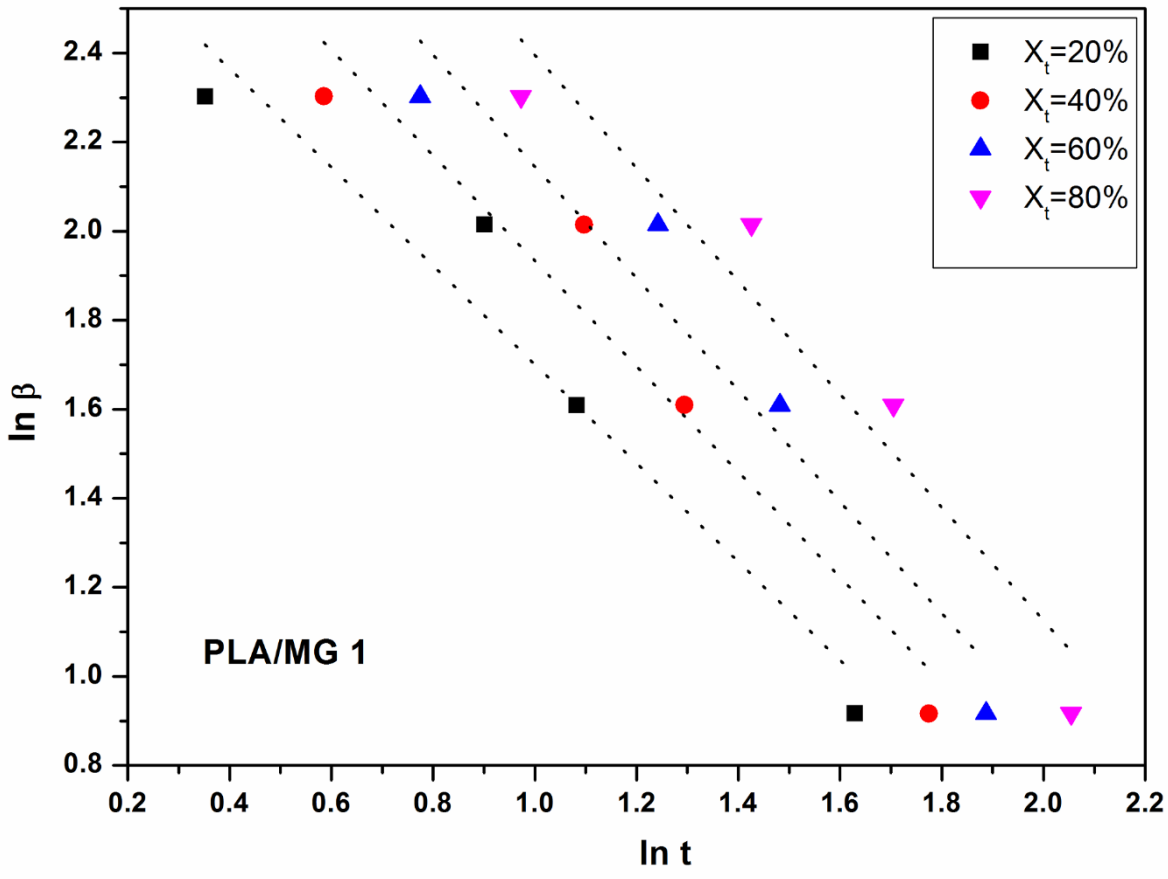

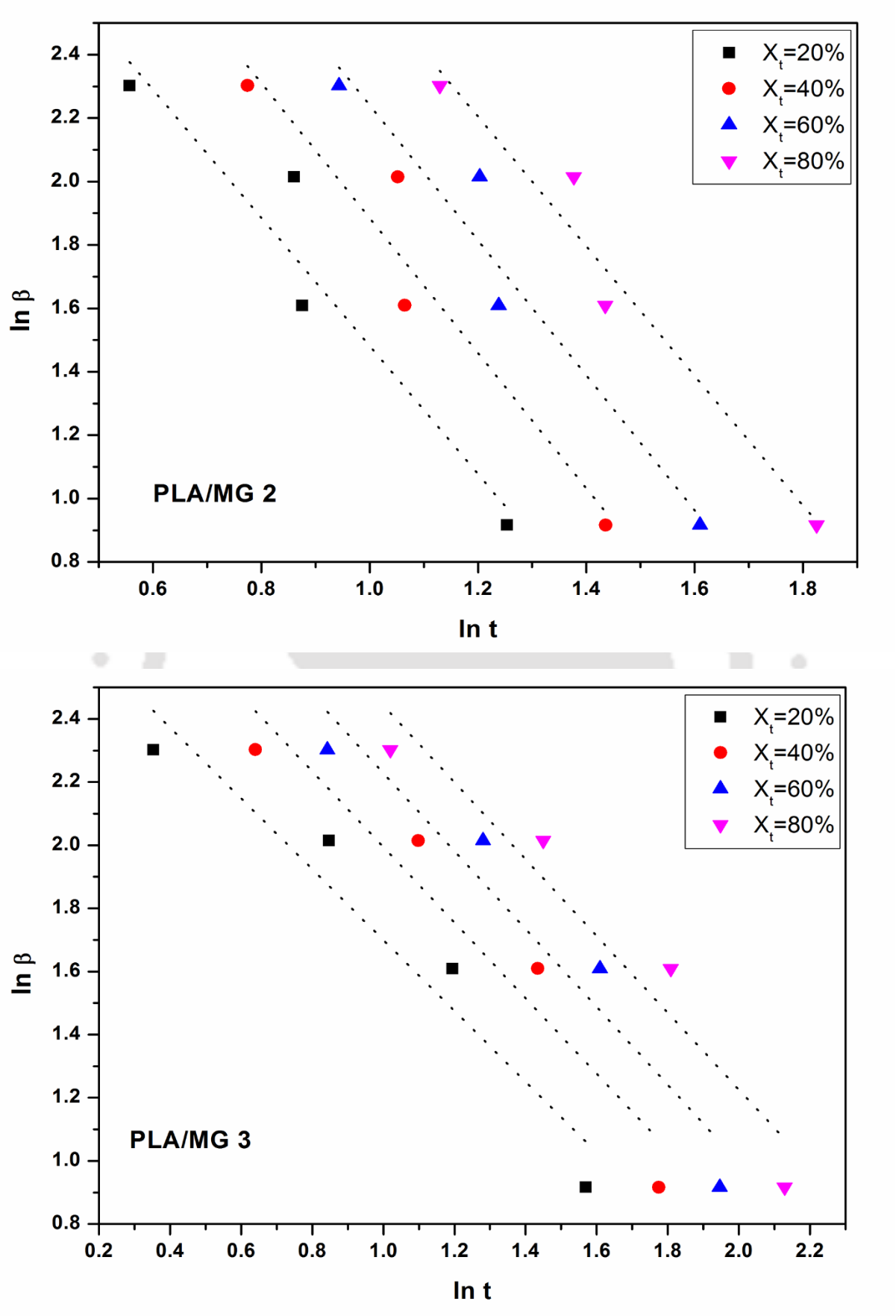

Fig. 5.15 Mo Plots for PLA and PLA/MG-based foams.

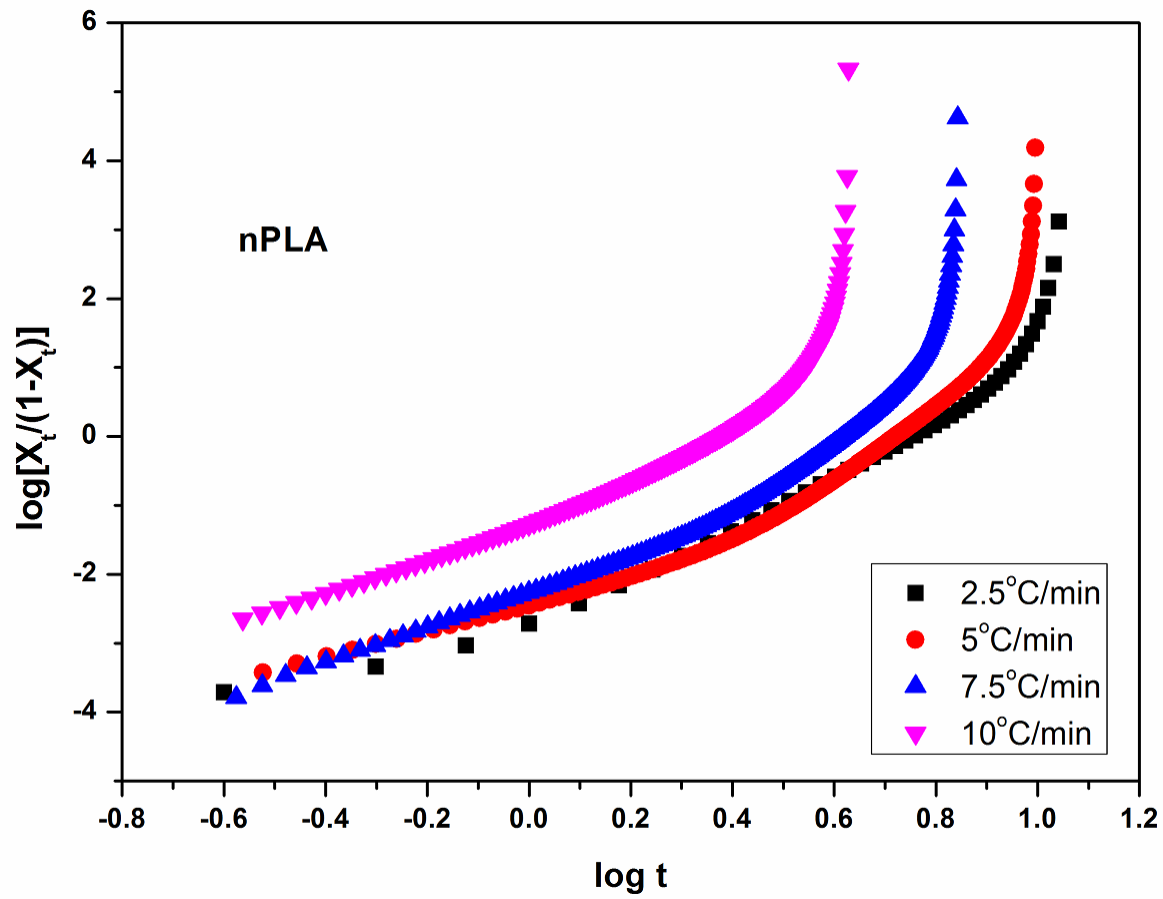
nPLA
log[X/(1-X)]
log t
2.5°C/min
5°C/min
7.5°C/min
10°C/min

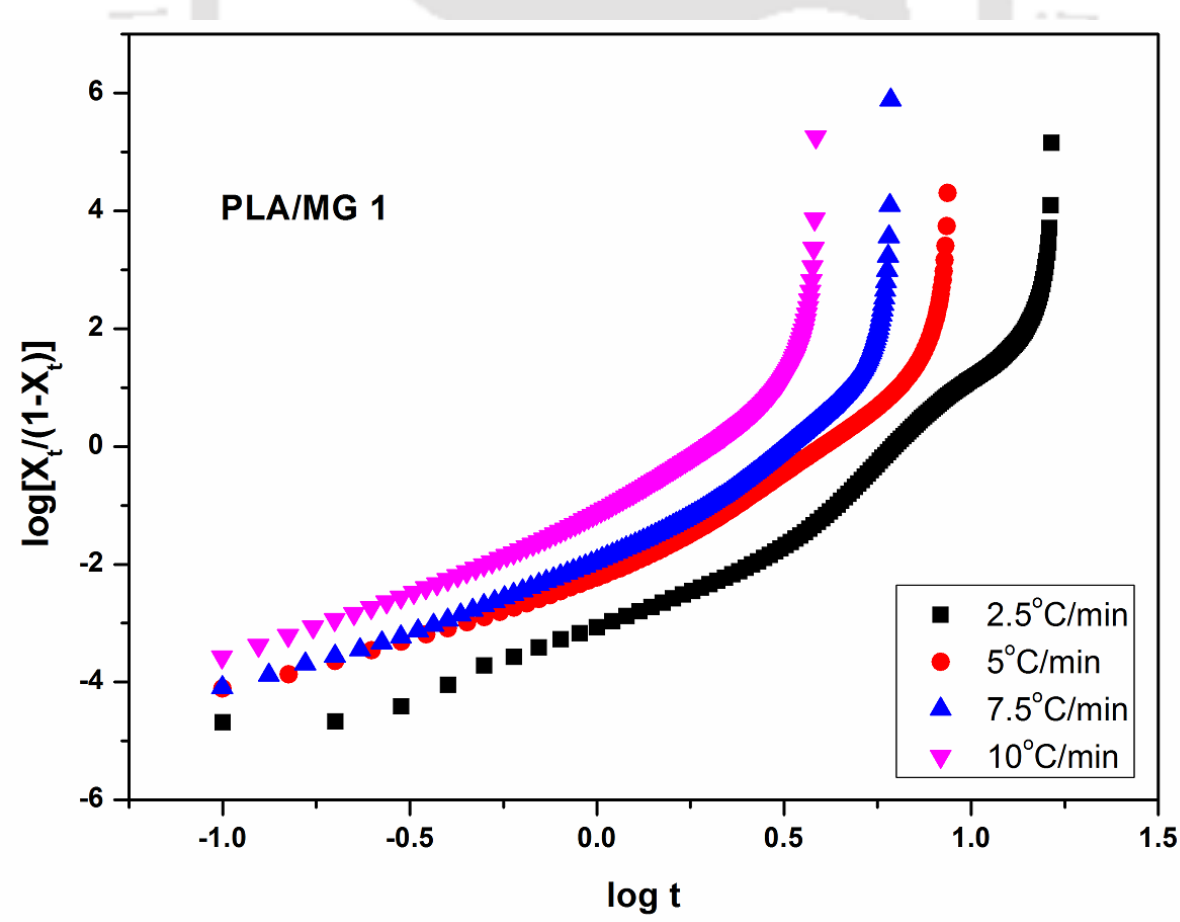
PLA/MG 1
log[X/(1-X)]
log t
2.5°C/min
5°C/min
7.5°C/min
10°C/min

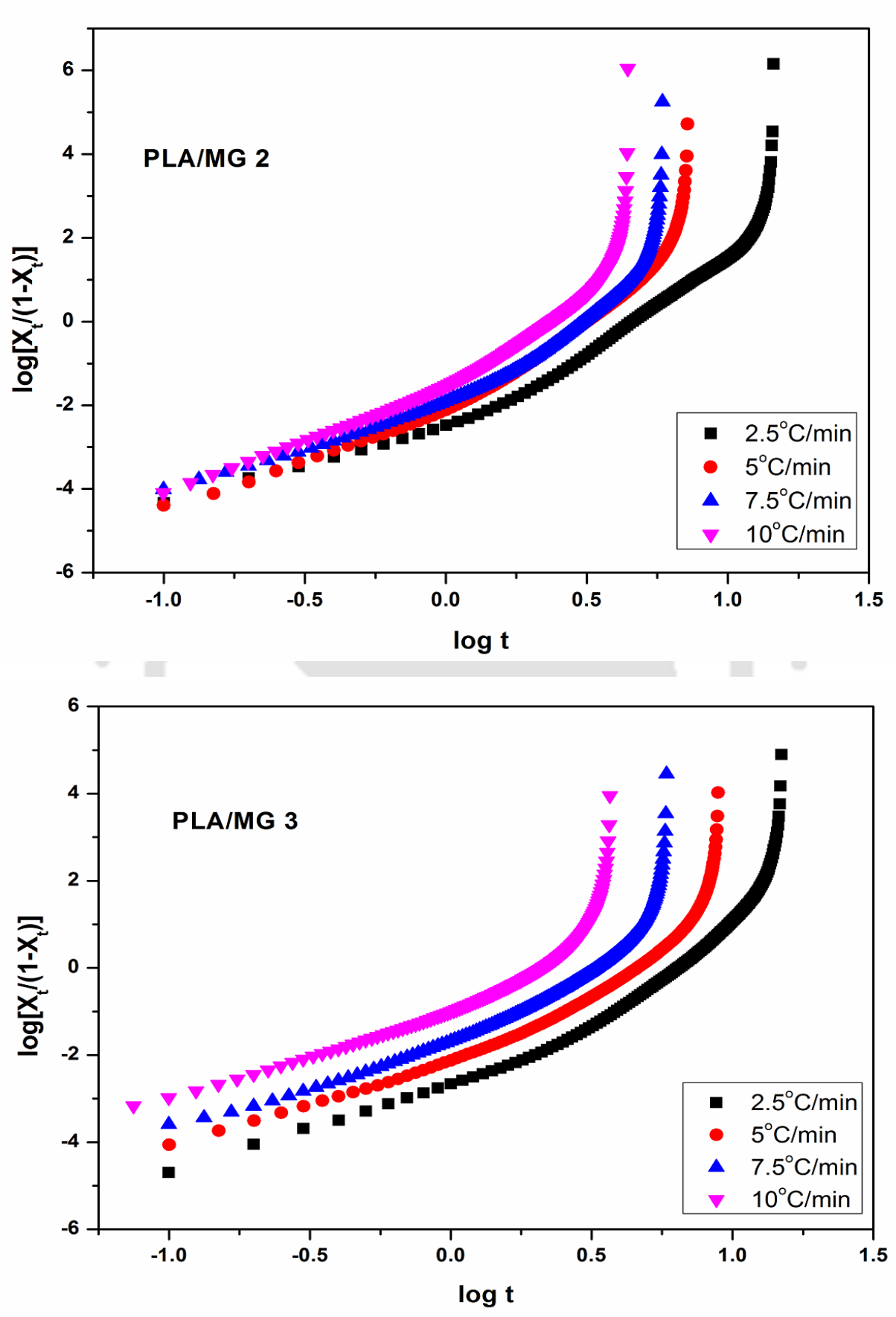

Fig. 5.16 Tobin Plots of PLA and PLA/MG-based foams.

5.4 Hydrolytic degradation studies of PLA and PLA/MG-based foams

The hydrolytic degradation investigations of the PLA and PLA/MG-based fabricated foam samples are shown in **Fig. 5.17**. The different analytical techniques are utilized to investigate the hydrolytic degradation of the fabricated foams. The samples are degraded at 35 °C and 55 °C and analyzed after 120 h of degradation. The temperatures are selected as per different literature available [158,159]. It can be visually observed from the figure that degradation is more prominent at elevated temperature as compared to lower temperature. The increase in degradation at elevated temperature might be due to the chain mobility and formation of low molecular weight products. Also from the figure, it is observed that degradation is more prominent in the basic and acidic medium compared to the neutral solution.

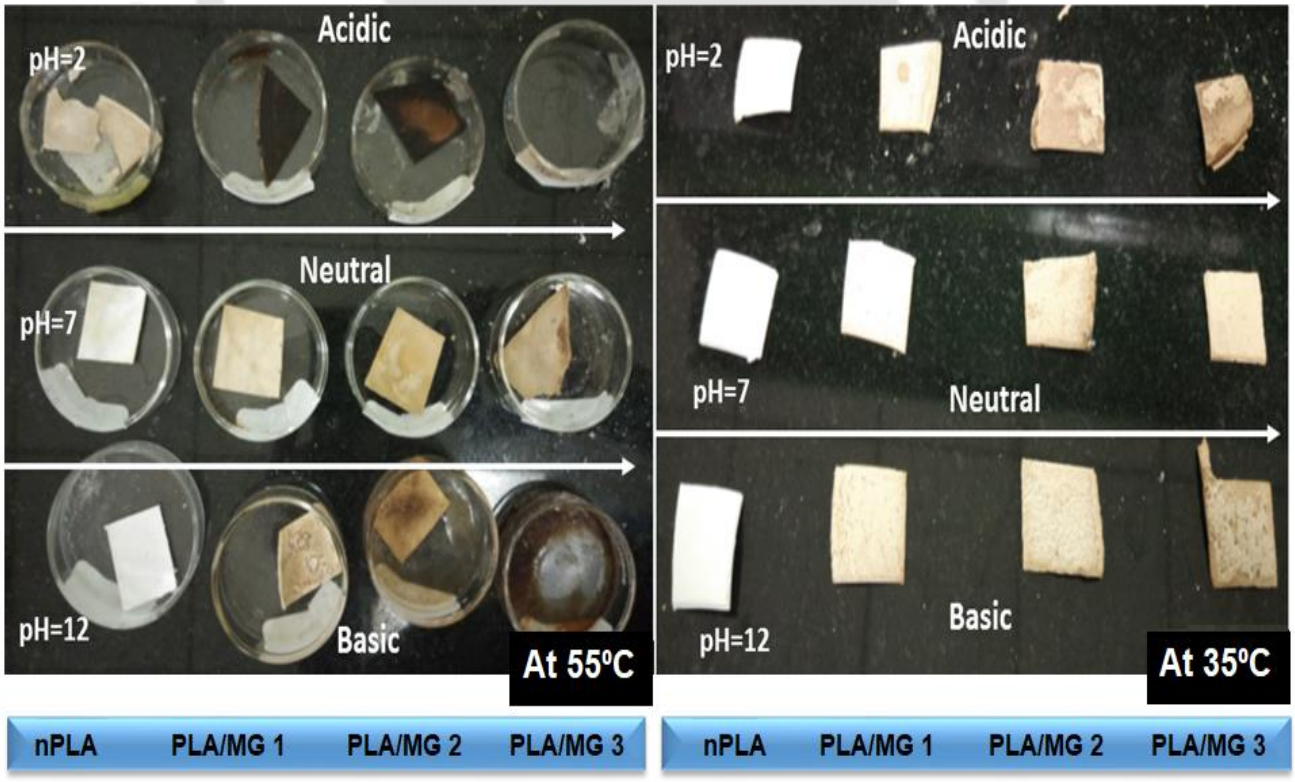

Fig. 5.17 Visual observation of degraded PLA and PLA/MG-based foams after 120 h.

The residual weight (%) of the hydrolytically degraded PLA and PLA/MG-based foams observed at an equal interval of time as represented in **Fig. 5.18**. It can be observed from the figure that degradation is more significant in the acidic medium and basic medium compared to neutral medium in hydrolytic degradation. At elevated temperature (55 °C), the weight residue (%) decreases than at 35 °C. The decrease in weight residue (%) might be due to the formation of short chains oligomers in the matrix and movements of PLA chains. Degradation proceeds via mechanisms like random chain scission, surface erosion, chain cleavage and so on [234,235]. The degradation at basic medium is more noticeable due to the presence of –OH group which attacks the ester linkage present in PLA structure [236,237]. The degradation rate observed from the figure can be divided into three regions: initially the degradation is faster followed by mid degradation stage and finally, a steady degradation region is observed in the figure. the similar trend is followed by all the fabricated PLA and PLA/MG-based foams [238–240].

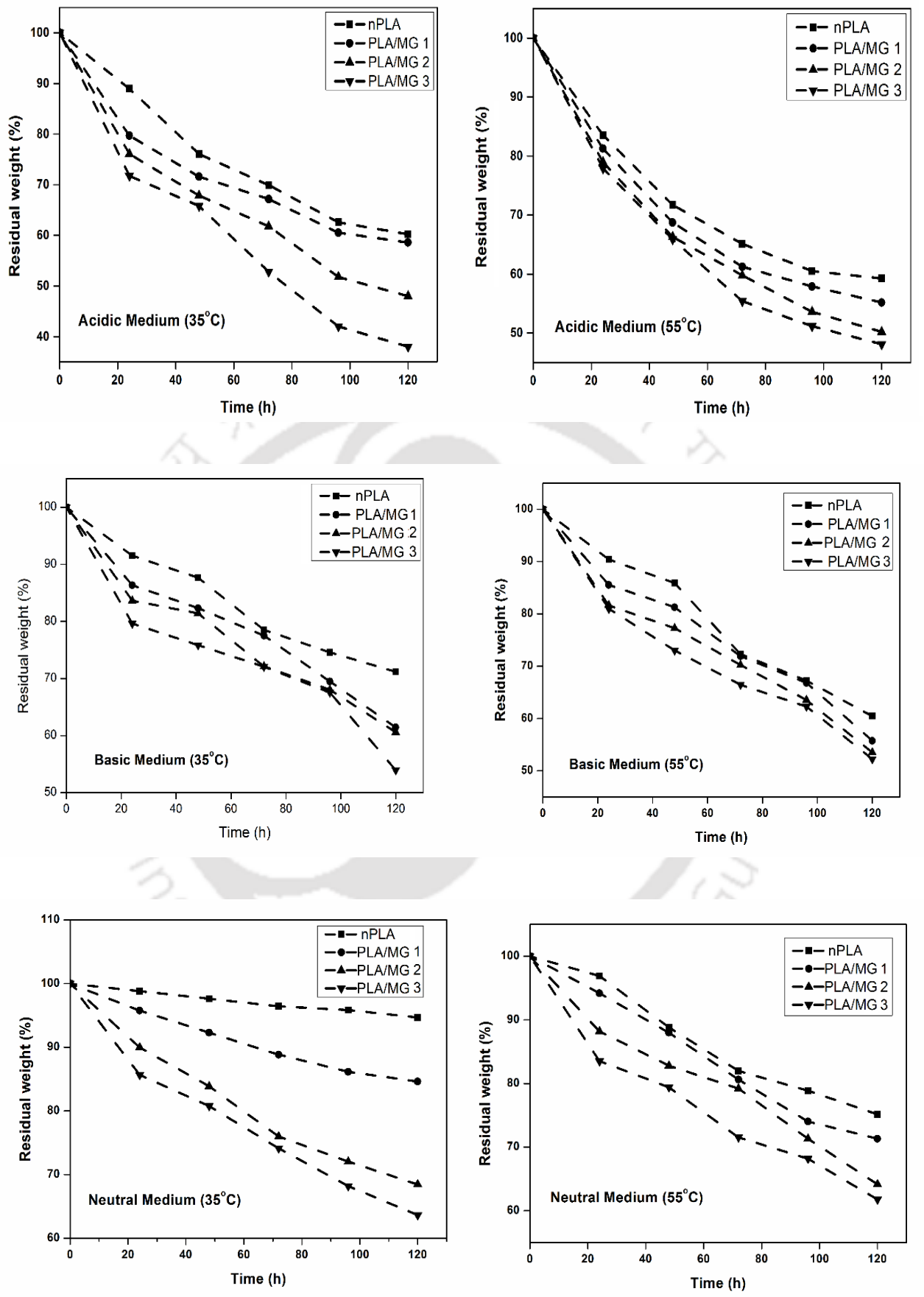

Fig. 5.18 Residual weight of PLA and PLA/MG-based foams for 120 h.

The degradation in presence of water in PLA-based foams can be represented by the following reaction

$$-COO- + H_2O \rightarrow -COOH + HO- \qquad (5.1)$$

The degradation in the alkaline medium of PLA-based foam proceeds via chain-end cleavage [241–243]. The morphology of the foamed structure and the available surface area for degradation is also responsible for the degradation rate. The generation of smaller pores in the PLA/MG-based foam increases the surface area, thus the available surface for degradation is higher, which generates of more degradation cites in the matrix. The hydrolytic degradation is more effective in the surface compared to the core [244]. Further, surface erosion are also taken place on the surface by the surrounding medium [245–248].

The XRD plots for degraded PLA and PLA/MG-based foams are shown in **Fig. 5.19** at 35 °C and 55 °C. The crystalline region of the PLA is more hydrolytic resistant compared to the amorphous region. In the initial stages of hydrolytic degradation, the assess ability of water molecules to the ordered crystalline region is difficult compared to the chains present in the amorphous region. The hydrolytic degradation initially takes place in the available amorphous region of the PLA by producing some water-soluble monomers and low molecular weight products. The crystalline region left over from the initial hydrolytic degradation in the polymer matrix is known as “crystalline residue” [244,249]. The second step of degradation is focused on the crystalline residues. The surrounding media has influenced the degradation of the chains present in the crystalline region and the amorphous chains present between the ordered crystalline region [250–254]. From the XRD the presence of crystalline residue in the PLA/MG-based system is clearly visible. The crystalline peaks are observed in the degraded foam samples indicating the degradation of the amorphous region. Sharp crystalline peaks are mainly observed in the acidic and basic medium compared to the neutral solution at 35 °C.

However, at elevated temperature (55 °C), crystalline peaks can be visualized from the plots in all the three mediums indicating the hydrolytic degradation of the amorphous region in all the fabricated PLA and PLA/MG-based foam samples. The peaks are more prominent in acidic and basic medium indicating the good agreements of results with a previously described section of residual weight (%)[255].

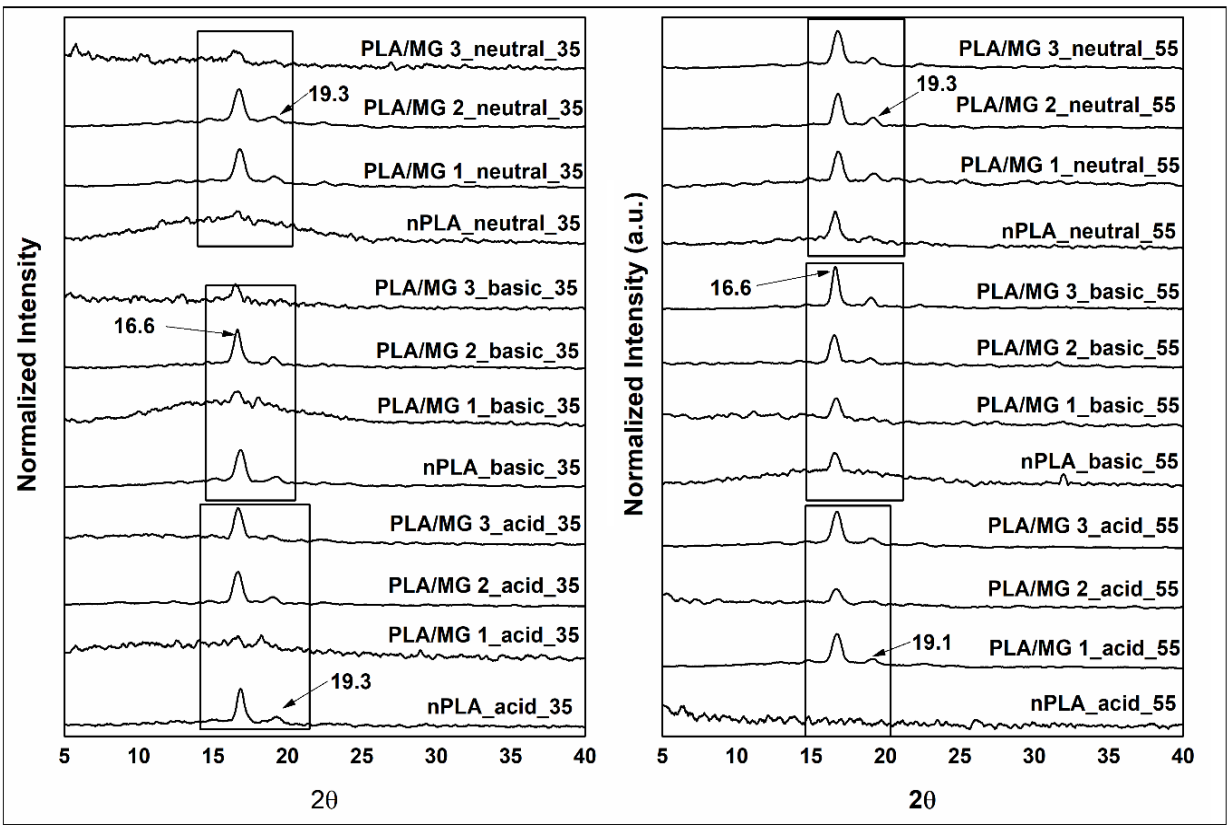

Fig. 5.19 XRD plots for degraded PLA and PLA/MG-based foams at 35 °C and 55 °C.

The morphological changes of the PLA and PLA/MG-based foams on hydrolytic degradation can be visualized from **Fig. 5.20.** The morphological changes in the degraded samples of PLA and PLA/MG-based foams can be easily visualized from the figure. Significant changes in surface morphology are visible in acidic medium samples of PLA/MG-based foam compared to untreated samples (**Fig. 5.2**). The rupture of cell wall and the development of cracks are more noticeable at an elevated temperature of degradation. The effect of degradation on surface

morphology of PLA/MG-based foam is more significant in acidic and basic medium. The change in morphology of the porous structure leads to the generation of larger pores in the structure, which may affect the wettability phenomena. From the morphological investigation, the effect of hydrolytic degradation on the cellular structure can be observed.

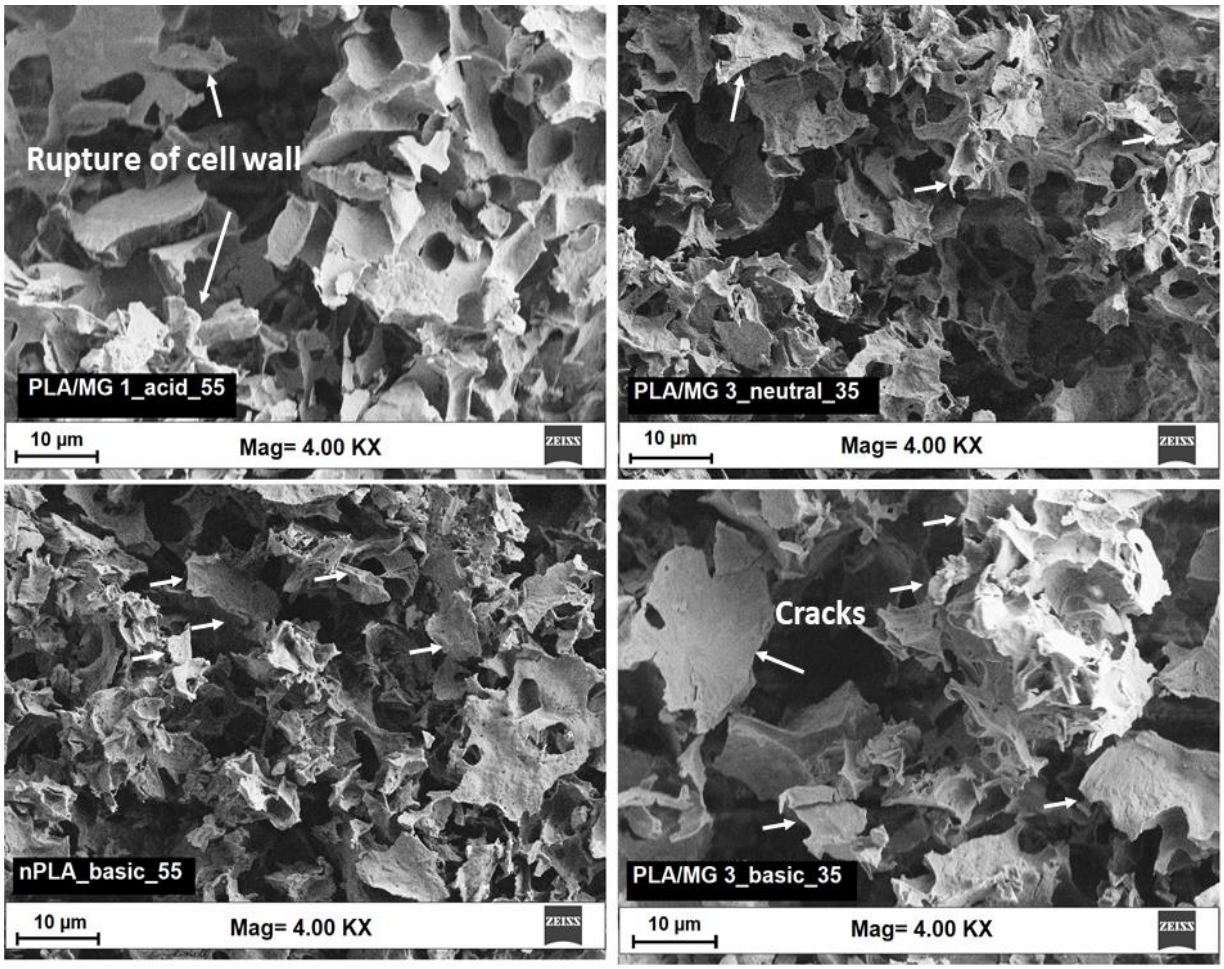

Fig. 5.20 FESEM micrograph of degraded PLA and PLA/MG-based foams.

The wettability phenomena of the hydrolytic degraded PLA and PLA/MG-based samples are investigated and the obtained contact angles are shown in **Fig. 5.21**. It is observed that the wettability is affected by degradation, where the change in contact angle is observed compared to the untreated PLA/MG-based foam samples. The change in wettability in the degraded samples might be due to the morphological changes as observed in FESEM. The breakage of

cell walls generated larger pores, which increases the water penetration in the foam structure and thus hydrophilicity increases. However, in the neutral medium, the contact angle is not effected much compared to other mediums. The decrease in contact angle is due to the cleavage of ester linkage by the hydrolytic degradation, resulting in formation of hydrophilic terminal end groups like hydroxyl and carboxyl groups in the PLA surface. Therefore, the hydrophilicity increases on increase in hydrolytic degradation [256–258].

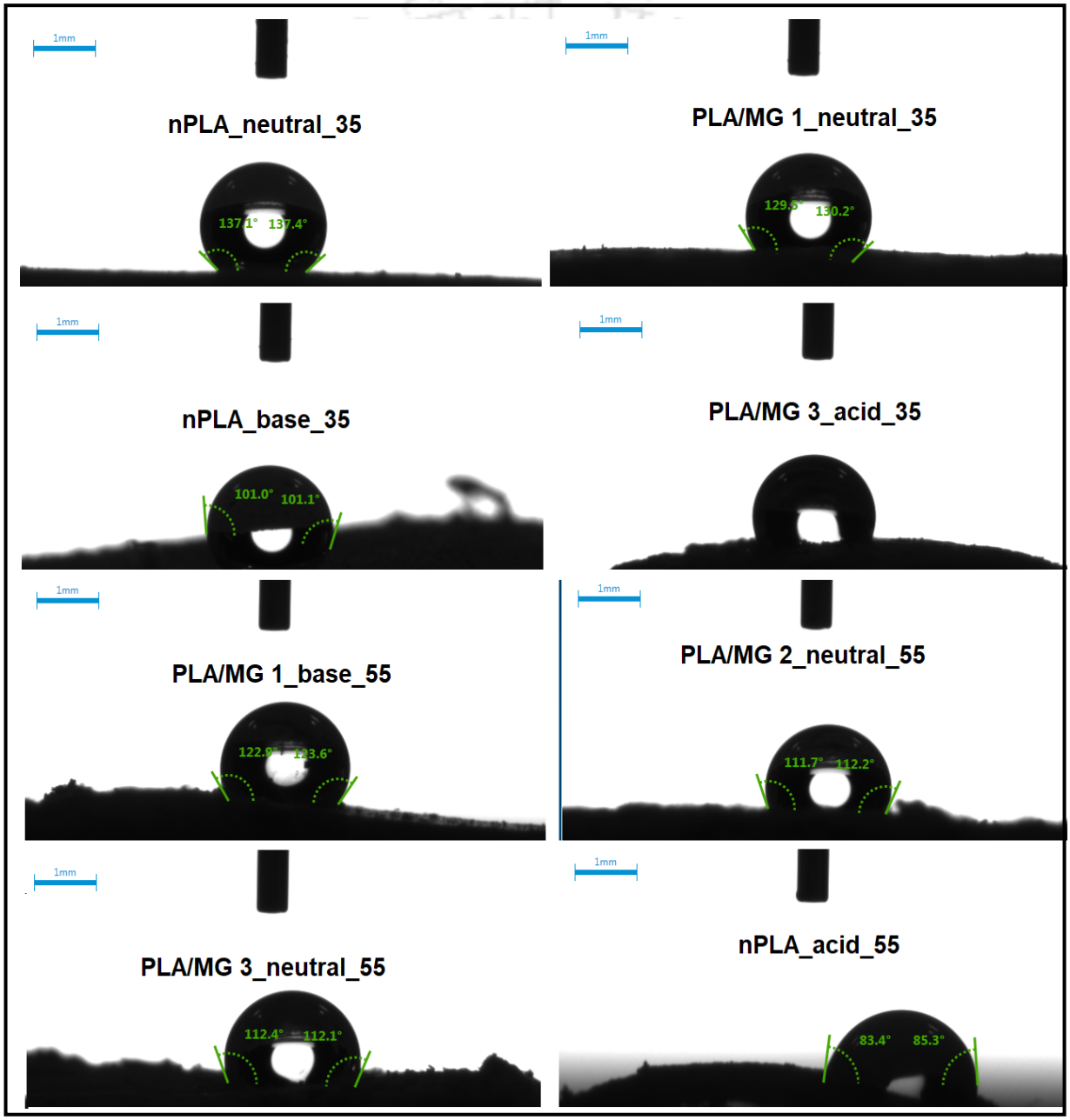

Fig. 5.21 Representative contact angle values for hydrolytic degraded PLA and PLA/MG-based foam.

The increase in hydrophilicity can be observed from the figure compared to untreated PLA and PLA/MG-based foam surfaces (**Fig. 5.10**).

Further, the molecular weight (M_w) investigation of the hydrolytically degraded PLA/MG-based samples are shown in **Fig. 5.22**.

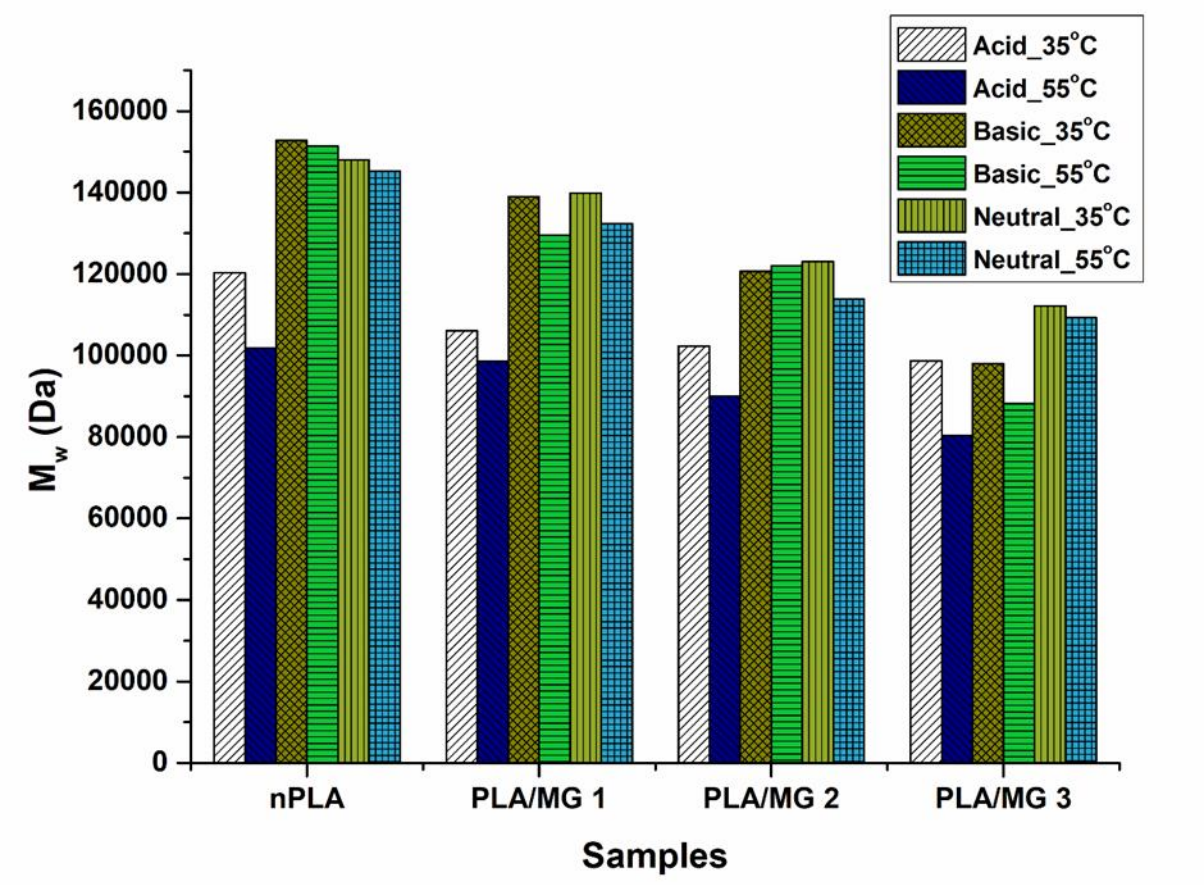

Fig. 5.22 Molecular weight investigations of the degraded PLA and PLA/MG-based foams.

The reduction in molecular weight can be observed in elevated temperature compared to lower temperature. Similarly, it is also observed from the figure that with an increase in MG, the molecular weight decreases due to the formation of short chains in the PLA matrix by the MG. MG acts as a plasticizing agent in the matrix by enhancing the chain mobility, which helps in the degradation process. In the elevated temperature, the mobility of polymeric chains increases, and thus increases the formation of low molecular weight monomers resulting in the

decrease of the molecular weight. The reduction in molecular weight is prominent in acidic medium and basic medium. In neutral medium, the reduction is comparatively less due to the fact that the degradation is low in the neutral medium as discussed in an earlier section.

The influence of hydrolytic degradation on thermal properties of PLA and PLA/MG-based foams has been investigated. The DSC thermograms of hydrolytic degraded samples are shown in **Fig. 5.23.**

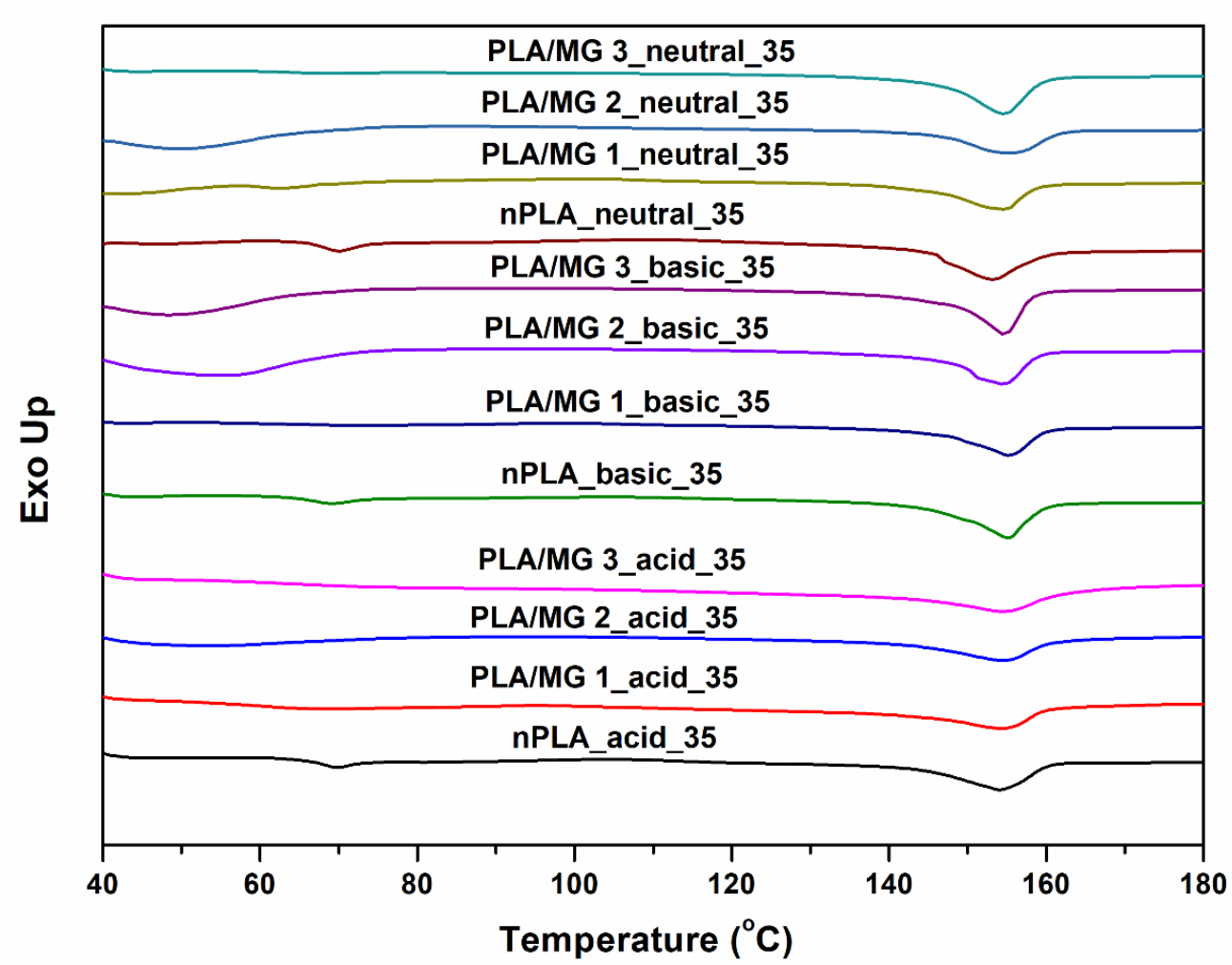

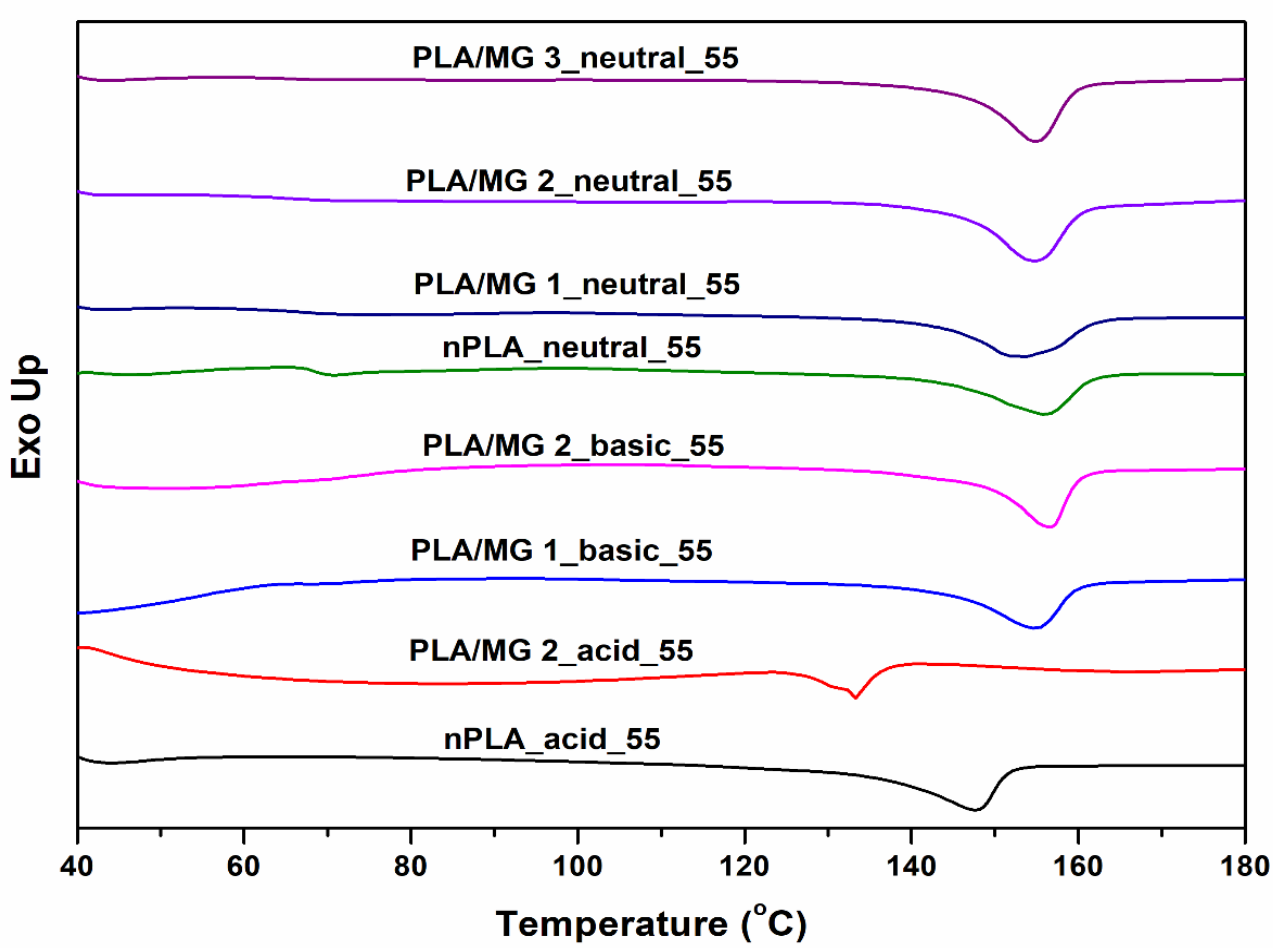

Fig. 5.23 DSC plots for PLA/MG-based foam at 35 °C and 55 °C.

From the DSC plots of the degraded samples, the decrease in the glass transition temperature (T_g) on hydrolytic degradation can be observed. The increase in chain mobility has occurred due to the reduction of molecular weights [255]. The decrease in melting point (T_m) of the hydrolytic degraded samples are observed from the figure above as compared to the untreated foam samples discussed earlier. However, the melting point reduction is more prominent in the acidic and basic medium compared to a neutral medium resulting from the decrement in the crystalline thickness and change in surface morphology of crystalline region [259]. The results obtained from DSC are in accordance with the previous results obtained in hydrolytic degradation as discussed earlier.

The thermal stability of the degraded PLA and PLA/MG-based foam samples are investigated by TGA. The TGA plots of the degraded foam samples are shown in **Fig. 5.24**. The onset temperature of degradation (T_{onset}) decreases on hydrolytic degradation. The reduction is prominent in acidic and basic medium as discussed earlier. It is also observed that on the incorporation of MG in the PLA matrix decreases the thermal stability on hydrolytic degradation. The plasticizing effect of MG is responsible for the reduction in thermal stability. MG enhances the molecular chain mobility in the PLA matrix. It can be observed that at elevated temperatures the thermostability reduces further due to the formation of low molecular weight oligomers. The maximum degradation temperature (T_{max}) is significantly reduced on the incorporation of MG in the acidic medium and basic medium as observed from the figure. A similar reduction in T_{max} can also be observed in the neutral medium but the magnitude of reduction is less compared to the acidic and basic medium.

From the above discussions on hydrolytic degradation investigations of PLA and PLA/MG-based foams, it can be concluded that hydrolytic degradation proceeds with surface erosion and breakage of cellular structure in the foam matrix and a change in morphology is observed in the foam surface. It is also noticed that the weight loss is more in acidic and basic medium.

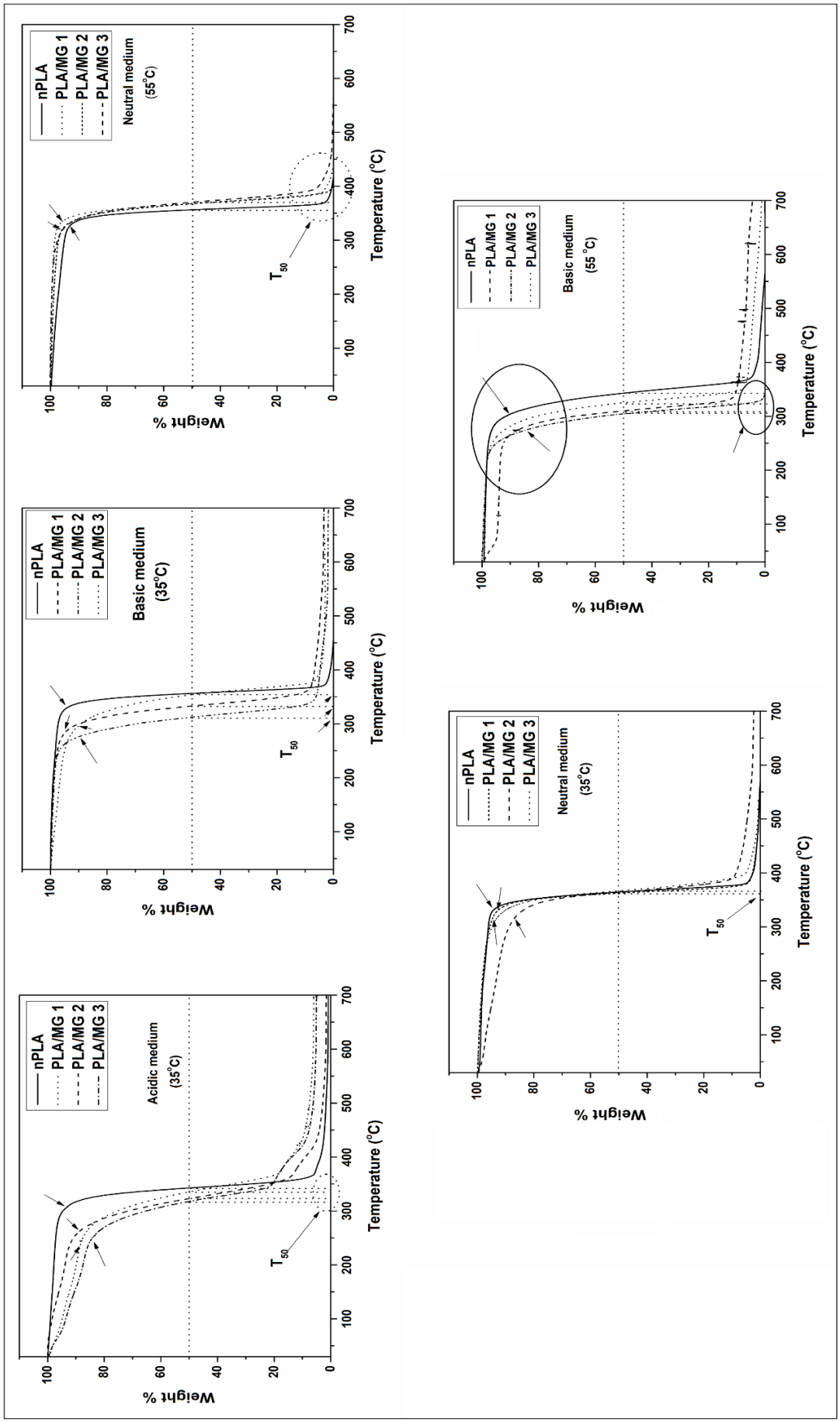

Fig. 5.24 TGA plots for hydrolytic investigation of PLA/MG-based foam.

The hydrolytic degradation also affects the wettability and thermal properties of the PLA/MG-based foam samples. It is also noticed that MG reduces the thermal stability on hydrolytic degradation and it is more prominent at elevated temperature.

5.5 Photodegradation (UV-irradiate) of PLA and PLA/MG based foams

The UV-irradiated photodegradation of the PLA and PLA/MG-based foams samples are investigated by using different analytical techniques. The fabricated foam samples are exposed to UV light and investigations has been performed after 1 week, 2 weeks and 3 weeks of exposure to UV light. The change in color of PLA/MG-based foam samples is observed after UV exposure. The fading of color is more significant after the higher time of UV exposure. The colorimetric investigations of the photodegraded foam samples are illustrated in **Fig. 5.25**.

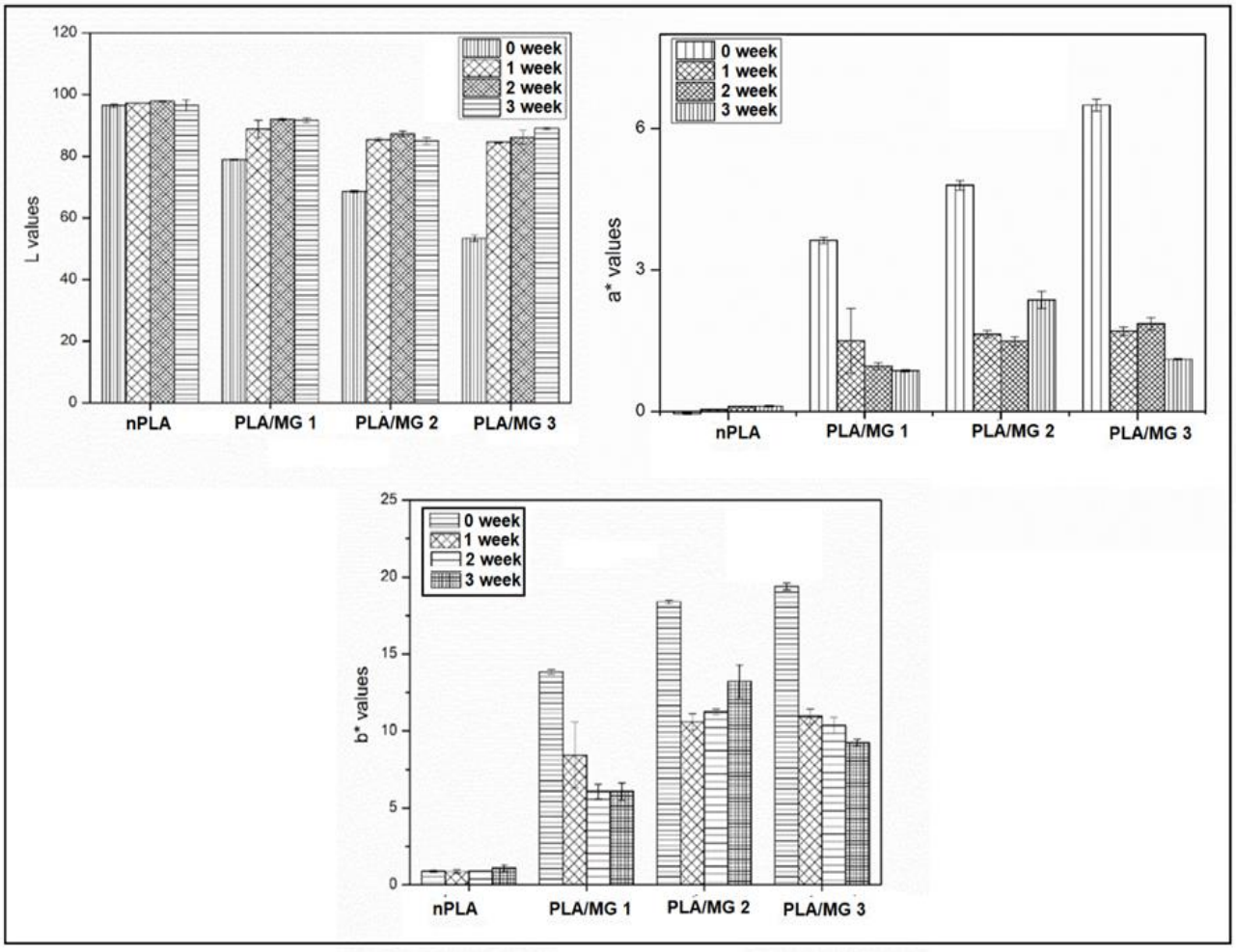

Fig. 5.25 Colorimetric values of photodegradation studies of PLA/MG-based foams.

The change in color parameters is observed on photodegradation due to the presence of MG in the matrix along with the photoexcitation of –C=O linkage present in the PLA structure. The photoexcitation causes some chemical reactions in the PLA like α and β cleavage, atom abstraction, radical addition and so on [260,261]. The –C=O chromophore group is highly reactive to UV radiation. Due to the photochemical reactions, the fading of color is observed in the PLA/MG-based foams. The change in color parameters on UV exposure is illustrated in **Fig. 5.25**. The change is more prominent in higher weeks of UV exposure. From the figure, it is observed that the change in L* parameter is more prominent in PLA/MG-based foams compared to PLA. The dark brown color of MG might be responsible for this change. On UV exposure, the fading of color is observed. The addition of MG affects the whiteness value of the fabricated PLA/MG-based foams. The increment in whiteness can be observed in PLA/MG-based foams with a higher period of UV exposure. The greenness of the PLA/MG-based foams is also increased on UV exposure. Similarly, form the figure it is observed that the value of b* parameter decreases on UV exposure suggesting the decrease in yellowness in the PLA/MG-based foams on UV exposure. The photochemical reactions like transfer of electrons (n-π*), atom abstraction etc. in the PLA under UV exposure might be the reason behind the change in color [118,262].

The morphological investigations of the photodegraded PLA and PLA/MG-based foam samples are illustrated in **Fig. 5.26**. The FESEM micrographs of the UV exposed surfaces of foam indicates the change in cellular morphology. The absorption of UV energy causes changes like the development of cracks and breakage of cellular structure in the PLA/MG-based foams as compared to the unexposed PLA/MG-based foams as discussed in earlier section 5.2.1 in **Fig. 5.2 and Fig. 5.3**. The change in morphology is more prominent at higher exposure periods. Development of cracks and rupture of cell walls is more significant in PLA/MG-based foams compared to nPLA. The change in surface morphology of the

photodegraded foam can influence various properties like wettability and thermal properties. The photodegradation also affects the molecular weight.

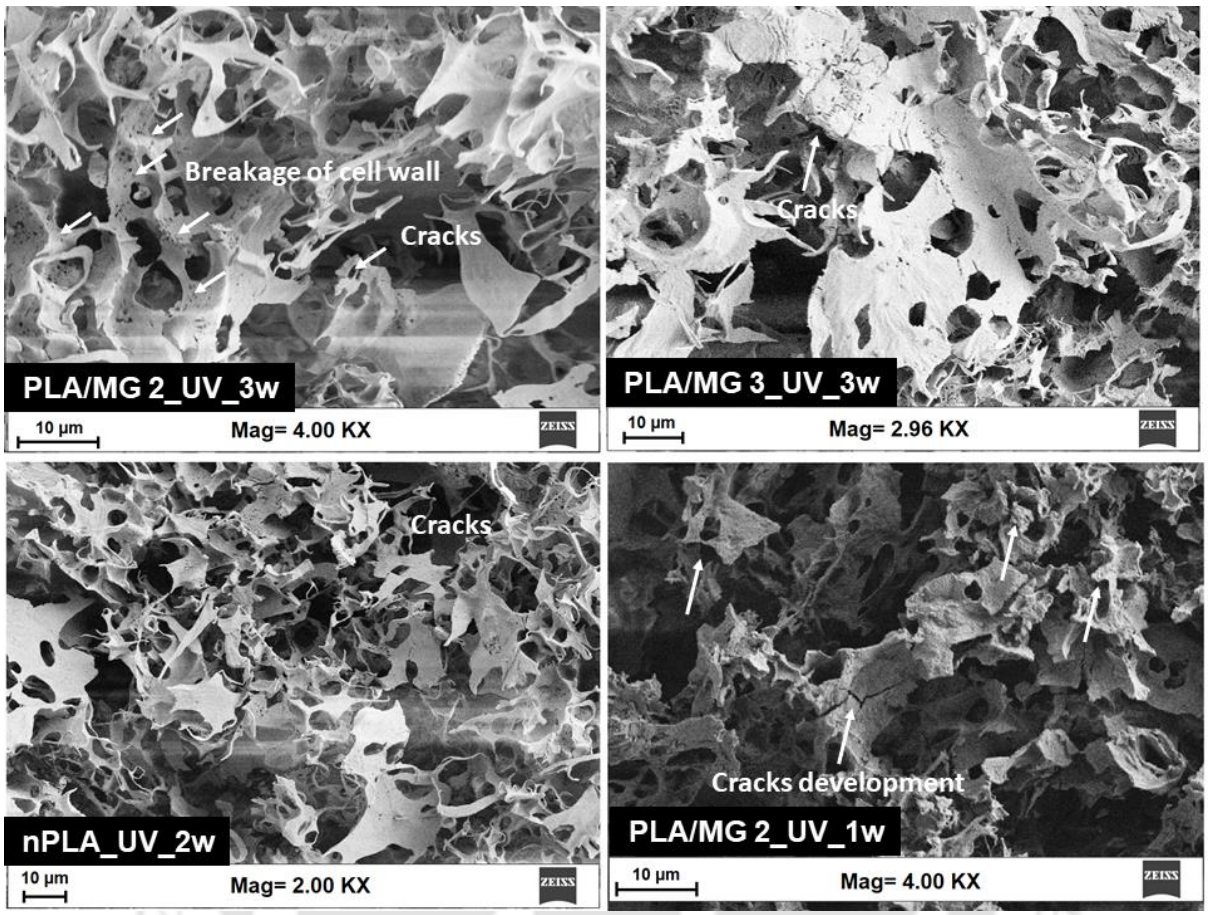

Fig. 5.26 FESEM micrographs of photodegraded PLA and PLA/MG-based foam.

The change in cellular morphology of the UV exposed foam samples can be clearly visible in FESEM micrographs. The MG effects the degradation of PLA/MG-based foams as compared to neat PLA as suggested by the FESEM above.

The wettability investigations of the photodegraded PLA and PLA/MG-based foams are shown in **Fig. 5.27**. The change in contact angle is observed for the PLA based photodegraded foams. The decrease in contact angle is observed for nPLA and PLA/MG 1 foams with UV exposure period. However, no such trend is observed for PLA/MG 2. However, at higher loading of MG (PLA/MG 3), the decrease in contact angle is observed. The change in wettability phenomena of the photodegraded PLA/MG-based foams might be due to the change in surface morphology

as suggested by FESEM. The development of cracks and breakage of the cell wall in the PLA/MG-based foams on photodegradation impacts the wettability. The incorporation of MG further enhances the degradation due to its plasticizing effect and formation of oligomers in the matrix. The wettability phenomena are influenced by the change in cellular morphology and the MG nanobiofiller present in the PLA matrix under the exposure of UV irradiation.

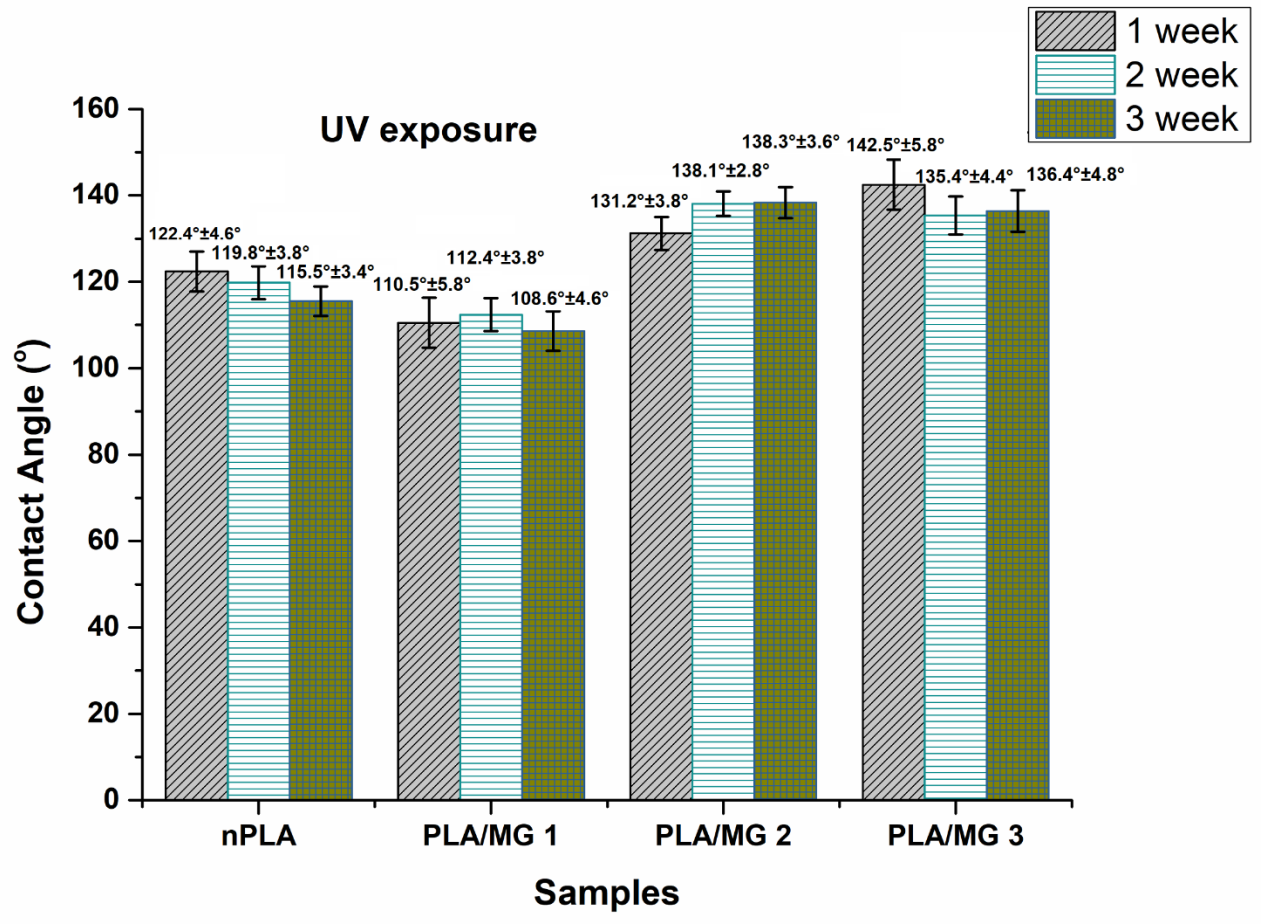

Fig. 5.27 Wettability investigation of PLA and PLA/MG-based foam.

The molecular weight (M_w) investigations of the photodegraded PLA/MG-based foam samples are shown in **Fig. 5.28**. It can be easily observed from the figure that the molecular weight decreases on UV irradiation. In all the cases of PLA and PLA/MG-based photodegraded foam samples, a reduction in molecular weight is observed with the UV irradiation. The reduction in molecular weight might be due to the photodegradation effect on the PLA. It can be easily noticed from the GPC results that reduction of molecular weight is more significant in the

PLA/MG-based foams compared to nPLA. The reduction of molecular weight is observed for PLA/MG-based photodegraded foams. The reduction is more prominent on samples of higher loadings of MG.

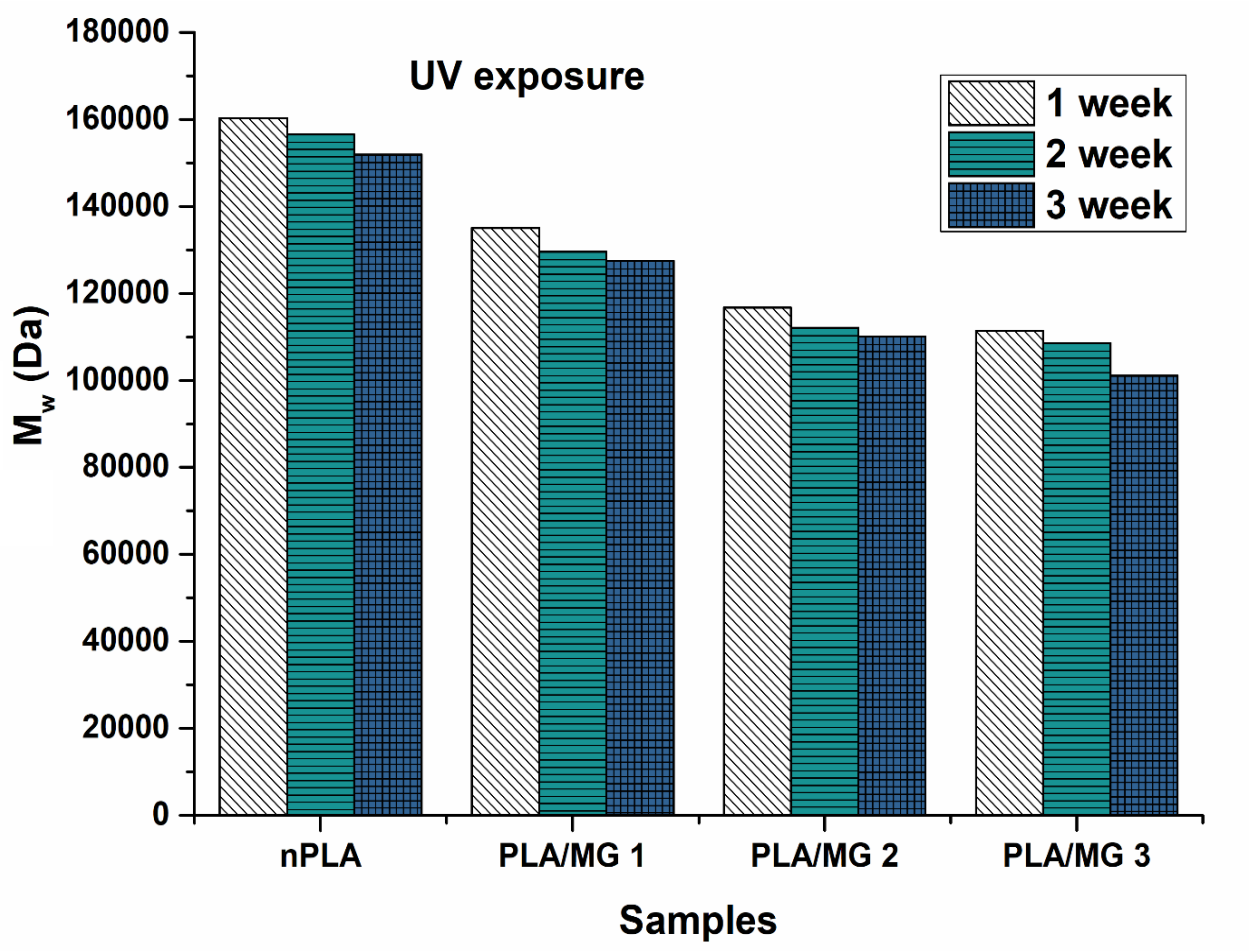

Fig. 5.28 Molecular weight investigation of photodegraded PLA and PLA/MG-based foam.

The highest decrement of molecular weight is observed for PLA/MG 3. The incorporation of MG in the PLA matrix has plasticizing effects, which increases the chain mobility and increases the formation of low molecular weight oligomers on UV irradiation. The degradation observed is mainly due to the absorption of UV light by C=O groups and via n-π* electron transfer and resulting in the formation of chromophores [4,260]. The other groups present in PLA such as C-C and C-H absorbs wavelengths below 180 nm. In the case of PLA/MG-based foams, the presence of MG influences the degradation of molecular weight in the presence of UV light.

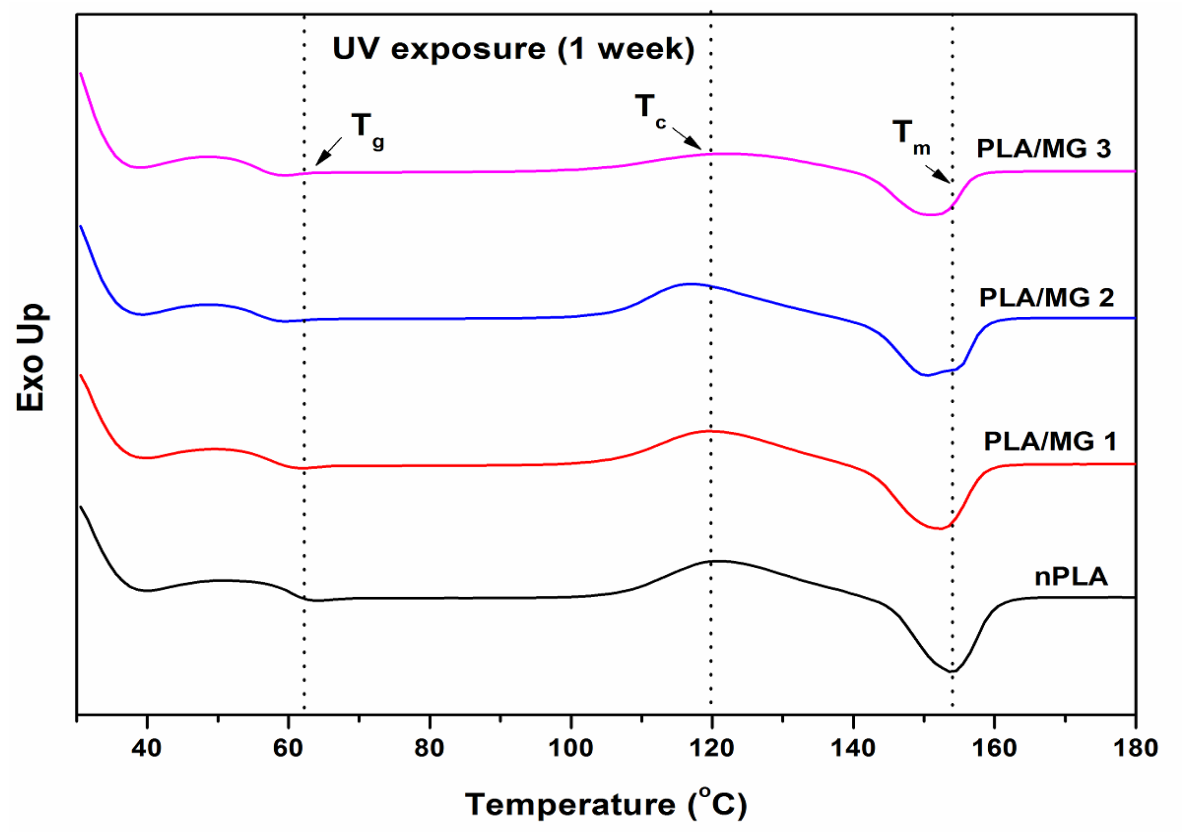

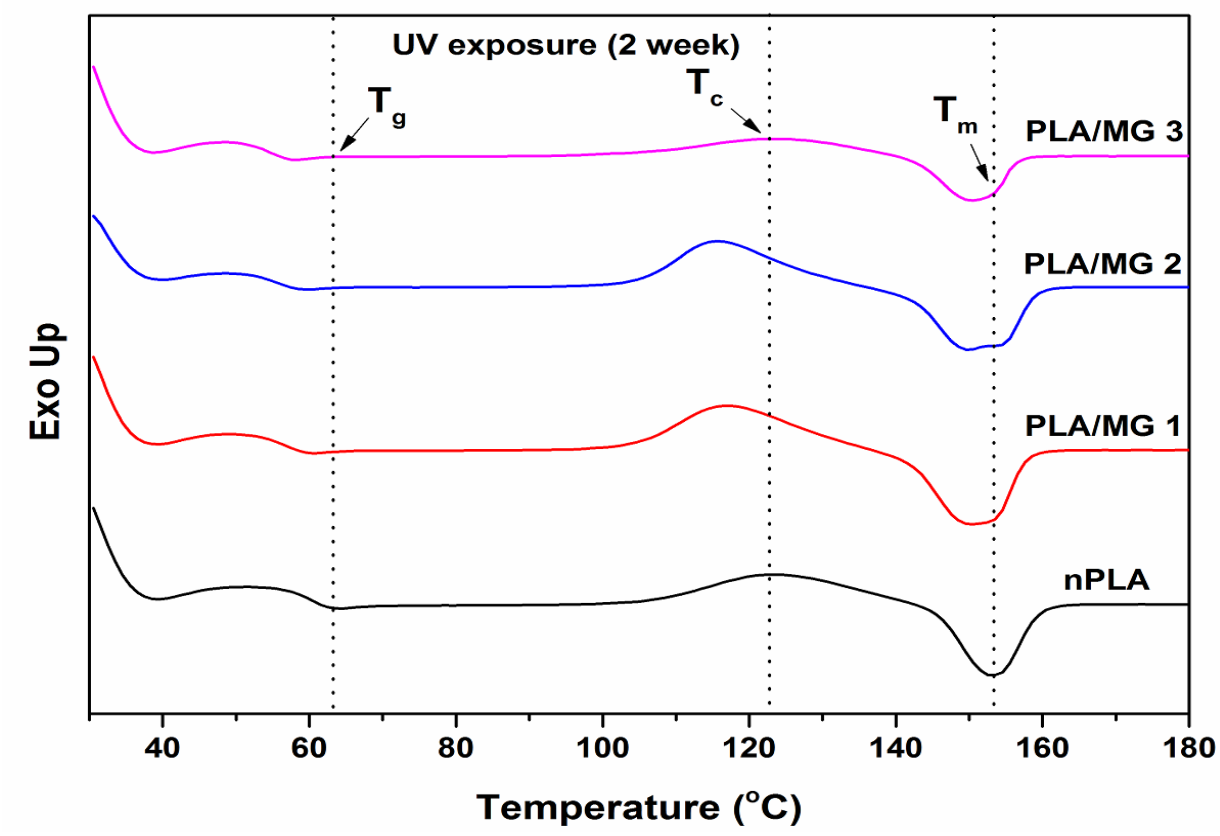

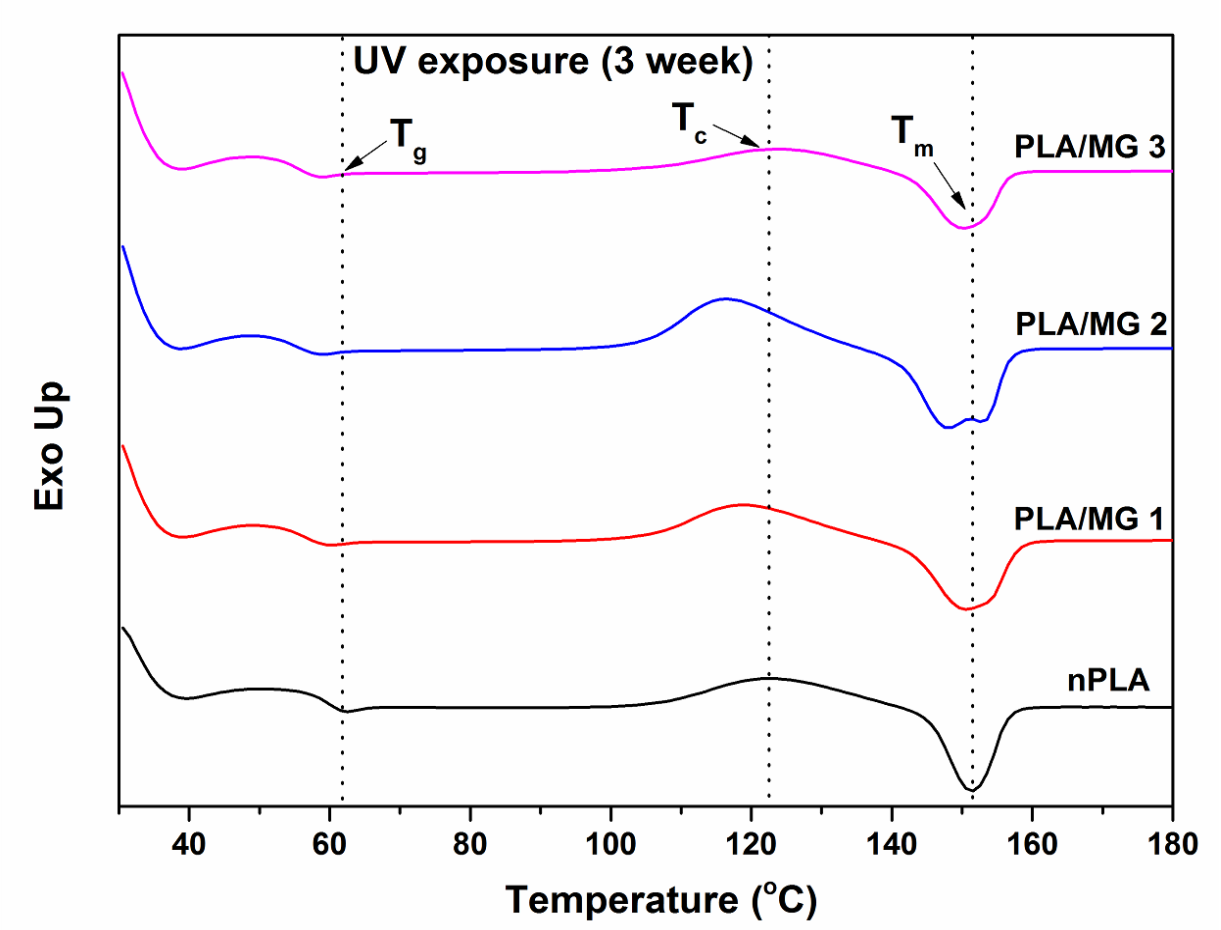

Fig. 5.29 DSC thermographs of photodegraded PLA and PLA/MG-based foam.

The thermal property of the photodegraded PLA and PLA/MG-based foams are investigated by DSC and TGA. The DSC plots of the PLA and PLA/MG-based foams under UV exposure of 1 week, 2 weeks and 3 weeks **(Fig. 5.29)**. The decrease in glass transition temperature (T_g) is observed with the increase in the concentration of MG in the PLA matrix. The decrease in glass transition is the evidence of the formation of short chains in the matrix. The decrease in T_g is more prominent in PLA/MG 3. On UV exposure, the T_g further decreases with time of exposure indicating the formation of short-chain low molecular weight products. Similarly, the reduction in melting point is also observed with an increase in UV exposure time indicating the structural change in the crystalline region and reduced size of the crystal. Therefore, it can be observed that UV influences the crystal structure along with structural surface changes in the foam matrix.

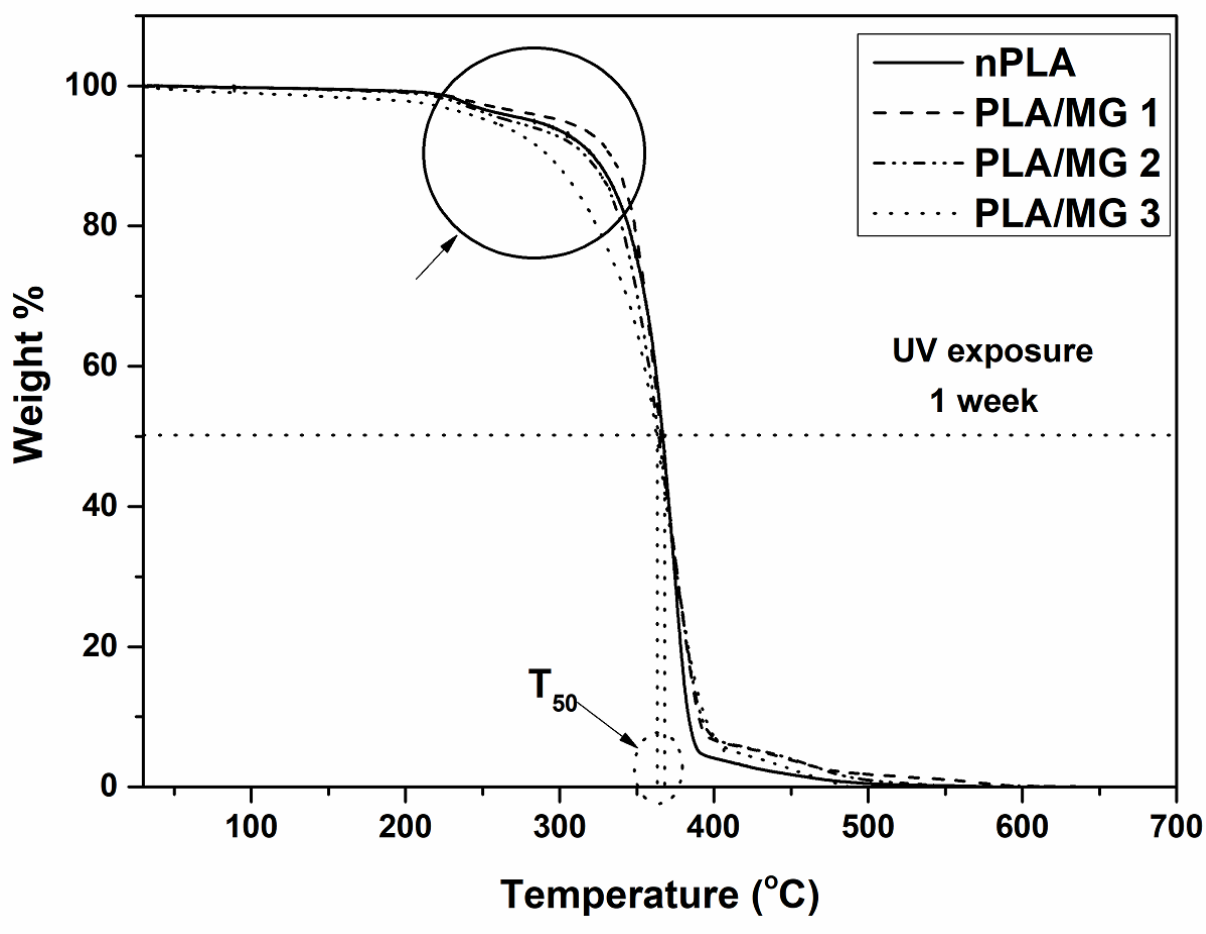

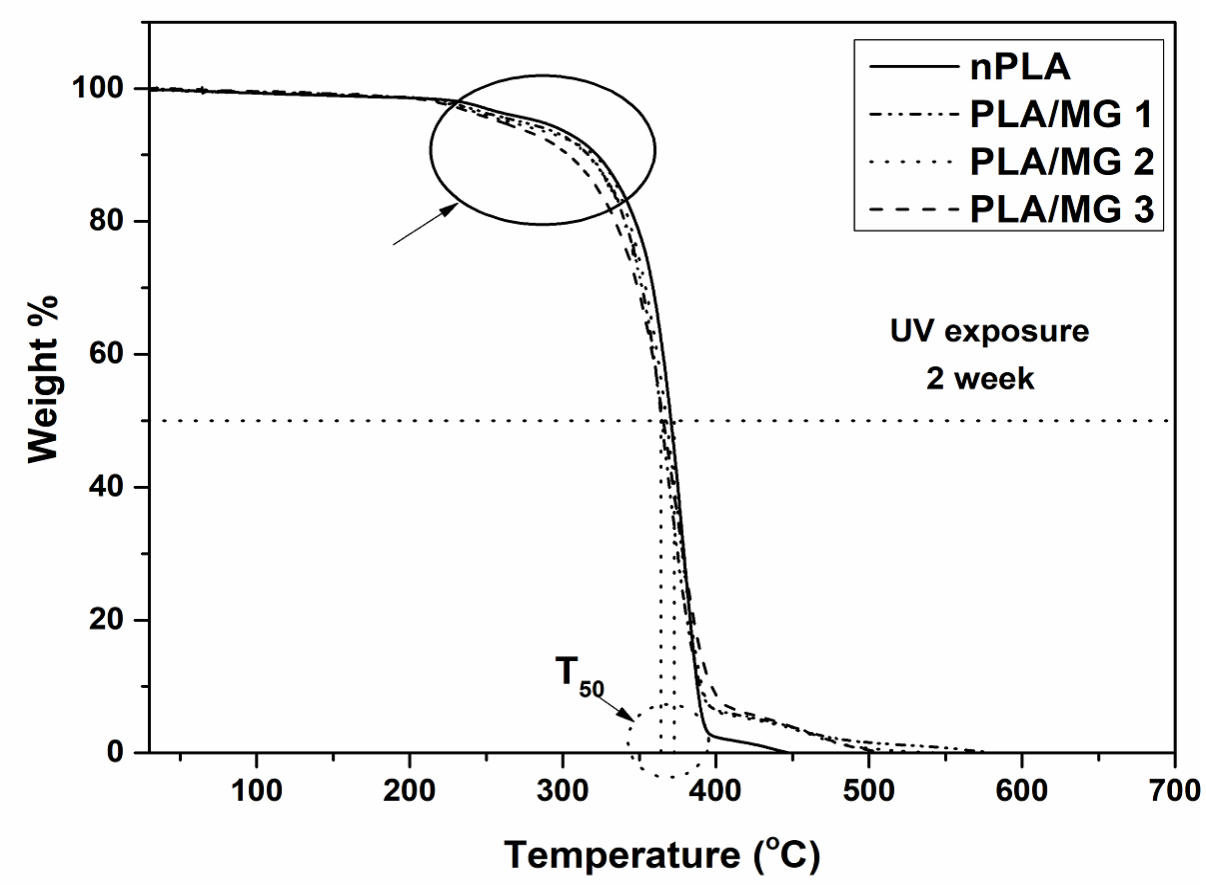

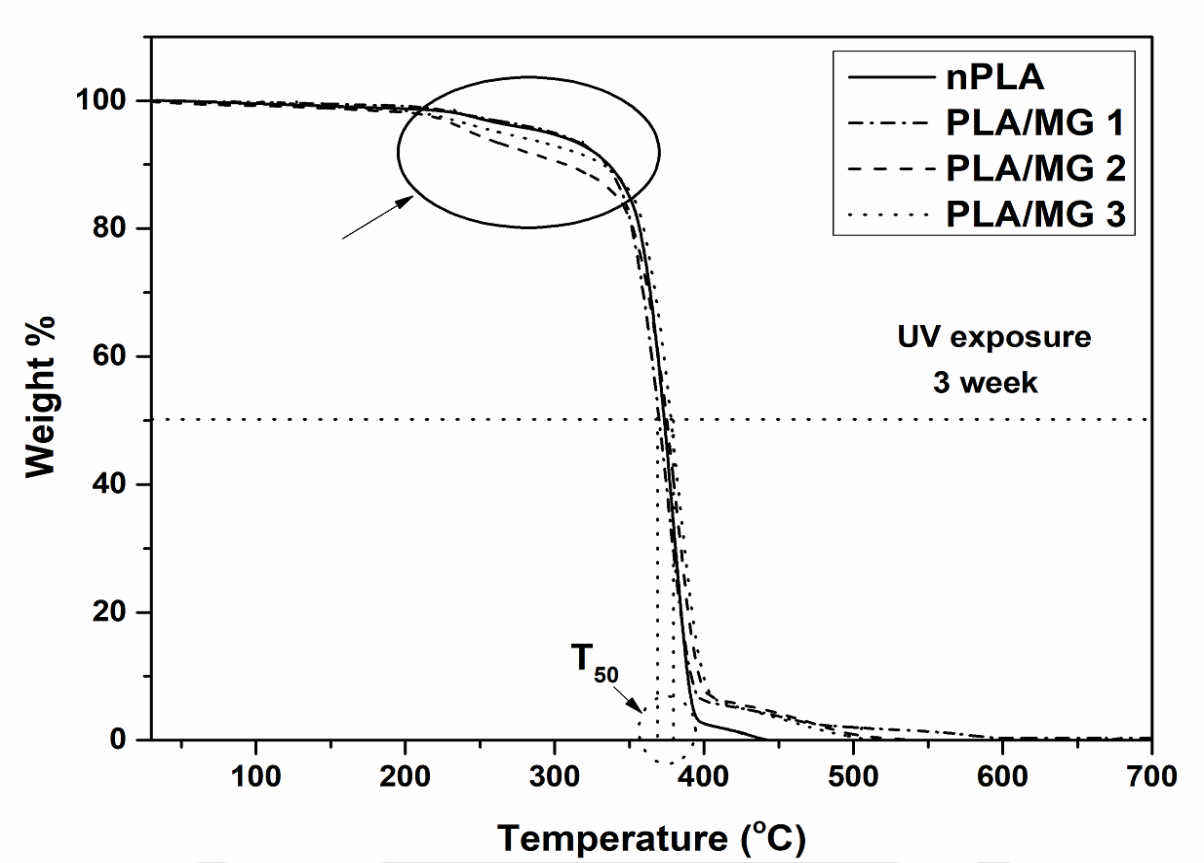

Fig. 5.30 TGA plots of photodegraded PLA and PLA/MG-based foams after UV exposure.

The TGA plots of the UV exposed PLA and PLA/MG-based foams can be observed in **Fig. 5.30.** From the figure, the reduction in onset degradation temperature (T_{onset}) can be observed with an increase in UV exposure time of the PLA and PLA/MG-based foams. It is also observed that with the incorporation of MG, the T_{onset} value further decreases. The decrement in T_{onset} is more prominent for samples of higher UV exposure compared to the low exposure time. The reduction in maximum degradation temperature (T_{max}) is also observed with UV exposure time. It is also observed that at a higher exposure time of 3 weeks under UV irradiation, the PLA/MG-based foams thermally degraded faster and the thermal stability is also affected. The thermal stability of nPLA is also reduced with UV exposure but the reduction is lesser than the PLA/MG-based foams.

From the photo degradation investigations of the PLA and PLA/MG-based foams, it can be concluded that UV irradiation effects the surface morphology of the fabricated foams. The wettability, molecular weight, and thermal properties are also deeply affected by UV degradation. The incorporation of MG enhances the degradation process and reduces the thermal stability and other properties under UV exposure.

5.6 Summary

This chapter demonstrates the fabrication of microcellular, interconnected, hydrophobic and highly porous PLA based foams applying an innocuous and cost-effective technique using sucrose as a porogen medium. A ~86% reduction in density is observed in PLA/MG based composites than PLA granules. Effect of MG in cell size and cell density of the fabricated foams can be observed from FESEM. A decrement of ~7% in crystallinity is also observed in fabricated foams might be due to the plasticizing effect of MG. The thermomechanical and thermal investigations also indicate the plasticizing effect of MG. An increment of ~16% in water contact angle is observed for the highest loading than the neat counterpart. The hydrophobic nature of MG along with the surface texture might be responsible for the change in wettability behavior with MG. Porosimetric investigation reveals the increment of surface area and decrement of pore diameter with MG indicating the nucleating effect of nanofiller at lower concentrations. The increase in surface area, decrease in pore size and hydrophobic nature is favorable for biomedical applications. Further, investigations like colorimetry also suggest the effect of MG in the color parameters. Crystallization studies also suggest the nucleating effect of MG in the PLA matrix and both primary and secondary crystallization. The chapter provides a thorough analysis of the structure-property relationship of bio-based composite foam material having the ability for applications in the area of biomedical such as tissue engineering for preparing scaffolds. From the hydrolytic investigation, it is observed that PLA/MG-based foams are more prone to degrade in the basic and acidic medium compared to the neutral medium. The incorporation of MG also

influences the thermal stability and wettability more prominently at elevated temperature. The hydrolytic degradation effects the cellular structure of the fabricated foam. The surface morphology, cell size, and surface area also have influence in hydrolytic degradation of the fabricated foams. The photodegradation investigation also suggesting the influence of MG on degradation. The photodegradation effects the thermal properties, wettability and structural morphology of the fabricated PLA and PLA/MG-based foams. The MG nanobiofiller enhances the degradation process of the fabricated foams.

Chapter 6

Development of Silk-based Poly (lactic acid) Microcellular Composite Foams

This chapter mainly deals with the fabrication and characterization of PLA/silk nanocrystal (SNC) based foams. The structure-property relationship of the developed foams has thoroughly been discussed in this chapter. The crystallization kinetics along with other foam properties like cell density, cell size etc. has been discussed in the chapter. Porosimetric investigations of the fabricated PLA/SNC-based foams reveals the nucleating effect of the SNC. A brief comparative study on available literature of non-porous PLA/SNC system with PLA/SNC foam system is also included in this chapter. Thermal stability of the fabricated PLA and PLA/SNC based foams are thoroughly analyzed with the help of thermogravimetric analysis. It is observed that SNC improves the thermal stability of the fabricated PLA based foams. The hydrolytic and photodegradation behavior of the developed foams has been investigated in this chapter. This chapter provides useful information of the fabrication, effect of SNC in PLA foam properties, thermal stability and mechanism of degradation of the fabricated PLA and PLA/SNC- based foams for their probable applications in different biomedical and commodity areas.

Parts of this chapter are ready for communication as:

1. Shasanka Sekhar Borkotoky, Rahul Patwa, Tabli Ghosh, and Vimal Katiyar *"Silk nanocrystal (SNC) based Poly (lactic acid) (PLA) foams: structure-property relationships."* **(To be submitted to "Composite Science and Technology", Elsevier)**

2. Shasanka Sekhar Borkotoky, Tabli Ghosh and Vimal Katiyar *"Degradation studies of PLA and PLA/SNC based microcellular nanocomposite foams."* **(To be submitted to "European Polymer Journal", Elsevier)**

6.1 Introduction

The demand for bio-based and environmentally friendly products for day-to-day commodity applications leads to the development of various biodegradable polymeric products. However, still, petro-based non-degradable plastics mainly dominates the polymer market [263,264]. Researchers are now mainly focused on the development of bio-based cost-effective, low density and lightweight products, which can be a replacement to the petrol-based non-degradable polymers for commodity applications [265]. One of the useful way to reduce the cost by less use of material, which can be easily achieved by polymer foams. Polymeric foams have many advantages like low density, lightweight and less requirement of materials, which ultimately leads to the reduction in the cost of production [216,266]. Foams have been utilized in the various commodity as well as sophisticated biomedical applications. It almost penetrates in every field of applications where lightweight and low density is a prerequisite condition along with some rigid structural dimensions. Recent developments on polymeric foams are in lines with the improvement of properties by the addition of additives, plasticizers, nanobiofillers [111]. Some researchers are focusing on the green replacement of non-degradable polymeric foams by bio-based and biodegradable foams by enhancing its property to a comparable level. The properties of PLA is comparable with the conventional petrol-based polymers and it comes from a bio-based route [4]. A wide range of applications of PLA-based foams is recently observed. Addition of bio-based and bio-derived nanobiofillers can further improve its properties and helps in the disposal of biodegradable foams. These nanobiofillers also helps in environmental friendliness in the handling of the disposal. Development of new bionanofillers for tuning of PLA-based foams is now a prominent area of research.

Silk can be termed as nature's own nylon. Silk can be extracted from different insects. Silk has also had UV resistant property as demonstrated by some of the researchers [267–269]. Silk nanoparticles can be utilized as nanobiofillers to PLA matrix [75]. Preparation of silk

nanoparticles from Mulberry, Eri, and Muga has been demonstrated by some of the researchers [270–272]. Another investigation regarding the preparation of silk nanoparticles from silk fibroin was reported by **Kundu et al.** where dimethyl sulphoxide (DMSO) as a desolvating agent [273]. **Zhang et al.** demonstrated the fabrication process of silk fibroin nanoparticles (SFNs) with sizes ranging from 35-125 nm [274]. Some investigations have been observed for crystalline silk nanoparticles in the literature. **Tao et al.** demonstrated the preparation of crystalline silk fibroin (CSFs). They have utilized CSFs in the polyurethane matrix and investigated the properties. Some investigations have been observed for PLA/silk-based nanocomposites in available literature [45]. PLA/silk-based porous structured scaffolds were fabricated by **Wang et al.** where they have utilized electrospinning techniques to fabricate the porous structure with PLA fibers in the outer layer and silk in the inner layer [275]. Fabrication of well-controlled microcellular biodegradable PLA/silk composite foams has been reported in previous literature using silk fibroin powder at different concentration [75]. Dispersion of silk nanocrystals (SNC) on PLA matrix has been investigated by some researchers along with its application in cancer therapy [276,277].

However, no literature is available for PLA/silk nanocrystal (SNC)-based fabricated foams as per our knowledge of concern. It is observed from the literature that a knowledge gap exists on the fabrication of PLA and PLA/SNC-based foams and to investigate the effect of SNC on the foam properties of PLA such as cell size, cell density, wettability, thermal and crystallization behavior. In addition, a detailed investigation in different degradation methods has to be thoroughly investigated in order to understand the effect of SNC on PLA foam matrix.

This chapter demonstrates the development of PLA and PLA/SNC-based foams using casting and leaching (C/L) technique. Detailed investigation of the structure-property relationship of PLA/SNC-based foams has been reported in this chapter. Effect of SNC on the wettability phenomena and the porosimetric investigation has been discussed thoroughly. Detailed

investigations on the effect of SNC in hydrolytic and photo-degradation (UV) has been performed. This chapter will provide enough information regarding the effect of SNC on the PLA foam matrix and the probable application area of the fabricated PLA/SNC-based foams.

6.2 Results and discussions

This section discusses the results and observations obtained from different investigations along with scientific explanations and conclusions.

6.2.1 Porogen size analysis

The particle size distribution of prepared finely grinded sucrose particle (porogens) after 7 h and 12 h under continuous magnetic rotations are shown in **Fig. 6.1**. From the Delsa Nano investigations, it was observed that the particle size of sucrose was ~7.6 µm. However, after 12 h of magnetic stirring the porogen particle size was found to be ~1.9 µm, which was dispersed in the PLA matrix for the fabrication of PLA and PLA/SNC-based foams. The decrease in porogen particle size after rigorous magnetic stirring might be due to the collision effect between the dispersed porogen particles in 1,4 dioxane.

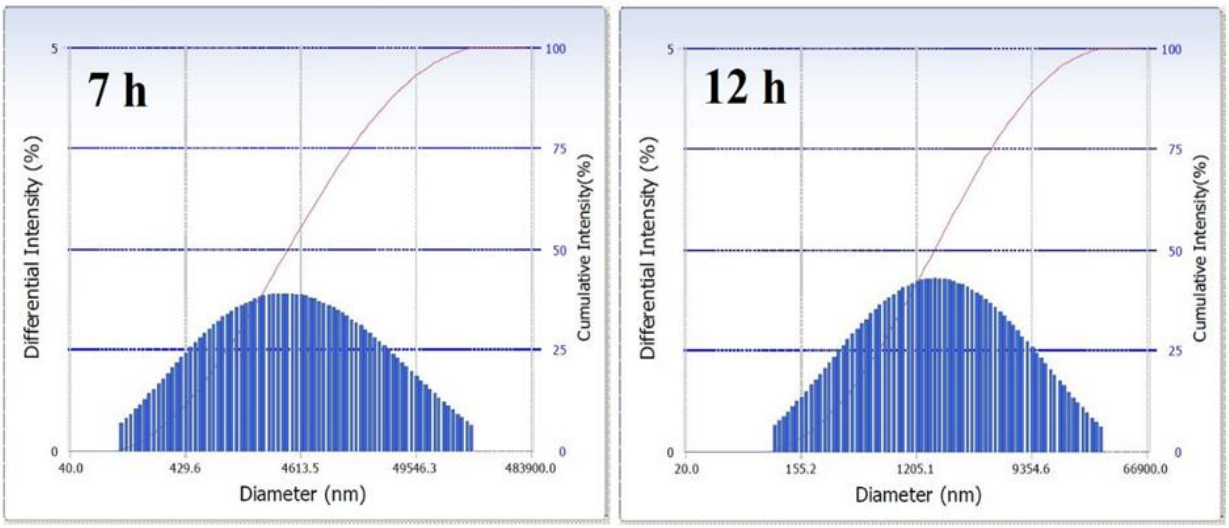

Fig. 6.1 Particle size analysis of sucrose (Delsa nano).

6.2.2 Morphological investigations

The morphological investigations of the fabricated PLA and PLA/SNC-based foams have been investigated by utilizing FESEM and FETEM. The FESEM micrographs of PLA and PLA/SNC-based foams are shown in **Fig. 6.2** (horizontal surface). The cross-sectional view of the fabricated PLA/SNC-based foams can be found in **Fig. 6.3**. From the FESEM micrographs, the open cellular, interconnected and highly porous structure of fabricated PLA and PLA/SNC-based foams can be confirmed. The dispersed SNC nanofiller in PLA matrix can be observed in **Fig. 6.3.** The uniform dispersion of SNC in the PLA matrix can be observed from the FESEM micrographs.

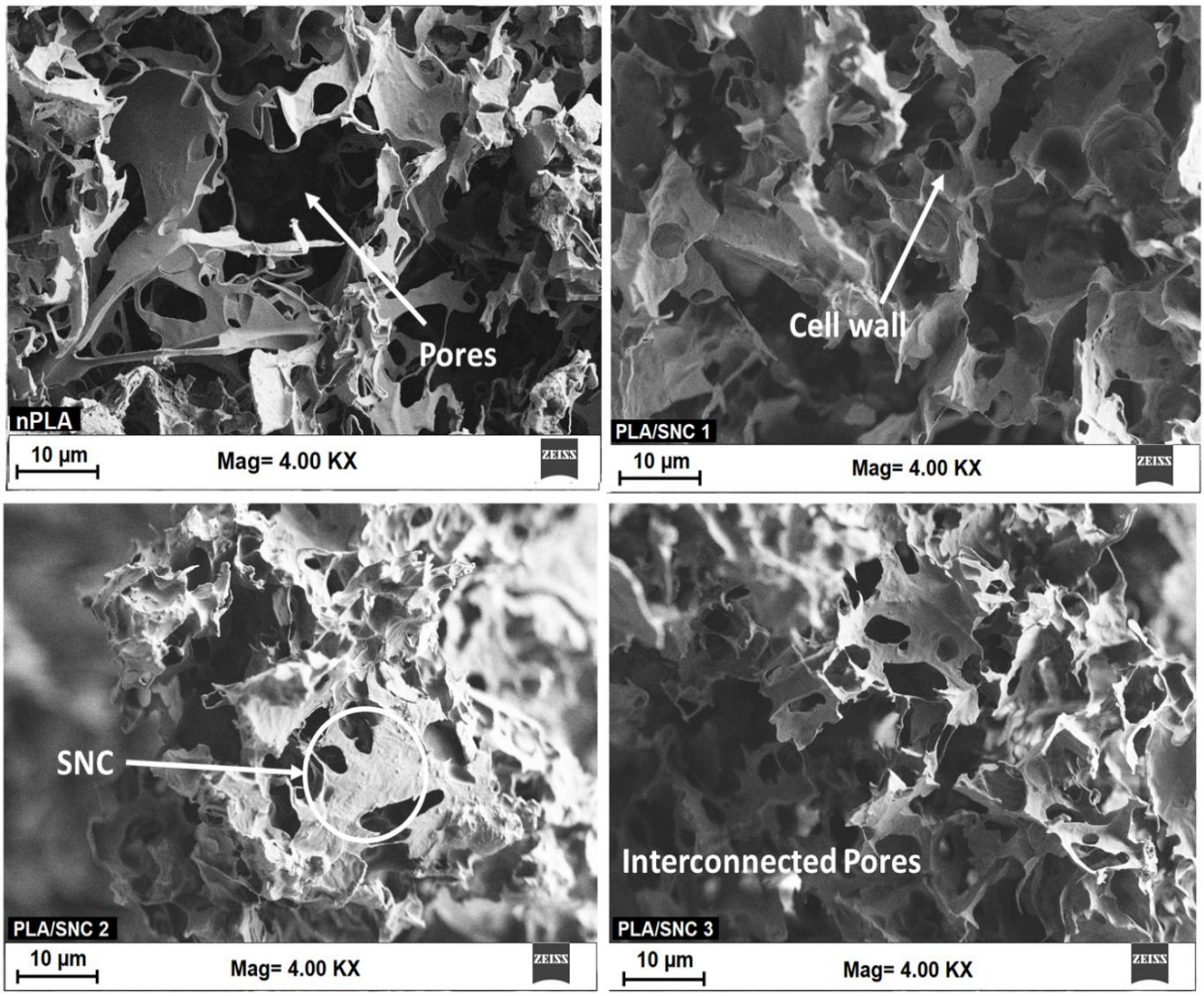

Fig. 6.2 FESEM view of PLA and PLA/SNC-based foams (Horizontal surface).

The size and shape of SNC nanofiller can be observed from TEM micrographs in **Fig. 6.4**. From the figure,, it can be observed that the prepared SNC nanofiller are in the range of 20 nm-50 nm. The disc type morphology of the fabricated SNC can be visualized from the TEM image. The underlying SNC nanobiofiller can also visualize from the SNC situated over them from the figure.

The average pore diameter of the fabricated PLA and PLA/SNC-based foams are calculated by using Image J® software. The average cell size of nPLA is measured as ~2.1±0.08 µm from the micrograph. The cell size and cell density of the fabricated PLA and PLA/SNC-based foams can be observed from **Fig. 6.5**. The cell size decreases up to ~1.9±0.07 µm for PLA/SNC 1. Similarly, ~23% and ~47% reduction in cell size is observed for PLA/SNC 2 and PLA/SNC 3 respectively. The cell size of the fabricated PLA/SNC-based foams decreases on increasing SNC.

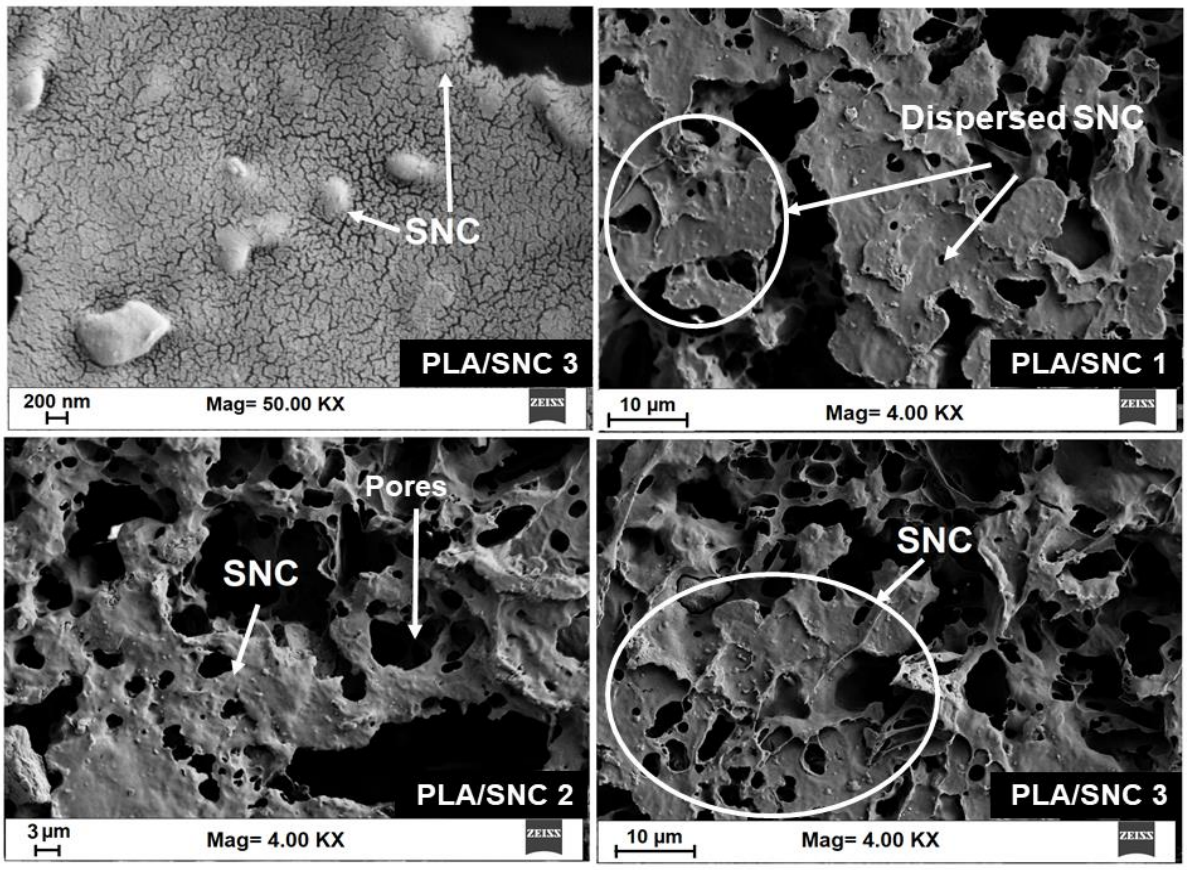

Fig. 6.3 FESEM micrograph of PLA/SNC-based foams (Cross-sectional surface).

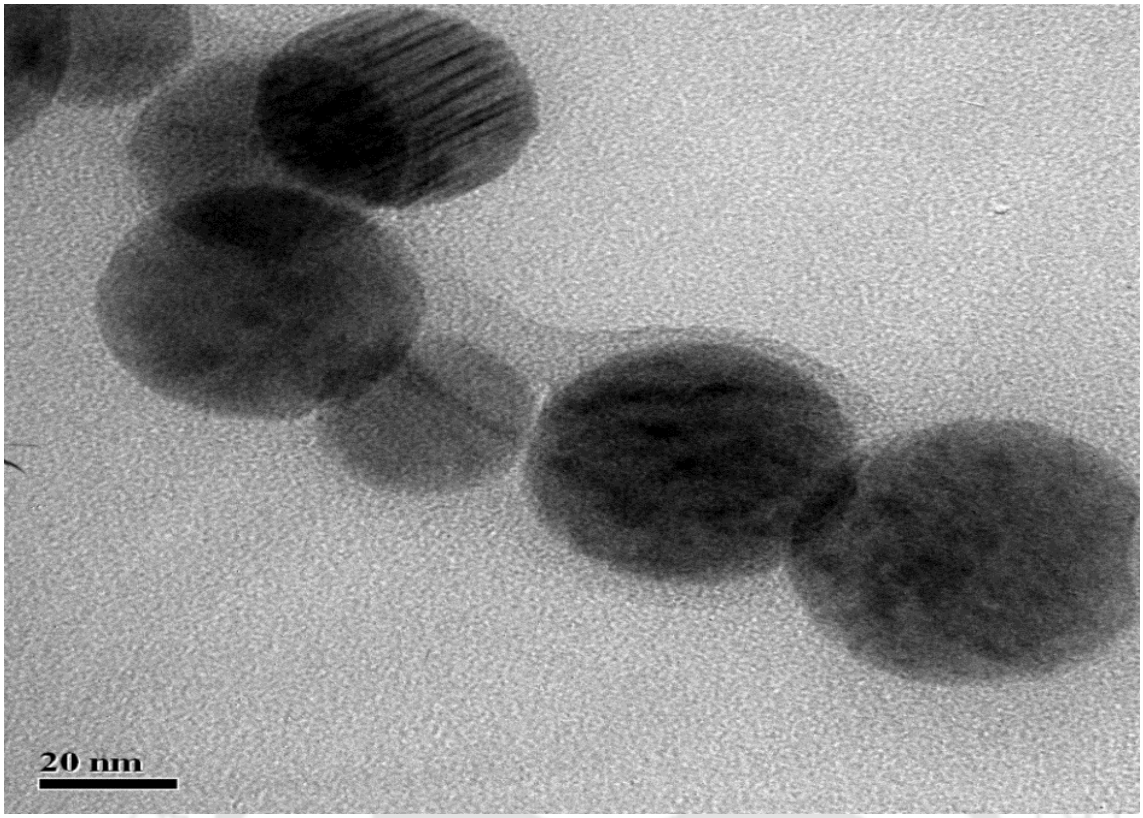

Fig. 6.4 FETEM micrographs of SNC nanobiofiller.

The decrease in the cell size of the fabricated foams might be due to the nucleating effect of SNC. The nanofiller generates nucleating sites in the PLA matrix in addition to the effect of porogen leaching increasing the number of smaller pores in the foam structure [30]. Simultaneously, the increase in cell density is also observed with increase in SNC. Number of smaller pores are accumulated in the same volume of the fabricated PLA/SNC-based foams, which effects in cell density. The cell density of the nPLA is observed as ~1.02×10^{10} cells/cm^3. The value is increased to ~1.9×10^{10} cells/cm^3 for PLA/SNC 1. The cell density further increases to ~2.3×10^{10} cells/cm^3 for PLA/SNC 2. For the highest concentration foam sample (PLA/SNC 3), the cell density drastically increases to ~1.3-times compared to the neat counterpart.

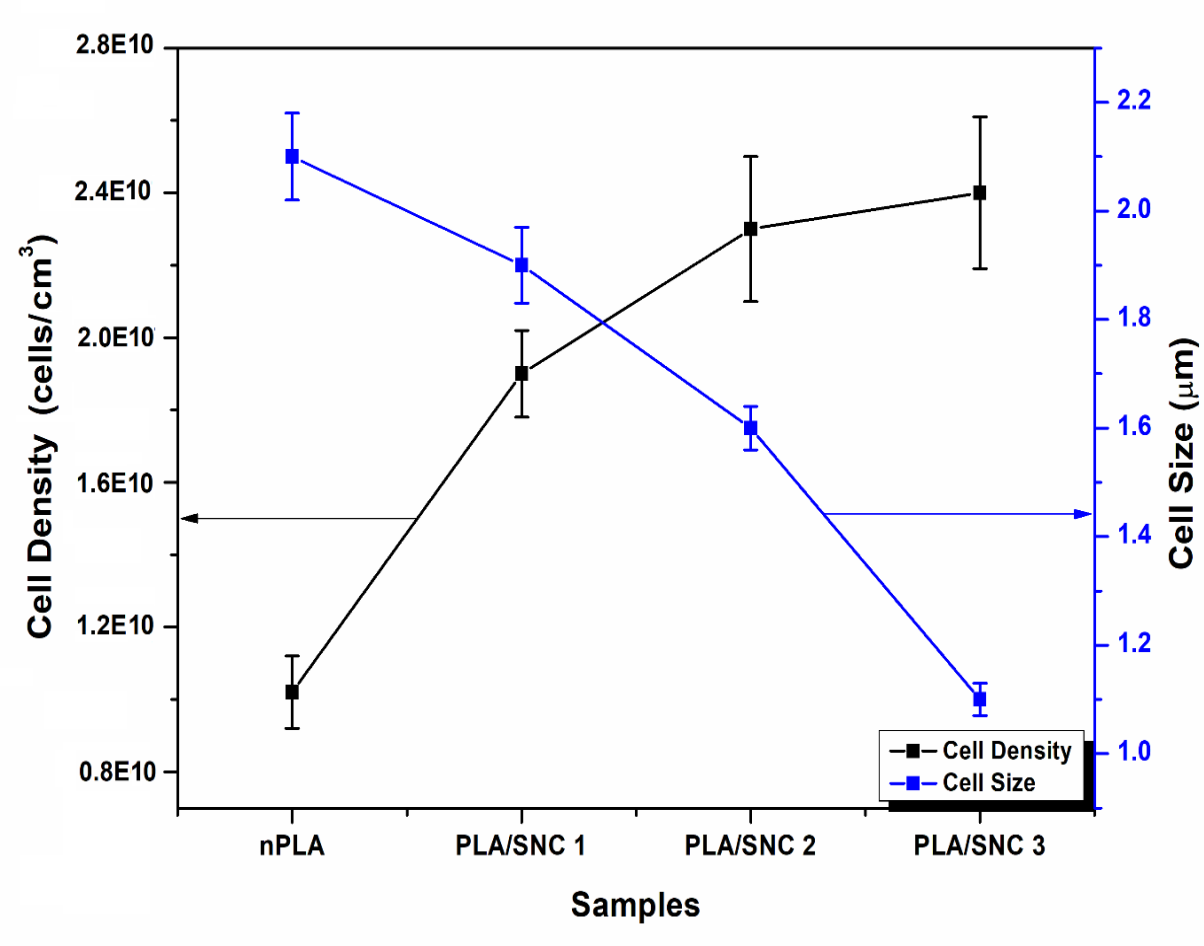

Fig. 6.5 Cell size and cell density of PLA and PLA/SNC-based foams.

It can be concluded from the morphological investigation of fabricated PLA/SNC-based foams that SNC nanofiller effects the foam morphology by generating more number of nucleating sites in the PLA matrix.

6.2.3 Chemo-physical investigation of PLA/SNC-based foam

The density of the fabricated PLA/SNC-based foams is measured and tabulated in **Table 6.1**. From the table, it is observed that a huge reduction of density (~85%) is observed for the fabricated foams compared to neat PLA granules (~1.23±0.04 g/cc). The reduction in density is more prominent at highest concentration (PLA/SNC 3) might be due to the generation of more nucleating sites by the nanobiofiller, which ultimately increases the cell density and

reduced the cell sizes. Presence of more gaseous voids in the matrix leads to the reduction in weight and affects the volume and density. Dry weight analysis of the fabricated foams (**Table 6.1**) indicates the removal of porogens from the PLA matrix eventually leads to the porous structure. From the VER values, it is observed that all foam can be categorized as medium density foam.

The FTIR spectrum of the fabricated PLA/SNC-based foams, SNC and sucrose are shown in **Fig. 6.6**. From the figure, characteristic peak of sucrose can be observed around ~908 cm^{-1} indicating –C-O- stretching, sharp peak around ~1235 cm^{-1} indicates bending vibrations of –OH group and peaks observed around ~3400 cm^{-1} and ~3500 cm^{-1} indicates the stretching vibrations of –OH groups of sucrose [177]. From the FTIR spectrum of SNC, peaks observed around ~963 cm^{-1} and ~1047 cm^{-1} attributes to alanine and glycine of amino acids present in the SNC [278]. Peaks around ~1222 cm^{-1} and ~1630 cm^{-1} indicates the amide III and amide I linkage present in SNC [279]. Another peak around ~1695 cm^{-1} (amide I) indicates the presence of highly ordered β-sheets in the SNC [124]. In case of nPLA, peaks are observed around ~890 cm^{-1}, ~1073 cm^{-1}, ~1189 cm^{-1}, ~1450 cm^{-1} and ~1740 cm^{-1} attributes the –C-O-C- stretching, $-CH_3$ asymmetric vibrations, -C-O- stretching, -CH bending vibrations and –C=O vibrations respectively. Similarly, for PLA/SNC-based foams, peaks are observed around ~1630 cm^{-1} and ~1695 cm^{-1} indicating the presence of amide I linkage and highly ordered β-sheets of SNC in the PLA/SNC-based foams [63].

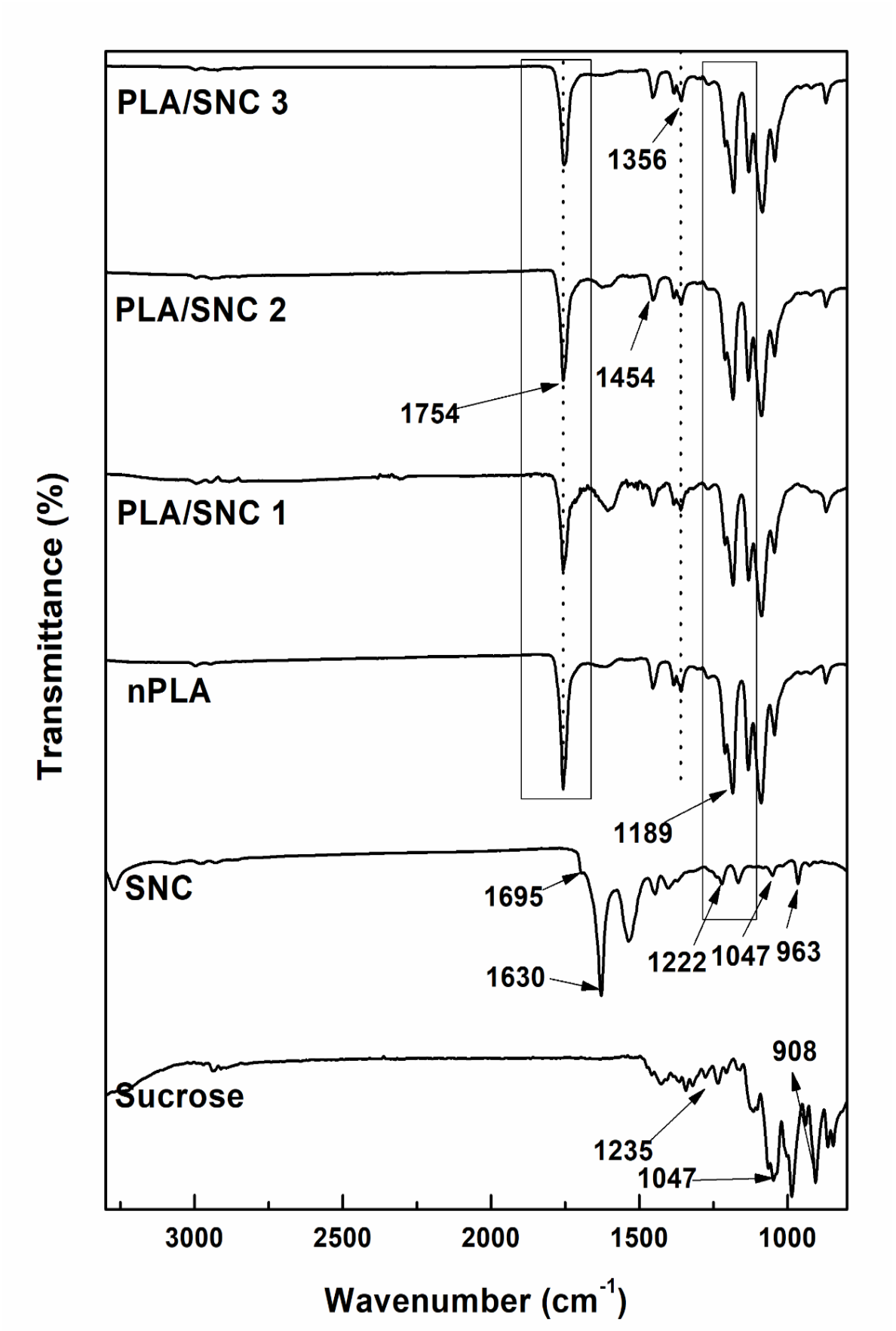

Fig. 6.6 FTIR spectra of PLA and PLA/SNC-based foam.

Table 6.1 Weight, density and volume expansion ratio of the nPLA and PLA/SNC based foams.

Sample	Avg. density (gm/cc)	VER	Dry Weight Analysis		Foam Type
			Before Leaching (g)	After Leaching (g)	
nPLA	0.23±0.04	5.4	34.6	3.1	Medium density
PLA/SNC 1	0.23±0.03	5.4	32.8	3.8	Medium density
PLA/SNC 2	0.21±0.01	5.9	34.8	3.6	Medium density
PLA/SNC 3	0.18±0.02	6.9	33.8	3.4	Medium density

The XRD spectrum of the PLA and PLA/SNC-based foams are shown in **Fig. 6.7**. It is observed from the figure that a distinct sharp peak is present around 2θ=16.6° associated with the [1 1 0]/[2 0 0] planes of PLA and also suggesting the presence of α-form of crystals [123,280,281]. This prominent peak is present in all the fabricated PLA/SNC-based foams suggesting the presence of ordered crystal structure in the PLA/SNC-based foams. Similarly, small intensity peaks observed around ~14.6°, ~19.1° and ~22.4° corresponds to [0 1 0], [2 0 3] and [0 1 5] planes respectively. From the XRD spectra of SNC, peaks are observed around ~16.8°, ~20.1° and ~23.8° indicating [2 0 1] and [0 0 3] lattice planes of orthorhombic β-sheet crystal structure respectively [271]. In case of PLA/SNC-based foams, the characteristic peak of ~16.7° of SNC is overlapped with PLA peak and thus producing a single intense peak around ~16.6° [63]. In the case of PLA/SNC-based foams, other peaks are observed around ~20.2° and ~~23.9° respectively indicating the presence of crystalline SNC structure in the PLA matrix. The crystallinity Index (C.I.) values of PLA and PLA/SNC-based foams are calculated. The C.I. value of nPLA is found to be ~52.3%. The value of C.I. increases with the increase of SNC loading in the matrix. The values of C.I. observed as ~54.8%, ~56.1% and ~61.1% for

PLA/SNC 1, PLA/SNC 2 and PLA/SNC 3 respectively. On the other hand, the crystallization index (C.I.) of SNC developed is found to be ~87.6%. Hence, it can be concluded that SNC helps in chain folding of the PLA and increases the formation of the more ordered region and hence crystallinity of PLA. The increase in crystallinity also helps in the improvement of different mechanical and thermal properties of PLA-based foams [282–284].

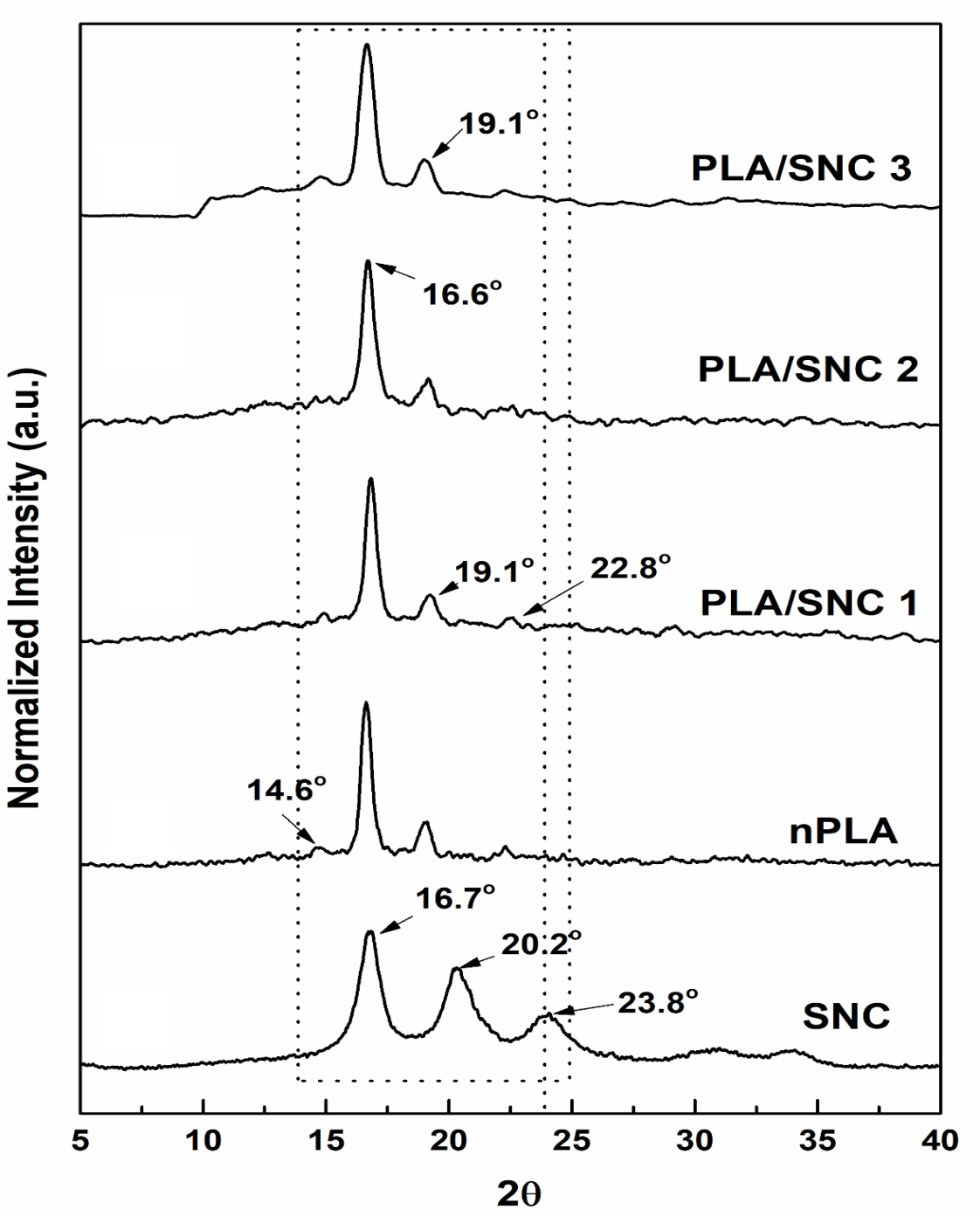

Fig. 6.7 XRD spectrum of PLA and PLA/SNC-based foams.

The molecular weight investigations of the fabricated PLA and PLA/SNC-based foams are shown in **Fig. 6.8**. There is no significant change in both M_w and M_n is observed for PLA/SNC-based foams as observed from the results. The PDI value of nPLA is found to be ~1.9. the PDI values of PLA/SNC 1, PLA/SNC 2 and PLA/SNC 3 are observed as ~1.9, ~1.8 and ~1.8 respectively. Hence, it can be concluded that SNC does not have any significant influence on the degradation of PLA and the molecular weight, which is useful for various probable applications.

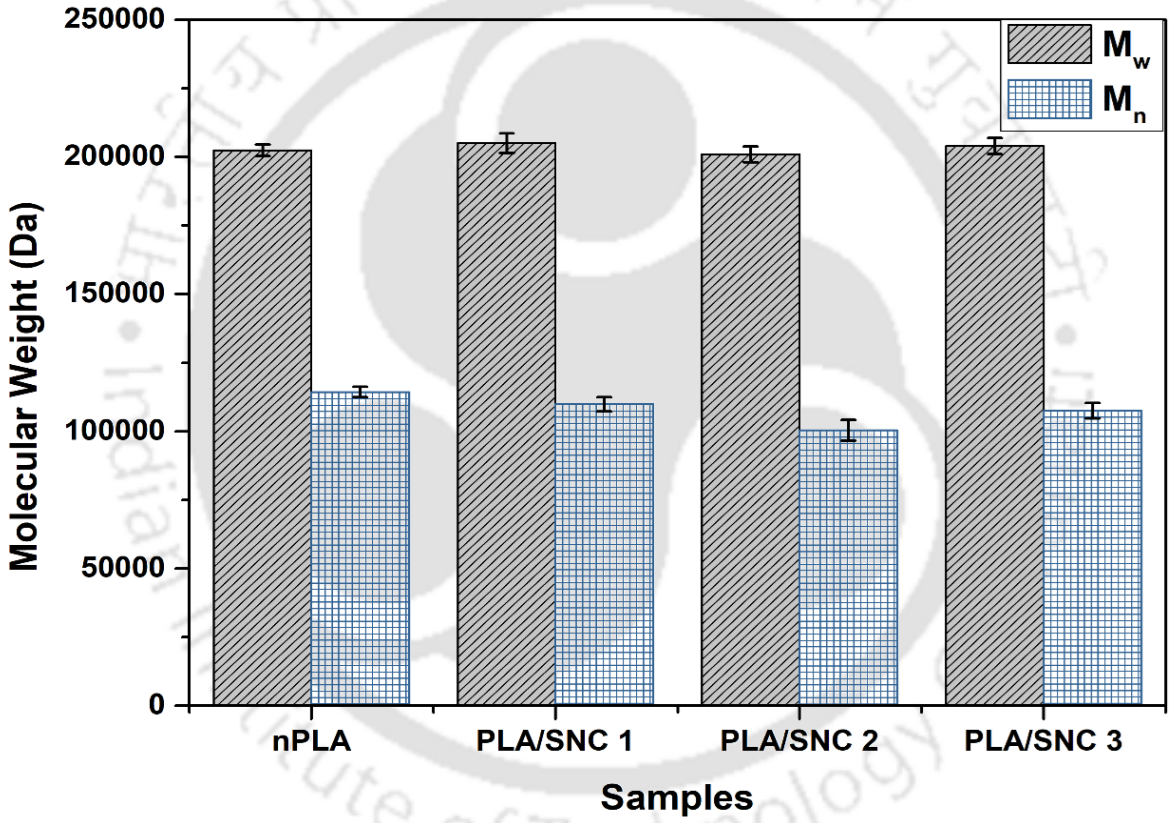

Fig. 6.8 Molecular weight investigations of PLA and PLA/SNC-based foams.

The colorimetric investigations of the fabricated PLA/SNC-based foams can be found in **Fig. 6.9**. It is observed from the colorimetric investigation that SNC has some effect in the ultimate color of the PLA/SNC-based foams. The L* parameter value of nPLA is observed as ~97.21, which is in close agreements with previous similar research [230]. However, no significant

change in the L* value is observed on the incorporation of SNC in the PLA matrix. Similarly, the hue value of the fabricated foams is also not significantly affected by the incorporation of SNC. On the other hand, a significant increase is observed for a* and b* parameters indicating the drastic changes from redness to greenness and improvement of yellow color present in the foam matrix. The chroma* parameter of the fabricated PLA/SNC-based foams are also influenced by the incorporation of SNC, indicates the increase in saturation values. The brown color of the SNC might be responsible for this change in color parameters. The improvements in yellowness might be due to the effect of temperature and color of SNC. The value of these parameters increases with increase in the concentration of SNC in the matrix.

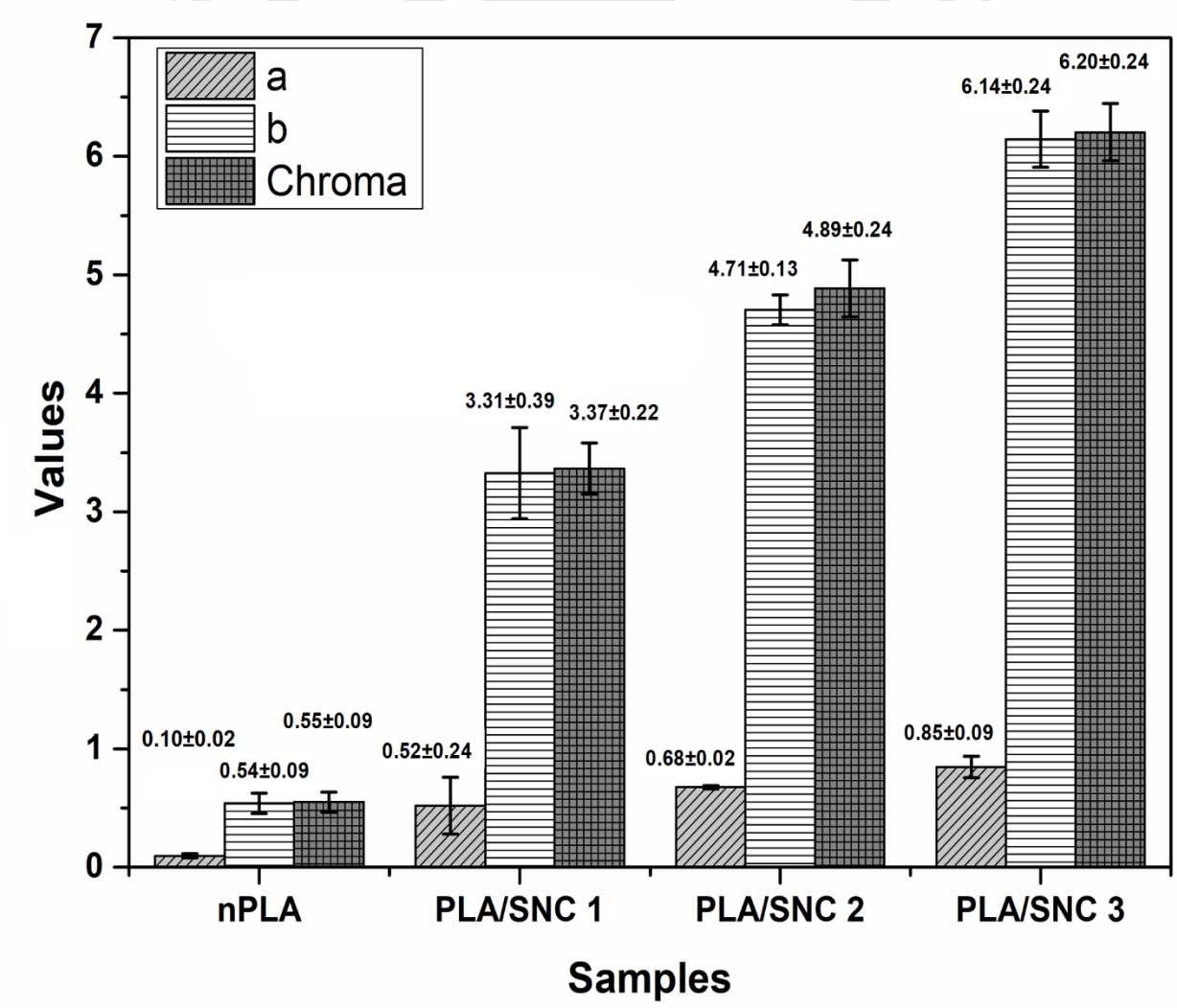

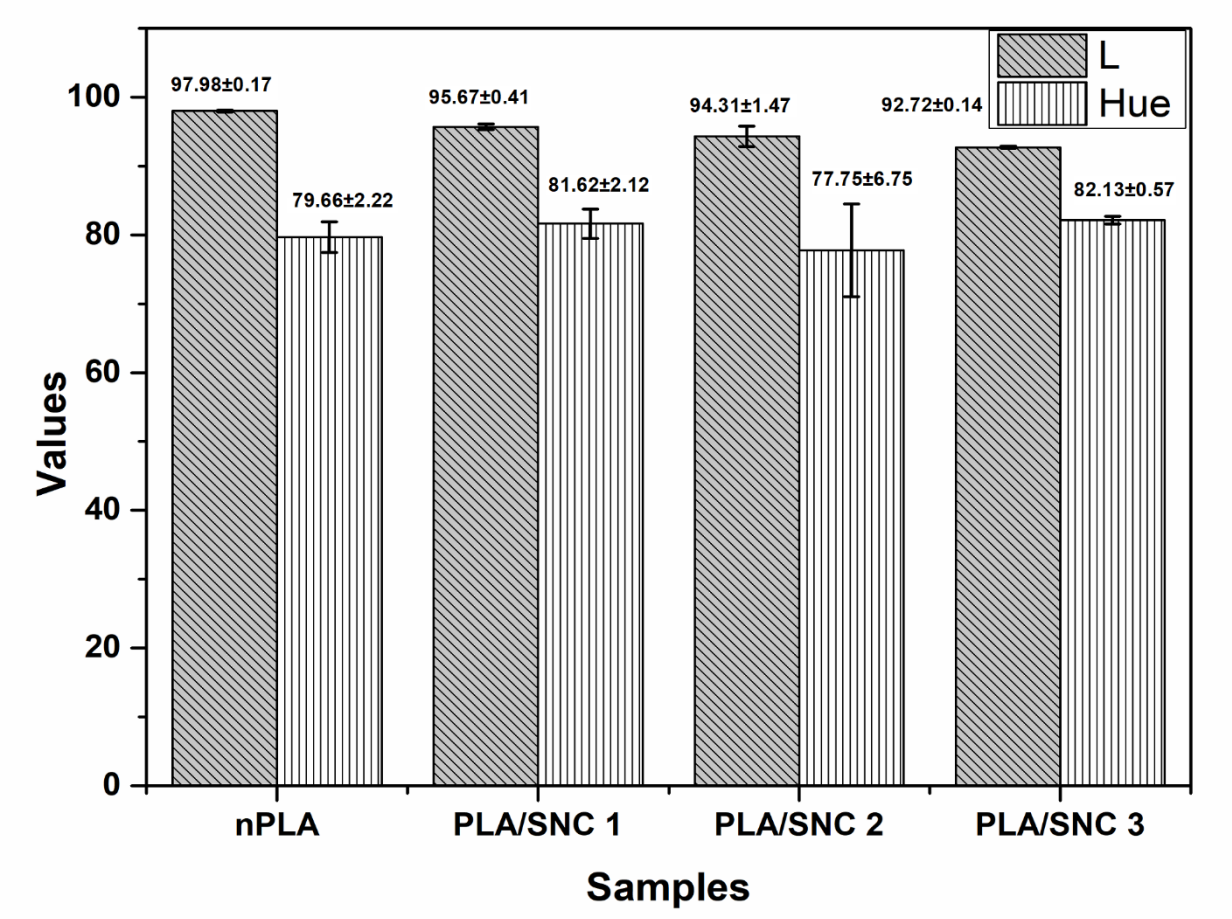

Fig. 6.9 Colour parameters of PLA and PLA/SNC-based foams.

6.2.4 Water absorption test of PLA and PLA/SNC-based foams

The investigation of water absorption test for the fabricated PLA and PLA/SNC-based foams are shown in **Fig. 6.10**. For the nPLA foam, ~86% of weight increase is observed. However, the value decreases to ~67% for PLA/SNC 1. Further increasing the concentration of SNC, the weight increase (%) value decreases. At highest loading (PLA/SNC 3) the value further decreases to ~55%. The decrement of percentage weight increase is due to the generation of smaller pores in the PLA matrix. In the case of nPLA foam, the pore size is bigger due to which water can easily penetrate the surface and thus more water can be accumulated. The hydrophobic nature of SNC might also be the reason behind this. However, in the case of PLA/SNC-based foams due to the generation of smaller pores, the water penetration is difficult compared to nPLA. Swelling of SNC nanobiofiller also blocked the pores and thus the rate of

water adsorption is drastically reduced. The surface area of PLA/SNC-based foam is also higher than the nPLA and it is difficult to penetrate the higher surface with smaller available pores, hence the percentage weight is reduced and accumulate less amount of water in the available pores.

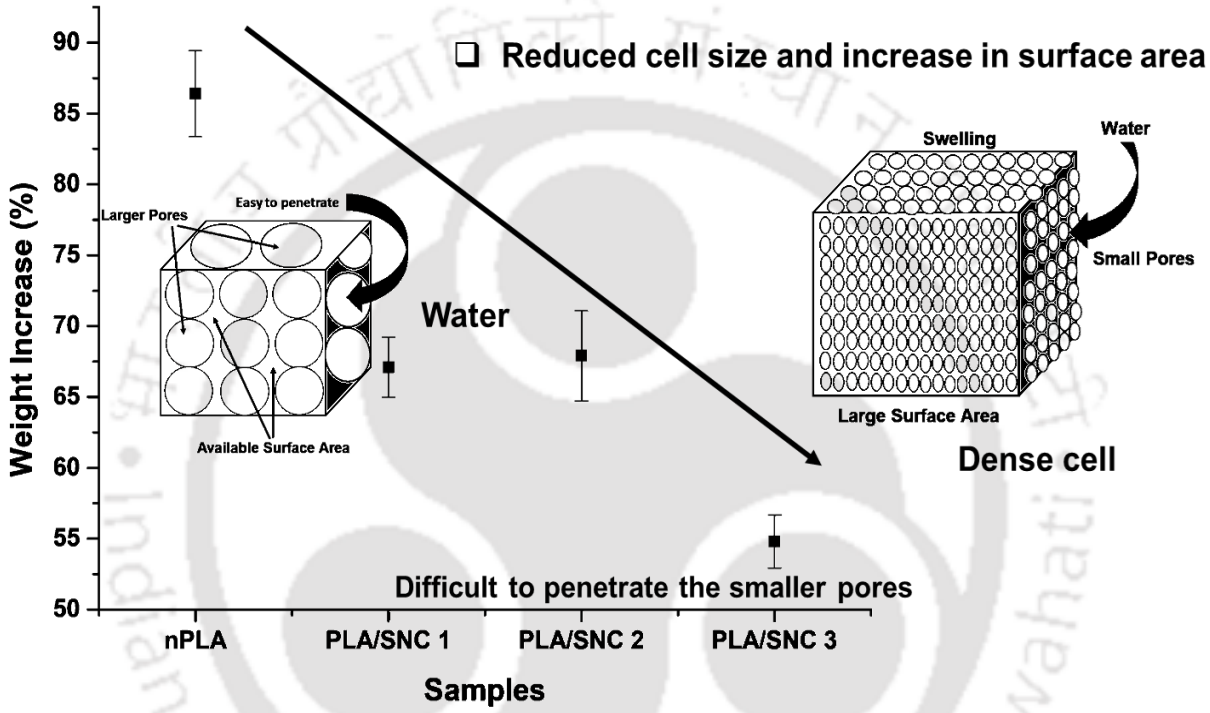

Fig. 6.10 Water absorption test for PLA and PLA/SNC-based foams.

6.2.5 Thermal investigations of PLA and PLA/SNC-based foams

The DSC curves of PLA and PLA/SNC-based foams are shown in **Fig. 6.11**. The glass transition (T_g), crystallization temperature (T_c) and temperature of melting (T_m) values of the fabricated foams can be observed from the figure. The glass transition value of nPLA is observed as ~61.2 °C. On incorporation of SNC, no significant change in T_g is observed for PLA/SNC-based foams, indicating the absence of short-chain formation. Good compatibility of the SNC with PLA can be concluded by observing single T_g for all the PLA/SNC-based

foams. The T_g values of PLA/SNC 1, PLA/SNC 2 and PLA/SNC 3 are observed as ~61.4 ºC, ~61.8 °C, and ~61.3 °C respectively.

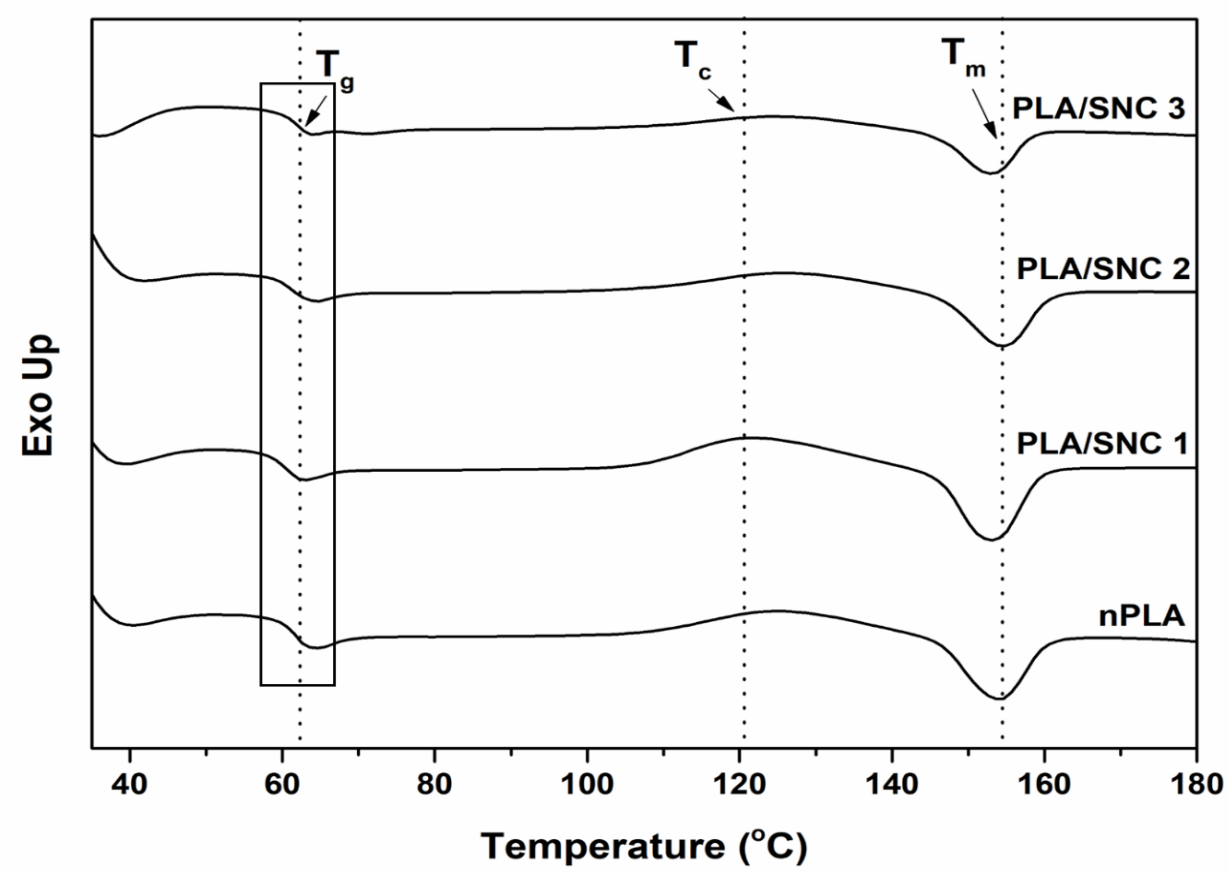

Fig. 6.11 DSC thermographs of PLA and PLA/SNC-based foams.

The temperature of crystallization value (T_c) of the fabricated PLA and PLA/SNC-based foams are observed around ~120 °C. However, a slight decrease in T_c can be observed on increasing SNC concentration indicates that SNC might enhance the chain folding of PLA. From the endothermic peaks of PLA and PLA/SNC-based foams, it can be noticed that SNC has no significant effect in melting point of PLA/SNC-based fabricated foams. Interestingly, a single peak in the endothermic melting region suggests the homogeneous distribution of the ordered crystals. The endothermic single peaks at higher temperatures (>150 °C) indicate the melting of perfect crystals [179].

The TGA isotherms of PLA and PLA/SNC-based foams is illustrated in **Fig. 6.12**. The thermostability of the fabricated foams can be observed from the figure. It can be observed that all the fabricated PLA and PLA/SNC-based foams are thermally stable until 200 °C.

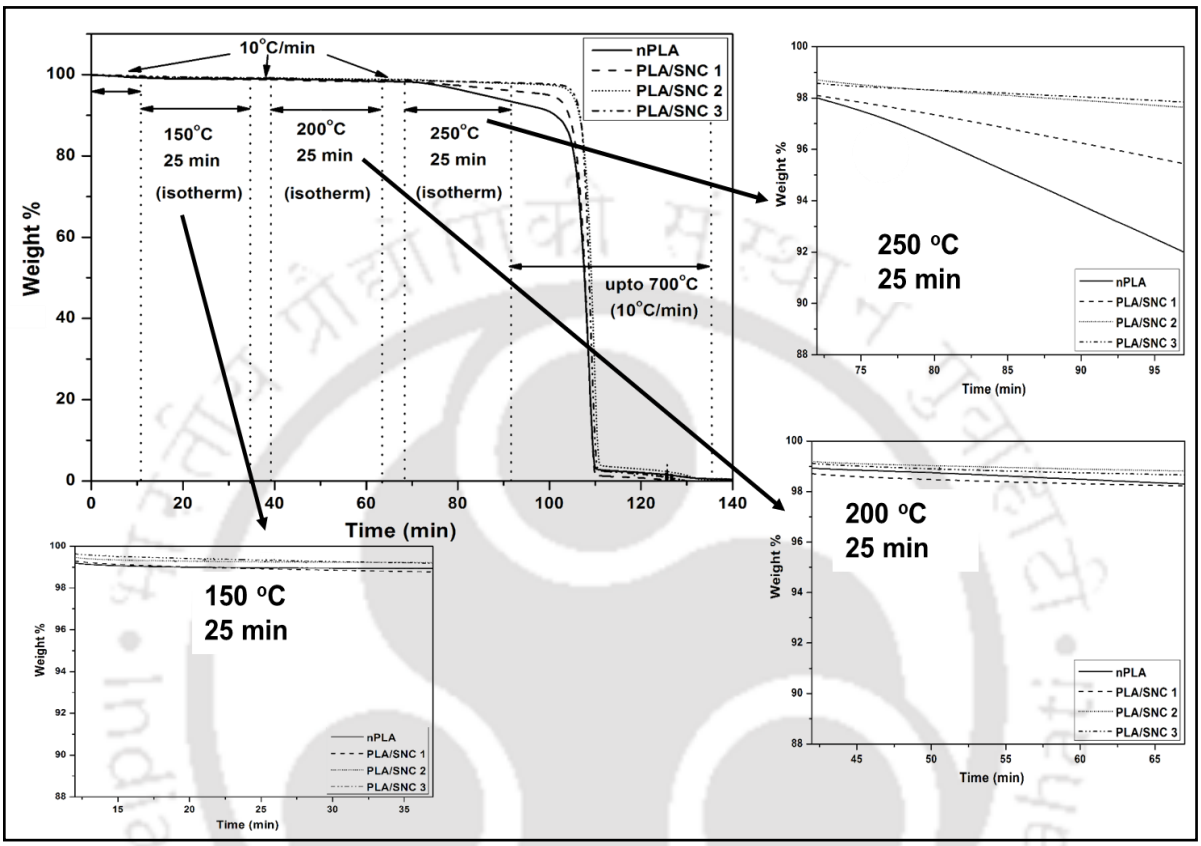

Fig. 6.12 TGA isotherm of PLA and PLA/SNC-based foams.

The PLA and PLA/SNC-based foams are found to be thermally stable at 150 °C and 200 °C after 25 min of the isotherm. No weight loss is observed. Interestingly, it can be observed from the isotherm at 250 °C that the thermostability of nPLA reduces as the weight % values decrease drastically. However, at 250 °C, in the case of PLA/SNC 1, reduction in weight % is observed, thought the reduction is lower compared to the neat counterpart. As the concentration of SNC increases in the PLA foam matrix, the increase in thermostability is observed from the graph and it can be seen that PLA/SNC 2 and PLA/SNC 3 is almost thermostable at 250 °C. From the investigation, it can be concluded that SNC improves the thermostability of the fabricated PLA/SNC-based foams and hence, SNC has not influenced enhancement of the

degradation of PLA. The enhancement of stability might be due to the uniform dispersion of SNC in the PLA matrix. Single step degradation is observed for all the fabricated PLA and PLA/SNC-based foams.

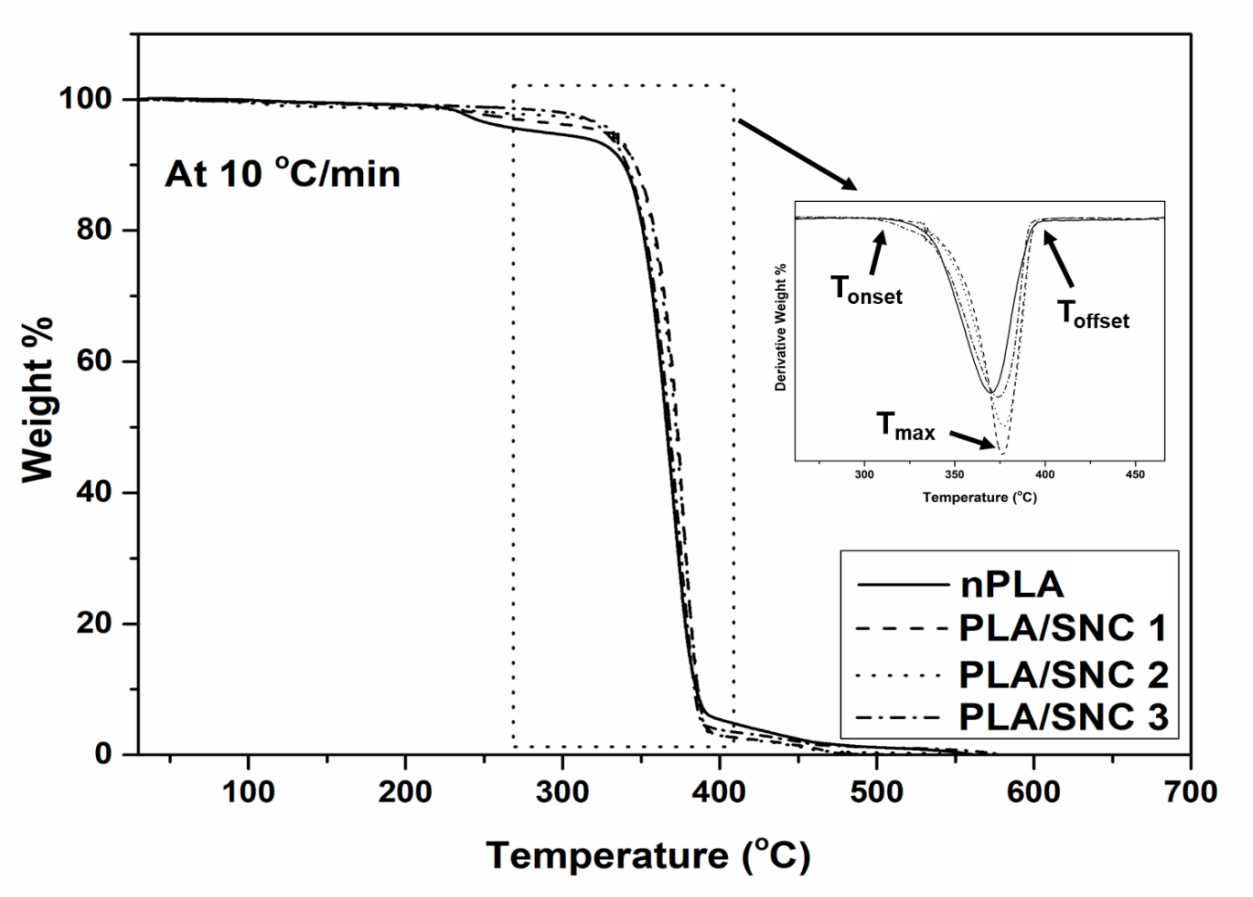

Fig. 6.13 TGA plots for PLA and PLA/SNC-based foams at 10 °C/min.

The onset temperature of degradation (T_{onset}), maximum degradation temperature (T_{max}) and offset of degradation (T_{offset}) of the fabricated PLA and PLA/SNC-based foams can be observed from the TGA plots (**Fig. 6.13**). The T_{max} of nPLA is observed around ~368.5 °C which might be due to the hydrolysis and oxidative scission of chains present in PLA matrix [178]. The T_{max} value slightly improves to a higher temperature on the incorporation of SNC and it is observed around ~373.3 °C for PLA/SNC 1, further increases to ~374.6 °C and ~376.8 °C for PLA/SNC 2 and PLA/SNC 3 respectively. Similarly, in the case of T_{onset} values of fabricated PLA/SNC-based foams, improvement is observed. The onset value increases on increasing SNC

concentration in PLA matrix. An increment of ~5 °C in onset temperature is observed for PLA/SNC 3. The thermal degradation kinetics behavior and the crystallization kinetics investigations of fabricated PLA and PLA/SNC-based foams will be thoroughly discussed in the later sections of this chapter.

The evolution of various gaseous products obtained from thermal degradation has been investigated by hyphenated TGA-FTIR system and the results are shown in **Fig. 6.14**.

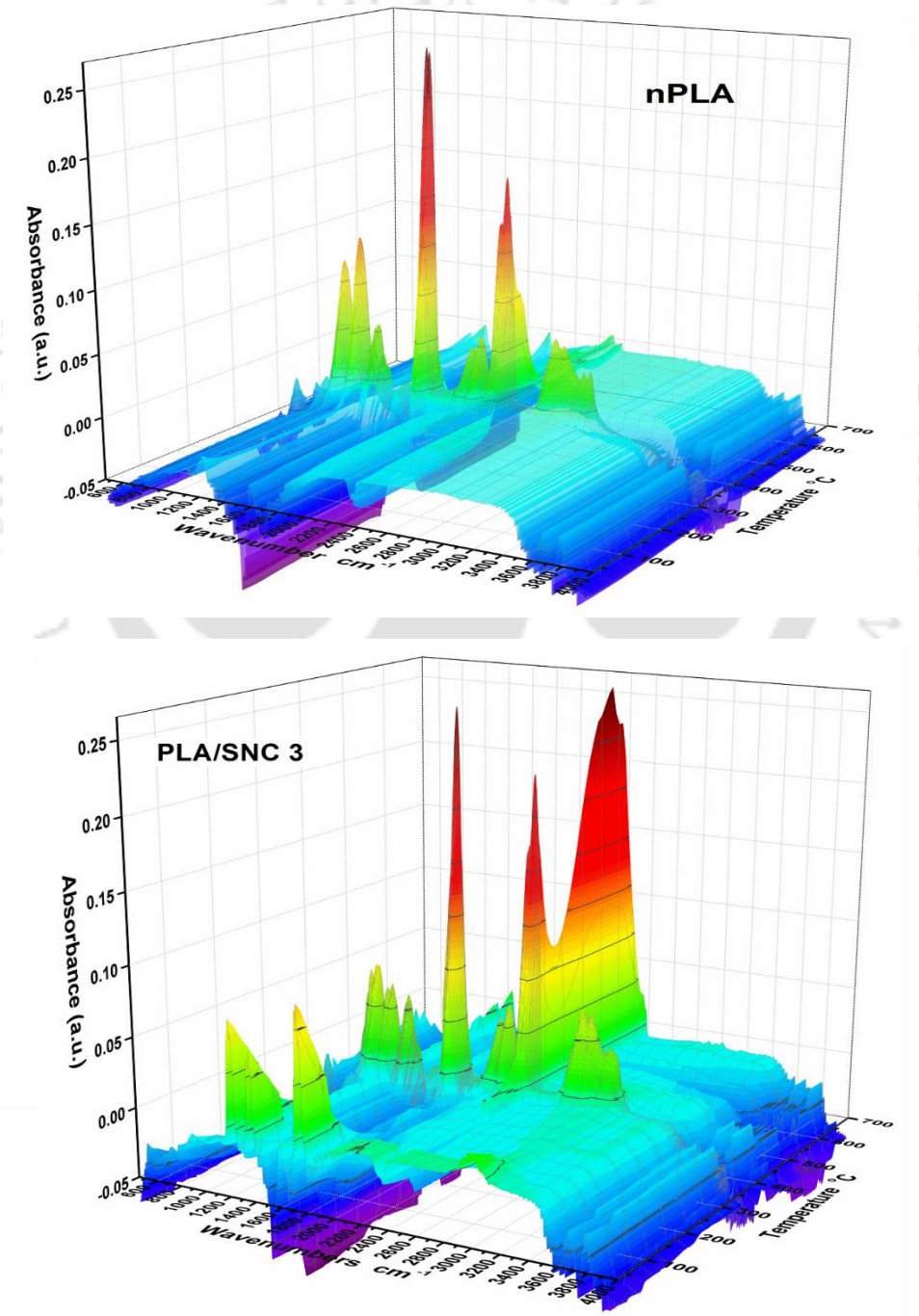

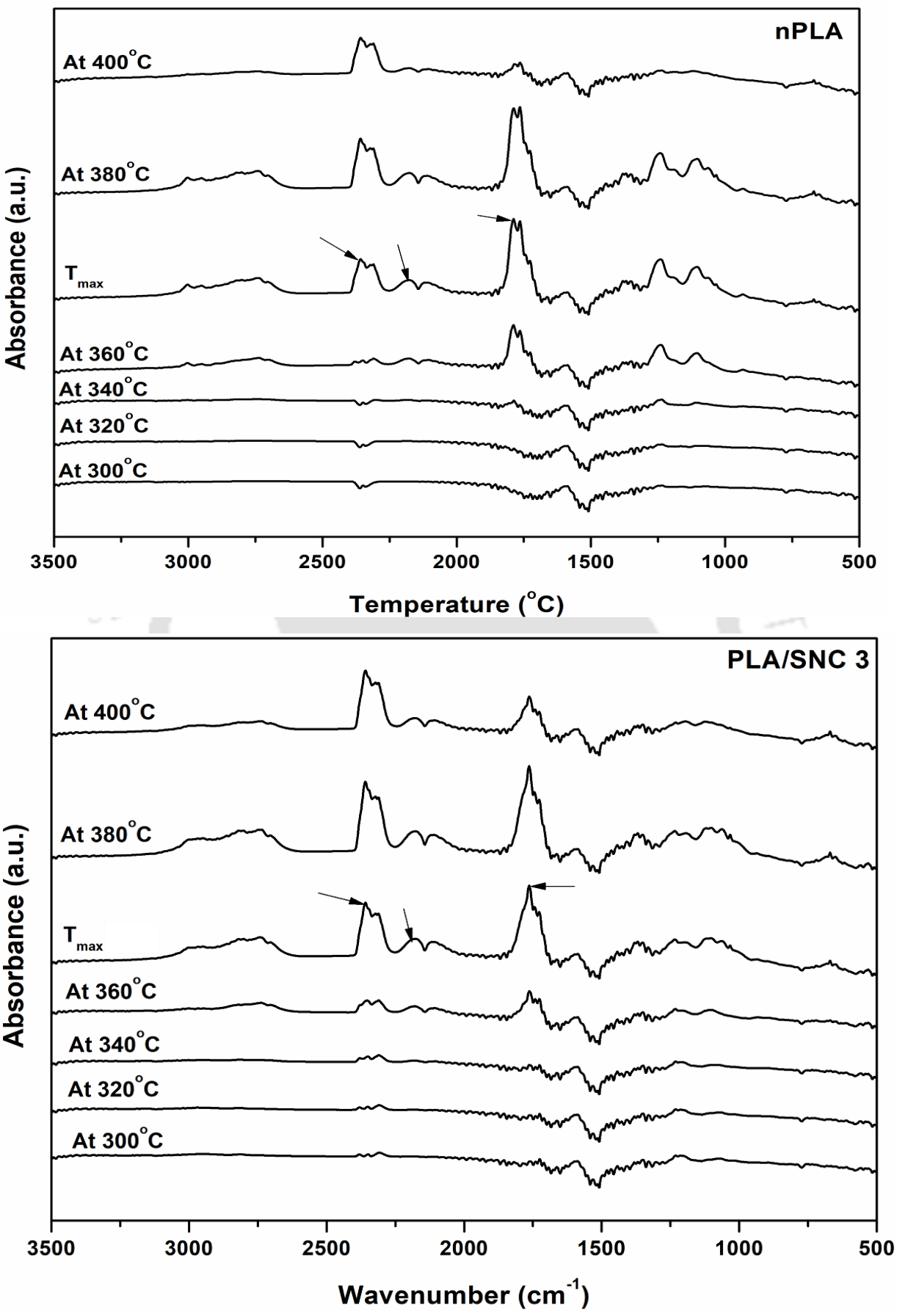

Fig. 6.14 TGA-FTIR spectrum of PLA and PLA/SNC-based foam.

The 3D FTIR spectrum and FTIR peaks corresponding to different degradation temperatures (~300 °C-~400 °C) are shown in **Fig. 6.14** with dynamic temperature ranging from 30°C to 700°C. The investigation was carried out for nPLA and PLA/SNC 3 and a single step degradation process was adopted as discussed earlier. The formation of various gaseous products was mainly noticed in the range of ~360 °C-~400 °C for the prepared foam. In the case of nPLA foams, at T_{max}, two prominent peaks were observed at ~1790 and ~2350 cm^{-1} representing cyclic oligomers and carbon dioxide, respectively. From the figure, it was observed that the intensity of the peaks is maximum at T_{max}. Other peaks observed in both the nPLA and PLA/SNC 3 are around ~3575 cm^{-1}, ~2950 cm^{-1} and ~3010 cm^{-1} for –OH group, $–CH_3$ symmetric stretching and asymmetric stretching, respectively. Two peaks around ~2180 and ~2106 cm^{-1} were observed in both the samples indicating the –C-O- bending vibrations of carbon monoxide (CO). It was observed that on the addition of SNC, the intensity of these peaks decreases compared to nPLA, which is a favorable result in terms of environmental issues concerned. Peaks were also observed at ~1375, ~1240, ~1100 and ~930 cm^{-1} indicating the –CH- stretching, -C=O- stretching, -C-O- stretching and –C-C- stretching, respectively. The presence of a β-sheet structure of SNC might be the reason for the presence of peaks around ~1230 cm^{-1} and ~1248 cm^{-1} (amide III) of –CH stretching in the PLA/SNC-based foam. Hence, we can conclude that the main degraded gaseous products evolved during the degradation of PLA and PLA/SNC-based foams are cyclic oligomers, carbon dioxide, water, and carbon monoxide. The formation of carbon dioxide in degradation might be due to the chain homolysis of PLA [123]. It was also noticed that carbon dioxide is present until the end of the degradation. Carbon monoxide formation might be due to decomposition of hydroxyl end initiated esters. The intensity of other gaseous products is decreasing after T_{max}. It can also be concluded that the degradation of PLA and PLA/SNC-based foams might be via random depolymerization, which ultimately leads to the formation of various gaseous products. In addition, it is found

that on the introduction of a small percentage of loading of SNC in the PLA foam matrix does not change the main degraded gaseous products [181,285–291].

6.2.6 Thermo-mechanical investigations of PLA and PLA/SNC-based foams

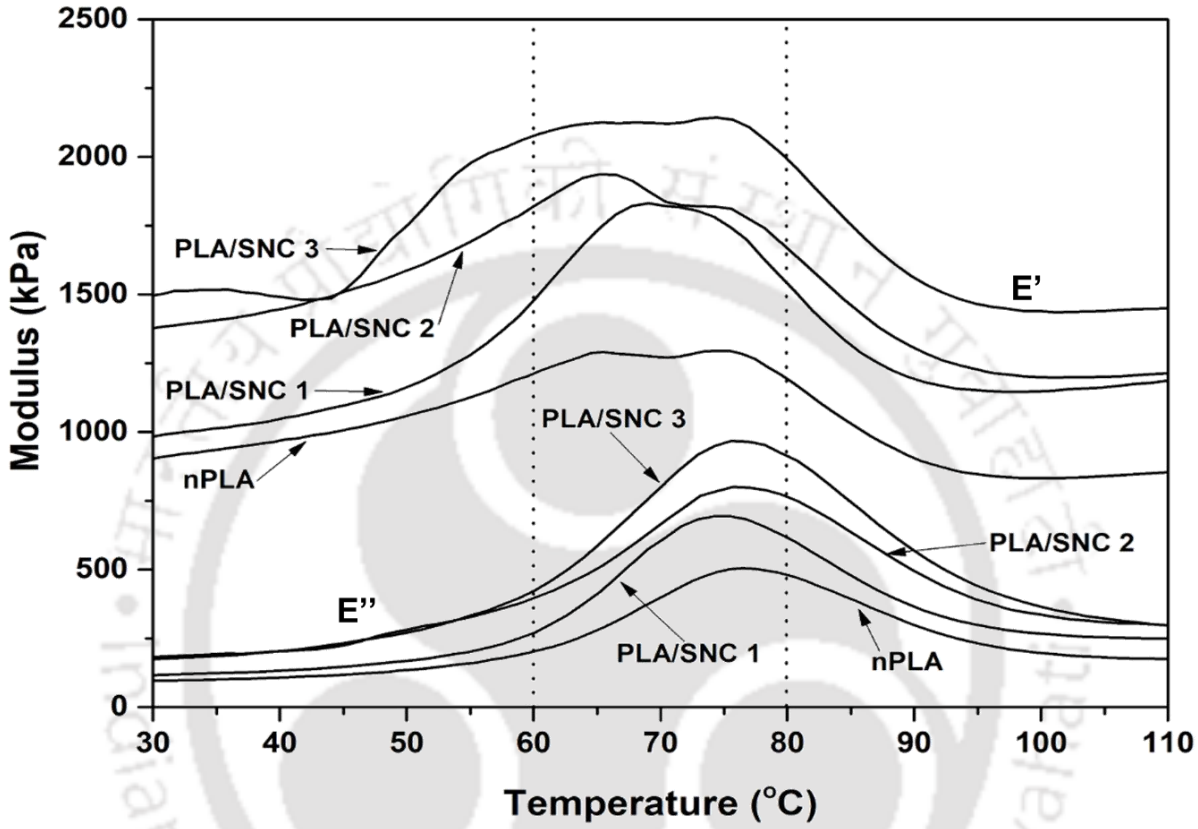

Fig. 6.15 DMA investigations of the PLA and PLA/SNC-based foams (Compressed mode).

The storage modulus (E') and loss modulus (E") of the fabricated PLA and PLA/SNC-based foams are shown in **Fig. 6.15** performed under compressed mode. The dynamic mechanical responses are presented as a function of temperature in the figure above. It can be observed from the figure that both the storage as well as loss modulus increases with increase in the concentration of SNC. The values of E' and E" are tabulated in **Table 6.2** at two different temperatures of 60 °C (near the T_g value of PLA) and 80 °C. It can be observed that in all the cases, the E' and E" curves are linear until 50 °C. Then an increase in E' and E" values are observed in the curves, which might be because at near T_g, rapid densification happens on

compression to the fabricated PLA and PLA/SNC-based foams [78]. The increase in storage modulus and loss modulus of PLA/SNC-based foams might be due to an increase in more ordered crystalline regions in the PLA matrix on the incorporation of SNC. The uniform dispersion of SNC in the PLA matrix is also responsible for the improvements in dynamic mechanical behaviors of the fabricated foams.

Table 6.2 Storage and loss modulus of PLA and PLA/SNC-based foams.

Samples	Storage Modulus (E') kPa		Loss Modulus (E'') kPa	
	60 °C	80 °C	60 °C	80 °C
nPLA	1209.1	1199.8	204.9	479.8
PLA/SNC 1	1479.2	1547.6	268.8	617.8
PLA/SNC 2	1821.8	1680.1	391.8	768.7
PLA/SNC 3	2076.6	1998.0	435.3	920.4

There is an increase of ~0.7-times is observed in storage modulus of PLA/SNC 3 compared to the neat counterpart. Similarly, in the case of loss modulus, an increase of ~1.2 times is observed for highest loading of SNC compared to nPLA.

6.2.7 Wettability phenomena of the fabricated PLA and PLA/SNC-based foams

The water contact angle (CA) values of the fabricated PLA and PLA/SNC-based foams can be observed from **Fig. 6.16**. The CA value of nPLA is found to be ~126° ± 3.1°. It is clearly visible from the figure that on the incorporation of SNC in the PLA matrix, the hydrophobicity of the fabricated PLA/SNC-based foams increases. An increment of ~13° is observed for PLA/SNC 3 compared to nPLA. The hydrophobicity depends on the surface morphology and the effect of nanobiofillers. To understand the effect of SNC in hydrophobicity, the wettability investigations on compressed foam surface was performed. A huge reduction in CA is observed

for compressed PLA and PLA/SNC-based surfaces compared to foamed samples. The reduction in CA might be due to the collapsing of the foamed morphology and reorganization of SNC nanofiller of PLA and PLA/SNC-based foams. The CA values obtained from compressed foam studies (surface without texture) are found to be ~74.6° ± 2.2°, ~76.4° ± 1.9°, ~78.8° ± 2.8° and ~80.8° ± 1.8° for nPLA, PLA/SNC 1, PLA/SNC 2 and PLA/SNC 3 respectively. Around ~8° increase in CA is observed for compressed PLA/SNC 3 compared to nPLA compressed foam. From the investigation on the compressed surface without texture, it can be concluded that SNC has also effected the increase in CA along with the surface morphology. The increase in hydrophobicity of the fabricated PLA/SNC-based foams might be due to the morphological changes in the PLA foam matrix. Incorporation of SNC generates number of smaller pores in the PLA matrix and also effects in cell density due to its nucleating effect.

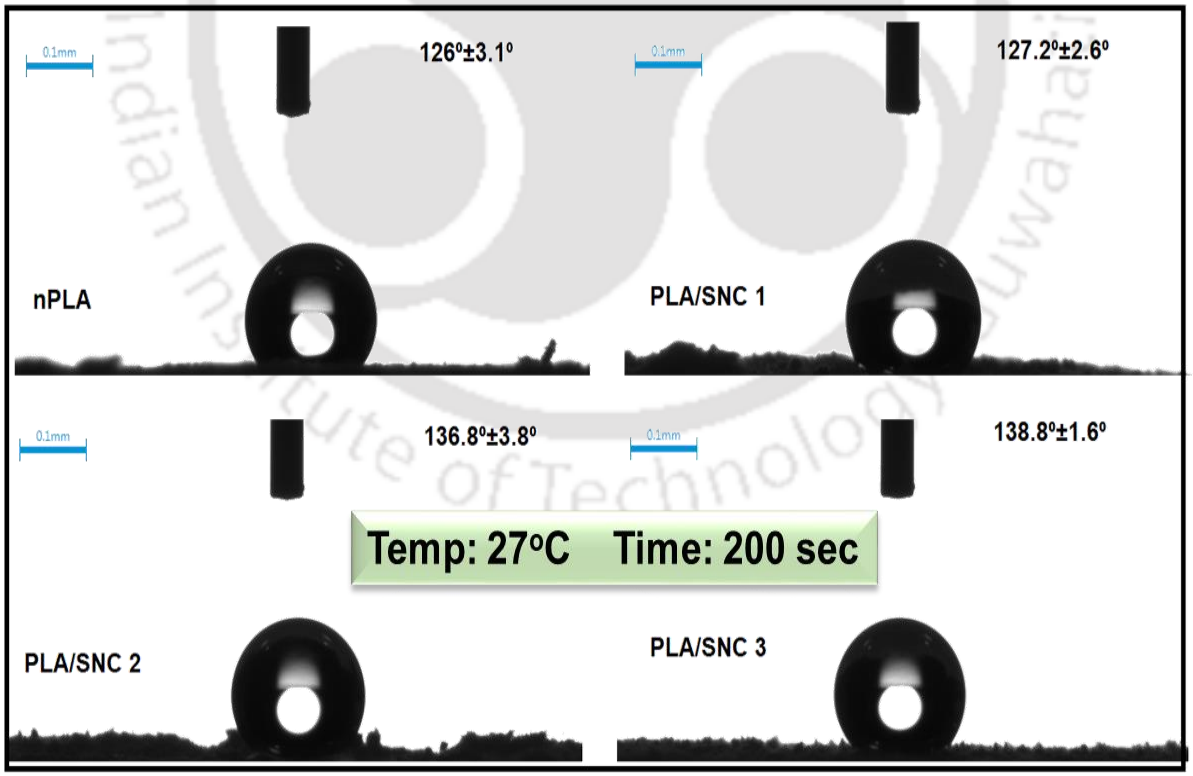

Fig. 6.16 Wettability phenomena of PLA and PLA/SNC-based foam.

6.2.8 Porosimetric investigations of PLA and PLA/SNC-based foams

The results obtained from MIP studies (porosimetric investigations) are tabulated in **Table 6.3**. The porosity of all the fabricated PLA and PLA/SNC-based foams are in the range of 78%-82%. The nPLA has the porosity of ~82%. The value has slightly reduced to ~80% for PLA/SNC 1, further reduced to ~78% for the highest loading of SNC (PLA/SNC 3). This slight reduction in porosity can be attributed to the generation of more nucleating sites in the PLA foam matrix, which ultimately leads to the generation of smaller pores and slightly decreases the porosity.

Table 6.3 Porosimetric investigations (MIP) of PLA and PLA/SNC-based foams.

Samples	Porosity (%)	Avg. Pore dia. (µm)	Surface Area (m^2/g)
nPLA	82	1.5	13.6
PLA/SNC 1	80	1.1	15.9
PLA/SNC 2	81	0.8	17.3
PLA/SNC 3	78	0.6	22.6

Similarly, in the case of average pore diameter of the fabricated foams, it can be observed from the table that nPLA has avg. pore dia. Value of ~1.5 µm. A reduction of ~26% in average pore diameter is observed for PLA/SNC 1. The average pore diameter further reduced to ~46% and ~60% for PLA/SNC 2 and PLA/SNC 3 respectively. It is observed that an increase of nanofiller concentration, the pore diameter decreases. The phenomena can be explained on the basis of nucleation theory of nanofiller. The results obtained from porosimetric investigations are in good accordance with the morphological investigation of the fabricated PLA and PLA/SNC-based foam as discussed in the earlier section. The increase in the concentration of the SNC

nanofiller enhances the number of nucleating sites in the PLA foam matrix, which helps a generation of an increasing number of smaller pores in the matrix. The generation of smaller pore leads to an increase in pore density. From the porosimetric results, it can be observed that the loading of SNC also affects the surface area of the fabricated PLA-based foam. Increase in surface area is observed for PLA/SNC-based foams with the increase in the concentration of SNC. An improvement of ~17% in surface area is observed for PLA/SNC 1. The surface area of the fabricated PLA/SNC-based foam is further increases up to ~27% for PLA/SNC 2. At higher concentration of SNC, the surface area drastically improves to ~66% compared to nPLA foam. The improvement in the surface area might be due to the generation of smaller pores and increase in pore density with SNC loading.

6.3 Crystallization behavior of PLA and PLA/SNC-based foams

DSC thermographs at four different heating rates are shown in **Fig. 6.17.** Crystallization is the ordered arrangement if polymeric chains in the matrix. It is observed from the previous discussion that SNC increases the crystallinity of PLA in PLA/SNC-based fabricated foams. The relative crystallinity (X_t) with time of crystallization plots can be observed from **Fig. 6.18**. It can be observed from the figure that the overall time for crystallization reduces with increase in SNC loading. At 2.5 °C/min heating rate, the overall time of crystallization value for nPLA foam is observed as ~21 min, which is reduced to ~20 min for PLA/SNC 1 foam. The value further reduced to ~11 min and ~9.5 min for PLA/SNC 2 and PLA/SNC 3 respectively. A similar trend can be noticed for higher heating rates from the figure. The crystallization half-time (t_{50}) at 2.5 °C/min is observed as ~7.8 min for nPLA. The value reduced to ~7.3 min, ~5.0 min and ~4.9 min for PLA/SNC 1, PLA/SNC 2 and PLA/SNC 3 respectively. For higher heating rates, also similar trend is observed. In case of 5 °C/min heating rate, the value observed as ~4.3 min, ~4.3 min, ~4.3 min and ~2.8 min for nPLA, PLA/SNC 1, PLA/SNC 2 and PLA/SNC 3 respectively. Similarly, in the case of 7.5 °C/min, the values are observed as ~3.0

min, ~2.8 min, ~2.8 min and ~2.4 min for nPLA, PLA/SNC 1, PLA/SNC 2 and PLA/SNC 3 respectively. A similar trend is observed in higher heating rate also. It can be concluded that SNC might be acting as a nucleating agent in the PLA matrix.

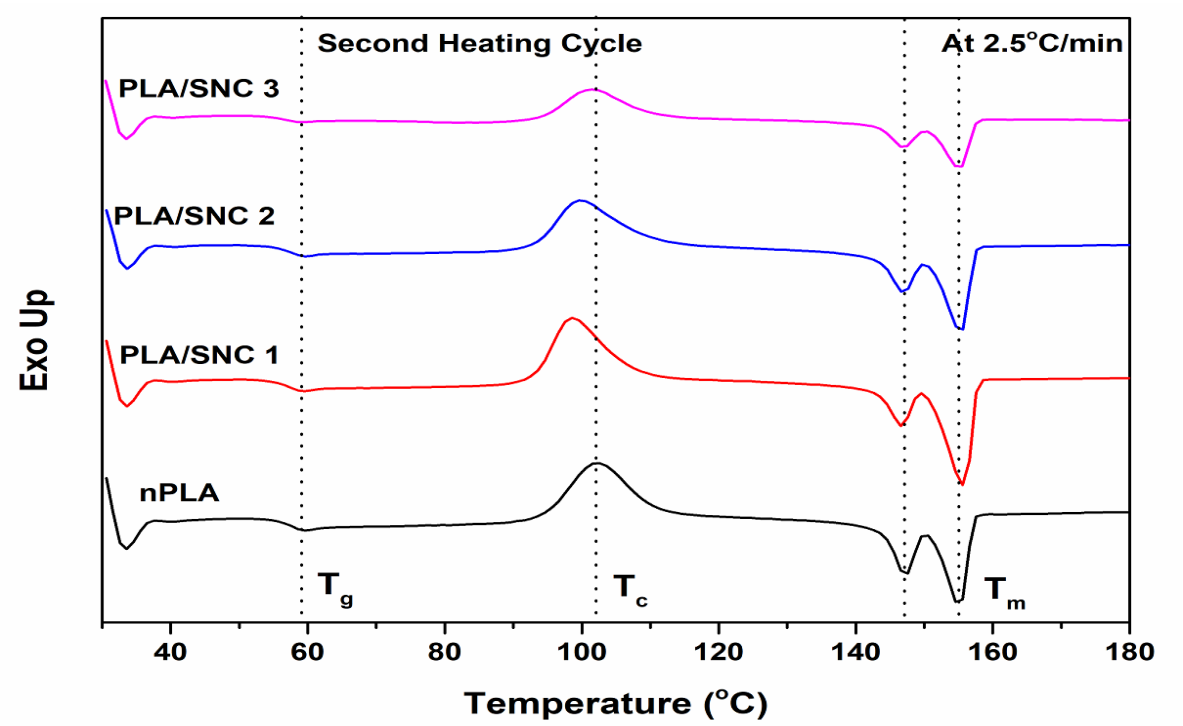

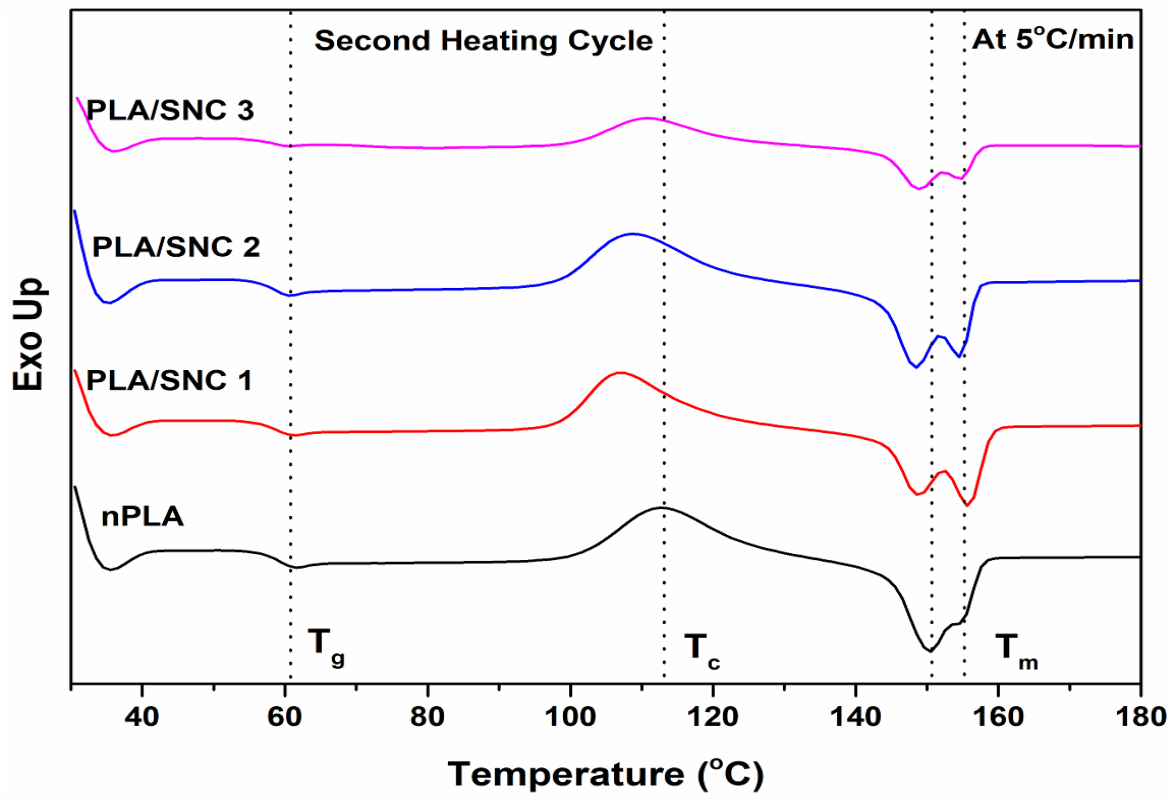

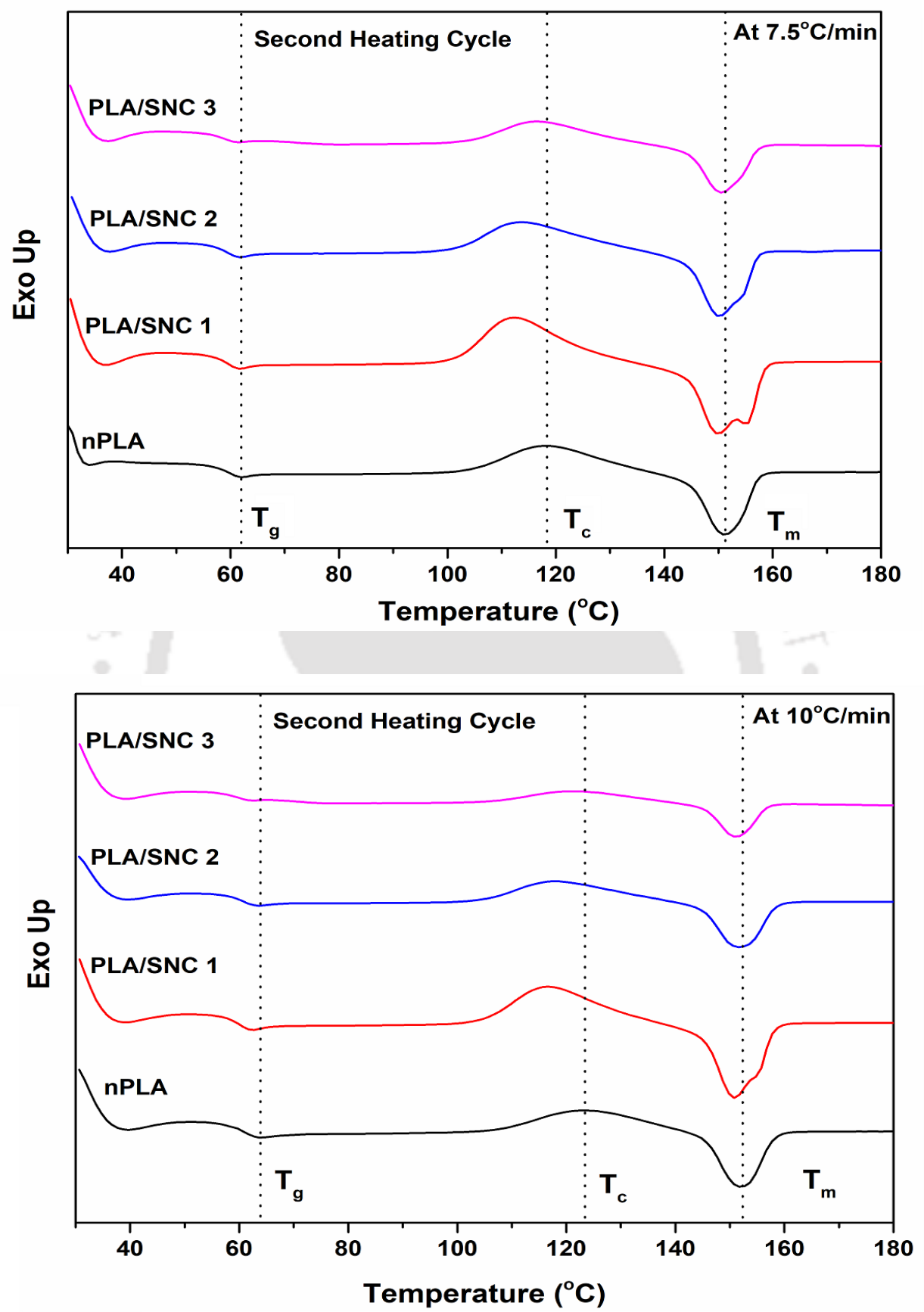

Fig. 6.17 DSC thermographs of PLA and PLA/SNC-based foams at different temperatures.

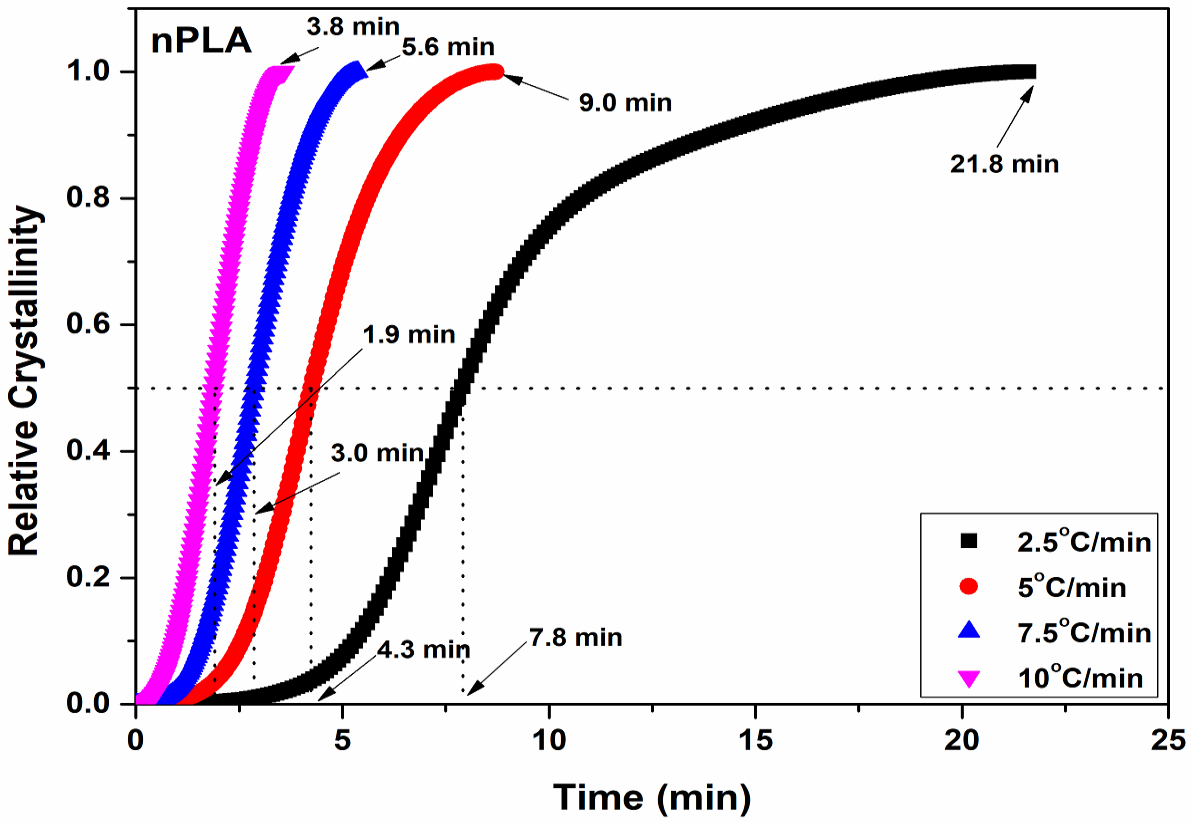

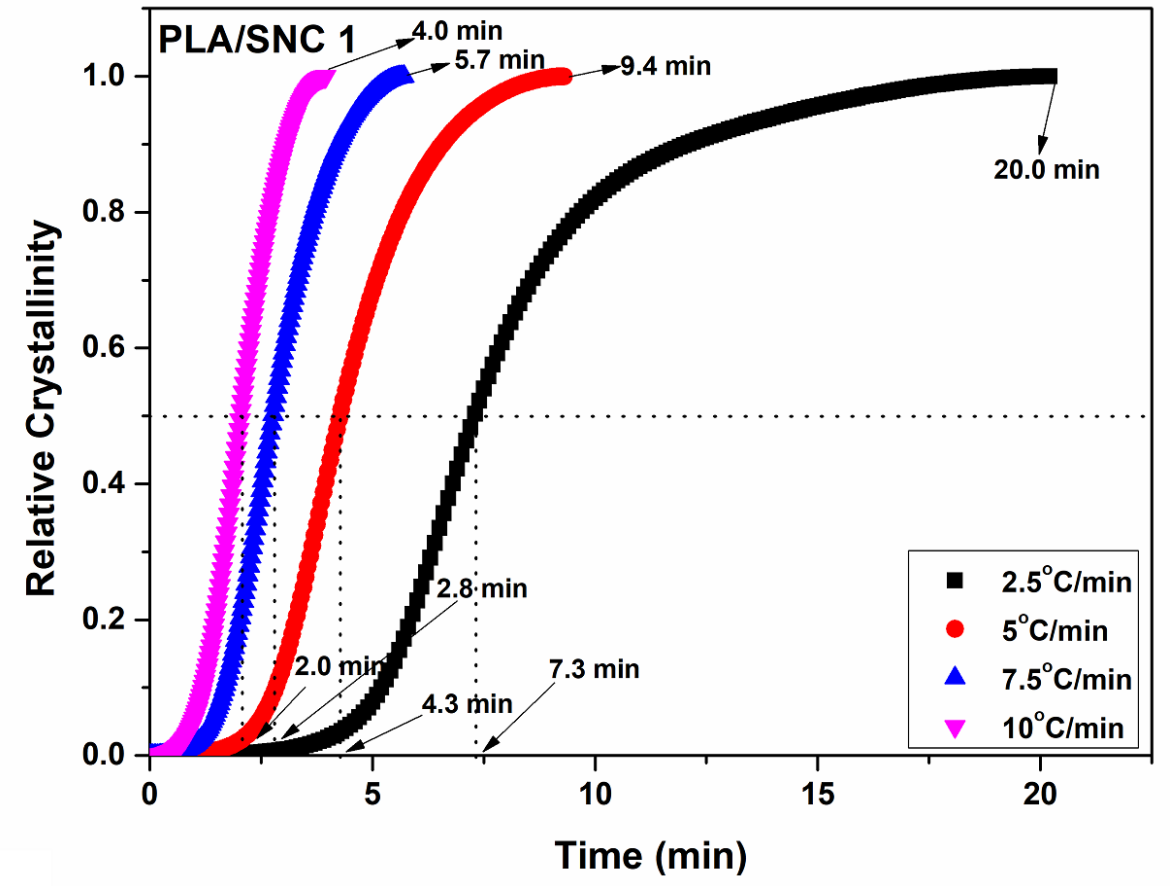

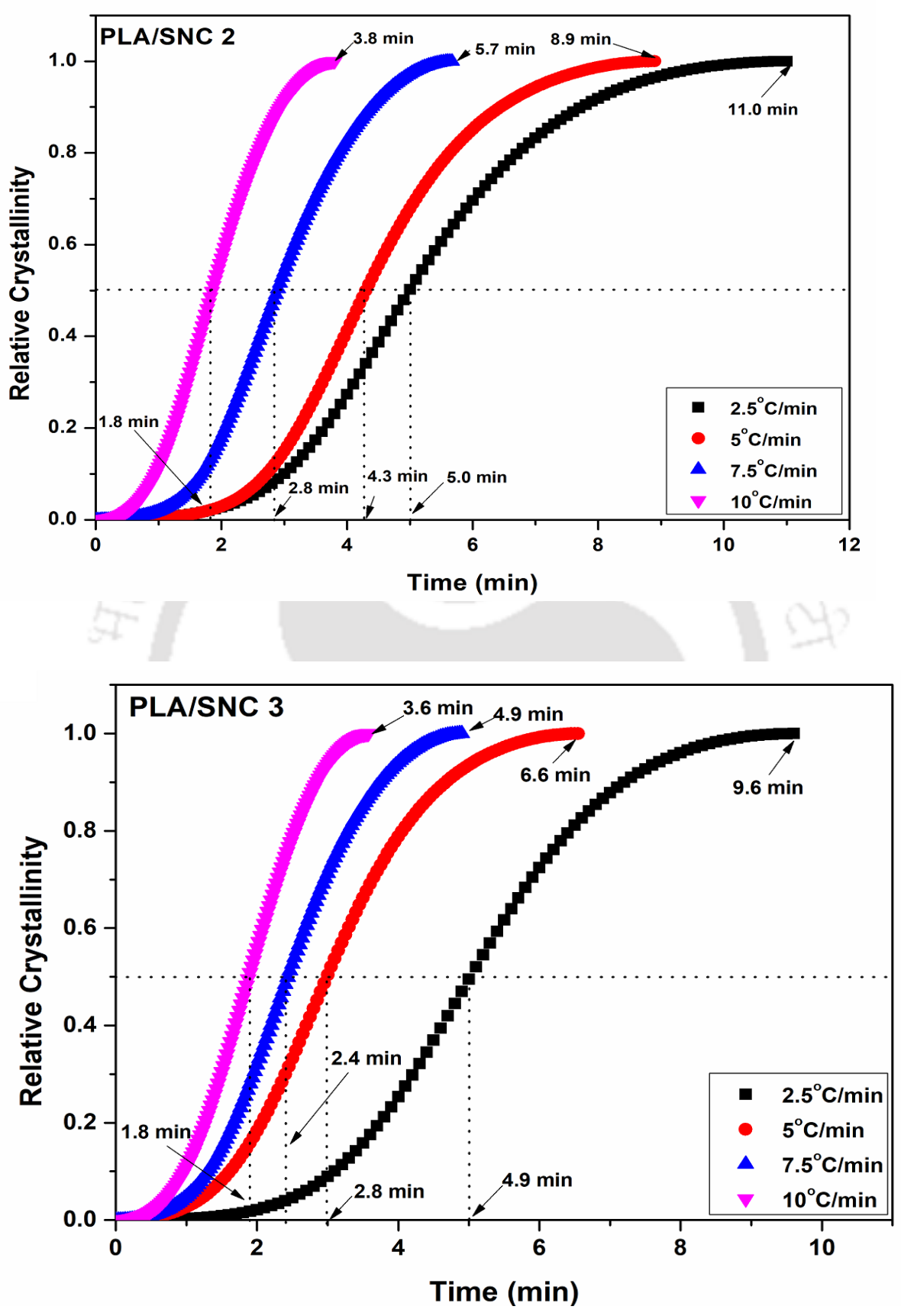

Fig. 6.18 Relative crystallinity vs. time plots of PLA and PLA/SNC-based foams.

The Avrami plots for PLA and PLA/SNC-based fabricated foams can be observed in **Fig. 6.19**. The crystallization rate constant "*k*" and Avrami exponent "*n*" values are calculated from slope and intercept of the plots and are summarized in **Table 6.4**. The values are very important to understand the crystallization behavior. A slight deviation from the linearity is observed in the Avrami plots indicating the presence of both primary and secondary crystallization in the PLA/SNC-based system.

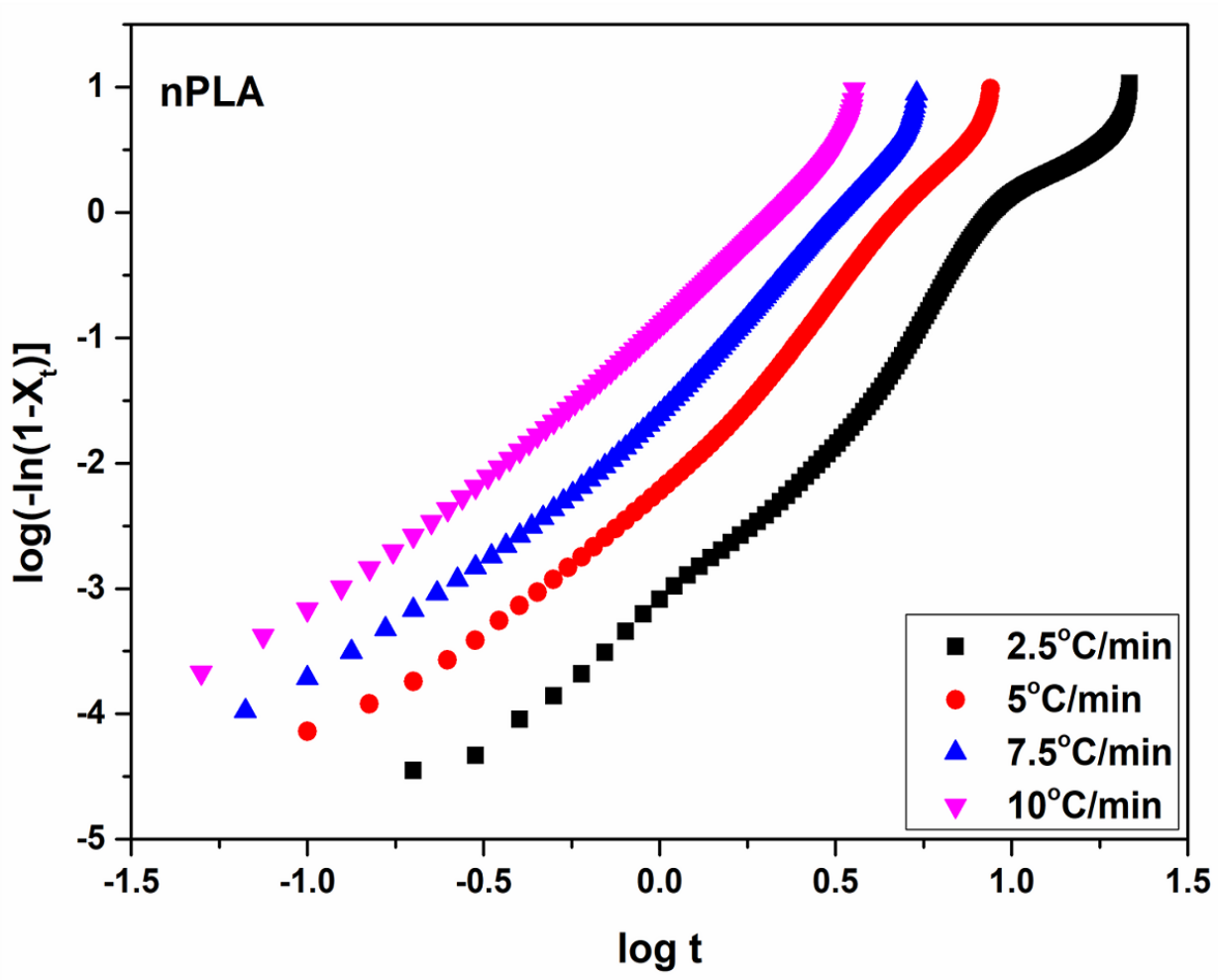

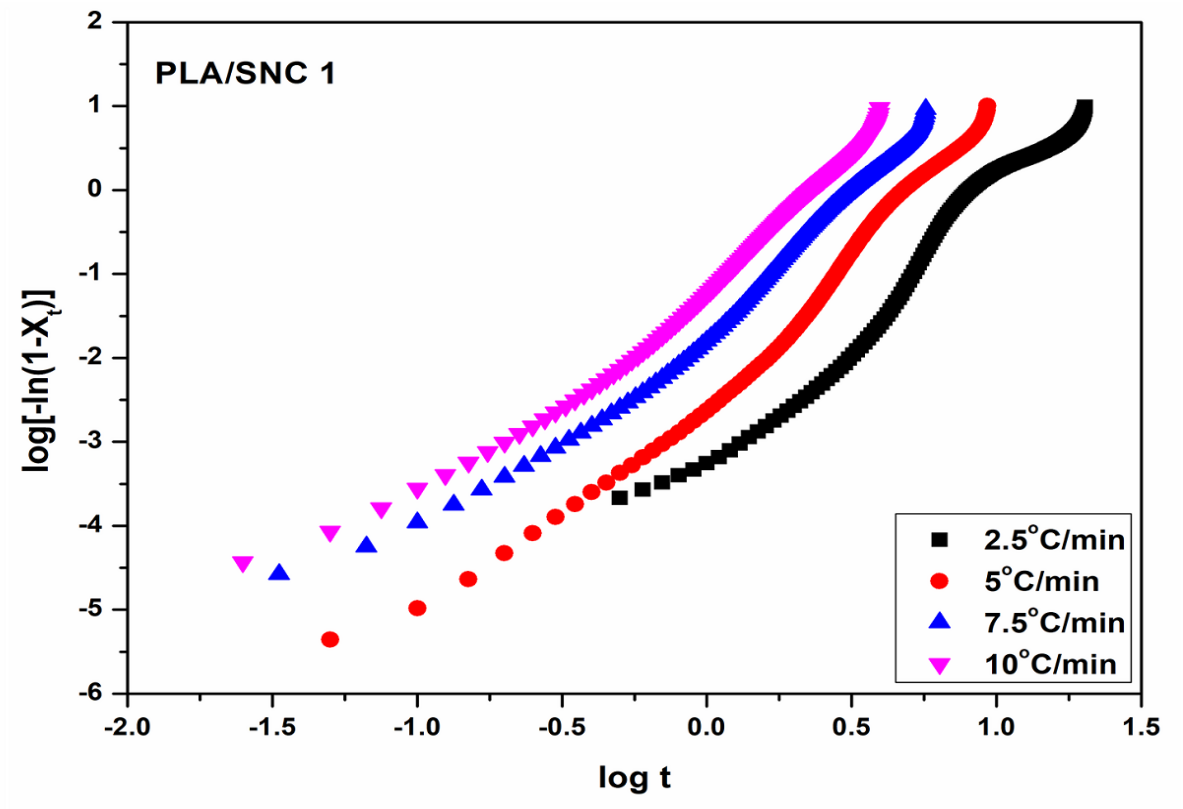

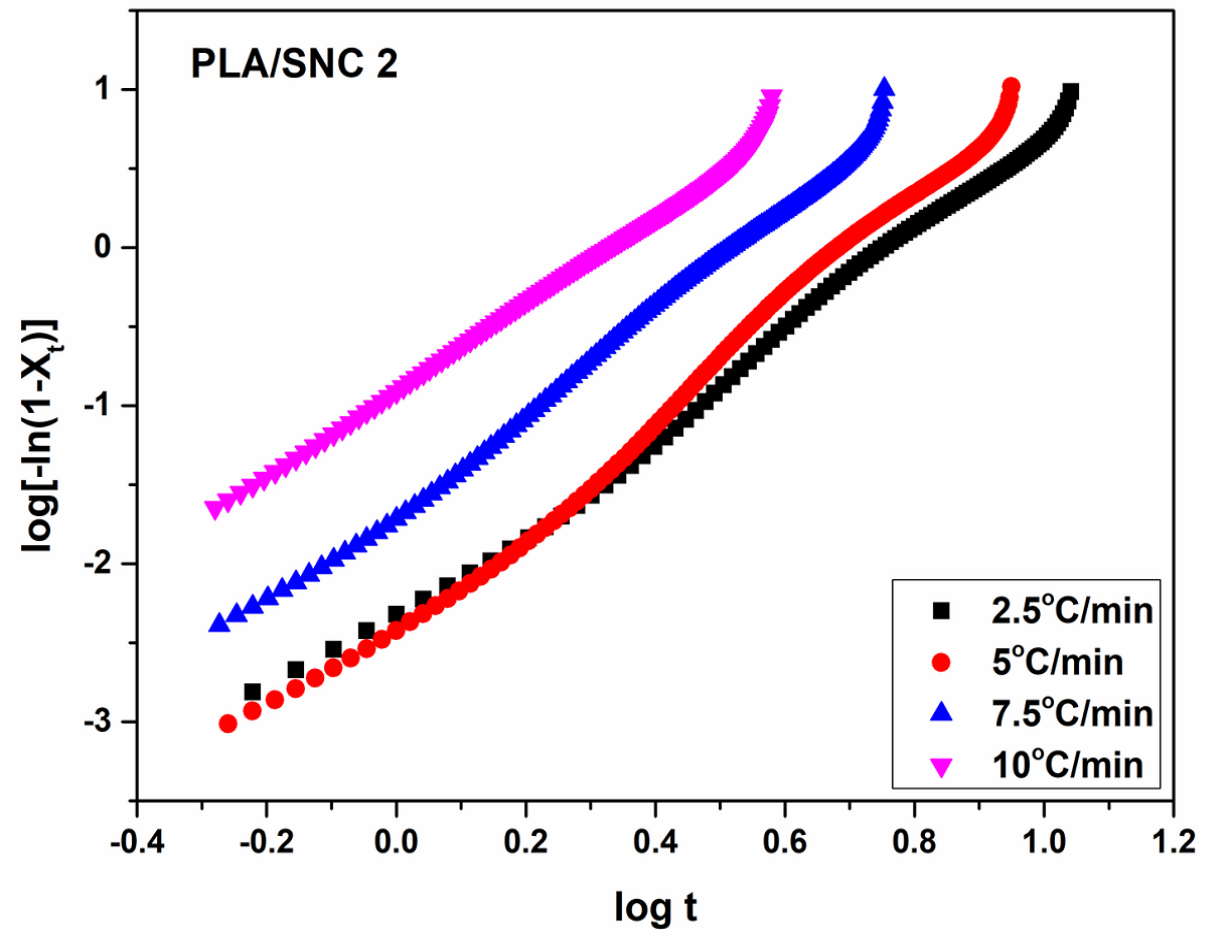

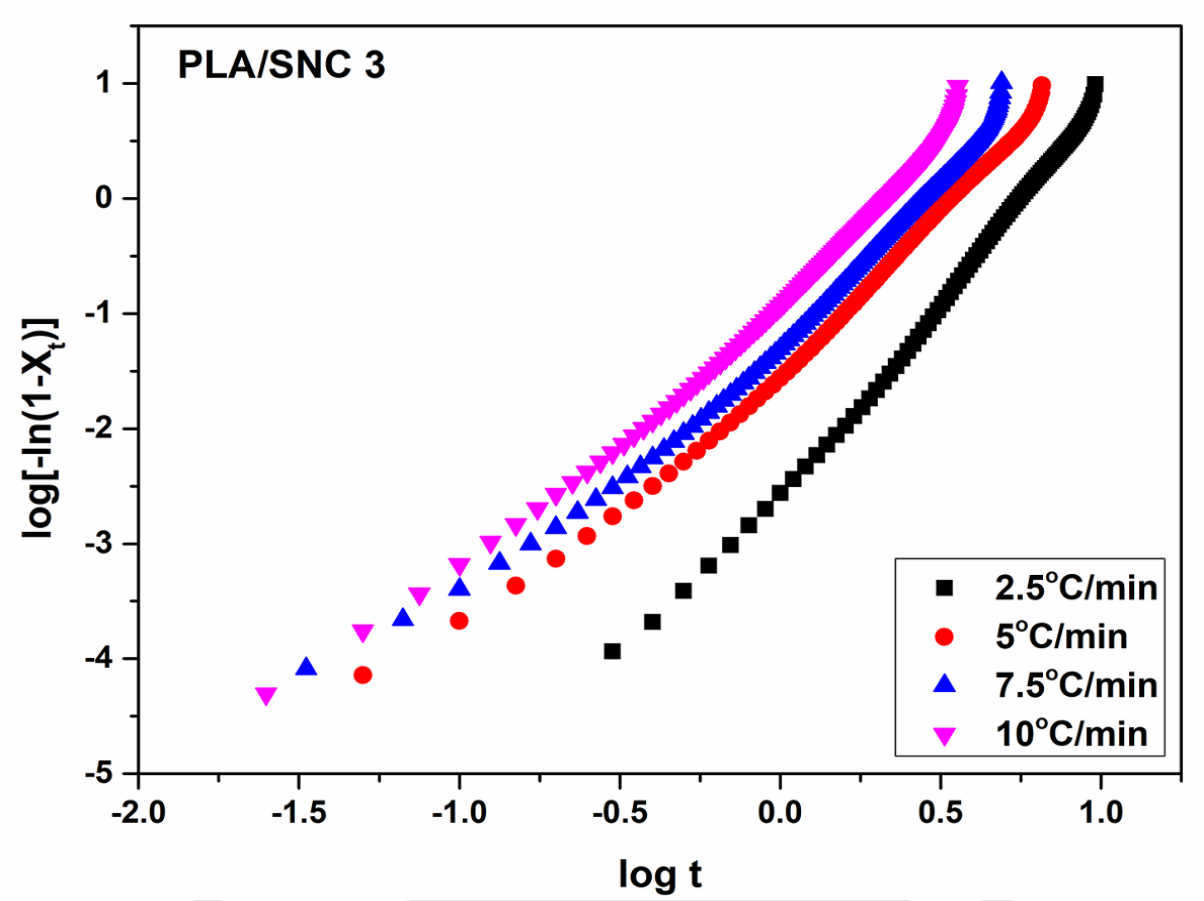

Fig. 6.19 Avrami plots for PLA and PLA/SNC-based foams.

From the Avrami plots, it can be observed that all the fabricated PLA/SNC-based foams behave similarly. From the value of "*n*" the nucleation mechanism of SNC can be understood by the crystal growth. The value of "*n*" observed in the range of ~2.1-~3.9 as observed from the table. The "*n*" value nearer to ~2 suggested the 2-dimensional growth of crystals and its value nearer to ~3 suggested the plate-like growth of crystals. Similarly, from the rate constant value, it can be noticed that "*k*" increases on increasing the heating rate for all the fabricated PLA and PLA/SNC-based foams. It can be concluded that SNC acts as a nucleating agent in the matrix and enhances the generation of smaller pores and also takes part in the crystallization process [123,231]. Similarly, Tobin plots of crystallization of PLA and PLA/SNC-based foams are shown in **Fig. 6.20**. The deviation from linearity in the Tobin plots are observed suggesting both primary and secondary crystallization in the PLA/SNC-based foams.

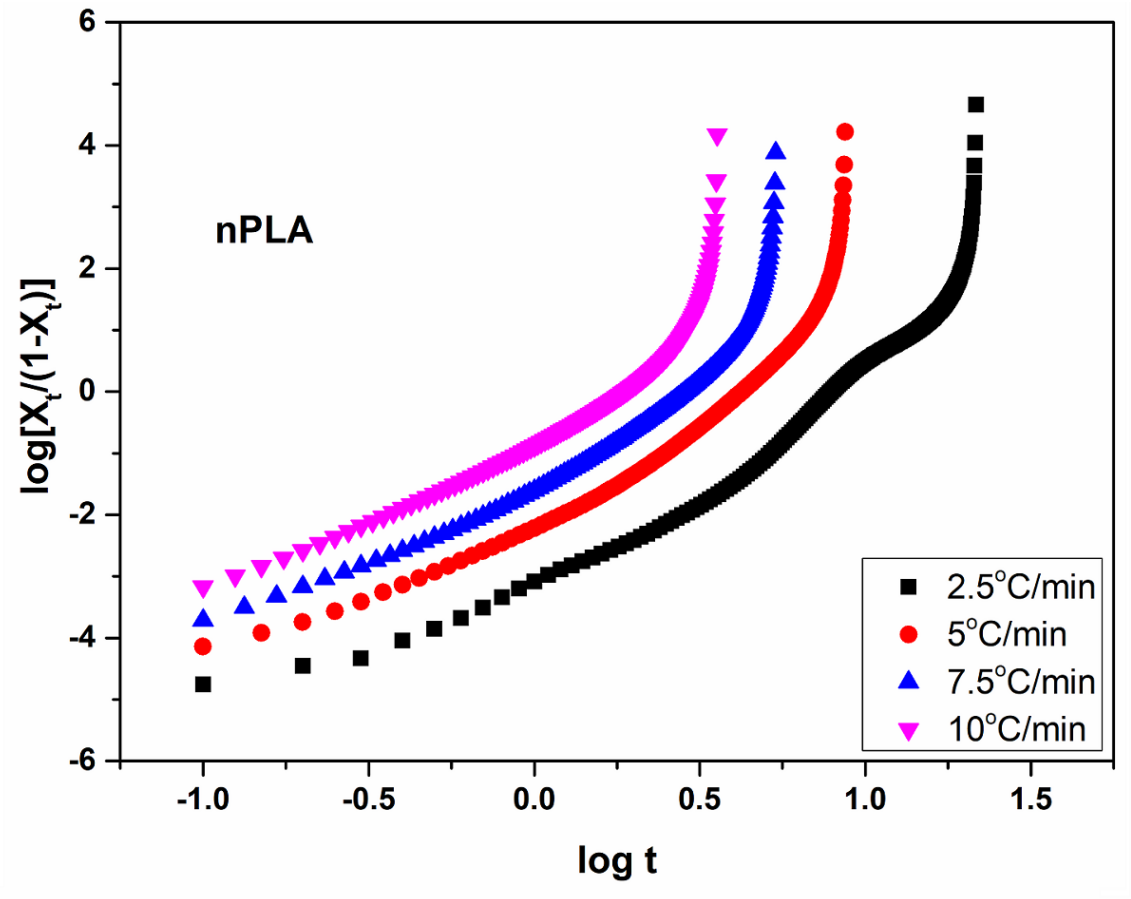
nPLA
log[X_t/(1-X_t)]
log t
2.5°C/min
5°C/min
7.5°C/min
10°C/min

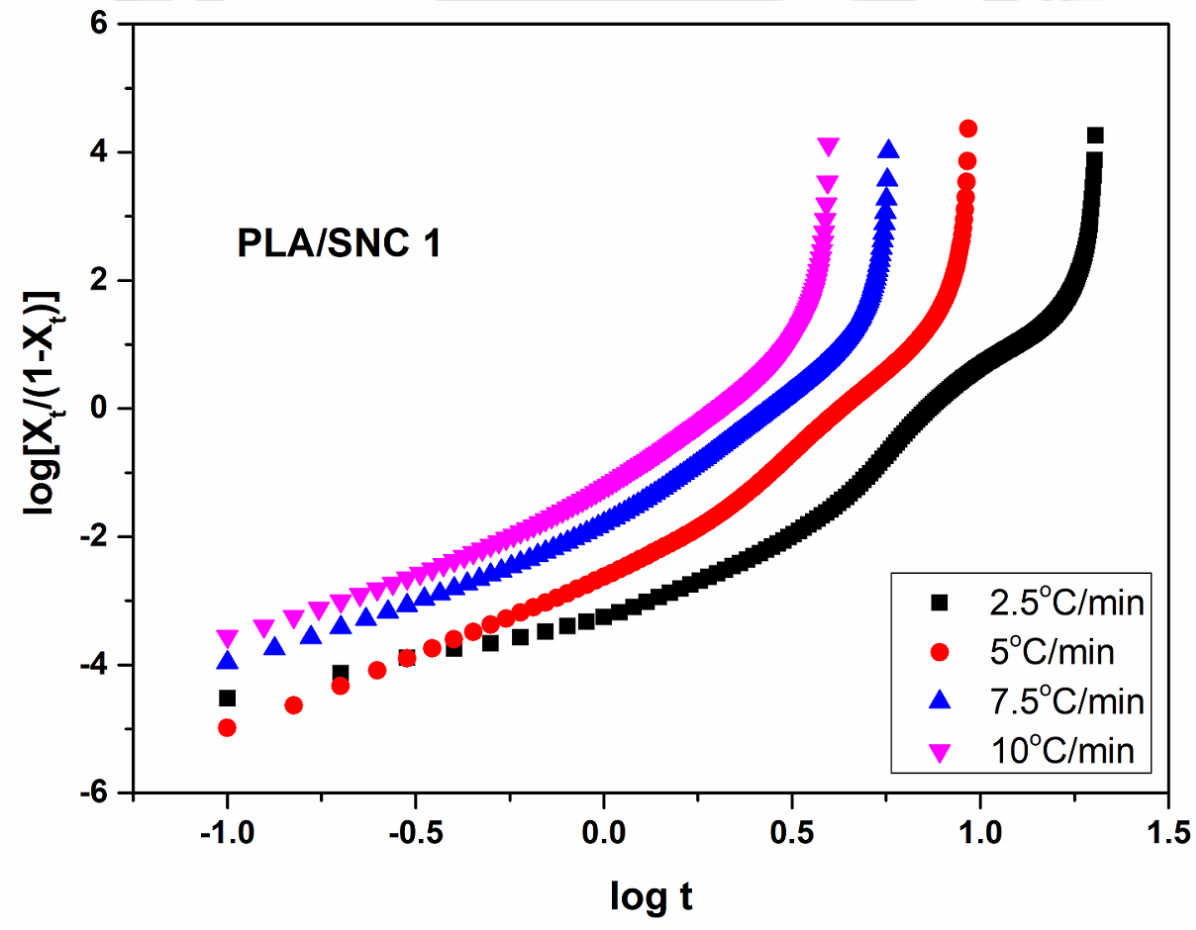
PLA/SNC 1
log[X_t/(1-X_t)]
log t
2.5°C/min
5°C/min
7.5°C/min
10°C/min

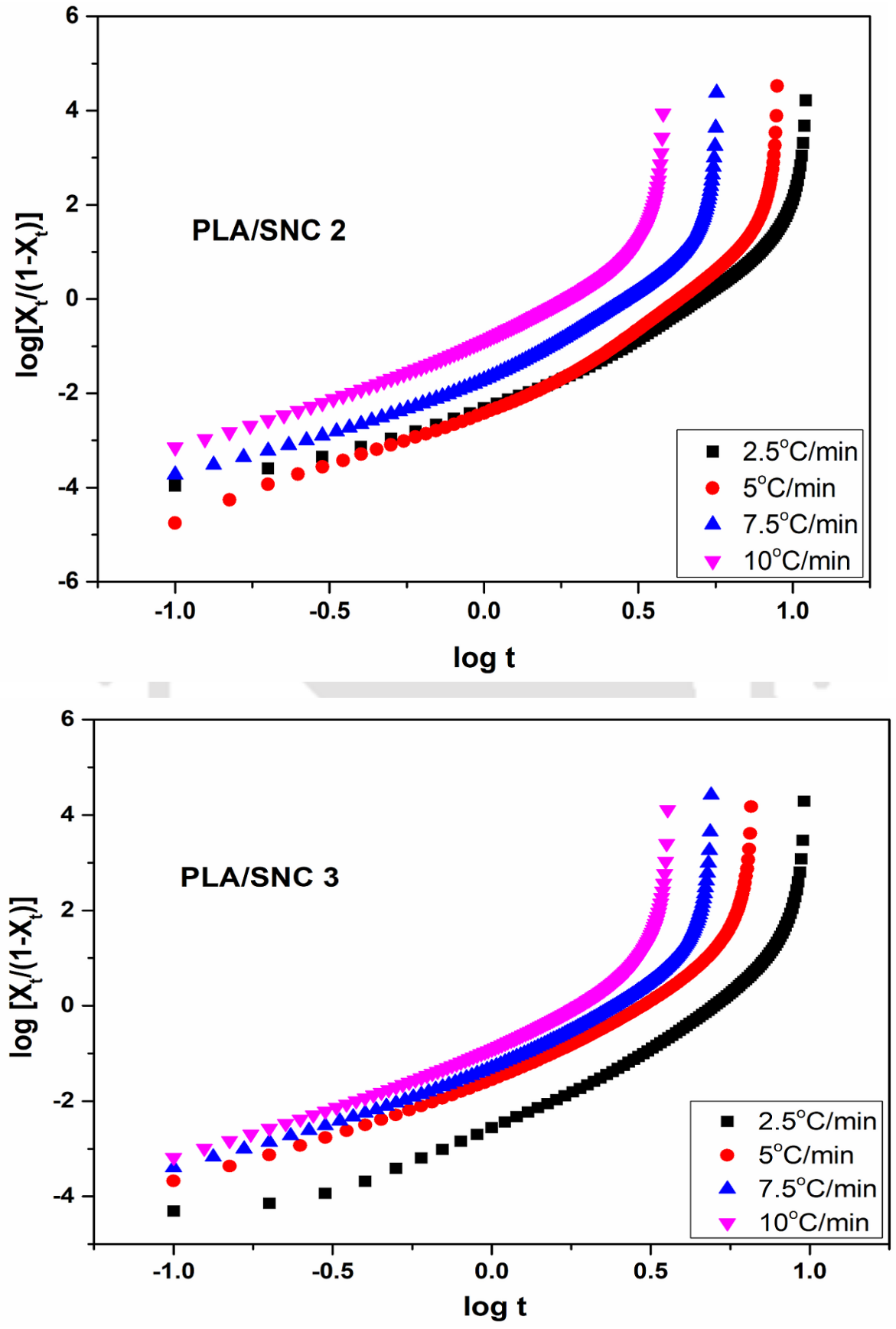

Fig. 6.20 Tobin plots for PLA and PLA/SNC-based foams.

Tobin plot is helpful in understanding the whole crystallization process along with Avrami. The value of Tobin parameters "n_T" and "K_T" are tabulated in **Table 6.5**. The observed value of "n_T" are in the range of ~3.1-~4.1 for PLA and PLA/SNC-based foams. The value is similar to the Avrami plots. The increase in the value of "K_T" is also observed with the increase in heating rates which also in agreements with Avrami constant. The observed Tobin parameters are higher than the Avrami parameters [192]. The Tobin parameters are in good accordance with the Avrami parameters.

The Kissinger plots for the energy of crystallization (ΔE) of PLA and PLA/SNC-based foams are shown in **Fig. 6.21**. The ΔE values are calculated from the slope of the linearly fitted Kissinger plot and are tabulated in **Table 6.4**.

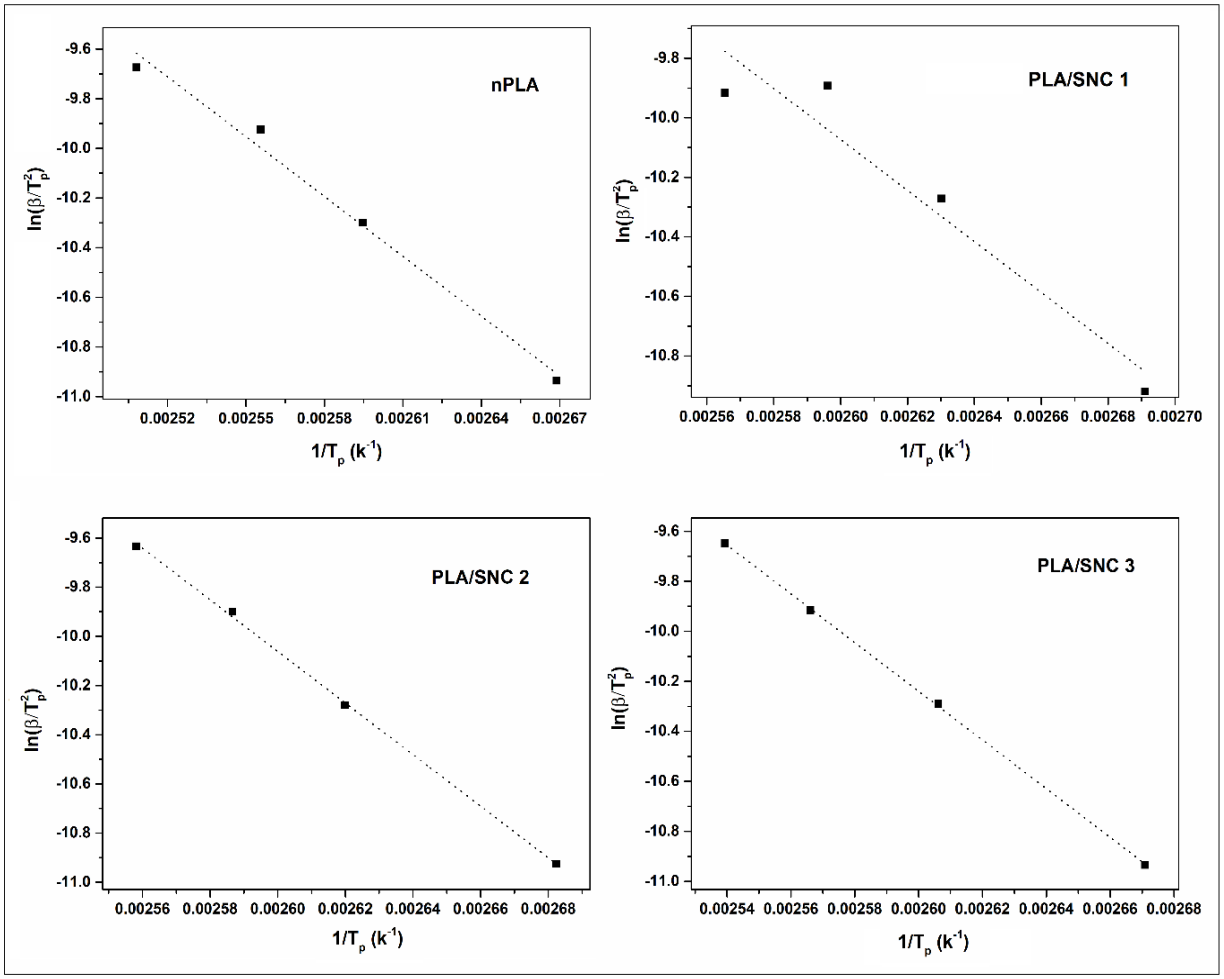

Fig. 6.21 Kissinger plots for crystallization energy of PLA and PLA/SNC-based foams.

It is observed from the table that ΔE value of nPLA foam is ~66.8 kJ/mol. The value slightly increases to ~71.2 kJ/mol for 1% loading of SNC nanobiofillers. The value of ΔE further increases to ~87.2 kJ/mol for PLA/SNC 2. At the highest loading of SNC (PLA/SNC 3), the value is observed as ~81.0 kJ/mol. The slight increase in ΔE value might be due to the hindrance of SNC in the chain folding behavior. Therefore, higher energy is required for crystallization. At higher loading, there might be some agglomeration of SNC, which requires more energy for crystallization [157].

Table 6.4 Crystallization parameters from the Avrami and Kissinger analysis.

Sample	**Heating Rate (°C/min)**	**$t_{0.5}$ (min)**	***k*** **(min^{-n})**	***n***	**ΔE (kJ/mol)**
nPLA	2.5	7.8	0.0008	2.9	66.8
	5	4.3	0.009	2.1	
	7.5	3.0	0.04	2.8	
	10	1.9	0.2	2.6	
PLA/SNC 1	2.5	7.3	0.0005	3.3	71.2
	5	4.3	0.004	3.3	
	7.5	2.8	0.03	2.9	
	10	2.0	0.1	2.8	
PLA/SNC 2	2.5	5.0	0.004	3.1	87.2
	5	4.3	0.004	3.5	
	7.5	2.8	0.02	3.2	
	10	1.8	0.1	2.8	
PLA/SNC 3	2.5	4.9	0.003	3.4	81.0
	5	2.8	0.04	2.6	
	7.5	2.4	0.1	2.6	
	10	1.8	0.2	2.6	

The Mo plots of crystallization of PLA and PLA/SNC-based foams can be observed in **Fig. 6.22.** The values of "*a*" and *"F(t)"* at different crystallization degrees are tabulated in **Table 6.5**.

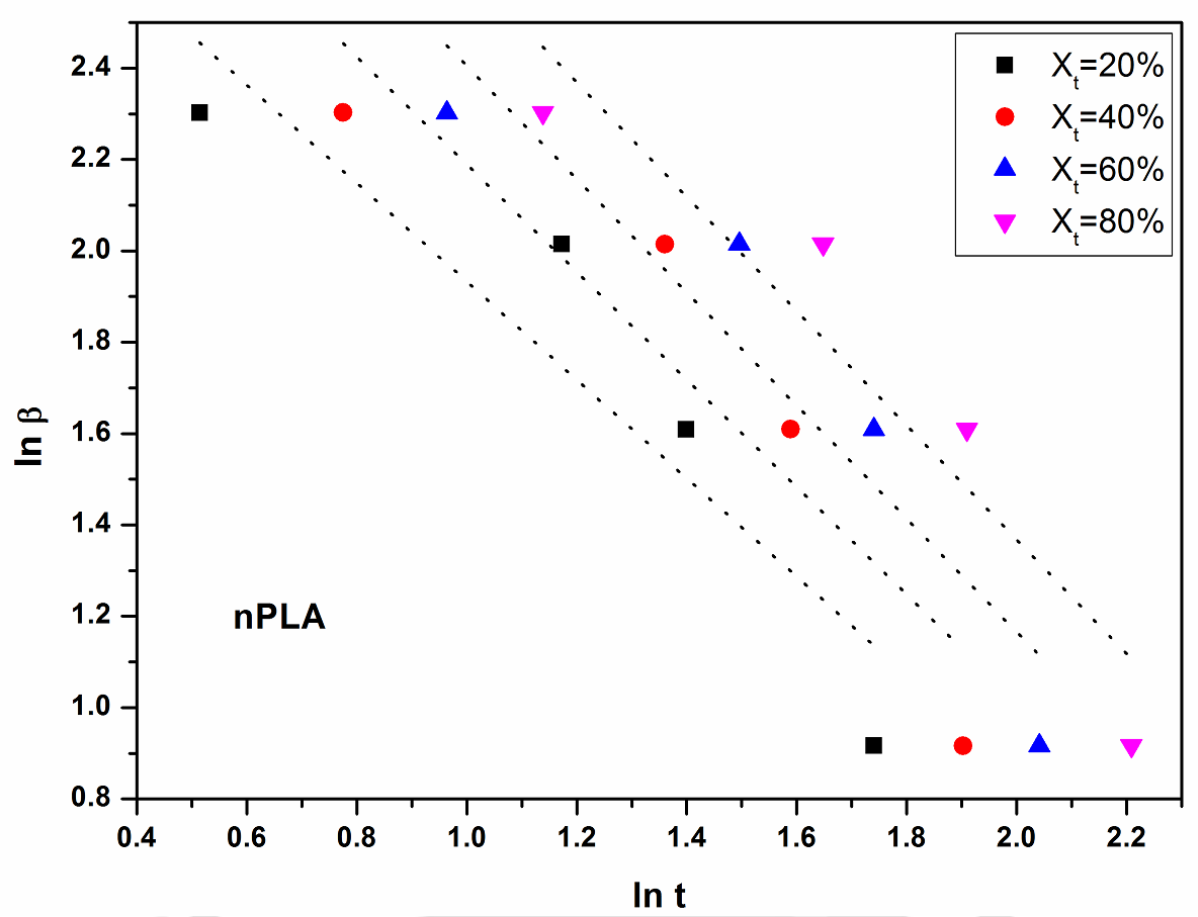

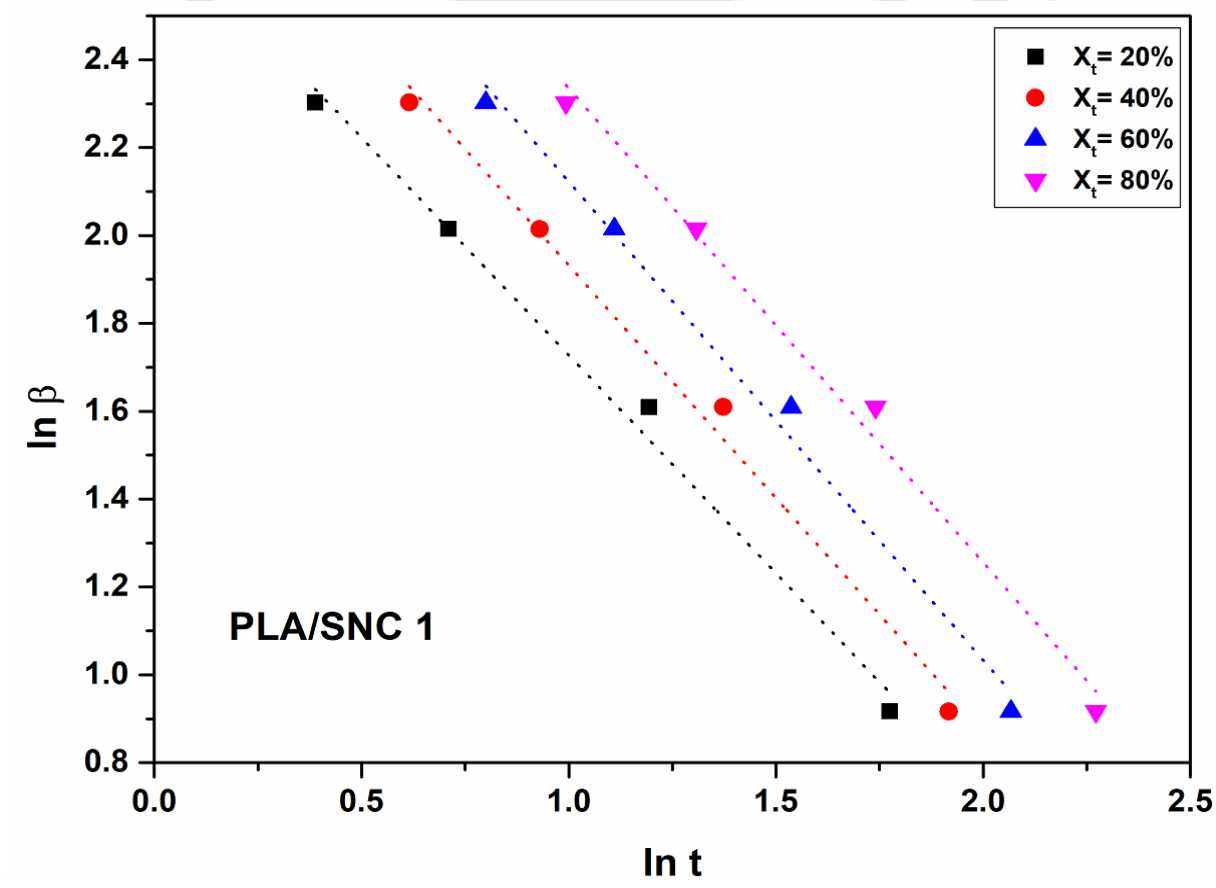

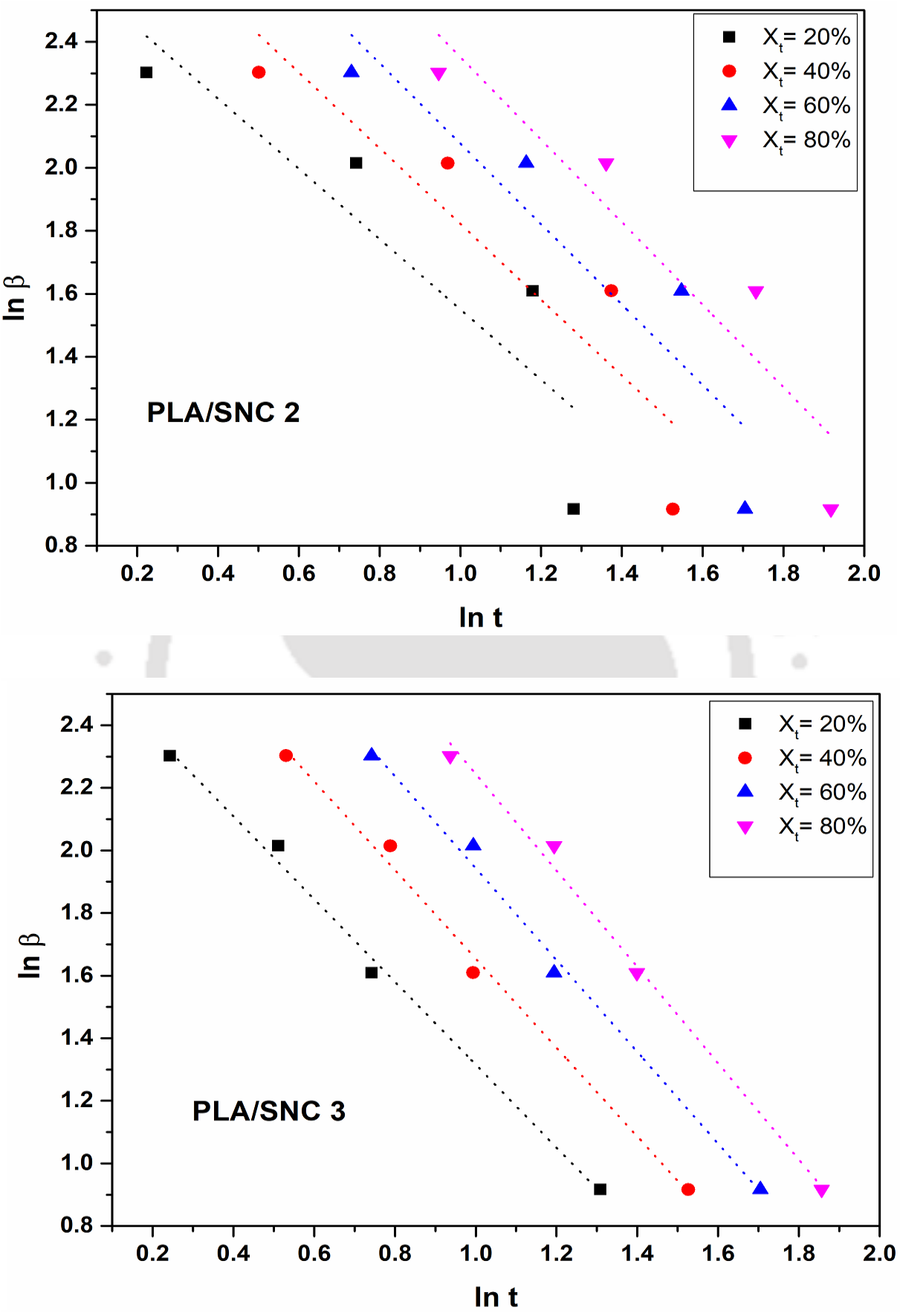

Fig. 6.22 Mo plots of PLA and PLA/SNC-based foams.

Table 6.5 Crystallization parameters from the Mo and Tobin analysis.

Sample	Mo			Heating Rate (°C/min)	Tobin	
	X_t (%)	$F(t)$	a		K_T	n_T
nPLA	20	20.3	1.1	2.5	0.04	3.1
	40	28.9	1.2	5	0.1	3.9
	60	38.2	1.2	7.5	0.3	3.7
	80	47.9	1.3	10	0.5	3.5
PLA/SNC 1	20	15.2	1.0	2.5	0.03	4.1
	40	19.9	1.1	5	0.08	4.1
	60	24.8	1.1	7.5	0.2	4.1
	80	30.4	1.1	10	0.4	4.0
PLA/SNC 2	20	14.4	1.1	2.5	0.1	3.8
	40	20.6	1.2	5	0.09	4.1
	60	28.6	1.3	7.5	0.2	3.8
	80	38.9	1.3	10	0.5	3.6
PLA/SNC 3	20	13.9	1.3	2.5	0.08	4.0
	40	21.6	1.4	5	0.2	3.7
	60	30.3	1.5	7.5	0.3	3.6
	80	43.9	1.5	10	0.5	3.5

The range of "*a*" value for nPLA are observed in the range of ~1.1, ~1.2, ~1.2 and ~1.3 at 20%, 40%, 60%, and 80% relative crystallinity. Similarly for the value lies in the range of ~1.0-~1.1, ~1.1-~1.3 and ~1.3-~1.5 for PLA/SNC 1, PLA/SNC 2 and PLA/SNC 3 respectively. The change in "*a*" value at different crystallization degree suggest the change in crystallization mechanism. The non-linearity observed in the Mo plots also suggesting the presence of primary and secondary crystallization, which are in good agreements with Avrami and Tobin plots. The increase in *F(t)* value with the increase in the degree of crystallinity is observed from the table. A similar trend is followed in all the fabricated PLA/SNC-based foams indicating the higher heating rate is required at higher crystallinity [155,156].

From the above discussions of crystallization of PLA and PLA/SNC-based foams, it can be concluded that SNC acts as a nucleating agent and both the primary along with the secondary process of crystallization are undergoing in the PLA foam matrix.

6.4 Degradation behavior of PLA and PLA/SNC-based foams

The hydrolytic and photodegradation behaviour of the fabricated PLA and PLA/SNC-based foams are discussed in this section.

6.4.1 Hydrolytic degradation of PLA and PLA/SNC-based foams

The hydrolytic degradation behavior of the fabricated PLA and PLA/SNC-based foams are investigated in three different mediums of acid, basic and neutral. The weight reduction of samples after an equal interval of time is shown in **Fig. 6.23**. Two different temperatures of 35 °C and 55 °C are taken for the investigation to study the effect of temperature on hydrolytic degradation. The ester linkage present in the PLA chain in more susceptible towards hydrolytic degradation [292,293]. It can be seen from the residual weight graphs that the degradation of PLA and PLA/SNC-based foams are comparatively higher at elevated temperature. This phenomenon can be explained on the basis that at higher temperature the polymeric chain movements are higher and it requires less energy of activation for bond breaking [245,294–296]. From the figure, it is observed that the degradation rate of the fabricated PLA and PLA/SNC-based samples are higher in acidic and basic solutions compared to neutral medium might be due to the fact that –OH group of alkaline medium attacks the ester linkage of PLA matrix. It is observed that in the neutral medium the degradation is slower than the other mediums [242]. The weight loss is measured in equal intervals till a steady region is observed.

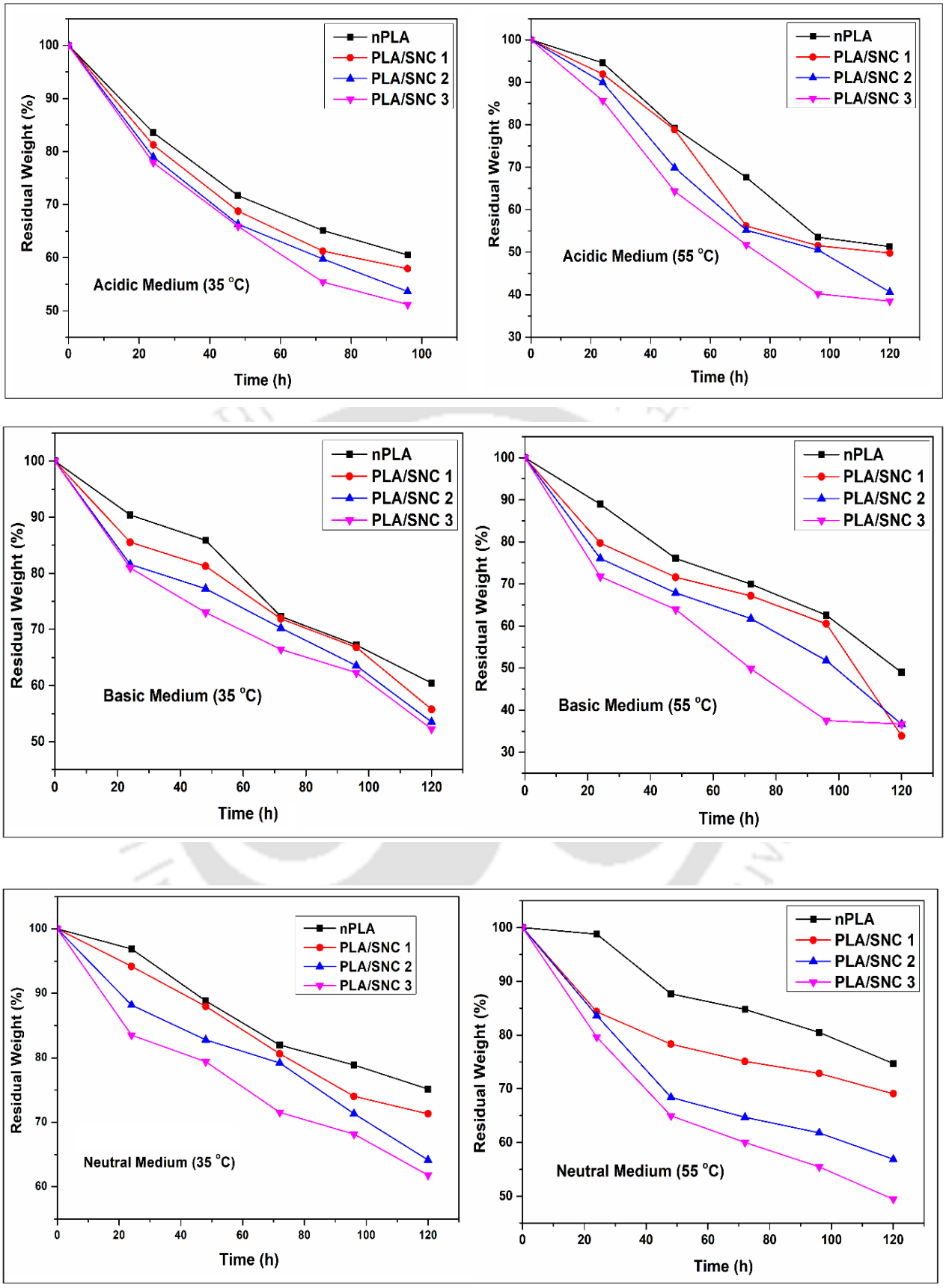

Fig. 6.23 Residual weight fraction vs. degradation time plots for degraded PLA and PLA/SNC-based foams.

Generally, hydrolytic degradation occurs in three stages: Initial or faster degradation stage, mid degradation stage, and slow and steady degradation stage. The weight loss observed in the degraded sample is due to the formation of low molecular weight oligomers and monomers by the cleavage of chains. Hydrolytic degradation mainly occurs in the surface of contact than the core of the surface [248,297,298].

6.4.1.1 Morphological changes due to hydrolytic degradation

Due to the hydrolytic degradation, some morphological changes are observed due to erosion occurred in the surface of the fabricated PLA and PLA/SNC-based foams.

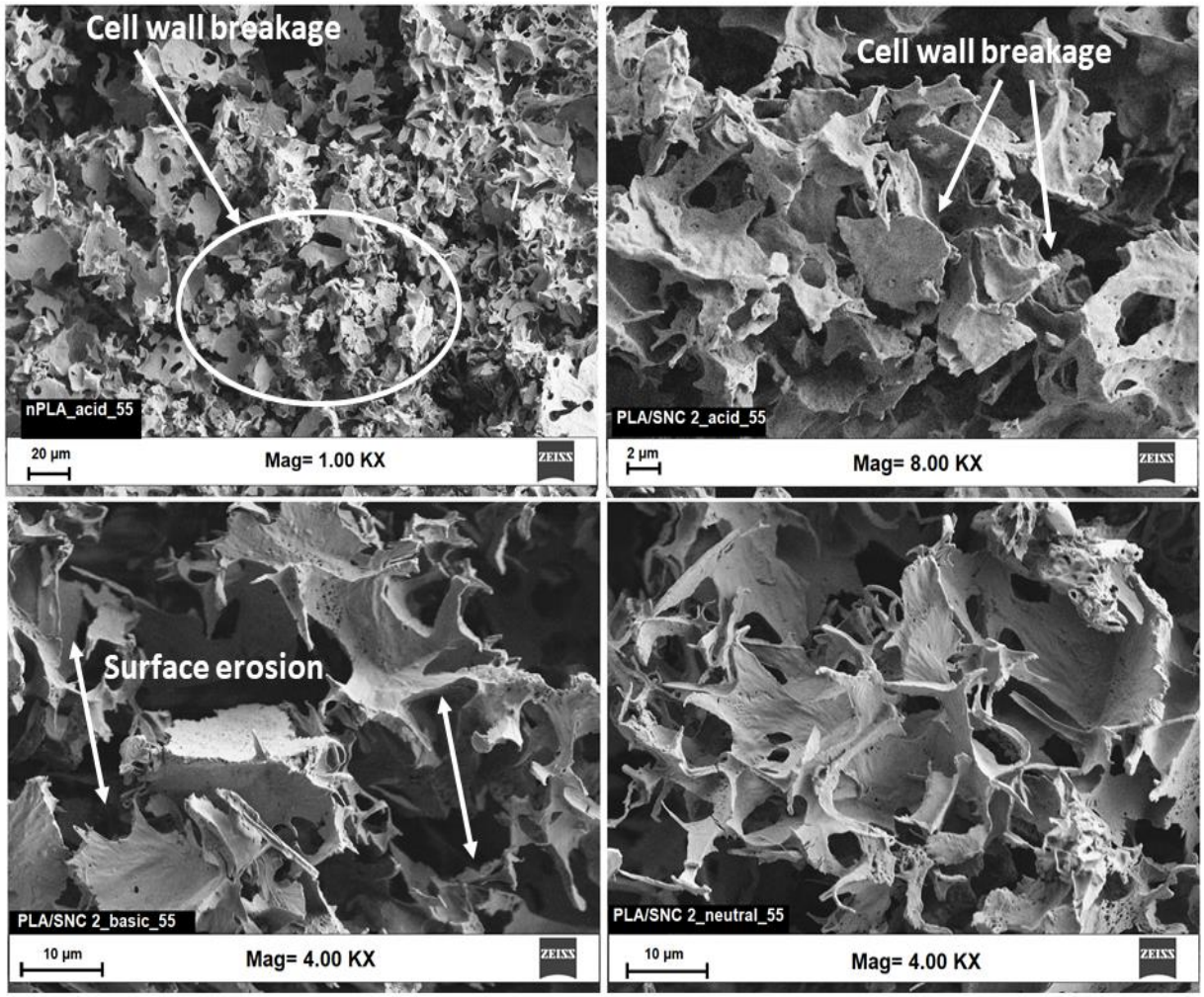

Fig. 6.24 Surface erosion and cellular breakage of PLA and PLA/SNC-based foams caused by hydrolytic degradation (at different magnifications).

The FESEM micrographs of hydrolytic degraded PLA and PLA/SNC-based foams after 120 h can be found in **Fig. 6.24**. The breakage of the cell wall and surface erosion of the fabricated foam samples are clearly visible from the micrographs as compared to **Fig. 6.2** of untreated foam samples. The cellular morphology of the foam changes and due to the breakage of cell walls, the pore size increases. It can also be observed that due to the degradation of the surface morphology of the fabricated foam changes, which might also effect in other properties like wettability. However, in the neutral medium, the degradation is a little bit less compared to acidic and basic medium also suggested by the residual weight fraction investigations [250,251].

6.4.1.2 Influence of hydrolytic degradation on wettability phenomena

The contact angle values of the hydrolytic degraded PLA and PLA/SNC-based samples at 35 °C and 55 °C are measured and shown in **Fig. 6.25**. It can be observed from the figure that the contact angle value decreases than the untreated samples as discussed in an earlier section (6.2.7). The drastic change in wettability might be due to the morphological changes observed in the foam surface and the erosion of the surface by the different medium used. The decrement is no so prominent compared to the untreated samples for neutral medium. The degradation and the change in surface morphology are comparatively lesser than the acidic and basic medium. However, from the wettability investigation, it is also observed that at elevated temperature, the decrement is more prominent in all the three medium used. From the previous section, it is confirmed that the degradation rate is faster at elevated temperature compared to low temperature. The region behind the decrements in contact angle at elevated temperature may be the more prominent surface morphological changes and erosion. The trend is similar as compared with the contact angles at 35 °C. So it can be concluded from this investigation that hydrolytic degradation has effects in wettability phenomena of the fabricated foams. The effect is more prominent in the acidic and basic medium compared to the neutral medium.

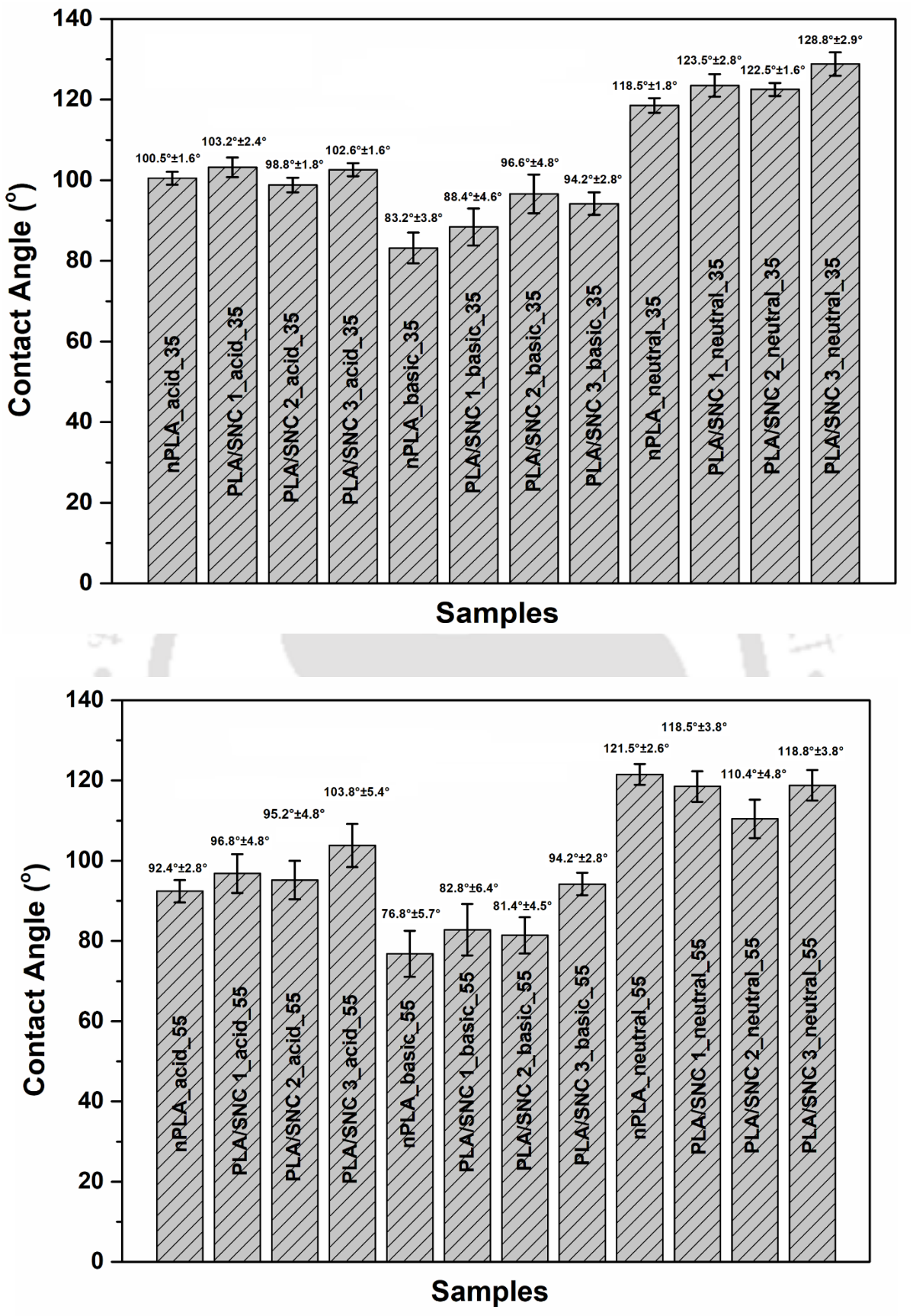

Fig. 6.25 Influence of hydrolytic degradation on the wettability of PLA and PLA/SNC-based foams.

6.4.1.3 Effect of hydrolytic degradation on the molecular weight

The molecular weight investigations of the hydrolytic degraded PLA and PLA/SNC-based foams can be found in **Fig. 6.26**. From the investigation, it can be observed that the molecular weight (both M_w and M_n) decreases on hydrolytic degradation compared to untreated PLA and PLA/SNC-based foams as observed in **Fig. 6.8.**

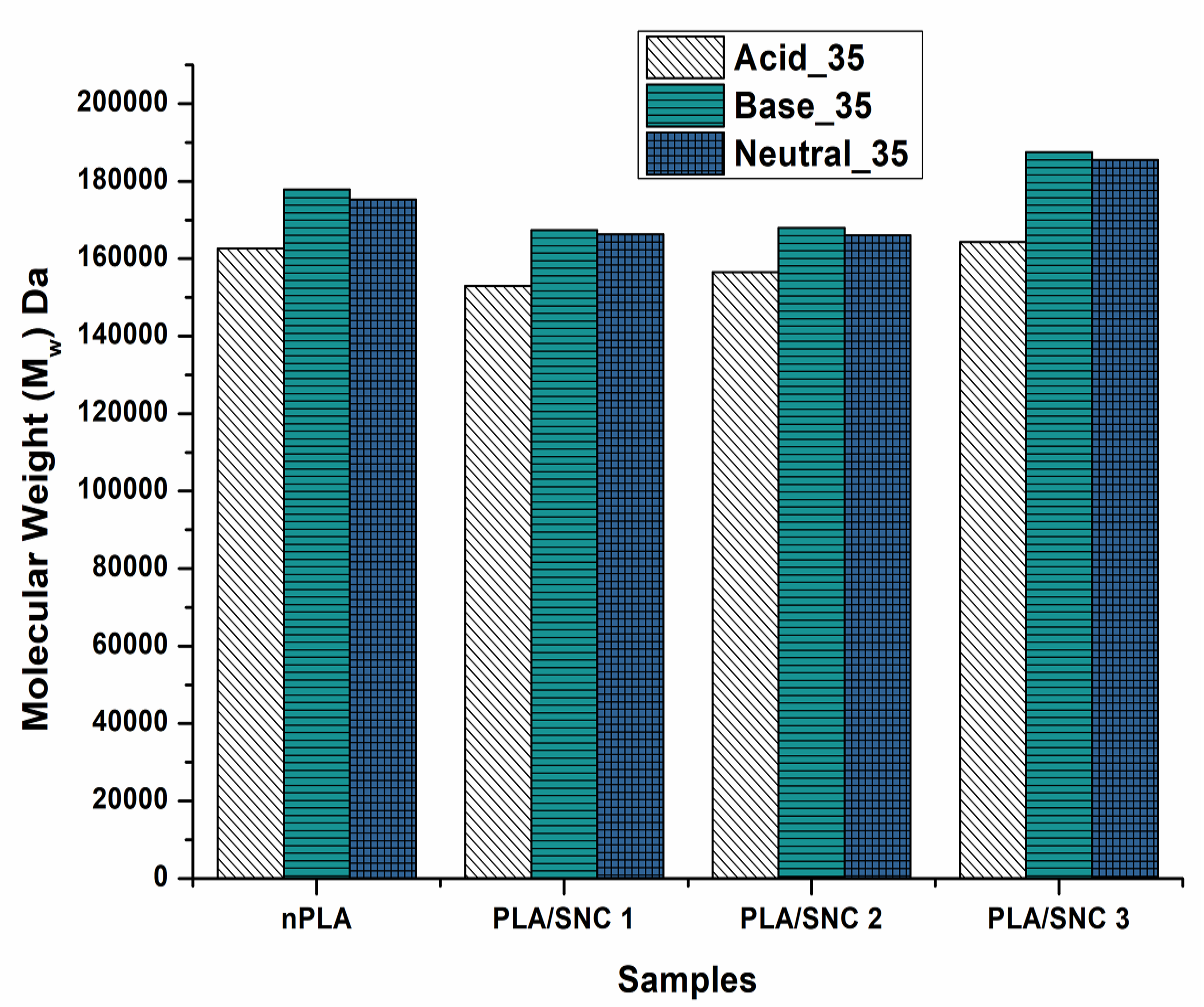

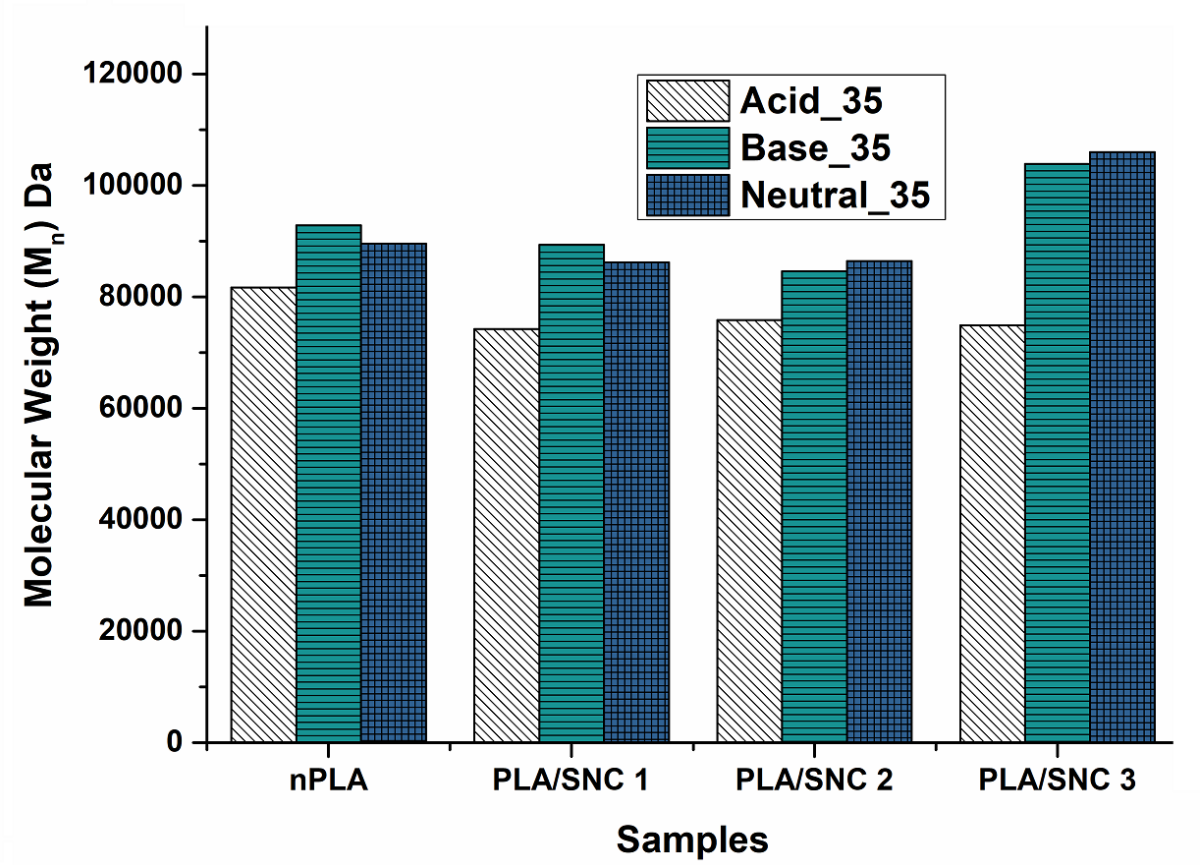

Fig. 6.26 Molecular weight (M_w and M_n) investigations of degraded PLA and PLA/SNC-based foams.

In neutral medium, the molecular weight reduction is less compared to other two mediums. The maximum reduction is observed in the acidic medium due to the degradation of the PLA in acidic medium. It can also be observed that the reduction of molecular weight is higher in PLA-based foams compared to the PLA/SNC-based fabricated foams in all the medium. This much be due to the hydrophobic nature of SNC and also the uniform dispersion in the PLA matrix [63]. The drastic reduction in molecular weight (M_w and M_n) might be due to the formation of more short chains at higher temperature and low molecular weight products [299]. The degradation process is followed by chain scission of ester linkages, producing carboxylic acid end groups. The porous structure of the developed PLA and PLA/SNC-based foams also affected the degradation. The larger surface area and penetration of the medium by the pores

also affected the degradation. In PLA/SNC-based foams the average pore size is smaller compared to PLA-based foams, makes it a little bit difficult to penetrate to the core of the matrix (as discussed in earlier section 6.2.4). At elevated temperature, the chain mobility increases that effects the faster degradation of the fabricated PLA and PLA/SNC-based foams by forming oligomers and monomers of low molecular weight, which ultimately reduced the molecular weight [241,242].

6.4.1.4 Effect of hydrolytic degradation on thermal properties of PLA and PLA/SNC-based foams

The TGA plots at a heating rate of 10 °C/min for the hydrolytic degraded PLA and PLA/SNC-based foams at 35 °C and 55 °C temperatures can be observed in **Fig. 6.27.** The thermal stability of the fabricated foam decreases on increasing in degradation temperature. The prominent degradation of thermal stability is observed for PLA/SNC-based foams in a basic medium. The thermal stability also reduced for the samples in acidic medium. The reduction in onset temperature of degradation (T_{onset}) is observed in an acidic and basic medium more significantly at 35 °C from the figure. The formation of oligomers might be the reason behind this change. At elevated temperature (55 °C), a similar trend can be observed. At elevated temperature, the mobility of polymeric chains increases and thus affecting the thermal stability. The thermal stability drastically reduced for nPLA foam in a basic medium at 55 °C. The results obtained are in good accordance with our previous observations from weight reduction and morphological analysis. From the analysis, it is also observed that PLA/SNC-based foams have more stability in neutral medium. The decrement of T_{onset} value is observed in acidic and basic medium. The reduction is more prominent at an elevated temperature of degradation.

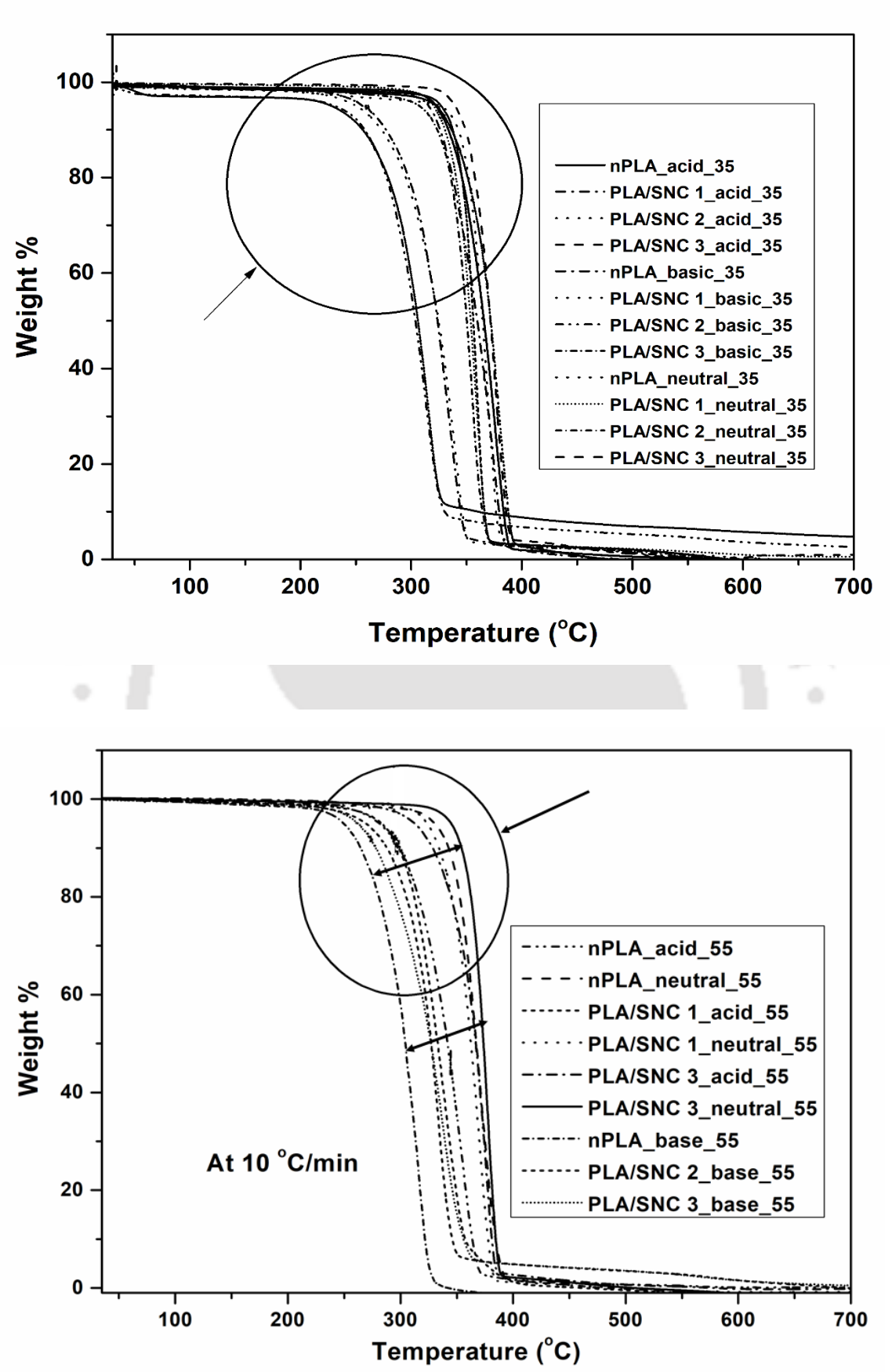

Fig. 6.27 TGA plots for degraded PLA and PLA/SNC-based foams at 35 °C and 55 °C.

The DSC plots of degraded PLA and PLA/SNC-based foams are shown in **Fig. 6.28**.

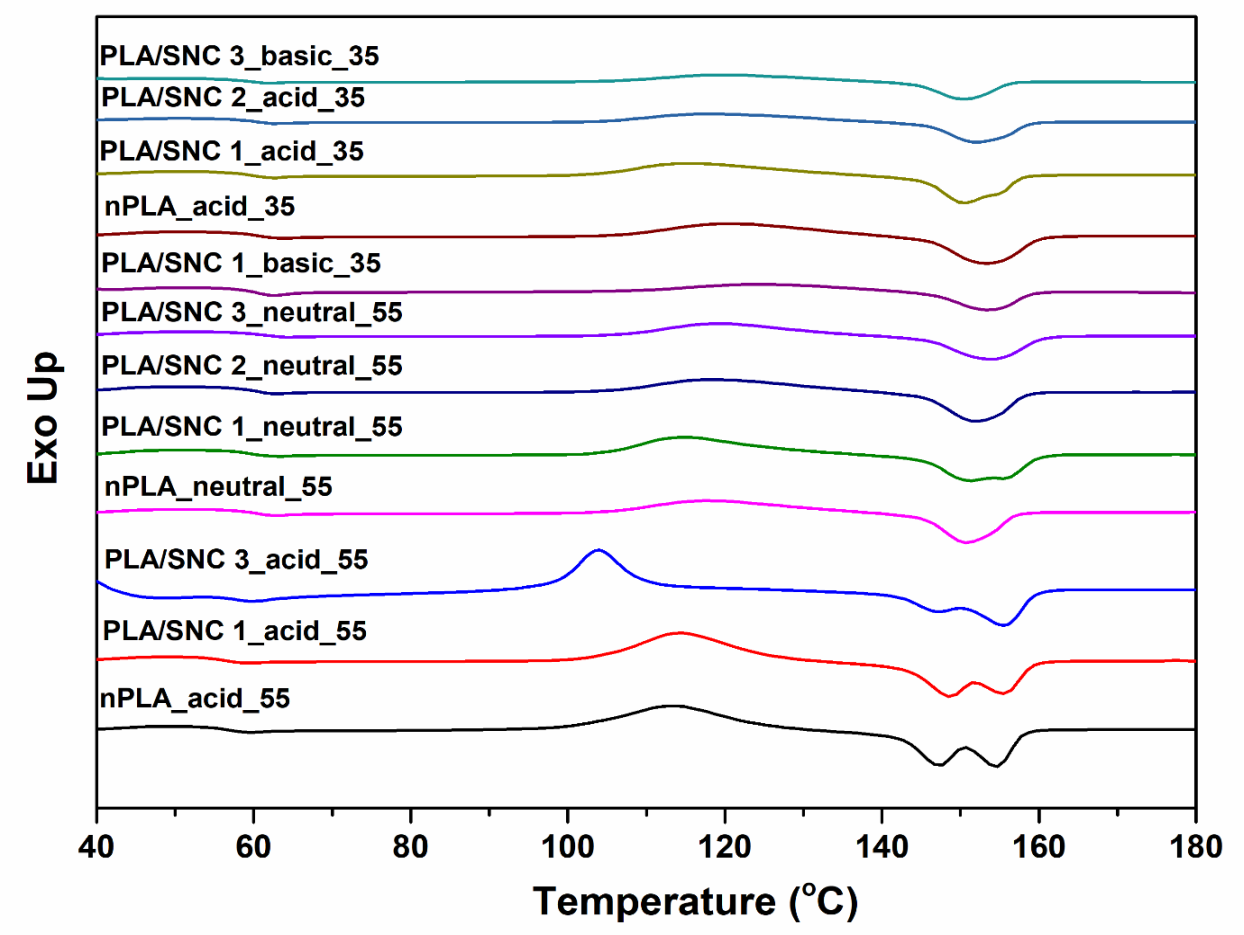

Fig. 6.28 DSC thermoplots for degraded PLA nd PLA/SNC-based foams.

From the DSC thermographs, it is clearly visible that the glass transition temperature decreases on hydrolytic degradation of the fabricated foams. The decrease in T_g might be due to the decrease in molecular weight on degradation. Formation of low molecular weight oligomers has plasticizing effects on PLA chains. The melting point of the hydrolytically degraded PLA and PLA/SNC-based foams increases compared to undegraded samples as discussed earlier (**Fig. 6.10**) [259]. The decrease in melting point is observed on hydrolytic degradation due to the increase in the formation of the short chain and a decrease in crystalline thickness on hydrolytic degradation. The initial stage of degradation consists of removal of amorphous regions and producing crystalline residue [249,299–302]. The sharp crystallization peak in

acidic samples indicates the crystalline residue in the sample since the amorphous region is wiped off by the acidic medium. It can also be observed here that for the samples in a neutral medium, the increase in melting point is less compared to other two medium. These results are also in accordance with the previously discussed outcomes of hydrolytic degradation of fabricated PLA and PLA/SNC-based foams.

The influence of hydrolytic degradation is also affected by the porous structure of the fabricated PLA and PLA/SNC-based foams. The cell size, breakage of the cell wall, available surface area for degradation and so on are the various parameters of hydrolytic degradation if we compare the porous system with different non-porous PLA/SNC-based systems [63]. Due to the cellular morphology, the available surface area for degradation is higher in foam system compared to the non-foamed system.

6.4.2 Photodegradation (UV) of PLA and PLA/SNC-based foams

The fabricated PLA and PLA/SNC-based foams are exposed under UV light and the degradation is investigated using different analytical techniques. The photodegradation is mainly caused by the absorption of light energy by the low molecular weight compounds present in the PLA matrix. The absorption leads to different chemical reactions like bond cleavage, chain scission, oxidation and cross-linking of polymeric chains [260,261]. The photodegradation studies of the fabricated PLA and PLA/SNC-based foams are carried out to understand the effect of SNC in the photodegradation. The main observation notices are the change in color or color fading of the surface and increase in brittleness [262]. The morphological investigation of the PLA and PLA/SNC-based foams after 1 week, 2 weeks and 3 weeks of exposure to UV light can be observed in **Fig. 6.29**.

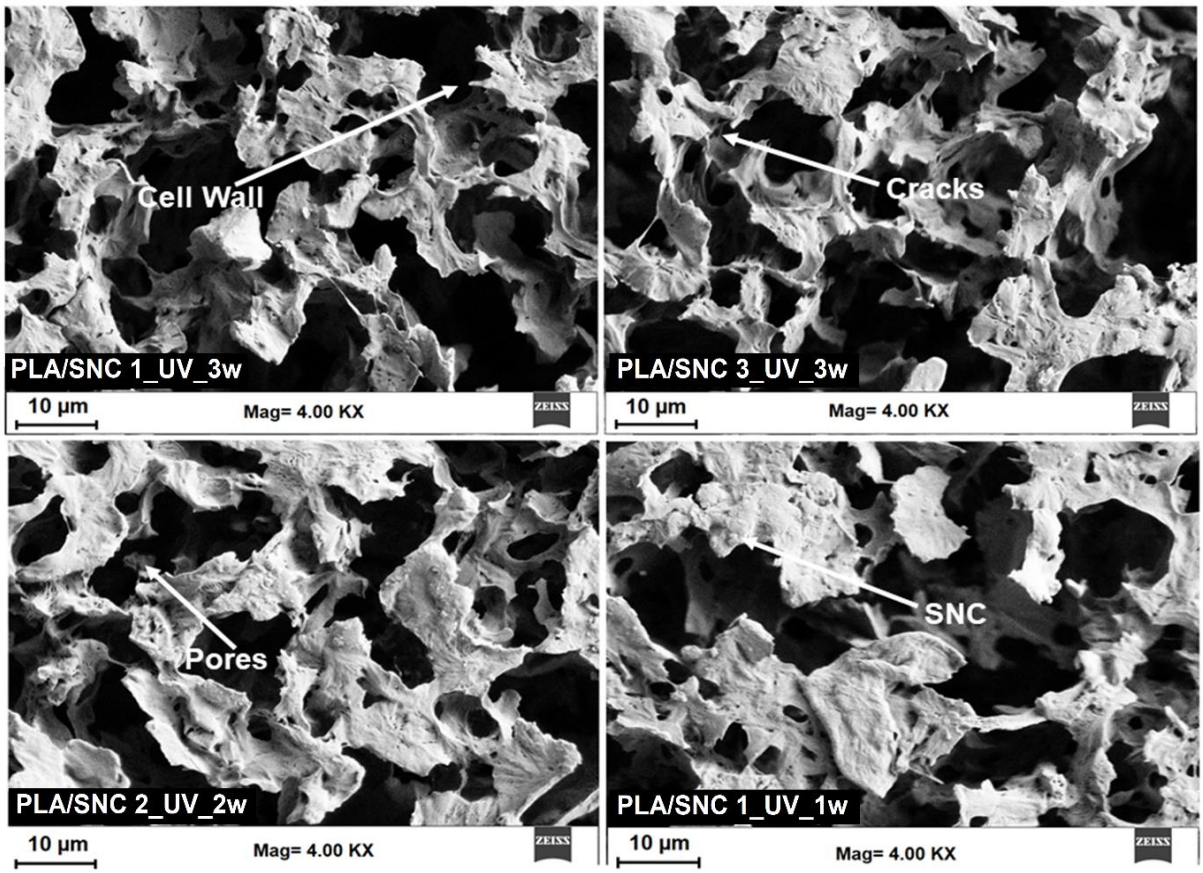

Fig. 6.29 FESEM of photodegraded PLA/SNC-based foams.

The morphological changes can be observed from the FESEM micrographs compared to unexposed samples as discussed in section 6.2.2. The UV exposed samples shows cell wall breakage and increasing pore sizes due to the rupture of cell walls. The morphological changes are more prominent at the higher exposure samples.

The colorimetric investigations of the UV exposed PLA and PLA/SNC-based foam samples are shown in **Fig. 6.30.** The change in color parameters is observed on exposure of UV light to the fabricated foam surfaces. The scientific representation of the color change can be demonstrated by a change in the value of color parameters. From the investigation, effects the color parameters on photodegradation and fading of color is observed in the fabricated foams on UV exposure. The intensity of change in color is more prominent at higher UV exposures. The change in color is due to the breaking of bonds. PLA has C-O, C-C, C=O and C-H bonds

in its chemical structure [303]. The C=O bond is generally a photoexcited bond. The absorption of a photon by this bond leads to different photochemical reactions like electron transfer, α and β cleavage, radical generation and so on [304].

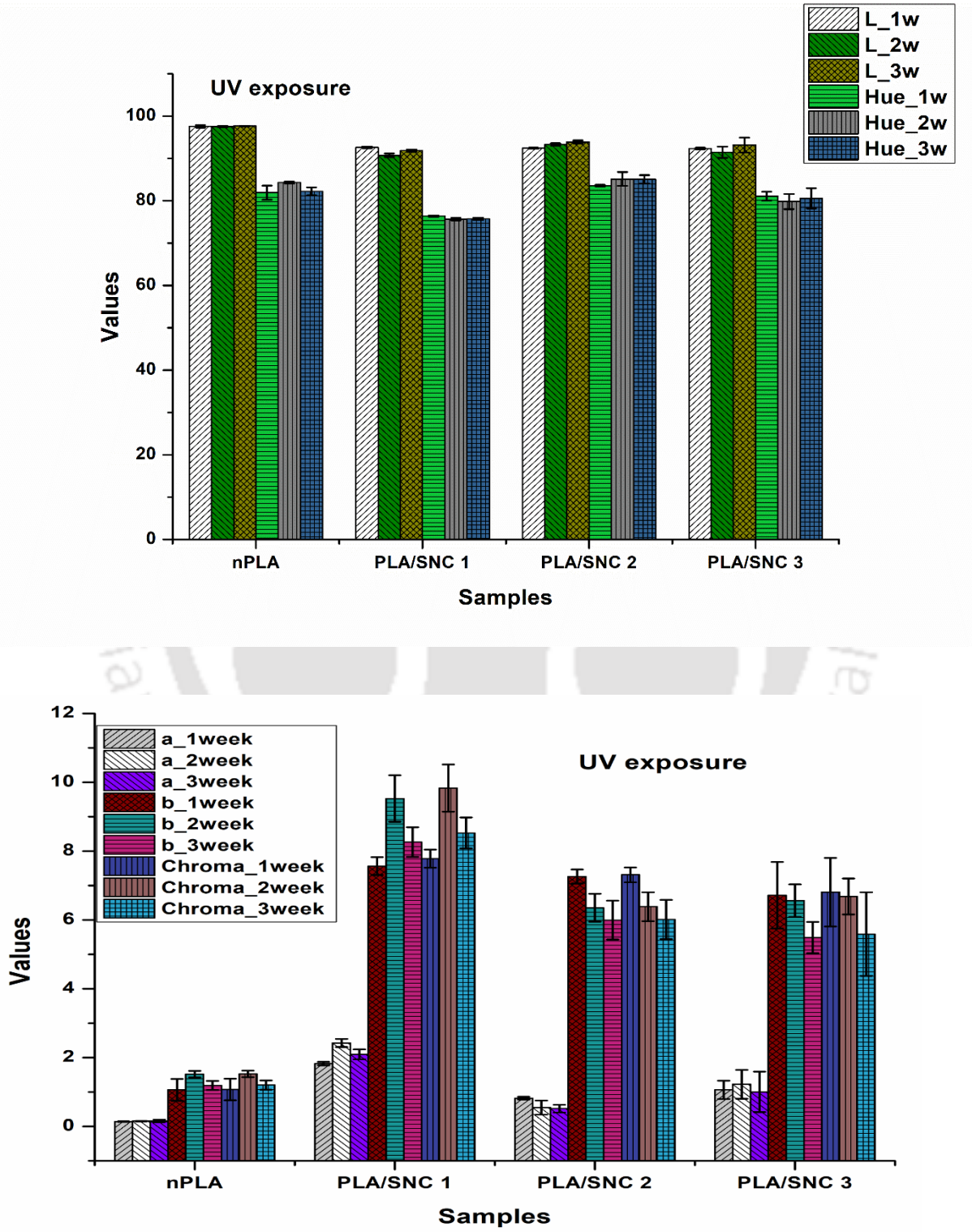

Fig. 6.30 Colorimetric investigation of UV exposed PLA and PLA/SNC-based foams.

The single bonds present in the structure of PLA can only absorb wavelength lesser than 180 nm. So the ultimate photodegradation process of PLA is depends on the excitation of the highly reactive C=O chromophore groups of ester linkage present in the structure. The carbonyl group absorbs UV radiation via an n-π^* electron transfer at a wavelength of ~280 nm [118]. From the figure, it is observed that, color parameters L, a, b, chroma and hue value changes with UV exposure. The huge difference in a, b and chroma value in PLA/SNC-based foams with nPLA is due to the presence of SNC. The brownish color of SNC is responsible for the reducing value of whiteness. Decreasing value of L indicates an increase in darkness. The UV exposure does not effect much in the whiteness of the fabricated PLA and PLA/SNC-based foams. However, the UV exposure affects the redness and greenness (a) and yellowness (b) of the fabricated PLA/SNC-based foams. The photochemical changes in PLA and PLA/SNC-based foams are responsible for the color fading observed in the PLA/SNC-based foams.

The TGA plots of the UV exposed PLA and PLA/SNC-based foams are shown in **Fig. 6.31**. it can be observed from the figure that thermostability changes with exposure time. Silk is a well-known UV resistant material. From the graph, it can be visualized that the thermostability of PLA based foams decreases on UV exposure. However, on the incorporation of SNC in the PLA matrix gives thermostability on UV exposure to the PLA/SNC-based foam. The PLA/SNC-based foams are observed to be more thermostable as compared to neat PLA foam. This is a very promising result for thermal properties of PLA/SNC-based foams. The onset degradation temperature (T_{onset}) of PLA-based foams decreases compared to PLA/SNC-based foams. The uniform dispersion of the SNC in the PLA foam matrix is also responsible for the improved thermostability of PLA/SNC-based foams.

The DSC plots of the UV exposed PLA/SNC-based foam samples are shown in **Fig. 6.32.** The glass transition temperature (T_g) of the PLA based foam decreases on increase in UV exposure as suggested by the figure. The decrease in T_g indicates the formation of short chains due to

the degradation of PLA. However, in the case of PLA/SNC-based foams, no such decrements in T_g is observed indicating that the degradation is slow compared to PLA based foam. A similar type of observations can be noticed from melting point (T_m) and temperature of crystallization (T_c) for the PLA/SNC-based foams. The results observed are in good agreements with the other investigations as discussed earlier.

The wettability investigations of the UV exposed PLA and PLA/SNC-based foam samples are tabulated in **Fig. 6.33.** From the investigation, it can be observed that the hydrophobicity of the fabricated foams decreases on UV exposure. The probable reason for these wettability phenomena is the change in morphology as wettability mainly depends on the surface morphology of the samples. The exposed surface morphology changes due to the formation of cracks and rupturing of cell walls. The pore size increases due to cell wall breakage and thus affecting the wettability phenomena of the PLA and PLA/SNC-based sample.

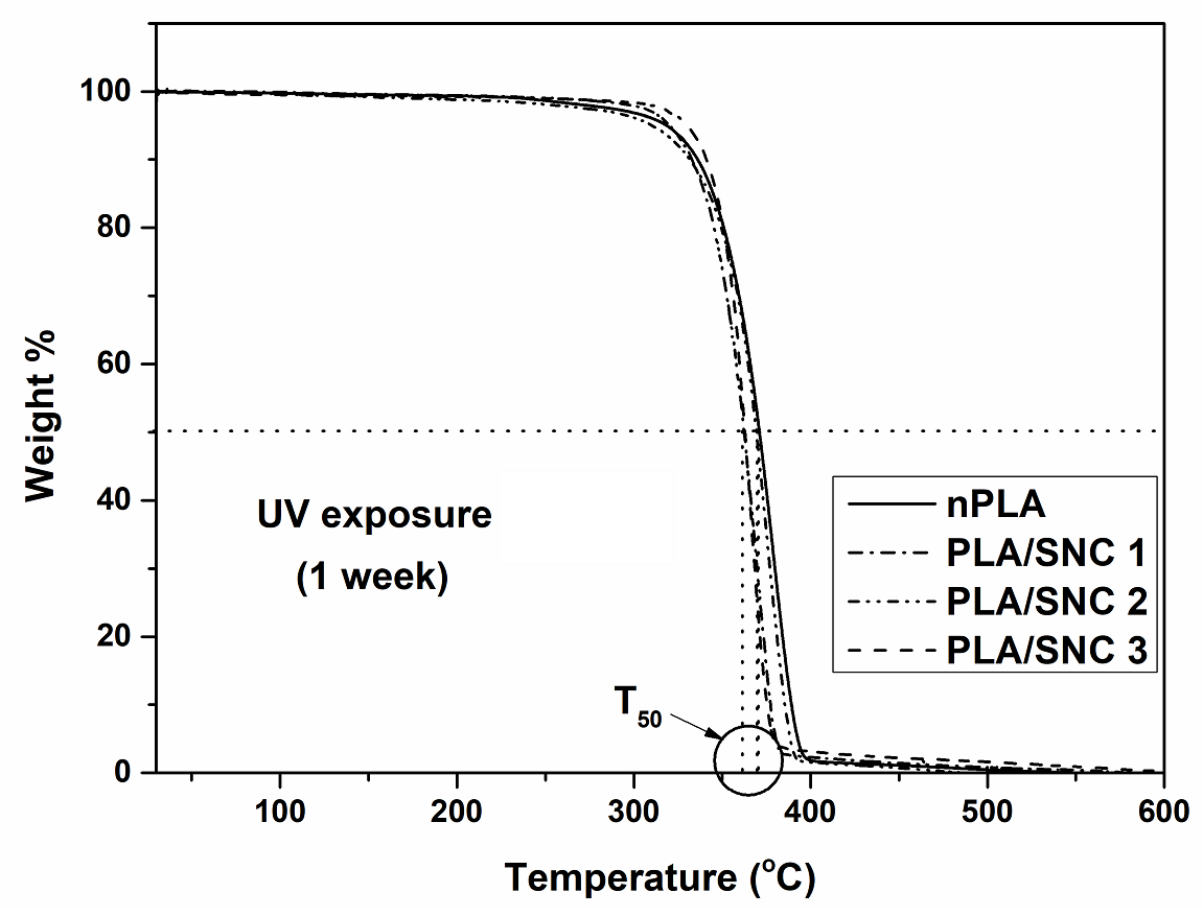

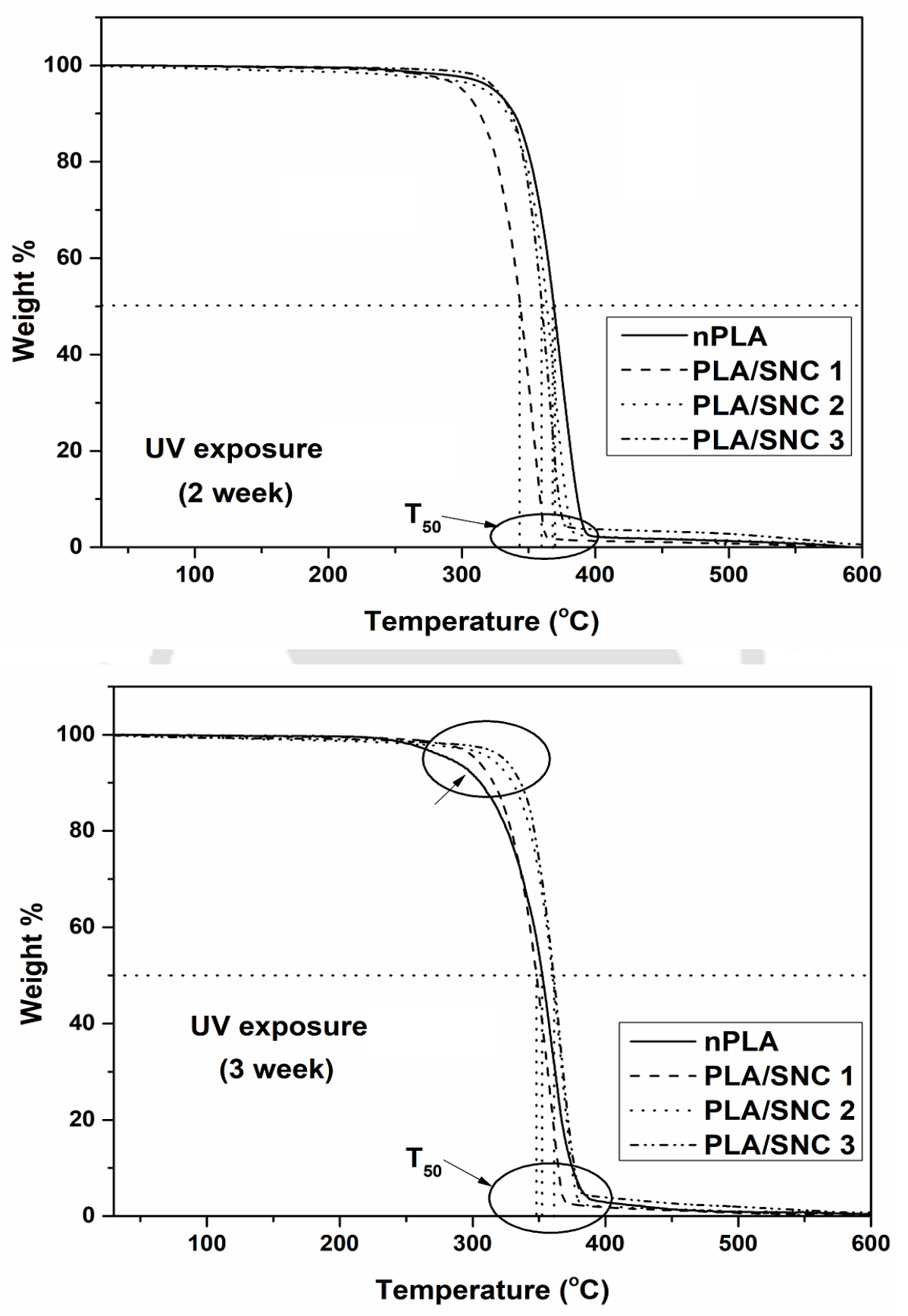

Fig. 6.31 TGA plots for the UV exposed PLA and PLA/SNC-based foams.

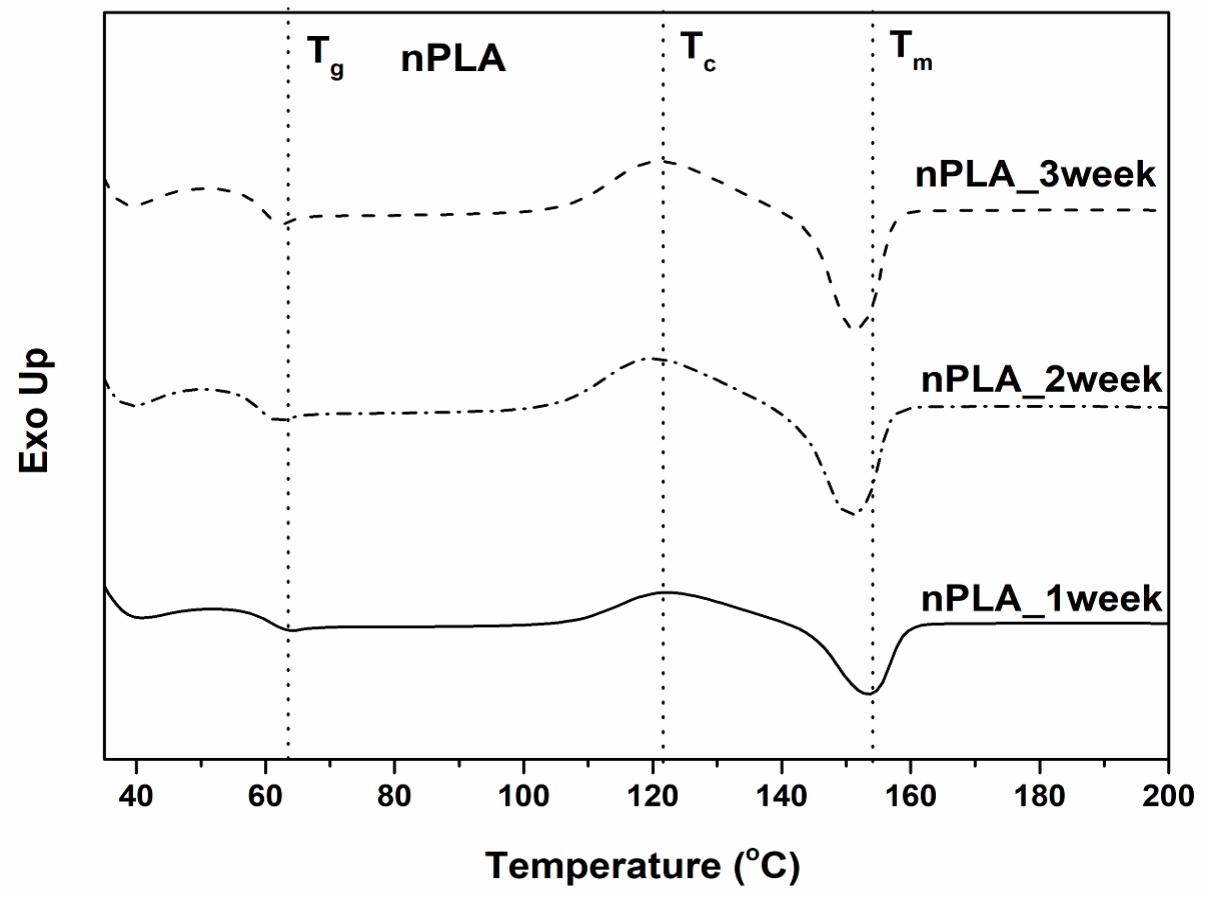

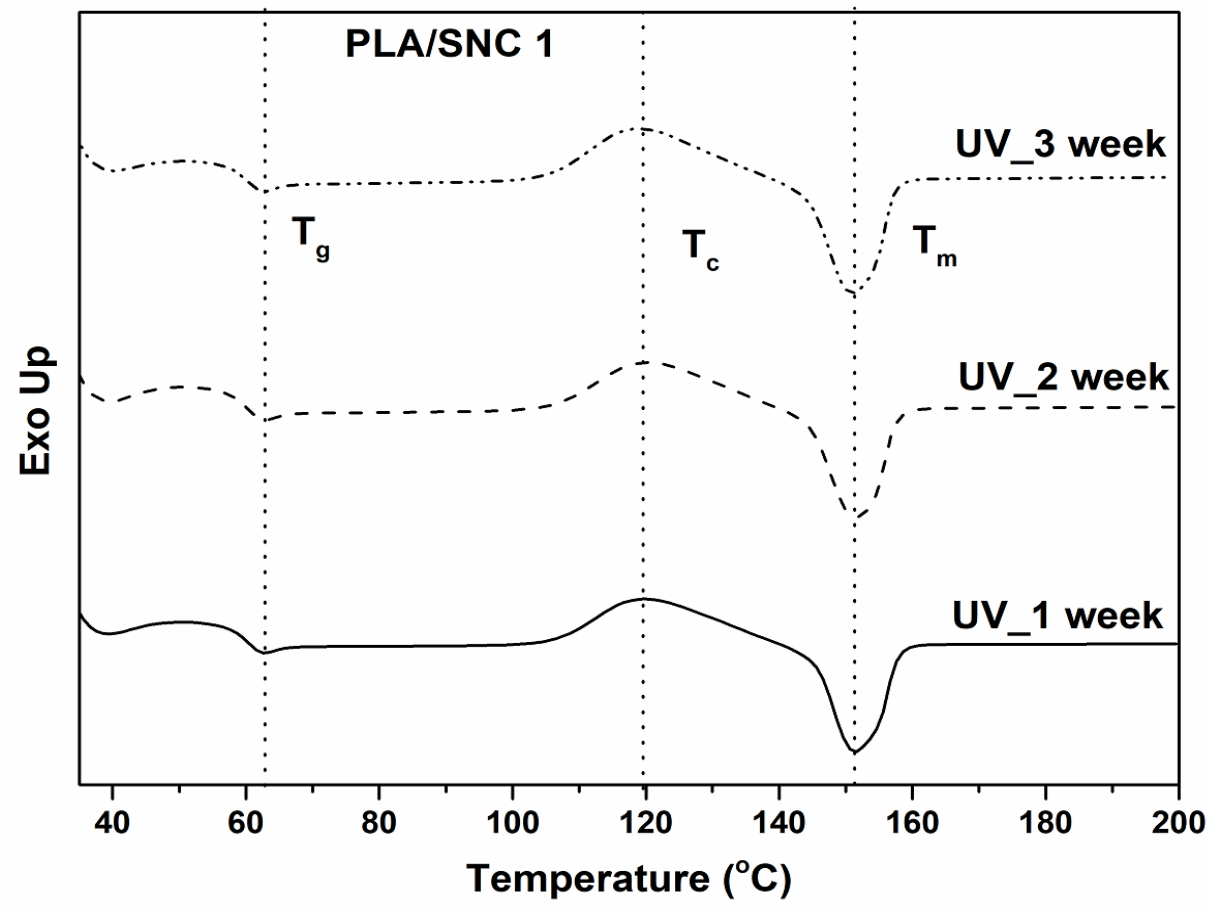

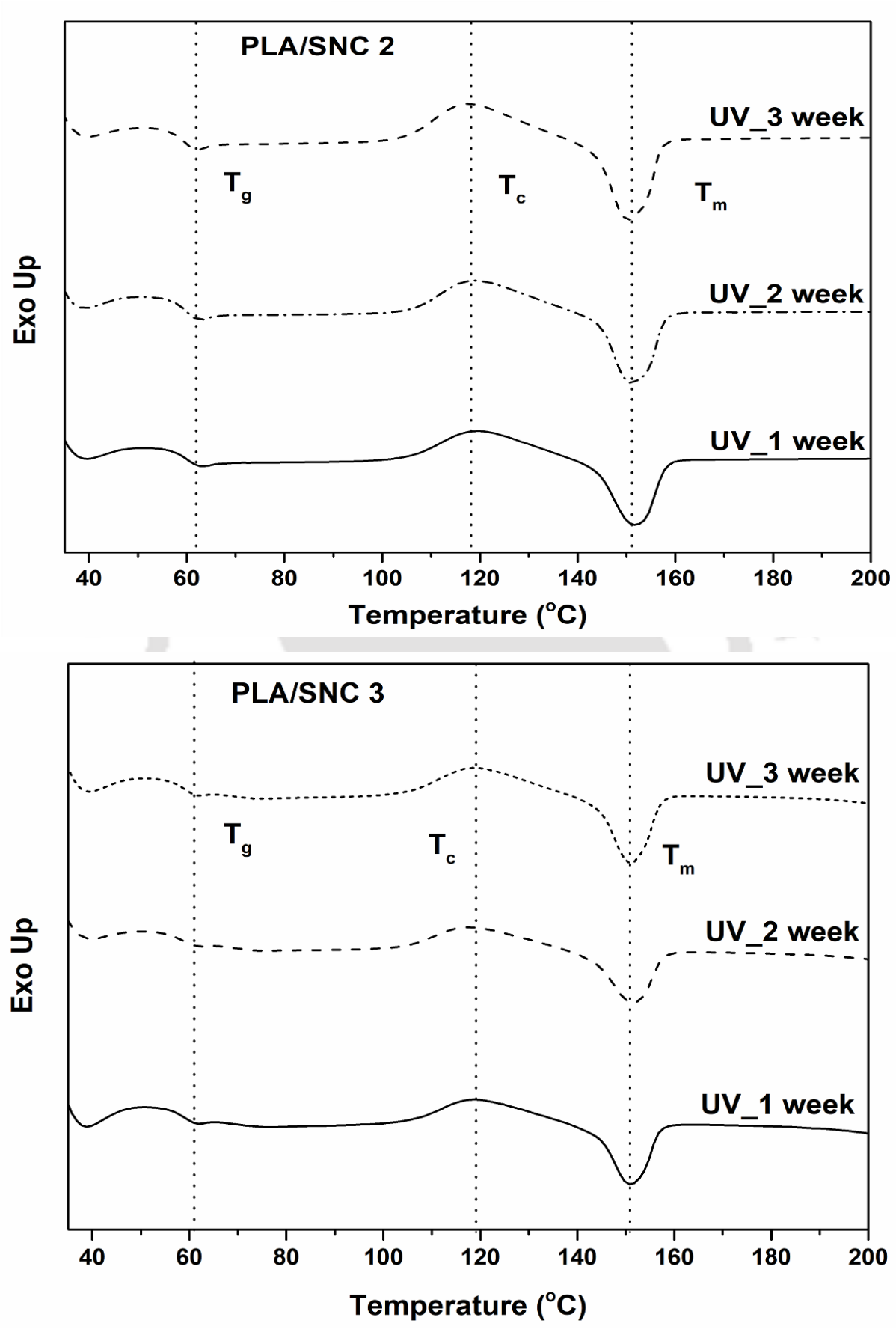

Fig. 6.32 DSC plots of UV exposed PLA and PLA/SNC-based foams.

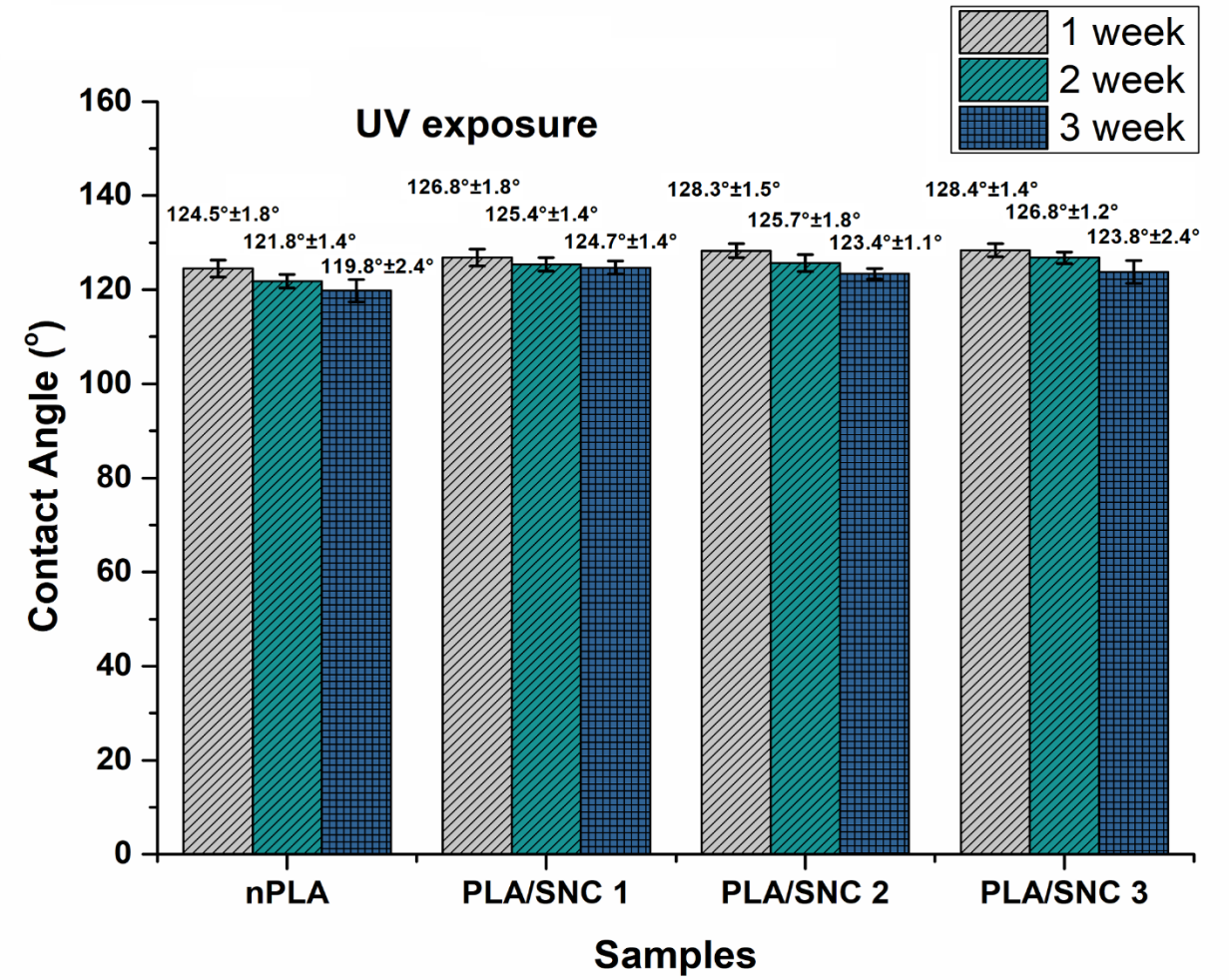

Fig. 6.33 Wettability of UV exposed PLA and PLA/SNC-based foams.

However, the change is not so prominent with UV exposure time as shown from the figure. Therefore, the wettability phenomena are not significantly affected by UV exposure.

The molecular weight investigations (M_w and M_n) of the UV exposed samples are shown in **Fig. 6.34.** It is observed that the molecular weight value decreases on UV exposure. The reduction in molecular weight is more prominent in nPLA compared to PLA/SNC-based foams. The reduction in molecular weight is due to the photochemical reactions, which causes chain scission, α, β cleavage, atom abstraction, electron transfer and radical addition in the PLA matrix and causes degradation [305,306]. It is observed at higher loading of SNC in PLA/SNC-based foams, the molecular weight change is very less compared to nPLA, might be due to the

presence of SNC, and uniformly dispersed in the matrix. Uniform dispersion makes the bond breakage more difficult and more energy is required to break the bond compared to nPLA.

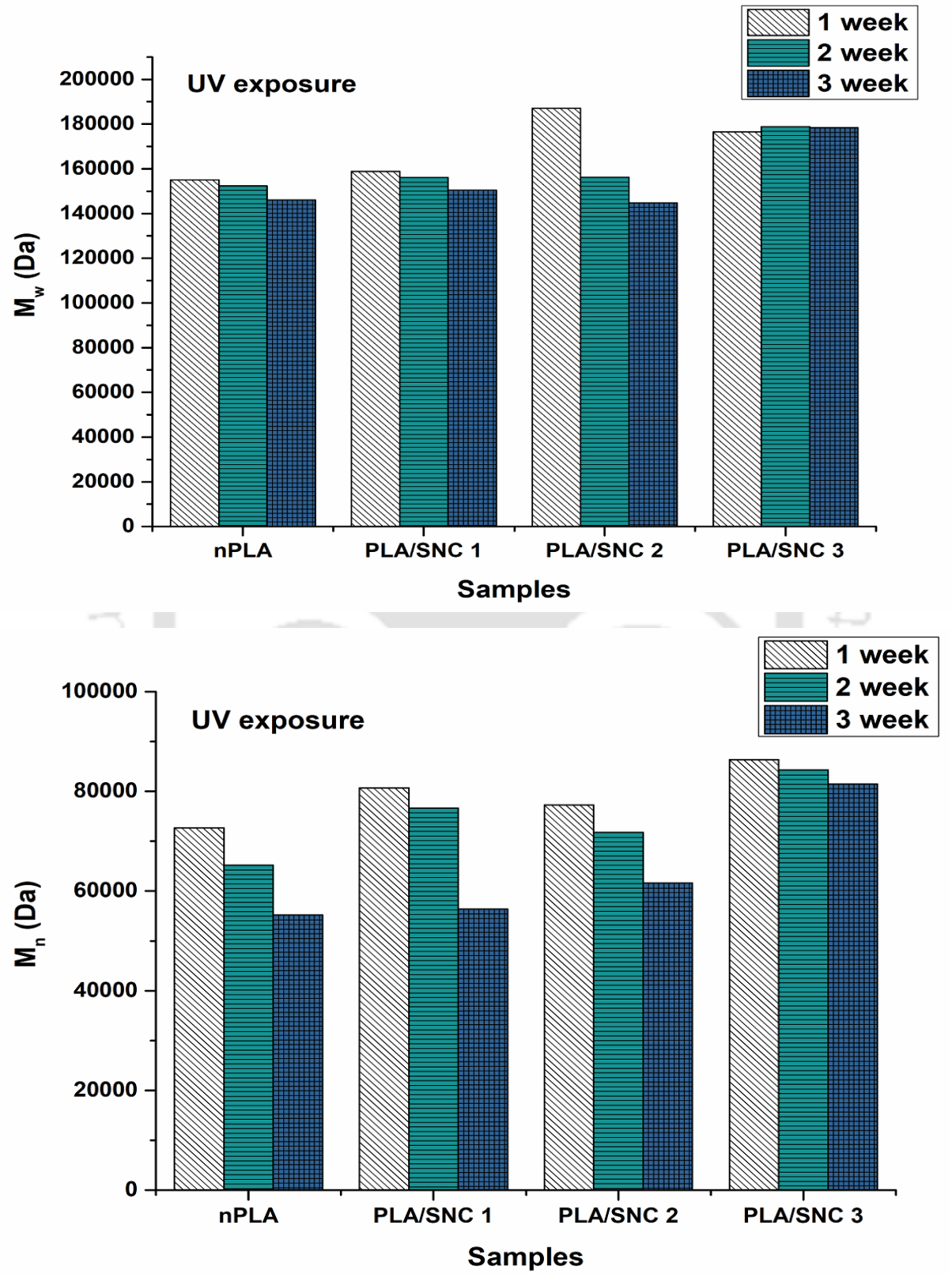

Fig. 6.34 Molecular weight of UV exposed PLA and PLA/SNC-based foams.

The FTIR spectra of UV exposed PLA and PLA/SNC-based foams are shown in **Fig. 6.35**.

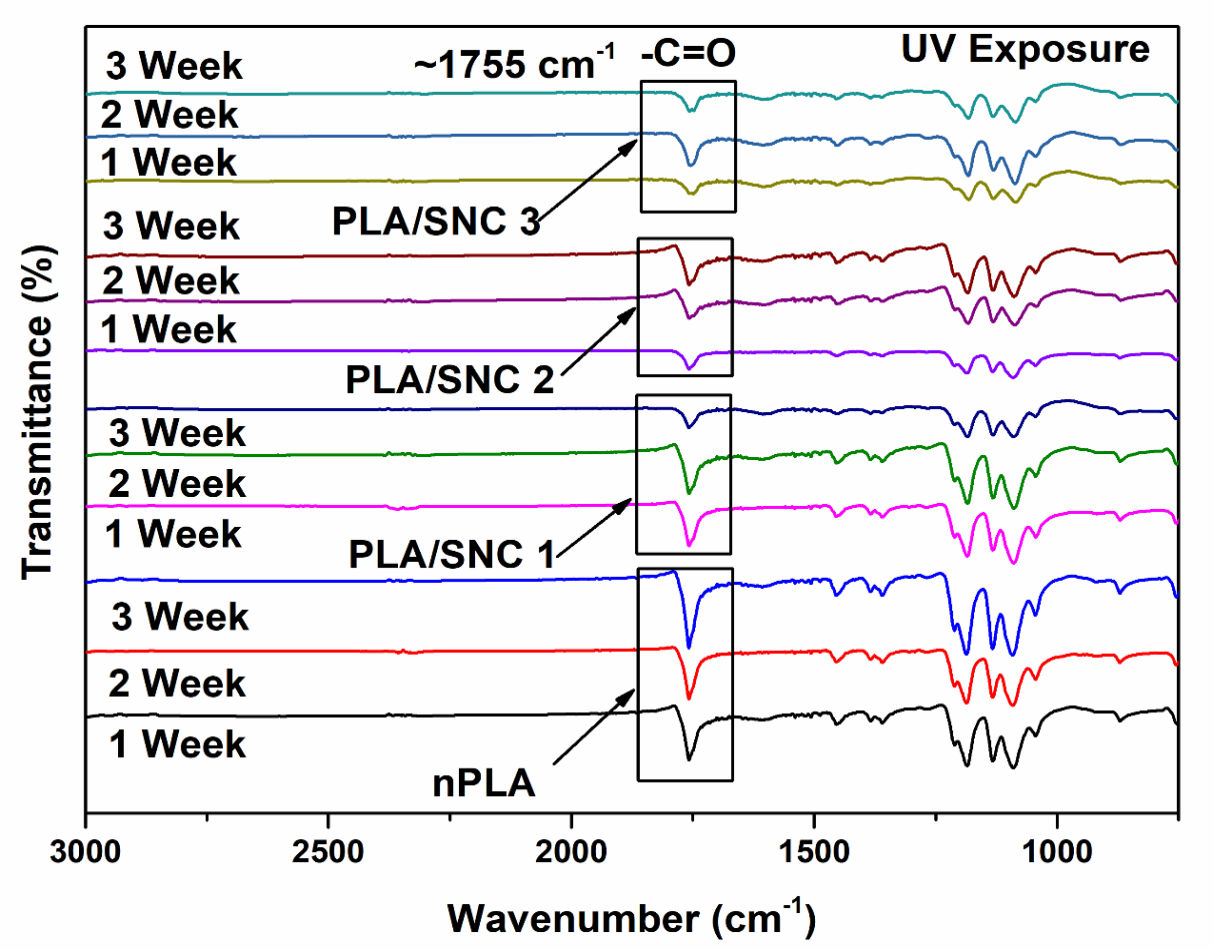

Fig. 6.35 FTIR spectra of UV degraded PLA and PLA/SNC-based foams.

From the spectra, the characteristic peaks of PLA and PLA/SNC-based foams can be observed as discussed in section 6.2.3. Prominent peaks are observed at ~1755 cm^{-1} indicating the presence of a carbonyl group in the PLA matrix. This carbonyl group is mainly responsible for the photodegradation of the fabricated PLA and PLA/SNC-based foams. The intensity of the carbonyl group is less in PLA/SNC-based foams compared to nPLA. The high-intensity carbonyl peak observed in PLA indicates the occurrence of chain scission reactions initiated by photoexcited C=O groups [307,308]. Therefore, the degradation of nPLA is higher than PLA/SNC-based foams.

The results observed in FTIR is in accordance with the previous results obtained for photodegradation of PLA and PLA/SNC-based foams. From this section, it can be concluded that the presence of SNC imparts UV resistance to the PLA matrix. The thermal stability is also improved in PLA/SNC-based foams compared to PLA-based foam. Therefore, silk-based SNC nanofiller can be effectively utilized in the PLA matrix for photoresistance.

6.5 Summary

This chapter mainly focuses in the development of PLA/SNC-based microcellular, highly porous and interconnected open cellular morphological foam by utilizing less expensive C/L technique taking easily available and cost-effective sugar as porogen medium. The results obtained in the development of PLA/SNC-based foams are very promising. It is observed that SNC improves the crystallinity of the PLA-based foams. SNC nanobiofiller mainly acts as a nucleating agent and helps to generate smaller pores in the matrix influencing foam properties. The decrement in cell size is observed up to ~60% at highest loading of SNC. The thermal stability of the fabricated PLA/SNC-based foams is also improved by the uniform dispersion of the SNC in the PLA matrix. The TGA isotherm suggests that the PLA/SNC-based foams are more thermally stable and applicable up to 250 °C compared to nPLA. Almost ~10 °C increments in T_{max} is observed for foam sample with the highest concentration of SNC. The change in color parameters is observed in the fabricated PLA/SNC-based foams; however, the change is not so prominent in visualization as compared to MC and MG as discussed in earlier chapters. SNC nanobiofillers are also helpful in improving the thermo-mechanical properties of PLA and PLA/SNC-based foams. The improvements in hydrophobicity are also observed in the PLA/SNC-based foams due to the surface changes and the effect of nanobiofillers. The nucleating behavior of SNC in the PLA matrix is also confirmed by the crystallization kinetics study. Both the primary and secondary crystallization is taking place in the polymer matrix.

From the hydrolytic degradation studies, it is observed that degradation is more prominent in the basic and acidic medium compared to the neutral solution. The degradation is also affected by the porous foam structure, cell size, and SNC. From the photodegradation studies of the PLA and PLA/SNC-based foam, it can be concluded that SNC improves the thermostability of PLA foam under UV exposure and morphological changes also observed due to photodegradation. PLA/SNC-based foams can be useful in some sophisticated biomedical applications where a higher surface area is required for the growth of cells and in tissue engineering applications. In addition, it can be applied in areas where biodegradability, hydrophobicity along with operations under sunlight is a prerequisite condition.

Chapter 7

Conclusions and Future Prospects

This chapter draws conclusions based on the current research work. This chapter also provides farsighted information regarding the future scope and directions for subsequent research work. In this research, we have successfully fabricated highly porous, interconnected cellular, hydrophobic biodegradable PLA based foams with average pore diameter <10 microns. The utilization of easily available sucrose particles as a porogen medium is also an interesting point of view in this research. The decrease in average pore size (<10 micron) achieved in the research might be due to the slight modification of the conventional C/L technique (pre-treatment of porogen).

7.1 Conclusions of the doctoral research

The current doctoral research is based on the fabrication of PLA and PLA/nanobiofiller-based microcellular composite foams and its investigation. The selection of the nanobiofillers is based on the abundant availability of bio-based resources from where it can be fabricated. The research is based on four different bionanofillers: Cellulose nanocrystals (CNC), modified chitosan (MC), modified gum arabic (MG) and silk nanocrystals (SNC). The fabrication of PLA/nanobiofiller-based foams has been carried out using cost-effective and innocuous method casting and leaching (C/L) technique with slight modifications. The use of easily available and non-toxic sugar as porogen particle in the C/L technique is one of the interesting aspect in the current research. The structure-property relationships, thermal, crystallization and different degradation methods are thoroughly investigated in the current research.

The major findings and observations drawn on the basis of overall doctoral research can be broadly organized into four chapters. The overall conclusions of the research work are discussed below.

7.1.1 Specific conclusions from PLA/CNC-based investigations

This research successfully demonstrates the fabrication of PLA/CNC-based microcellular composite foams with improved hydrophobicity and interconnected porous structure. The reduced density is observed for the fabricated PLA/CNC-based foams compared to PLA granules. It is witnessed from the investigations that CNC acts as a nucleating agent in the PLA matrix. CNC helps in generation of more number of smaller pores in the PLA foam matrix, thus affecting properties of fabricated PLA/CNC-based foams. Porosimetric investigation suggests the increase up to ~2-fold in surface area for PLA/CNC 2. The minimum average pore diameter achieved up to ~0.45 µm for PLA/CNC 2. The uniform dispersion of CNC in the PLA matrix as suggested by FESEM also improves the thermo-mechanical properties of PLA/CNC-

based fabricated foams. Improvements in storage and loss modulus are observed with increase in CNC concentration. CNC also positively affects the crystallinity of the fabricated PLA/CNC-based foams. The crystallinity is observed as ~55.6% for the highest concentration foam sample (PLA/CNC 3). At higher loading of CNC, a reduction in thermal properties is observed due to the probable agglomeration of CNC and the increasing number of sulfate groups. The thermal degradation kinetics investigation of fabricated PLA/CNC-based foams suggests the increase in activation energy (E_a) with CNC and optimum thermal stability is observed at PLA/CNC 1. However, the value decreases to some extent due to the agglomeration. The E_a value of the fabricated PLA/CNC-based porous system is more than ~40 kJ/mol-~50 kJ/mol higher than the PLA/CNC-based film system as observed from literature. The increase in activation energy might be due to the presence of gaseous voids in the foam system, which eventually retards the heat transfer due to the tortuous path length. Similarly, from the crystallization investigation, it can be concluded that CNC acts as the nucleating agent in lower loadings and give hindrance to chain folding at higher loadings. It is also concluded from the investigation that effect of porosity, the morphology of surface and surface area mainly influences the thermal degradation than in crystallization phenomena. It is also observed that CNC does not have any significant influence in volatile product released during degradation and the degradation mechanism of the PLA-based foams. From the results discussed above, it can be concluded that the fabricated PLA/CNC-based foams have the probable applications in areas of interest in degradability and in packaging sectors. It has also the potential to replace some of the non-degradable polymeric foams in some of the commodity applications.

7.1.2 Specific conclusions from PLA/MC-based investigations

The fabrication of highly porous, interconnected cellular PLA/MC-based foams is successfully carried out using the C/L technique. From the investigation, it is observed that MC acts as a plasticizing agent in the matrix due to the presence of low molecular weight oligomers. MC also helps in generating a number of smaller pores in the PLA matrix and an increase of ~2.3 fold in cell density is observed compared to the PLA-based foams. The change in surface morphology due to the presence of MC influences the wettability phenomena and an increase in ~9° in case of static contact angle and ~10° in case of dynamic Young's contact angle is observed. MC influences the thermal stability of the fabricated PLA/MC-based foams. Porosimetric studies of the fabricated foam suggest an increase in the surface area up to ~30.2% and reduction in cell size up to ~33.3% on the incorporation of MC in the PLA matrix. The decrease in activation energy for thermal degradation and reduction in energy of crystallization is also observed, which further confirms the plasticizing effect of MC in the PLA matrix. Based on the above discussions, it can be concluded that the fabricated PLA/MC-based foams might be effectively used in some sophisticated biomedical applications, where degradability, hydrophobicity and surface area is a major concern.

7.1.3 Specific conclusions from PLA/MG-based investigations

In the current research, we have successfully developed a highly porous, interconnected microcellular PLA/MG-based foam utilizing C/L technique. From the investigation, it is observed that MG helps in the generation of smaller pores in the PLA matrix along with the influence of porogen size and shape. An improvement in the surface area up to ~60% and reduction in cell size up to ~53% is observed on the incorporation of MG in the PLA matrix. The results also suggests the plasticizing effect of MG in the PLA matrix. The decrease in glass transition and thermal properties of PLA/MG-based foams is observed with MG. The

improvement in hydrophobicity is observed due to the change in surface morphology and MG. The crystallization studies suggesting the nucleating effects of nanobiofiller in the matrix and simultaneous happening of both primary and secondary crystallization. The hydrolytic degradation investigation of the fabricated PLA/MG-based foams indicates that degradation is more prominent in the basic and acidic medium compared to the neutral solution. The hydrolytic degradation proceeds via surface erosion and rupture of a cellular structure for the fabricated foams. MG also enhances the degradation process. The photodegradation studies suggest that the fabricated PLA/MG-based foams are more prone to degrade under UV exposure than neat counterpart. From the investigation, it can be concluded that the fabricated PLA/MG-based foams can demonstrate its applications in biomedical fields, where the surface area is a major concern and, further, it can be used in food storage packaging due to the proven reduced oxygen permeability [123].

7.1.4 Specific conclusions from PLA/SNC-based investigations

The development of PLA/SNC-based microcellular composite foams has been performed by C/L technique utilizing sugar as porogen medium. The results suggests that SNC is acting as a nucleating agent in the PLA matrix. A reduction of ~60% in average cell size is observed on the incorporation of SNC. It has also been noticed that SNC improves the thermostability of PLA/SNC-based foams. Isothermal TGA investigation suggests that PLA/SNC-based foams are thermally stable up to ~250 °C, whereas nPLA foam starts to thermally degrade at that temperature. Enhancement in thermomechanical properties is also observed for PLA/SNC-based foams than the neat counterpart. Improvements in hydrophobicity are also observed in PLA/SNC-based foams due to the change in surface morphology. Hydrolytic investigation suggests that degradation is more prominent in basic and acidic solutions. One of the major findings of PLA/SNC-based foams is that SNC improves the thermal stability under UV irradiation compared to neat PLA. This result can open a wide window in the area of

applications of the developed PLA/SNC-based foams under sunlight/open atmospheric conditions. From the result obtained, it can be concluded that the developed PLA/SNC-based foams have probable applications in some biomedical sophisticated areas and some commodity applications under sunlight. The PLA/SNC-based foams have the potential to replace some conventional petro-based polymeric foams in their fields of application and thus it may develop a sustainable approach towards the environment.

7.1.5 Overall conclusions of the research work

From the above discussions, it can be concluded that the bionanofillers used in the current research have good compatibility with the PLA foam matrix. The incorporation of these nanobiofillers in the PLA matrix helps in improvement of various foam properties. Improvements in thermal and thermomechanical properties are mainly witnessed in PLA/CNC and PLA/SNC foams compared to neat PLA counterpart. On the contrary, a reduction in thermomechanical and thermal properties are observed for PLA/MC and PLA/MG-based foams due to presence of oligo pendent group in MC and MG. These reductions in properties for PLA/MG and PLA/MC-based foam limits its applications where thermal and mechanical enhancement is required. However, the increase in surface area and the nanobiofillers used (as chitosan and gum arabic are regarded as safe by USFDA) in the matrix makes these foams more suitable for different biomedical and food-related applications. Similarly, reduction in cell size is observed in all the four different developed PLA-based foams. In such a way, the current research can be utilized towards the sustainability of the environment and overall development of mankind.

The overall major findings of the current doctoral research are summarized in **Table 7.1**. It can be observed from the table that CNC and SNC mainly act as a nucleating agent in the PLA

foam matrix. On the other hand, MC and MG mainly act as a plasticizing agent in the PLA-based foam matrix. The pictorial illustration of the research can be observed in **Fig. 7.1**.

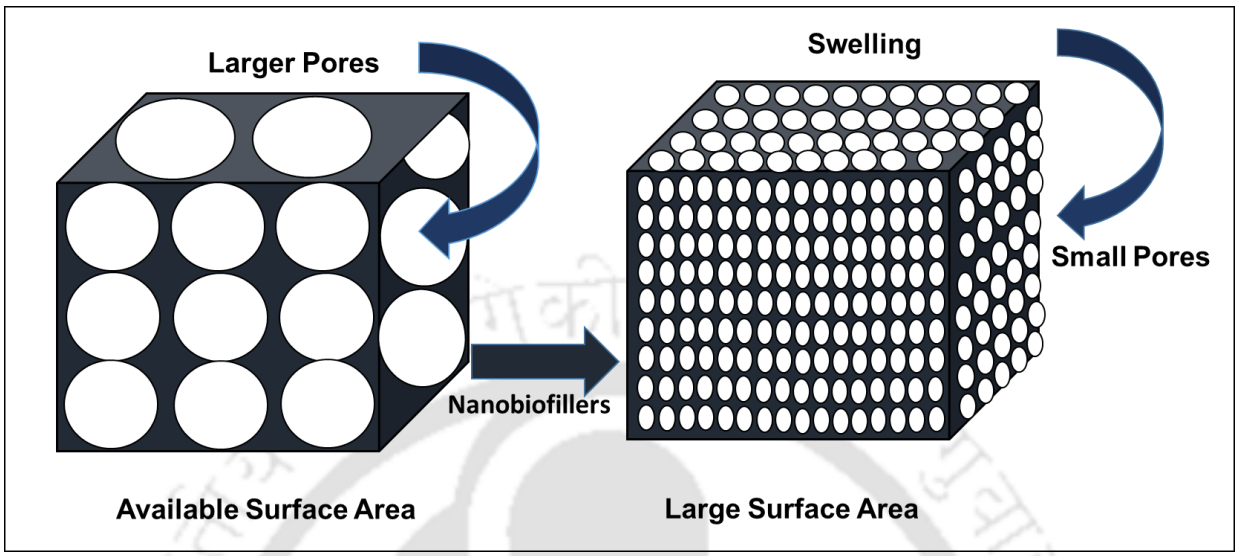

Fig. 7.1 Effect of nanobiofillers on PLA-based foam.

Table 7.1 Summary of major findings of the research work.

PLA/nanobiofiller based Foams	Research Findings
PLA/cellulose nanocrystals (CNC)	✓ CNC mainly acts as a nucleating agent and helps in crystallization at lower loadings. ✓ Improvements observed in mechanical, thermal, wettability phenomena of the PLA based foam. An increase in surface area is observed. ✓ The combined effect of porosity and CNC is observed in thermal degradation, not in crystallization.
PLA/modified chitosan (MC)	✓ MC acts as a plasticizing agent in the PLA matrix. ✓ Improvements are mainly observed in wettability, cell density etc. ✓ MC has not any significant effect in improvement in thermal properties. ✓ The combined effect of porosity and MC is observed in thermal degradation
PLA/modified gum arabic (MG)	✓ Nucleating and plasticizing effect of MG is mainly observed in PLA/MG based foams. ✓ MG degrades PLA based foams under UV exposure. ✓ MG induced the crystallization of PLA matrix.
PLA/silk nanocrystals (SNC)	✓ SNC mainly acts as a nucleating agent in the PLA matrix. ✓ Average cell size up to ~0.6 microns is achieved. ✓ Improves thermal and mechanical properties. ✓ SNC imparts thermal stability under UV exposure.

7.2 Future directives of the doctoral research

Based on the major outcomes of the current research, few recommendations and suggestions for future research directives can be made as given below.

- The cell proliferation study can be performed in the fabricated PLA based foams. The decrease in cell size and an increase in the surface area of the foam has an added advantage in this regards.
- The fabrication of the PLA/nanobiofillers-based foams can be performed by utilizing other methods of fabrication of foams such as extrusion foaming, high-pressure foaming, by using TIPS method, using inert supercritical gases and so on.
- Scale up the production of PLA/nanobiofillers-based foams.
- Investigation in the direction of biomedical applications of the fabricated foams.
- Investigations can be carried out for different probable applications like acoustic, insulation, structural and so on with the incorporation of different additives in the PLA/nanobiofiller matrix.
- The other established nanobiofillers extracted from the abundantly available resources from nature can be utilized in PLA matrix for enhancement in various properties.

References

[1] N. Karak, Fundamentals of polymers: raw materials to finish products, PHI Learning Pvt. Ltd., 2009.

[2] E. Kosior, R.M. Braganca, P. Fowler, Lightweight compostable packaging: literature review, Waste Resour. Action Program. 26 (2006) 1–48.

[3] R. Narayan, Drivers & rationale for use of biobased materials based on life cycle assessment (LCA), GPEC Pap. Abstr. (2004).

[4] R.A. Auras, L.-T. Lim, S.E.M. Selke, H. Tsuji, Poly (lactic acid): synthesis, structures, properties, processing, and applications, John Wiley & Sons, 2011.

[5] W. Zhai, Y. Ko, W. Zhu, A. Wong, C.B. Park, A study of the crystallization, melting, and foaming behaviors of polylactic acid in compressed CO_2, Int. J. Mol. Sci. 10 (2009) 5381–5397.

[6] L.M. Mathieu, M. Montjovent, P. Bourban, D.P. Pioletti, J. Månson, Bioresorbable composites prepared by supercritical fluid foaming, J. Biomed. Mater. Res. Part A An Off. J. Soc. Biomater. Japanese Soc. Biomater. Aust. Soc. Biomater. Korean Soc. Biomater. 75 (2005) 89–97.

[7] C.R. Kothapalli, M.T. Shaw, M. Wei, Biodegradable HA-PLA 3-D porous scaffolds: effect of nano-sized filler content on scaffold properties, Acta Biomater. 1 (2005) 653–662.

[8] D. Preechawong, M. Peesan, P. Supaphol, R. Rujiravanit, Preparation and characterization of starch/poly (L-lactic acid) hybrid foams, Carbohydr. Polym. 59 (2005) 329–337.

[9] Y.-M. Corre, A. Maazouz, J. Duchet, J. Reignier, Batch foaming of chain extended PLA with supercritical CO_2: Influence of the rheological properties and the process parameters on the cellular structure, J. Supercrit. Fluids. 58 (2011) 177–188.

[10] V. Katiyar, Bio-based Plastics for Food Packaging Applications, Smithers Pira, 2017.

[11] S.-T. Lee, C.B. Park, N.S. Ramesh, Polymeric foams: science and technology, CRC press, 2006.

[12] H. Zhao, Z. Cui, X. Sun, L.-S. Turng, X. Peng, Morphology and properties of injection molded solid and microcellular polylactic acid/polyhydroxybutyrate-valerate (PLA/PHBV) blends, Ind. Eng. Chem. Res. 52 (2013) 2569–2581.

[13] A.G. Mikos, A.J. Thorsen, L.A. Czerwonka, Y. Bao, R. Langer, D.N. Winslow, J.P. Vacanti, Preparation and characterization of poly (L-lactic acid) foams, Polymer (Guildf). 35 (1994) 1068–1077.

[14] L.J.M. Jacobs, M.F. Kemmere, J.T.F. Keurentjes, Sustainable polymer foaming using high pressure carbon dioxide: a review on fundamentals, processes and applications, Green Chem. 10 (2008) 731–738.

[15] M. Nofar, C.B. Park, Poly (lactic acid) foaming, Prog. Polym. Sci. 39 (2014) 1721–1741. doi:10.1016/j.progpolymsci.2014.04.001.

[16] W.L. Murphy, R.G. Dennis, J.L. Kileny, D.J. Mooney, Salt fusion: an approach to improve pore interconnectivity within tissue engineering scaffolds, Tissue Eng. 8 (2002) 43–52.

[17] P. Krishnamachari, J. Zhang, J. Lou, J. Yan, L. Uitenham, Biodegradable poly (lactic acid)/clay nanocomposites by melt intercalation: a study of morphological, thermal, and mechanical properties, Int. J. Polym. Anal. Charact. 14 (2009) 336–350.

[18] Y. Di, S. Iannace, E. Di Maio, L. Nicolais, Poly (lactic acid)/organoclay nanocomposites: thermal, rheological properties and foam processing, J. Polym. Sci. Part B Polym. Phys. 43 (2005) 689–698.

[19] M. Mihai, M.A. Huneault, B.D. Favis, H. Li, Extrusion Foaming of Semi-Crystalline PLA and PLA/Thermoplastic Starch Blends, Macromol. Biosci. 7 (2007) 907–920.

[20] L. Yu, H. Liu, K. Dean, L. Chen, Cold crystallization and postmelting crystallization of PLA plasticized by compressed carbon dioxide, J. Polym. Sci. Part B Polym. Phys. 46 (2008) 2630–2636.

[21] S. Pilla, S.G. Kim, G.K. Auer, S. Gong, C.B. Park, Microcellular extrusion-foaming of polylactide with chain-extender, Polym. Eng. Sci. 49 (2009) 1653–1660.

[22] S.Y. Cho, H.H. Park, Y.S. Yun, H.-J. Jin, Influence of cellulose nanofibers on the morphology and physical properties of poly (lactic acid) foaming by supercritical carbon dioxide, Macromol. Res. 21 (2013) 529–533.

[23] S.-T.S.-T. Lee, D.P.K. Scholz, C.B. Park, R. Gendron, Foam extrusion: principles and practice, CRC press, 2008.

[24] S.-T. Lee, Polymeric Foams: Innovations in Processes, Technologies, and Products, CRC Press, 2016.

[25] R. Gendron, Thermoplastic foam processing: principles and development, CRC press, 2004.

[26] S.-T. Lee, D.P.K. Scholz, Polymeric foams: Technology and developments in regulation, process, and products, CRC Press, 2008.

[27] S.-T. Lee, Introduction: Polymeric Foams, Mechanisms, and Materials, in: Polym. Foam., CRC press, 2004: pp. 15–29.

[28] J.H. Saunders, R.H. Hansen, The mechanism of foam formation, Plast. Foam. Part I, Marcel Dekker, New York. (1972) 23–108.

[29] J.H. Saunders, D. Klempner, Fundamentals of foam formation, Handb. Polym. Foam. Foam Technol. (1991) 5–15.

[30] S. Mane, Effect of porogens (type and amount) on polymer porosity: a review, Can. Chem. Trans. 4 (2016) 210–225.

[31] V. La Carrubba, F.C. Pavia, V. Brucato, S. Piccarolo, PLLA/PLA scaffolds prepared via Thermally Induced Phase Separation (TIPS): tuning of properties and biodegradability, Int. J. Mater. Form. 1 (2008) 619–622.

[32] L.M. Matuana, O. Faruk, C.A. Diaz, Cell morphology of extrusion foamed poly (lactic acid) using endothermic chemical foaming agent, Bioresour. Technol. 100 (2009) 5947–5954.

[33] S. Arif, G. Burgess, R. Narayan, B. Harte, Evaluation of a biodegradable foam for protective packaging applications, Packag. Technol. Sci. An Int. J. 20 (2007) 413–419.

[34] J.L. Willett, R.L. Shogren, Processing and properties of extruded starch/polymer foams, Polymer (Guildf). 43 (2002) 5935–5947.

[35] S.Y. Lee, H. Chen, M.A. Hanna, Preparation and characterization of tapioca starch–poly (lactic acid) nanocomposite foams by melt intercalation based on clay type, Ind. Crops Prod. 28 (2008) 95–106.

[36] M. Ajioka, K. Enomoto, A. Yamaguchi, K. Suzuki, T. Watanabe, Y. Kitahara, Degradable foam and use of same, (1995).

[37] C. Zhou, L. Ma, W. Li, D. Yao, Fabrication of tissue engineering scaffolds through solid-state foaming of immiscible polymer blends, Biofabrication. 3 (2011) 45003.

[38] E. Feese, H. Sadeghifar, H.S. Gracz, D.S. Argyropoulos, R.A. Ghiladi, Photobactericidal porphyrin-cellulose nanocrystals: Synthesis, characterization, and antimicrobial properties, Biomacromolecules. 12 (2011) 3528–3539. doi:10.1021/bm200718s.

[39] N. Lin, A. Dufresne, Nanocellulose in biomedicine: Current status and future prospect, Eur. Polym. J. 59 (2014) 302–325. doi:10.1016/j.eurpolymj.2014.07.025.

[40] R.R. Devi, P. Dhar, A. Kalamdhad, V. Katiyar, Fabrication of cellulose nanocrystals from agricultural compost, Compost Sci. Util. 23 (2015). doi:10.1080/1065657X.2014.972595.

[41] M.P. Arrieta, E. Fortunati, F. Dominici, E. Rayón, J. López, J.M. Kenny, PLA-PHB/cellulose based films: Mechanical, barrier and disintegration properties, Polym. Degrad. Stab. 107 (2014) 139–149.

[42] X. Wang, T. Yucel, Q. Lu, X. Hu, D.L. Kaplan, Silk nanospheres and microspheres from silk/pva blend films for drug delivery, Biomaterials. 31 (2010) 1025–1035.

[43] A. Nova, S. Keten, N.M. Pugno, A. Redaelli, M.J. Buehler, Molecular and nanostructural mechanisms of deformation, strength and toughness of spider silk fibrils, Nano Lett. 10 (2010) 2626–2634.

[44] K. Numata, P. Cebe, D.L. Kaplan, Mechanism of enzymatic degradation of beta-sheet crystals, Biomaterials. 31 (2010) 2926–2933.

[45] Y. Tao, W. Xu, Y. Yan, Y. Cao, Preparation and characterization of silk fibroin nanocrystals, Polym. Int. 61 (2012) 760–767.

[46] D. Knorr, Functional properties of chitin and chitosan, J. Food Sci. 47 (1982) 593–595.

[47] A.T. Paulino, J.I. Simionato, J.C. Garcia, J. Nozaki, Characterization of chitosan and chitin produced from silkworm crysalides, Carbohydr. Polym. 64 (2006) 98–103.

[48] A.M. Islam, G.O. Phillips, A. Sljivo, M.J. Snowden, P.A. Williams, A review of recent developments on the regulatory, structural and functional aspects of gum arabic, Food Hydrocoll. 11 (1997) 493–505.

[49] J. Sethi, M. Illikainen, M. Sain, K. Oksman, Polylactic acid/polyurethane blend reinforced with cellulose nanocrystals with semi-interpenetrating polymer network (S-IPN) structure, Eur. Polym. J. 86 (2017) 188–199.

[50] B. Braun, J.R. Dorgan, L.O. Hollingsworth, Supra-molecular ecobionanocomposites based on polylactide and cellulosic nanowhiskers: synthesis and properties, Biomacromolecules. 13 (2012) 2013–2019.

[51] J.R. Capadona, K. Shanmuganathan, S. Trittschuh, S. Seidel, S.J. Rowan, C. Weder, Polymer nanocomposites with nanowhiskers isolated from microcrystalline cellulose, Biomacromolecules. 10 (2009) 712–716.

[52] X. Zhang, Y. Zhang, Reinforcement effect of poly (butylene succinate)(PBS)-grafted cellulose nanocrystal on toughened PBS/polylactic acid blends, Carbohydr. Polym. 140 (2016) 374–382.

[53] A.N. Frone, S. Berlioz, J. Chailan, D.M. Panaitescu, D. Donescu, Cellulose fiber-reinforced polylactic acid, Polym. Compos. 32 (2011) 976–985.

[54] M. Martínez-Sanz, R.T. Olsson, A. Lopez-Rubio, J.M. Lagaron, Development of electrospun EVOH fibres reinforced with bacterial cellulose nanowhiskers. Part I: Characterization and method optimization, Cellulose. 18 (2011) 335–347.

[55] M. Martínez-Sanz, A. Lopez-Rubio, J.M. Lagaron, Optimization of the dispersion of unmodified bacterial cellulose nanowhiskers into polylactide via melt compounding to significantly enhance barrier and mechanical properties, Biomacromolecules. 13 (2012) 3887–3899.

[56] A. Gupta, W. Simmons, G.T. Schueneman, D. Hylton, E.A. Mintz, Rheological and thermo-mechanical properties of poly (lactic acid)/lignin-coated cellulose nanocrystal composites, ACS Sustain. Chem. Eng. 5 (2017) 1711–1720.

[57] M.M.-U. Haque, D. Puglia, E. Fortunati, M. Pracella, Effect of reactive functionalization on properties and degradability of poly (lactic acid)/poly (vinyl acetate) nanocomposites with cellulose nanocrystals, React. Funct. Polym. 110 (2017) 1–9.

[58] D. Bondeson, K. Oksman, Dispersion and characteristics of surfactant modified cellulose whiskers nanocomposites, Compos. Interfaces. 14 (2007) 617–630.

[59] K. Cai, K. Yao, S. Lin, Z. Yang, X. Li, H. Xie, T. Qing, L. Gao, Poly (D, L-lactic acid) surfaces modified by silk fibroin: effects on the culture of osteoblast in vitro, Biomaterials. 23 (2002) 1153–1160.

[60] Y.-Q. Zhao, H.-Y. Cheung, K.-T. Lau, C.-L. Xu, D.-D. Zhao, H.-L. Li, Silkworm silk/poly (lactic acid) biocomposites: Dynamic mechanical, thermal and biodegradable properties, Polym. Degrad. Stab. 95 (2010) 1978–1987.

[61] H.-Y. Cheung, K.-T. Lau, Y.-F. Pow, Y.-Q. Zhao, D. Hui, Biodegradation of a silkworm silk/PLA composite, Compos. Part B Eng. 41 (2010) 223–228.

[62] J. He, Y. Qin, S. Cui, Y. Gao, S. Wang, Structure and properties of novel electrospun tussah silk fibroin/poly (lactic acid) composite nanofibers, J. Mater. Sci. 46 (2011) 2938–2946.

[63] R. Patwa, A. Kumar, V. Katiyar, Effect of silk nano-disc dispersion on mechanical, thermal, and barrier properties of poly (lactic acid) based bionanocomposites, J. Appl. Polym. Sci. 135 (2018) 46671.

[64] N. Niamsa, Y. Baimark, Preparation and characterization of highly flexible chitosan films for use as food packaging, Am. J. Food Technol. 4 (2009) 162–169.

[65] A.J. Svagan, A. Åkesson, M. Cárdenas, S. Bulut, J.C. Knudsen, J. Risbo, D. Plackett, Transparent films based on PLA and montmorillonite with tunable oxygen barrier properties, Biomacromolecules. 13 (2012) 397–405.

[66] S.B. Schreiber, J.J. Bozell, D.G. Hayes, S. Zivanovic, Introduction of primary antioxidant activity to chitosan for application as a multifunctional food packaging material, Food Hydrocoll. 33 (2013) 207–214.

[67] Y. Peng, Y. Wu, Y. Li, Development of tea extracts and chitosan composite films for active packaging materials, Int. J. Biol. Macromol. 59 (2013) 282–289.

[68] F. Li, P. Biagioni, M. Finazzi, S. Tavazzi, L. Piergiovanni, Tunable green oxygen barrier through layer-by-layer self-assembly of chitosan and cellulose nanocrystals, Carbohydr. Polym. 92 (2013) 2128–2134.

[69] F. Croisier, C. Jérôme, Chitosan-based biomaterials for tissue engineering, Eur. Polym. J. 49 (2013) 780–792.

[70] G. Wyasu, N.Z.J. Okereke, Improving the film forming ability of gum Arabic, J. Nat. Prod. Plant Resour. 2 (2012) 314–317.

[71] D. Sakloetsakun, D. Preechagoon, A. Bernkop-Schnürch, T. Pongjanyakul, Chitosan–gum arabic polyelectrolyte complex films: physicochemical, mechanical and mucoadhesive properties, Pharm. Dev. Technol. 21 (2016) 590–599.

[72] A. Ali, M. Maqbool, S. Ramachandran, P.G. Alderson, Gum arabic as a novel edible coating for enhancing shelf-life and improving postharvest quality of tomato (Solanum lycopersicum L.) fruit, Postharvest Biol. Technol. 58 (2010) 42–47.

[73] A. Tsimpliaraki, I. Tsivintzelis, S.I. Marras, I. Zuburtikudis, C. Panayiotou, The effect of surface chemistry and nanoclay loading on the microcellular structure of porous poly (d, l lactic acid) nanocomposites, J. Supercrit. Fluids. 57 (2011) 278–287.

[74] S. Pilla, A. Kramschuster, J. Lee, C. Clemons, S. Gong, L.-S. Turng, Microcellular processing of polylactide–hyperbranched polyester–nanoclay composites, J. Mater. Sci. 45 (2010) 2732–2746.

[75] D.J. Kang, D. Xu, Z.X. Zhang, K. Pal, D.S. Bang, J.K. Kim, Well-Controlled Microcellular Biodegradable PLA/Silk Composite Foams Using Supercritical CO2, Macromol. Mater. Eng. 294 (2009) 620–624.

[76] T.-R. Kuang, H.-Y. Mi, D.-J. Fu, X. Jing, B. Chen, W.-J. Mou, X.-F. Peng, Fabrication of poly (lactic acid)/graphene oxide foams with highly oriented and elongated cell structure via unidirectional foaming using supercritical carbon dioxide, Ind. Eng. Chem. Res. 54 (2015) 758–768.

[77] P.X. Ma, J.-W. Choi, Biodegradable polymer scaffolds with well-defined interconnected spherical pore network, Tissue Eng. 7 (2001) 23–33.

[78] J.J. Blaker, V. Maquet, R. Jérôme, A.R. Boccaccini, S.N. Nazhat, Mechanical properties of highly porous PDLLA/Bioglass® composite foams as scaffolds for bone tissue engineering, Acta Biomater. 1 (2005) 643–652.

[79] L. Ma, W. Jiang, W. Li, Solvent-free fabrication of tissue engineering scaffolds with immiscible polymer blends, Int. J. Polym. Mater. Polym. Biomater. 63 (2014) 510–517.

[80] J. Pinto, A. Athanassiou, D. Fragouli, Effect of the porous structure of polymer foams on the remediation of oil spills, J. Phys. D. Appl. Phys. 49 (2016) 145601.

[81] J. Wang, Q. Ren, W. Zheng, W. Zhai, Improved flame-retardant properties of poly (lactic acid) foams using starch as a natural charring agent, Ind. Eng. Chem. Res. 53 (2014) 1422–1430.

[82] J. Dlouhá, L. Suryanegara, H. Yano, Cellulose nanofibre–poly (lactic acid) microcellular foams exhibiting high tensile toughness, React. Funct. Polym. 85 (2014) 201–207.

[83] X. Sun, H. Kharbas, J. Peng, L.-S. Turng, A novel method of producing lightweight microcellular injection molded parts with improved ductility and toughness, Polymer (Guildf). 56 (2015) 102–110.

[84] J.J. Song, H.H. Chang, H.E. Naguib, Design and characterization of biocompatible shape memory polymer (SMP) blend foams with a dynamic porous structure, Polymer (Guildf). 56 (2015) 82–92.

[85] Y. Di, S. Iannace, E. Di Maio, L. Nicolais, Reactively modified poly (lactic acid): properties and foam processing, Macromol. Mater. Eng. 290 (2005) 1083–1090.

[86] S. Lee, M.A. Hanna, Preparation and characterization of tapioca starch-poly (lactic acid)-Cloisite NA+ nanocomposite foams, J. Appl. Polym. Sci. 110 (2008) 2337–2344.

[87] S. Hwang, P.P. Hsu, J. Yeh, K. Chang, Y. Lai, The mechanical/thermal properties of microcellular injection-molded poly-lactic-acid nanocomposites, Polym. Compos. 30 (2009) 1625–1630.

[88] G. Ji, J. Wang, W. Zhai, D. Lin, W. Zheng, Tensile properties of microcellular poly (lactic acid) foams blown by compressed CO2, J. Cell. Plast. 49 (2013) 101–117.

[89] K. Taki, D. Kitano, M. Ohshima, Effect of growing crystalline phase on bubble nucleation in poly (L-lactide)/CO_2 batch foaming, Ind. Eng. Chem. Res. 50 (2011) 3247–3252.

[90] L. Tang, W. Zhai, W. Zheng, Autoclave preparation of expanded polypropylene/poly (lactic acid) blend bead foams with a batch foaming process, J. Cell. Plast. 47 (2011) 429–446.

[91] A. Ameli, D. Jahani, M. Nofar, P.U. Jung, C.B. Park, Development of high void fraction polylactide composite foams using injection molding: Mechanical and thermal insulation properties, Compos. Sci. Technol. 90 (2014) 88–95.

[92] J. Wang, W. Zhu, H. Zhang, C.B. Park, Continuous processing of low-density, microcellular poly (lactic acid) foams with controlled cell morphology and crystallinity, Chem. Eng. Sci. 75 (2012) 390–399.

[93] S.C. Frerich, Biopolymer foaming with supercritical CO_2—Thermodynamics, foaming behaviour and mechanical characteristics, J. Supercrit. Fluids. 96 (2015) 349–358.

[94] M. Bitou, M. Okamoto, Fabrication of porous 3-D structure from poly (L-lactide)-based nano-composite foams. Effect of foam structure on enzymatic degradation, Polym. Degrad. Stab. 93 (2008) 1081–1087.

[95] E. Richards, R. Rizvi, A. Chow, H. Naguib, Biodegradable composite foams of PLA and PHBV using subcritical CO_2, J. Polym. Environ. 16 (2008) 258–266.

[96] A. Hao, Y. Geng, Q. Xu, Z. Lu, L. Yu, Study of different effects on foaming process of biodegradable PLA/starch composites in supercritical/compressed carbon dioxide, J. Appl. Polym. Sci. 109 (2008) 2679–2686.

[97] J. Zhang, X. Sun, Biodegradable foams of poly (lactic acid)/starch. I. Extrusion condition and cellular size distribution, J. Appl. Polym. Sci. 106 (2007) 857–862.

[98] J. Zhang, X. Sun, Biodegradable foams of poly (lactic acid)/starch. II. Cellular structure and water resistance, J. Appl. Polym. Sci. 106 (2007) 3058–3062.

[99] H. Yuan, Z. Liu, J. Ren, Preparation, characterization, and foaming behavior of poly (lactic acid)/poly (butylene adipate-co-butylene terephthalate) blend, Polym. Eng. Sci. 49 (2009) 1004–1012.

[100] S. Pilla, S.G. Kim, G.K. Auer, S. Gong, C.B. Park, Microcellular extrusion foaming of poly (lactide)/poly (butylene adipate-co-terephthalate) blends, Mater. Sci. Eng. C. 30 (2010) 255–262.

[101] S. Pilla, A. Kramschuster, J. Lee, G.K. Auer, S. Gong, L.-S. Turng, Microcellular and solid polylactide–flax fiber composites, Compos. Interfaces. 16 (2009) 869–890.

[102] Y. Fujimoto, S.S. Ray, M. Okamoto, A. Ogami, K. Yamada, K. Ueda, Well-controlled biodegradable nanocomposite foams: from microcellular to nanocellular, Macromol. Rapid Commun. 24 (2003) 457–461.

[103] Y. Di, S. Iannace, E. Di Maio, L. Nicolais, Poly (lactic acid)/organoclay nanocomposites: thermal, rheological properties and foam processing, J. Polym. Sci. Part B Polym. Phys. 43 (2005) 689–698.

[104] Y. Ema, M. Ikeya, M. Okamoto, Foam processing and cellular structure of polylactide-based nanocomposites, Polymer (Guildf). 47 (2006) 5350–5359.

[105] L.M. Matuana, C.A. Diaz, Study of cell nucleation in microcellular poly (lactic acid) foamed with supercritical CO2 through a continuous-extrusion process, Ind. Eng. Chem. Res. 49 (2010) 2186–2193.

[106] J. Dlouhá, L. Suryanegara, H. Yano, The role of cellulose nanofibres in supercritical foaming of polylactic acid and their effect on the foam morphology, Soft Matter. 8 (2012) 8704–8713.

[107] C. Hopmann, S. Latz, Foaming technology using gas counter pressure to improve the flexibility of foams by using high amounts of CO_2 as a blowing agent, Polymer (Guildf). 56 (2015) 29–36.

[108] D.U. Shah, F. Vollrath, D. Porter, Silk cocoons as natural macro-balloon fillers in novel polyurethane-based syntactic foams, Polymer (Guildf). 56 (2015) 93–101.

[109] R. Huang, X. Zhu, H. Tu, A. Wan, The crystallization behavior of porous poly (lactic acid) prepared by modified solvent casting/particulate leaching technique for potential use of tissue engineering scaffold, Mater. Lett. 136 (2014) 126–129.

[110] P. Jia, J. Hu, W. Zhai, Y. Duan, J. Zhang, C. Han, Cell morphology and improved heat resistance of microcellular poly (l-lactide) foam via introducing stereocomplex crystallites of PLA, Ind. Eng. Chem. Res. 54 (2015) 2476–2488.

[111] J. Ludwiczak, M. Kozlowski, Foaming of polylactide in the presence of chain extender,

J. Polym. Environ. 23 (2015) 137–142.

[112] M. Zhou, P. Zhou, P. Xiong, X. Qian, H. Zheng, Crystallization, rheology and foam morphology of branched PLA prepared by novel type of chain extender, Macromol. Res. 23 (2015) 231–236.

[113] J. Goswami, N. Bhatnagar, S. Mohanty, A.K. Ghosh, Processing and characterization of poly (lactic acid) based bioactive composites for biomedical scaffold application., Express Polym. Lett. 7 (2013).

[114] N.J. Mills, R. Stämpfli, F. Marone, P.A. Brühwiler, Finite element micromechanics model of impact compression of closed-cell polymer foams, Int. J. Solids Struct. 46 (2009) 677–697.

[115] J.J. Yoon, T.G. Park, Degradation behaviors of biodegradable macroporous scaffolds prepared by gas foaming of effervescent salts, J. Biomed. Mater. Res. An Off. J. Soc. Biomater. Japanese Soc. Biomater. Aust. Soc. Biomater. Korean Soc. Biomater. 55 (2001) 401–408.

[116] C. Liao, C. Chen, J. Chen, S. Chiang, Y. Lin, K. Chang, Fabrication of porous biodegradable polymer scaffolds using a solvent merging/particulate leaching method, J. Biomed. Mater. Res. An Off. J. Soc. Biomater. Japanese Soc. Biomater. Aust. Soc. Biomater. Korean Soc. Biomater. 59 (2002) 676–681.

[117] E. Lizundia, P. Mateos, J.L. Vilas, Tuneable hydrolytic degradation of poly (l-lactide) scaffolds triggered by ZnO nanoparticles, Mater. Sci. Eng. C. 75 (2017) 714–720.

[118] E. Ikada, Photo-and bio-degradable polyesters. Photodegradation behaviors of aliphatic polyesters, J. Photopolym. Sci. Technol. 10 (1997) 265–270.

[119] G. Schliecker, C. Schmidt, S. Fuchs, R. Wombacher, T. Kissel, Hydrolytic degradation of poly (lactide-co-glycolide) films: effect of oligomers on degradation rate and crystallinity, Int. J. Pharm. 266 (2003) 39–49.

[120] M.A. Elsawy, K.-H. Kim, J.-W. Park, A. Deep, Hydrolytic degradation of polylactic acid (PLA) and its composites, Renew. Sustain. Energy Rev. 79 (2017) 1346–1352.

[121] P. Dhar, D. Tarafder, A. Kumar, V. Katiyar, Effect of Cellulose Nanocrystal Polymorphs on Mechanical, Barrier and Thermal Properties of Poly(lactic acid) based bionanocomposites, RSC Adv. 5 (2015) 60426–60440. doi:10.1039/C5RA06840A.

[122] N. Tripathi, V. Katiyar, PLA/functionalized-gum arabic based bionanocomposite films for high gas barrier applications, J. Appl. Polym. Sci. 133 (2016).

[123] A.K. Pal, V. Katiyar, Nanoamphiphilic chitosan dispersed poly (lactic acid) bionanocomposite films with improved thermal, mechanical, and gas barrier properties, Biomacromolecules. 17 (2016) 2603–2618.

[124] M. Tesfaye, R. Patwa, R. Kommadath, P. Kotecha, V. Katiyar, Silk nanocrystals stabilized melt extruded poly (lactic acid) nanocomposite films: Effect of recycling on thermal degradation kinetics and optimization studies, Thermochim. Acta. 643 (2016) 41–52.

[125] A. Mohebbi, F. Mighri, A. Ajji, D. Rodrigue, Current issues and challenges in polypropylene foaming: a review, Cell. Polym. 34 (2015) 299–338.

[126] P. Dhar, D. Tarafder, A. Kumar, V. Katiyar, Thermally recyclable polylactic acid/cellulose nanocrystal films through reactive extrusion process, Polymer (Guildf). 87 (2016) 268–282.

[127] D. Kohlhoff, M. Ohshima, Open Cell Microcellular Foams of Polylactic Acid (PLA)-based Blends with Semi-Interpenetrating Polymer Networks, Macromol. Mater. Eng. 296 (2011) 770–777.

[128] K. Grundke, K. Pöschel, A. Synytska, R. Frenzel, A. Drechsler, M. Nitschke, A.L. Cordeiro, P. Uhlmann, P.B. Welzel, Experimental studies of contact angle hysteresis phenomena on polymer surfaces—Toward the understanding and control of wettability for different applications, Adv. Colloid Interface Sci. 222 (2015) 350–376.

[129] H.B. Eral, J.M. Oh, Contact angle hysteresis: a review of fundamentals and applications, Colloid Polym. Sci. 291 (2013) 247–260.

[130] T.S. Meiron, A. Marmur, I.S. Saguy, Contact angle measurement on rough surfaces, J. Colloid Interface Sci. 274 (2004) 637–644. doi:10.1016/j.jcis.2004.02.036.

[131] F.J. Montes Ruiz-Cabello, M.A. Rodriguez-Valverde, A. Marmur, M.A. Cabrerizo-Vílchez, Comparison of sessile drop and captive bubble methods on rough homogeneous surfaces: a numerical study, Langmuir. 27 (2011) 9638–9643.

[132] L. Gao, T.J. McCarthy, Contact angle hysteresis explained, Langmuir. 22 (2006) 6234–6237.

[133] E. Bormashenko, Y. Bormashenko, G. Whyman, R. Pogreb, A. Musin, R. Jager, Z. Barkay, Contact angle hysteresis on polymer substrates established with various experimental techniques, its interpretation, and quantitative characterization, Langmuir. 24 (2008) 4020–4025. doi:10.1021/la703875b.

[134] R.-D. Schulze, W. Possart, H. Kamusewitz, C. Bischof, Young's equilibrium contact angle on rough solid surfaces. Part I. An empirical determination, J. Adhes. Sci. Technol. 3 (1989) 39–48.

[135] M.A. Rodríguez-Valverde, F.J.M. Ruiz-Cabello, P.M. Gea-Jódar, H. Kamusewitz, M.A. Cabrerizo-Vílchez, A new model to estimate the Young contact angle from contact angle hysteresis measurements, Colloids Surfaces A Physicochem. Eng. Asp. 365 (2010) 21–27.

[136] K. Pielichowski, J. Njuguna, Thermal degradation of polymeric materials, iSmithers Rapra Publishing, 2005.

[137] O. Bianchi, J.D.N. Martins, R. Fiorio, R.V.B. Oliveira, L.B. Canto, Changes in activation energy and kinetic mechanism during EVA crosslinking, Polym. Test. 30 (2011) 616–624.

[138] A. Khawam, D.R. Flanagan, Complementary use of model-free and modelistic methods in the analysis of solid-state kinetics, J. Phys. Chem. B. 109 (2005) 10073–10080.

[139] A.K. Pal, V. Katiyar, Theoretical and analyzed data related to thermal degradation kinetics of poly (L-lactic acid)/chitosan-grafted-oligo L-lactic acid (PLA/CH-g-OLLA) bionanocomposite films, Data Br. 10 (2017) 304–311.

[140] H.L. Friedman, Kinetics of thermal degradation of char-forming plastics from thermogravimetry. Application to a phenolic plastic, in: J. Polym. Sci. Part C Polym.

Symp., Wiley Online Library, 1964: pp. 183–195.

[141] H.E. Kissinger, Reaction kinetics in differential thermal analysis, Anal. Chem. 29 (1957) 1702–1706.

[142] A. Aboulkas, K. El Harfi, Study of the Kinetics and Mechanisms of Thermal Decomposition of Moroccan Tarfaya Oil Shale and Its Kerogen., Oil Shale. 25 (2008).

[143] J. Opfermann, E. Kaisersberger, An advantageous variant of the Ozawa-Flynn-Wall analysis, Thermochim. Acta. 203 (1992) 167–175.

[144] J.H. Flynn, L.A. Wall, A quick, direct method for the determination of activation energy from thermogravimetric data, J. Polym. Sci. Part B Polym. Lett. 4 (1966) 323–328.

[145] T. Ozawa, A new method of analyzing thermogravimetric data, Bull. Chem. Soc. Jpn. 38 (1965) 1881–1886.

[146] K. Chrissafis, Kinetics of thermal degradation of polymers, J. Therm. Anal. Calorim. 95 (2009) 273–283.

[147] H. Wang, J. Yang, S. Long, X. Wang, Z. Yang, G. Li, Studies on the thermal degradation of poly (phenylene sulfide sulfone), Polym. Degrad. Stab. 83 (2004) 229–235.

[148] B. Danon, N.M. Mkhize, P. Van Der Gryp, J.F. Görgens, Combined model-free and model-based devolatilisation kinetics of tyre rubbers, Thermochim. Acta. 601 (2015) 45–53.

[149] A. Aboulkas, A. El Bouadili, Thermal degradation behaviors of polyethylene and polypropylene. Part I: Pyrolysis kinetics and mechanisms, Energy Convers. Manag. 51 (2010) 1363–1369.

[150] J.M. Criado, Kinetic analysis of DTG data from master curves, Thermochim. Acta. 24 (1978) 186–189.

[151] S. Mallakpour, M. Taghavi, Kinetics and thermal degradation study of optically active and thermally stable aromatic polyamides with flame-retardancy properties, Polym. J. 41 (2009) 308.

[152] X. Lu, J.N. Hay, The effect of physical aging on the rates of cold crystallization of poly (ethylene terephthalate), Polymer (Guildf). 41 (2000) 7427–7436.

[153] N. Vasanthan, N.J. Manne, A. Krishnama, Effect of Molecular Orientation on the Cold Crystallization of Amorphous–Crystallizable Polymers: The Case of Poly (trimethylene terephthalate), Ind. Eng. Chem. Res. 52 (2013) 17920–17926.

[154] M. Avrami, Kinetics of phase change. I General theory, J. Chem. Phys. 7 (1939) 1103–1112.

[155] M. Liu, Q. Zhao, Y. Wang, C. Zhang, Z. Mo, S. Cao, Melting behaviors, isothermal and non-isothermal crystallization kinetics of nylon 1212, Polymer (Guildf). 44 (2003) 2537–2545.

[156] G.Z. Papageorgiou, D.S. Achilias, D.N. Bikiaris, Crystallization kinetics of biodegradable poly (butylene succinate) under isothermal and non-isothermal conditions, Macromol. Chem. Phys. 208 (2007) 1250–1264.

[157] P. Dhar, S.M. Bhasney, A. Kumar, V. Katiyar, Acid functionalized cellulose

nanocrystals and its effect on mechanical, thermal, crystallization and surfaces properties of poly (lactic acid) bionanocomposites films: A comprehensive study, Polymer (Guildf). 101 (2016) 75–92.

[158] G. Gorrasi, R. Pantani, Effect of PLA grades and morphologies on hydrolytic degradation at composting temperature: assessment of structural modification and kinetic parameters, Polym. Degrad. Stab. 98 (2013) 1006–1014.

[159] K. Fukushima, D. Tabuani, M. Dottori, I. Armentano, J.M. Kenny, G. Camino, Effect of temperature and nanoparticle type on hydrolytic degradation of poly (lactic acid) nanocomposites, Polym. Degrad. Stab. 96 (2011) 2120–2129.

[160] N. Mills, Polymer foams handbook: engineering and biomechanics applications and design guide, Elsevier, 2007.

[161] V. Mittal, Polymer nanotubes nanocomposites: synthesis, properties and applications, John Wiley & Sons, 2014.

[162] D. Klempner, V. Sendijarevic, Polymeric foams and foam technology, 2nd. Ed. (2004).

[163] S. Alavi, S. Thomas, K.P. Sandeep, N. Kalarikkal, J. Varghese, S. Yaragalla, Bio-based Nanocomposites: Prospects in green packaging applications, in: Polym. Packag. Appl., Apple Academic Press, 2014: pp. 281–306.

[164] R. Auras, B. Harte, S. Selke, An overview of polylactides as packaging materials, Macromol. Biosci. 4 (2004) 835–864.

[165] J.H. Lee, S.H. Park, S.H. Kim, Surface modification of cellulose nanowhiskers and their reinforcing effect in polylactide, Macromol. Res. 22 (2014) 424–430.

[166] M. Sauceau, J. Fages, A. Common, C. Nikitine, E. Rodier, New challenges in polymer foaming: A review of extrusion processes assisted by supercritical carbon dioxide, Prog. Polym. Sci. 36 (2011) 749–766.

[167] A. Wong, S.F.L. Wijnands, T. Kuboki, C.B. Park, Mechanisms of nanoclay-enhanced plastic foaming processes: Effects of nanoclay intercalation and exfoliation, J. Nanoparticle Res. 15 (2013). doi:10.1007/s11051-013-1815-y.

[168] X. Cao, Y. Habibi, L. a. Lucia, One-pot polymerization, surface grafting, and processing of waterborne polyurethane-cellulose nanocrystal nanocomposites, J. Mater. Chem. 19 (2009) 7137–7145. doi:10.1039/b910517d.

[169] J.V. Edwards, N. Prevost, K. Sethumadhavan, A. Ullah, B. Condon, Peptide conjugated cellulose nanocrystals with sensitive human neutrophil elastase sensor activity, Cellulose. 20 (2013) 1223–1235. doi:10.1007/s10570-013-9901-y.

[170] J.K. Jackson, K. Letchford, B.Z. Wasserman, L. Ye, W.Y. Hamad, H.M. Burt, The use of nanocrystalline cellulose for the binding and controlled release of drugs., Int. J. Nanomedicine. 6 (2011) 321–330. doi:10.2147/IJN.S16749.

[171] F. Carrasco, L.A. Pérez-Maqueda, P.E. Sánchez-Jiménez, A. Perejón, O.O. Santana, M.L. Maspoch, Enhanced general analytical equation for the kinetics of the thermal degradation of poly (lactic acid) driven by random scission, Polym. Test. 32 (2013) 937–945.

[172] G. Guo, Q. Ma, F. Wang, B. Zhao, D. Zhang, Kinetic evaluation of the size-dependent

decomposition performance of solvent-free microcellular polylactic acid foams, Chinese Sci. Bull. 57 (2012) 83–89.

[173] H. Tsuji, I. Fukui, Enhanced thermal stability of poly (lactide) s in the melt by enantiomeric polymer blending, Polymer (Guildf). 44 (2003) 2891–2896.

[174] A.K. Pal, V. Katiyar, Thermal degradation behaviour of nanoamphiphilic chitosan dispersed poly (lactic acid) bionanocomposite films, Int. J. Biol. Macromol. 95 (2017) 1267–1279.

[175] Y. Fan, H. Nishida, Y. Shirai, Y. Tokiwa, T. Endo, Thermal degradation behaviour of poly (lactic acid) stereocomplex, Polym. Degrad. Stab. 86 (2004) 197–208.

[176] P. Dhar, U. Bhardwaj, A. Kumar, V. Katiyar, Improved structural properties of polyhydroxybutyrate composites, Plast. Res. Online. (2016) 1–4. doi:10.2417/spepro.006379.

[177] A.B. Brizuela, L.C. Bichara, E. Romano, A. Yurquina, S. Locatelli, S.A. Brandán, A complete characterization of the vibrational spectra of sucrose, Carbohydr. Res. 361 (2012) 212–218.

[178] M. Pracella, M.M.-U. Haque, D. Puglia, Morphology and properties tuning of PLA/cellulose nanocrystals bio-nanocomposites by means of reactive functionalization and blending with PVAc, Polymer (Guildf). 55 (2014) 3720–3728.

[179] K. Bocz, T. Tábi, D. Vadas, M. Sauceau, J. Fages, G. Marosi, Characterisation of natural fibre reinforced PLA foams prepared by supercritical CO2 assisted extrusion, Express Polym. Lett. 10 (2016) 771–779.

[180] X. Zhao, F.R. Guerrero, J. Llorca, D.-Y. Wang, New superefficiently flame-retardant bioplastic poly (lactic acid): flammability, thermal decomposition behavior, and tensile properties, ACS Sustain. Chem. Eng. 4 (2015) 202–209.

[181] N. Tudorachi, R. Lipsa, F.R. Mustata, Thermal degradation of carboxymethyl starch–g-poly (lactic acid) copolymer by TG–FTIR–MS analysis, Ind. Eng. Chem. Res. 51 (2012) 15537–15545.

[182] H. Zou, C. Yi, L. Wang, H. Liu, W. Xu, Thermal degradation of poly (lactic acid) measured by thermogravimetry coupled to Fourier transform infrared spectroscopy, J. Therm. Anal. Calorim. 97 (2009) 929.

[183] H. Kamusewitz, W. Possart, D. Paul, The relation between Young's equilibrium contact angle and the hysteresis on rough paraffin wax surfaces, Colloids Surfaces A Physicochem. Eng. Asp. 156 (1999) 271–279.

[184] R. Valapa, S. Hussain, P.K. Iyer, G. Pugazhenthi, V. Katiyar, Influence of graphene on thermal degradation and crystallization kinetics behaviour of poly (lactic acid), J. Polym. Res. 22 (2015) 175.

[185] R. Zong, Z. Wang, N. Liu, Y. Hu, G. Liao, Thermal degradation kinetics of polyethylene and silane-crosslinked polyethylene, J. Appl. Polym. Sci. 98 (2005) 1172–1179.

[186] P. Dhar, V. Katiyar, Thermal degradation kinetics of polylactic acid/acid fabricated cellulose nanocrystal based bionanocomposites, Int. J. Biol. Macromol. 104 (2017) 827–836.

[187] D.H. Sebastian, J.A. Biesenberger, Principles of polymerization engineering, Wiley New York, 1983.

[188] N. Tripathi, V. Katiyar, Poly (lactic acid)/modified gum arabic based bionanocomposite films: Thermal degradation kinetics, Polym. Eng. Sci. 57 (2017) 1193–1206.

[189] F. Auriemma, C. De Rosa, G.C. Alfonso, Polymer Crystallization II From Chain Microstructure to Processing Preface, (2017).

[190] L. Mandelkern, Crystallization of Polymers: Volume 2, Kinetics and Mechanisms, Cambridge University Press, 2004.

[191] G. Reiter, G.R. Strobl, Progress in understanding of polymer crystallization, Springer, 2007.

[192] P. Supaphol, N. Dangseeyun, P. Srimoaon, M. Nithitanakul, Nonisothermal melt-crystallization kinetics for three linear aromatic polyesters, Thermochim. Acta. 406 (2003) 207–220.

[193] E. Lizundia, J.L. Vilas, L.M. León, Crystallization, structural relaxation and thermal degradation in Poly (l-lactide)/cellulose nanocrystal renewable nanocomposites, Carbohydr. Polym. 123 (2015) 256–265.

[194] S. Camarero-Espinosa, D.J. Boday, C. Weder, E.J. Foster, Cellulose nanocrystal driven crystallization of poly (d, l-lactide) and improvement of the thermomechanical properties, J. Appl. Polym. Sci. 132 (2015).

[195] C. Xu, Q. Lv, D. Wu, Z. Wang, Polylactide/cellulose nanocrystal composites: a comparative study on cold and melt crystallization, Cellulose. 24 (2017) 2163–2175.

[196] J. Chen, D. Wu, K.C. Tam, K. Pan, Z. Zheng, Effect of surface modification of cellulose nanocrystal on nonisothermal crystallization of poly (β-hydroxybutyrate) composites, Carbohydr. Polym. 157 (2017) 1821–1829.

[197] T. Xu, Y. Wang, Q. Han, D. He, Q. Li, C. Shen, Nonisothermal crystallization kinetics of poly (lactic acid) nucleated with a multiamide nucleating agent, J. Macromol. Sci. Part B. 53 (2014) 1680–1694.

[198] S.-T. Lee, C.B. Park, Foam extrusion: principles and practice, CRC press, 2014.

[199] N.E. Suyatma, A. Copinet, L. Tighzert, V. Coma, Mechanical and barrier properties of biodegradable films made from chitosan and poly (lactic acid) blends, J. Polym. Environ. 12 (2004) 1–6.

[200] X. Niu, Q. Feng, M. Wang, X. Guo, Q. Zheng, In vitro degradation and release behavior of porous poly (lactic acid) scaffolds containing chitosan microspheres as a carrier for BMP-2-derived synthetic peptide, Polym. Degrad. Stab. 94 (2009) 176–182.

[201] S.K. Sahoo, A.K. Panda, V. Labhasetwar, Characterization of porous PLGA/PLA microparticles as a scaffold for three dimensional growth of breast cancer cells, Biomacromolecules. 6 (2005) 1132–1139.

[202] Y. Jiao, Z. Liu, C. Zhou, Fabrication and characterization of PLLA–chitosan hybrid scaffolds with improved cell compatibility, J. Biomed. Mater. Res. Part A. 80 (2007) 820–825.

[203] Z. Zhang, H. Cui, Biodegradability and biocompatibility study of poly (chitosan-g-lactic

acid) scaffolds, Molecules. 17 (2012) 3243–3258.

[204] A.-M. Haaparanta, E. Järvinen, I.F. Cengiz, V. Ellä, H.T. Kokkonen, I. Kiviranta, M. Kellomäki, Preparation and characterization of collagen/PLA, chitosan/PLA, and collagen/chitosan/PLA hybrid scaffolds for cartilage tissue engineering, J. Mater. Sci. Mater. Med. 25 (2014) 1129–1136.

[205] Y. Hu, D.W. Grainger, S.R. Winn, J.O. Hollinger, Fabrication of poly (α-hydroxy acid) foam scaffolds using multiple solvent systems, J. Biomed. Mater. Res. An Off. J. Soc. Biomater. Japanese Soc. Biomater. Aust. Soc. Biomater. Korean Soc. Biomater. 59 (2002) 563–572.

[206] J. Málek, J.M. Criado, J. Šesták, J. Militký, The boundary conditions for kinetic models, Thermochim. Acta. 153 (1989) 429–432.

[207] A. Anitha, S. Sowmya, P.T.S. Kumar, S. Deepthi, K.P. Chennazhi, H. Ehrlich, M. Tsurkan, R. Jayakumar, Chitin and chitosan in selected biomedical applications, Prog. Polym. Sci. 39 (2014) 1644–1667.

[208] G. Chakraborty, A. Gupta, G. Pugazhenthi, V. Katiyar, Facile dispersion of exfoliated graphene/PLA nanocomposites via in situ polycondensation with a melt extrusion process and its rheological studies, J. Appl. Polym. Sci. 135 (2018) 46476.

[209] S. Turmanova, S. Genieva, L. Vlaev, Kinetics of nonisothermal degradation of some polymer composites: change of entropy at the formation of the activated complex from the reagents, J. Thermodyn. 2011 (2011).

[210] S. Ramukutty, E. Ramachandran, Reaction rate models for the thermal decomposition of ibuprofen crystals, J. Cryst. Process Technol. 4 (2014) 71.

[211] M. Poletto, A.J. Zattera, R.M.C. Santana, Thermal decomposition of wood: kinetics and degradation mechanisms, Bioresour. Technol. 126 (2012) 7–12.

[212] S.-J. Sheng, F. Wang, Q.-Y. Ma, X. Hu, Impact of foaming air on melting and crystallization behaviors of microporous PLA scaffolds, J. Therm. Anal. Calorim. 122 (2015) 1077–1088.

[213] D. Li, T. Liu, L. Zhao, X. Lian, W. Yuan, Foaming of poly (lactic acid) based on its nonisothermal crystallization behavior under compressed carbon dioxide, Ind. Eng. Chem. Res. 50 (2011) 1997–2007.

[214] I. Bružauskaitė, D. Bironaitė, E. Bagdonas, E. Bernotienė, Scaffolds and cells for tissue regeneration: different scaffold pore sizes—different cell effects, Cytotechnology. 68 (2016) 355–369.

[215] A. Kumar Pal, A. Das, V. Katiyar, Chitosan from Muga silkworms (Antheraea assamensis) and its influence on thermal degradation behavior of poly (lactic acid) based biocomposite films, J. Appl. Polym. Sci. 133 (2016).

[216] N.S.R. Shau-Tarng Lee, Chul B. Park, Polymeric Foams: Science and Technology, CRC Press, Boca Raton, 2007.

[217] W. Li, S. Liu, Preparation and characterization of polyurethane foam/activated carbon composite adsorbents, J. Porous Mater. 19 (2012) 567–572.

[218] S. Yu, H. Tan, J. Wang, X. Liu, K. Zhou, High porosity supermacroporous polystyrene

materials with excellent oil–water separation and gas permeability properties, ACS Appl. Mater. Interfaces. 7 (2015) 6745–6753.

[219] S. Cotugno, E. Di Maio, G. Mensitieri, S. Iannace, G.W. Roberts, R.G. Carbonell, H.B. Hopfenberg, Characterization of microcellular biodegradable polymeric foams produced from supercritical carbon dioxide solutions, Ind. Eng. Chem. Res. 44 (2005) 1795–1803.

[220] J.I. Lim, H.-K. Park, Fabrication of macroporous chitosan/poly (l-lactide) hybrid scaffolds by sodium acetate particulate-leaching method, J. Porous Mater. 19 (2012) 383–387.

[221] P. Netti, Biomedical foams for tissue engineering applications, Elsevier, 2014.

[222] R.E. Lee, Y. Guo, H. Tamber, M. Planeta, S.N.S. Leung, Thermoforming of polylactic acid foam sheets: Crystallization behaviors and thermal stability, Ind. Eng. Chem. Res. 55 (2016) 560–567.

[223] M. Ranjbar-Mohammadi, M.P. Prabhakaran, S.H. Bahrami, S. Ramakrishna, Gum tragacanth/poly (l-lactic acid) nanofibrous scaffolds for application in regeneration of peripheral nerve damage, Carbohydr. Polym. 140 (2016) 104–112.

[224] W. Calame, A.R. Weseler, C. Viebke, C. Flynn, A.D. Siemensma, Gum arabic establishes prebiotic functionality in healthy human volunteers in a dose-dependent manner, Br. J. Nutr. 100 (2008) 1269–1275.

[225] Y.D. Kim, C. V Morr, T.W. Schenz, Microencapsulation properties of gum arabic and several food proteins: liquid orange oil emulsion particles, J. Agric. Food Chem. 44 (1996) 1308–1313.

[226] L. Zhang, F. Yu, A.J. Cole, B. Chertok, A.E. David, J. Wang, V.C. Yang, Gum arabic-coated magnetic nanoparticles for potential application in simultaneous magnetic targeting and tumor imaging, AAPS J. 11 (2009) 693.

[227] K.K. Nishi, A. Jayakrishnan, Preparation and in vitro evaluation of primaquine-conjugated gum arabic microspheres, Biomacromolecules. 5 (2004) 1489–1495.

[228] C. Sanchez, G. Mekhloufi, D. Renard, Complex coacervation between β-lactoglobulin and Acacia gum: A nucleation and growth mechanism, J. Colloid Interface Sci. 299 (2006) 867–873.

[229] S.S. Banerjee, D.-H. Chen, Fast removal of copper ions by gum arabic modified magnetic nano-adsorbent, J. Hazard. Mater. 147 (2007) 792–799.

[230] H. Samsudin, H. Soto-Valdez, R. Auras, Poly (lactic acid) film incorporated with marigold flower extract (Tagetes erecta) intended for fatty-food application, Food Control. 46 (2014) 55–66.

[231] D. Battegazzore, S. Bocchini, A. Frache, Crystallization kinetics of poly (lactic acid)-talc composites, Express Polym Lett. 5 (2011) 849–858.

[232] V.J. Mkhabela, Novel bio-nanocomposite scaffolds for tissue engineering application, (2015).

[233] D. Wu, L. Wu, L. Wu, B.I.N. Xu, Y. Zhang, M. Zhang, Nonisothermal cold crystallization behavior and kinetics of polylactide/clay nanocomposites, J. Polym. Sci.

Part B Polym. Phys. 45 (2007) 1100–1113.

[234] H. Tsuji, Polylactides, Biopolym. Polyesters III, Y. (2002) 129–177.

[235] H. Tsuji, Degradation of poly (lactide)--based biodegradable materials, Nova Science Publishers, 2008.

[236] G.B. Kharas, F. Sanchez-Riera, D.K. Severson, Polymers of lactic acid, Plast. from Microbes Microb. Synth. Polym. Polym. Precursors. (1994) 93–137.

[237] A. Södergård, M. Stolt, Properties of lactic acid based polymers and their correlation with composition, Prog. Polym. Sci. 27 (2002) 1123–1163.

[238] K. Makino, M. Arakawa, T. Kondo, Preparation and in vitro degradation properties of polylactide microcapsules, Chem. Pharm. Bull. 33 (1985) 1195–1201.

[239] K. Makino, H. Ohshima, T. Kondo, Mechanism of hydrolytic degradation of poly (L-lactide) microcapsules: effects of pH, ionic strength and buffer concentration, J. Microencapsul. 3 (1986) 203–212.

[240] C. Migliaresi, L. Fambri, D. Cohn, A study on the in vitro degradation of poly (lactic acid), J. Biomater. Sci. Polym. Ed. 5 (1994) 591–606.

[241] C. Braud, R. Devarieux, H. Garreau, M. Vert, Capillary electrophoresis to analyze water-soluble oligo (hydroxyacids) issued from degraded or biodegraded aliphatic polyesters, J. Environ. Polym. Degrad. 4 (1996) 135–148.

[242] C.F. van Nostrum, T.F.J. Veldhuis, G.W. Bos, W.E. Hennink, Hydrolytic degradation of oligo (lactic acid): a kinetic and mechanistic study, Polymer (Guildf). 45 (2004) 6779–6787.

[243] C. Shih, A graphical method for the determination of the mode of hydrolysis of biodegradable polymers, Pharm. Res. 12 (1995) 2036–2040.

[244] H. Tsuji, Biodegradable polymers, (2002).

[245] A. Kulkarni, J. Reiche, A. Lendlein, Hydrolytic degradation of poly (rac-lactide) and poly [(rac-lactide)-co-glycolide] at the air–water interface, Surf. Interface Anal. An Int. J. Devoted to Dev. Appl. Tech. Anal. Surfaces, Interfaces Thin Film. 39 (2007) 740–746.

[246] T. Tarvainen, T. Karjalainen, M. Malin, S. Pohjolainen, J. Tuominen, J. Seppälä, K. Järvinen, Degradation of and drug release from a novel 2, 2-bis (2-oxazoline) linked poly (lactic acid) polymer, J. Control. Release. 81 (2002) 251–261.

[247] F. von Burkersroda, L. Schedl, A. Göpferich, Why degradable polymers undergo surface erosion or bulk erosion, Biomaterials. 23 (2002) 4221–4231.

[248] C. Jie, K.J. Zhu, Preparation, Characterization and Biodegradable Characteristics of Poly (D, L-lactide-co-1, 3-trimethylene carbonate), Polym. Int. 42 (1997) 373–379.

[249] H. Tsuji, K. Ikarashi, In vitro hydrolysis of poly (l-lactide) crystalline residues as extended-chain crystallites: II. Effects of hydrolysis temperature, Biomacromolecules. 5 (2004) 1021–1028.

[250] T. Yoshioka, N. Kawazoe, T. Tateishi, G. Chen, In vitro evaluation of biodegradation of poly (lactic-co-glycolic acid) sponges, Biomaterials. 29 (2008) 3438–3443.

[251] S. Li, Hydrolytic degradation characteristics of aliphatic polyesters derived from lactic and glycolic acids, J. Biomed. Mater. Res. An Off. J. Soc. Biomater. Japanese Soc. Biomater. Aust. Soc. Biomater. 48 (1999) 342–353.

[252] J.W. Leenslag, A.J. Pennings, R.R.M. Bos, F.R. Rozema, G. Boering, Resorbable materials of poly (L-lactide): VII. In vivo and in vitro degradation, Biomaterials. 8 (1987) 311–314.

[253] Y. Matsusue, T. Yamamuro, M. Oka, Y. Shikinami, S. Hyon, Y. Ikada, In vitro and in vivo studies on bioabsorbable ultra-high-strength poly (L-lactide) rods, J. Biomed. Mater. Res. 26 (1992) 1553–1567.

[254] M. Therin, P. Christel, S. Li, H. Garreau, M. Vert, In vivo degradation of massive poly (α-hydroxy acids): validation of in vitro findings, Biomaterials. 13 (1992) 594–600.

[255] H. Tsuji, K. Ikarashi, N. Fukuda, Poly (L-lactide): XII. Formation, growth, and morphology of crystalline residues as extended-chain crystallites through hydrolysis of poly (L-lactide) films in phosphate-buffered solution, Polym. Degrad. Stab. 84 (2004) 515–523.

[256] Y.S. Nam, J.J. Yoon, J.G. Lee, T.G. Park, Adhesion behaviours of hepatocytes cultured onto biodegradable polymer surface modified by alkali hydrolysis process, J. Biomater. Sci. Polym. Ed. 10 (1999) 1145–1158.

[257] T. Chandy, C.P. Sharma, Effect of plasma glow, glutaraldehyde and carbodiimide treatments on the enzymic degradation of poly (L-lactic acid) and poly (γ-benzyl-L-glutamate) films, Biomaterials. 12 (1991) 677–682.

[258] G.E. Park, M.A. Pattison, K. Park, T.J. Webster, Accelerated chondrocyte functions on NaOH-treated PLGA scaffolds, Biomaterials. 26 (2005) 3075–3082.

[259] M.F. Gonzalez, R.A. Ruseckaite, T.R. Cuadrado, Structural changes of polylactic-acid (PLA) microspheres under hydrolytic degradation, J. Appl. Polym. Sci. 71 (1999) 1223–1230.

[260] W. Schnabel, Polymer Degradation: Principles and Practice, (1981).

[261] J.F. Rabek, Photodegradation of polymers: physical characteristics and applications, Springer Science & Business Media, 2012.

[262] N.J. Turro, Photoaddition and photosubstitution reactions, Mod. Mol. Photochem. 607 (1978) 362–409.

[263] J. Hopewell, R. Dvorak, E. Kosior, Plastics recycling: challenges and opportunities, Philos. Trans. R. Soc. B Biol. Sci. 364 (2009) 2115.

[264] M. Sogancioglu, E. Yel, G. Ahmetli, Pyrolysis of waste high density polyethylene (HDPE) and low density polyethylene (LDPE) plastics and production of epoxy composites with their pyrolysis chars, J. Clean. Prod. 165 (2017) 369–381.

[265] R.E. Drumright, P.R. Gruber, D.E. Henton, Polylactic acid technology, Adv. Mater. 12 (2000) 1841–1846.

[266] S.T. Lee, N.S. Ramesh, Polymeric Foams: Mechanisms and Materials, 2004. doi:10.1109/MEI.2005.1412232.

[267] Y.-Q. Zhang, Applications of natural silk protein sericin in biomaterials, Biotechnol.

Adv. 20 (2002) 91–100.

[268] T. Matsuhira, K. Yamamoto, S. Osaki, Effects of UV irradiation on the molecular weight of spider silk, Polym. J. 45 (2013) 1167.

[269] S. Osaki, K. Yamamoto, A. Kajiwara, M. Murata, Evaluation of the resistance of spider silk to ultraviolet irradiation, Polym. J. 36 (2004) 623.

[270] R. Rajkhowa, L. Wang, X. Wang, Ultra-fine silk powder preparation through rotary and ball milling, Powder Technol. 185 (2008) 87–95.

[271] N. V Bhat, G.S. Nadiger, Crystallinity in silk fibers: Partial acid hydrolysis and related studies, J. Appl. Polym. Sci. 25 (1980) 921–932.

[272] N. V Bhat, G.S. Nadiger, K.M. Paralikar, S.M. Betrabet, Electron diffraction studies on Indian silk, J. Appl. Polym. Sci. 25 (1980) 635–640.

[273] J. Kundu, Y.-I. Chung, Y.H. Kim, G. Tae, S.C. Kundu, Silk fibroin nanoparticles for cellular uptake and control release, Int. J. Pharm. 388 (2010) 242–250.

[274] Y.-Q. Zhang, W.-D. Shen, R.-L. Xiang, L.-J. Zhuge, W.-J. Gao, W.-B. Wang, Formation of silk fibroin nanoparticles in water-miscible organic solvent and their characterization, J. Nanoparticle Res. 9 (2007) 885–900.

[275] S. Wang, Y. Zhang, H. Wang, G. Yin, Z. Dong, Fabrication and properties of the electrospun polylactide/silk fibroin-gelatin composite tubular scaffold, Biomacromolecules. 10 (2009) 2240–2244.

[276] R. Patwa, N. Soundararajan, N. Mulchandani, S.M. Bhasney, M. Shah, S. Kumar, A. Kumar, V. Katiyar, Silk nano-discs: A natural material for cancer therapy, Biopolymers. 109 (2018) e23231.

[277] R. Patwa, A. Kumar, V. Katiyar, Crystallization kinetics, morphology, and hydrolytic degradation of novel bio-based poly (lactic acid)/crystalline silk nano-discs nanobiocomposites, J. Appl. Polym. Sci. 135 (2018) 46590.

[278] G. Fang, Y. Tang, Z. Qi, J. Yao, Z. Shao, X. Chen, Precise correlation of macroscopic mechanical properties and microscopic structures of animal silks—using Antheraea pernyi silkworm silk as an example, J. Mater. Chem. B. 5 (2017) 6042–6048.

[279] M. Tsukada, G. Freddi, P. Monti, A. Bertoluzza, N. Kasai, Structure and molecular conformation of tussah silk fibroin films: Effect of methanol, J. Polym. Sci. Part B Polym. Phys. 33 (1995) 1995–2001.

[280] A. Gupta, V. Katiyar, Cellulose Functionalized High Molecular Weight Stereocomplex Polylactic Acid Biocomposite Films with Improved Gas Barrier, Thermomechanical Properties, ACS Sustain. Chem. Eng. 5 (2017) 6835–6844.

[281] A. Gupta, A. Prasad, N. Mulchandani, M. Shah, M. Ravi Sankar, S. Kumar, V. Katiyar, Multifunctional Nanohydroxyapatite-Promoted Toughened High-Molecular-Weight Stereocomplex Poly (lactic acid)-Based Bionanocomposite for Both 3D-Printed Orthopedic Implants and High-Temperature Engineering Applications, ACS Omega. 2 (2017) 4039–4052.

[282] B. Yuan, C. Bao, L. Song, N. Hong, K.M. Liew, Y. Hu, Preparation of functionalized graphene oxide/polypropylene nanocomposite with significantly improved thermal

stability and studies on the crystallization behavior and mechanical properties, Chem. Eng. J. 237 (2014) 411–420.

[283] L. Suryanegara, A.N. Nakagaito, H. Yano, The effect of crystallization of PLA on the thermal and mechanical properties of microfibrillated cellulose-reinforced PLA composites, Compos. Sci. Technol. 69 (2009) 1187–1192.

[284] G. Perego, G.D. Cella, C. Bastioli, Effect of molecular weight and crystallinity on poly (lactic acid) mechanical properties, J. Appl. Polym. Sci. 59 (1996) 37–43.

[285] F.-D. Kopinke, M. Remmler, K. Mackenzie, M. Möder, O. Wachsen, Thermal decomposition of biodegradable polyesters—II. Poly (lactic acid), Polym. Degrad. Stab. 53 (1996) 329–342.

[286] I.C. McNeill, H.A. Leiper, Degradation studies of some polyesters and polycarbonates—2. Polylactide: degradation under isothermal conditions, thermal degradation mechanism and photolysis of the polymer, Polym. Degrad. Stab. 11 (1985) 309–326.

[287] O. Wachsen, K. Platkowski, K.-H. Reichert, Thermal degradation of poly-l-lactide—studies on kinetics, modelling and melt stabilisation, Polym. Degrad. Stab. 57 (1997) 87–94.

[288] H. Yu, N. Huang, C. Wang, Z. Tang, Modeling of poly (L-lactide) thermal degradation: Theoretical prediction of molecular weight and polydispersity index, J. Appl. Polym. Sci. 88 (2003) 2557–2562.

[289] M. Herrera, G. Matuschek, A. Kettrup, Thermal degradation studies of some aliphatic polyamides using hyphenated techniques (TG-MS, TG-FTIR), J. Therm. Anal. Calorim. 59 (2000) 385–394.

[290] C.A. Wilkie, TGA/FTIR: an extremely useful technique for studying polymer degradation, Polym. Degrad. Stab. 66 (1999) 301–306.

[291] T. Provder, M.W. Urban, H.G. Barth, Hyphenated techniques in polymer characterization, American Chemical Society, 1994.

[292] M. Vert, S. Li, H. Garreau, More about the degradation of LA/GA-derived matrices in aqueous media, J. Control. Release. 16 (1991) 15–26.

[293] D.H. Lewis, Controlled release of bioactive agents from lactide/glycolide polymers, Biodegrad. Polym. as Drug Deliv. Syst. (1990) 1–41.

[294] M. Hakkarainen, S. Karlsson, A.-C. Albertsson, Rapid (bio) degradation of polylactide by mixed culture of compost microorganisms—low molecular weight products and matrix changes, Polymer (Guildf). 41 (2000) 2331–2338.

[295] P.N. Thanki, E. Dellacherie, J.-L. Six, Prevailing mechanisms of the hydrolytic degradation of oligo (d, l-lactide)-grafted dextrans, Eur. Polym. J. 41 (2005) 1546–1553.

[296] M. V Chaubal, G. Su, E. Spicer, W. Dang, K.E. Branham, J.P. English, Z. Zhao, In vitro and in vivo degradation studies of a novel linear copolymer of lactide and ethylphosphate, J. Biomater. Sci. Polym. Ed. 14 (2003) 45–61.

[297] J.L. Espartero, I. Rashkov, S.M. Li, N. Manolova, M. Vert, NMR analysis of low molecular weight poly (lactic acid) s, Macromolecules. 29 (1996) 3535–3539.

[298] V. De Simone, G. Maglio, R. Palumbo, V. Scardi, Synthesis, characterization, and degradation of block polyesteramides containing poly (l-lactide) segments, J. Appl. Polym. Sci. 46 (1992) 1813–1820.

[299] H. Tsuji, Y. Ikada, Properties and morphology of poly (L-lactide). II. Hydrolysis in alkaline solution, J. Polym. Sci. Part A Polym. Chem. 36 (1998) 59–66.

[300] T. Iwata, Y. Doi, Alkaline hydrolysis of solution-grown poly (L-lactic acid) single crystals, Sen'i Gakkaishi. 57 (2001) 172–177.

[301] P. Taddei, P. Monti, R. Simoni, Vibrational and thermal study on the in vitro and in vivo degradation of a poly (lactic acid)-based bioabsorbable periodontal membrane, J. Mater. Sci. Mater. Med. 13 (2002) 469–475.

[302] K. Tomihata, M. Suzuki, Y. Ikada, The pH dependence of monofilament sutures on hydrolytic degradation, J. Biomed. Mater. Res. An Off. J. Soc. Biomater. Japanese Soc. Biomater. Aust. Soc. Biomater. Korean Soc. Biomater. 58 (2001) 511–518.

[303] A. V Janorkar, A.T. Metters, D.E. Hirt, Degradation of poly (L-lactide) films under ultraviolet-induced photografting and sterilization conditions, J. Appl. Polym. Sci. 106 (2007) 1042–1047.

[304] H. Tsuji, Y. Echizen, Y. Nishimura, Enzymatic degradation of poly (l-lactic acid): Effects of UV irradiation, J. Polym. Environ. 14 (2006) 239–248.

[305] A. Copinet, C. Bertrand, A. Longieras, V. Coma, Y. Couturier, Photodegradation and biodegradation study of a starch and poly (lactic acid) coextruded material, J. Polym. Environ. 11 (2003) 169–179.

[306] A. Copinet, C. Bertrand, S. Govindin, V. Coma, Y. Couturier, Effects of ultraviolet light (315 nm), temperature and relative humidity on the degradation of polylactic acid plastic films, Chemosphere. 55 (2004) 763–773.

[307] P. Baishya, D. Saikia, M. Mandal, T.K. Maji, Biodegradability, flammability, dimensional stability, and UV resistance study of green wood starch gluten nanocomposites, Polym. Compos. (n.d.).

[308] Y. Li, A. Hayashi, M. Saito, M. Vacha, S. Murase, H. Sato, Degradation of aliphatic polyesters by vacuum ultraviolet irradiation, Polym. J. 38 (2006) 395.

Research Outputs

Peer-reviewed journal publications (published)

1. Shasanka Sekhar Borkotoky, Prodyut Dhar and Vimal Katiyar. "Biodegradable poly (lactic acid)/Cellulose nanocrystals (CNCs) composite microcellular foam: Effect of nanofillers on foam cellular morphology, thermal and wettability behavior." *International Journal of Biological Macromolecules* 106 (2018): 433-446. **(Impact Factor: ~4)**

2. Shasanka Sekhar Borkotoky, Gourhari Chakraborty and Vimal Katiyar. *"Thermal degradation behavior and crystallization kinetics of poly (lactic acid) and cellulose nanocrystals (CNC) based microcellular composite foams." International Journal of Biological Macromolecules* 108 (2018): 1518-1531. **(Impact Factor: ~4)**

3. Shasanka Sekhar Borkotoky, Akhilesh Kumar Pal and Vimal Katiyar. *"Poly (lactic acid)/Modified Chitosan-based Nanocomposite Foams: Non-isothermal Crystallization and Thermal Degradation Kinetics with Wettability and Porosimetric Investigations." Journal of Applied Polymer Science (JAPS),* 136 (2019), 47236 **(Impact Factor: ~2)**

4. Shasanka Sekhar Borkotoky, Tabli Ghosh, Purabi Bhagabati and Vimal Katiyar. "Poly (lactic acid)/Modified Gum Arabic (MG) based microcellular composite foam: Effect of MG on foam properties, thermal and crystallization behavior." *International Journal of Biological Macromolecules* 125 (2019): 159-170. **(Impact Factor: ~4)**

Journal articles (Ready for communication)

1. Shasanka Sekhar Borkotoky, Tabli Ghosh and Vimal Katiyar. *"Hydrolytic and UV irradiate degradation of Modified Gum Arabic (MG) reinforced Poly (lactic acid)-based microcellular nanocomposite foams: A mechanistic approach"* **(To be submitted to "Polymer Degradation and Stability", Elsevier).**

2. Shasanka Sekhar Borkotoky, Rahul Patwa, Tabli Ghosh, and Vimal Katiyar. *"Silk nanocrystal (SNC) based Poly (lactic acid) (PLA) foams: structure-property relationships."* **(To be submitted to "Composite Science and Technology", Elsevier)**

3. Shasanka Sekhar Borkotoky, Tabli Ghosh and Vimal Katiyar. *"Degradation studies of PLA and PLA/SNC based microcellular nanocomposite foams."* **(To be submitted to "European Polymer Journal", Elsevier)**

4. Review article on "*Recent advances in biodegradable polymeric foams/scaffold for biomedical applications."* **(Under preparation)**

Book Chapter (Published/Ready for communication)

1. Narendren Soundarajan, **Shasanka Sekhar Borkotoky,** and Vimal Katiyar, book chapter titled as "*Up to date Advances of Biobased and Biodegradable Polymers in Food Packaging*" in book 'Bio-based Plastics for Food Packaging Applications'. (Smithers Rapra, ISBN: 9781910242582)

2. Shasanka Sekhar Borkotoky and Vimal Katiyar, *Biodegradable Nanocomposite Foam: Processing, Structure, and Properties.* (**Book chapter: to be submitted to "Advances in Sustainable Polymers, Springer**)

3. Tabli Ghosh, **Shasanka Sekhar Borkotoky,** Vimal Katiyar, *Porous and Non-Porous Structures of Green Composites: Processing and Application.* **(Book chapter: to be submitted to "Advances in Sustainable Polymers, Springer)**

Conference proceedings/workshop/seminar attended

1. Shasanka Sekhar Borkotoky and Vimal Katiyar, V. *"Fabrication of Tuneable Biodegradable Polymeric Foams"*, Chemcon 2015, 27-30 December 2015, Guwahati, India.

2. Shasanka Sekhar Borkotoky and Vimal Katiyar, V. *"Effect of Chitosan and Cellulose Nanocrystals in the Surface Morphology and Wetting of Biodegradable Poly(lactic acid) Foams"*, Advances in Sustainable Polymers(ASP-2016), August 3-6, 2016, Kyoto, Japan.

3. Shasanka Sekhar Borkotoky and Vimal Katiyar, "*Surface Wettability Behaviour of Functionalized-Gum Arabic Dispersed Poly (lactic acid) Bionanocomposite Foams"*, Macro 2017, January 9-11, 2017, Thiruvananthapuram, Kerala, India.

4. Shasanka Sekhar Borkotoky, Rahul Patwa and Vimal Katiyar, "*Effect of silk nanoparticles on thermal and wetting behavior of poly (lactic acid) based foams"*. International Conference on Sophisticated Instruments in Modern Research, IIT Guwahati, 30 June-1 July 2017.

5. Shasanka Sekhar Borkotoky, Vimal Katiyar, *"Thermal Degradation Behaviour of PLA/CNC based Porous Microcellular Composite Foams."* Indo-Japan Bilateral Symposium on Future Perspective of Bioresource Utilization in North-East India, IJBS-17, February 1-4, 2018.

6. Shasanka Sekhar Borkotoky, Tabli Ghosh and Vimal Katiyar, *"Biodegradable Polylactic acid/ Modified Gum Arabic (MG) based Microcellular Composite Foam: Effect of MG on Foam properties and Thermal Behaviour."* International Symposium on Advances in Sustainable Polymers, ASP-17, January 8-11, 2018

7. Workshop on *"Training program on confocal laser scanning microscopy and its applications"* during 27-29 June 2016 at Guwahati Biotech Park, IIT Guwahati.

8. Attended *"3D-printing workshop"* during 21-22 March 2015 at IIT Guwahati (SEISMECH 15).

9. Attended "*GIFU-U/IITG and GIFU-U/UKM joint symposium*" on 1st August 2016 at Gifu University, Gifu Prefecture, Japan.

10. Attended short-term course on "Transport process and optimization techniques in polymers" during 15-20 December 2014 at IIT Guwahati.

11. Participated in a seminar on *"Extended rheology characterization"* on 18th September 2017 at IIT Guwahati.

12. Participated in the national symposium on *"IPR in innovation and entrepreneurship"* on 16th March 2015 at IIT Guwahati.

International Journal of Biological Macromolecules 118 (2018) 1518–1531

Contents lists available at ScienceDirect

International Journal of Biological Macromolecules

journal homepage: http://www.elsevier.com/locate/ijbiomac

Thermal degradation behaviour and crystallization kinetics of poly (lactic acid) and cellulose nanocrystals (CNC) based microcellular composite foams

Shasanka Sekhar Borkotoky, Gourhari Chakraborty, Vimal Katiyar *

Indian Institute of Technology Guwahati, Guwahati, Assam 781039, India

ARTICLE INFO

Article history:
Received 10 April 2018
Received in revised form 28 June 2018
Accepted 30 June 2018
Available online 5 July 2018

Keywords:
Poly (lactic acid) (PLA)
Foam
Cellulose nanocrystals (CNC)

ABSTRACT

The current investigation addresses the thermal degradation and non-isothermal crystallization behaviour of the fabricated poly (lactic acid) foam (nPLA) and poly (lactic acid) (PLA)/cellulose nanocrystal (CNC) based foams at three different loadings of CNC (i.e. 1%, 2% and 3%) as PLA/CNC 1, PLA/CNC 2 and PLA/CNC 3 having highly porous, interconnected and microcellular morphology. The formation of various gaseous products at two different conversions ($\alpha = 0.3$ and $\alpha = 0.7$) are investigated by using thermogravimetric analyser hyphenated Fourier transmission infrared spectroscopy (TGA-FTIR) analysis in isothermal condition. Effect of porosity and CNC reinforcement towards thermal degradation and crystallization of the PLA is thoroughly investigated by using mercury intrusion porosimetry (MIP). "Model-free" and "modelistic" approaches like Friedman, Flynn-Wall-Ozawa (FWO), Kissinger-Akahira-Sinouse (KAS), Kissinger and Augis & Bennet have been utilized for non-isothermal degradation kinetics of the fabricated foams. Non-isothermal melt crystallization kinetics of fabricated foams reveals that both primary and secondary crystallization process taking place. The apparent activation energy calculated from FWO are ~175.8 kJ/mol, ~198.6 kJ/mol, ~175.5 kJ/mol and ~174.7 kJ/mol for nPLA, PLA/CNC 1, PLA/CNC 2 and PLA/CNC 3 respectively. It is also observed that at higher conversions, complex three dimensional diffusion mechanism of degradation might be taking place in accordance with Criado plots.

1. Introduction

The demand of biodegradable polymeric substances is growing day by day due to environmental hazards caused by the conventional non-degradable petroleum based polymers [1]. The requirement of green technology for bringing more and more biodegradable polymers to the market has become one of prime interest for academia as well as industries. However, some properties of the biodegradable polymers are not upto the mark and can be tuned to compete with major commercial polymers like polystyrene (PS) and polypropylene (PP). Biodegradable polymers from natural feedstock like poly (ε-caprolactone) (PCL), polyhydroxybutyrate (PHB), starch and poly (lactic acid) (PLA) is now started to flourish in the market. Now days many researchers are focusing on PLA due to its bio based, biodegradable and biocompatible nature along with comparable strength, modulus with conventional petroleum based non-degradable polymers [2].

One of the concerning factor of biodegradable polymers is the cost of production. The cost of production of a material can easily be reduced by converting it to foam. Foam production required less material usage compared to unfoamed products which also effects the cost of production of the materials. Foaming technology is used to create gaseous voids in polymeric materials to produce lightweight products [3,4]. Development of biodegradable foam is a current hot topic due to its applicability in various biomedical related fields like drug delivery [5], tissue engineering [6] etc. where degradability is a factor. Researches are going to establish biobased foams like PLA (due to its comparable properties) as a green replacement [7] of conventional petro based polymer foams for different applications [8,9]. The various foam properties can be tuned by addition of nanofillers, additives [10,11] etc. Biobased nanofillers like cellulose nanocrystals (CNC) can be used for PLA based biodegradable foams. CNC is a smart biomaterial comes from natural feedstock. Lots of researches are going on CNC based biomaterials due to its advantages like high surface area, non-toxicity and biodegradable nature [10,12].

Polymer foaming is generally done in batch or in continuous process [13]. Solid state foaming of polymers is done by using inert gases like nitrogen (N_2) [14], carbon dioxide (CO_2) in supercritical state under high temperature and pressure [15,16]. Foaming can also be done by using chemical foaming agents (CFA) in the polymer matrix [17], by using thermally induced phase separation (TIPS) process [18] and by using casting and leaching method [10]. In C/L method, normally a water soluble porogen particles are used to fabricate the porous polymer structure. In this technique the pore size and morphology of the fabricated foams can be controlled by the amount and size of the porogen particles [19,20].

* Corresponding author.
E-mail address: vkatiyar@iitg.emet.in (V. Katiyar).

https://doi.org/10.1016/j.ijbiomac.2018.06.202
0141-8130/

International Journal of Biological Macromolecules 106 (2018) 433–446

Contents lists available at ScienceDirect

International Journal of Biological Macromolecules

journal homepage: www.elsevier.com/locate/ijbiomac

Biodegradable poly (lactic acid)/Cellulose nanocrystals (CNCs) composite microcellular foam: Effect of nanofillers on foam cellular morphology, thermal and wettability behavior

Shasanka Sekhar Borkotoky, Prodyut Dhar, Vimal Katiyar*

Department of Chemical Engineering, Indian Institute of Technology Guwahati, Guwahati 781039, Assam, India

ARTICLE INFO

Article history:
Received 20 June 2017
Received in revised form 19 July 2017
Accepted 4 August 2017
Available online 7 August 2017

Keywords:
Poly (lactic acid)
Foam
Cellulose nanocrystals (CNCs)

ABSTRACT

This article addresses the elegant and green approach for fabrication of bio-based poly (lactic acid) (PLA)/cellulose nanocrystal (CNCs) bionanocomposite foam (PLA/CNC) with cellular morphology and hydrophobic surface behavior. Highly porous (porosity >80%) structure is obtained with interconnected pores and the effect of CNCs in the cell density (N_f) and cell size of foams are thoroughly investigated by morphological analysis. The thermo-mechanical investigations are performed for the foam samples and almost ~1.7 and ~2.2 fold increase in storage modulus is observed for the compressive and tensile mode respectively. PLA/CNC based bionanocomposite foams displayed similar thermal stability as base PLA foam. Detailed investigations of decomposition behavior are studied by using hyphenated thermogravimetric analysis-fourier transmission infrared spectroscopy (TGA-FTIR) system. Almost ~13% increment is observed in crystallinity at highest loading of CNCs compared to neat counterpart. To investigate the splitting and spreading phenomenon of the wettability of the samples, linear model is used to find the Young's contact angle and contact angle hysteresis (CAH). Besides, ~6.1 folds reduction in the density of PLA and the nanocomposite foams compared to PLA carries much significance in specialized application areas where weight is an important concern.

1. Introduction

The importance of bio-based and biodegradable polymers is growing day by day due to the generation of plastic waste and the problem of their ultimate disposal [1]. PLA is a bio-based, biocompatible and biodegradable material and getting global importance due to possible adverse impact on the environment by the use of petrochemical based synthetic polymers [2,3]. PLA is a linear aliphatic polymer, which can be derived from ring opening polymerization of lactide. Lactide is produced from natural bio feedstock like corn, sugar etc. [4]. However, the cost of production of PLA is relatively higher than other synthetic petroleum based polymers for similar applications. In order to match its applications with conventional polymers, it is demand of time to adopt strategies by which, the cost of production of articles made of PLA can be reduced. In order to fulfil the above criteria, foaming process seems to be a viable process where significantly less polymeric material can be used because foam contains enormous gaseous voids in its structure. In recent years, the need of polymeric foam has increased dramatically. Porous materials have some very important properties like high surface area, low thermal conductivity, light weight, high permeability, low density etc. [5]. Foams can be prepared from all three types of materials e.g. metal, ceramic and elastomers. However, the use of elastomeric foam is tremendous in our daily life. The polymeric foams got attention in the market due to the demand of materials such as shock and sound absorbers, light weight materials etc. [6]. Due to its huge demand in the above fields, the annual production of polymeric foams has a large share in the total polymer production in the world [7]. At present, the major market players for polymeric foams are the conventional non-degradable foams like polyurethane, polystyrene, polypropylene etc. [8]. But due to the ultimate disposal problem of these non-degradable polymers, biodegradable polymeric foams can play a major role in the future [9]. Recently, a lots of investigations has been done in biodegradable PLA foams. Poly (lactic acid) foams can be a better replacement in green packaging to the non-degraded foams [10]. PLA foams have potential to compete with conventional non-degradable petroleum based foams like polyurethane, polystyrene etc. in some of the applications where degradability is a major area of concern [11]. Foam materials have to fulfil some requirements for specific type

* Corresponding author.
E-mail address: vkatiyar@iitg.ernet.in (V. Katiyar).

http://dx.doi.org/10.1016/j.ijbiomac.2017.08.036
0141-8130/

International Journal of Biological Macromolecules 125 (2019) 159–170

Contents lists available at ScienceDirect

International Journal of Biological Macromolecules

journal homepage: http://www.elsevier.com/locate/ijbiomac

Poly (lactic acid)/modified gum arabic (MG)based microcellular composite foam: Effect of MG on foam properties, thermal and crystallization behavior

Shasanka Sekhar Borkotoky, Tabli Ghosh, Purabi Bhagabati, Vimal Katiyar *

Indian Institute of Technology Guwahati, Assam 781039, India

ARTICLE INFO

Article history:
Received 20 September 2018
Received in revised form 12 November 2018
Accepted 26 November 2018
Available online 28 November 2018

Keywords:
Poly (lactic acid)
Foam
Gum arabic

ABSTRACT

The article demonstrates a simple and innocuous method for fabrication of poly (lactic acid) (PLA)/modified gum arabic (MG)based hydrophobic, microcellular, highly porous and interconnected composite foam. The observed density of the composite foams was remarkably reduced by ~86% in comparison to PLA granules. Further, there was noticed an increase in cell density and a decrease in cell size due to the addition of MG nanofiller. The thermogravimetric analysis (TGA) of developed foam showed no significant effect of MG in maximum degradation temperature (T_{max}). Dynamic mechanical analysis (DMA) and differential scanning calorimetry (DSC) investigations suggested the plasticizing effect of MG nanofiller in the PLA matrix. The hydrophobicity of fabricated foam was found to increase with an increase in loading of MG and an increment of ~20° in contact angle was observed for highest loading of MG (3%) in comparison to neat PLA foam. Further, an increase in the surface area up to ~60% and a decrease in pore diameter up to ~53% were observed for PLA/MG based foam by porosimetric investigations. Based on this investigation, the fabricated PLA/MG based foams have the potential for specialized applications as an alternative to non-degradable petro-based foams in various fields of life.

1. Introduction

Recently, polymeric foams have gained a lot of attention over non-foamed materials due to its unique advantages such as lightweight, less usage of materials etc. that positively affects the production cost [1]. Foaming process is generally carried out by using different established techniques such as casting and leaching (C/L) [2], thermally induced phase separation (TIPS) [3,4], using inert gases CO_2, N_2 [5,6], using supercritical gases [7] etc. Among all available techniques, solvent casting and particulate leaching is one of the simple and less expensive methods compared to other techniques of foaming. In this technique, porogens like salt, sugar etc. are used which on leaching left a porous structure in the polymer matrix [8]. In recent times, the polymeric foam market is mainly dominated by petroleum based, non-degradable conventional foams like polyurethane (PU) foam [9], polystyrene (PS) foam etc. [10]. The leftover carbon footprint and the disposal of these materials is an environmental concern [11]. The detrimental effects of non-degradable polymeric foams can be overcome by replacing with biodegradable polymeric foams [12]. Biodegradable polymeric foams are now showing their presence in different acoustic, thermal insulation, commodity, biomedical and commodity applications. However, to compete with conventional non-degradable polymeric foams, it needs some tuning in properties [13]. Among available biodegradable polymers, poly (lactic acid) (PLA) is maintaining a significant interest in providing a wide application in the area of biodegradable polymeric materials for tissue engineering application. Nowadays, the use of PLA based polymeric foam is increasing due to their potentiality in the field of food packaging, tissue engineering for developing scaffolds for tissue [14,15]. In recent researches, it is observed that nanofillers like clay [16], cellulose nanocrystals (CNC) [13,17], starch [18], graphene oxide [19], etc. are utilized to tune various properties of the PLA based microcellular and nanocellular foams. In a greener approach, bio-based and biodegradable PLA foams are now commercialized for packaging applications and are projected as an alternative to nondegradable conventional polystyrene (PS) foams [20]. Blaker et al. formulated poly D, L lactic acid (PDLA)/Bioglass® based foams, which is highly porous, degradable foam providing a remarkable application in the field of bone tissue engineering [21]. Interestingly, increase in surface area and a decrease in the cell size of the foam are two important parameters for biomedical applications like cell proliferation study, tissue engineering an so on. [22]. In current situation, researchers are mainly interested in the biobased, biocompatible nanofillers for tuning the properties of biodegradable foams. In literature, some investigations are found on the effect of polysaccharide-based gums like gum tragacanth, gum karaya and so on in PLA matrix. Recently, investigations on

* Corresponding author.
E-mail address: vkatiyar@iitg.ernet.in (V. Katiyar).

https://doi.org/10.1016/j.ijbiomac.2018.11.257
0141-8130/

JOURNAL OF Applied Polymer SCIENCE

Poly(lactic acid)/modified chitosan-based microcellular foams: Thermal and crystallization behavior with wettability and porosimetric investigations

Shasanka Sekhar Borkotoky, Akhilesh Kumar Pal, Vimal Katiyar
Indian Institute of Technology Guwahati, Guwahati, 781039, Assam, India
Correspondence to: V. Katiyar (vkatiyar@iitg.ernet.in)

ABSTRACT: This article addresses a less expensive and elegant method for the fabrication of hydrophobic poly(lactic acid) (PLA)/modified chitosan (MC)-based bionanocomposite foams with high porosity (>~80%) and open cellular interconnected morphology. An increment of ~2.3-fold of cell density and reduction of ~1.3-fold of cell size are observed at highest loading of MC (i.e. 3 wt %). The MC also influences the hydrophobicity (up to ~10 increment in contact angle) of the foams. Structure–property relationship of the fabricated foams has been investigated along with wettability behavior. Thermal degradation kinetics and degradation mechanism of the fabricated foams have been investigated by using different approaches like modified Coats Redfern (modified CR), Flynn-Wall-Ozawa (FWO), Kissinger, and Criado. Crystallization behavior of the fabricated foams are also investigated. Increase in surface area with MC-loading and nucleating behavior of MC in the PLA matrix is confirmed by the porosimetric investigation of the fabricated foams. © 2018 Wiley Periodicals, Inc. J. Appl. Polym. Sci. **2018**, *00*, 47236.

KEYWORDS: biodegradable; biomaterials; crystallization; foams; porous materials

Received 18 June 2018; accepted 15 September 2018
DOI: 10.1002/app.47236

INTRODUCTION

Recently polymeric foams gain many attentions in research due to its unique characteristics over non-foamed counterparts like lightweight and low density. These unique properties make it suitable to penetrate in almost all aspects in our daily life. The cost of production of these materials are also comes down due to the less usage of material.[1] Polymeric foams are mainly fabricated by using established techniques like casting and leaching (C/L),[2,3] solid state foaming using inert gases,[4] thermally induced phase separation (TIPS),[5] and so on. Currently, polymeric foam market is mainly dominated by conventional petroleum-based polymeric foams like polystyrene (PS), polypropylene (PP), and so on.[6] The ultimate disposal and recycle of these polymers have some detrimental effects in nature. Due to this reason, now researchers are mainly focus on development of green biodegradable foams, which can be easily fed to the ecological system.[7] Foamed materials already made their strong presence in some sophisticated areas of application like drug delivery, tissue engineering, and other biomedical applications. The need of new greener sustainable polymeric foam for the environmental point of view is opening new opportunities for biobased, non-toxic, and biodegradable polymers like poly(lactic acid) (PLA), polycaprolectum, and so on. In some sophisticated applications, biodegradability is a major area of concern.[8] In the recent past, PLA-based foams gets more attention in the research community due to its comparable properties with petroleum-based conventional polymeric foams. It can be used as a green packaging for various applications.[9] The requirements of foam properties (like cell size, cell density etc.) varies with the applications. The limitations of PLA like low melt strength and brittleness can be tuned to desired level depending on applications by incorporating nanofillers,[10] plasticizing agent,[11] chain extender,[12] and so on in the PLA matrix. Nanofillers like organically modified montmorillonite,[13–15] organically modified layered silicates (organoclay)[16] has been used in the recent past to tune various properties of PLA foam according to applications. Silk composite,[17] graphene oxide,[18] chain extenders,[12] and paraffin spheres[19] are also used by the researchers for various improvement in properties. PLA foam can be a possible candidate for biomedical sophisticated applications if some of its properties can be tuned by using bio-based, bio derived, and biodegradable materials.[20]

More greener approach of development and improvement of PLA foams can be done by using some naturally derived

Additional Supporting Information may be found in the online version of this article.